IAEA-TECDOC-1682

Advances in Nuclear Power Process Heat Applications

IAEA
International Atomic Energy Agency

Advances in Nuclear Power Process Heat Applications

The following States are Members of the International Atomic Energy Agency:

AFGHANISTAN
ALBANIA
ALGERIA
ANGOLA
ARGENTINA
ARMENIA
AUSTRALIA
AUSTRIA
AZERBAIJAN
BAHRAIN
BANGLADESH
BELARUS
BELGIUM
BELIZE
BENIN
BOLIVIA
BOSNIA AND HERZEGOVINA
BOTSWANA
BRAZIL
BULGARIA
BURKINA FASO
BURUNDI
CAMBODIA
CAMEROON
CANADA
CENTRAL AFRICAN REPUBLIC
CHAD
CHILE
CHINA
COLOMBIA
CONGO
COSTA RICA
CÔTE D'IVOIRE
CROATIA
CUBA
CYPRUS
CZECH REPUBLIC
DEMOCRATIC REPUBLIC OF THE CONGO
DENMARK
DOMINICA
DOMINICAN REPUBLIC
ECUADOR
EGYPT
EL SALVADOR
ERITREA
ESTONIA
ETHIOPIA
FINLAND
FRANCE
GABON
GEORGIA
GERMANY
GHANA
GREECE
GUATEMALA
HAITI
HOLY SEE
HONDURAS
HUNGARY
ICELAND
INDIA
INDONESIA
IRAN, ISLAMIC REPUBLIC OF
IRAQ
IRELAND
ISRAEL
ITALY
JAMAICA
JAPAN
JORDAN
KAZAKHSTAN
KENYA
KOREA, REPUBLIC OF
KUWAIT
KYRGYZSTAN
LAO PEOPLE'S DEMOCRATIC REPUBLIC
LATVIA
LEBANON
LESOTHO
LIBERIA
LIBYA
LIECHTENSTEIN
LITHUANIA
LUXEMBOURG
MADAGASCAR
MALAWI
MALAYSIA
MALI
MALTA
MARSHALL ISLANDS
MAURITANIA
MAURITIUS
MEXICO
MONACO
MONGOLIA
MONTENEGRO
MOROCCO
MOZAMBIQUE
MYANMAR
NAMIBIA
NEPAL
NETHERLANDS
NEW ZEALAND
NICARAGUA
NIGER
NIGERIA
NORWAY
OMAN
PAKISTAN
PALAU
PANAMA
PARAGUAY
PERU
PHILIPPINES
POLAND
PORTUGAL
QATAR
REPUBLIC OF MOLDOVA
ROMANIA
RUSSIAN FEDERATION
SAUDI ARABIA
SENEGAL
SERBIA
SEYCHELLES
SIERRA LEONE
SINGAPORE
SLOVAKIA
SLOVENIA
SOUTH AFRICA
SPAIN
SRI LANKA
SUDAN
SWEDEN
SWITZERLAND
SYRIAN ARAB REPUBLIC
TAJIKISTAN
THAILAND
THE FORMER YUGOSLAV REPUBLIC OF MACEDONIA
TUNISIA
TURKEY
UGANDA
UKRAINE
UNITED ARAB EMIRATES
UNITED KINGDOM OF GREAT BRITAIN AND NORTHERN IRELAND
UNITED REPUBLIC OF TANZANIA
UNITED STATES OF AMERICA
URUGUAY
UZBEKISTAN
VENEZUELA
VIETNAM
YEMEN
ZAMBIA
ZIMBABWE

The Agency's Statute was approved on 23 October 1956 by the Conference on the Statute of the IAEA held at United Nations Headquarters, New York; it entered into force on 29 July 1957. The Headquarters of the Agency are situated in Vienna. Its principal objective is "to accelerate and enlarge the contribution of atomic energy to peace, health and prosperity throughout the world''.

IAEA-TECDOC-1682

ADVANCES IN NUCLEAR POWER PROCESS HEAT APPLICATIONS

INTERNATIONAL ATOMIC ENERGY AGENCY
VIENNA, 2012

For further information on this publication, please contact:

Nuclear Power Technology Development Section
International Atomic Energy Agency
Vienna International Centre
PO Box 100
1400 Vienna, Austria
email: Official.Mail@iaea.org

Printed by the IAEA in Austria
May 2012

IAEA Library Cataloguing in Publication Data

Advances in nuclear power process heat applications. –
Vienna : International Atomic Energy Agency, 2012.
p. ; 30 cm. – (IAEA-TECDOC series, ISSN 1011-4289 ; no. 1682)
ISBN 978-92-0-130210-6
Includes bibliographical references.

1. Gas cooled reactors – Design and construction.
2. Gas cooled reactors – Safety measures. 3. Saline water conversion. 4. Hydrogen – Research.
I. International Atomic Energy Agency. II. Series.

IAEAL 12-00742

FOREWORD

The coordinated research programme (CRP) on the Potential of High-Temperature Gas cooled Reactors for Process Heat Applications was organized in the framework of the technical working group on gas cooled reactors (TWG-GCR) established in 1978 with the purpose of advising the Director General of the IAEA and promoting the exchange of technical information on national programmes in the field of gas cooled reactors.

The project has been conducted within the Nuclear Power Technology Development Section of IAEA. It was actually launched in 2007, with research proposals received from nine Member States and completed by 2009. The participants were: Argentina, China, France, Germany, Japan, India, the Russian Federation, South Africa, and the Syrian Arab Republic. Some specific objectives of this CRP were to:

- Address and update the status of R&D on technical and economic prospects of coupling HTGR to process heat applications;
- Focus on potential use of HTGR for nuclear hydrogen production and seawater desalination, representing high temperature and low temperature process heat applications;

The outcome of the CRP was expected to include the following:

- Collection of data, analysis of design features, characteristics of couplings, and safety and environmental aspects of HTGR and their process heat applications;
- Analysis of configuration of nuclear hydrogen production plants and layout and design approaches of high temperature heat exchangers;
- Analysis of waste heat from HTGR and its potential use for seawater desalination.

The basic aim of the present publication is to summarize the outputs from the Member States, participating in this CRP. The publication therefore follows the same objectives and scope as those established for the CRP. Indeed, this publication is intended to present the results of participants to this CRP and highlight major advances, difficulties and recommendations in the area of non-electric applications of nuclear energy which are of importance to the nuclear communities at large and to scientists and engineers focusing on safety aspects and economics of the overall nuclear power plant coupled to applications of process heat.

Previous activities of the GCR project relevant to this CRP were an IAEA Technical Committee Meeting (TCM) on the subject of high temperature applications of nuclear energy, held in Japan in 1992, and several meetings with OECD/NEA on issues such as prospects for hydrogen in future energy structures and role of nuclear power, status of nuclear hydrogen R&D efforts around the globe, nuclear hydrogen technologies and design concepts, integrated nuclear hydrogen production systems, and basic and applied science in support of nuclear hydrogen production.

This publication has been prepared through the collaboration of all the participants to the CRP. The IAEA appreciates this support and thanks all the authors who provided their reviews and contributions. Especially appreciated is the contribution of K. Verfondern (Germany) in the compilation and preparation of this IAEA-TECDOC. The IAEA officer responsible for this publication was I. Khamis of the division of nuclear power.

EDITORIAL NOTE

The use of particular designations of countries or territories does not imply any judgement by the publisher, the IAEA, as to the legal status of such countries or territories, of their authorities and institutions or of the delimitation of their boundaries.

The mention of names of specific companies or products (whether or not indicated as registered) does not imply any intention to infringe proprietary rights, nor should it be construed as an endorsement or recommendation on the part of the IAEA.

CONTENTS

1. INTRODUCTION

1.1. OBJECTIVES

The increased interest in nuclear power process heat applications, such as hydrogen production and seawater desalination was one of the major drivers for the IAEA to initiate a coordinated research project (CRP) on Advances in Nuclear Power for Process Heat Applications which was completed in 2009. The challenges which were addressed by this CRP are related to process technologies, coupling safety, high temperature material technology and the economic merits of centralized vs distributed production units.

In addition to increasing the cooperation among member states on information exchange on nuclear process heat applications and to serve as a platform for collaborative research on the technical and economic aspects of coupling high temperature gas cooled reactors (HTGR) to process heat applications such as hydrogen production and seawater desalination, the overall objective was to assess the potential of high temperature gas cooled reactors in process heat applications and to update the status of related research and development.

The CRP was effective in reaching specific objectives as in establishing a solid background on HTGR and its potential applications for process heat applications. During the implementation of CRP, results have been obtained from leading institutes and offered up-to-date information on R&D in both analytical and experimental areas, permitting to derive useful conclusions and recommendations. The CRP offered a platform for nine experts from eight member states jointly analyzing the potential of HTGR for two main applications of process heat applications: hydrogen production and seawater desalination. The collaboration among these experts, specifically within each application proved to be an effective means of reaching the overall objective of the CRP. However, heterogeneity of the participants to the CRP as they formed two groups working independently from each other namely: the hydrogen group whom are not interested in desalination, and the desalination group whom they have no direct knowledge on hydrogen productions and related issues. Another factor was the budget constraints, specifically limitation in grants for research contracts

1.2. NUCLEAR PROCESS HEAT APPLICATIONS

Nuclear heat applications have been considered for long time, but not much has succeeded. Effective and practical measures to gain the advantages of aspects of climate change — green house gas reduction — need to be taken now. Nuclear industry and related branches should advance and address to the real world as other technologies and environmental institutions do. Practical application would be possible based on exchange of experiences and further international collaboration.

Since nuclear energy is nearly carbon free generation and is long term sustainable solution and potentially cost-competitive with fossil fuels, it is necessary to consider it as a choice for desalination projects. Particularly in cases when power and heat for desalination is generated from using heavy crude oil or coal, which requires significant cost for pollution control and is an inefficient generation solution, resulting in significant increase of the penalty for CO_2 emission and greenhouse impact.

As an alternative path to the current fossil fuel economy, a hydrogen economy is envisaged in which hydrogen would play a major role in energy systems and serve all sectors of the economy, substituting for fossil fuels. Hydrogen as an energy carrier can be stored in large quantities, unlike electricity, and converted into electricity in fuel cells, with only heat and

water as by-products. It is also compatible with combustion turbines and reciprocating engines to produce power with near-zero emission of pollutants.

Nuclear-generated hydrogen has important potential advantages over other sources that will be considered for a growing hydrogen economy. Nuclear hydrogen requires no fossil fuels, results in lower greenhouse gas emissions and other pollutants, and lends itself to large scale production. These advantages do not ensure that nuclear hydrogen will prevail, however, especially given strong competition from other hydrogen sources. There are technical uncertainties in nuclear hydrogen processes, certainly, which need to be addressed through a vigorous research and development effort. The hydrogen storage and distribution are also important area of research to be undertaken for bringing in a successful hydrogen economy regime in future.

1.3. SCOPE OF THE REPORT

The scope of this CRP was to enable the member states to investigate the potential of using high temperature reactors for cogeneration of electricity and hydrogen, and for other process heat applications.

The report includes an overview of current progress on HTGR coupling schemes for different process heat applications, such as hydrogen production and desalination. Apart from the coupling schemes, a more detailed description is also provided on the actual work that was performed and the corresponding results. These include both technical work on the different processes as well as techno–economic studies. A major focus was on the qualitative assessment of using waste heat generated by such reactors for seawater desalination and the optimal thermochemical processes for hydrogen production. The important safety aspects of coupling high temperature reactors to hydrogen and desalination facilities are highlighted.

As this report includes results achieved by participants to the CRP, it will benefit scientists and engineers working in the areas of nuclear hydrogen production and desalination, safety and design aspects of integrated nuclear desalination systems, and economics of such systems. In addition, decision makers/their advisors, physicists and specialists in the area of thermo chemical processes related to hydrogen production and desalination technologies, and the general public as well.

2. PROCESS HEAT HIGH TEMPERATURE REACTOR CONCEPTS

2.1. DESIGN ASPECTS

Development of the high temperature gas cooled reactor is pursued as an environmentally agreeable efficient power source for electricity generation and other industrial applications. One of its main objectives is to provide energy for facilitating combined production of desalinated water, electricity and hydrogen. The high exit temperature of the coolant of about 900°C is useful for hydrogen production. The reject heat is utilized for electricity generation. The waste heat can be utilized for the desalination of seawater for producing potable water.

The HTGR is considered as one of the leading candidates for future nuclear power plants for the following advantages

- Higher thermodynamic efficiency;
- Lower waste quantity;
- Higher safety margins;
- High burnup (~100 GW·d/t of uranium).

2.1.1. General design of HTGR

An HTGR plant is contained in two or more interconnected pressure vessels and enclosed in general in an underground concrete containment structure. In the example of the design shown in Fig. 2.1, one vessel contains the reactor system and the second vessel contains the entire power conversion system. The turbo-machinery is composed of a generator, turbine and two compressor sections mounted on a single shaft rotating on magnetic bearings. The vessel also contains three compact heat exchangers.

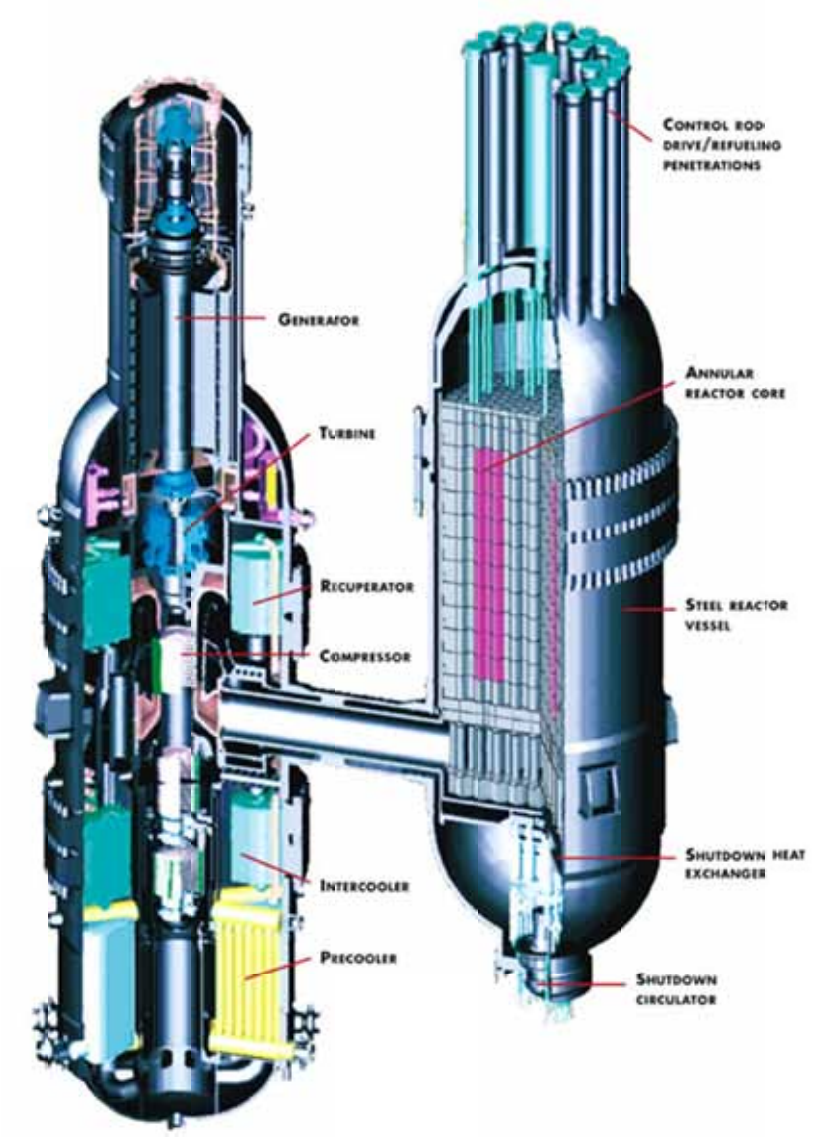

FIG. 2.1. High temperature gas cooled reactor.

The power conversion unit (PCU) consists of two turbo-compressors, power turbine, recuperator, precooler and intercooler. The turbo-compressors are placed in a chamber called pressure vessel, which is also used as the duct between the high pressure compressor (HPC) outlet and the recuperator cold side inlet.

At present, all modern HTGR designs are based on the modular concept providing for increased safety because of inherent self-protection properties and passive cool down. There are the well-known two types of reactor. One has a core with block type fuel elements and the other has a pebble-bed core. Power sizes of the reactors with a pebble bed and prismatic fuel

blocks, and with annular active core geometry are limited to about 400 MW(th) and 600 MW(th), respectively. These values are determined by the maximum allowable fuel temperature (< 1600°C) in the case of loss of forced convection (LOFC) in the depressurized reactor with residual heat removal through the reactor vessel to the reactor cavity cooling system.

Some of the main characteristic features of HTGR designs with either block or pebble core are compared in Table 2.1.

TABLE 2.1. MAIN CHARACTERISTICS OF PLANT DESIGNS WITH BLOCK TYPE CORE AND PEBBLE BED TYPE CORE

Reactor type	Block core	Pebble-bed core
Power and efficiency		
Thermal power (MW(th))	600	200–500
Electric power (MW(e))	274–284	80–200
Cycle/net thermal efficiency (%)	47.2–48.4/45.6–46.2	44–49.5/45.5
Main Gas Conditions		
Reactor inlet/outlet temperature (°C)	460–587/850	280–550/750–950
Helium gas pressure (MPa)	7–7.15	5.5–9
Mass flow rate (kg/s)	296.4–440	~203
Fuel		
Fuel element	Monolithic pin-in-block	60 mm diameter sphere
Average enrichment (%)	15	10
Packing fraction	29–35	4–11
Average burnup (GW·d/t U)	110–120	100
Fuel cycle (days)	450–730	903
Fuel exchange working time (days)	33–82 (incl. reflector exchange)	On power loading
Core		
Equivalent diameter (m) cylindrical annular	 3.70/5.48 (inner/outer)	≤ 3.0 2.70/4.50 (inner/outer)
Effective height (m)	8.1–8.4	9.4
Average power density (MW/m^3)	5.44–5.77	4.2
Pressure drop (%)	0.65–1.42	3.3
Maximum fuel temperature during normal operation (°C) in accident (°C)	 1108–1286 1546–1575	 1130 1520
Reactor vessel		
Inner diameter (m)	7.62–7.89	≤ 7.3
Height (m)	23.4–24.4	≤ 32.4
Weight (ton) upper/lower part	285–398/838–923	134/975
Material	9Cr–1Mo–V or SA533/SA508 steel	SA 533
Dose rate due to fission product plate out on the turbine rotor (mSv/h)	160	5440

In case of a block type core, the modest reactor outlet gas temperature of 850°C for power generation reactor designs [1–3] and of 900-950°C for process heat reactor designs including for nuclear hydrogen production [4–6] has been selected. The range of design values listed for the block core in Table 2.1 have been reported of the power generation reactor designs. In case of pebble-bed core, the higher reactor outlet gas temperature of 900°C could be achieved easily during normal operation. In this type of core, the maximum temperature at the depressurization accident is most critical.

Pebble Bed Modular Reactor (Pty) Ltd. has been developing advanced helium cooled, graphite-moderated HTGRs during the past decade. The PBMR technology is expected to be the basis of a family of products that has multiple applications. It is ideal for electricity generation where small energy demand markets prevail or distributed generation is required. The PBMR is also an ideal source of high temperature and pressure (high energy) steam. With follow-on development it is also an ideal source for direct high temperature process heat applications.

The early market PBMR process heat plant (PHP) is envisaged to operate at power levels between 200 and 250 MW(th) with reactor outlet temperatures up to 750°C, delivering steam, electricity or both. Based on development and qualification of an acceptable intermediate heat exchanger design, the direct high temperature process heat applications can be addressed by this plant. The configuration of the pebble-bed process heat plant and the requirements associated with the IHX depends on the specific process heat application. The business cases for various selected process applications have been prepared. The initial development of the process heat plant is expected to result from an industry consortium approach.

Current development work for the pebble-bed process heat plant is focused on the following time frames and technology windows:

- Applications operating at reactor outlet temperatures less than 750°C to produce high temperature and high pressure steam and cogeneration. Component engineering development requirements and application integration engineering requirements are such that deployment in the latter part of the next decade will be feasible.

- The follow-on development phase will meet the requirements for operating at reactor outlet temperatures up to 950°C. This phase matches timeframes for associated developments in high temperature materials and hydrogen production processes including thermochemical water splitting processes.

2.1.2. Power cycles of HTGR

The helium Brayton cycle is ideally applied to HTGR (Fig. 2.2). Key factors affecting the efficiency of Brayton cycle include the turbine inlet temperature, compressor and turbine adiabatic efficiencies, recuperator effectiveness, and cycle fractional pressure loss. The compression ratio is also important.

2.1.3. HTGR details

The major heat exchangers of gas turbine cycle are recuperator, precooler and intercooler. Direct heat exchangers are integrated together with the turbomachinery in the PCU vessel. Some of the essential parameters are given in above Table 2.2 for the reactor concepts GT-MHR, GTHTR300, and PBMR.

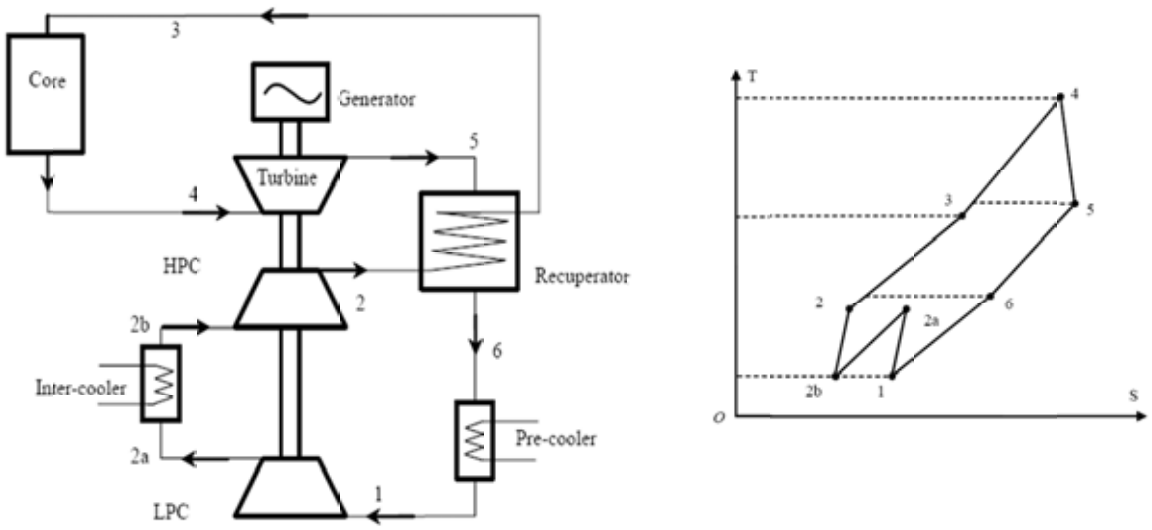

FIG. 2.2. Brayton cycle HTGR and respective temperature–entropy (T–S) plot.

TABLE 2.2. TECHNICAL PARAMETERS FOR GT-MHR, GTHTR300, AND PBMR [2, 7–8]

Parameter	GT-MHR	GTHTR300		PBMR [a]
Net plant efficiency (%)	46.7/45.2	45.6	47.6	42
Inlet/outlet temperature (°C)	490/850	587/850		536/900
Number of cycle intercooling stages	1	none	1	1
Cycle recuperation effectiveness (%)	95	95	95	96
Cycle compression ratio	2.86	2.0	2.4 [b]	2.7
Turbomachine shaft rotation speed (rpm)	3000/4400	3000		15 200 (HP-TC) 14 200 (LP-TC) 3000 (turbo-generator)
Turbine adiabatic efficiency (%)	93.0	93.8	93.5	90 (generator turbine) 89 (compress. turbine)
Compressor adiabatic efficiency LPC/HPC (%)	88.0/87.0	89.5	89.0	89
Relative pressure losses in the helium circuit (%)	7.49/8.1	6.4	7.1	~5
Generator efficiency/Frequency converter (%)	98.65/97.7/98.5	98.7		98.5

[a] There are no published detailed data on a new PCU.
[b] The final design selects non-intercooled cycle. The intercooled cycle option is shown here for comparison purpose only.

2.1.3.1. Recuperator

The recuperator in GT-MHR with direct gas turbine cycle allows the reactor and the turbine to be operated at high temperatures. The hot helium from the core outlet flows directly through the turbine where it is expanded. Then it is cooled before being compressed and flowing back to the core. The turbine drives the electric generator. The high efficiency of the cycle can be still further improved (up to 50%) using a helium/helium heat exchanger called recuperator

between the low and high pressures sides. In this case, the remaining gas energy at the turbine outlet is recuperated by this exchanger and is used to preheat the helium at the core inlet. The recuperator needs to have a high efficiency (95%), but also requires good mechanical characteristics as it operates at high pressure and high temperature. Furthermore, it should be as small as possible to limit the size of the vessel. For the example of the GT-MHR as a commercial-size power reactor, the steady state operating conditions are summarized in Table 2.3.

TABLE 2.3. RECUPERATOR TECHNICAL CHARACTERISTICS FOR A GT-MHR TYPE REACTOR

Parameter	Hot side (LP side)	Cold side (HP side)
Thermal capacity (MW)	630	630
Inlet temperature (°C)	507	107
Outlet temperature (°C)	127	487
Inlet pressure (MPa)	2.6	7.2
Flow rate (kg/s)	320	320

2.1.3.2. Precooler and intercooler

The precooler and intercooler ensure operation of compressors at low temperatures, thereby increasing the thermodynamic efficiency.

As can be seen from Fig. 2.3, the arrangement of two intercooling stages considerably increases the cycle efficiency from 44% up to 50%. The highest increase (~4.5%) takes place when one stage is added. Using intercooled or non-intercooled helium cycle has a strong influence on the design of the turbo-machinery and its layout, when arranging it in the limited space of the PCU.

Tables 2.4 and 2.5 give the characteristics of selected steam cycle HTGRs and modular HTGR gas turbine plants, respectively.

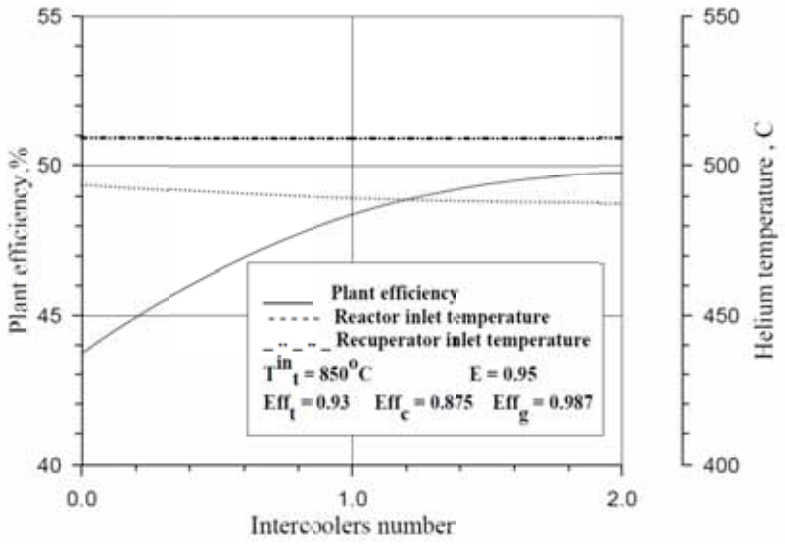

FIG. 2.3. Impact of number of intercoolers on plant efficiency, reactor and recuperator inlet helium temperature [9].

TABLE 2.4. CHARACTERISTICS OF SELECTED STEAM CYCLE HTGRS (AS OF 2001) [10]

	AVR	Peach Bottom	Ft. St. Vrain	THTR-300	HTR-500	VG-400	HTR-Modul	MHTGR
Country of origin	Germany	USA	USA	Germany	Germany	Russian Federation	Germany	USA
Core type	Pebble	Sleeve	Block	Pebble	Pebble	Pebble	Pebble	Block
Thermal power (MW(th))	46	115	842	750	1390	1060	200	350
Net electric power (MW(e))	13	40	330	300	550	Cogeneration	80	139
Power density (MW/m^3)	2.5	8.3	6.3	6.0	6.6	6.9	3.0	5.9
Core outlet temperature (°C)	950	725	775	750	700	950	700	686
Helium pressue (MPa)	1.1	2.25	4.8	3.9	5.5	5.0	6.6	6.4
Steam Temperature (°C)	505	538	538	530	530	535	530	538

TABLE 2.5. CHARACTERISTICS OF SELECTED MODULAR HTGRS GAS TURBINE PLANTS (AS OF 2001) [10]

	GT-MHR	PBMR [a]	MHTGR-IGT	ACACIA	GTHTR300	HTGR-GT	MPBR
Country of origin	USA/Russian Federation	South Africa	China	The Netherlands	Japan	Japan	USA
Core Type	Block	Pebble	Pebble	Pebble	Block	Pin/Block	Pebble
Cycle Type	Direct	Direct	Indirect	Direct	Direct	Direct	Indirect
Thermal power (MW(th))	600	265	200	40	600	600	250
Net electric power (MW(e))	278	116	~96	Cogeneration	273	287	112
Power density (MW/m^3)	6.5	4.3	3.0	—	—	5.77	—
Core outlet temperature (°C)	850	900	900	800	850	850	850
Helium pressure (MPa)	7.15	7.0	6.0	2.3	6.8	6.0	7.9

[a] There are no published detailed data on a new PCU.
— Data not available.

2.2. NUCLEAR HEAT SUPPLY SYSTEM (COUPLING)

2.2.1. Dedicated HTGR for heat-only applications

The HTGR configurations for heat only are currently envisaged as steam only solutions, however, the reactor could be configured for other heat-only applications as well. Steam-only applications include in-situ oil sands recovery using the so-called "steam assisted gravity drainage' (SAGD) process as well as other applications requiring lower pressure steam. Process requirements for oil sands recovery typically include steam at pressures up to 16 MPa, depending on the depth of the deposits. This steam pressure is beyond that normally produced by water moderated nuclear reactors and thus gives a significant advantage to modular HTGRs. The output of a PBMR steam unit is also well matched to the incremental energy requirements currently planned for regional oil sands expansion schemes.

Figure 2.4 presents a layout of the PBMR conceptual design for the indirect production of process heat at intermediate reactor outlet temperatures (up to 800°C) which can be used for petrochemical complexes (the intermediate helium loop piping and steam generator is not shown). This layout is typical of applications where an additional barrier is required between the heat supply and the reactor, such as in hydrogen and ammonia processes, thus the inclusion of the IHX.

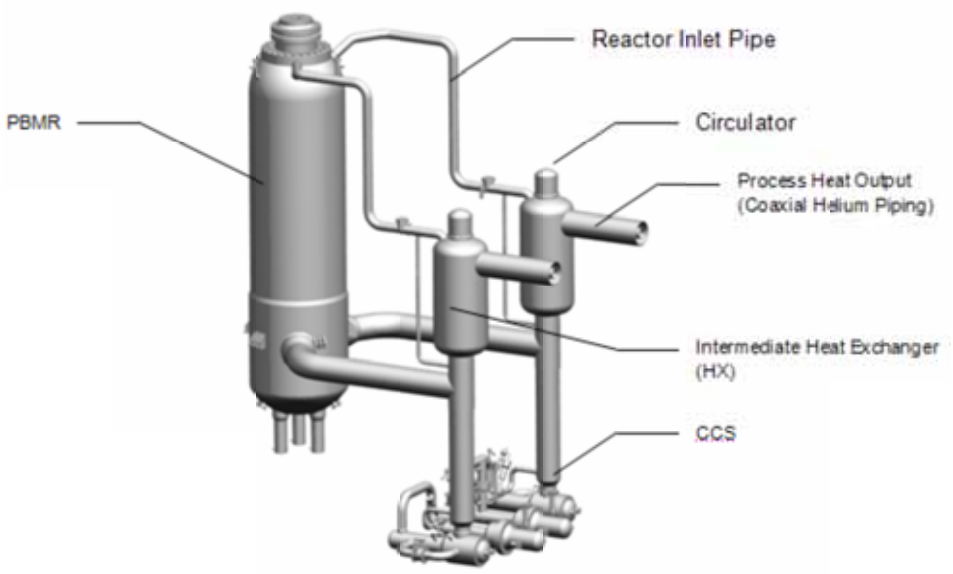

FIG. 2.4. Example of PBMR indirect heat production plant with IHX.

An additional steam-only configuration is presented in Fig. 2.5. In this configuration the hot helium leaving the PBMR first passes through the steam generator after which the blower returns the helium to the reactor inlet. This configuration has some advantages such as utilizing the least number of components while also catering for a range of process temperatures while it does not necessarily fully utilize the high temperature capabilities of the nuclear heat source.

2.2.2. Requirements for cogeneration systems

Cogeneration HTGR systems produce electricity, high temperature process heat for hydrogen production or other applications, and low temperature process steam if desalination system is coupled. Reactor power is shared for electricity generation and process heat supply (Fig. 2.6).

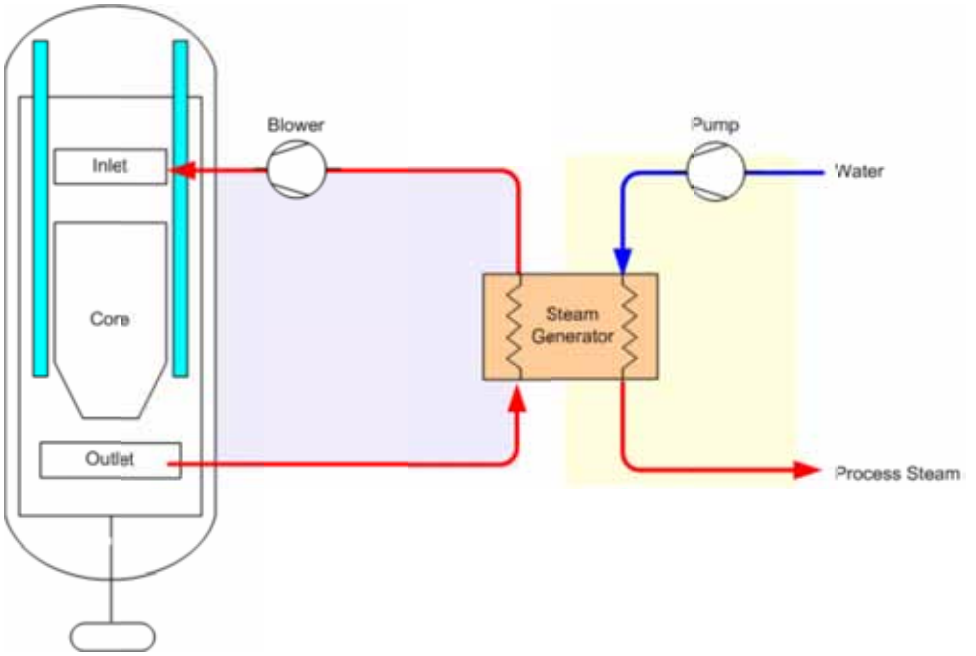

FIG. 2.5. Possible steam-only configuration.

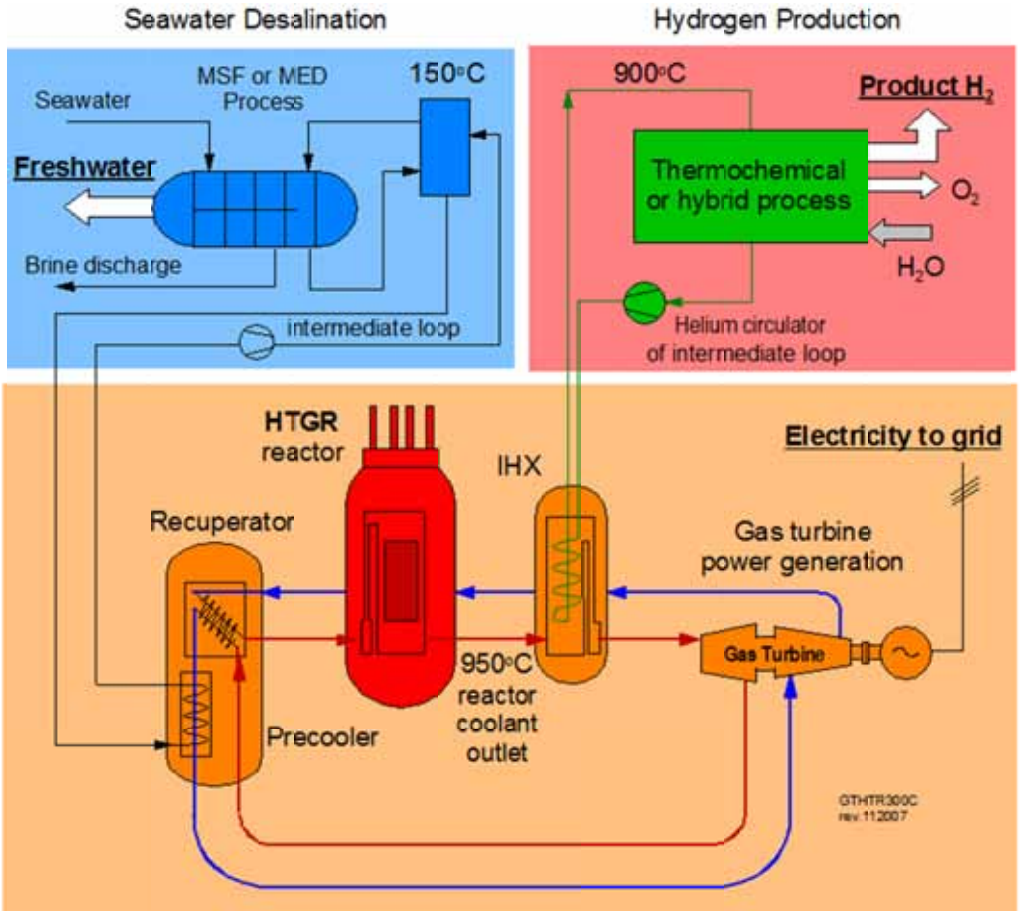

FIG. 2.6. HTGR cascade energy plant for efficient cogeneration of electricity, hydrogen, and fresh water.

The HTGR will employ a gas turbine system to produce electricity economically and effectively. Two system configurations are considered for the gas turbine power generation system. Direct cycle provides a gas turbine system in the primary coolant loop and indirect cycle provides it in the secondary helium loop. Direct cycle has an advantage of power conversion efficiency because of its operation temperature and pressure. But radiation contamination of the gas turbine system is a concern and should be considered. Indirect cycle is proposed to prevent radiation contamination of the gas turbine system. But power conversion efficiency decreases and a large IHX and a secondary loop to transfer nuclear heat from primary to secondary loop is needed so that plant cost will increase.

The major hydrogen production processes of steam methane reforming and thermochemical water splitting process which are expected to be coupled with HTGR, require process heat of 800°C or above for their chemical reactions. The process heat supply system is connected upstream of the gas turbine system in the primary coolant system of the HTGR to generate high temperature secondary helium to supply process heat for the hydrogen production plant. The process heat supply system consists of an IHX which transfers nuclear heat to the secondary helium, a secondary helium piping which couples the HTGR and the hydrogen production plant, and a helium circulator which circulates secondary helium in the piping.

Reactor outlet coolant temperature of the HTGR is required at 900°C or above to supply high temperature process heat. The IHX must withstand the static and dynamic loading at high temperature operation when a hydrogen production plant is in operation or not, because the IHX represents the reactor coolant boundary.

There are two candidates of the IHX configuration. One is the helical tube and shell type IHX and the other one is the plate type IHX. The helical tube and shell type IHX has been developed and demonstrated in test loops in Germany and in the high temperature engineering test reactor (HTTR) in Japan (see also chapter 2.2.6). Plate type IHX with their compact design promise an excellent heat exchanger performance, but they are still under development with regard to their employment under nuclear conditions. Early HTGR cogeneration systems may employ the proven helical tube and shell type IHX. They may be later replaced with plate type IHX, after their development has been completed and demonstration was done in out-of-pile test loops.

HTGR cogeneration system is the base load power generation station. It must supply continuously electricity to the consumer with high plant reliability when hydrogen production plant is shutdown. Power generation system and hydrogen production system should be able to operate independently. The intermediate heat transfer loop has a function to separate physically the hydrogen production system from the nuclear power generation system. Thermal load variation of the hydrogen production plant must be controlled in the power generation system or in the heat transfer loop when the hydrogen production plant has undergone an emergency shutdown.

Other design requirements for HTGR cogeneration system are

(1) to provide safety items to ensure nuclear safety in all operational states against accident in the hydrogen production plant;

(2) to be able to operate load-follow of the hydrogen production plant;

(3) to prevent fission products from transferring to the hydrogen production plant to protect contamination in the products; and

(4) to prevent oxygen and/or water ingress into reactor coolant system from hydrogen production plant.

The cogeneration options that were investigated at PBMR covered a broad spectrum of steam requirements and feedwater conditions with steam pressures ranging from 4 MPa up to 16 MPa and steam temperatures from 312°C up to 510°C. A reference of 4 MPa and 440°C was selected based on requirements from specific petrochemical plants together with the need for electricity generation.

The steam and electricity can be produced with two separate nuclear plants where one is dedicated to steam production and another to electricity production. Alternatively the steam and electricity can be produced with a single nuclear plant. The possible nuclear cycle configurations that were identified for the production of high temperature steam and electricity (cogeneration) is as follows:

(A) Configuration 1

This configuration consists of the PBMR reactor with a topping Brayton Cycle which is connected to a steam generator. The steam generator operates at 18 MPa and makes use of reheating in an open loop bottoming Rankine cycle (Fig. 2.7). The steam is dispended after passing through the open loop Rankine cycle. This configuration will typically favor process plants requiring lower pressure steam and more electricity than process steam. Additionally this configuration can also favor locations where electricity sales provide an economic advantage.

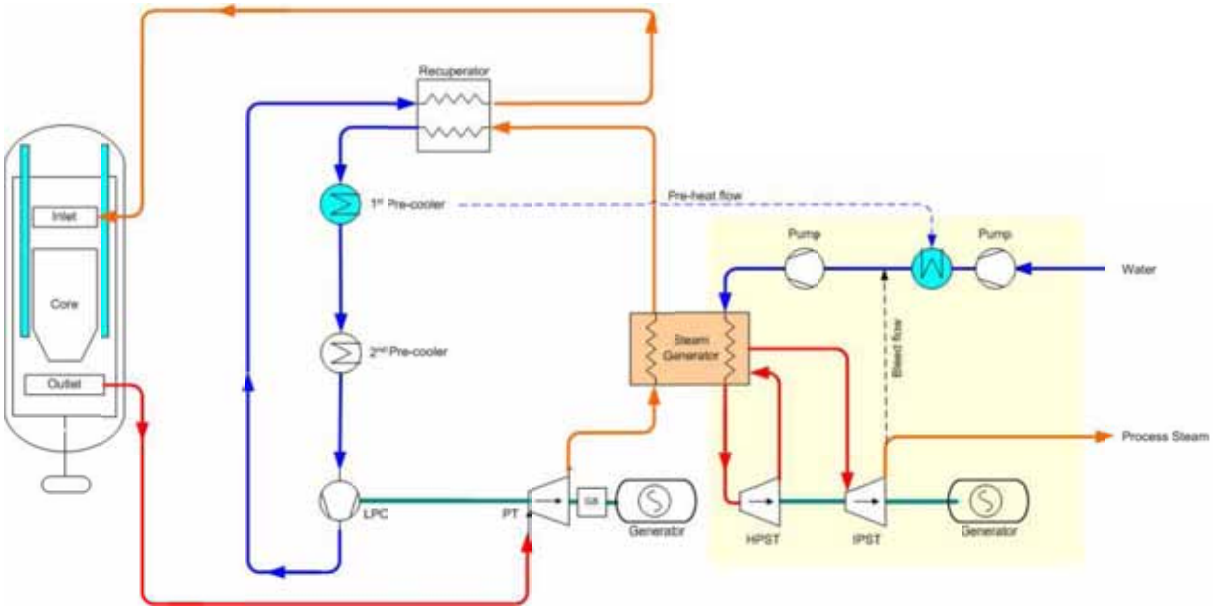

FIG. 2.7. Cogeneration configuration 1.

(B) Configuration 2

Configuration 2 is illustrated in Fig. 2.8 and consists of the PBMR reactor with a topping Brayton cycle. This is in turn connected to a steam generator which operates at the required steam pressure. This configuration will favor typically process plants requiring higher pressure steam and more process steam than electricity, but again does not fully utilize the high temperature capabilities of the nuclear heat source.

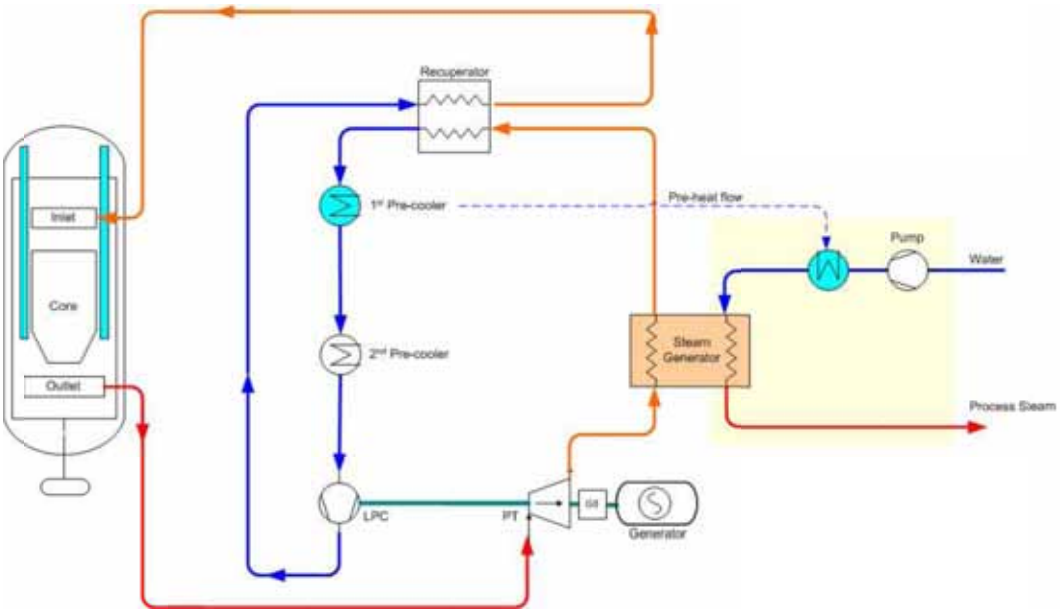

FIG. 2.8. Cogeneration configuration 2.

(C) Configuration 3

Configuration 3 is illustrated in Fig. 2.9 and consists of the PBMR reactor with the steam generator directly coupled to the reactor and providing high temperature and pressure steam to an exhaust turbine. This configuration will favor typically process plants requiring lower pressure steam and more process steam than electricity. Although it utilizes the high temperature capabilities of the nuclear heat source and is very efficient, it will require significant feedwater treatment consideration.

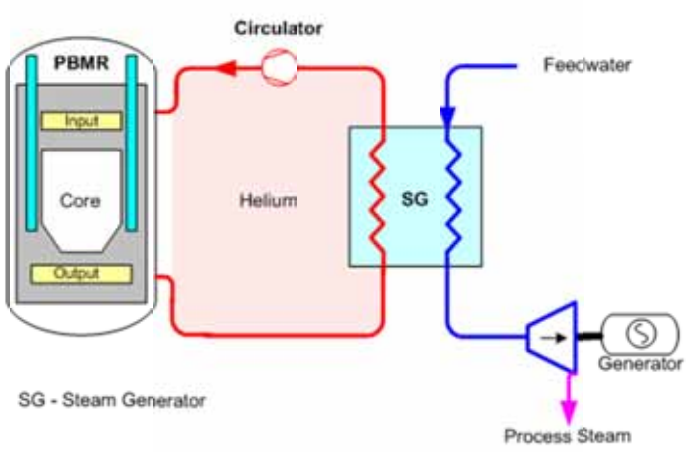

FIG. 2.9. Cogeneration configuration 3.

2.2.3. Method of thermal integration of HTGR for cogeneration

2.2.3.1. Introduction

Purpose of this section is to estimation in detail the resource stream (in terms of quality and quantity) from an HTGR for cogeneration by thermal integration techniques. BARC has carried out the thermal integration of HTGR by so-called 'pinch technology'. Objectives for these studies are:

1. Maximize process to process heat recovery;
2. Minimize the utility requirement;
3. Design of the heat exchanger network.

2.2.3.2. Methodology of the thermal integration: pinch analysis

'Pinch analysis' is the application of the tools and algorithm of the 'pinch technology'. It is carried out in several steps [11, 12]:

First step is the identification of streams in the process:

i. Hot streams are those streams which must be cooled or available to be cooled, i.e. hot helium gas which is coming out from turbine outlet and needs to be cooled before entering the compressor.
ii. Cold streams are those streams which must be heated, i.e. compressed helium from HP compressor need to be heated before entering the reactor.
iii. Utility streams (hot utility & cold utility), i.e. cooling water or steam.

Second step is the extraction of thermal data of all process and utility streams:

i. Supply temperature (T_{supply})
ii. Target temperature (T_{target})

Enthalpy change (ΔH), $\Delta H = MC_p (T_{supply} - T_{target})$

Third step is the selection of the initial ΔT_{min} value:

ΔT_{min} = Hot stream temperature (T_H) – Cold stream temp. (T_C)

This is the minimum positive temperature difference to allow the heat transfer between streams. The temperature level at which ΔT_{min} is observed in the process is referred to as 'pinch point' or 'pinch condition'. A so-called 'problem table algorithm' (PTA) is used for determining the utility needs of a process and the location of the process pinch.

Fourth step is the construction of the 'grand composite curve' (GCC):

It shows the net heat available in various temperature intervals within the process.

Fifth step is the estimation of the minimum energy of the utility:

GCC diagrams are used to estimate minimum utility requirements and aim to maximize the use of cheaper utility levels and minimize the use of expensive utility levels.

Sixth and final step is the design of the heat exchanger network and its optimization.

2.2.4. Thermal integration of 600 MW(th) HTGR plant

Flow diagram for the 600 MW(th)t HTGR plant is shown in Fig. 2.10. It is a helium cooled direct cycle nuclear power plant having relatively high thermal efficiency (45–50%) and enhanced safety and environmental characteristics. It includes the nuclear heat source, i.e. the reactor system, and power conversion system consisting of equipment needed for electric power generation (turbo-compressor, recuperator, generator, precooler and intercooler).

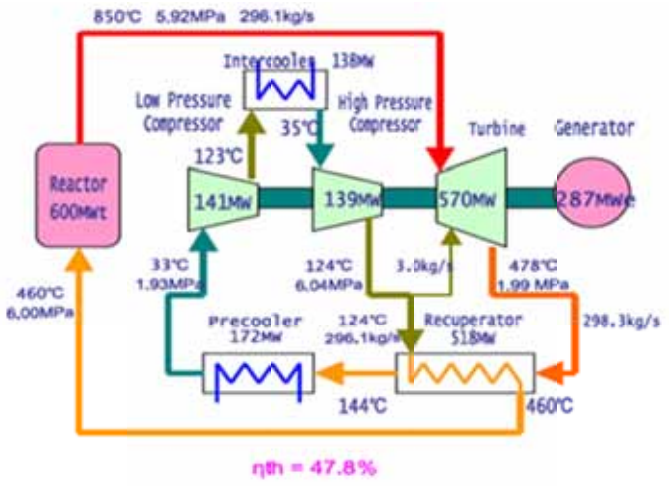

FIG. 2.10. Flow diagram for the 600 MW(th) HTGR plant [13].

2.2.4.1. Energy targeting

First streams were identified from the flow diagram for the 600 MW(th) HTGR plant as listed in Table 2.6.

As stream H1 is utilized solely for power generation in turbine, the pinch analysis considers the rest of the stream for thermal integration.

ΔT_{min} is assumed as 10°C. Shifting the temperature of the hot stream down by ½ ΔT_{min} and also shifting the temperature of the cold stream up by ½ ΔT_{min}, the shifted temperatures of all streams are obtained as shown in Table 2.7. Energy targeting was done by constructing the PTA assuming ΔT_{min} = 10°C (Table 2.8).

TABLE 2.6. STREAM DATA FOR THE 600 MW(th) HTGR PLANT

Stream	T_{supply} (°C)	T_{target} (°C)	M (kg/s)	Cp (kJ/(kg·K))	MCp (kW/K)	ΔH (MW(th))
H1	850	478	296.1	5.2	1539.72	572.77584
H2	478	33	296.1	5.2	1539.72	665.1754
H3	123	35	296.1	5.2	1539.72	135.49536
C1	124	460	296.1	5.2	1539.72	-517.34592

TABLE 2.7. SHIFTED TEMPERATURE

	$T_{shifted}$ (°C)	MCp (kW/K)
Internal supply	473	1551.16
	118	1551.16
	129	1539.72
Internal demand	28	1551.16
	30	1551.16
	465	1539.72

TABLE 2.8. PROBLEM TABLE ALGORITHM (ΔT = 10°C)

$T_{decreasing}$ (°C)	MCp (kW/K)	Cum MCp (kW/K)	Q_{inter} (MW)	Q_{Cas} (MW)
473	1551.16	1551.16	0	0
465	-1539.72	11.44	12.40928	12.40928
129	1539.72	1551.16	3.84384	16.25312
118	1551.16	3102.32	17.06276	33.31588
30	-1551.16	1551.16	273.0042	306.32
28	-1551.16	0	3.10232	309.4224

Plotting the values of Q_{cas} vs. T of Table 2.8 yields the GCC for the process (Fig. 2.11). From the grand composite curve, the minimum cold utility target is obtained as Q_c = 310 MW.

2.2.4.2. Heat exchanger network design

The heat exchanger network diagram is shown in Fig. 2.12 which is similar to the original HTGR flow diagram where cooler C1 represents the precooler and cooler C2 represents the intercooler. Cold utility, i.e. cold demineralized water is used as the cooling media in coolers.

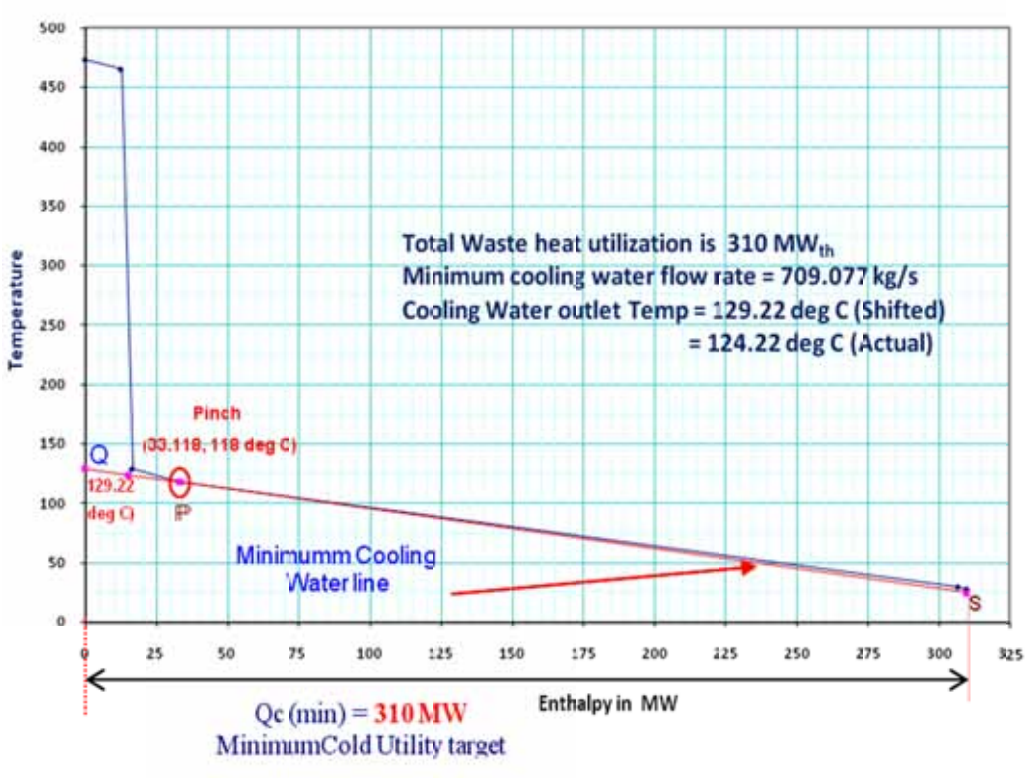

FIG. 2.11. Grand composite curve for 600 MW(th) HTGR plant (ΔT = 10°C).

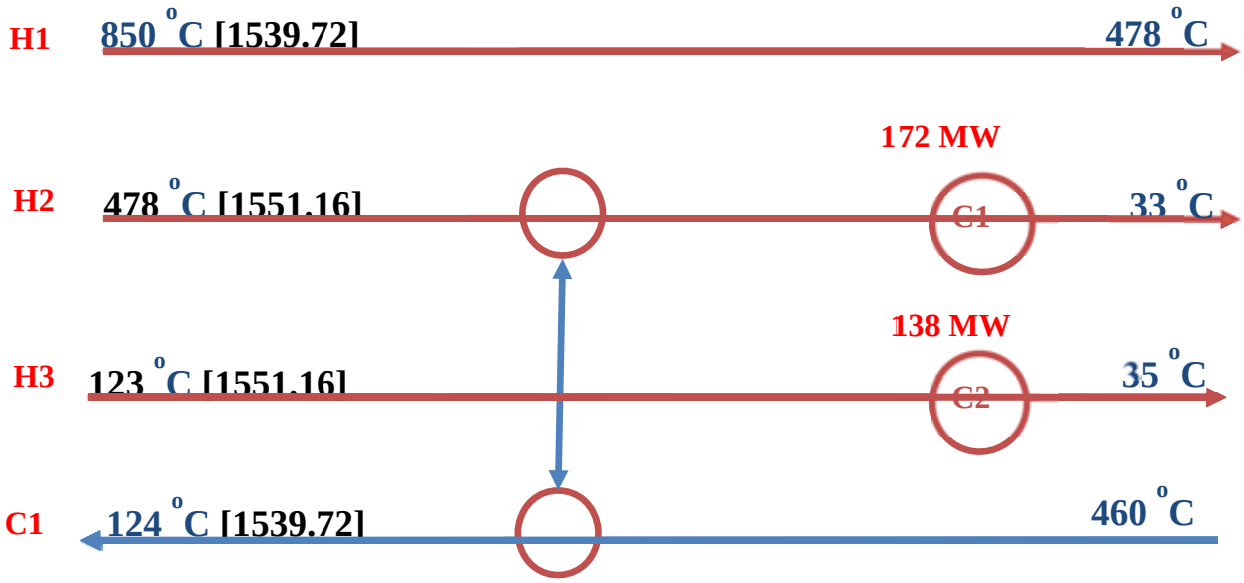

FIG. 2.12. Heat exchanger network diagram for 600 MW(th) HTGR plant.

2.2.4.3. Targeting minimum cooling water flow rate and maximum coolant outlet temperature

Next step is to minimize the cooling water flow rate to save the utility cost and its pumping cost. Minimization of cooling water flow rate also leads to the maximization of the coolant outlet temperature as the heat duty for the coolers is already fixed. This is also advantageous as this heated cooling water will be useful for desalination. The higher the temperature of this cooling water, the larger will be the capacity of the desalination plant. From the plotted GCC, the generation of cold utilities has been targeted (Fig. 2.11).

Cold water supply temperature = 20°C

Cold water supply shifted temperature = 25°C

Point S in Fig. 2.11 denotes the cooling water inlet condition. The line drawn from this point is the cooling water line.

For maximum cooling water outlet temperature and minimum cooling water flow rate, a line is drawn from point S which is the tangent to the GCC. This tangent represents the minimum cooling water line. It touches the GCC at point P which is the pinch point. The slope of this tangent gives the required minimum cooling water flow rate.

The minimum cooling water line is found to touch the GCC at 118°C (shifted temperature). From the slope, the minimum cooling water flow rate can be calculated as F_{min} = 709.077 kg/s. This cooling water is heated up to 124.22°C.

2.2.4.4. Desalination utilizing waste heat from 600 MW(th) HTGR

By the thermal integration of the 600 MW(th) HTGR and pinch analysis, hot water of 124.2°C at a rate of 709.077 kg/s is achieved. This water can be utilized for water production by desalination purposes. To transfer the thermal energy from the HTGR cycle to the desalination plant, an isolation loop is incorporated.

BARC has developed an in-house software InDesal-HTGR in visual basic for doing the preliminary design calculation for the hybrid desalination system coupled to the HTGR utilizing its waste heat. It provides a graphical user interface and performs calculations for

- HTGR power cycle and available waste heat;
- Isolation loop for coupling the HTGR with the desalination plant;
- Hybrid desalination plant coupled to HTGR.

Results of the calculations for the 600 MW(th) HTGR by InDesal-HTGR are shown in Figs 2.13 and 2.14.

2.2.4.5. Summary

- Waste heat from the HTGR cycle is utilized for desalination.
- HTGR plant is coupled to hybrid desalination plant consisting of LT-MED plant and preheats RO plant.
- Waste heat from HTGR is used to heat water in the desalination loop. It is then flashed in the flash chamber. Steam is then used in the MED plant. Capacity of the MED with a gain output ratio (GOR) of 6 is 1467 t/h.
- Seawater heated in the heat sink is used as feed stock to the RO plant. For 40% recovery in the RO plant, desalination capacity is 715 t/h.
- Total desalination capacity is = 2182 m^3/h.
- Total waste heat utilization is 310 MW(th).

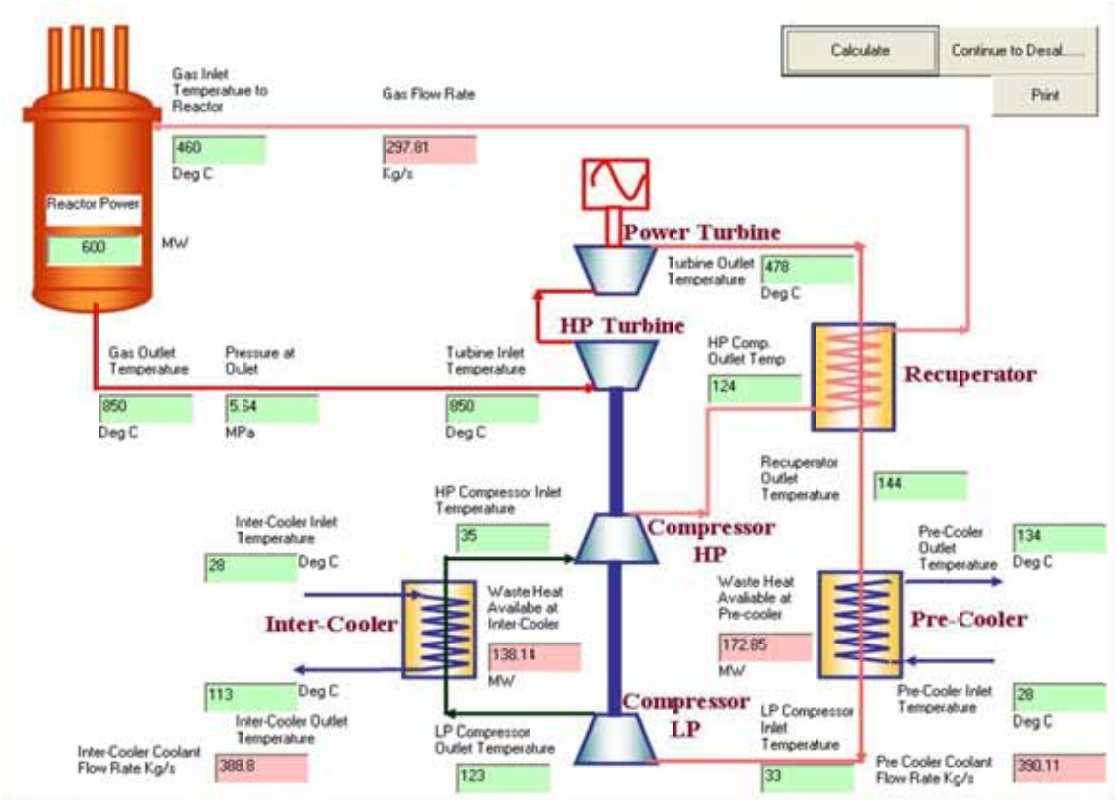

FIG. 2.13. Available waste heat in a 600 MW(th) HTGR plant as calculated by InDesal-HTGR.

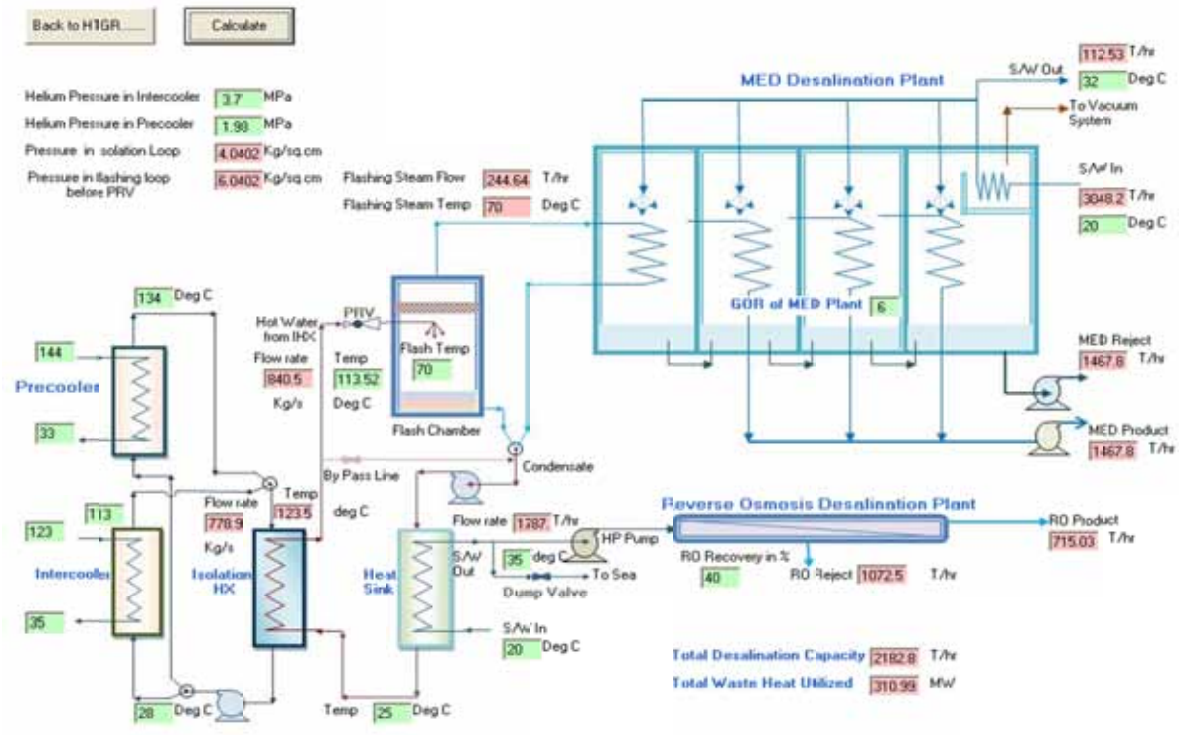

FIG. 2.14. Seawater desalination utilizing waste heat of 600 MW(th) HTGR as calculated by InDesal-HTGR.

2.2.5. Thermal integration of 400 MW(th) PBMR plant

A flow diagram for the 400 MW(th) PBMR plant as of 2001 [13] is shown in Fig. 2.15. It is a helium cooled direct cycle nuclear power plant having relatively high thermal efficiency (45–50%) and enhanced safety and environmental characteristics. It includes the nuclear heat source, i.e. the reactor system, and power conversion system consisting of equipment needed for electric power generation (turbo-compressor, recuperator, generator, precooler and intercooler).

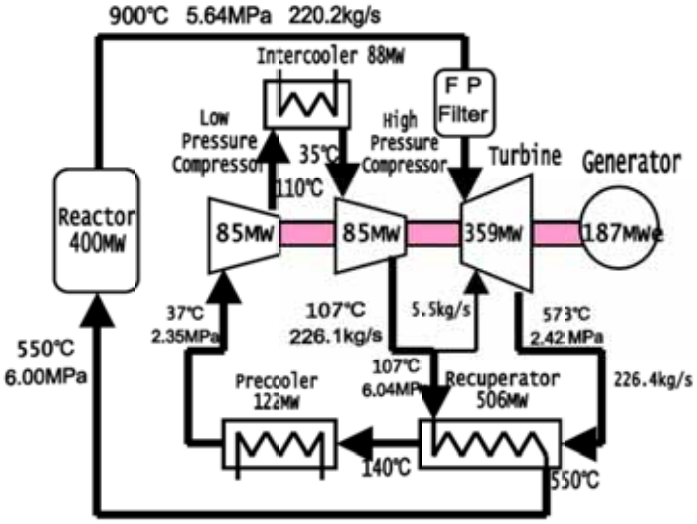

FIG. 2.15. Flow diagram for the 400 MW(th) PBMR plant [13].

2.2.5.1. Energy targeting

At first, streams were identified from the flow diagram for the 400 MW(th) PBMR listed in Table 2.9.

TABLE 2.9. STREAM DATA OF THE 400 MW(th) PBMR PLANT

Stream	T_{supply} (°C)	T_{target} (°C)	M (kg/s)	Cp (kJ/(kg·K))	MCp (kW/K)	ΔH (MW(th))
H1	900	573	220.2	5.2	1145.04	374.42
H2	573	37	226.4	5.17	1171.62	627.98
H3	110	35	226.4	5.17	1171.62	87.87
C1	107	550	220.9	5.17	1143.15	-506.4

Plotting the values of Q_{cas} vs. T of Table 2.11 yields the GCC for the process as shown in Fig. 2.16. From the grand composite curve, the minimum cold utility target is obtained as Q_c = 209.4 MW.

As stream H1 is utilized solely for power generation in turbine, the pinch analysis considers the rest of the stream for thermal integration.

ΔT_{min} is assumed as 10°C. Shifting the temperature of the hot stream down by ½ ΔT_{min} and also shifting the temperature of the cold stream up by ½ ΔT_{min}, the shifted temperatures of all streams are obtained as shown in Table 2.10.

TABLE 2.10. SHIFTED TEMPERATURES

	$T_{shifted}$ (°C)	MCp (kW/K)
Internal supply	568	1171.62
	105	1171.62
	112	1143.15
Internal demand	32	1171.62
	30	1471.62
	555	1143.15

TABLE 2.11. PROBLEM TABLE ALGORITHM (ΔT = 10°C)

$T_{decreasing}$ (°C)	MCp (kW/K)	Cum MCp (kW/K)	Q_{inter} (MW)	Q_{Cas} (MW)
568	1171.62	1171.62	0	0
555	-1143.1575	28.4625	15.23106	15.23106
112	1143.1575	1171.62	12.60889	27.83995
105	1171.62	2343.24	8.20134	36.04129
32	-1171.62	1171.62	171.0565	207.0978
30	-1171.62	0	2.34324	209.441

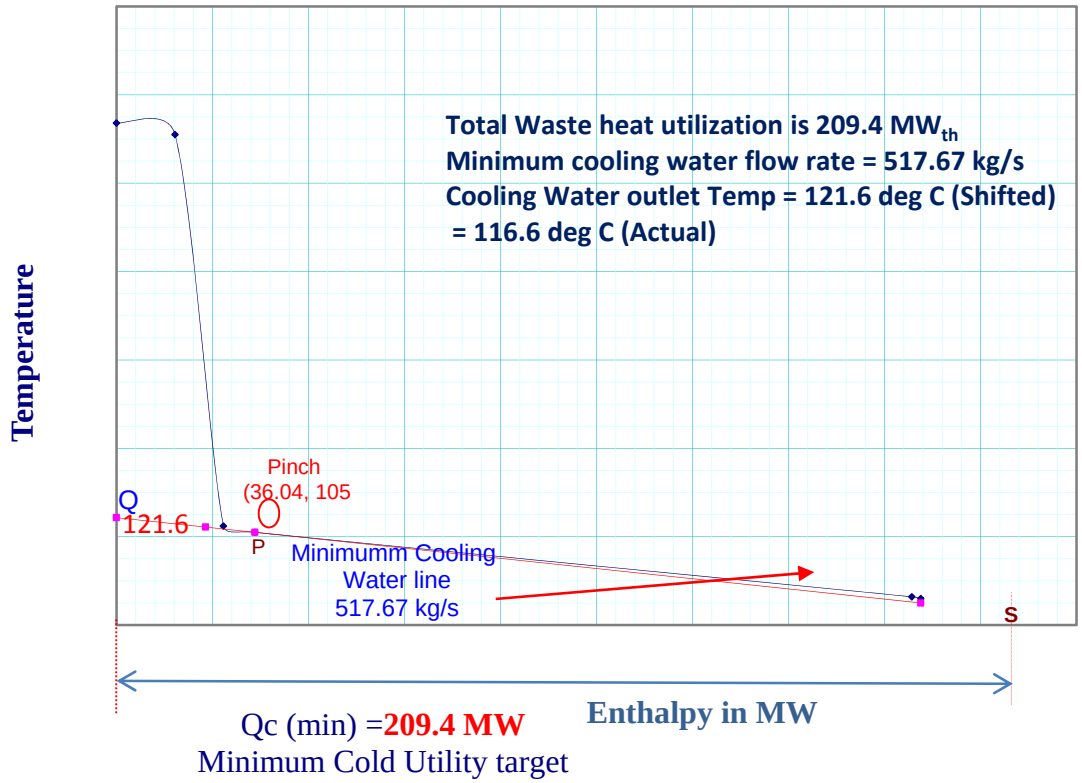

FIG. 2.16. Grand composite curve for 400 MW(th) HTGR plant (ΔT = 10°C).

2.2.5.2. Heat exchanger network design

The heat exchanger network diagram is shown in Fig. 2.17 which is similar to the original PBMR flow diagram where cooler C1 represents the precooler and cooler C2 represents the intercooler. Cold utility, i.e. cold demineralized water is used as the cooling media in coolers.

2.2.5.3. Targeting minimum cooling water flow rate and maximum coolant outlet temperature

Next step is to minimize the cooling water flow rate to save the utility cost and its pumping cost. Minimisation of cooling water flow rate also leads to the maximization of the coolant outlet temperature as the heat duty for the coolers is already fixed. This is also advantageous as this heated cooling water will be useful for desalination. The higher the temperature of this cooling water, the larger will be the capacity of the desalination plant.

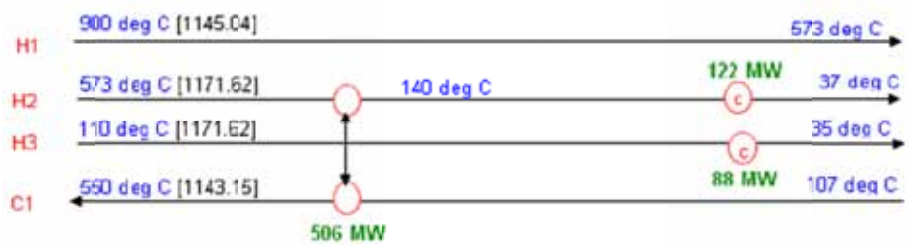

FIG. 2.17. Heat exchanger network for 400 MW(th) PBMR plant.

From the plotted GCC, the generation of cold utilities has been targeted (Fig. 2.16).

Cold water supply temperature = 20°C

Cold water supply shifted temperature = 25°C

Point S in Fig. 2.16 denotes the cooling water inlet condition. The line drawn from this point is the cooling water line.

The minimum cooling water line is found to touch the GCC at 110°C (shifted temperature). From the slope, the minimum cooling water flow rate can be calculated as F_{min} = 517.67 kg/s. This cooling water is heated up to 116.6°C.

2.2.5.4. Desalination utilizing waste heat from PBMR

By the thermal integration of the 400 MW(th) PBMR and pinch analysis, hot water of 116.6°C at a rate of 517.67 kg/s is achieved. To transfer the thermal energy from the PBMR cycle to the desalination plant, an isolation loop is incorporated.

Results of the calculation for 400 MW(th) PBMR by InDesal-HTGR are shown in Figs 2.18 and 2.19.

2.2.5.5. Summary

- Multiple hot utilities are targeted by thermal integration of the PBMR cycle.
- PBMR plant is coupled to hybrid desalination plant consisting of LT-MED plant and preheats RO plant.
- Waste heat from PBMR is used to heat water in the desalination loop. It is then flashed in the flash chamber. Steam is then used in the MED plant. Capacity of the MED with a GOR of 6 is 863.7 t/h.
- Seawater heated in the heat sink is used as feed stock to the RO plant. For 40% recovery in the RO plant, desalination capacity is 571.2 t/h.
- Total desalination capacity is = 1435 m^3/h
- Total waste heat utilization is 209.4 MW(th).

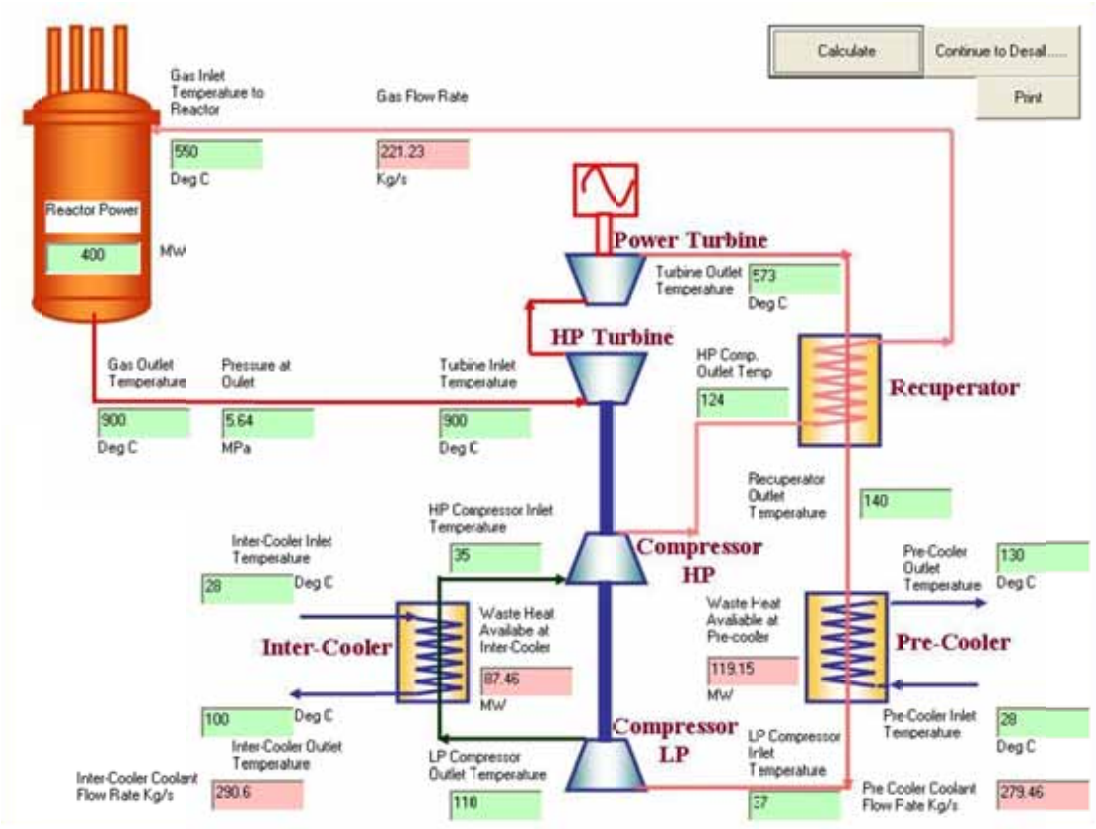

FIG. 2.18. Available waste heat in the 400 MW(th) PBMR plant as calculated by InDesal-HTGR.

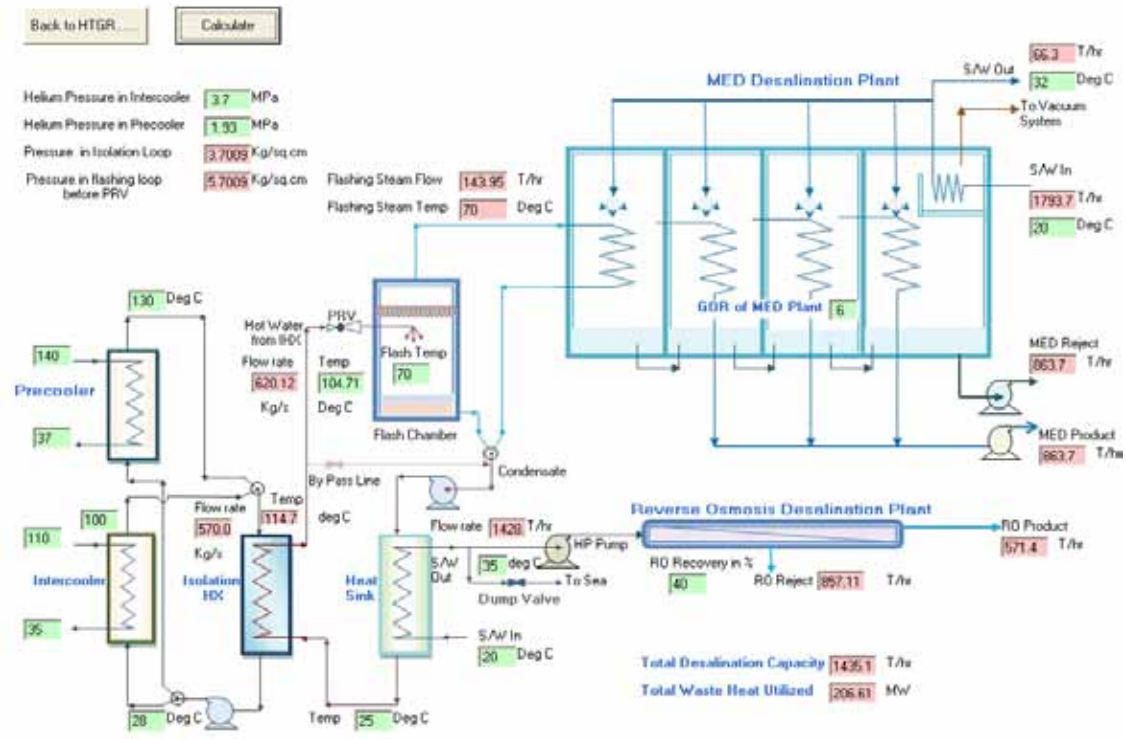

FIG. 2.19. Seawater desalination utilizing waste heat of 400 MW(th) PBMR plant as calculated by InDesal-HTGR.

2.2.6. Comparative analysis of configuration of nuclear hydrogen production plants

HTGR hydrogen production application is based on processes with high thermodynamic and technical–economic efficiency. Such processes shall eliminate consumption of organic fuel, especially coal, oil, and gas, and include hydrogen production by water electrolysis, thermochemical decomposition and high temperature steam electrolysis (HTSE). Their cost does not depend on constantly increasing oil and gas prices in contrast to methane-based hydrogen production. However, the processes of methane-based hydrogen production are considered for the first stage of hydrogen power application at relative low gas prices. Currently, water electrolysis and steam methane reforming (SMR) are the main industrially mastered technologies suitable for the first stage of HTGR hydrogen production integration. Water electrolysis allows using reactor modules with gas turbine power conversion units of 48% electricity generation efficiency.

When considering HTGR applications in various hydrogen production processes, two basic types of reactor plant may be distinguished:

- with intermediate helium circuit transferring heat from the reactor to the plant, based on thermochemical water decomposition with highly aggressive fluids and at high temperature of 950–1000°C;
- with heat transfer directly in the primary circuit, in high temperature heat exchangers, based on SMR or HTSE; the latter case requires electric power generation in the power conversion units located downstream the heat exchanger.

SMR efficiency depends on gas prices and temperature of consumed heat. Heat at temperature up to 850°C shall be supplied; further increase of this temperature does not have any impact on efficiency (Fig. 2.20).

Since steam-gas mixture to be converted includes 80% of water steam, a reactor plant configuration is considered where heat is transferred directly in the primary circuit, from helium to hydrogen production process facilities via the high temperature heat exchanger (Fig. 2.21) [15].

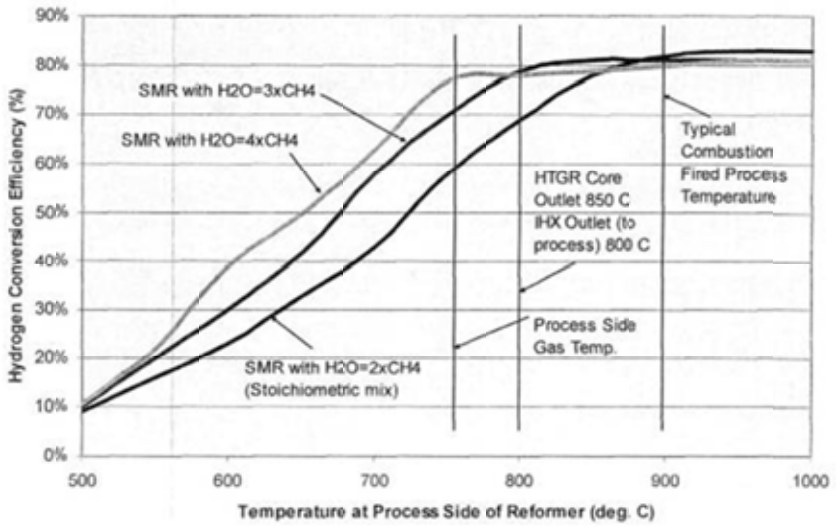

FIG. 2.20. SMR efficiency as a function of temperature [14].

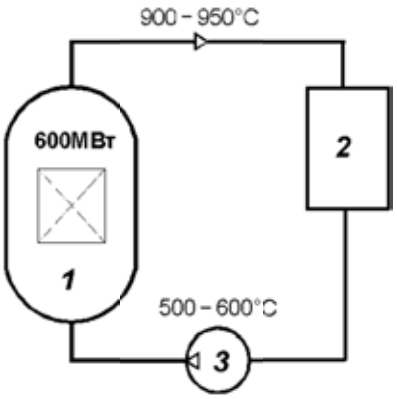

1: reactor; 2: high temperature heat exchanger of the hydrogen production facility; 3: gas circulator.

FIG. 2.21. Reactor plant with primary circuit heat transfer from the reactor to the hydrogen production facility.

In operating plants such as Fort St. Vrain (USA), THTR-300 (Germany), VG-400 and VGM (Russian Federation), heat of primary circuit helium is transferred directly to steam in the steam generator. Operation analysis and experience confirm that the effects of supply and limitation of supply of hydrogen bearing products to the reactor in potential accidents with depressurization of the steam generator or high temperature heat exchanger are reliably regulated by reactor control and protection systems.

The high temperature heat exchanger is pressure boundary of the primary circuit. Boundary integrity is provided through implementation of prerequisites and conditions eliminating brittle fracture of boundaries, including the high temperature heat exchanger casing. In case of possible primary circuit leaks, radioactive fluid is retained due to arrangement of the reactor with the high temperature heat exchanger and other primary circuit equipment in a reinforced concrete leak-tight containment. In case of depressurization of heat exchange surface of the high temperature heat exchanger, coolant leak from the primary circuit beyond the containment shall be limited by closing quick-response isolation valves. Such layout solutions are adopted in the French (Fig. 2.22) and the Russian Federationn (Figs 2.23 and 2.24) design of the hydrogen production reactor plant.

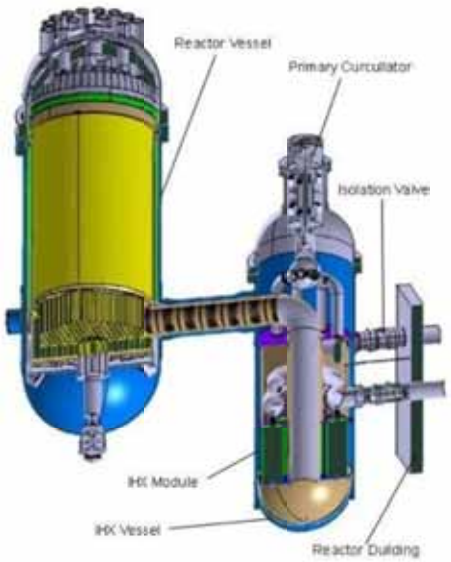

FIG. 2.22. Layout of Areva ANTARES VHTR of 600 MW transferring primary circuit heat from the reactor to process facilities via the intermediate heat exchanger [16].

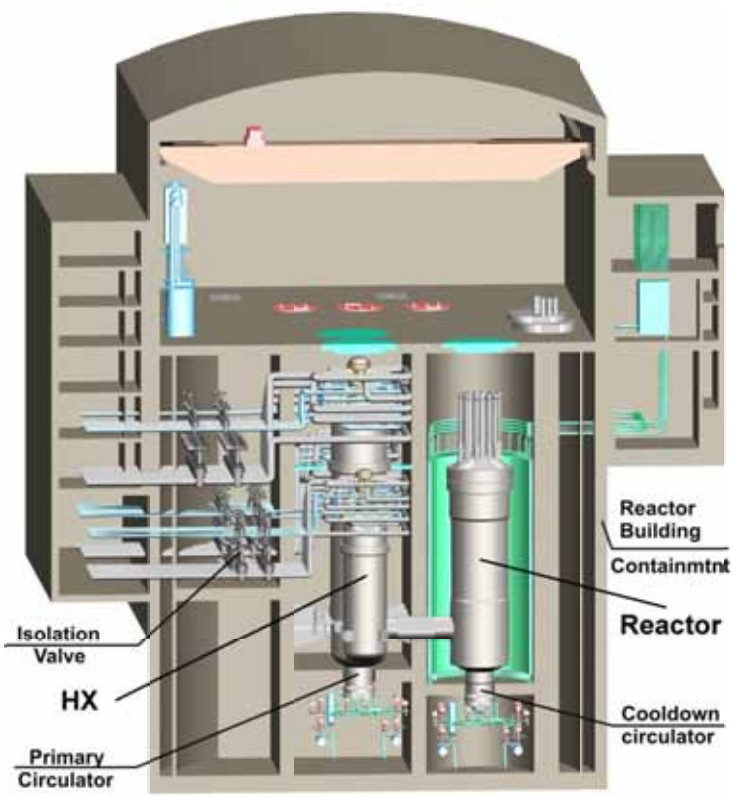

FIG. 2.23. Layout of Russian design VHTR of 200 MW transferring directly primary circuit heat from the reactor to process facilities [17, 18].

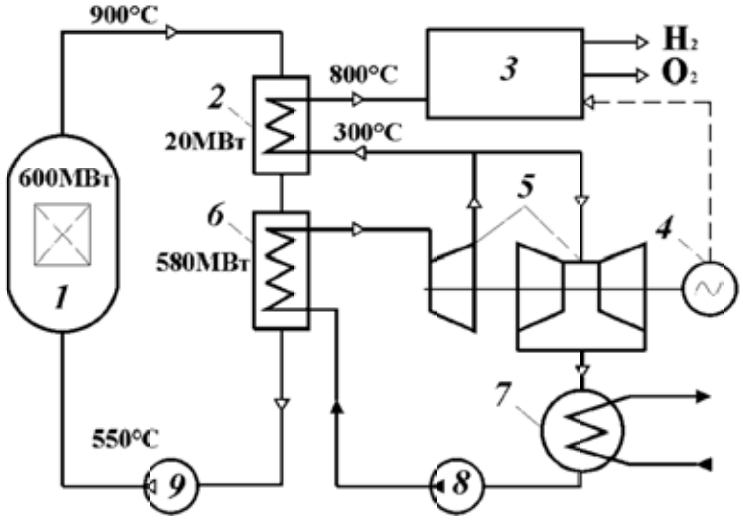

1: reactor; 2: high temperature steam superheater; 3: hydrogen production facility; 4: generator; 5: steam turbine; 6: steam generator; 7: condenser; 8: feed pump; 9: primary circuit gas circulator (MB_T = MW(th))

FIG. 2.24. Reactor plant transferring primary circuit heat from the reactor to hydrogen production facilities and power conversion unit for electric power generation.

High temperature steam electrolysis (HTSE) (see also chapter 3.1.2) allows using facilities which transfer high temperature heat from the reactor directly via the high temperature heat exchanger to steam whereby heating it up to 800°C. Steam electrolysis efficiency depends on electricity prices and temperature of consumed heat (Fig. 2.25). Electrolysis is implemented for steam with operational parameters of 3–7 MPa and up to 800°C.

In this design, the high temperature heat exchanger serves as high temperature steam superheater. Heat of lower temperature is converted into electric power in the power conversion unit located downstream the high temperature heat exchanger. The PCU may be either equipped with a gas turbine or steam turbine cycle, depending on technical–economic indices. In order to heat steam up to 800°C, the helium temperature at the reactor outlet shall not be lower than 900°C.

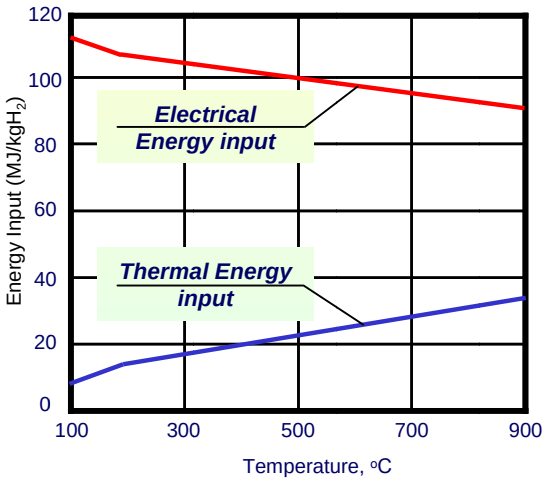

FIG. 2.25. Balance of input power at HTSE as a function of temperature [19].

At further development stages, HTGR heat may be used in thermochemical processes with high efficiencies. Thermochemical decomposition of water in a sulphur–iodine cycle is the most investigated process. Its efficiency mainly depends on the temperature of the supplied heat (Fig. 2.26). Effective hydrogen production in such a cycle requires supply of heat with the temperature from 900 to 950°C. In view of temperature differences in the high temperature intermediate heat exchanger, the required helium temperature at the reactor outlet increases up to 1000°C.

Proper selection of materials to sustain the aggressive sulphur–iodine environment at high temperatures is one of the key problems impeding development of such thermochemical cycles. Due to the absence of corrosion-resistant materials, reactor heat will be transferred in this cycle via the intermediate circuit (Fig. 2.27).

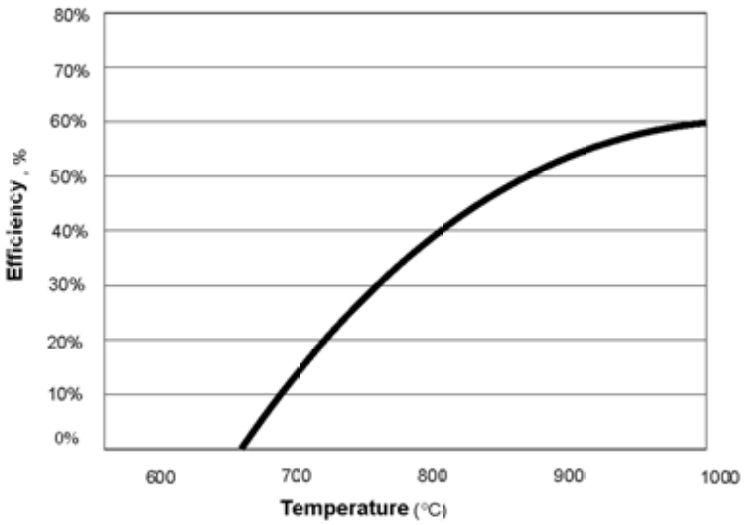

FIG. 2.26. Sulfur–iodine cycle efficiency as a function of temperature [14].

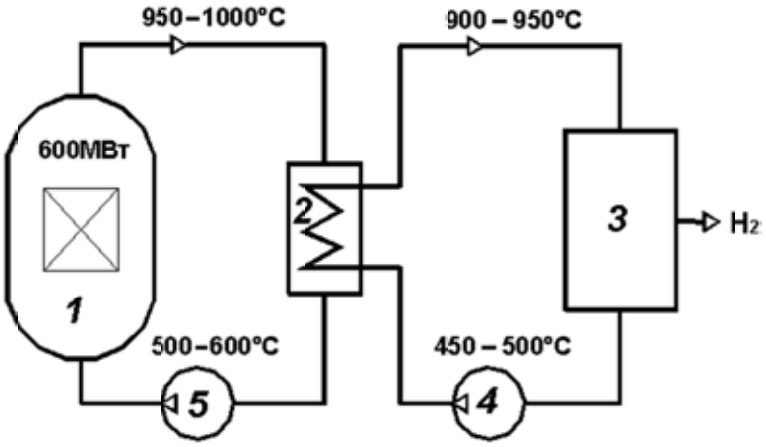

1: reactor; 2: intermediate heat exchanger; 3: hydrogen production facility;
4: primary circuit gas circulator; 5: intermediate circuit gas (MB_T = MW(th))

FIG. 2.27. Reactor plant transferring heat from the reactor to the hydrogen production facility via intermediate circuit [15].

Application of intermediate circuit has the following advantages:

- possible unification of the reactor core, i.e. usage of a single reactor type in various industries;
- less probable radioactive contamination of final product and on the contrary ingress of excited environments from technological process in the primary circuit at emergency depressurized as compared to a plant without intermediate circuit;
- spatial separation of the reactor and thermochemical process units to ensure fire and explosion safety.

However, the following negative factors should be taken into account as well:

- decrease of temperature potential of heat transferred to production facilities due to heat losses into the environment;
- reduction of plant efficiency;
- increase of capital costs.

VGM-P design included a comparative analysis of three types of reactor plant intermediate circuit coolants: helium, Pb–Bi melt and silicon oil [20].

Minimum total heat exchange area of the IHX and the 3rd circuit heat exchanger is achieved when using a Pb–Bi intermediate circuit. A helium intermediate circuit requires a surface which is 1.5 times larger, and silicon oil requires a 1.9 times larger surface.

The helium intermediate circuit is characterized by maximum costs for coolant pumping along the intermediate circuit (N = 3000 kW). Pb–Bi pumping requires 2.3 times less power (N = 1280 kW), and silicon oil requires 8.3 times less power (N = 360 kW). But effectiveness of Pb–Bi or silicon oil pumping in the intermediate circuit is reduced due to an increase of 3rd circuit pump efficiency caused by increased coolant flow from its lower temperature (G = 422 kg/s at t = 450°C for Pb–Bi and silicon oil, in contrast to G = 318 kg/s at t = 500°C for helium). Total power of 3rd circuit pumps and intermediate circuit gas circulator for the helium intermediate circuit is N = 10.7 MW. For Pb–Bi, it is N = 7.9 MW, and for silicon oil, it is N = 5.1 MW. Intermediate circuit helium coolant has minimum mass and lowest cost (m = 0.8 t and C = 1 relative unit). Silicon oil mass and cost are higher by a factor of 120 and 35,

respectively, (m = 97 t and C = 35). Pb–Bi mass and cost are by factors of 1625 and 468, respectively, higher (m = 1300 t and C = 468).

Helium is the most preferable coolant for the intermediate circuit in terms of VGM-P reactor plant safety. It prevents ingress of 3rd circuit coolant into the primary helium circuit and excess of allowable 3rd circuit coolant temperatures. Pb–Bi or silicon oil intermediate circuit coolants can ingress into the primary helium circuit. In an accident with intermediate circuit pump shutdown (for example, at de-energization) and further non-opening of isolation valves on main gas circulator, the intermediate circuit coolant is heated up to 750°C in the IHX, which is much higher than the allowable Pb–Bi and silicon oil operation temperatures. Therefore, it is necessary to study the behavior of these materials at temperatures up to 750°C. Thus, the analysis shows that intermediate circuit coolant shall be helium.

Preliminary technical–economic estimates [14] of hydrogen production in advanced processes with HTGR heat and electric power demonstrate that SMR with helium temperature at the reactor outlet 950°C can compete with conventional technologies at current gas prices even without taking account of potential taxes for CO_2 emissions. In view of the tendency for further gas price increase, the most economically efficient technology will be thermochemical water decomposition in a sulphur–iodine cycle. SMR and thermochemical water decomposition at a temperature of 950°C can compete with conventional low temperature electrolysis. HTSE advantages at a temperature of 950°C are not clear so far and will finally depend on capital costs of heat application for electricity production. Estimates were performed for processes which may be implemented with helium temperature at the reactor outlet not higher than 950°C. Temperature increase up to 1000°C allows an enhanced efficiency of hydrogen production processes, but increases the cost of creation of a safe reactor plant. Therefore, a thorough technical–economic analysis shall be performed when selecting the temperature level at the reactor outlet and hydrogen production process pattern.

2.3. SPECIFIC HTGR DESIGN PROPOSALS

2.3.1. Germany

2.3.1.1. Process heat reactor concept

Within the German prototype nuclear process heat (PNP) project, a significant part of the efforts was dedicated to the design and demonstration of the ability of HTGRs to be used for process heat applications. Of special importance for process heat projects was the 46 MW(th) AVR test reactor in Jülich which was operated between 1967 and 1988. It became the world's first pebble-bed reactor to successfully achieving a coolant outlet temperature of 950°C proving the feasibility of the pebble-bed HTGR concept under high temperature process heat conditions with a high availability. (The same helium outlet temperatures were later demonstrated for the Japanese block reactor HTTR as well.) As most chemical processes are performed at lower pressures some adaptation of the reactor design and of the chemical process has been necessary.

The choice of the pressure is also important to reduce the loads on the high temperature barriers in case of depressurization accidents either in the primary or in the secondary circuit. Other important aspects of reactor design are the amount of cogenerated electricity, high availability as well as an optimization towards significant simplification of the nuclear island. Heat transfer under varying operational load conditions, hot gas mixing in the core bottom, or the lifetime of hot gas thermal insulation have been comprehensively investigated in experiments.

In comparison to the electricity generating nuclear plant, several modifications are necessary for the process heat variant:

- reduced power density to compensate for the higher core outlet temperature level (for the HTR-Modul: 3 → 2.55 MW/m^3, 200 → 170 MW(th));
- reduced system pressure as compromise between a high pressure desired for its favorable effect on operating and accident conditions of the nuclear reactor and a low pressure desired for chemical process reasons in the secondary and tertiary circuit. The pressures in the different circuits should be in the same range, slightly increasing towards the outside (for the HTR-Modul: 7 → 5 (4 with IHX) MPa);
- two fuel zones in the pebble bed to minimize the occurrence of hot/cold gas strains in the core to achieve a radial temperature profile as uniform as possible;
- ceramic (graphite) liner to replace the metallic liner because of the higher temperatures.

2.3.1.2. Prototype nuclear process heat (PNP) reactor designs

The concept for a German nuclear process heat reactor was originally based on thermal power sizes of 500 MW (PR-500) and 3000 MW (PNP-3000), respectively. The PR-500 pebble bed reactor (Fig. 2.28) was designed to produce 523 t/h of steam at a temperature of 265°C and a pressure of 2 MPa plus an electric power of 55 MW. The coolant helium was heated up from 265°C to 865°C. The reactor was placed in a prestressed concrete pressure vessel surrounded by three units each containing heat exchanger and blower [21]. The large-size reactor concept of the PNP-3000 was foreseen to be connected to steam reforming with 1071 MW heat input (to eight units in four loops) and electricity cogeneration with 540°C/19.5 MPa turbine steam. The reactor pressure was fixed to 4 MPa being much below the pressure for electricity generating plants (~7 MPa).

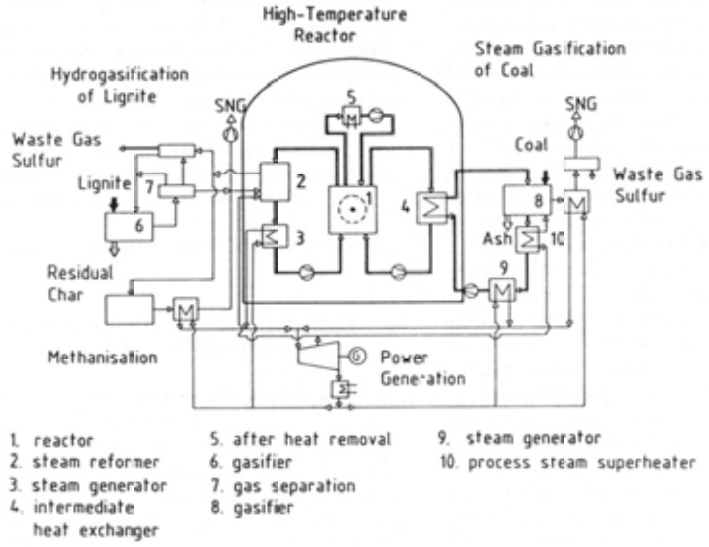

FIG. 2.28. System diagram of the PNP-500 plant.

A part of the safety concept was the employment of a non-integrated arrangement with separate vessels for the generation and the conversion of heat, and a containment to enclose the total primary circuit. A placement of the nuclear unit underground ensures an enhanced protection against atmospheric explosions of gas clouds, fire, or aircraft crash. A particular significance has the hot gas duct which is the direct connection between heat source and heat sink, and whose rupture would cause the maximum possible pressure transient. The coaxial

ducts are designed as pressure vessels according to the leak-before-break principle, where the early detection of a leakage would allow the immediate plant shutdown. Furthermore, the inside pipe containing the hot helium is also designed for a pressure of 4 MPa, although the pressure difference to the annular space around containing the returning cold helium is not more than 100 kPa during normal operation.

More concepts of nuclear process heat HTGRs of smaller size have been proposed later, among them the modified version of the HTR-500, the 170 MW(th) HTR-Modul concept, and the AVR-50. All were characterized by a supply of energy at high temperature levels in the order of 950°C, which allows the achievement of high chemical reaction rates.

2.3.1.3. Coupling between nuclear and chemical plant

For the PNP nuclear steam coal gasification process, it was foreseen that the heat from the reactor coolant be transferred to an additional intermediate circuit via a helium–helium intermediate heat exchanger (He–He IHX). The main reason was to avoid the handling of coal and ash in the primary system of the reactor, and a much more complex way for repair and maintenance work. Primary helium of 950°C flowing on the outside of the IHX tubes passes its heat to the secondary helium entering the steam gasifier at 900°C. Also pressure is slightly higher than on the primary side for the purpose of preventing radioactivity to enter the secondary circuit in case of a leak. The hot steam produced is routed into the coal bed to be gasified. Unlike conventional fossil-fueled components, the helium-heated components of the HTGR have to meet the more stringent requirements of a „nuclear' component in terms of construction, quality assurance, and scheduled re-testing. They have the important function of forming a radioactivity barrier between the primary helium and the process gas.

Two different He–He IHX components were constructed by German companies (see Fig. VI.7 in Appendix VI), one with a helical tube bundle and the other one with U-tubes, designed for a power level (~125 MW) representative for large and medium-sized plants. Both components were tested with 950°C helium on the primary side. The hot helium entering the heat exchanger at the bottom, flows upwards through the bundle, and is cooled down to 300°C. The secondary helium with a temperature of 200°C is entering the component at the top into a ring conduit where it is uniformly distributed over the tube bundle and heated up to 900°C in counter-current flow. The hot helium is leaving the IHX again at the top of the component. The maximum wall temperature in the tubes in normal operation is 920°C, the maximum pressure difference between primary and secondary side is 0.2 MPa under operational conditions. In depressurization accidents, they have to withstand the full pressure difference in a limited time period.

For the PNP nuclear hydro-gasification of coal, it was foreseen to use the steam–methane reformer directly for heat transfer from the hot helium to the methane–steam mixture. An intermediate heat exchanger was, at least in those days, not deemed necessary. The drawback seen was the more complicated exchange of the catalyst in the nuclear steam reformer.

Both IHX components were tested under nuclear coal gasification conditions in a 10 MW(th) component test loop (KVK), operated within the PNP project [22]. The facility consisted of a primary and a secondary helium loop. The helium flow rate was 3 kg/s in both circuits. Heat sources were a natural gas fired heater and an electrical heater. The test components examined included, apart from the two IHX, hot gas ducts with a total length of 140 m, hot gas valves, water cooler, and a steam generator (as the heat sink). KVK was operated for 18 400 h with 7 000 h above 900°C and 11 000 h above 700°C, respectively, demonstrating the industrial feasibility of the tested components at a high reliability and an almost 100% availability. The nuclear steam reformer component was tested as part of the EVA–ADAM system at FZJ.

According to the BBC/HRB strategy, the IHX for a nuclear heat supply system based on the HTR-500 concept was designed as a tandem-type He–He heat exchanger separated into a high temperature and a low temperature section. This arrangement offers the chance of a separate replacement of the high temperature part, if necessary, and the use of cheaper materials for the low temperature part. The materials of choice, at that time, were Inconel 617 for the high temperatures and Incoloy 800 for the low temperatures. Selecting a split-up temperature of ~700°C, the low temperature range would be covered by conventional material technology.

2.3.2. Japan

2.3.2.1. Concept of the GTHTR300C

Japan Atomic Energy Agency (JAEA) has constructed and operated a 30 MW(th) HTGR, named high temperature engineering test reactor (HTTR) [23]. HTTR has the extreme design feature to generate reactor outlet coolant temperature of 950°C intending to provide process heat for hydrogen production plant. Initial criticality of the HTTR was achieved in 1998. First full power operation at 850°C was carried out in 2001, and that at 950°C in 2004. Some safety demonstration tests, which include reactivity insertion test and forced cooling reduction test, have been performed since 2001. Design specifications are listed in Table 2.12. The cooling system of the HTTR is shown in Fig. 2.29.

TABLE 2.12. MAJOR DESIGN SPECIFICATIONS OF THE HTTR

Parameter	Value
Reactor thermal power (MW(th))	30
Reactor outlet coolant temperature (°C)	850 or 950
Reactor inlet coolant temperature (°C)	395
Primary coolant pressure (MPa)	4.0
Primary pressurized water cooler (MW(th))	30 or 20
Intermediate heat exchanger (MW(th))	10

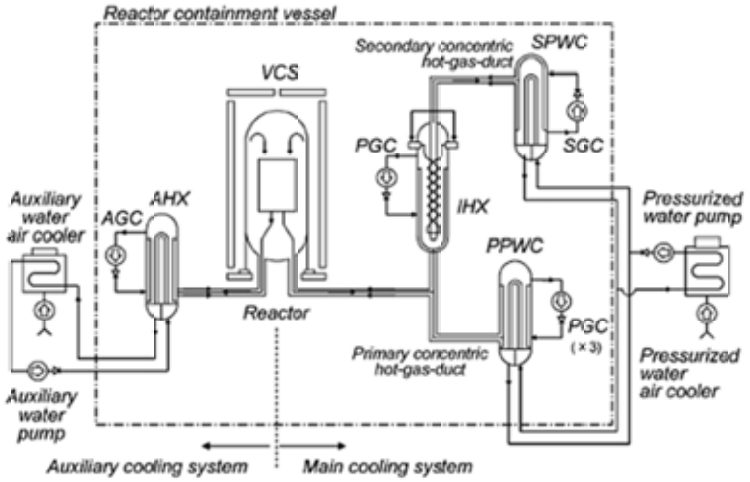

IHX: Intermediate heat exchanger
PGC: Primary gas circulator
SGC: Secondary gas circulator
AGC: Auxiliary gas circulator
PPWC: Primary pressurized water cooler
SPWC: Secondary pressurized water cooler
AHX: Auxiliary heat exchanger
VCS: Vessel cooling system

FIG. 2.29. Cooling system layout of the HTTR.

Based on the experiences with HTTR, JAEA has developed the conceptual design of a commercial scale HTGR hydrogen cogeneration system named GTHTR300C [24, 25]. The GTHTR300C is based on an electricity generation HTGR with a gas turbine electricity generation system named 'gas turbine high temperature reactor' (GTHTR300) [3, 5]. The GTHTR300C employs fully passive reactor safety, high fuel burnup, conventional steel reactor pressure vessel, non-intercooled direct Brayton cycle power conversion, horizontal single shaft gas turbine and electric generator, and a modular system arrangement. Reactor design specifications of the GTHTR300 and the GTHTR300C are the same except for the reactor outlet and inlet helium temperature and the helium flow rate. Major design specifications of the GTHTR300 and the GTHTR300C are shown in Table 2.13. Figure 2.30 shows the system layout of the GTHTR300C. GTHTR300C consists of four modules including a reactor module, a gas turbine module, a heat exchanger module, and an intermediate heat exchanger module. The cooling system layout of the GTHTR300C is shown in Fig. 2.31. The reactor coolant temperature is limited to 850°C to avoid turbine blade cooling and use conventional turbine blade materials. Deletion of an intercooling system reduces the power generation efficiency by 2%. But system arrangement is simplified and cost of construction becomes smaller.

TABLE 2.13. MAJOR DESIGN SPECIFICATIONS OF THE GTHTR300 AND GTHTR300C

	GTHTR300	GTHTR300C
Reactor thermal power (MW(th))	600	600
Core coolant flow (kg/s)	439	322
Core inlet/outlet temperature (°C)	587/850	594/950
Gas turbine inlet temperature (°C)	850	850
Core coolant pressure (MPa)	6.9	5.1
Electricity generation (MW(e))	274	202
Intermediate heat exchanger (MW(th))	n.a.	170

n.a. not applicable.

2.3.2.2. GTHTR300C core design

The reactor core of the GTHTR300C consists of 90 fuel columns in annular arrangement, 73 inner reflector columns, 48 outer reflector columns and 18 sectors of fixed reflector as shown in Fig. 2.32. The effective annular core diameters are 3.6 m at the inside and 5.5 m at the outside. The core height is 8 m. Eight fuel blocks are stacked in each fuel column. Iin the hexagonal fuel block which has a height of 1.05 m and across flat distance is 0.41 m (Fig. 2.33), 57 fuel rods are inserted. A fuel rod is composed of 12 hollow fuel compacts supported by a graphite center rod. Outer diameter of the fuel compact is 26 mm and inner diameter is 9 mm as shown in Fig. 2.34. TRISO coated fuel particles are bonded with graphite matrix in the fuel compact. The diameter of a TRISO coated fuel particle is 1 mm. Seven kinds of enriched uranium are used and average uranium enrichment is 14%. The average fuel burnup is 120 GW·d/t and the age power density is 5.4 MW/m^3. Refueling interval is 18 months. Maximum fuel temperature is estimated at 1244°C during normal operation and 1535°C in a loss of forced convection accident, which are lower than the design temperature limit of 1600°C.

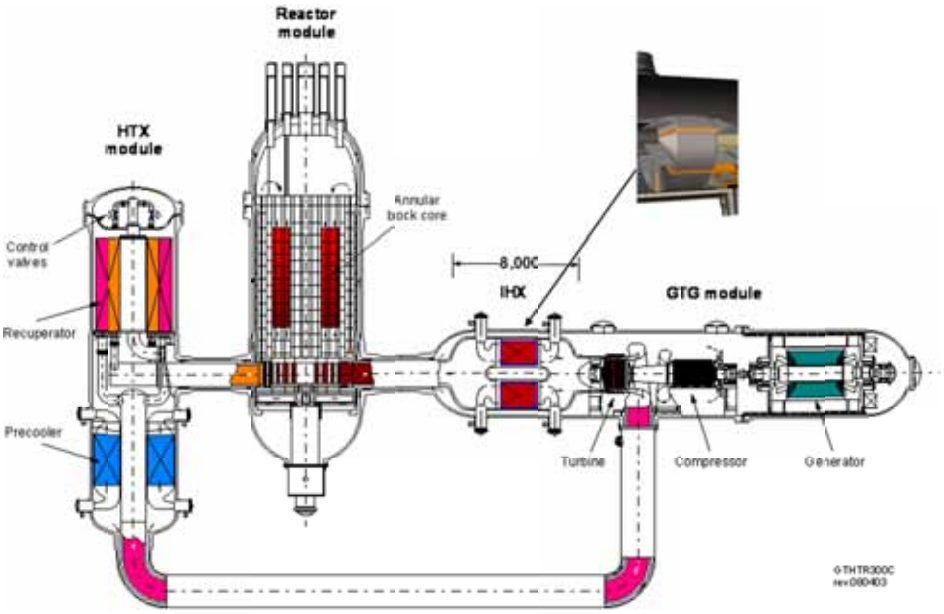

FIG. 2.30. System layout of the GTHTR300C.

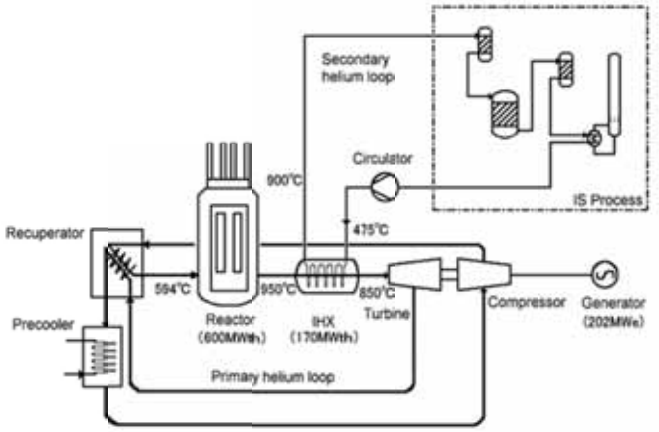

FIG. 2.31. Cooling system of the GTHTR300C.

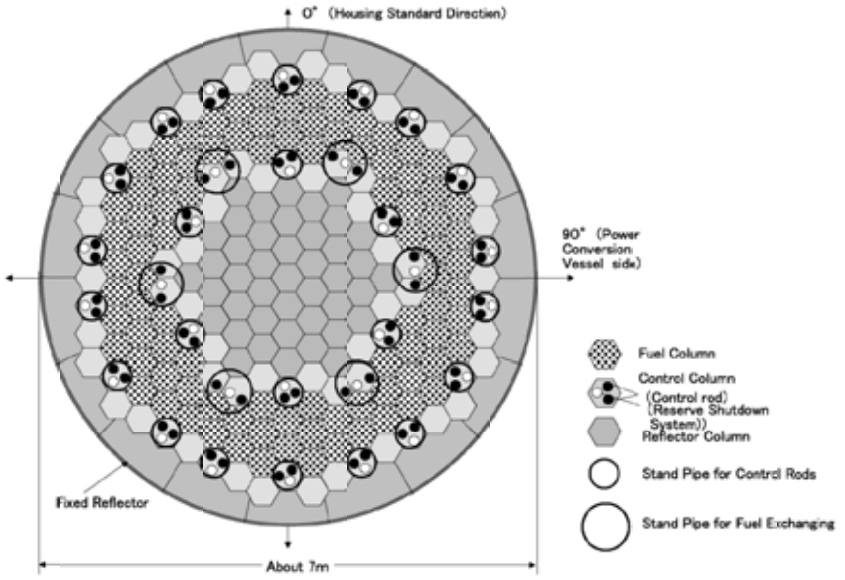

FIG. 2.32. Core horizontal cross section of the GTHTR300C.

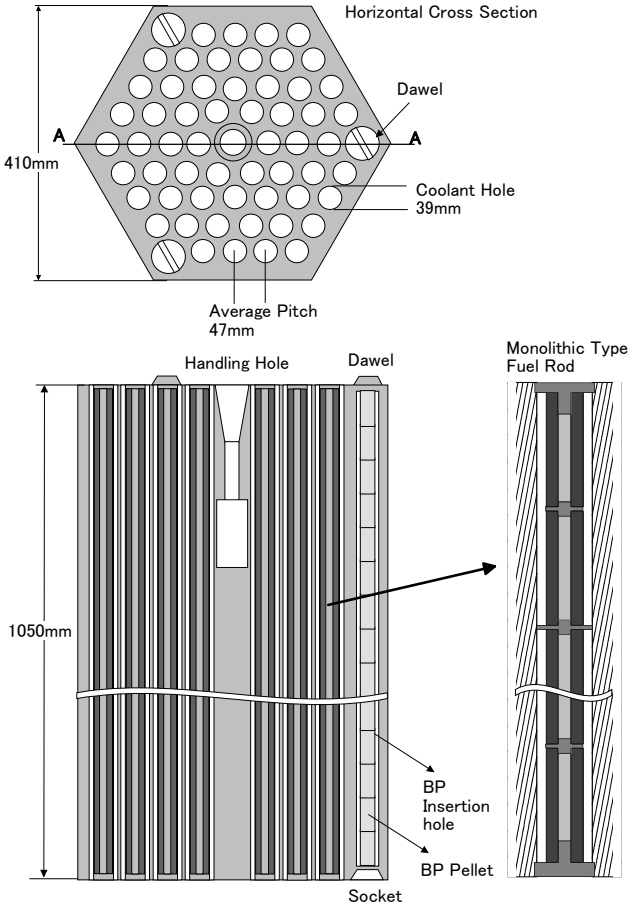

FIG. 2.33. Fuel block of the GTHTR300C.

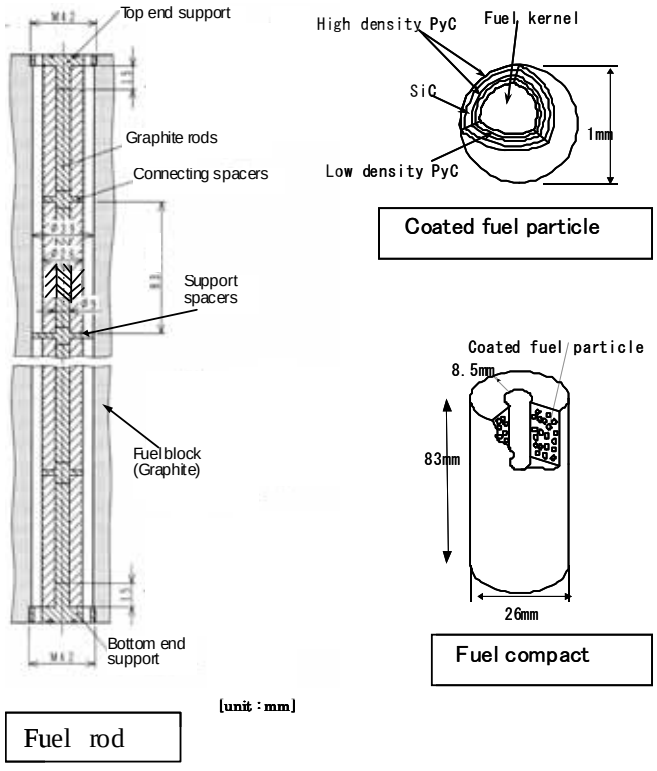

FIG. 2.34. Fuel rod, fuel compact, and coated fuel particle of the GTHTR300C.

2.3.2.3. GTHTR300C reactor coolant system

The reactor outlet coolant flows into the IHX to generate high temperature secondary helium to supply nuclear heat to the hydrogen production plant as shown in Fig. 2.31. Inlet and outlet helium temperature are 950°C and 850°C, respectively. A thermal power of 170 MW is transferred from the primary to the secondary helium in the IHX. The secondary helium can be heated up to 900°C.

The GTHTR300C employs a gas turbine electricity generation system for power conversion. Gas turbine, compressor and generator are placed in the gas turbine module. They are connected by a single rotor and supported by magnetic bearings. The gas turbine is a six-stage axial-flow turbine. Rotor speed is 3600 rpm.

The recuperator recovers turbine exhaust heat. The efficiency of the recuperator affects significantly the electricity cost. Compact and high efficient plate heat exchangers operating in high pressure helium gas are employed. The recooler cools helium gas to 28°C by cooling water to enhance the compression efficiency. The compressor is a 21-stage axial flow compressor. The compressor inlet helium temperature is designed at 28°C and the compressor pressure ratio is 2.0. Compressor outlet helium gas flows into the recuperator and is heated up to 594°C.

The turbine and the compressor are waiting to work at low reactor power in startup and shutdown operation states. Residual heat from the core is removed by a shutdown cooling system and a reactor cavity cooling system (RCCS) as shown in Fig. 2.35. The shutdown cooling system is placed at the bottom of the reactor vessel and consists of water cooler and helium gas circulator. This system must not operate during a depressurization accident to prevent air ingress into the core. In this case, the RCCS removes the residual heat from the core passively by radiation from the reactor vessel to the cooling panels surrounding the vessel, and by natural convection of the cooling air in the cooling panels. The fuel temperature during a LOFC accident is shown in Fig. 2.36 and does not exceed the design limit of 1600°C. The RCCS can cool the core under any set of conditions.

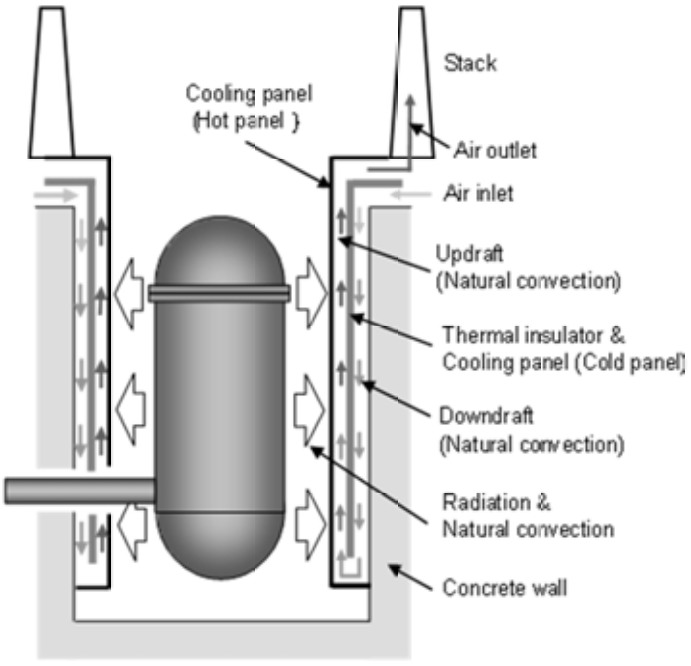

FIG. 2.35. Reactor cavity cooling system.

2.3.2.4. Reactivity control system of the GTHTR300C

The reactivity control system is composed of the control rod system and the reserve shutdown system. The control rods are separate from their driving mechanisms and are automatically inserted into the channels of the control rod columns, as shown in Fig. 2.32, by gravity when a reactor shutdown signal is received from the control system. In the event of control rod system failure, the reserve shutdown system drops B_4C/C pellets into the exclusive channels of the control rod column which shuts the reactor down from the rated operation condition to the hot subcriticality condition. These two systems are redundant and different in their actuation methods.

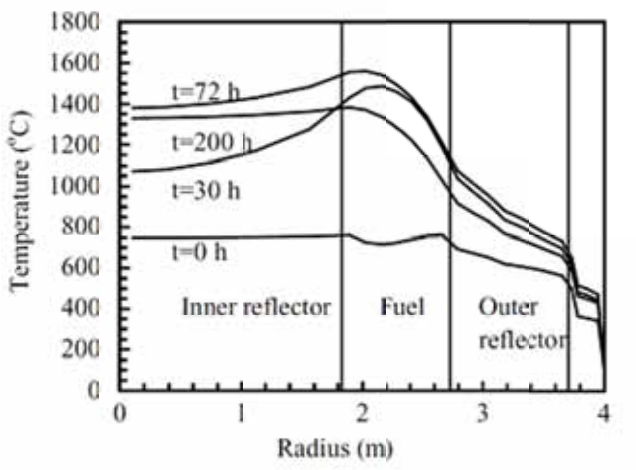

FIG. 2.36. Analysis result of fuel temperature in the loss of coolant accident.

2.3.2.5. GTHTR300C reactor confinement system

The RCCS can remove the residual heat from the core in the LOFC accident, but a long time is required to significantly decrease fuel temperatures. When the core temperatures are high, the fuel may be damaged from oxidation caused by air ingress. The amount of air ingress into the core shall be restricted during the depressurization accident. The GTHTR300C does not employ a containment reactor vessel, but rather a confinement reactor building to prevent excessive air ingress and the release of radioactive material to the environment. A schematic of the reactor building confinement system is shown in Fig. 2.37.

As a large amount of helium blows out within the confinement system in the loss of coolant accident, the pressure in the confinement increases. Pressure release panels are provided in the stacks to automatically release the helium gas into the environment to prevent a failure of the confinement system by overpressure. After the pressure drops, the stack closing panels prevent air ingress into the confinement through the stacks.

The secondary helium pipes in the heat transfer loop penetrate the reactor confinement building. Failure of heat transfer tubes in the IHX and the secondary helium pipe outside the reactor building can create a flow path to release helium coolant to the environment and to flow air into the reactor. However, multiple isolation valves are installed on the secondary helium piping near the penetration of the reactor building to mitigate the consequences of the beyond design basis event.

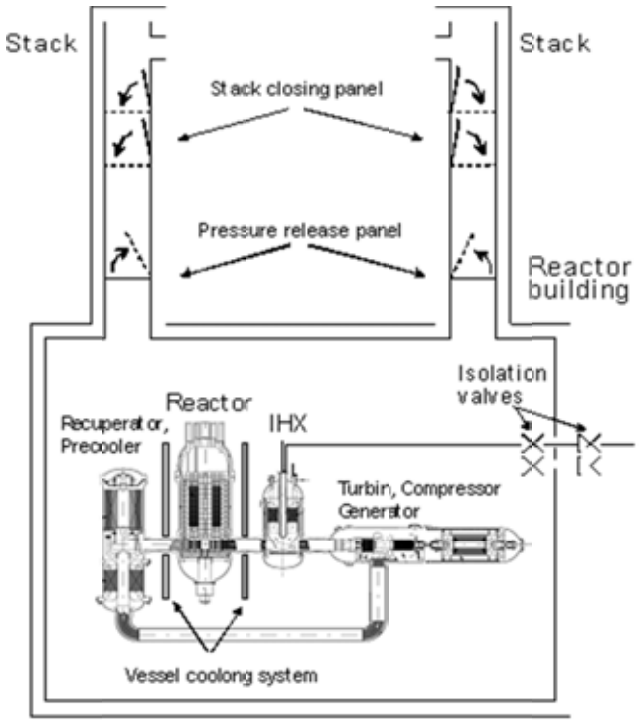

FIG. 2.37. Schematic of reactor confinement system.

2.3.2.6. diate heat exchanger for the GTHTR300C

A conceptual design of the shell and tube type IHX for the GTHTR300C was developed. Design specification are listed in Table 2.14 and a conceptual drawing is shown in Fig. 2.38 [26]. The IHX of the GTHTR300C is used at high temperature of 950°C. Reduction of creep damage by primary stress is significant to extend the design lifetime of the IHX heat exchanger tubes. Primary stress originates from pressure loads and the tubes' own weight. The pressure load is a plant design parameter and independent of the IHX design. The large diameter of the tube bundle increases a span of tube support so that primary stress of the outer tube bundle originating from the weight becomes large. In sizing of the heat exchanger tube, both weight of the tube and diameter of the tube bundle should be minimized.

A large heat transfer area is required for the IHX of the GTHTR300C to transfer heat of 170 MW. To provide such a large heat transfer area, it is required to enlarge the diameter of the tube, to increase the number of tubes or to extend the tube length. Extension of the tube length increases the pressure drop and pump load so that the system efficiency decreases. Increasing the number of the tubes causes an increase in the coiled layers and an enlargement of the pressure vessel diameter. The tube length, diameter, thickness, and number have been evaluated and are shown in Table 2.14.

2.3.3. India

2.3.3.1. Nuclear heat supply system for hydrogen production

The nuclear heat supply system (NHSS) that is proposed for the process heat applications is based on the 400–500 MW(th) PBMR reactor, and developed in conjunction with the PBMR/Westinghouse electric company consortia. This is in fulfilment of the next generation nuclear plant (NGNP) proposal as required by the US Department of Energy (DOE).

TABLE 2.14. MAJOR DESIGN SPECIFICATIONS OF THE SHELL AND TUBE TYPE IHX FOR THE GTHTR300C

Parameter	Value
Thermal rating (MW(th))	170
Heat transfer area (m^2)	1448
Shell side flow	
Flow rate (kg/s)	324.2
Temperature (inlet/outlet) (°C)	950/850
Inlet pressure (MPa)	5.0
Tube side flow	
Flow rate (kg/s)	80.3
Temperature (inlet/outlet) (°C)	500/900
Inlet pressure (MPa)	5.15
Tube size (outer dia/thickness) (mm)	45.0/5.0
Tube effective length (m)	14.2
Tube bundle diameter (ID/OD) (mm)	1.84/4.57
Number of tubes	724
Number of coiled columns	22
Pressure vessel	
Outer diameter (m)	5.7
Thickness (mm)	100

ID = inner diameter.
OD = outer diameter.

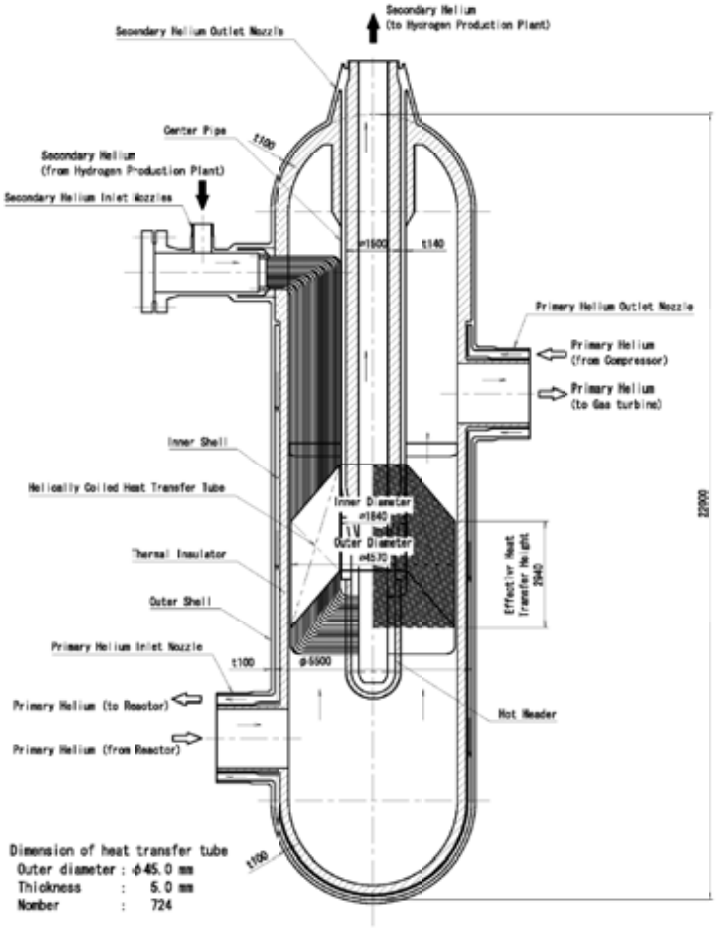

FIG. 2.38. Conceptual design of the shell and tube type IHX for the GTHTR300C.

The reactor of the NGNP serves to heat the fluid in the primary heat transport system (PHTS) by means of a nuclear reaction in the reactor unit system (RUS). The PHTS circulates the primary coolant from the RUS to the intermediate heat exchangers, where the heat from the RUS is transferred to the secondary heat transport system (SHTS). The SHTS transports heat to the hydrogen production system (HPS) and the power conversion system (PCS), where the heat is either utilized or, in certain plant operating modes, rejected to the environment. A simplified diagram illustrating this configuration is presented in Fig. 2.39.

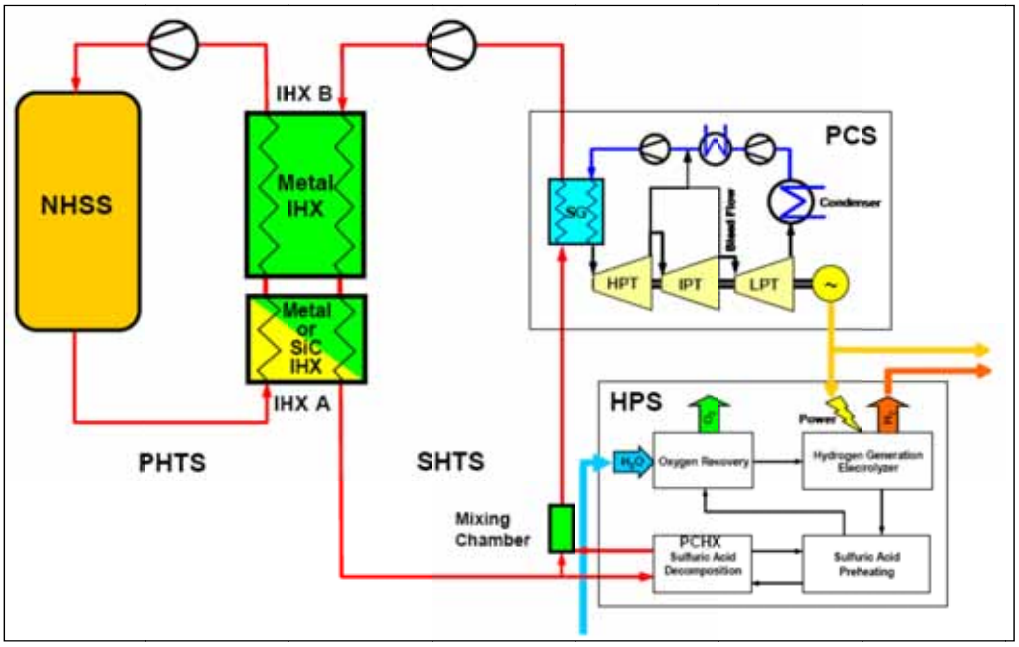

FIG. 2.39. NGNP with hydrogen demonstration preconceptual design schematic.

The NHSS design is based on the PBMR's initial power plant reactor design, which uses the HTGR technology which was originally developed in Germany. This implies the use of spherical fuel elements, referred to as pebbles, which are in size and physical characteristics the same as the fuel which was developed for the German HTGR programmes. Similar to the German pebble bed reactors, the PBMR design uses an online refueling scheme.

For application in the NGNP project, the most significant change to this reactor is an up rating of the continuous power level from 400 MW(th) to 500 MW(th). This was accomplished by changing the reactor inlet/outlet temperatures from 500ºC/900ºC to 350ºC/950ºC, while the reactor mass flow was decreased from 193 kg/s to 161 kg/s.

Another important change to the reactor design for NGNP application is that the core barrel bonditioning system (CBCS) is not necessary, due to the lowering of the reactor inlet temperature. For the NGNP application, the function of the CBCS is fulfilled by re-routing the flow path of the primary coolant, which is at a lower temperature than the first reactor. The change in primary coolant flow path necessitates moving the PHTS cold pipe (reactor inlet) from the bottom part of the RUS to the top of the reactor pressure vessel.

2.3.3.2. Nuclear heat supply system for steam production

During 2008, the US-DOE recognized that the NGNP development path directly to hydrogen production carried schedule risk and consequently reduced the operating requirements for the NGNP to those that support the production of steam and electricity, in order to support an

earlier deployment of the NHSS. In response to this change, the PBMR/Westinghouse consortium is proposing the configuration as illustrated in Fig. 2.40.

The SHTS transports heat to the steam generator which supplies high temperature and pressure steam to the power conversion system (PCS) which utilizes the steam to make electricity while extracting the steam at the desired conditions for use in the process.

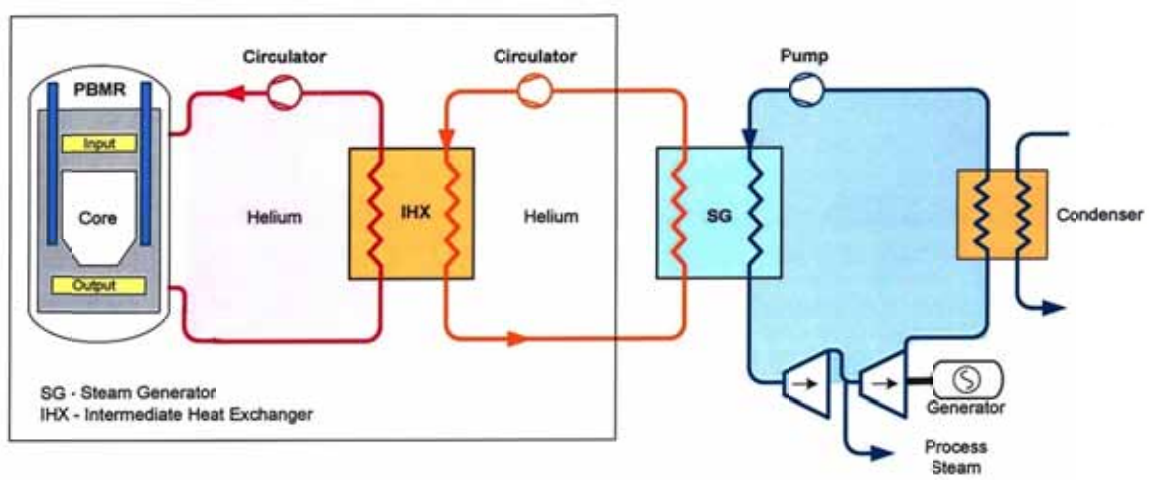

FIG. 2.40. NGNP demonstration cogeneration design schematic.

The NHSS design basis is as described above and has a reactor outlet temperature of 750°C and a reactor inlet temperature of 280°C. The SHTS supplies helium to the steam generator at 700°C while the steam generator supplies the steam to the extraction turbine at about 565°C and 17 MPa. Consideration is currently being given to fitting the steam generator directly into the PHTS, but this decision is subject to a complete analysis of all the advantages and disadvantages of both configurations.

3. PROCESS HEAT HTGR APPLICATIONS

3.1. NUCLEAR HYDROGEN PRODUCTION

Hydrogen can be produced by thermochemical and/or electrochemical processes using nuclear energy as the primary thermal energy source. Nuclear energy can be used in hydrogen production mainly in three ways:

- By using the electricity from the nuclear plant for conventional liquid water electrolysis (electricity + H_2O [liquid] → H_2 + O_2).
- By using both the high temperature heat and electricity from the nuclear plant for the high temperature steam electrolysis (electricity + H_2O [steam] → H_2 + O_2) or the hybrid processes (electricity + heat + H_2O → [cyclic chemical reactions] → H_2 + O_2).
- By using the heat from the nuclear plant for thermochemical processes (heat + H_2O → [cyclic chemical reactions] → H_2 + O_2).

Even the conventional liquid water electrolysis is a commercially proven technology that can be driven by the present generation of low temperature water cooled nuclear power reactors, it may not present an energy efficient hydrogen production method for the long term since higher process temperatures are required for more efficient thermochemical and electrochemical hydrogen production reactions. Consequently, nuclear technologies capable of producing reactor coolant temperatures on the order of 700ºC or higher are expected to be

suitable for large scale hydrogen production in the future. Since they can reach the required high temperatures, gas cooled reactors, molten salt cooled reactors, and heavy metal cooled reactors, appear to be the most promising technologies to be coupled to the hydrogen plants for efficient production [27–29].

High temperature operation of both nuclear and hydrogen plant imposes stringent heat transfer associated design requirements that demand materials development as well as intricate design requirements for integrated plant layouts, which consequently affect the cost of each technology. Furthermore, the safety of the three components of the complex, the hydrogen plant, the nuclear reactor, and the coupling of the two, should be carefully analyzed.

In the following, the main processes under development for hydrogen production using HTGRs as a primary energy source are analyzed.

3.1.1. High temperature steam electrolysis

The history of water electrolysis starts as early as the first industrial revolution when, in the year 1800, Nicholson and Carlisle discovered the capability of electrolytic water splitting. At present, conventional liquid water electrolysis including alkaline water electrolysis, high pressure electrolysis, and solid polymer electrolyte water electrolysis, is basically applied to produce hydrogen if a cheap source of electricity is available, since it involves high electrical energy consumption. Furthermore, the overall efficiency of the process is too small, about 27% [30].

Instead, the high temperature steam electrolysis (HTSE) that is a reverse process of a solid oxide fuel cell (SOFC), offers several advantages from both thermodynamic and kinetic standpoints [27], as can be appreciated in Fig. 3.1.

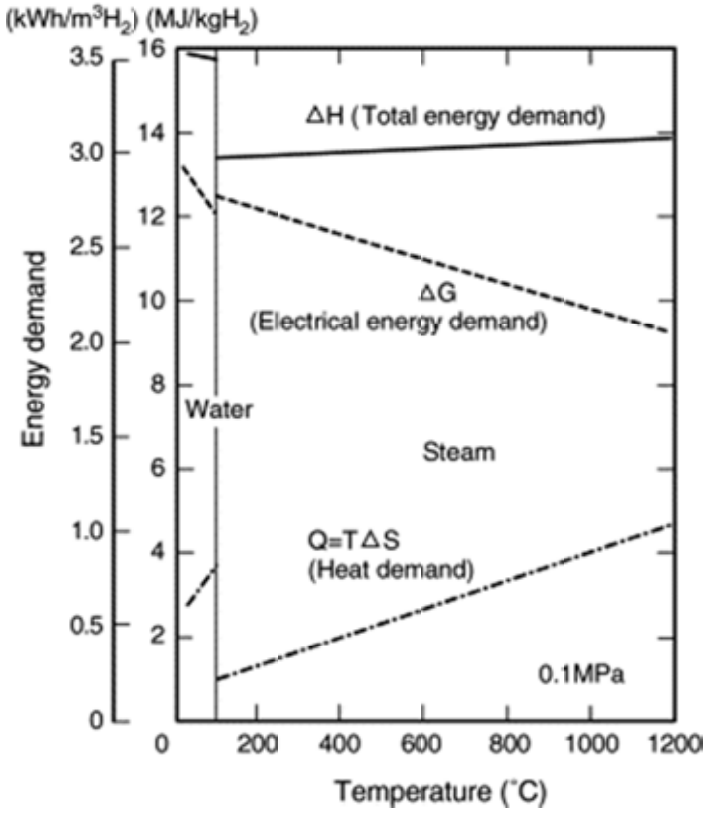

FIG. 3.1. Energy demand for high temperature steam electrolysis [31].

The total energy required, ΔH, which is composed of the required thermal energy, Q, and the Gibbs free energy (electrical energy demand), ΔG, increases with increasing temperature leading to increased direct heat requirement. The decrease in electrical energy demand drives the thermal-to-hydrogen energy conversion efficiency to higher values. On the other hand, the higher temperatures also favor the electrode activity and help lower the cathodic and anodic over-voltages. Therefore, it is possible to increase the electric current density at higher temperatures and, consequently, lower the polarization losses yielding an increase in the process efficiency.

The HTSE process uses a combination of thermal energy and electricity to split water in an electrolyzer that is similar to a SOFC and operates at high temperatures in the range between 800ºC and 1000ºC. A schematic picture of both devices with the corresponding electrochemical reactions is shown in Fig. 3.2.

Steam is dissociated with electrons from externally provided electricity on the surface of a cathode. In presence of an oxygen ionic conductor used as a solid electrolyte, hydrogen molecules form on this surface while, simultaneously, oxygen ions migrate through the solid electrolyte and form oxygen molecules on the surface of an anode with the release of electrons. The products, hydrogen and oxygen, are separated by the gastight electrolyte and the hydrogen produced by this process has high purity. Only the gases H_2O, O_2 and H_2 have to be circulated in the electrolysis plant and no other chemicals are involved that could rise to safety or environmental problems.

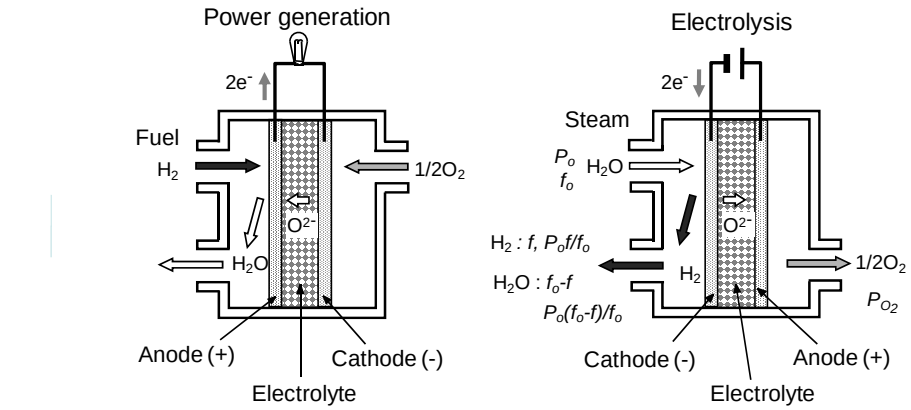

FIG. 3.2. Principle of high temperature steam electrolysis, reverse reaction of solid oxide fuel cell [32].

Development of electrolysis cells for HTSE process is being undertaken vigorously around the world [33, 34]. An yttrium-stabilized zirconium oxide membrane was introduced as a solid oxide electrolyte and its applicability to a high temperature electrolysis to produce hydrogen was examined by the Japan Atomic Energy Agency (JAEA) [32, 35]. In 2004, the Idaho National Laboratory (INL) also proposed the high temperature electrolysis concept to produce hydrogen using the nuclear energy from HTGRs [36] and an electrolysis cell was tested [37].

Even the specific materials for the electrodes and electrolyte and the geometry of the unit cell can change, depending on the operating temperature for providing optimized performance, a representative electrolysis cell is shown in Fig. 3.3. It consists of a ceramic solid membrane of

10 μm in thickness, a porous Ni–ZrO_2 cathode of 50 μm in thickness, and a porous Sr-doped lanthanum manganite anode of 150 μm in thickness. The electrodes are deposited on either side of the electrolyte. The outsides of the electrodes are enveloped by a 2.5 mm stainless steel plate. The cell size is 10 cm × 10 cm × 4.06 cm and the effective electrode area is 64 cm^2. A stack composed of 10 cells can produce the hydrogen at 60 Nl/hour [38].

The mechanism of the HTSE in the unit cell can be described as follows. A mixture of 90% steam and 10% hydrogen is introduced into the high temperature cathode chamber though a pipe. The gas mixture penetrates the porous cathode via the interface between the cathode and the solid oxide electrolyte. A water molecule is electrically split into hydrogen and an oxygen anion by two electrons transported from the anode through an external cable. The hydrogen produced is back-diffused to the cathode chamber. The cathode is graded with a nickel–zirconia cermet layer immediately adjacent to the electrolyte and a pure nickel outer layer.

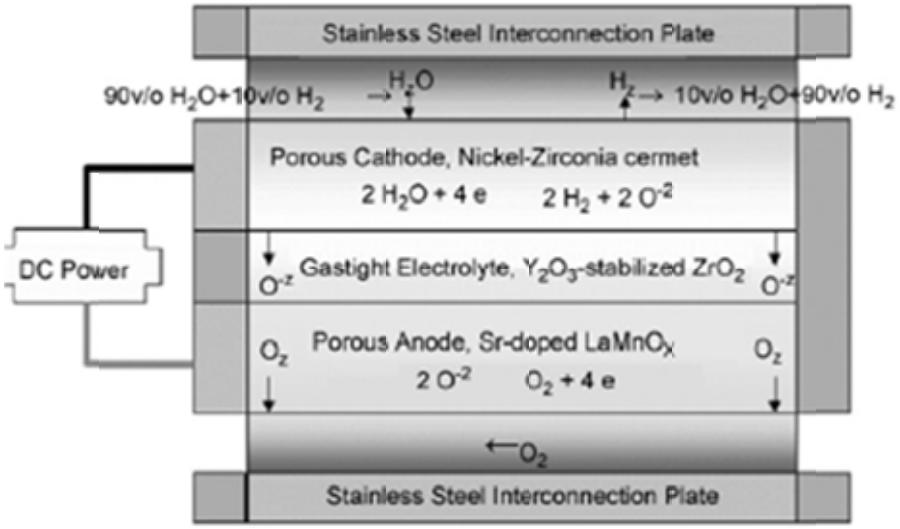

FIG. 3.3. Unit cell for high temperature steam electrolysis [38].

The partially oxidized nickel element of Ni–ZrO_2 cathode material must be reduced before conducting an electrolytic chemical reduction of steam. Besides, a reduction environment for keeping the pure nickel metal is demanded continuously during operation and shutdown by introducing hydrogen inside the cathode chamber. The reduced oxygen anion is drawn to the anode through the solid oxide electrolyte by the electrochemical potential driven by a AC/DC potentio-stat, thus liberating the two electrons, and then is oxidized to oxygen. The oxidized oxygen continuously penetrates the porous anode and is collected and evacuated at the anode chamber. The liberated electrons are also transported to the cathode through the electric cable.

The HTSE process is particularly advantageous when coupled to high efficiency power cycles and can, consequently, yield very high overall thermal-to-hydrogen efficiency. The HTSE concept can be coupled to a range of nuclear technologies, such as supercritical water cooled reactors, gas cooled reactors, lead–bismuth cooled reactors, and molten salt reactors, all of which can deliver relatively high temperatures and high net power cycle efficiencies.

Based on the very high temperature reactor (VHTR) introduced by Generation IV nuclear energy systems [39], a conceptual flow diagram of the HTSE process for hydrogen production was developed [38]. As presented in Fig. 3.4, the process consists of the VHTR to produce high temperature thermal energy, the power cycle to generate electricity, the AC/DC converter to supply DC power to the electrolyzer, two heat exchangers to supply thermal

energy to the superheated steam generator, the high temperature electrolyzer to produce hydrogen from steam, the heat recuperating condenser, the hydrogen–water separator, and the dehumidifier to remove the residual water from the hydrogen.

The second high temperature heat exchanger supplies superheated steam to the electrolyzing cell at a temperature of about 850–950ºC, and a pressure of around 5 MPa. The superheated steam introduced into the electrolyzer contains a small portion of hydrogen in order to maintain the reducing conditions at the cathode. Argon gas can be used as an inert carrier gas. The argon and hydrogen mixture is mixed with steam to maintain the proper humidity and partial pressures of the gas mixture. The net conversion rate is measured by using a precision dew point sensor at the inlet and outlet points of the cathode chamber.

The hydrogen stream produced by operating the high temperature electrolysis cell including 10% of water is introduced into the heat recuperating condenser in which the steam is condensed and separated from the hydrogen stream. Most of the heat of the hot gas product stream exiting the electrolyzer is recovered at the recuperating condenser by the demineralized and deionized water. The preheated water is mixed with hydrogen at a humidifier and introduced into the intermediate heat exchanger. The hydrogen stream separated from the condensed water is introduced into a dehumidifier and finally stored in a storage vessel. Consequently, the overall thermal efficiency of the system is affected by the performance of the electrolyzer, the thermal recuperating fraction at the condenser, and the gas turbine efficiency.

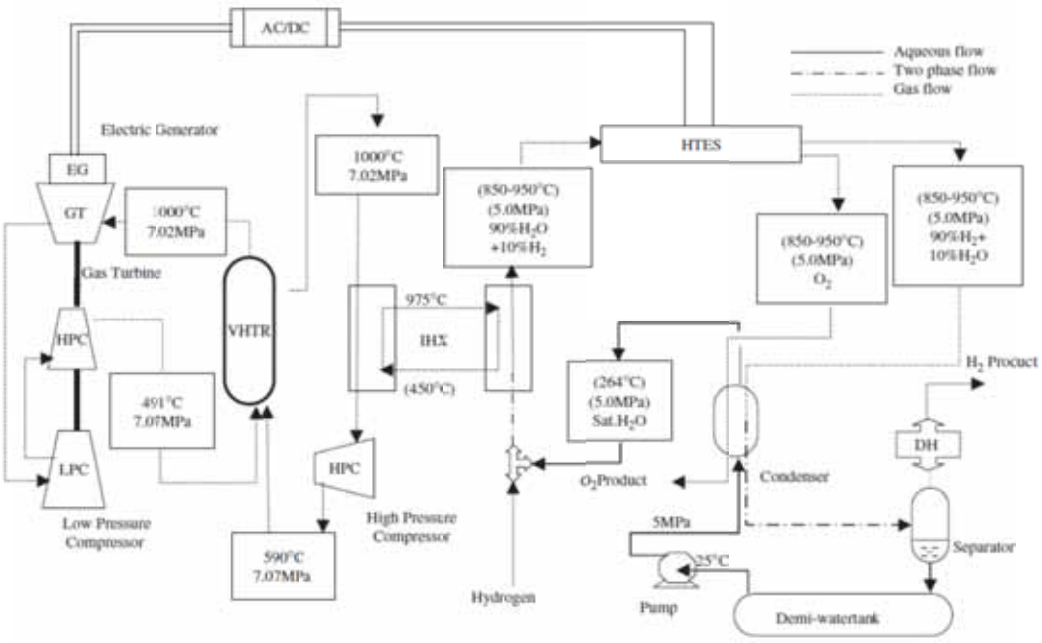

FIG. 3.4. Conceptual flow diagram of the VHTR-based hot electrolysis for hydrogen production [38].

In Ref. [27], two alternatives were considered for both the nuclear reactor and the electrical power cycle in a preliminary evaluation stage. The first alternative for the nuclear plant is the modular helium reactor (MHR) with helium power conversion cycle. This approach has also started to be evaluated at INL [40]. The second alternative is a proposal to couple an advanced version of the currently operating advanced gas reactors (AGR) to a direct supercritical CO_2 power conversion cycle. In both cases the nuclear reactor is coupled with a HTSE hydrogen plant called high operating temperature electrolysis (HOT ELLY) developed by Dornier GmbH, Lurgi GmbH and Robert Bosch GmbH [41]. The electric net cycle efficiencies of both

alternatives corresponding to the respective ranges of reactor exit temperatures of the working fluid were calculated. Results are given in Fig. 3.5.

It is clear from Fig. 3.5 that attaining high power cycle efficiency can have a more important effect on the hydrogen production efficiency than solely attaining a high operating temperature. Even though the AGR-HTSE system is proposed to attain a lower range of operating temperature than that of the MHR-HTSE system, thermodynamically, the electrical net efficiency is higher for the first alternative.

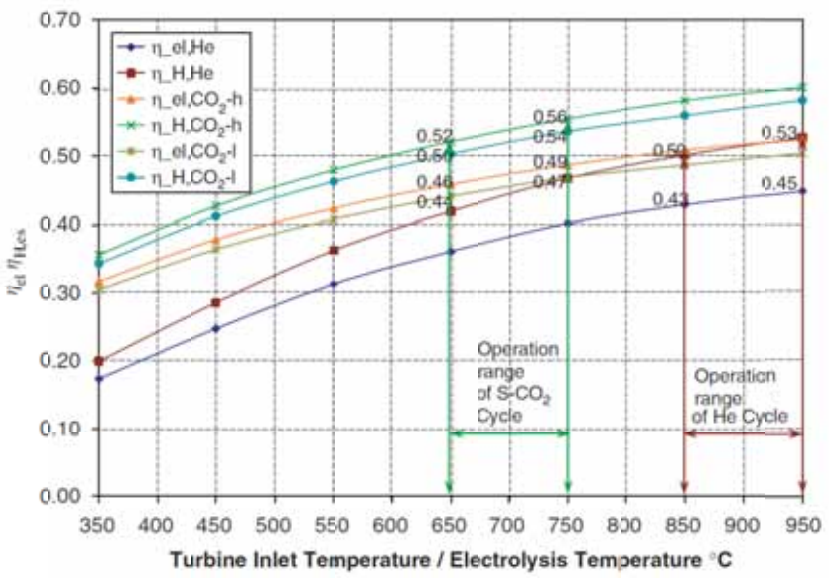

FIG. 3.5. Power cycle net efficiency and thermal-to-hydrogen energy efficiency for the MHR-HTSE and AGR-HTSE technologies [27].

3.1.2. Thermochemical cycles

3.1.2.1. General

Thermochemical processes for hydrogen production involve thermally assisted chemical reactions that release the hydrogen from hydrocarbons or water. While the most widespread thermochemical process for hydrogen production at present is the steam methane reforming process (SMR), it is not favored for a long term hydrogen economy since it yields considerable greenhouse gas emissions. Therefore, alternative thermochemical processes which split the water into hydrogen and oxygen through a series of thermally driven chemical reactions are being developed in several countries. This approach is called the thermochemical water splitting process.

The simplest thermochemical process to split water would involve heating the water molecule to a high temperature and separating the hydrogen molecule from the equilibrium mixture. Unfortunately the decomposition of water is only completed at temperatures above 2600ºC. The problems with materials and separations at such high temperatures make direct decomposition not feasible at this time. However, by combining high temperature endothermic chemical reactions and low temperature exothermic chemical reactions, in which the net chemical change resulting from the sequence of component chemical reactions is the water decomposition, it is possible, in principle, to decompose water with the heat of about 900ºC [42]. Using intermediate compounds, a sequence of chemical and physical processes can decompose water into hydrogen and oxygen, without releasing any pollutants externally to the atmosphere since the intermediate compounds are recycled internally in a closed loop.

Even over 200 thermochemical cycles have been identified for the water splitting [43, 44], very few of them have progressed beyond theoretical calculations to working experimental demonstrations that establish the technical feasibility of the thermochemical processes. Currently the leading alternatives are the sulphur–iodine cycle (S–I) and the hybrid sulphur process (HyS). Other processes have been also proposed but are less developed, such as the copper–chloride (Cu–Cl) cycle and the UT-3 thermochemical process. The main characteristics of these thermochemical processes for hydrogen production which can be supported by nuclear energy are described below.

3.1.2.2. Sulfur–iodine cycle

i. S–I Cycle Basics

The S–I cycle was originally proposed by General Atomics (USA) in the 1980s [45, 46], and was studied also in Europe [47], Canada [48], and Japan [49]. At present, active development is underway at General Atomics (USA), Sandia National Laboratory, SNL (USA), Japan Atomic Energy Agency, JAEA (Japan), Commissariat à l'energie atomique, CEA (France), Korean Atomic Energy Research Institute, KAERI (Republic of Korea), Institute of Nuclear and New Energy Technology, INET (China), and others.

The S–I cycle is the most developed thermochemical water splitting process. The equipment has been scaled to a laboratory level in Japan, where approximately 30 Nl/hour of hydrogen were produced for 175 hours [50]. For these experiments, electrically heated helium was used for supplying heat to the chemical reactors but, in the near future, a hydrogen production system based on the S–I cycle is planned to be connected to the operating high temperature engineering test reactor (HTTR) [51]. The scale-up to a pilot plant with an expected H_2 production rate of 30 Nm^3/h is currently under construction.

The S–I process involves the decomposition of sulphuric acid (H_2SO_4) and hydrogen iodide (HI), and the regeneration of these reagents using the Bunsen reaction, as it is schematically shown in Fig. 3.6. Process heat is supplied at temperatures greater than 800ºC to concentrate and decompose sulphuric acid. The exothermic Bunsen reaction is performed at temperatures below 120ºC and releases waste heat to the environment. Hydrogen is generated during the decomposition of hydrogen iodide, using process heat at temperatures higher than 300ºC [52]. The process works like a chemical engine to produce hydrogen by absorbing high temperature heat in the endothermic decomposition and discharging low temperature heat in the exothermic Bunsen reaction.

The sulphur–iodine process, an HTGR-based pure thermochemical cycle, basically consists of three chemical reactions and is considered suitable for large scale cost effective production of hydrogen through environmentally attractive option [42].

Bunsen reaction (exothermic at 20–120°C):

(1) $I_2 + SO_2 + 2\ H_2O \leftrightarrow H_2SO_4 + 2HI$

Hydriodic acid decomposition (endothermic at 300–450°C):

(2) $2\ HI \leftrightarrow H_2 + I_2$

Sulphuric acid decomposition (endothermic at 800–900°C):

(3) $H_2SO_4 \leftrightarrow H_2O + SO_2 + 0.5\ O_2$

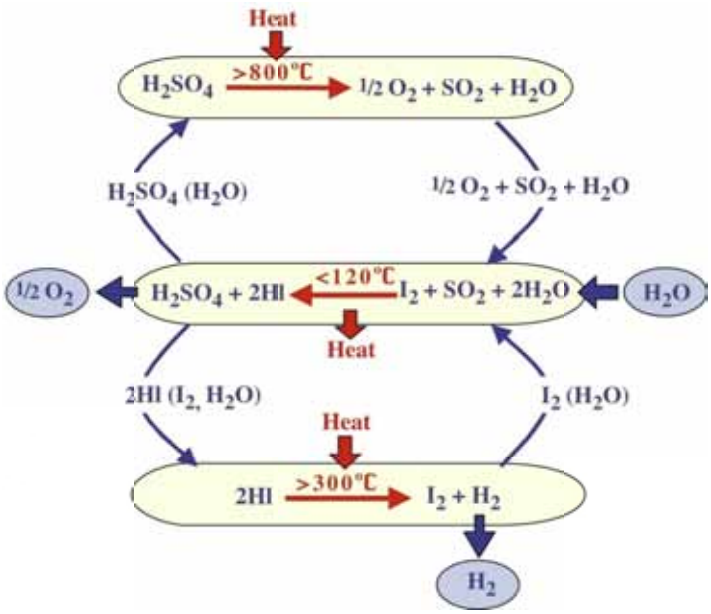

FIG. 3.6. Schematic of the sulphur–iodine cycle [52].

Apart from R&D efforts on the feasibility and process optimization, a few technological breakthroughs in key issues like materials, membrane-based processing, coupling to nuclear reactor, integration and optimization of heat distribution within the cycle are called for fully harnessing the potential of the S–I cycle.

Reaction (1) is typically operated in aqueous medium (water acting as solvent and reactant) with large excess of iodine to facilitate separation of the two product acids, to improve chemical equilibrium, and to eliminate side reactions. It can be represented by

$$(4) \qquad (x+1)I_2 + SO_2 + (2+y+z)H_2O \quad \leftrightarrow \quad \begin{matrix}(2HI + xI_2 + yH_2O)\ HI_x\ \text{Phase} \\ + (H_2SO_4 + zH_2O)\ H_2SO_4\ \text{Phase}\end{matrix}$$

where x,y,z are the iodine and water molar excess quantities respectively.

This cycle has values of x=8, y= 4, z=10. The more detailed steps and recycled streams of the S–I cycle can be schematically represented as given in Fig 3.7. The addition of excess iodine and water in S–I process penalizes the cycle in terms of efficiency, complexity of processing steps, recycling of large quantities with associated complications(all have bearing on economics). These are being researched seeking innovative solutions. Attempts are directed towards minimizing excess quantities and/or seeking alternative routes to carryout process operations in various sections [53–55].

One of the key technical concerns of S–I cycle is that excess amounts of water and iodine added for a good purpose in the Bunsen reaction section become a burden in the downstream sections where those excesses are recovered and sent back to the Bunsen reaction section. Much energy is demanded and lost during the recovery processes through heating, separation, cooling, and pumping. As a consequence, the overall cycle efficiency decreases. To improve the efficiency, the excess water and iodine should be minimized or optimized because the HI/H_2O liquid solution has an azeotrope at relatively low concentration and it is inefficient to concentrate HI above the azeotrope [56].

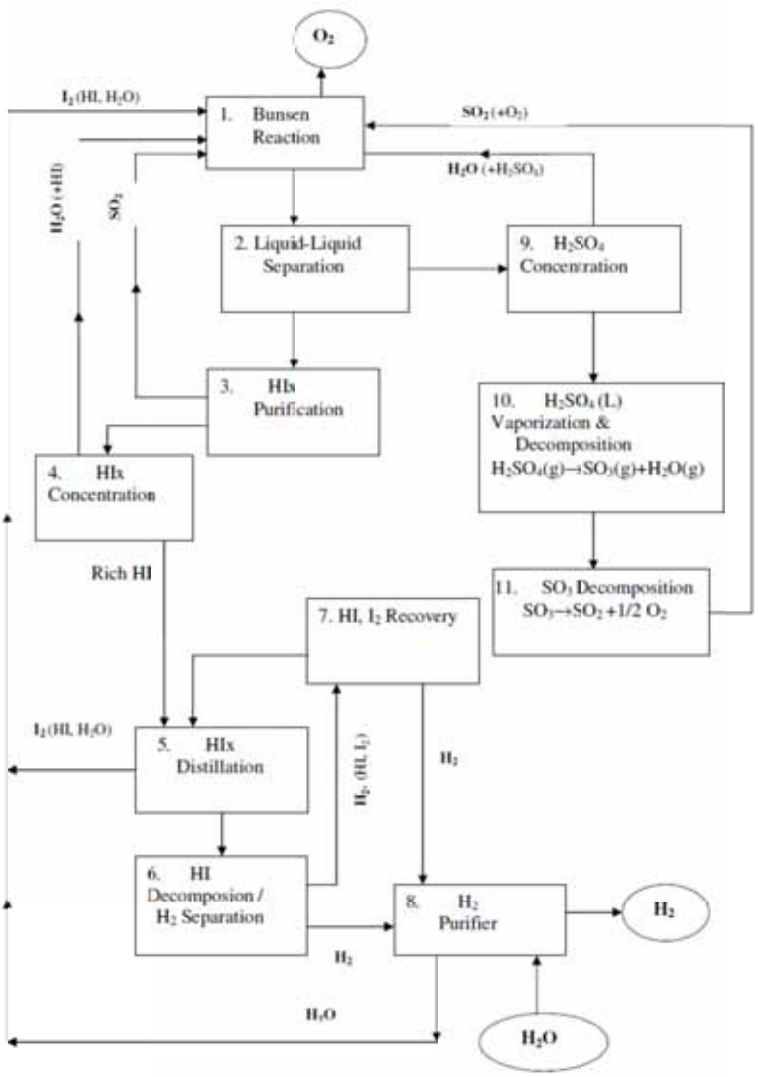

FIG. 3.7. S–I process — typical schematic of steps and recycled streams.

To solve this problem, several different approaches are being developed. General Atomics proposed an extractive distillation technique that uses phosphoric acid (H_3PO_4) as a medium to concentrate the HI solution above the azeotrope [43]. However, the phosphoric acid itself should be recovered through a separate cycle consuming a large amount of energy. In Germany, the Aachen University introduced a reactive distillation column, in which concentration and decomposition processes occur simultaneously [57]. Upward along the distillation column, the HI content in the liquid phase gets richer, and so more HI molecules are likely to escape. Then the vapour phase HI content in the upper region of the column is higher than in the lower region. JAEA in Japan is developing an electro–electro dialysis technology to overcome the azeotrope of HI solution [58], and its technical challenges arise from the fact that electro–electro dialysis demands much electrical energy and the low mechanical strength of the required membranes causes difficulties for scaling up the facility to a larger plant.

Another technical issue of the S–I process is corrosion. Since sulphuric acid, hydriodic acid and iodine are very corrosive substances, selection of the structural materials is very important. So far, screening tests have been carried out on corrosion resistant materials in the representative process environments by General Atomics, JAEA, and others. The main results can be summarized as follows:

(a) in the gaseous environment of sulphuric acid decomposition, refractory alloys that have been used in conventional chemical plants show good corrosion resistance;

(b) in the gaseous environment of HI decomposition, a Ni–Cr–Mo–Ta alloy presents a good corrosion resistance;

(c) in the case of the Bunsen reaction section, glass-lining materials show a suitable corrosion behavior;

(d) in the environment of HI_x distillation, tantalum shows excellent corrosion resistance;

(e) for the severest environmental condition that is the boiling of concentrated H_2SO_4 under high pressure, e.g. 2 MPa, ceramic materials containing silicon as SiSiC, SiC, and Si_3N_4 are the only materials that show good corrosion resistance [59].

Major uncertainties in the S–I process also relate to the estimation of an overall efficiency. Figure 3.8 and Table 3.1 give some clue about the potential and development efforts required to improve the process.

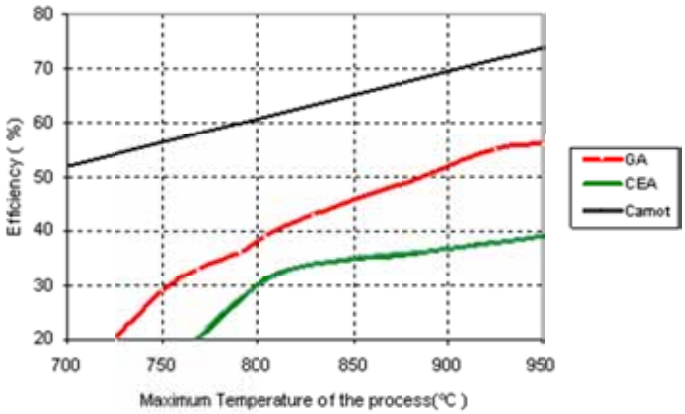

FIG. 3.8. Thermodynamic efficiency curves [63].

TABLE 3.1. ESTIMATED VALUES OF THERMAL EFFICIENCY IN PROCESS SCHEMES PROPOSED BY DIFFERENT GROUPS

Process scheme	Efficiency (% (HHV))	Reference
HI section Extractive distillation using phosphoric acid Sulphuric acid section Concentration with multistage flash evaporation	47 (BE)	[45]
HI Section — Reactive distillation	42 (BE)	[47]
Sulfuric acid section — Direct contact process	56 (BE)	[64]
HI section Reactive distillation Reducing the recycle of HI back to Bunsen section Side stream eliminated from reactive distillation Sulfuric acid section — Direct contact process	39 (BE)	[65]
HI Section — Reactive distillation Sulfuric acid section — Direct contact process	51 (max) 33–36 (BE)	[66]
EED cell for HI concentration and HPMR for HI decomposition	57 (max) 34 (BE)	[67]
EED and HPMR coupled with HTTR	44 (BE)	[51]
Enrichment of HI by simple flash process before decomposition and the same for sulphuric acid section	47–48 (BE)	[56]

BE = best estimate.

The realistic S–I cycle as was given in (4) can be split into the following process steps [66]:

(1)	$(9I_2)_l + (SO_2)_g + (16H_2O)_l$	→	$(2HI+10H_2O+8I_2)_l + (H_2SO_4+4H_2O)_l$	[120°C]
(2)	$L2 = (2HI + 10H_2O + 8I_2)_l$	→	$(2HI)_g + (10H_2O+8I_2)_l$	[227°C]
(3)	$(2\ HI)_g$	→	$H_2 + (I_2)_g$	[327°C]
(4)	$L1 = (H_2SO_4 + 4H_2O)_l$	→	$(H_2SO_4)_l + (4H_2O)_l$	[297°C]
(5)	$(H_2SO_4)_l$	→	$(H_2SO_4)_g$	[357°C]
(6)	$(H_2SO_4)_g$	→	$(SO_3)_g + (H_2O)_g$	[397°C]
(7)	$(SO_3)_g$	→	$(SO_2)_g + 0.5\ O_2$	[867°C]

The temperatures between brackets are approximate and depend upon the pressure that is not necessarily uniform in the different parts of the process.

The Bunsen reaction (1) proceeds exothermally in liquid phase, and produces two immiscible aqueous acid phases which compositions are indicated in parentheses: L1 phase which is aqueous sulphuric acid and L2 phase which is a mixture of hydrogen iodide, iodine and water, named HI_x. In step (2), HI is separated from L2. It is the most critical phase of the cycle. Reaction (3) is the thermal decomposition of HI, while step (4) is the separation of L1 into H_2SO_4 and H_2O. Process steps (5) to (7) proceed in the gas phase and produce H_2O, SO_2 and O_2. These gases are cooled down before bubbled in the Bunsen reactor to separate oxygen from SO_2 and H_2O. Due to the fact that reaction (7) is incomplete, a residual amount of SO_3 is found in the hot gases following the reaction. This SO_3 is recombined to H_2O in a reactor where the reverse of reaction (6) is performed and the diluted H_2SO_4 produced is recycled in step (4).

ii. Process concepts and implications

To overcome thermodynamic limitations like low chemical equilibrium values, azeotropes in phase equilibria and also to tackle energy and exergy issues, a variety of concepts like membrane-based processing, reactive distillation, etc., which involve process intensification, integration principles are pursued. Application of these process concepts in each of the section is described below.

Bunsen reaction (section I):

Although the Bunsen reaction looks less critical due to negligible energy demand and relatively mild temperatures of operations, it represents a key process step to be optimized since the compositions of its product streams strongly affect energy consumption in the operations downstream [68]. The reaction system consisting of SO_2, H_2O, I_2, HI, H_2SO_4 has a very complex solution chemistry due to strong electrolytic behavior, formation of tri-iodides (I_3^-), polyiodides (I_4^{2-}, I_5^-, etc.) and solvation reactions. The system displays partial miscibility behavior. A large data base of the reaction is needed at different pressures of SO_2. Figure 3.9 pictures the domain of R&D for data generation. Domain knowledge to elucidate the processes in Bunsen reactor is indicated in Fig. 3.10.

This heterogeneous reaction (G–L–S or G–L–L) can be construed as ‘pseudo first order system’ (Fig. 3.11) as the reaction rate is dependent only on SO_2 partial pressure. A multistage counter current contactor like oscillatory baffled column reactor (Fig 3.12) to enhance mass transfer, heat transfer, product purity is considered [70, 71].

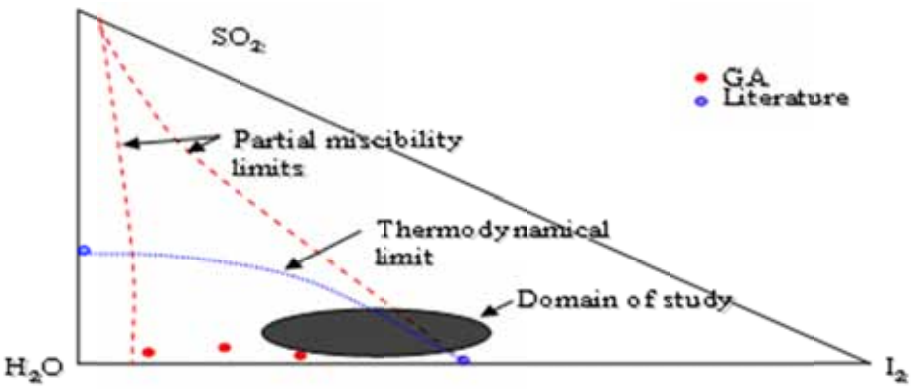

FIG. 3.9. Bunsen reaction study [69].

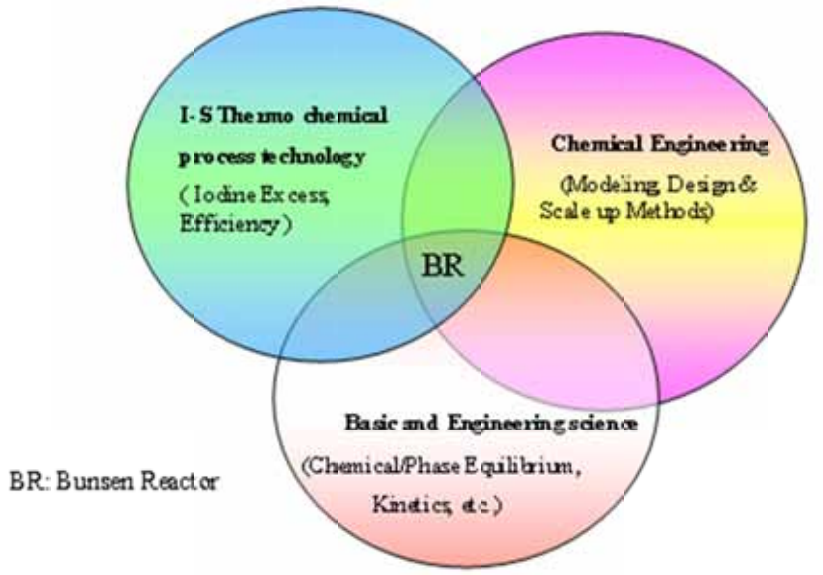

FIG. 3.10. Domain knowledge for Bunsen reactor [70, 71].

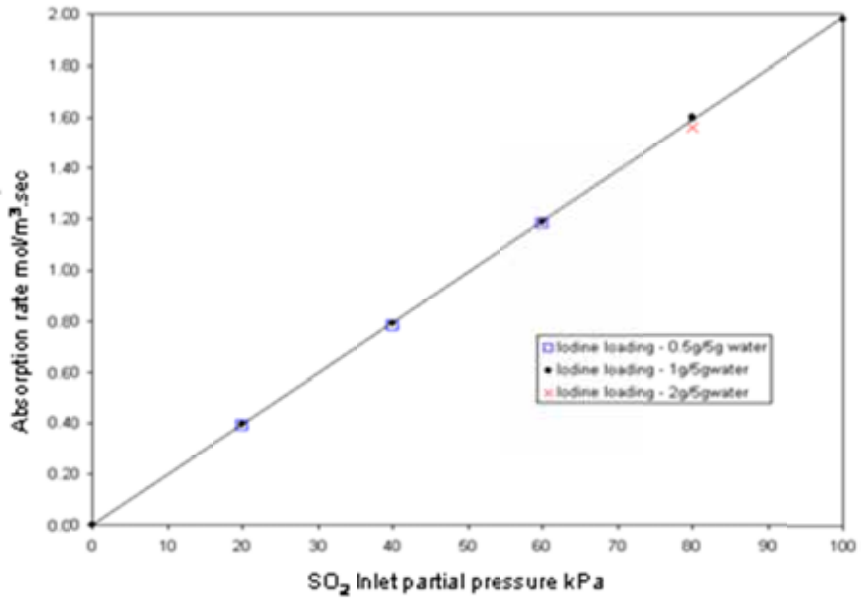

FIG. 3.11. Absorption behavior of SO_2 at different pressures of SO_2.

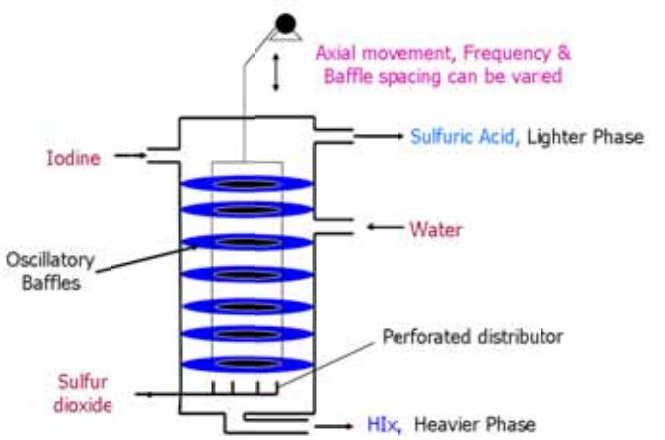

FIG. 3.12. Oscillatory baffled Bunsen reactor [70, 71].

A survey of other Bunsen reaction routes to overcome excess iodine and water in the cycle is also undertaken (Table 3.2). The electrochemical route, vigorously being pursued at JAEA, Japan and ENEA, Italy, is considered to be an attractive option [53–55]. This route as depicted in the process schematic in Fig. 3.13 combines reaction and product separation steps and vastly reduces the iodine load of the cycle.

TABLE 3.2. BUNSEN SECTION PROCESS CONCEPTS

	Process concepts	Comments	Ref
1.	Electrochemical Bunsen reactor (ECBR) (Fig. 3.13)	1. Reduction of usage of large quantities of I_2 and H_2O (advantage) 2. Integration of reaction and separation (advantage) 3. Improvements in overall efficiency (even though electrochemical option) as the I_2 and H_2O contents are decreased.	[53–55, 72]
2.	Use of reaction solvent other than water (Fig. 3.14) a. Liquid SO_2 b. Tri butyl phosphate (TBP)	1. Reduction of amount of iodine in the system. Increase in the overall process efficiency (advantage) 2. Pressurized reactor operation to keep SO_2 in liquid phase (disadvantage) 3. Introduction of additional chemical in to the cycle (disadvantage)	[53, 73]
3.	Use of precipitation agent ($PbSO_4$) to selectively precipitate insoluble salts (PbI_2) (Fig. 3.15)	1. Reduction of use of iodine in the system thus increase in the overall process efficiency (advantage) 2. Breakage of HI–H_2O azeotrope (advantage) 3. More processing steps (disadvantage) 4. Introduction of new chemical (disadvantage) 5. Solid PbI_2 handling (disadvantage)	[53]

However, membranes of required properties have to be developed to generate concentrated product solutions without cross contamination by eliminating permeation, electro-osmotic drag etc. In this process, the Bunsen reaction can be carried out electrochemically as a redox process with anodic oxidation to H_2SO_4 and cathodic I_2 reduction to HI according to

(1) $SO_2 + 2\ H_2O \rightarrow H_2SO_4 + 2\ H^+ + 2\ e^-$ (anode E_o = +0.172 V)

(2) $I_2 + 2\ H^+ + 2\ e^- \rightarrow 2\ HI$ (cathode E_o = +0.535 V)

Theoretically this system has to work like a voltaic cell, but over-potentials due to electrode, membrane, electrolyte necessitates input of electrical energy to drive the reaction. This option, although negating the pure thermochemical nature of S–I process, is worth being pursued. Development efforts for finding suitable electrodes, membranes, and cell configurations with good fluid flow, heat and mass transfer characteristics are suggested. Apart from the issues of efficiency, other techno–economic parameters like membrane service life, electrode life, throughput, and size of the electrochemical membrane reactor need to be studied.

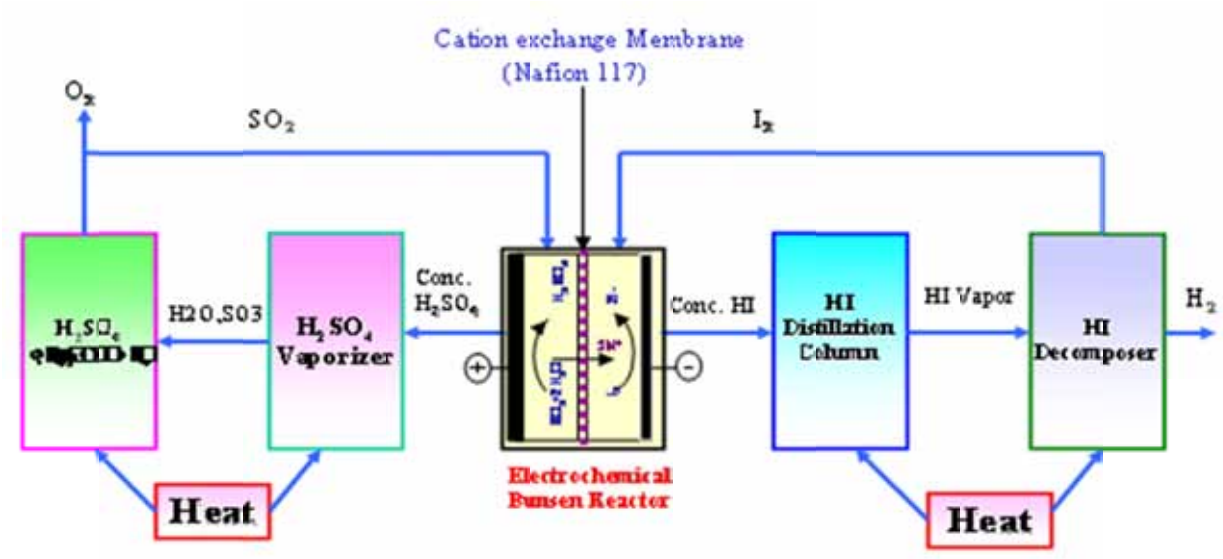

FIG. 3.13. Process scheme of S–I process using electrochemical Bunsen reactor.

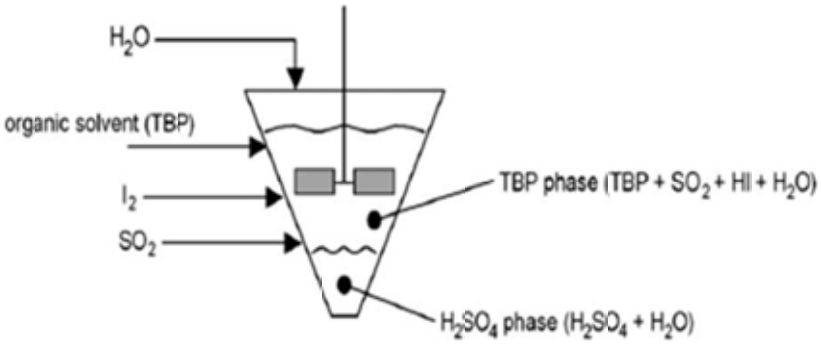

FIG. 3.14. Process concept with solvent other than water, tributylphosphate (TBP).

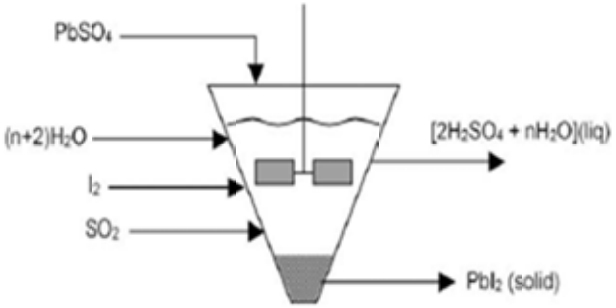

FIG. 3.15. Process concept with use of precipitation agent ($PbSO_4$) to selectively precipitate insoluble salt (PbI_2).

Other alternative Bunsen reaction routes include the use of a solvent other than water like tributylphosphate (TBP) (Fig. 3.14), liquid SO_2, and the use of precipitating agents and solid salt formation (Fig. 3.15). These routes also suffer from some critical drawbacks which are yet to be resolved [53]. The introduction of other chemicals to affect separation and application of high pressures or very low temperatures to keep SO_2 in a liquid state, have to be considered for assessing the overall merit of these options versus others (Table 3.2).

H_2SO_4 concentration and decomposition (Section II):

Even though the chemicals (H_2SO_4, SO_3, SO_2) handled in this section are relatively conventional for process industry, the temperatures (up to 950°C) and pressures make the unit operations and processes technologically challenging. Sintering of catalysts, low chemical equilibrium values, excessive corrosion, creep, etc., are a few issues which the designers have to contend. In addition, heat exchange between hot fluids from the nuclear reactor and process fluids needs to be carried out effectively keeping exergy and energy aspects in mind utilizing pinch analysis techniques. Innovative integrated process units (heat exchanger reactors) are being conceived/developed. Diffusion bonded plate type printed circuit heat exchangers (PCHE) having catalyst coated small semicircular flow channels (3 to 4 mm diameter) and self-catalyzing heat exchanger reactors made of platinum (1–5 wt%) incorporated alloy 800H, Inconel 617, etc., are two designs being considered for applications in this section. These concepts make the units compact for carrying out multiple operations like heat exchange, chemical reaction etc, effectively. R&D efforts are directed towards developing fabrication methods and procedures to build structurally rugged units for high temperature and high pressure operations. Corrosion resistant membrane reactor–separator–heat exchanger units are also being developed. Figure 3.16 depicts the process steps involved in this section.

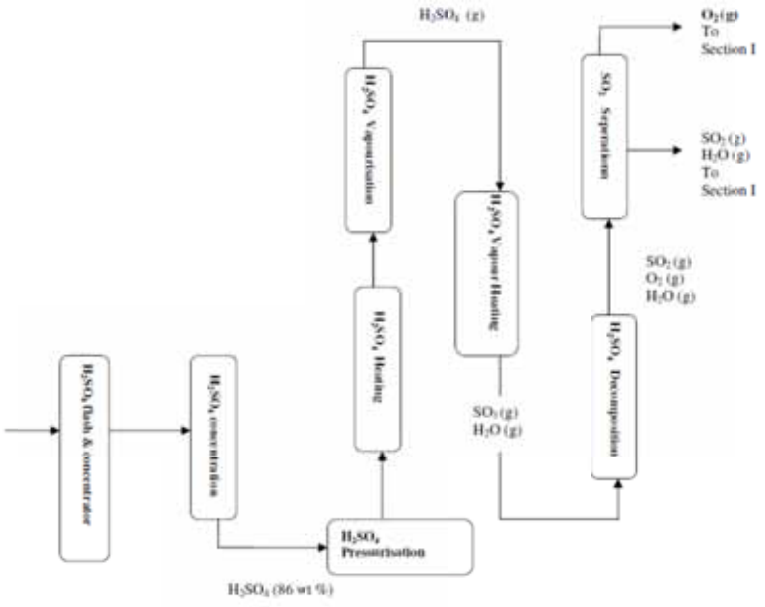

FIG. 3.16. H_2SO_4 concentration and decomposition.

HI concentration and decomposition (section III):

Separation of iodine and water from HI, decomposition of HI into hydrogen and iodine, and recycling of iodine and water to Bunsen section constitute the main operations in this section of the S–I process. These operations are highly energy intensive due to

(a) low chemical equilibrium and slow kinetics of decomposition;

(b) azeotrope formation of HI–H_2O binary or pseudo azeotrope formation of HI–H_2O–I_2 ternary system and consequent energy demands for concentration and separation;

(c) requirement to recycle large quantities of iodine and water bearing process streams.

In addition, higher temperatures (up to 450°C) and pressures (up to 5 MPa) aggravate the corrosion problem and necessitate the use of exotic and costly materials of construction. Table 3.3 mentions some of the process options for operations in this section. Process integration and intensification concepts are being evaluated to tackle the problems mentioned above. For example, in extractive distillation (Fig. 3.17), a third body (H_3PO_4) is added to destroy the azeotrope by first separating the iodine before the HI is distilled and then decomposed. Reactive distillation (Fig. 3.18) integrates separation (HI from H_2O and I_2) and decomposition reaction (HI into H_2 and I_2) with use of appropriate tower internals, process streams and catalyst. Similarly electro–electro dialysis (Fig. 3.19) combines concentration and electrochemical separation. Membrane-based processing is invoked to intensify operation by simultaneous withdrawal of one of the species to overcome azeotropic/chemical equilibrium limitations (Fig. 3.20).

TABLE 3.3. HI SECTION

	Process concepts	Comments	Ref
1.	Distillation	1. Suitable only for lab scale demonstration 2. Energy intensive due to necessity of evaporating the solvent water 3. Azeotropic HI input to the decomposer (disadvantage) 4. Overall low efficiency (disadvantage)	
2.	Extractive distillation (Fig. 3.17)	1. Can overcome azeotropic limit of HI–H_2O system(advantage) but introduces additional chemicals(disadvantage) 2. Corrosion problems due to H_3PO_4 (disadvantage) 3. Huge amount of energy required to concentrate H_3PO_4 which decreases process efficiency.	[77]
3.	Reactive distillation (Fig. 3.18)	1. Separation and reaction can be integrated (advantage) 2. High pressure operation (disadvantage) 3. Severe corrosion problem (disadvant.) 4. Costly equipment (disadvantage)	[81]
4.	Electro–electro dialysis (Fig. 3.19)	1. Helps to concentrate HI above azeotrope and decrease water and I_2 content (advantage) 2. Even though electrochemically driven, attractive overall efficiency (advantage) 3. Cationic membrane development effort is called for 4. Techno–economics for large scale deployment needs to be studied	[82–84]
5.	Pervaporation	1. Helps to concentrate HI above azeotropic concentration 2. Use of Nafion-112, Nafion-117 containing both hydrophilic and hydrophobic domains	[85]
6.	Coupled distillation and membrane decomposition (Fig. 3.20)	1. High concentration of HI and high yield of H_2 can be achieved	[86, 87]
7.	Membrane distillation	1. Helps to concentrate HI above azeotropic concentration 2. Use of Poly-Propylene, PTFE hydrophobic membrane	[88]

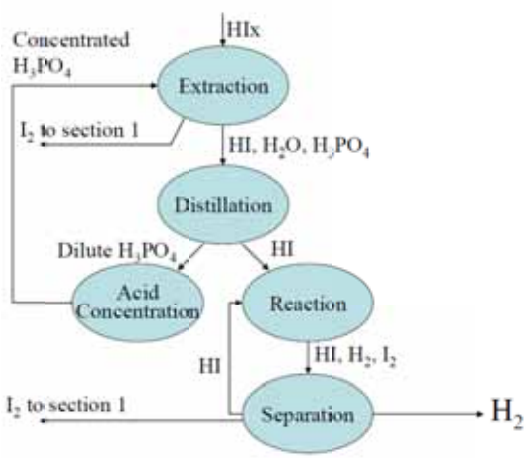

FIG. 3.17. Extractive distillation.

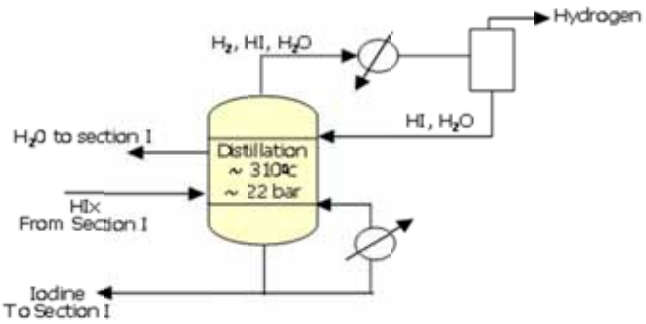

FIG. 3.18. Reactive distillation.

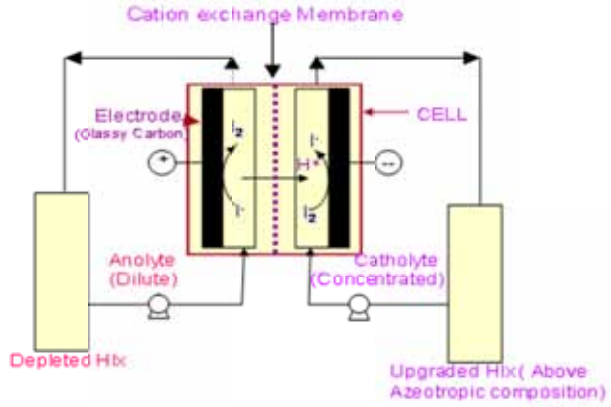

FIG. 3.19. Electro–electro dialysis.

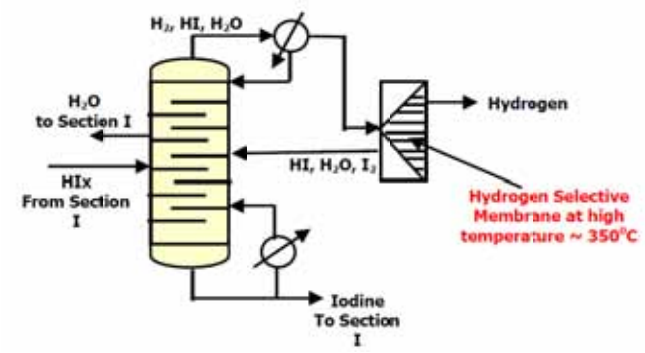

FIG. 3.20. Membrane-based electro–electro dialysis.

However, a lot of development effort is required to perfect these concepts. In reactive distillation, the development of a catalyst for HI decomposition (in gas/liquid phase) is underway. Design of columns with appropriate internals and materials of construction is a process engineering and technological challenge. Lots of theoretical and experimental investigations are underway.

Pt /Pd/Ru reported as active metal catalysts for this reaction. Other catalysts tried are ceria (CeO_2), nickel, and carbon. For HI decomposition in the gas phase, the theoretical equilibrium conversion calculated from free energy values varies from ~14% at 150 ^oC to ~25% at 600 ^oC. With Pt on carbon catalyst, a conversion very close to this equilibrium is achievable. Furthermore, by theoretical analysis with reactive distillation, where decomposing gas will be replenished with much higher moles of liquid, the overall conversion will be further enhanced by 10 to 15%. This reflux liquid also improves the reactive distillation column performance by taking away iodine from the reacting system.

Process simulation and property models employed by different research groups for different sections of the S–I process are:

- ASPEN Plus [74–78];
- SRNL OLI [79];
- JAEA OLI [80];
- ProSimPlus [80].

VLE, LLE, SLE experimental data are mentioned in Table 3.4 with references given in [60].

In the case of membrane-based processing, development of durable membranes for handling high concentration fluids with good separation factors and flux characteristics is the focus area of research.

TABLE 3.4. EXPERIMENTAL DATA AVAILABLE IN LITERATURE FOR HI_X SYSTEM AND ITS BINARY SUBSYSTEM [60]

	Data type	$T_{min} – T_{max}$ [°C]	$P_{min} – P_{max}$ [MPa]	Data number
H_2O–HI	VLE (T,P,x)	77.8–280.9	0.022–5.38	80
	VLE (T,x,y)	60.0–126.5	0.1013	38
	VLE (T,x,y)	0.6–126.8	0.1013	30
	VLE (P,x)	25.0	0.003–0.747	21
	Azeotropic point	127.0	0.1013	1
	LLE (T,x,x')	24.0–70.0	—	2
	LLE	25.0	0.747	1
H_2O–I_2	LLE (T,x,x')	77.1–220.0	—	10
	SLE (T,x)	0.0–60.0	—	10
HI–I_2	SLE (T,x)	25.0–90.0	—	5
H_2O–HI–I_2	VLE (T,P,x)	100–280	0.4–64.0	280
	LLE tie line	24.0–152.1	7.0–62.2	19

VLE vapour–liquid equilibrium.
LLE liquid–liquid equilibrium.
SLE solid–liquid equilibrium.
— data not available.

iii. Low-pressure reactive distillation for HI_x system

Reactive distillation represents simultaneous reaction and separation step in a same volume. Reactive distillation is considered to be the most attractive option for S–I thermochemical closed loop water splitting cycle at third stage. Commercial viability of the process lies in the feasibility demonstration of reactive distillation which requires high pressure and high temperature operation with highly corrosive HI_x mixture for achieving high efficiency. Any reduction in pressure, even at the cost of reduced efficiency, will make the process much more implementable.

An important stage of the S–I cycle is decomposition of HI into H_2 and I_2 from an aqueous HI_x ($HI+H_2O+I_2$) solution and separation of iodine from the system. Simultaneous separation of iodine from the reacting phase shifts the equilibrium towards forward direction, thereby improving yield. HI decomposition reaction is very slow and requires catalyst. 300°C operating temperature is normally fixed based on compromise between hydrogen yield and material stability in terms of material corrosion and pressure rating. However, this approach has the limitation of a corresponding high saturation pressure corresponding to 300°C. Reactive distillation of HI_x feasibility needs low pressure distillation but high temperature in the reaction zone operation.

Modeling

Reactive distillation of HI_x system is extremely complex due to presence of $HI–H_2O$ hetero azeotrope and non-condensable hydrogen in the system. Azeotropic composition changes marginally with pressure and iodine concentration. Further complication is due to strong electrolytic nature of the aqueous HI_x system. In most of the literature, reactive distillation concept is considered for liquid phase kinetic controlled reactions with or without catalyst.

In reactive distillation, three simultaneous states of equilibrium exist. First there will be a vapour–liquid equilibrium of HI between two phases. Next based on the assumption that the HI decomposition reaction is equilibrium-controlled but not kinetically controlled, there exists an equilibrium between reactant HI and products hydrogen (H_2) and iodine (I_2). Finally, there will be again a vapour–liquid equilibrium of I_2 between two phases. Apart from these, there will be vapour–liquid equilibrium of water and complex formation in the liquid phase. It is shown here in the diagram in Fig. 3.21.

Equilibrium constant of HI_x decomposition in vapour phase reaction, plotted against temperature in the graph (Fig. 3.22) is based on JANAF data from standard state Gibbs free energy data. For modeling purpose, generally equilibrium constants are related to temperature as follows:

$$\ln\left(K^{eq}\right) = A + \frac{B}{T} + c\,\ln(T) + DT$$

where A, B, C and D – empirical constants.

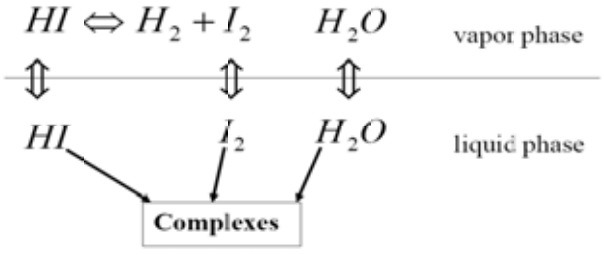

FIG. 3.21. Schematic of HI decomposition.

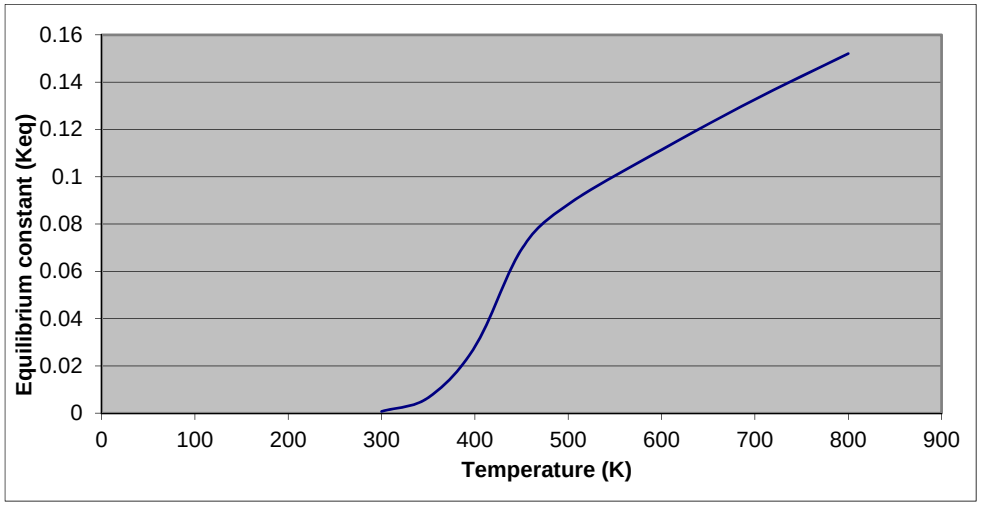

FIG. 3.22. Equilibrium constant of HI decomposition in vapour phase reaction based on JANAF table standard Gibbs free energy values.

So far reactive distillation of HIX phase for section III of S–I process is conceptualized at higher operating pressure (about 2.2 to 5.0 MPa). Due to extreme corrosive nature of the HI_x phase, it is difficult to construct a commercial plant with suitable material which can withstand the environment. This high pressure requirement comes from the corresponding high saturation temperature where both equilibrium yield (Fig. 3.23) and kinetics of reaction are improved. As far as physical distillation for iodine separation is concerned, pressure does not have much appreciable effect. Therefore, it is expected to be advantageous in terns of material of construction, if the process can be operated at lower pressure (close to ambient). For low pressure reactive distillation of HI_x to be functional, the whole physical distillation will be operated at low pressure saturated temperature condition for iodine stripping and reactive distillation section also will be operated with low pressure, but HI vapour phase catalytic decomposer only will be isolated from liquid reflux and elevated to higher temperature (approximately 300°C) to facilitate hydrogen production. The whole process will be integrated in a single reactive distillation column with additional heating facility at the HI vapour phase decomposer section.

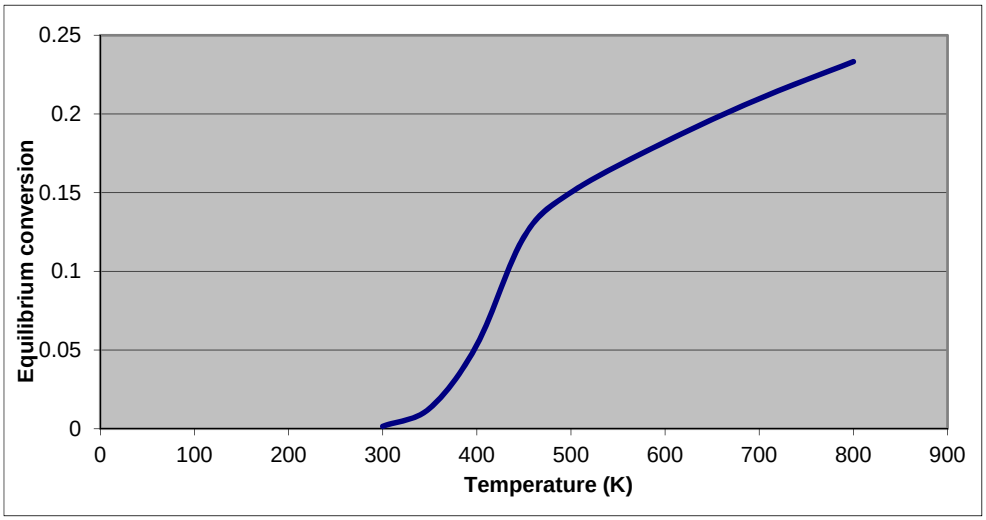

FIG. 3.23. Equilibrium conversion of HI in vapour phase reaction based on JANAF table standard Gibb's free energy values.

Thermodynamic models

At any temperature and pressure condition, when HI_x mixture vapour and liquid is at equilibrium, liquid and vapour fugacities will be equal for all individual components. Based on this postulate we can write;

$$f_i^V(T,P,y_i) = f_i^L(T,P,x_i)$$

where y_i and x_i are the vapour phase and liquid phase mole fraction of component 'i', respectively.

There are two approaches used for present-day simulation: (1) Φ–Φ –Φ approach. In the first homogeneous Φ–Φ approach, each phase component fugacity is calculated from phase fugacity coefficients $\Phi_i^V(T,P,y_i)$ and $\Phi_i^L(T,P,x_i)$ assuming fugacities as well as fugacity coefficients also are equal. Fugacity coefficients are calculated from any unique suitable real gas equation of states. In the second heterogeneous γ–Φ approach, vapour and liquid phasea are handled separately. Similar to the first approach, vapour phase component fugacity is calculated from fugacity coefficient, which is calculated by any suitable equation of state, but liquid phase component fugacity is calculated by introducing activity coefficients γ_i to consider non-ideality of the liquid phase. Thus when gas and liquid phase fugacities are equated, the expression becomes:

$$\Phi_i^V(T,P,y_i)P = \gamma_i(T,x_i)x_i\, f_i^{0L}(T,P)$$

where $f_i^{0L}(T,P)$ is the liquid state fugacity of component 'i' at reference state.

To calculate vapour phase fugacity coefficient of HI_x system, mostly three equations of state are used, these are PR (Peng–Robinson) [89], RK (Redlich–Kwong) [90] and SRK (Soave–Redlich–Kwong) [91].

PR equation of state: $p = \dfrac{R\,T}{V_m - b} - \dfrac{a\,\alpha}{V_m^2 + 2bV_m\, b^2}$

with $a = \dfrac{0.45724\,R^2\,T_c^2}{p_c}$, $b = \dfrac{0.0778\,R\,T_c}{p_c}$, and

$\alpha = \left[1 + \left(0.37464 + 1.5422\,\omega - 0.26992\,\omega^2\right)\left(1 - T_r^{0.5}\right)\right]^2$

where $T_r = T/T_c$, and ω is the acentric factor, equal to $\left\{-\log_{10}(p_r) - 1\right\}$ at $T_r = 0.7$;

RK is the equation of state: $p = \dfrac{R\,T}{V_m - b} - \dfrac{a}{\sqrt{T}\,V_m\left(V_m + b\right)}$

with $a = \dfrac{0.42748\,R^2\,T_c^{2.5}}{p_c}$, $b = \dfrac{0.08662\,R\,T_c}{p_c}$.

Soave modified Redlich–Kwong (SRK) equation of state: $p = \dfrac{R\,T}{V_m - b} - \dfrac{a\,\alpha}{V_m\left(V_m + b\right)}$

with $a = \frac{0.42747\, R^2\, T_c^2}{p_c}$, $b = \frac{0.08664\, R\, T_c}{p_c}$, and

$$\alpha = \left[1 + \left(0.48508 + 1.5517\,\omega - 0.17613\,\omega^2\right)\left(1 - T_r^{0.5}\right)\right]^2$$

where

V_m is the molar volume,
R is the universal gas law constant,
T is the temperature,
T_r is the reduced temperature,
T_c is the critical temperature,
p is the pressure,
p_r is the reduced pressure, and
p_c is the critical pressure.

For liquid phase activity coefficient calculation of a highly non-ideal electrolyte HI_x system, mostly two thermodynamic methods are used, 'elec NRTL' (electrolyte non-random two liquid model) [92] and UNIQUAC (universal quasi chemical) [93].

For the 'elec NRTL' model, molecule–electrolyte and molecule–molecule interaction parameters (τ_{ij}) between two species, i and j, are calculated as follows:

$$\tau_{ij} = \alpha_{ij} + \frac{b_{ij}}{T} + e_{ij}\left(\frac{T_{ref} - T}{T} + \ln\frac{T}{T_{ref}}\right)$$

where

a_{ij} and b_{ij} are the binary interaction parameters,
e_{ij} is the binary electrical interaction parameter,
T is the temperature, and
T_{ref} is the reference temperature [61].

For UNIQUAC activity coefficient model, component Gibbs excess free energy is correlated to activity coefficient and Engel's salvation parameters as follows:

$$\frac{g^{ex}}{R\,T} = f_{combinatorial}(x, r, q) + f_{residual}\left(x, q, A_{ij}, A_{ji}\right)$$

where the combinatorial term handles molecular-size difference effects and the residual term handles fluid–fluid interaction. The terms r and q are UNIQUAC structural parameters and A_{ij} and A_{ji} are binary interaction parameters [60].

Summary and conclusion

Simulation studies are conducted for the above specific cases where only physical distillation will be conducted to separate iodine at 0.15 to 0.2 MPa pressure, followed by vapour phase HI decomposition reactor and subsequent iodine stripping at the top of the physical distillation column at the same pressure with desired superheated conditions. With this modification, it is expected that overall performance of the reactive distillation column will not alter and column can be operated at low pressure at the expense of additional heat load at each decomposition reactor section. Low-pressure reactive distillation scheme is shown in Fig. 3.24.

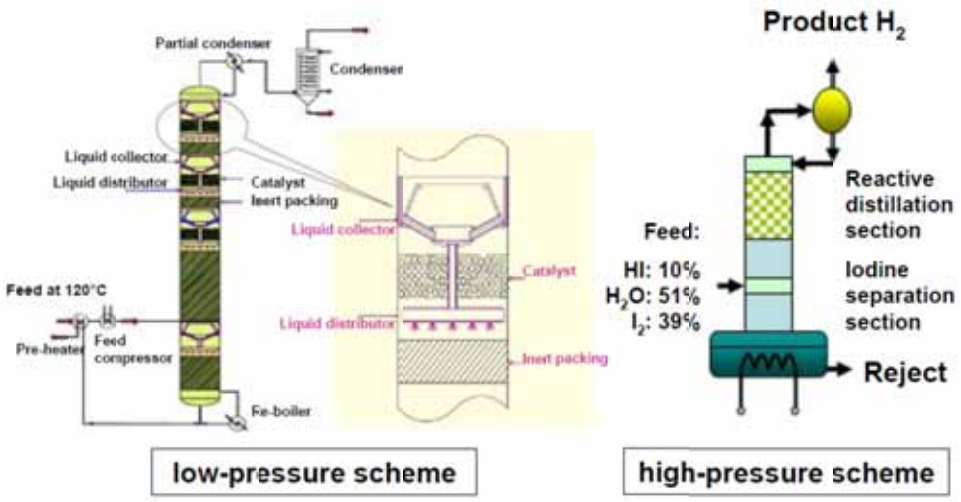

FIG. 3.24. Low pressure reactive distillation of HI_x Scheme with column internals and high pressure conventional reactive distillation scheme.

iv. HTGR concepts with S–I cycle

Since temperatures in excess of 800ºC are required for the S–I thermochemical water splitting process, different concepts of HTGRs are being investigated for the coupling between the nuclear plant and the hydrogen production chemical plant based on the S–I cycle.

In Japan, JAEA has launched the preliminary design of a hydrogen production system based on the HTTR with a thermal power of 30 MW and a reactor outlet temperature of 950ºC, achieved for the first time in April 2004. Development of the so-called HTTR-IS system started in 2005 with a conceptual design study where available structure and heat mass balance of the system were evaluated. Basic design of the HTTR-IS is expected to be completed in 2010 [51].

Figure 3.25 shows a schematic of a candidate HTTR-IS system [51]. Heat produced by the HTTR core is transferred to the secondary helium gas at the intermediate heat exchanger. The secondary helium flows through the inner pipe of the concentric hot gas duct and a high temperature valve, and supplies heat to the chemical reactors of the S–I process such as SO_3 decomposer, H_2SO_4 vapourizer, and HI decomposer. Finally, after cooled by a steam generator and a helium cooler, secondary helium is circulated by a helium circulator back to the IHX through the annular pipe of the concentric hot gas duct. Chemical impurities in the secondary helium are removed by the secondary helium purification system.

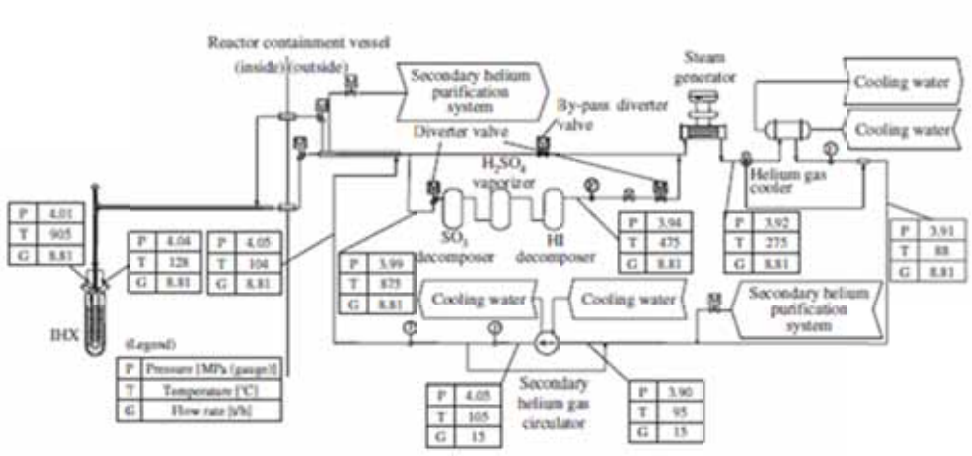

FIG. 3.25. Schematic diagram of a candidate HTTR-IS system [51].

As for the reactor technology, the HTTR operational experience is accumulated and tests on safety demonstration and up-grade are being performed. For developing the S–I process, (i) close cycle test, (ii) high efficiency component test, and (iii) material test are under way [94]. The close cycle test aiming at establishing of reaction control has been carried out with a bench scale test apparatus using high temperature helium gas heated by electric heaters to drive the process. In parallel with these process studies, materials for the pilot scale facility having hydrogen production rate of 30 Nm^3/h are being developed to meet the corrosive process conditions such as boiling sulphuric acid and SO_2–SO_3–H_2O–O_2 gaseous mixture at about 800ºC.

In USA, the Department of Energy (DOE) has sponsored a research project addressed to use the MHR for driving the hydrogen production based on the S–I thermochemical cycle and the HTSE process. The project is directed by General Atomics and involves the participation of the Idaho National Laboratory and Texas A&M University [95].

The GT-MHR is a modular, passively safe version of the HTGR, designed to operate at a power level of 600 MW(th) and, for hydrogen production, is referred as H2-MHR. The plant consists of four 600 MW(th) MHR modules, with each module coupled to an IHX to transfer the heat to a secondary helium loop. The heat is then transferred to the S–I-based hydrogen production system. The IHX design is based on the PCHE which consists of metal plates that are diffusion bonded to restore the properties of the base metal. Fluid flow channels are chemically milled into the plates using a technique that is similar to that used for etching printed electrical circuits. The IHX design consists of 40 modules and associated manifolds within an insulated steel vessel, with each module transferring about 15 MW(th) [96].

Several different concepts for coupling the H2-MHR to the S–I process are being evaluated, including running the H_2SO_4 and HI decomposition reactions in series, as shown in Fig. 3.26, and running them in parallel with a power topping cycle. The series configuration was

heat exchanger pinch points, and because the power topping cycle used with the parallel configuration adds complexity without significant improvement in the overall efficiency [96].

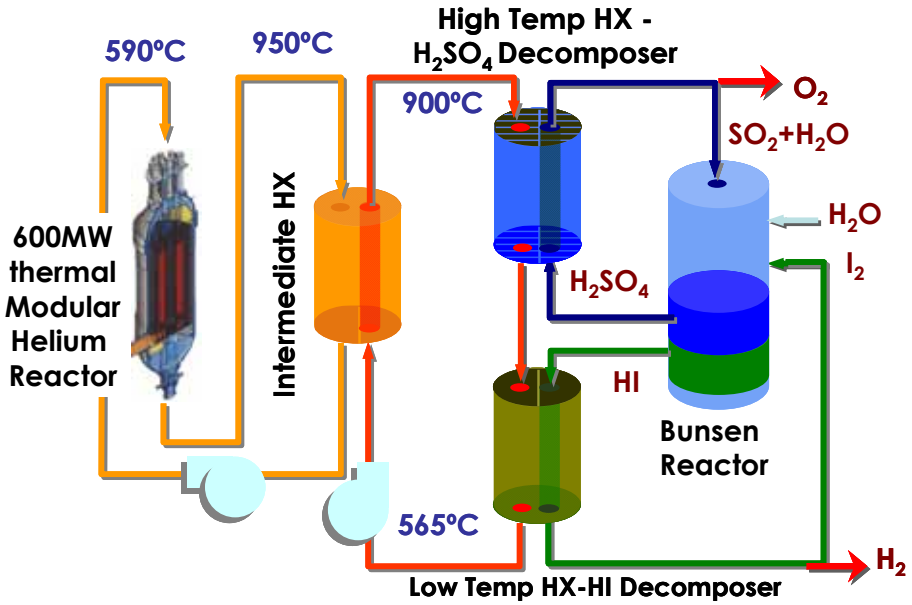

FIG. 3.26. H2-MHR system coupled to S–I process with series configuration [96].

In Europe, a cooperative research project named HYTHEC – HYdrogen THErmochemical Cycles – has been established for searching a long term massive hydrogen production route using solar and nuclear technologies [97]. The objective of HYTHEC is to investigate the effective potential of the S–I cycle, and to compare it with the Westinghouse HyS cycle. The project was funded by the European Community and involved six partners from five countries (France, United Kingdom, Italy, Germany and Spain). HYTHEC aimed to conduct flow sheeting, industrial scale-up, safety and cost modeling, to improve the fundamental knowledge and efficiency of the S–I cycle, and to demonstrate a solar primary energy source for the H_2SO_4 decomposition step which is common to both the cycles.

A preliminary reference sheet of the sulphur–iodine cycle has been reviewed and optimized to a 'reference' flow sheet with coupling to an indirect cycle VHTR (Fig. 3.27) delivering both heat and electricity (self-sustaining concept) to run the hydrogen production process at a rate of 110 t/d and an overall plant efficiency of ~35% [97]. This scheme represents a self-sustainable plant concept in which, in addition to the heat supply to the S–I cycle, the electrical demand of the internal consumers is provided by the nuclear reactor. The high temperature heat from the reactor is passed to an IHX that transfers the heat to a secondary helium loop which interacts with the S–I cycle components, improving heat recovery. A part of the heat flow goes to the S–I cycle, another part to a Brayton cycle for an electricity production that equals the S–I cycle consumption.

The HYTHEC project was terminated in 2008 and succeeded by the HYcycleS project aiming at the qualification of materials and reliability of components for the essential reactions in thermochemical cycles.

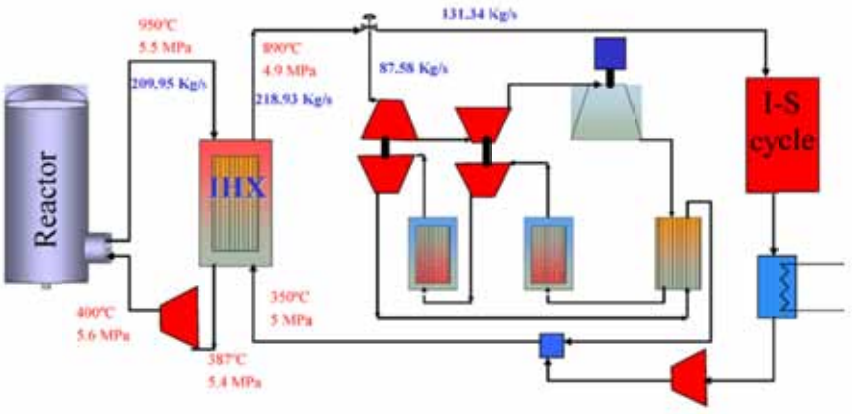

FIG. 3.27. Coupling between S–I cycle and a nuclear reactor [97].

China has developed a high temperature test reactor, HTR-10 which reached first criticality in 2000. Based on the HTR-10, China is constructing a larger demonstration HTGR nuclear power plant, HTR-PM. The aim is to complete the plant by 2013 [98]. As a part of the HTR-PM project, R&D on nuclear hydrogen has been carried out in INET. The sulphur–iodine thermochemical cycle and high temperature steam electrolysis (HTSE) for splitting water have been selected as potential processes of nuclear hydrogen production. Since 2005, INET has conducted preliminary studies on the S–I process and HTSE process. The laboratory of nuclear hydrogen with facilities for process studies has been established. The HTR-10 in INET will provide a suitable nuclear reactor facility for future research and development of nuclear hydrogen production technology. Development of nuclear hydrogen in China will proceed in three phases: phase I (2009–2013) is on the process verification of both hydrogen processes and bench scale testing; phase II (2014–2020) mainly involves R&D

works on pilot scale testing, coupling technology with the reactor, nuclear hydrogen production safety; finally phase III (2020~) is dedicated to the engineering scale development of nuclear hydrogen production [99].

In addition, China is exploring the concept of an ‘open loop’ S–I thermochemical cycle for the production of hydrogen, sulphuric acid and electric power based on two important domestic facts: (1) the chemical reactants are inexpensive and abundantly available; (2) the products, in addition to hydrogen, are valuable and marketable [100].

In the Republic of Korea, within the framework of the so-called ‘nuclear hydrogen production technology development and demonstration (NHDD) project’ for the ultimate purpose to design, construct a prototype VHTR, and demonstrate nuclear hydrogen production, KAERI is performing several research activities related with VHTR design technology development and fuel technology development [101], as well as the study of several alternatives of flow sheets for the S–I thermochemical cycle. Main objectives are to overcome the problems associated with the excess of water and iodine observed in the original S–I cycle [56, 102].

v. Simulation of the hydrogen production plant based on S–I cycle with heat exchanger

In order to calculate the quantities of chemical materials used in each of the three sections of the S–I cycle, the previous chemical equations (1), (2), (3) are used together with the following assumptions:

$$X = m(I_2)\ ,\ Y = m(SO_2)\ ,\ Z = m(H_2SO_4)\ ,\ W = m(H_2O)$$

$$Q = m(SO_3)\ ,\ M = m(O_2)\ ,\ N = m(HI)\ ,\ R = m(H_2)$$

where

m is the mass of material,
X1, Y1, … are the masses of materials in section 1,
X2, Y2, … are the masses of materials in section 2,
X3, Y3, … are the masses of materials in section 3,
X, Y, … are the masses of materials which are not reacted, and
V is the recovery of hydrogen production.

Therefore, each section can be described by the following equations:

- Section 1 (as shown in Fig. 3.28)

with the main reaction

$$I_2 + SO_2 + 2\ H_2O \rightarrow H_2SO_4 + 2\ HI$$

$$X_1 = N_1 \times 0.992;\ Y_1 = N_1 \times 0.25;\ W_1 = N_1 \times 0.111;\ Z_1 = N_1 \times 0.383$$

- Section 2 (as shown in Fig. 3.29)

with the main reactions

$$H_2SO_4 \rightarrow SO_3 + H_2O$$

$$SO_3 + H_2O \rightarrow SO_2 + O_2 + H_2O$$

$$Q_2 = Z_1 \times 0.816\ ;\ Y_2 = Q_2 \times 0.8\ ;\ W_2 = Q_2 \times 0.225\ ;\ M_2 = Q_2 \times 0.2\ ;\ Z_2 = Z_1$$

- Section 3 (as shown in Fig. 3.30)

with the main reaction

$$2\ HI \rightarrow H_2 + I_2$$

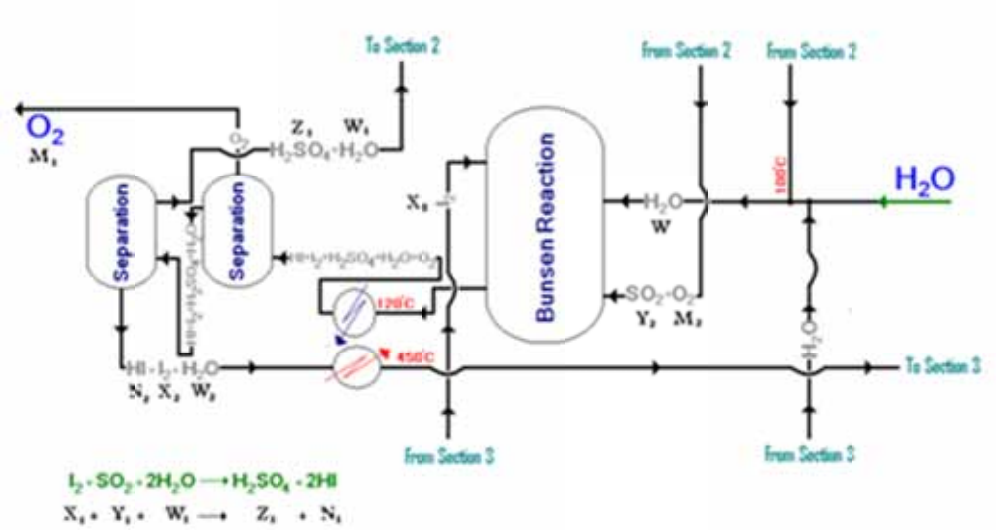

FIG. 3.28. Section 1 – Bunsen reaction.

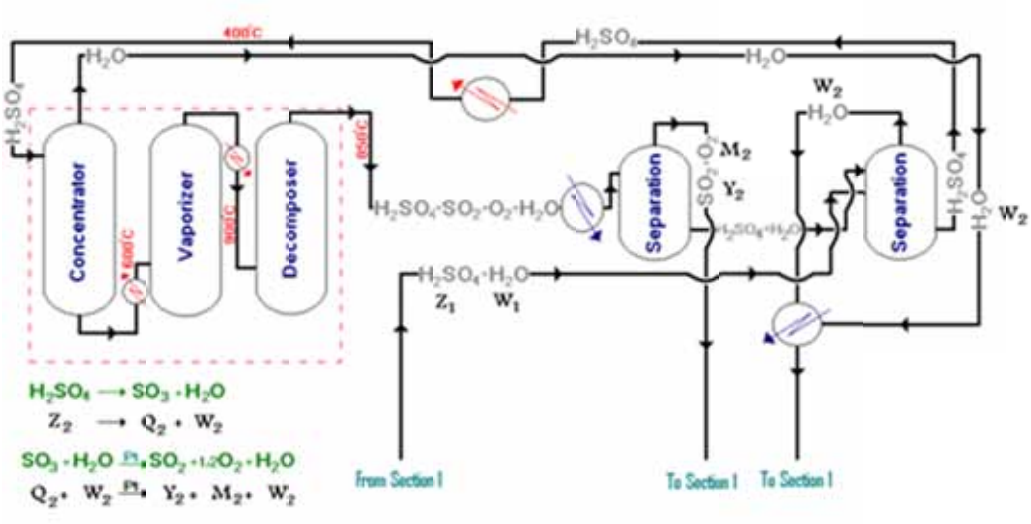

FIG. 3.29. Section 2 – sulphuric acid decomposition.

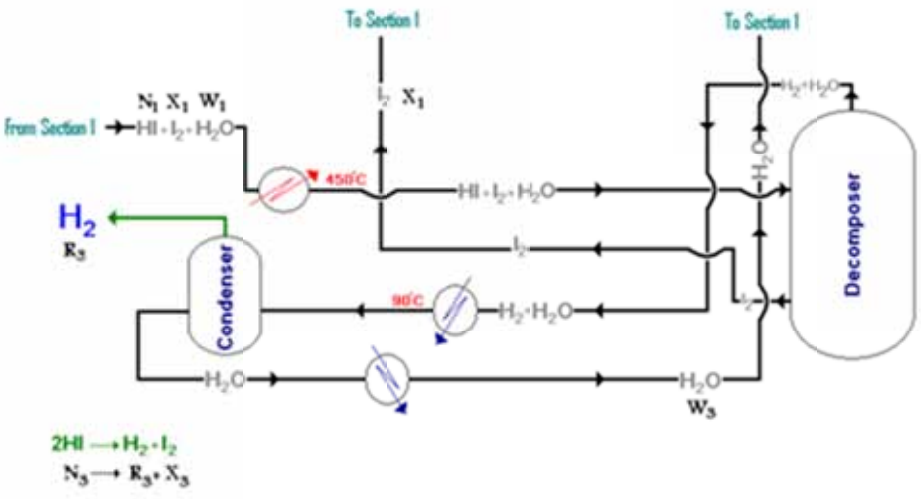

FIG. 3.30. Section 3 – hydriotic acid decomposition.

$$N_3 = R_3 \times 128;\ X_3 = R_3 \times 127,\ N_3 = N_1$$

- Recycled (not reacted) quantity of materials:

$$X = X_3 \times 5.8;\ N = N_1 \times 1.381;\ Z = Z_1 \times 0.031$$

The above reactions and material balance are being programmed in order to get a simulator for nuclear hydrogen production.

vi. Heat exchanger

The heat exchanger which is responsible for heat transfer from the HTGR to the hydrogen production plant (Fig. 3.31) consist of two main steps: the first is the closed loop which transfers heat from the reactor to the sections 2 and 3 in the S–I cycle, and the second step consists of two separate heat exchangers, one is to feed heat to section 2 and the other one is to feed heat to section 3 [103].

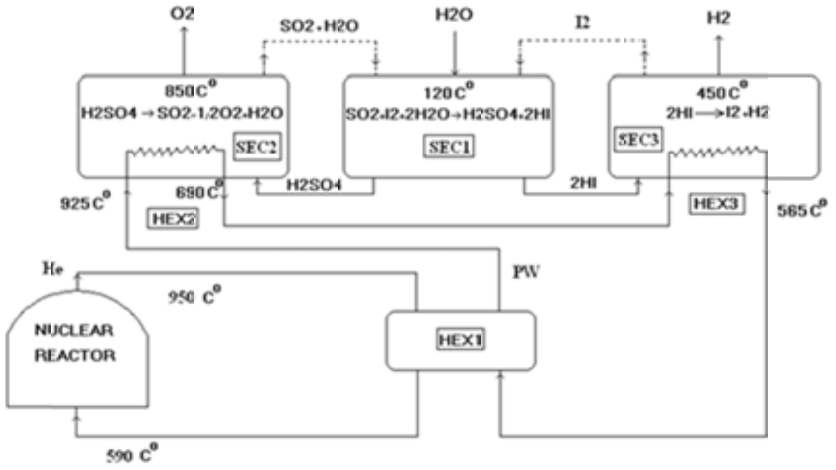

FIG. 3.31. Intermediate heat exchangers between the reactor and the hydrogen plant.

Thermodynamic analysis of HEX

The heat transfer area, in general, is the main parameter which is needed to be calculated for the heat exchanger. It is given by

$$A = \frac{Q}{K \cdot \Delta t_{Log}}$$

where Q is the transferred thermal energy through the HX given by

$$Q = m.Cp.\left(t'' - t'\right)$$

where

m is the mass flux of the medium,
t', t'' are the inlet and outlet temperatures, and
Cp is the heat capacity of the medium.

K is the heat transfer coefficient of the heat exchanger given by

$$K = \frac{1}{\frac{1}{\alpha_1} + \frac{\delta}{\lambda} + \frac{1}{\alpha_2}}$$

The logarithmic temperature difference, $\Delta t_{\log}$, is given by

$$\Delta t_{\log} = \frac{\left(t'_1 - t'_2\right) - \left(t''_1 - t''_2\right)}{\mathrm{Ln}\dfrac{t'_1 - t'_2}{t''_1 - t''_2}}$$

The above four equations can be used to determine the HEX heat exchangers needed for the hydrogen production plant by using the data specifications of all three sections of the S–I cycle as assumed in the CEA studies [104]. Results are shown in Tables 3.5 through 3.8. They show some agreement with the CEA studies.

vii. Material issues:

Material issues are crucial for a successful deployment of the S–I process on commercial scale. Material research areas relate to development of construction materials, catalysts, and membranes. Efforts are ongoing to find solutions which render the S–I process efficient and economical. Reference [105] gives an excellent overview of the research findings and directions. Suggested R&D areas include

- Development of fabrication methods for components made of tantalum alloys, silicon carbide, etc.;
- Study of long term creep characteristics of candidate materials for sulphuric acid decomposition at higher temperatures;
- Study of long term stability and economics of membrane reactor/separators;
- Development of platinum and oxide-based catalysts and their substrates for SO_3 decomposition;
- Catalysts suitable for HI decomposition.

TABLE 3.5. INPUT DATA OF THE 1 MOL/S HYDROGEN PRODUCTION PLANT

	Section 2 (H_2SO_4)	Section 3 (HI)
Mass (kg)	24.225	146.28
Time (s)	5	60
Mass flow rate (kg/s)	4.85	2.44
Input temperature (°C)	120	120
Output temperature (°C)	850	450
Heat capacity (kJ/(kg·K))	1.42	2.51
Density (kg/m^3)	1.84×10^{-3}	5.686

TABLE 3.6. PROPERTIES OF PRESSURIZED WATER IN HEX1, HEX2, AND HEX3

Parameter	Value
Input temperature (°C)	925
Output temperature (°C)	690
Heat capacity (kJ/(kg·K))	2.465
Density (kg/m^3)	20.58
Heat conductivity (W/(m·K))	112.9×10^{-3}
Kinetic viscosity (m^2/s)	1.99×10^{-6}
Prandtl number	0.894
Pressure (MPa)	8
Dynamic viscosity (kg/(m·s))	40.94×10^{-6}

TABLE 3.7. PROPERTIES OF HELIUM IN HEX1

Parameter	Value
Input temperature (°C)	590
Output temperature (°C)	950
Heat capacity (kJ/(kg·K))	5.193
Density (kg/m^3)	3.53
Heat conductivity (W/(m·K))	64 192.2
Kinetic viscosity (m^2/s)	9.96×10^{-12}
Prandtl number	6.726
Pressure (MPa)	7.65
Dynamic viscosity (kg/(m·s))	83 138.7

For the HI decomposition section, Ta–40NB, Nb–1Zr are excellent metallic materials for construction, where as Ta–2.5W, Ta–10W and Ta are also good materials. Hastelloy B-2 can be used as sacrificial material only, because cost of the better materials is very high. Hastellow C-276 and SS are inappropriate for HI_x system. Glass, quartz, mullite and silicon carbide are ceramic materials which have very good corrosion resistance against HI_x. They can be used for packing material, high temperature heat exchanger material, etc.

TABLE 3.8. CALCULATED SPECIFICATIONS OF THE HEXS

Section 2	Concentration		Decomposer		SO_3/SO_2 Reactor	
	calculated	CEA study	calculated	CEA study	calculated	CEA study
Q (MW(th))	6.079	6.4	20.236	20.4	11	11
K (W/(m^2·K))	375.22	356	83.88	83	387.193	395
A (m^2)	108.16	104	1818.329	1535	355.38	370
LMTD (K)	149.76	176	132.67	159	79.9	74
Hex. type	Tube in tube	Shell & tube	Tube in tube	Shell & tube	Tube in tube	Shell & tube
$d_{1,in/out}$ (mm)	60/65	—	60/65	—	60/65	—
$d_{2,in/out}$ (mm)	50/55	—	50/55	—	25/30	—
$d_{tube,in/out}$ (mm)	—	27/31	—	27/31	—	27/32
d_{shel1} (mm)	—	1067/1500	—	2.5 × 1.7 × 2.6	—	2.65 × 9
Section 3	**E302**		**E305**		**E306**	
	calculated	CEA study	calculated	CEA study	calculated	CEA study
Q [MW(th)]	21.912	21.5	0.55	—	8.608	21.4
K [W/(m^2·K)]	314.26	305	39.03	—	195.24	305
A [m^2]	225.7	218	128	—	322	218
LMTD [K]	308.925	322	109	—	136.53	321.85
Hex. type	Tube in tube	Shell & tube	Tube in tube	—	Tube in tube	Shell & tube
$d_{1,in/out}$ [mm]	60/65	—	60/65	—	60/65	—
$d_{2,in/out}$ [mm]	20/25	—	20/25	—	20/25	—
$d_{tube,in/out}$ [mm]	—	21/25	—	—	—	21/25
d_{shel1} [mm]	—	4 × 26.1	—	—	—	2.4 × 3.2

— data not available.

viii. Analytical and measurement technology issues

In different process units of the S–I process, various chemical species displaying diverse interactions (ionic, dipole–dipole, van der Waals, molecule–ionic) are encountered. These interactions in turn lead to complex phase behavior, chemical equilibria, etc. To fully characterize and elucidate the complex behavior of the physico–chemical processes, reliable sensors, measurement techniques and computational tools are essential. Development of analytical and measurement technologies is further complicated due to corrosive, toxic and opaque nature of the chemicals. Conventional measurement techniques have to be fine-tuned or new techniques have to be developed. A standard apparatus used for generating thermodynamic data needs to be re-engineered. Developing on-line measuring techniques which permit real time concentration measurements, etc., are required for process control to achieve stable, efficient operation for a given throughput. In addition, special techniques with high special resolution are required to understand the structure and properties of the materials.

The following list shows some of the techniques which are being developed:

- Raman spectroscopy for speciation (eg., I_4H^+, I_6H^+, I_8H^+ and hydrogen without iodine) studies of HI–I_2–H_2O ternary system at ENEA, Italy [106];
- UV/visible spectrometry for I_2 studies and FTIR for HI and H_2O [68];
- Design and development of calorimeters, ebulliometers [107].

ix. Conclusion

S–I process R&D can be labeled as high potential and high cost research spanning diverse areas such as process engineering, materials, analytical techniques, integration with nuclear reactor, and safety. An attempt has been made to mention process concepts being studied and indicate how research findings described here address some of the issues. Notwithstanding the diversity and complexity, the R&D effort increasingly being made by the developed and developing countries will surely make large scale commercial production of hydrogen by the S–I process a reality alongside development of the high temperature nuclear reactor. This paves the way for establishing a nuclear–chemical industry which can mitigate problems of greenhouse gas emissions or fossil fuel depletion.

3.1.2.3. Hybrid-sulphur process

The HyS cycle was first proposed by Brecher and Wu at Westinghouse Electric Corporation, where the process was extensively studied in the 1970s and 1980s and patented [108]. As a result, it has come to be known as the Westinghouse process [109]. HyS is one of the simplest thermochemical cycles comprising only two reaction steps and having only fluid reactants. The term ‘hybrid’ acknowledges the electrochemical nature of one of the reaction steps which requires that electric as well as thermal energy be supplied to the process. It is a sulphur cycle because it involves sulphur oxidation and reduction and, in fact, sulphur is the only element in the cycle other than hydrogen and oxygen. A simple schematic showing the reaction steps is given in Fig. 3.32 [110].

The first reaction step

$$H_2SO_4(aq) \rightarrow H_2O(g) + SO_2(g) + \tfrac{1}{2}\, O_2(g)\ (> 800^oC) \quad (1)$$

is common to all sulphur cycles and, as a matter of fact, the result of two separate reactions. As H_2SO_4 is vapourized and superheated, it spontaneously decomposes into water and sulphur trioxide (SO_3):

$$H_2SO_4(aq) \rightarrow H_2O(g) + SO_3(g) \quad (1a)$$

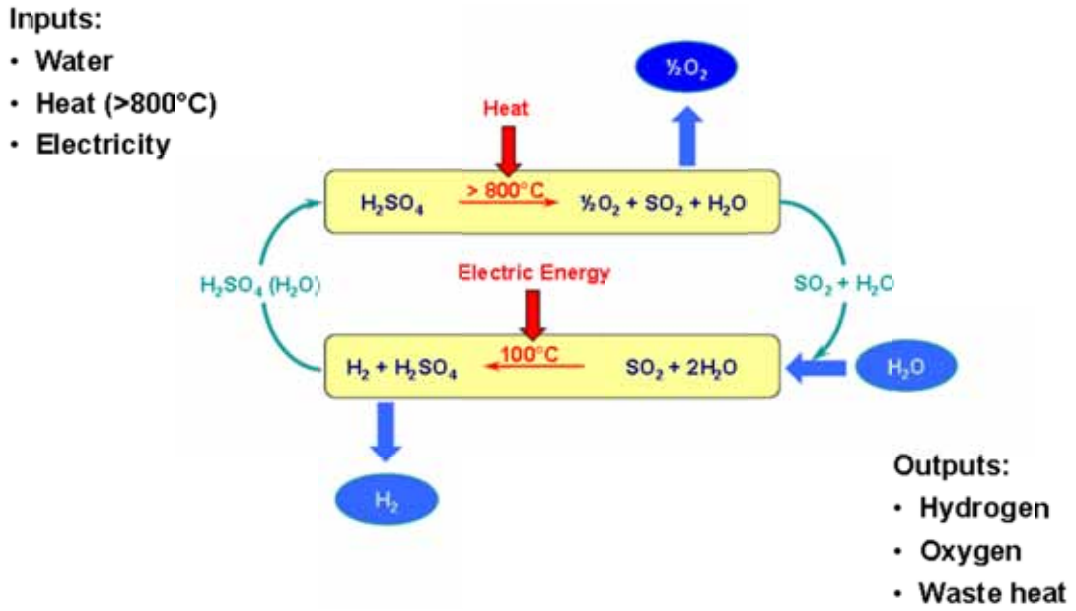

FIG. 3.32. The hybrid sulphur (HyS) cycle reaction steps [110].

Further heating the vapour to high temperatures in the presence of a catalyst drives the endothermic decomposition of SO_3 into oxygen and sulphur dioxide (SO_2):

$$SO_3(g) \rightarrow SO_2(g) + \tfrac{1}{2}\, O_2(g) \qquad (1b)$$

After O_2 is removed as a co-product, the SO_2 and H_2O are combined with make-up H_2O (and recycled H_2SO_4) and fed to the anode of an electrolyzer where the second reaction takes place. This is the SO_2 depolarized electrolysis of water:

$$SO_2(aq) + 2H_2O(l) \rightarrow H_2SO_4(aq) + H_2(g)\ (< 100^oC) \qquad (2)$$

A schematic diagram of an SO_2-depolarized electrolyzer is illustrated in Fig. 3.33 [110]. SO_2 is electrochemically oxidized at the anode to form H_2SO_4, protons and electrons, according to the reaction

$$SO_2(aq) + 2H_2O(l) \rightarrow H_2SO_4(aq) + 2H^+ + 2e^- \qquad (2a)$$

Protons are conducted across the electrolyte separator to the cathode where they recombine with electrons which pass through an external circuit to form H_2:

$$2H^+ + 2e^- \rightarrow H_2(g) \qquad (2b)$$

The net result is the H_2SO_4 production at the anode and H_2 production at the cathode. H_2SO_4 is recycled to the high temperature decomposition step to complete the cycle, while H_2 is removed as the principal product.

What makes the HyS cycle attractive is the standard cell potential for SO_2 depolarized electrolysis which is only -0.158V at 25ºC in water [111]. The reversible potential increases in magnitude to -0.243V if SO_2 is dissolved to saturation at 0.1 MPa total pressure in 50 wt% H_2SO_4–H_2O solution. This means that the SO_2 depolarized electrolyzer will consume much less electricity per mole of H_2 product than water electrolysis which has a reversible cell potential of -1.229V at 25ºC.

As the hydrogen generation step in the HyS cycle involves low temperature electrolysis instead of the heat transfer at high temperature, the coupling with a nuclear power reactor should be easier compared to the S–I cycle, since this step of the process can be located away from the nuclear plant at a distance that may be required for safety concerns. At the same time, the stage of the process that requires the high temperature heat from the nuclear reactor is not involved with hydrogen generation, and hence can be kept close to the reactor. This configuration can help to improve the overall efficiency of the process.

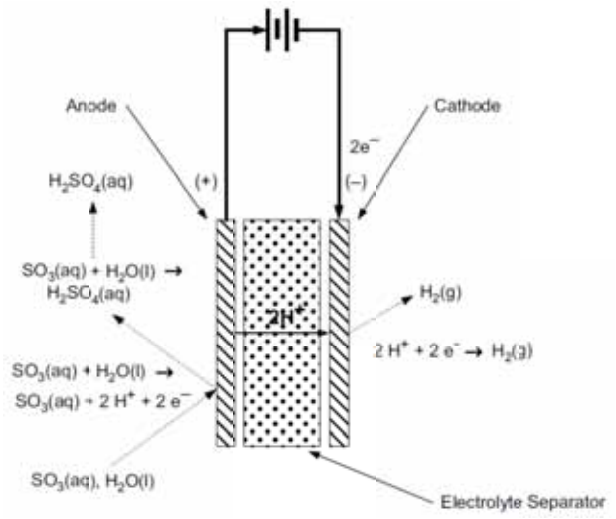

FIG. 3.33. Schematic diagram of an SO_2-depolarized electrolyser [110].

There is still much scope for further improvements in efficiency of HyS cycle by reducing the electrode potential and investigating structural materials stable at the high temperatures involved. For this reason, several research groups around the world are working in the development of the HyS cycle for hydrogen production. For instance, the European Union funded the HycycleS project which started in January 2008 and will investigate high temperature materials and catalysts as well as the H_2SO_4 decomposition reactor and product separator [112]. At Savannah River National Laboratory (SRNL), a single cell electrolyzer has been built and operated for 100 hours, and testing of a multi-cell electrolyzer is planned [113]. Westinghouse is also investigating the electrolyzer and decomposition reactor [114].

A major challenge for the HyS Process is the development of an efficient, cost-effective electrochemical reactor, or SDE (SO_2 depolarized electrolyzer). The SRNL is leading efforts supported by the US-DOE nuclear hydrogen initiative (NHI) to develop the SDE. In contrast to previous efforts to develop an SDE, SRNL has based its work on the use of proton exchange membrane (PEM) technology. The advantages of this design concept include high electrochemical efficiency, small footprint, and potential for competitive capital cost, all of which are crucial for successful implementation on a commercial scale. Since PEM technology is also the subject of intense development efforts for use in water electrolyzers and automotive fuel cells, there is the opportunity for leveraging that work for improving the SDE. The application is challenging, however, since the SDE must react SO_2 with water to produce hydrogen in the presence of strong sulphuric acid under elevated temperature and pressure. SRNL has successfully built and tested both single cell and multi-cell stacks for the SDE application using PEM technology.

The second step in the HyS Process involves the thermal decomposition of sulphuric acid using heat from the nuclear reactor. One of the most difficult challenges in decomposing sulphuric acid at high temperatures (> 800°C) and pressures (up to 9 MPa) is finding a

material that can contain the process at the required conditions without significantly corroding or deteriorating, while providing adequate heat transfer characteristics. Silicon carbide is among the handful of substances identified so far that meet these requirements. The SNL, as part of the NHI programme, has devised an innovative solution that makes use of readily available SiC shapes and does not have any high temperature connections. Their bayonet decomposition reactor features internal recuperation and allows all of the connections to be made at relatively low temperatures, where polytetrafluoroethylene (PTFE) and similar materials can be used for seals. The bayonet acid decomposer approach was used as the basis of the HyS process design in the related study.

Reference PBMR hybrid sulphur design

The current PBMR reference design features indirect heating of the high temperature sulphuric acid decomposition reactor by a secondary helium coolant loop between the primary helium heat transfer loop and the HyS Process. This provides separation between the nuclear heat supply facility and the hydrogen production plant. The basic configuration for integrating the PBMR and the HyS hydrogen plant is illustrated in Fig. 3.34.

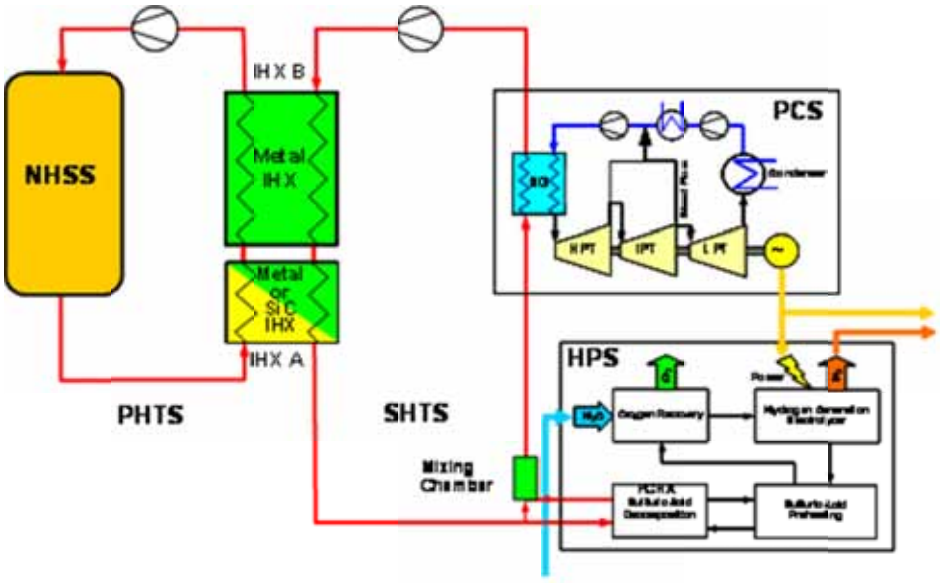

FIG. 3.34. PBMR/HyS integration.

The benchmark against which the PBMR/HyS system will frequently be judged is the use of conventional nuclear power generation coupled with water electrolysis. Since these are proven technologies that could be deployed almost immediately, the more complex PBMR/HyS system needs to provide a significant advantage in terms of higher process thermal efficiency in order to overcome development risk and expected higher initial capital costs. The results of this study indicate that this is the case. Detailed analysis was performed to determine both the HyS process efficiency, as well as the preferred integrations between the HyS process and the PBMR system. The overall process efficiency for the PBMR/HyS system is estimated to be 36.7% based on the higher heating value of the hydrogen product. The results are shown in Table 3.9. This compares to an estimated efficiency of 25–27% for a light water reactor (LWR) combined with conventional water electrolysis. This means that it would require over 40% more nuclear energy to generate an equivalent amount of hydrogen using conventional water cooled nuclear reactors combined with water electrolysis compared to the proposed PBMR/HyS plant design as described here. Different coupling configurations were also evaluated to transfer the nuclear heat to the HyS process with Figs 3.35 and 3.36 indicating two of the possible configurations.

TABLE 3.9. PBMR/HYS PLANT PERFORMANCE SUMMARY

PBMR power rating (MW(th))	500
Hydrogen output	
Mass flow rate (Mt/day)	160.1
Thermal value (HHV) (MW(th))	262.8
Thermal energy requirements (MW(th))	
High temperature heat to decomposition	312.8
Steam to acid concentration	70.6
Steam for power generation	132.9
Electric power requirements (MW(e))	
Helium circulators	20.3
HyS electrolyzer power supply (AC)	110.8
HyS pumps, circulators, etc.	4.7
NHSS, PGS, and BOP	8.2
Total electric demand	144.0
Onsite power generation	54.8
Net electric power from grid	89.2
Overall plant efficiency	
Reactor thermal input (MW(th))	500.0
Thermal equivalent of import electricity (MW(th))	216.5
Total thermal input (MW(th))	716.5
Overall plant efficiency (HHV) (%)	36.7

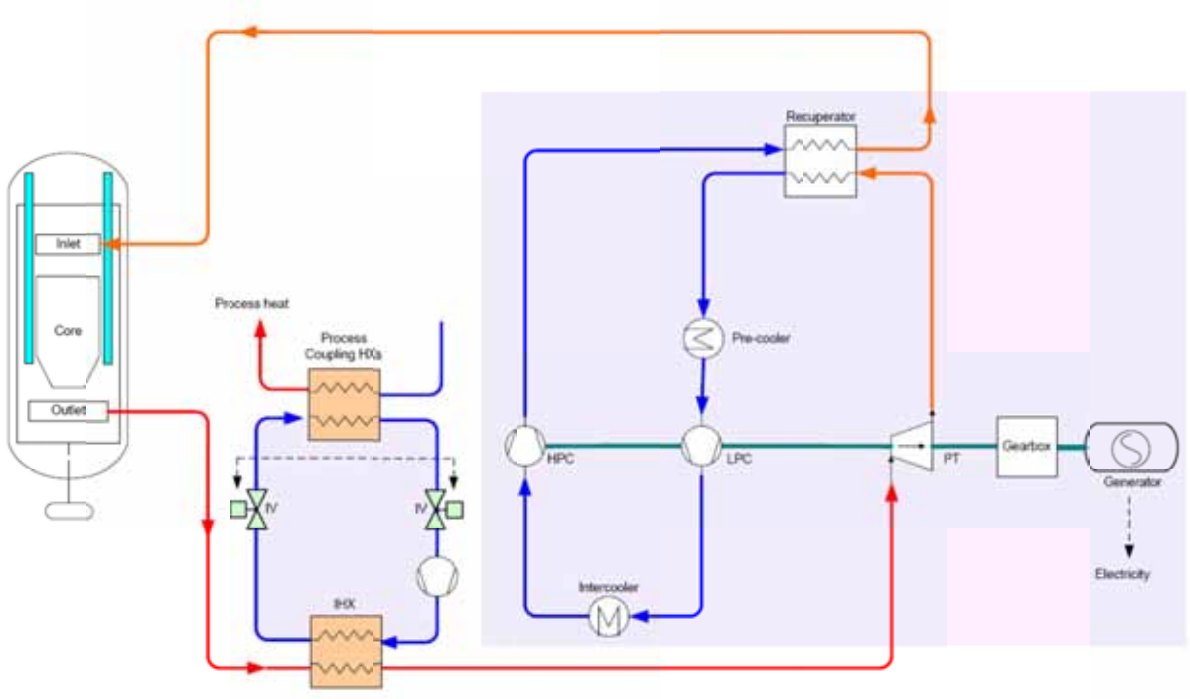

FIG. 3.35. Configuration 1 – possible PBMR/HyS integration.

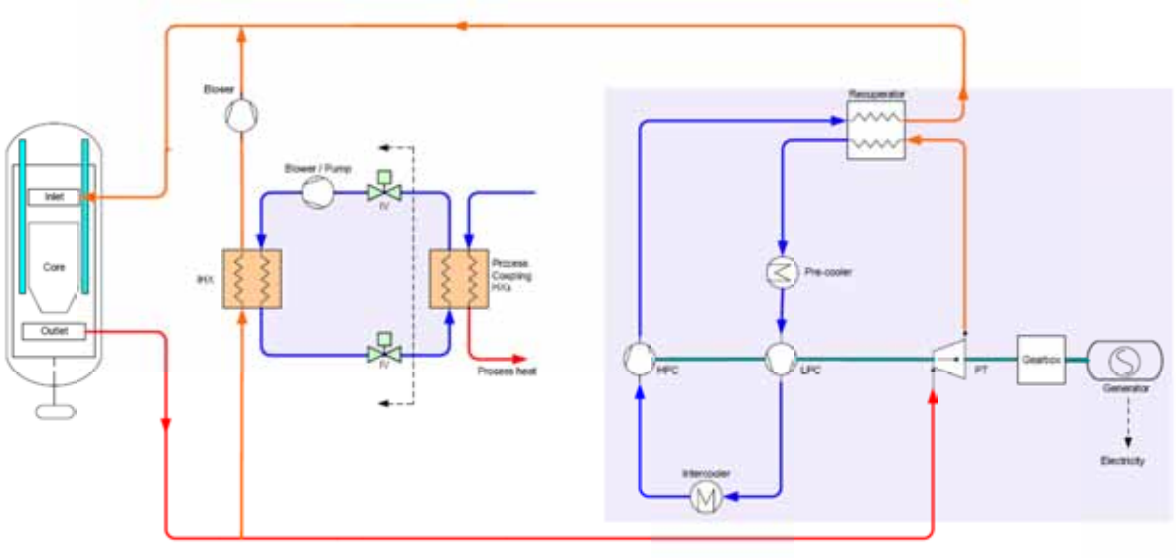

FIG. 3.36. Configuration 2 – possible PBMR/HyS integration.

3.1.2.4. Metallic chloride cycles

Since the S–I and HyS water splitting processes require heat supply at temperatures above 800ºC, several alternative thermochemical cycles were investigated for the hydrogen production, with the goal of reducing the process temperatures to the order of 500–600ºC. Lower operating temperatures reduce the costs of materials and maintenance, and they can effectively use low grade waste heat, thereby improving the cycle and power plant efficiencies. Additional advantages of lower operating temperatures include the use of common chemical agents and reactions going to completion without side reactions.

At the end of 1960s, an international round table on direct production of hydrogen with nuclear heat was held in Ispra, Italy. As result of that meeting, a research programme on hydrogen production from water was approved by the European Community for the period 1973–1983, and an initial searching for suitable reactions were investigated at the Joint Research Center (JRC), Ispra, by means of thermodynamic calculations and verification of theoretical feasibility. A summary of that research work has been published in [115], and a list of all the cycles studied is shown in Table 3.10 [42].

The second phase of the research programme was focused on the iron–chlorine (Fe–Cl) family of cycles, which had been proposed in the early of 1970 at the Aachen University, in Germany. An example of these cycles is the so-called Mark 15 cycle that involves the following reactions for the water splitting process at temperatures in the order of 650ºC [42]:

(1) $3\ FeCl_2 + 4\ H_2O \rightarrow Fe_3O_4 + 6\ HCl + H_2$

(2) $Fe_3O_4 + 8\ HCl \rightarrow FeCl_2 + 2\ FeCl_3 + 4\ H_2O$

(3) $2\ FeCl_3 \rightarrow 2\ FeCl_2 + Cl_2$

(4) $Cl_2 + H_2O \rightarrow 2\ HCl + ½\ O_2$

Two critical problems were identified for this Fe–Cl cycle: thermal decomposition of $FeCl_3$ and hydrolysis of $FeCl_2$. Many attempts were made to solve these problems, but no suitable solution was found. At that time, it was concluded that even though the reactions in the Fe–Cl family of cycles were chemically and practically feasible, the economics were not competitive [42].

Most recently, and after considering factors of availability and abundance of materials, simplicity, chemical viability, thermodynamic feasibility and control/safety issues, six cycles in addition to the S–I process were identified in the NHI as the most promising thermochemical water splitting processes [116]:

- copper–chlorine (Cu–Cl) [117];
- cerium–chlorine (Ce–Cl) [118];
- iron–chlorine (Fe–Cl) [118];
- vanadium–chlorine (Va–Cl) [118];
- copper–sulfate ($Cu–SO_4$) [118]; and
- hybrid chlorine [118].

Proof of principle demonstrations have been completed for these cycles and the chemical viability has been proven.

TABLE 3.10. SUMMARY OF THE JRC ISPRA THERMOCHEMICAL CYCLES [42]

No.	Mark	Max. terms elements	Max. temperature (K)	No. of reactions
1	Mark 1	Hg, Ca, Br	1050	4
2	Mark 1B	Hg, Ca, Br	1050	5
3	Mark 1C	Cu Ca, Br	1070	4
4	Mark 1S	Hg, Sr, Br	1070	3
5	Mark 2	Mn, Na (K)	1070	3
6	Mark 2C	Mn, Na (K), C	1120	4
7	Mark 3	V, Cl, O	1070	4
8	Mark 4	Fe, Cl, S	1070	4
9	Mark 5	Hg, Ca, Br, C	1120	5
10	Mark 6	Cr, Cl, Fe (V)	1070	4
11	Mark 6C	Cr, Cl, Fe (V), Cu	1070	5
12	Mark 7	Fe, Cl	1070	5
13	Mark 7A	Fe, Cl	1070	5
14	Mark 7B	Fe, Cl	1120	5
15	Mark 8	Mn, Cl	1120	3
16	Mark 9	Fe, Cl	920	3
17	Mark 10	I, S, N	1120	6
18	Mark 11	S (hybrid)	1120	2
19	Mark 12	I, S, N, Zn	1120	4
20	Mark 13	Br, S (hybrid)	1120	3
21	Mark 14	Fe, Cl	920	5
22	Mark 15	Fe, Cl	920	4
23	Mark 16	S, I	1120	3
24	Mark 17	S, I	1120	3

Due to lower operating temperatures of about 530–550ºC, the Cu–Cl cycle is a promising alternative for hydrogen production. The thermochemical cycle decomposes water into oxygen and hydrogen through intermediate copper and chlorine compounds. These chemical reactions form a closed internal loop that recycles all chemicals on a continuous basis without emitting any greenhouse gases.

The chemical reaction steps in the Cu–Cl cycle are as follows:

(1)	$(2\ Cu)_s + (2\ HCl)_g$	→	$(2\ CuCl)_l + (H_2)_g$	[430–475°C]
(2)	$(4\ CuCl)_{aq}$	→	$(2\ CuCl_2)_{aq} + (2\ Cu)_s$	[30–70°C, electrolysis]
(3)	$(2\ CuCl_2)_{aq}$	→	$(2\ CuCl_2)_s$	[> 100°C]
(4)	$(2\ CuCl_2)_s + (H_2O)_g$	→	$(CuO.CuCl_2)_s + (2\ HCl)_g$	[400°C]
(5)	$(CuO.CuCl_2)_s$	→	$(2\ CuCl)_l + (0.5\ O_2)_g$	[500°C]

The cycle consists of three main thermally driven reactions and one electrochemical reaction, and involves five steps: hydrogen production, copper production, drying, HCl(g) production using such equipment as a fluidized bed, and oxygen production. A chemical reaction takes place in each step, except in the drying step [119].

When compared to other methods of hydrogen production, the Cu–Cl cycle has its own unique advantages, challenges, risks, and limitations. Main advantages are its lower operating temperatures, inexpensive raw materials, and reactions that proceed nearly to completion without significant side reactions. Technical challenges include the transport of solids (between steps 1–2, 3–4, and 4–5) and electrochemical processes of copper electrowinning (or electroextraction), which are not needed by other cycles like the S–I cycle. These processes are challenging due to solids injection/removal that can block the equipment operation and generate undesirable side reactions in downstream chemical reactors.

A conceptual layout of a Cu–Cl cycle is illustrated in Fig. 3.37 [120]. As can be seen, only water and nuclear heat enters the cycle and, at the end of the process, only H_2 and O_2 are produced.

Liquid water at ambient temperature enters the cycle and passes through several heat exchangers where it evaporates and increases in temperature to 400ºC. Heat for this process is obtained from cooling the hydrogen and oxygen gases before they exit the cycle. Steam at 400ºC and solid copper chloride ($CuCl_2$) at 400ºC from the dryer enter the fluidized bed where a chemical reaction occurs. This reaction is endothermic and yields hydrochloric gas (HCl) and Cu_2OCl_2. HCl gas is compressed and Cu_2OCl_2 is transferred to another process step after its temperature is increased to the oxygen production reaction temperature of 500ºC.

In the second step, an endothermic chemical reaction takes place, in which Cu_2OCl_2 is heated and O_2 and copper monochloride (CuCl) are produced. Liquid copper monochloride is solidified by cooling it to 20ºC, after which it enters the third process step together with the solid copper monochloride from the fifth step.

In the third process step, solid copper monochloride and water react together at 20ºC, endothermically. However, in this reaction water acts as a catalyst, and does not react with the other elements or compounds. Another specification with this third reaction that differentiates this step from others and makes it the most expensive (based on the price of electricity) is that electrolysis takes place in this reaction. Solid copper and copper chloride–water solutions are produced in this reaction. A mixture of copper chloride and water is transferred to the dryer, and solid copper enters the fifth process step after its temperature is increased to that step's operating temperature.

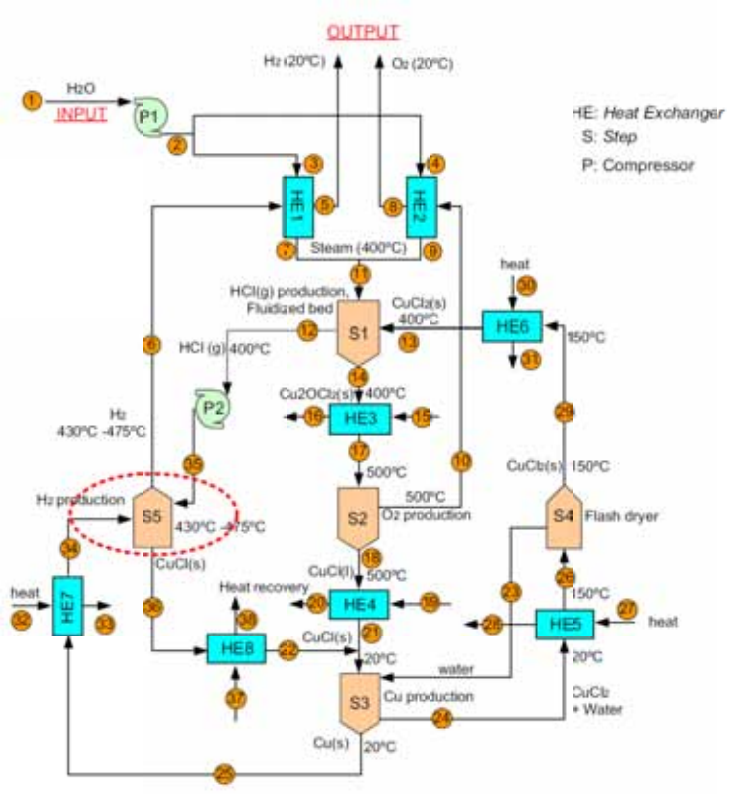

FIG. 3.37. Schematic view of the Cu–Cl thermochemical cycle [120].

In the hydrogen production step, hydrogen chloride gas and copper enter and are converted to hydrogen gas and solid cuprous monochloride (CuCl). The reaction takes place at 450ºC at steady state. The hydrogen generation reaction $2HCl(g) + 2Cu(s) \rightarrow 2CuCl(l) + H_2(g)$ is heterogeneous, exothermic, and reversible in the sense that the reaction can proceed forwards and backwards. The preferred operation temperature is 425–450ºC so that the formation of CuCl does not passivate the copper metal surface. Passivation is prevented by running the reaction above the melting point of the CuCl, at about 425ºC.

In reality, there are different variations of the Cu–Cl cycle that are being evaluated. Rosen et al [121] reported a conceptual loop consisting of five process steps. Lewis et al. [122] outlined four-step and five-step Cu–Cl cycles. Ewan and Allen [123] proposed a purely thermal reaction to produce hydrogen with low yield. Even decades ago, Dokiya and Kotera [124] reported two-step and three-step Cu–Cl cycles. The numbers of steps and the methods of grouping them have influences on the scale-up challenges and overall energy efficiency.

At present, the Atomic Energy of Canada Limited (AECL) and the ANL in the U.S. are actively investigating the Cu–Cl family of thermochemical cycles for integrating them with nuclear reactors through the Generation IV International Forum (GIF), taking into account that Generation IV nuclear reactor temperatures are 600ºC [116, 117]. Several Cu–Cl cycles with different numbers of process steps have been examined in the laboratory and various alternative configurations were identified [125]. Furthermore, a scale of 3 kg/day of hydrogen production is under development by the University of Ontario Institute of Technology (UOIT) in Canada, in collaboration with its partners [126, 127].

Nowadays, in the National Atomic Energy Commission, a research group is working on the optimization of metal chloride cycles. In Appendix V, the most recent results are presented.

3.1.2.5. Metallic bromide cycles

The bromine–calcium–iron (Br–Ca–Fe) water splitting thermochemical cycle is known as the UT-3 cycle (University of Tokyo, Br, Ca and Fe) and was developed in Japan during the 1980s [128]. The process consists of hydrolysis and bromination of calcium and iron compounds which are gas–solid heterogeneous reactions and, consequently, require a high reactivity and durability of solid reactants for the industrialization of the process. All the reactions of the UT-3 cycle are performed continuously in reactors by circulating only the gaseous reactants while the solid reactants are fixed in the reactors and exposed, alternately, to two reactions of both hydrolysis and bromination [129].

The UT-3 process is based on a cycle of the following four reactions to produce the chemical decomposition of water [130]:

(1)	$CaBr_2(s) + H_2O(g)$	$\longrightarrow$	$CaO(s) + 2\ HBr(g)$	[700–750°C]
(2)	$CaO(s) + Br_2(g)$	$\longrightarrow$	$CaBr_2(s) + 0.5\ O_2(g)$	[500–600°C]
(3)	$Fe_3O_4(s) + 8\ HBr(g)$	$\longrightarrow$	$3\ FeBr_2(s) + 4\ H_2O + Br_2(g)$	[200–300°C]
(4)	$3\ FeBr_2(s) + 4\ H_2O(g)$	$\longrightarrow$	$Fe_3O_4(s) + 6\ HBr(g) + H_2(g)$	[550–600°C]

The temperatures in brackets are approximate since the choice of temperature and pressure conditions depends on the physical and chemical properties of the reactants and the thermodynamics of the reactions. As reactions (1) and (4) are endothermic, heat must be supplied from an external heat source like an HTGR.

The UT-3 process has been extensively investigated in the 1980s and early 1990s, and an operating mode has been proposed as implemented in the so-called MASCOT (model apparatus for the study of cyclic operation in Tokyo) bench scale mockup [131]. Based on the operation of the bench scale model plant, a commercial size UT-3 hydrogen plant producing 20 000 Nm^3/hour was designed at a conceptual level, having a membrane gas separator [129].

Figure 3.38 shows the flow sheet of the UT-3 hydrogen plant coupled with an HTGR nuclear power plant which supplies the process heat required for the endothermic reactions [129]. Helium gas is introduced to the hydrogen plant at 850ºC and 4 MPa, and returned to the steam generator in the upstream of the HTGR at 700ºC and 4 MPa.

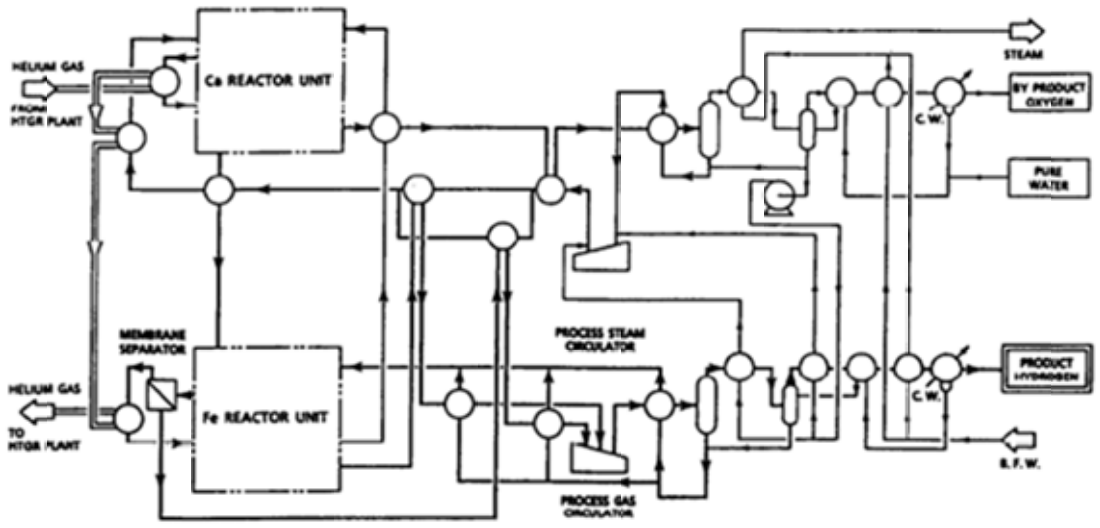

FIG. 3.38. Simplified flow sheet of the UT-3 hydrogen plant with a membrane gas separator [129].

The UT-3 plant consists mainly of Ca reactor units, Fe reactor units, hydrogen separation units, oxygen separation units, gas circulation units and membrane separation units. The reactant gases must always be heated up to a certain temperature level required for each reaction, because they cannot reach that temperature by heat exchange with product gases alone.

Heating as well as cooling of the solid reactants is carried out by use of the sensible heat of reactant gas mixtures with high steam content. The gaseous products from reactions (2) and (4) must be separated. In reaction (2), oxygen can be easily recovered from the mixture by condensation while hydrogen produced from the reaction (4) is also separated by condensation from the other two constituents, hydrogen bromide and steam. A condensed mixture of hydrogen bromide and steam can be utilized as gas reactant for reaction (3). Process waste heat generated in the hydrogen and oxygen separation unit is recovered as byproduct steam used for generating power.

More recent work has suggested that an adiabatic form of the UT-3 cycle could reach a higher efficiency than the previous version [132]. In comparison with non-adiabatic processes, theoretical calculations showed that energy and exergy economies could be increased approximately by 20% while the total power of the equipment is expected to be reduced by more than half.

The physiochemical properties of the solid and gaseous reactants, for instance the sintering of the solid, along with the toxicity of the reactants (bromide), make the practicabilities of the process very difficult. To overcome the first problem, a new flow sheet was developed which employed two asymmetric torus reactors with fluidized beds of solid reactants in each leg. This has the advantage of avoiding the energy intensive reactant preparation step and also improves the reaction kinetics [133].

A modified version of the UT-3 process is the calcium–bromine (Ca–Br) thermochemical cycle that is being investigated at ANL [134]. Compared to the UT-3 cycle, the current Ca–Br cycle is a marked departure in four ways:

1. molten calcium bromide ($CaBr_2$) is employed rather than a solid monolith, to overcome the heat and mass transfer limitations of the UT-3 process;
2. electrolysis (or possibly a plasma-chemical stage) will be used for the recovery of HBr as hydrogen and bromine, in contrast to the UT-3 cycle which employed two iron beds that swung semicontinuously between the oxide and bromide states;
3. all the steps in the Ca–Br cycle will be continuous;
4. the process is ‘hybrid’ since it requires the use of electricity. As a result, the hydrogen will be produced at much lower temperatures than those required by the UT-3 cycle and at much higher molar concentrations.

The three reactions in the hybrid Ca–Br cycle are given by [135]:

$CaBr_2$ hydrolysis with HBr formation:

(1) $CaBr_2(s) + H_2O(g) \longrightarrow CaO(s) + 2\ HBr(g)$ [740–777°C]

$CaBr_2$ regeneration with oxygen formation:

(2) $CaO(s) + Br_2(g) \longrightarrow CaBr_2(s) + 0.5\ O_2(g)$ [577–777°C]

Br_2 regeneration-PEM electrochemical:

(3) $2\ HBr(g) \longrightarrow H_2(g) + Br_2(g)$ [≈60°C]

In the framework of Generation IV nuclear energy systems initiative for the development of a proliferation resistant, sustainable, nuclear-based energy supply system, the hybrid Ca–Br cycle is being investigated for coupling with the so-called STAR-H2 system [136, 137]. STAR (for: secure transportable autonomous reactor) is a fast neutron spectrum, 400 MW(th) modular-sized reactor that is based on Russian submarine reactor technology. The reactor coolant is liquid lead (Pb) with a reactor core outlet temperature of 800ºC for future design at atmospheric pressure.

The thermal energy from the STAR-H2 system can drive the hybrid Ca–Br thermochemical process for hydrogen production. It is particularly attractive because nearly one half of the required thermodynamic energy for water splitting is delivered as nuclear heat at around 750ºC, and it is envisioned that this temperature will facilitate the engineering of materials when compared to other, higher temperature thermochemical cycles.

3.1.3. Steam methane reforming

Based on efficiency and economy reasons, most of the industrial hydrogen production is currently based on the steam methane reforming (SMR) process, although the use of this method generates significant CO_2 emissions into the atmosphere due to the nature of SMR reactions as well as the fact that it requires high process temperatures, and the most common practice for providing the needed heat is via burning natural gas [138].

The SMR process consists of breaking the link between the carbon and the hydrogen in the methane (CH_4) molecule, with the help of heat and steam. This causes the carbon to oxidize generating carbon dioxide (CO_2) and hydrogen (H_2). The conventional SMR process is composed of a steam reformer, a shift converter, and a hydrogen purifier. A mixture of desulphurized natural gas and steam is introduced into a catalyst bed in the steam reformer, where the steam reforming reaction proceeds on nickel-based catalyst, according to the following reaction:

$$CH_4 + H_2O \quad \rightarrow \quad 3\,H_2 + CO \qquad [700–800°C]$$

Furthermore, the reformed gas is supplied to a shift converter, where carbon monoxide is converted into carbon dioxide to produce more hydrogen by the shift reaction given by

$$CO + H_2O \quad \rightarrow \quad H_2 + CO_2$$

Often a 300% excess of steam is used so that more CO_2 is produced, moving the equilibrium in the water gas shift reaction and so achieving higher hydrogen yield and avoiding carbon deposition due to the Boudouard reaction which is also catalyzed by nickel. Finally the reformed gas is passed to a pressure swing adsorption (PSA) process for purification of H_2 or to a CO removal reactor by using preferential oxidation.

One option to mitigate the CO_2 emission problem associated with hydrogen production via SMR process is to use nuclear reactors for providing the heat necessary for the steam reforming reaction.

Compared to the water splitting thermochemical processes, hydrogen production by nuclear-heated SMR process is considered to be much closer to commercialization and is viewed as an intermediate step to nuclear-driven hydrogen production from water [139]. Nevertheless, the nuclear-heated SMR process is not believed to be an appropriate technology for the long term taking into account that, due to the nature of the reforming and shifting processes, there is still a need for natural gas feedstock and, consequently, CO_2 would still be emitted as byproduct of chemical reactions [140].

The advantageous effect of nuclear heat supply on the SMR process with a membrane reformer operating at 500oC is schematically illustrated in Fig. 3.39 [139]. The advantage increases with reforming temperature.

Even assuming an idealistic case for the conventional SMR process, in which all the heat generated by combustion of CH_4 is used for the heat of endothermic reaction of steam reforming, the consumption of CH_4 for the nuclear-heated SMR reaction is 3.3/4=83% (or 17% less) of that of conventional SMR reaction for producing the same amount of hydrogen. In the actual case of conventional SMR reaction, as ~2.7 mol of H_2 are really produced from 1 mol of CH_4 feed, the nuclear-heated SMR process is expected to save about 30% natural gas consumption, or reduce about 30% CO_2 emissions.

SMR process can potentially be coupled to an MHR plant that can function as the high temperature heat source operating at about 850ºC, to replace the natural gas burning furnace. The high operating temperature can enable the process to take place at about 80% efficiency. This alternative has been estimated to be potentially cost competitive in the near future with the conventional SMR process [141, 142].

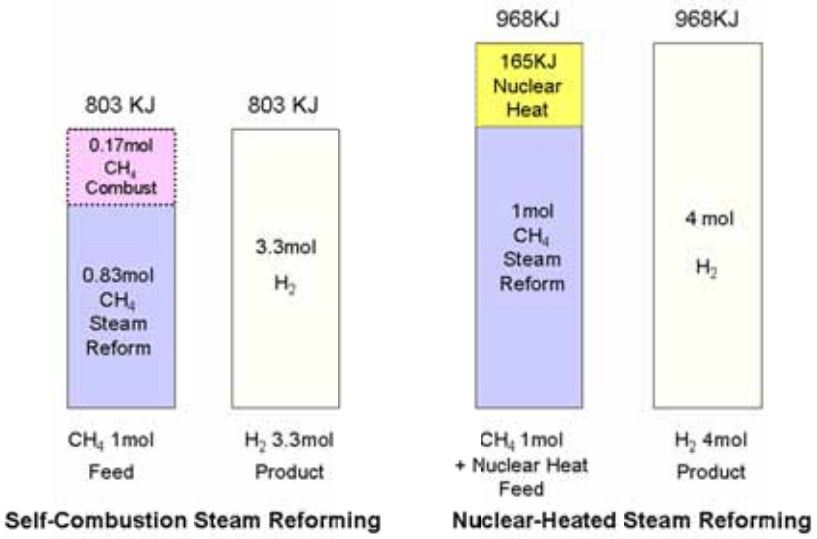

FIG. 3.39. Theoretical efficiencies of conventional and nuclear-heated SMR processes [139].

3.1.3.1. Nuclear SMR with HTTR

In Japan, JAEA has been evaluating the feasibility of hydrogen production under the SMR process coupled with the HTTR test reactor. The flow diagram developed for the nuclear/chemical plant is given in Fig. 3.40 [143].

The thermal energy of 10 MW produced by HTTR is transferred via the IHX to the secondary helium circuit, which is pressurized up to 4.2 MPa in order to prevent release of radioactivity from the core to the environment in case of a depressurization accident. The reactor provides high temperature helium gas of 905ºC at the outlet of the IHX. Inside the steam reformer, the helium flows outside the catalyst tubes transferring heat by forced convection flow. The catalyst tubes contain packings of Ni/Al_2O_3 reforming catalysts, through which the process feed gases (natural gas and steam) are routed. The helium enters the steam reformer at the bottom, then flows upwards outside the catalyst tubes, squeezed by multiple plates of orifice baffles, and finally exits at a temperature of 585ºC.

The process feed gas mixture of natural gas and steam, after preheated to 450ºC at a pressure of 4.5 MPa, enters the steam reformer at the top and then flows downwards in an annular gap

between the walls of outer and inner tube through the catalyst bed, where methane and other lighter hydrocarbons together with steam are reformed. The reformed gas, having reached a maximum temperature of 830ºC, flows then upwards inside the inner tubes transferring at the same time heat to the feed gas and, eventually, leaving the steam reformer at a temperature of 580ºC and a pressure of 4.1 MPa. This gas is cooled down by the water cooler and separated into steam and dry gas compositions including hydrogen, carbon monoxide, carbon dioxide and residual methane in the separator. The conversion ratio from methane to hydrogen is expected to be 68%, and the residual methane is burned in the flare stack together with the other combustible gases.

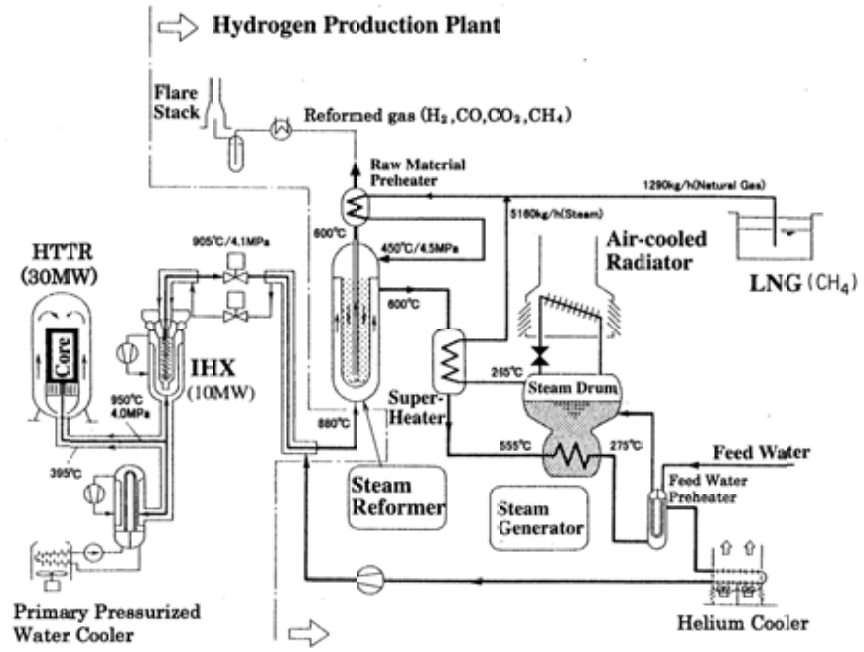

FIG. 3.40. HTTR plant with hydrogen production using SMR process [143].

Particular safety aspects for a combined nuclear/chemical complex have been investigated using the probabilistic safety assessment methodology. Possible accident sequences were identified, and their consequences for public health and frequencies of occurrence were estimated. Results of analyses showed that the dominant sequences are those that result in a methane explosion, and they are expected to occur with a frequency that is two orders of magnitude smaller than the frequency of core melting in the case of a boiling water reactor (BWR) [144].

3.1.3.2. Nuclear SMR with PBMR

Analyses have shown that the heat from the PBMR can be used to replace approximately 30% of the natural gas burned to get the right temperatures for the endothermic reforming reaction, and can also be used to heat the feed steam to the reaction. Figure 3.41 illustrates a possible layout of a nuclear SMR plan with the main advantages being:

- Possibility for near term implementation since SMR is commercially proven technology;
- Economic analyses have shown that PBMR SMR is competitive with current SMR at today's natural gas prices in most international markets;
- Syngas is a fundamental building block for several important processes;

- Lends itself to pipeline supply serving many off-site users of syngas or hydrogen with immediate markets;
- Nuclear technology replaces valuable natural gas feedstock;
- Reduces CO_2 and heat rejection;
- Good match between PBMR and process temperatures and size;
- Hydrogen produced from SMR can be a first step towards a hydrogen economy.

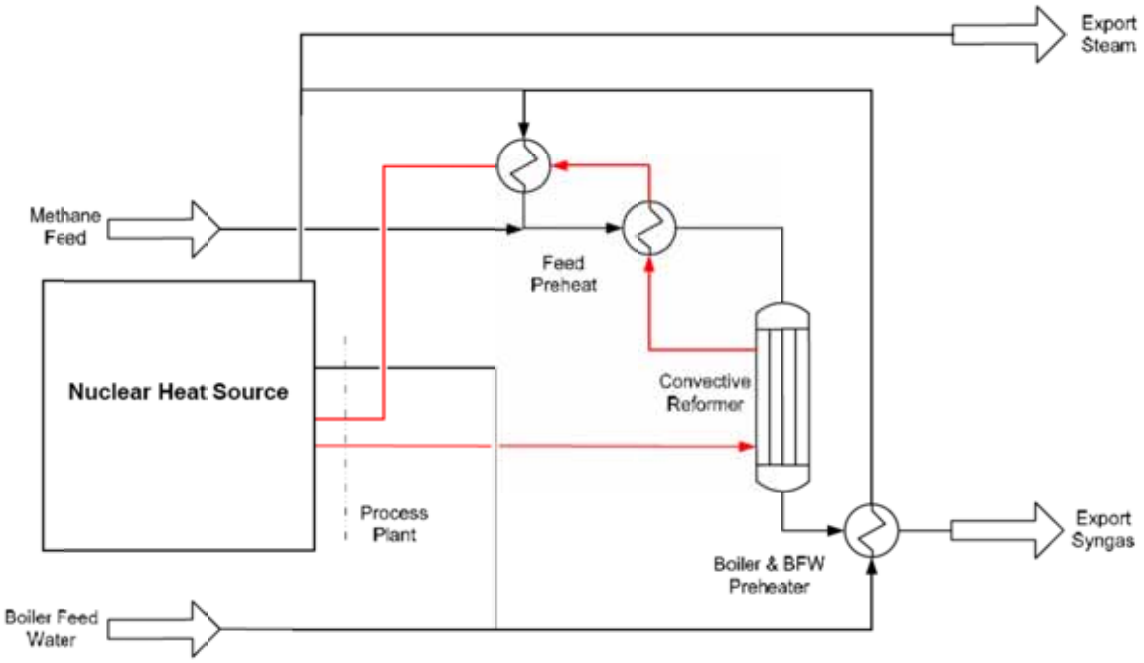

FIG. 3.41. Possible schematic for utilizing nuclear heat in an SMR plant.

In order to utilize this heat, different configurations were also evaluated to transfer the nuclear heat to the steam methane reforming plant. Two configurations were identified as the most promising and are presented in Figs 3.42 and 3.43, respectively.

Configuration 1 transfers all the nuclear heat through an intermediate heat exchanger to the SMR plant. All feed steam is produced at the SMR plant. Configuration 2 transfers high temperature heat through an intermediate heat exchanger while the rest of the heat is transferred through a steam generator. The steam generator is used to supply the steam feed for the SMR process. A brief summary of some of the advantage and disadvantages of these configurations is provided in Table 3.11.

3.1.4. Coal gasification

3.1.4.1. Coal – more than just a fuel to be burnt

Because of its abundant resources on earth, the conversion of coal to gaseous or liquid fuels has been worldwide commercially applied. The coke furnace process was already in use more than 100 years ago for the production of low energy gas (5–12.7 MJ/m^3), synthesis gas (~12.7 MJ/m^3), town gas (16.7–20 MJ/m^3), or substitute natural gas, SNG, (25–42 MJ/m^3). In Germany, hydrogen-rich (~50%) coal gas was fed as town gas into the municipal gas grids [145].

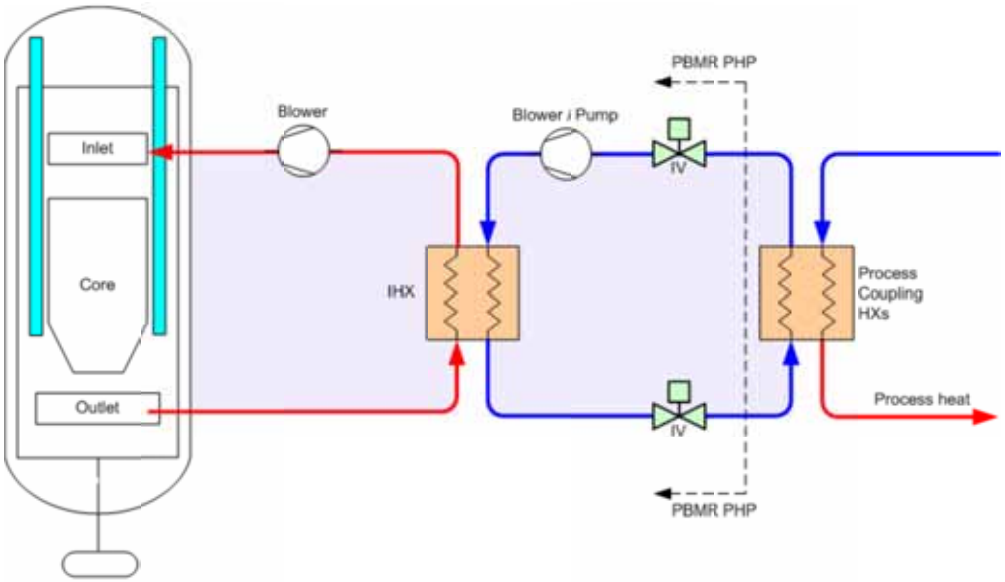

FIG. 3.42. SMR configuration 1.

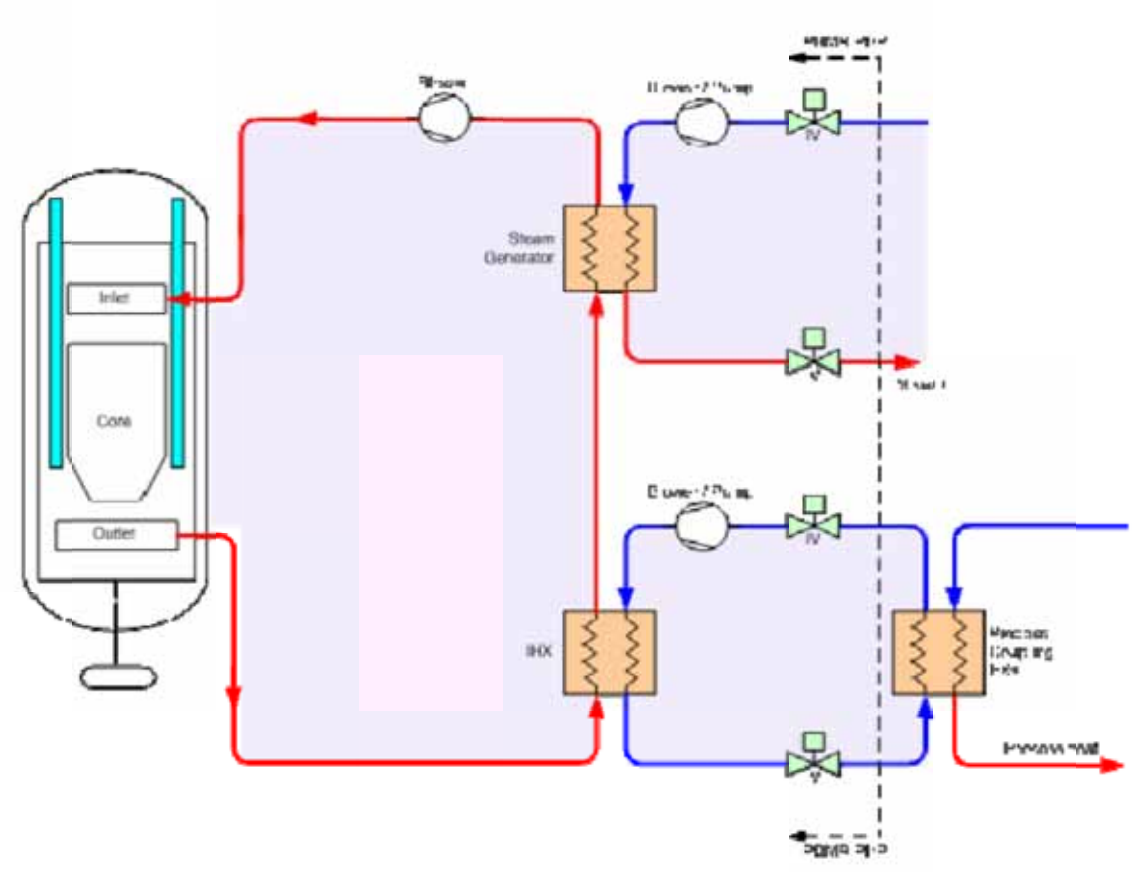

FIG. 3.43. SMR configuration 2.

TABLE 3.11. COMPARISON BETWEEN DIFFERENT CONFIGURATIONS

Configuration 1	Configuration 2
Advantages	
Fewer components coupled to the nuclear cycle	Smaller IHX required
Smaller citadel footprint in nuclear island	Better to withstand loss of process and failure to trip primary circulator
	Additional decay heat removal reliability
Disadvantages	
Difficult to withstand loss of process and failure to trip primary circulator	Possible leaks in steam generator need to be evaluated (more licensing scrutiny)

In order to bring together the requirements of a sustainable economic growth with the environmental protection, Argentine as most of the developed countries are encouraging strategies for the rational and integral utilization of their coal ores. This tendency will increase with time, as the gas and petroleum reserves become exhausted.

Coproduction of power, fuels and chemicals offers an innovative, economically advantageous mean of achieving these long term energy goals. Coproduction involves the integration of three major building blocks:

- gasification of coal to produce synthesis gas (‘syngas’);
- conversion of a portion of the syngas to high value products such as high purity hydrogen, liquid fuels and chemicals;
- combustion of syngas and unreacted syngas from the conversion processes to produce electric power in a combined cycle system.

In the coproduction concept, an energy complex produces not only power, but also fuels and/or chemicals. This greatly increases the flexibility of the complex and offers economic advantages compared with dedicated plants, one producing only power and the other only fuels or chemicals.

The present project in Argentina is addressed to introduce the concept of coproduction for the integral exploitation of the Rio Turbio coal, which is by far the most important domestic coal reserve. For this purpose, early research and development activities are planned, comprising both theoretical and experimental studies for understanding the mechanisms of the coal gasification reactions in presence of oxygen and steam, in order to determine the optimum parameter condition for the syngas production and the further cleanup steps for the harmful contaminants removal, transforming the synthesis gas in a clean fuel for electric power production in a combined cycle system, with efficiencies and emissions comparable to the natural gas fired plants.

Additionally taking into account the increasing international interest for developing renewable energy sources, and with the aim of taking understanding in the management of these sustainable technologies, preliminary studies will be carried out for the conversion of the synthesis gas in two high value products: (1) hydrogen by separation through diffusion membranes, in order to obtain ultra pure hydrogen for fuel cells; (2) liquid fuels through the Fischer–Tropsch synthesis.

With the first oil crisis at the beginning of the 1970s, the coal resources in Germany were become to play a central role and a revival of the coal conversion programme was starting as a contribution to an away-from-oil policy. Large markets were seen for synthesis gas, heating gas, reduction gas as a consumer-friendly type of energy. Extensive experimental and

theoretical studies included coal gasification, liquefaction, and advanced combustion systems aiming at improved methods for the generation of SNG, liquid hydrocarbons, and other raw materials for the chemical industries. Numerous coal gasification projects nearby mining locations were launched to investigate on pilot plant scale various processes and reactor types and optimize operational conditions [146]. Interest in coal refinement faded away again with cheap oil prices since the 1980s. Today coal gasification is primarily used for ammonia synthesis in the fertilizer industry and for synthesis gas production to be used in the synthesis of methanol and other hydrocarbons.

3.1.4.2. Coal conversion processes

If expressed in carbon and hydrogen, coal can be described with the formula of ~$(CH_{0.8})_n$. For the production of higher grade hydrocarbons, either the carbon must be reduced or hydrogen must be added. The conversion of coal into a gas is realized by means of a gasification agent which reacts with the coal at temperatures > 800°C similar to an incomplete combustion. All organic constituents will be converted at long enough residence times. The gasification agent is either steam (steam coal gasification) or hydrogen (hydro-gasification). If air or oxygen is injected into the gasifier, a part of the coal is directly burnt allowing for an autothermal reaction. Both processes have in common that high pressures are needed to achieve a high methane yield, whereas for an optimal synthesis gas output, high temperatures and low pressures are required.

i. Steam coal gasification

Steam gasification of coal is since long a mature and well established technology practiced on industrial scale. In the conventional steam–coal gasification process, a part of the coal is partially oxidized in a preceding step, before in the much slower heterogeneous water gas reaction, the residual organic solids are converted to synthesis gas with some CO_2 and steam.

In the steam–coal gasification process, a first step is the pyrolysis reaction during the heatup phase (400–600°C) where all volatile constituents of the coal are rapidly expelled. The gasification reaction with the agent ‘steam’ is given by the heterogeneous water gas reaction and the homogeneous water gas (shift) reaction with a further increase of the H_2 fraction:

$$C + H_2O \rightarrow H_2 + CO \qquad -118.5 \text{ kJ/mol C}$$
$$CO + H_2O \rightarrow H_2 + CO_2 \qquad +43.3 \text{ kJ/mol C}$$

where the residual organic solids are converted to synthesis gas. It is followed by a methanation step if the desired end product is SNG. Heat must be quickly withdrawn to avoid reverse chemical reactions.

$$CO + 3\,H_2 \rightarrow CH_4 + H_2O \qquad +206.0 \text{ kJ/mol C}$$

Gasification processes are classified according to the type of reactor. The principal lines mainly used today are those by Lurgi (since 1931), Winkler (since 1922), Koppers–Totzek (since 1941). They all were developed in Germany and exist at a large scale (Fig. 3.44). Modified process variants, such as Texaco, Shell–Koppers and many others have been developed aiming at an adjustment to the feedstock quality, an optimization of the product gas composition and, of course, an efficiency improvement. Variants differ by temperature and pressure range, grain size of the coal, and residence time. Partial oxidation of pulverized coal by oxygen/air (pure O_2 for hydrogen production) and steam in a fluidized bed takes place at about atmospheric pressure, where 30–40% of the coal is transformed to CO_2 to supply splitting energy of steam.

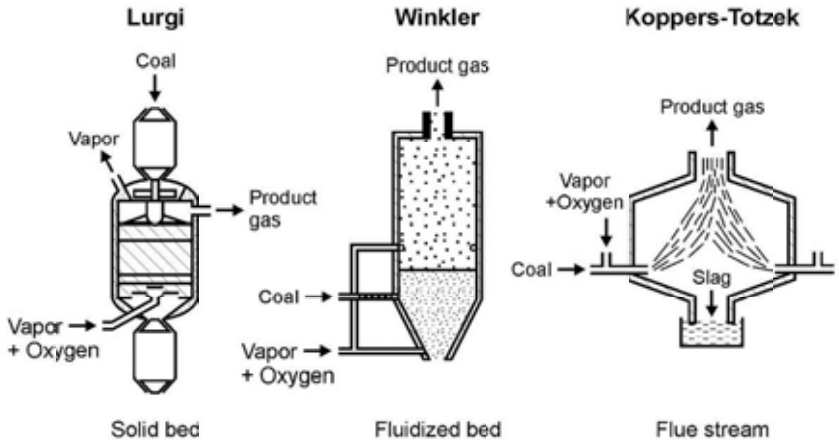

FIG. 3.44. Three principal lines of steam coal gasification, all developed in Germany and today applied at a large scale.

Commercial scale plants typically run in an autothermal mode. Autothermal gasification reactors are of relatively simple design in that they do not need heat input or heat exchanging devices. Higher temperatures are possible and thus higher reaction velocities which result in a higher coal throughput. Disadvantage is the larger specific CO_2 generation, since part of the feedstock is burnt to provide the process heat for the gasification reactions. This problem is not given if a CO_2-emission-free, external heat source is applied (allothermal gasification). For example, with an HTGR, the heat provided by the hot helium coolant can be introduced directly into the gas generator, another part being used for the steam production, and the rest still usable for electricity production.

Depending on the customers' requirements, respective downstream processing allows the optimized generation of either hydrogen or methane or synthesis gas. Coal conversion is estimated to be around 95% and the total efficiency (based on higher heating value) to be ~70%. Main disadvantages of coal gasification are the handling of solid material streams and the large amounts of CO_2, SO_2, and ash requiring a complex cleaning system. Table 3.12 lists some of the major characteristic features of the different types of steam–coal gasification processes [145].

(A) Solid bed

In the Lurgi pressure gasification, a solid bed of coal moving from top to bottom is gasified by adding steam and oxygen from the bottom at a pressure of 1.5–3 MPa forming different reaction zones at different temperatures. The amount of methane generated is depending on pressure, temperature, the oxygen-to-steam ratio, reactivity of the coal, and the contents of volatile substances in the coal. In a solid bed, the coal should be in smaller pieces (but not too small) and must not cake to allow for a sufficient permeability of the gases. The counter-current flow arrangement leads to higher conversion rates and thermal efficiencies. A drawback is that the product gases before exiting pass through a zone of fresh coal (which is given to the reactor from top), where it receives a significant load of tar and higher hydrocarbons, and therefore, necessitates extensive purification. The Lurgi gasifier is the only that is operated under pressure at a large-technical scale producing synthesis gas for the Fischer–Tropsch process.

TABLE 3.12. CHARACTERISTIC FEATURES OF DIFFERENT STEAM–COAL GASIFICATION PROCESSES

	Lurgi	Winkler	Koppers–Totzek
Reactor	Solid bed	Fluidized bed	Flue stream
Grain size (mm)	10–30	1–10	< 0.1
Steam-to-oxygen ratio	9–5	2.5–1	0.5–0.02
Movement of reactants, products	Counter-current flow	Vortex co-current flow	Co-current flow
Residence time of fuel (min)	60–90	15–60	< 0.02
Requirements to fuel	Mu	Highly reactive, must not decay	Melting point of ash < 1450°C
Maximum gas outlet temperature (°C)	370–600	800–950	1400–1600
Pressure (MPa)	2–3	0.1	0.1
Composition of product gas (vol.%)			
$CO + H_2$	62	84	60 + 29
CH_4	12	2	0.1
Byproducts	Tar, oil, phenols, gasoline, waste water	none	none

The Sasol company in South Africa became and still is the world's largest commercial applier of coal conversion technology operating a total of 97 units. Most Sasol–Lurgi standard fixed bed reactors have an inner diameter of 3.85 m (Mark IV), able to produce 65 000 Nm^3/h of dry gas with a raw coal throughput of 54 t/h. Sasol is also operating a 4.7 m diameter reactor (Mark V) with a capacity of 100 000 Nm^3/h [146, 147]. The plants in Secunda and Sasolburg convert more than 30 million tons per year of bituminous coal to yield about 5.1 million Nm3 per hour of 'pure synthesis gas' (containing 56% of H_2, 32% of CO, 11% of CH_4) corresponding to almost 30% of the world's production. It is the basis of manufacture of numerous fuels and chemicals [148].

(B) Fluidized bed

The high temperature Winkler (HTW) process takes place in a fluidized bed where fine-grain brown coal is reacted with oxygen and steam which are fed in at the bottom with high speed. The fluidized bed has no reaction zones, but rather forms a homogeneous distribution of solids. Operational conditions are high temperatures and atmospheric pressure. The temperature, however, must be below the ash melting point to prevent a softening and agglomeration of the ash, which would lead to a collapse of the fluidized bed. The product gas composition changes with height and contains almost no higher hydrocarbons at the exit. It carries, however, a large amount of dust which can be recirculated to the reactor to further raise the carbon conversion rate reaching up to 90%.

The Winkler gasification is characterized by simple coal pretreatment, low oxygen consumption, and good performance over a broad load range. The process was proven successful for highly reactive coal grades. Several large scale plants were constructed in Germany and other countries with coal throughputs of up to 35 t/h. Industrial scale is at ~60 000 Nm^3/h. Following the atmospheric Winkler process, the gasification was later done at higher pressures up to 1 MPa in order to raise unit capacity and gas quantity, and also to save

compression energy for the product gas. Gasifier plants have shown simple startup and shutdown as well as good partial load behavior and high reliability. Of advantage is also the low oxygen consumption.

(C) Flue stream

In the flue stream gasifier, dry coal dust is mixed with steam and oxygen/air and gasified at atmospheric pressure in an autothermal way. The reaction zone is limited to the flame area with a co-current flow of coal and gasification agent. The Koppers–Totzek process runs at very high temperatures above the ash melting point. It has the advantage that tar formation is suppressed and other organic substances are destroyed. The conversion rate is at almost 100% with a methane content in the product gas of < 0.1%. Industrial plant capacities are in the order of 50 000 Nm^3/h. The Shell process applies the Koppers–Totzek principle under pressures up to 4 MPa. Gasification temperatures achieved are up to 2000°C. In the Texaco gasification process, fine-grained coal is mixed with water to a suspension. The oxygen is added at the burner. The reactor operates at pressures of ~5.5 MPa and high steam contents. The conversion rate is about 99%, the thermal efficiency about 92%. The synthesis gas typically contains 34% of H_2 and 48% of CO. Hydrogen gas can be obtained with a purity > 97% and at a pressure of 4 MPa.

ii. Hydro-gasification

In the hydro-gasification process of coal, hydrogen is added to convert in an exothermic reaction the coal into a methane-rich raw gas, ideal for the production of substitute natural gas (SNG). The hydrogen can be provided either by taking the coke left from the hydro-gasification and convert it with oxygen and steam in a high temperature Winkler process, or by taking a part of the product methane for steam reforming. Both processes need high temperatures which could be provided by nuclear. The gasification reaction with the agent ‘hydrogen’ and the main product methane is:

$$C + 2\,H_2 \rightarrow CH_4 \quad + 87.5\ kJ/mol\ C$$

Kinetics of the process is more complex compared to steam gasification. The above reaction runs in several steps, a pyrolytic step, where primary methane is formed plus volatile hydrocarbons. The remainder is a highly reactive coke which either reacts with H_2 to methane or converts to slowly reacting coke, which then undergoes a slow hydrogenating gasification to form methane.

The other chemical reactions are the endothermic steam methane reforming and again the water gas shift reaction, both of which serve the purpose to provide the gasification agent:

$$CH_4 + H_2O \rightarrow CO + 3\,H_2 \quad - 206\ kJ/mol\ C$$

$$CO + H_2O \rightarrow + CO_2 \quad + 43.3\ kJ/mol\ C$$

A high gasification degree can be obtained already with relatively short residence times of 9–80 min. In order to obtain a high conversion rate of coal, the CH_4 fraction should not be higher than 5%, which requires a low temperature separation step. The advantage of hydro-gasification compared with steam coal gasification is its 200 K lower preheating temperature which reduces potential corrosive attack. A major drawback, however, is the low conversion rate, i.e. the large amount of residual coke of up to 40%. But again, subsequent processes would allow the generation of SNG or methanol. In contrast to steam gasification, the hydro-gasification process still needs to be demonstrated at a larger commercial scale.

iii. Coal liquefaction

Also coal liquefaction processes were developed in the first half of the 20th century. Bergius or Pott/Broche used a direct method to convert coal by a hydrogenation process. Coal is mixed with oil and catalyst to convert to an oily medium-sized interim product which is either reprocessed to a coal oil or, in a subsequent step, after mixing with H_2 passes through a series of hydrogenation reactors at 450–490°C and 20 MPa, and at presence of an iron oxide powder as catalyst to a coal oil. Here the coal having a molecular weight of > 5000 splits into smaller pieces with the concomitant accretion of hydrogen. Thermodynamic conditions determine quantity and type of products and they can be adjusted to the educts.

In contrast, Fischer and Tropsch were starting from synthesis gas. In this indirect liquefaction process, coal is gasified in a first step to synthesis gas followed by a catalytical (iron-based) hydrogenation of the CO where the synthesis gas is reacted in a Fischer–Tropsch process to high quality clean fuels:

$$2n\ H_2 + n\ CO \quad \rightarrow \quad (\text{-}CH_2\text{-})_n + n\ H_2O + \text{heat}$$

An alternative to Fischer–Tropsch is the Mobil–Oil process which is principally based on a new catalyst allowing an easy production of liquid fuels from methanol.

Both direct and indirect methods were developed to industrial maturity in Germany applying brown coal and stone coal. The indirect process is superior to the direct one because of the lower operational pressures necessary and thus a higher reliability of the plant. Maximum production rates amounted to ~4 million t/a of gasoline [145]. Coal liquefaction in Germany, however, eventually became uneconomic and was abandoned later. Renewed interest in the 1970s resulted in the operation of a pilot plant with a production rate of 200 kg/d. Since then only a few joint international projects, e.g. with South Africa, remained, the only country to apply this technology still today at a large scale. Since 1955, Sasol in Secunda, South Africa, is producing oil products from coal, today at an output of 150 000 barrels/d of fuels and petrochemicals [148]. A coal liquefaction plant has also been constructed in Shenhua, China, with a throughput of 9.7 million t/a of coal to be converted into 5 million t of gasoline, kerosine, diesel, and others. For the next years, China is planning the construction of 27 coal liquefaction plants.

Argentina has begun from 2007 the so-called AiCRT project (‘Integral exploitation of Rio Turbio Carbon, Argentine’) for producing diesel fuel through the Fischer–Tropsch synthesis with the synthesis gas obtained by the gasification of a sub-bituminous carbon.

3.1.4.3. Nuclear process heat for coal gasification

There are several drivers for nuclear energy to be introduced as a primary heat source into the coal gasification process [149]:

- In the conventional gasification process, a significant additional amount of feedstock is necessary to provide process heat at the required temperature level. Substitution for nuclear would allow resource savings of up to 40%. A respective reduction in CO_2 and other, coal-specific emissions will be achieved at the same time.
- The conversion to liquid hydrocarbons will reduce and diversify dependency on oil imports.
- If cost of nuclear heat is sufficiently low, it may help to meet growth rates in energy consumption, substitute for expensive electricity generation with fossil fuels, also replace old plants.

In Germany, the concept of the pebble-bed HTGR has been developed and became subject of various projects, for example the so-called PNP (prototype nuclear process heat) project. Motivation for this project was to take advantage of the large resources of the energy carriers coal and uranium and to find for the coal an additional spot on the heat market in order to diversify the energy supply in Germany and to reduce its dependency on imports of oil and natural gas. Furthermore, a great advantage was seen in the nuclear production of easy-to-handle energy carriers such SNG, synthesis gas, reductive gas, or — on a longer term — hydrogen by thermochemical water splitting cycles, and having at the same time a reduction of the specific noxious gaseous emissions.

Figure 3.45 shows a flow sheet of the PNP nuclear steam coal gasification process. For this gasification method, the heat from the reactor coolant was foreseen to be transferred to an additional intermediate circuit via a helium–helium intermediate heat exchanger (He–He IHX). The main reason was to avoid the handling of coal and ash in the primary system of the reactor, and a much more complex way for repair and maintenance work. Primary helium of 950°C flowing on the outside of the IHX tubes passes its heat to the secondary helium entering the steam gasifier at 900°C. Also pressure is slightly higher than on the primary side for the purpose of preventing radioactivity to enter the secondary circuit in case of a leak. The hot steam produced is routed into the coal bed to be gasified.

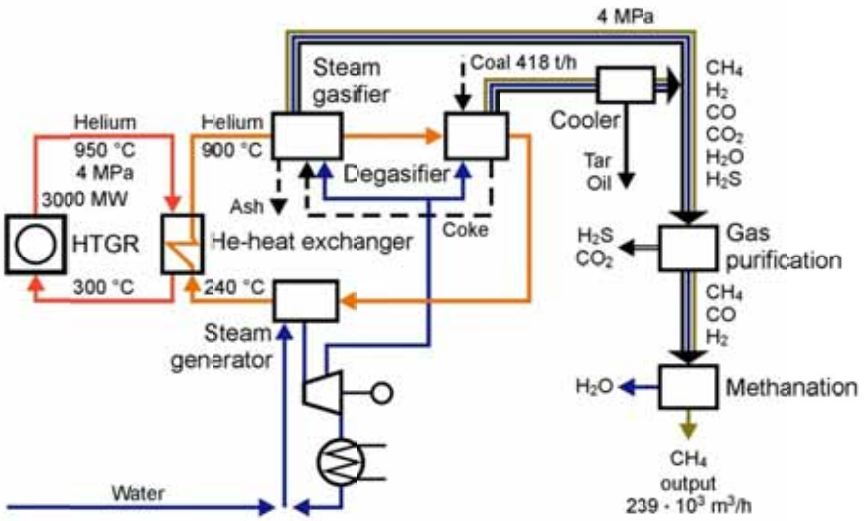

FIG. 3.45. Schematic of steam gasification of hard coal with nuclear process heat plant PR-3000.

3.1.5. Techno–economics: elements and methodology of costing

The economic viability of each technology was assessed based on capital costs, operating costs, technical risk, safety, and operability. Standard industry practice with respect to process engineering and cost estimating were used to assess the economic viability of each technology for commercial implementation while limited credit was given for cost improvements from technology breakthroughs.

Operating costs were based on first-of-a-kind process availability. All of these technologies are at an early stage of development, and the individual operability and safety concerns were identified and evaluated to further define risks to commercialization. To that end, an analysis was performed that evaluated the sensitivity of hydrogen cost, per kilogram of hydrogen produced, against variations in the range of the HTGR outlet temperature (i.e. from 950°C to 700°C).

3.1.5.1. Cost estimate for PBMR plant with HyS cycle

i. Capital costs

A capital cost estimate and cost-of-hydrogen estimate were made for the reference plant design. The HyS plant components were selected and sized in detail on the basis of the process flow sheet and the physical properties of the process streams. The available output data was suitably modified to get input for the component sizing process. Only commercially existing equipment was chosen, other than the sulphuric acid decomposer reactor and the SDE modules, which are technology in development.

Costs for the PBMR and associated NHSS equipment were based on previous estimates prepared by the Westinghouse/PBMR team. For the analysis of hydrogen selling price, a mature, four-PBMR unit hydrogen plant is modeled, in order to represent the full commercial potential of the application. Economies derive from sharing of facilities and other cost savings that would come from a mature supply infrastructure. The results are given for both the four-unit plant and a 'nominal' one-unit plant (where the one-unit plant still has the four-unit economies). Total costs for a PBMR/HyS water splitting plant are shown in Table 3.13.

ii.Costs of production

The cost-of-hydrogen for the plant was determined based on a specific tool for the comparison of hydrogen production technologies developed by DOE. This is a result of the H2A production analysis programme, which is part of the national Hydrogen Fuel Initiative, and which was conducted by a team from the various DOE divisions, the national laboratories and industrial participants. The H2A tool was, therefore, used as the basis for the hydrogen price calculations in this study.

TABLE 3.13. TOTAL COSTS OF PBMR HYS WATER SPLITTING PLANT

	Total cost		Specific cost
	Four-unit (2000 MW) NHSS (million US $)	One-unit (500 MW) NHSS (million US $)	Unit cost (US $)
Total direct depreciable cost	4432	1108	—
Indirect (owner's and other) cost	77.9	19.5	—
Total base construction cost	4510	1128	2200/kW(t)
Contingency	443.2	110.8	—
Land	2.0	0.5	5000/acre [a]
Total overnight capital cost	4962	1240	2500/kW(t) 7700/(kg·day) 5600/kW(t) of H_2 [b]

[a] 1 acre = 4046.86 $m^{2.}$

[b] based on LHV.

— data not available.

The results for the PBMR/HyS reference design are shown in Table 3.14. The results are given for both a base case (Shaw) and a case labeled 'Icarus'. The base case uses capital cost estimates for the HyS plant as determined by Shaw using their in-house estimating programme which draws data from recent purchasing. The Shaw estimate was prepared by an experienced professional estimator and equipment size estimated by an experienced process

engineer. The Icarus case uses HyS capital costs, which are significantly less, determined by SRNL using a commercial cost estimating programme. Although somewhat less rigorous than the Shaw estimate, the Icarus estimate is more consistent with other thermochemical hydrogen plant cost estimates that have been published. One reason for the higher costs estimated by Shaw was the use of equipment and commodity costs taken at a time (2nd Quarter 2008) at which industrial commodities were at a peak, which have since retreated. A second factor is that there is no specific industry experience with HyS or other large scale plants for similar production of pure hydrogen. For this second reason, subjective factors in the cost estimating process are unavoidable, and in accounting for unknowns, there is a natural tendency to be conservative.

The effects on hydrogen price were calculated for uncertainties in major parts of the costs, including capital cost factors and other factors, such as rate of return, power costs, etc. The base case using the Shaw estimates for the HyS equipment resulted in a levelized hydrogen price of US $6.18/kg H_2. The sensitivity analysis showed a price range from US $5.00 to US $7.10/kg of H_2. When the SRNL/Icarus equipment costs were used for the HyS plant, the levelized hydrogen price was US $5.34/kg of H_2, and the sensitivity range was US $4.15 to US $6.25/kg H_2.

TABLE 3.14. HYDROGEN PRICE COMPONENTS SUMMARY FOR PBMR HYS WATER SPLITTING PLANT

	Shaw		Icarus	
	(US $/kg)	%	(US $/kg)	%
Capital charge	4.01	65	3.19	59
Fixed O&M: Labor, taxes, insurance, annual licencing, permits and fees, material cost for maintenance and repairs, nuclear decommissioning funding, helium make-up	0.68	11	0.68	13
Variable O&M: Nuclear fuel, process catalyst and chemical consumption and waste disposal	0.56	9	0.56	11
Utilities and feed: electric power and process water	1.23	20	1.22	23
Byproduct credit (O_2)	-0.32	-5	-0.32	-6
Total hydrogen cost (year 2008)	6.18	100	5.34	100

Analysis was also performed to determine how the projected hydrogen costs compared to hydrogen produced by conventional natural gas steam reforming and water electrolysis. At the presently estimated base case costs, according to the H2A model with the assumptions and groundrules as stated in this report, the HyS nuclear water splitting plant competes with natural gas at a gas price of US $16/MMBTU[1] and with electrolysis at between US $60 and US $70/MW(e)-h. Using the Icarus-based process costs, the competitive range is approximately US $13/MMBtu natural gas price and between US $50 and US $60/MW(e)·h for electrolysis. These represent a high energy cost scenario, but they are not an unreasonable expectation.

Hydrogen production system utilizes heat and electricity generated in the HTGR. Cost information of heat and electricity is necessary to estimate hydrogen cost. Plant costs of HTGR consist of preconstruction costs, construction costs, operation and maintenance costs,

[1] 1 MMBTU = 1 million BTU (British thermal unit) = 293.1 kWh.

supplementary costs, fuel cycle costs. The heat and electricity cost is typically given as units of US $/kWh and US $/MJ.

3.1.5.2. Cost estimate for the Japanese GTHTR300C plant with S–I cycle

A preliminary cost evaluation of power plant with a gas turbine, GTHTR300, was performed [150]. To estimate construction cost of the GTHTR300, the following conditions were considered:

- Four reactor units in one plant;
- N^{th} of a kind (NOAK) plant;
- Modular construction and standardized design.

Construction cost of a unit of the GTHTR300 is given as listed in Table 3.15.

TABLE 3.15. CONSTRUCTION COST OF THE GTHTR300 FOR POWER GENERATION

Component	Million US $
Reactor components Reactor pressure vessel, Core components, Reactivity control system, Shutdown cooling system, Vessel cooling system, Fuel handling and storage system, Radioactive waste treatment system	170.8
Power conversion system Turbine and compressor, Generator, Heat exchanger, Power conversion vessel, Heat exchanger vessel, Hot piping	140.1
Auxiliary system Helium purification system, Cooling water system, Helium storage and supply system, Radioactive management system, Ventilation and air conditioning system, Others	67.2
Electric system	40.0
Control and instrumentation system	17.8
Buildings	110.7
Total	546.7

Power generation cost consists of the capital cost, the operation cost, and the fuel cost. The capital cost includes the depreciation cost, the interest cost, the property cost, and the decommissioning cost. The operation cost includes the maintenance cost, miscellaneous cost, the personnel cost, the head office cost, and the business tax. The fuel cost includes the uranium purchase and conversion cost, the enrichment cost, the fabrication cost, the storage cost, the reprocessing cost, and the waste disposal cost. A sample estimation result of power generation cost in the GTHTR300 as functions of load factor and discount rate is listed in Table 3.16.

TABLE 3.16. POWER GENERATION COST

Parameter	Value			
Load factor (%)	80		90	
Discount rate (%)	3	4	3	4
Capital cost (US cent/kWh)	1.57	1.74	1.40	1.55
Operation cost (US cent/kWh)	1.11	1.11	0.99	0.99
Fuel cost (US cent/kWh)	1.46	1.44	1.46	1.44
Total (US cent/kWh)	4.14	4.28	3.84	3.97

The GTHTR300C scales down of the power conversion system of the GTHTR300 including gas turbine and the compressor and adds the IHX and the secondary helium loop to supply process heat for a hydrogen production system. The construction cost of the GTHTR300C which excludes a hydrogen production plant is preliminary estimated as listed in Table 3.17. The GTHTR300C produces 202 MW of electricity and 170 MW of high temperature process heat. The cost of the power conversion system is evaluated by a scale-factor of 0.6. The cost of the IHX and the secondary helium loop is estimated from the HTTR construction cost. Electricity and heat costs are evaluated as listed in Table 3.18.

TABLE 3.17. CONSTRUCTION COST OF THE GTHTR300C FOR HYDROGEN GENERATION

Component	Million US $[(1)]
Reactor components	170.8
Power conversion system	114.7
Auxiliary system	67.2
Electric system	40.0
Control and instrumentation system	17.8
Buildings	110.7
IHX, secondary helium loop	69.0
Total	590.3

TABLE 3.18. POWER AND PROCESS HEAT GENERATION COST IN THE GTHTR300C

Parameter	Value
Load factor (%)	80
Discount rate (%)	3
Capital cost (US cent/kWh)	1.70
Operation cost (US cent/kWh)	1.18
Fuel cost (US cent/kWh)	1.46
Total (US cent/kWh)	4.34
Total (US cent/MJ)	5.40

Steam methane reforming is a mature technology. Detailed plant construction and operation costs can be estimated. However, thermochemical hydrogen production processes are at a stage of conceptual design, and performance of system and components are at R&D level. There is not enough technical data to estimate the plant cost at present. Then experimental factors are applicable to estimate plant construction cost of thermochemical processes. The Lang–Chilton factor listed in Table 3.19 is one of the conventional experimental cost estimation factors in the chemical industry. The lower value of the factor can be applied to estimate the construction cost of NOAK plant. The construction cost can be estimated from the component cost which can be preliminary calculated based on the conceptual design of thermochemical hydrogen production system.

Hydrogen production cost is estimated by the following equation:

$$\text{Hydrogen production cost} = \frac{\text{Capital cost} + \text{Operation cost} + \text{Energy cost} + \text{Material cost}}{\text{Amount of produced hydrogen}}$$

TABLE 3.19. LANG–CHILTON FACTOR

Item	Factor	
Components	1.0	
Installation	0.43	× (a)
Piping	0.1~0.3	× {(a)+(b)}
Instrumentation	0.05~0.1	× {(a)+(b)}
Outdoor wiring	0.05~0.15	× {(a)+(b)}
Auxiliary system	0.25~1.0	× {(a)+(b)}
Buildings	0.05~0.2	× {(a)+(b)}

Capital cost includes depreciation cost, property tax and business income. Operation cost includes maintenance cost, miscellaneous cost, personnel cost, and insurance cost. Energy cost includes heat cost and electricity cost. Material cost includes water cost and catalyst cost.

Table 3.20 shows an example of cost factor in chemical industry plant in Japan. Depreciation cost of 10% means that key components will be replaced every 10 years depending on their lifetime under corrosive conditions. Each thermochemical hydrogen production process is different in energy and material consumption rate. It is assumed that heat consumption rate is α MJ/Nm^3, electricity consumption rate is β kWh/Nm^3 and material consumption rate γ US cents/Nm^3. Operator fee is assumed at δ cents/ Nm^3. If hydrogen plant component cost is X million US $ for the thermal power of 170 MW, hydrogen production efficiency is 50% and load factor is 80%, the hydrogen production plant construction cost is 2.1×X million $ and the amount of hydrogen production is 168.2 million Nm^3/a.

$$\text{Capital cost} = \frac{0.2919 \times \text{million US\$}}{168.2 \text{ million Nm}^3} = 0.174 \times \text{UScents/Nm}^3$$

$$\text{Operation cost} = \frac{0.1029 \quad \text{million US\$}}{168.2 \text{ million Nm}^3} + \delta \text{ UScents/Nm}^3 = \left(0.061X + \delta\right) \text{UScents/Nm}^3$$

$$\text{Energy cost} = 5.4 \text{ UScents/MJ} \times \alpha \text{ MJ/Nm}^3 + 4.34 \text{ UScents/kWh} \times \beta \text{ kWh/Nm}^3$$

$$= \left(5.4\,\alpha + 4\ 34\,\beta\right) \text{UScents/Nm}^3$$

Then the hydrogen production cost is estimated by the following equation:

$$\text{Hydrogen production cost} = (0.235 \times +5.4\alpha + 4.34\beta + \gamma + \delta) \text{ cents/Nm}$$

	Factor
Depreciation cost (%)	10
Property tax (%)	1.4
Business income (%)	2.5
Maintenance cost (%)	3
Insurance (US cent/kWh)	0.6
Miscellaneous cost (%)	1.3

3.2. NUCLEAR DESALINATION

3.2.1. Cogeneration (thermal/membrane)

The nuclear reactor supplies energy to desalination systems either in the form of heat or mechanical/electrical energy. It supplies thermal energy for distillation processes such as MSF, MED, or MED/TVC, as for desalination processes that require energy in the form of electricity such as RO and MVC. The power is supplied from a dedicated plant or electrical grid to drive the high pressure pump for the RO process and the main compressor of MVC. Apart from the basic energy for desalination, all desalination processes require electricity for pumping, auxiliaries and other services.

Steam can also be bled off at suitable points in the secondary circuit of the power plant for use by the desalination plant. However, protective barriers must be included in all modes to prevent potential carry-over of radioactivity. The power plant condenser cooling water is usually discharged to the sea as waste heat. In a contiguous plant, it is possible to use this heated seawater as feed to an RO desalination plant, thereby improving the performance of the desalination plant. In this arrangement, waste heat from the power reactor is used to improve the efficiency of the RO plant.

The steam needed for heating in desalination plants is at a low temperature and pressure in general. The high temperature version of MSF and MED plants use saturated steam in the range of 100°C to a maximum of 140°C. Some plants use saturated steam of 80°C to 100°C, while the LT-HTME system operates with steam in the range of 60°C to 80°C.

Desalination plants can be coupled as a single purpose plant or a cogeneration plant. In the case of a single purpose nuclear desalination plant, energy is exclusively used for the desalination process, and the desalted water is the only product output. The nuclear reactor is fully dedicated to supplying energy for desalting. In case of a cogeneration plant, only a part of the energy is utilized for desalting. A cogeneration plant produces both electricity and water simultaneously.

When a nuclear reactor is used to supply steam for desalination, the method of coupling has a significant technical and economic impact. The optimum method of coupling depends on the size and type of the reactor, the specific characteristics of the desalination process, and the desirability and value of electricity generation as a co-product. In the next two sections some types of nuclear reactors which can play the role of cogeneration plants are listed and also the most important desalination processes are analyzed [151, 152].

3.2.1.1. MED desalination processes

i. MED (multi-effect desalination)

The multi-effect desalination process is an old process and as the result of the scaling problems which are associated with the old design of these early units, the multi-stage flash process was introduced as an alternative in the 1960s. Recently considerable improvements in MED desalination systems have been introduced to reduce the undesirable characteristics of the old MED submerged tube evaporators such as low heat transfer rate and high scale rate formation. Falling film evaporators such as vertical tube evaporator and the horizontal tube evaporator of new MED plants have a number of distinct advantages. They provide higher overall heat transfer coefficients and low specific heat transfer surface area if compared to MSF desalination systems. They do not employ recycling and are thus based on the once through principle and have low requirements for pumping energy. Using compressed vapour can enhance the performance of the plant and therefore reduce the power consumption of

MED/TVC plants which can be only around 2 kWh/m^3 as there are no requirements to recirculate large quantities of brine. The combination of high performance ratio and low power consumption results in lower overall energy costs. Multi-effect distillation also offers the possibility of reducing plant size and footprint. However, there are some problems which are associated with MED systems such as the complexity of morphology and the limitation of production capacities [153].

MED consists of a series of evaporators (effects) with each subsequent effect operated at a lower pressure. This permits the feed seawater to undergo multiple boiling without supplying additional heat after the first effect. In an MED plant, the seawater is heated to the boiling point after being preheated in tubes and then enters the first effect. Seawater is either sprayed or otherwise distributed onto the surface of evaporator tubes in a thin film to promote rapid boiling and evaporation. The tubes are heated by steam from a boiler, or other sources, which is condensed on the opposite side of the tubes. The condensate from the boiler steam is recycled to the boiler for reuse.

Only a portion of the seawater applied to the tubes in the first effect is evaporated. The remaining feed water is fed to the second effect, where it is again applied to a tube bundle. In turn, these tubes are heated by the vapours created in the first effect. This vapour is condensed to form the product water, while giving up heat to evaporate a portion of the remaining seawater feed in the next effect. This continues for several effects, with up to 20 effects being found in a typical large plant.

In order to analyze this process thermodynamically, the balances of the system need to be determined.

(a) Mass balance

$$M_f = M_D + M_b \quad [m^3/d]$$

where

M_f is the feed flow rate,
M_D is the distillate flow rate, and
M_b is the brine flow rate.

(b) Salt balance

$$X_f \times M_f = X_b \times M_b$$

where X_f is the feed-TDS (total dissolved salts), and X_b is the brine-TDS.

(c) Distillate mass flow rate

$$M_D = \sum_{k=1}^{n} D_k + \sum_{k=2}^{n} d_k$$

where

D_k is the distillate by boiling,
d_k is the distillate by flashing, and
n is the number of effects.

(d) Energy balance

- First effect:

$$M_h \times \lambda_h = M_f C_P (T_1 - t_2) + D_1 \times \lambda_D$$

where

M_h is the heating steam flow rate,
λ_h is the latent heat of heating steam,
C_p is the heat capacity,
T_1 is the boiling temperature,
t_2 is the feed temperature,
D_1 is the distillate in first effect,
λ_D is the latent heat of distillate.

- Second effect:

$$d_2 = (M_f - D_1) \times C_P \frac{T_1 - T_{2'}}{\lambda_{VJ'}}$$

where

$T_{2'}$ is the flashing vapour temperature,
$\lambda_{VJ'}$ is the latent heat of flashing vapour temperature.

- Other effects:
  - the amount of vapour formed by boiling in the effect i

$$D_i = \frac{D_{i-1} \times \lambda_{i-1}}{\lambda_i}$$

  - the amount of vapour formed by brine flashing in the effect i

$$d_i = \left(M - \sum_{j=1}^{i-1} D - \sum_{j=2}^{i-1} d_j \right) \times C_P \times \frac{T_{i-1} - T_i'}{\lambda_i}$$

  - the amount of produced water M_d:

$$M_d = \sum_{j=1}^{n} D_j + \sum_{j=2}^{n} d_j$$

  - the gain output ratio:

$$GOR = \frac{M_D}{M_h} = M_D \frac{2330}{Q_{th}}$$

    with the thermal heating steam energy, Q_{th} [kW(t)]:

$$Q_{th} = M_h \times \lambda_h$$

    where M_h is the heating steam flow rate and λ_h is the latent heat of the heating steam.

  - The electrical power consumption [154]:

$$q_{di} = \frac{M_D \times Q_{sdp}}{24 \times 1000}$$

    where $Q_{sdp} = 0.03\ Q_{th}$ [155].

ii. MED/TVC (thermal vapour compression)

The thermal vapour compression desalination technology utilizes the MED process with a steam jet compressor as the heat pump (Fig. 3.46). Steam jet compressors use motive steam at pressures ranging between 0.3 to 1 MPa.

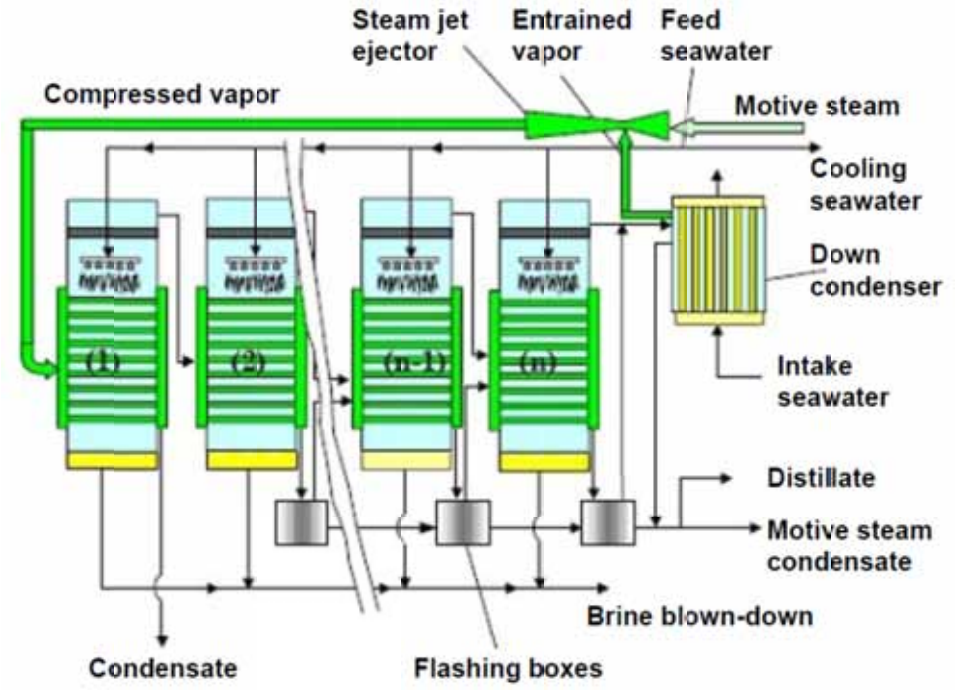

FIG. 3.46. Multi-effect evapouration with thermal vapour compression (MEE/TVC).

The design of the steam jet ejector (Fig. 3.47) depends, in general, upon the entrainment ratio which is defined as [154]:

$$Ra = \frac{m_1}{m_m}$$

where

m_1 is the entrained vapour mass flow rate, [m^3/d],
m_m is the motive steam mass flow rate, [m^3/d].

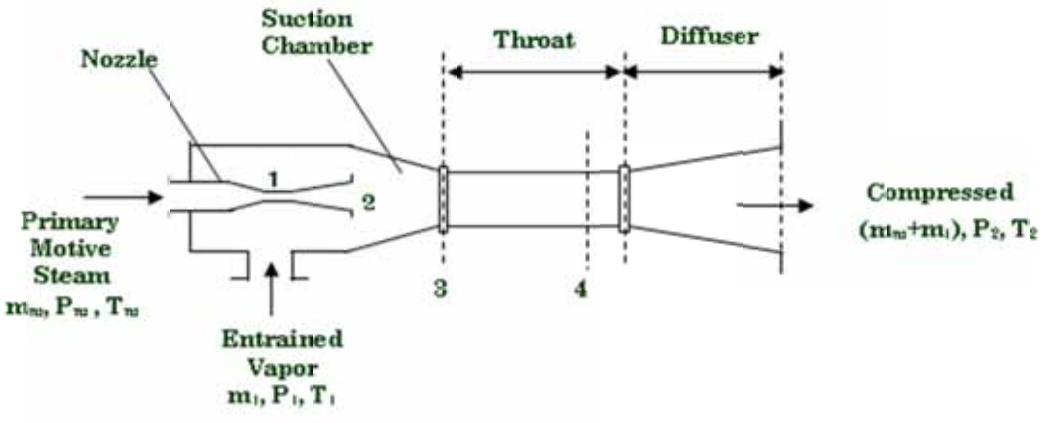

FIG. 3.47. Steam jet ejector.

The entrainment ratio can be calculated by the following empirical equation [154]:

$$Ra = 0.296 \times \frac{P_2^{1.19}}{p_1^{1.04}} * \left(\frac{p_m}{p_1} \right)^{0.015} \times \left(\frac{PCF}{TCF} \right)$$

where

p_2 is the compressed vapour pressure,
p_1 is the entrained vapour pressure,
p_m is the motive steam pressure,
PCF is the pressure correction factor, and
TCF is the temperature correction factor,
and with the last two factors defined as:

$$PCF = 3 \times 10^{-7} (p_m)^2 - 0.0009 (p_m) + 1.6101$$

$$TCF = 2 \times 10^{-8} (T_1)^2 - 0.0006 \ (p_m) + 1.0047$$

The mass balance equation through the ejector is:

$$m_2 = m_m + m_1$$

where m_2 is the compressed vapour flow rate at the steam jet ejector outlet.

Therefore, the plant performance ratio can be defined as follows:

$$PR = \frac{m_d \times 2253}{m_m \times \lambda_{Tm}} \times \eta$$

where η is the ejector efficiency defined as

$$\eta = \frac{\text{Total Energy Output}}{\text{Total Energy Input}}$$

iii. RO (reverse osmosis)

Osmosis is the natural process by which water flows through a semi-permeable membrane from pure or dilute solution to a more concentrated solution. The flow continues until the resulting osmotic head equals the osmotic pressure of the solution. If a pressure higher than the natural osmotic pressure of the solution is applied, the direction of the water flow is reversed. The solution becomes more concentrated, and purified water is obtained on the other side of the membrane, hence the term ‘reverse osmosis’ [156].

The RO desalination process was developed in the USA in the 1960s, and a first test plant was built in 1965. Since its commercial application to seawater in 1970, plants of larger and larger capacities have been designed, constructed and successfully operated.

An RO desalination plant mainly consists, as shown in Fig. 3.48, of a pretreatment section, a high pressure pump section, a membrane module section, and a posttreatment section. In general all modern large scale RO plants use power recovery turbines where the pressure of the concentrate is utilized to reduce the overall power consumption of the system. Membranes can be sensitive to pH, temperature, chemicals, etc., and are highly sensitive to fouling and clogging. Proper design of the system and pretreatment of the water can minimize these problems and hence protect the membranes.

The principles governing the operation of RO plants are:

1. The water flux through any given membrane is proportional to the effective pressure difference across it.

2. Salt also diffuses through the membranes. This diffusion is independent of the pressure difference, and depends only on the difference in concentration between the feed and product waters and the nature of the membrane.

In the process, saline water is pumped to pressurize it against a membrane in a container. As desalted water from the feed solution passes through the membrane, the remaining solution becomes more concentrated. A valve allows a portion of the feed water to be discharged without passing through the membrane. Without this discharge (or blow down), the concentration of dissolved salts in the feed solution would continually increase, requiring the pump to add ever-increasing energy to overcome the increased osmotic pressure, and precipitation of super-saturated constituents in the brine would occur.

The product water emerging from the membrane assembly generally needs some type of posttreatment before being distributed as potable water. Such posttreatment includes pH adjustment, usually by the addition of a base, removal of dissolved gases such as H_2S and CO_2 by air stripping, and/or disinfecting.

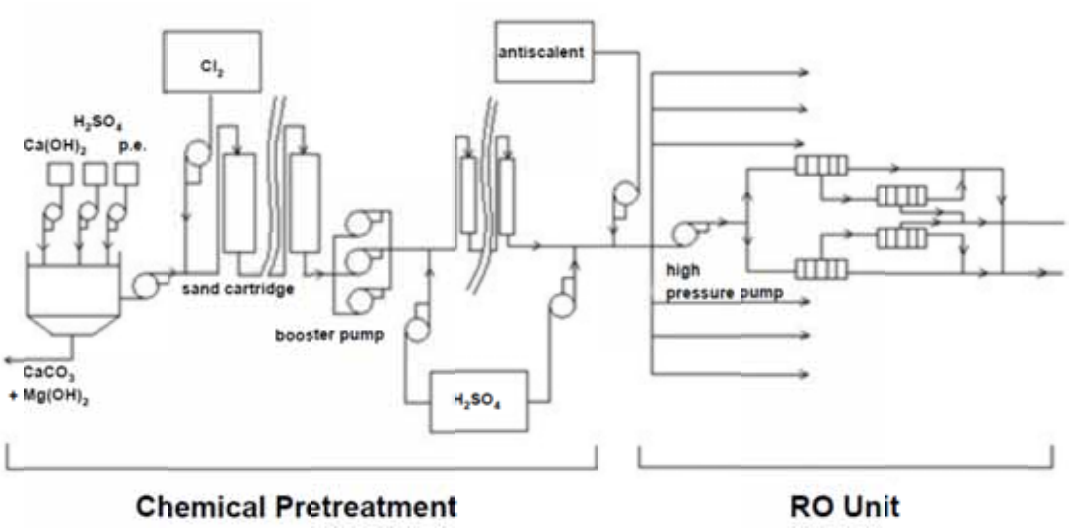

FIG. 3.48. Schematic representation of the RO plant.

3.2.1.2. Merits of cogeneration

There are benefits arising from the use of the standard reactor design. First there is the use of waste heat from the nuclear power generation process and the ability to optimize the overall system design, while other benefits result from an innovative cogeneration system design. A fully integrated cogeneration design based on co-located nuclear energy and desalination systems allows for shared land acquisitions and commonality of many on-site facilities including water intake and outfall structures, staff, maintenance as well as administrative facilities. These all have clear economic benefits. Fresh water and electrical transportation costs may also be reduced through the use of common rights-of-way to bring these two resources to their markets. By designing the power plant and desalination facility to operate independently even though they are thermally coupled, show that the system allows for flexibility of phased increases in the size of the desalination plant with no collateral requirement to modify the power plant.

Additionally coupling the reactor with the desalination system in this manner provides the flexibility of varying water production without adversely impacting the operation of the power plant. The nuclear power plant can be operated at maximum electrical production

efficiency, while the desalination plant is operated so that fresh water production meets or exceeds requirements under various operating conditions, including annual variations in site specific feed water conditions and daily variations in demand. During periods where the power plant is off-line and the feed water preheat is unavailable to the desalination plant, the desalination process can still continue, at a reduced efficiency. Through this combination of design and performance optimization, the unique electrical and thermal coupling of the energy source and desalination system shows significant improvements in water production efficiency and reductions in desalination plant capital cost. The result is a reduction in levelized water production costs. Although the costs for any given facility are highly specific to the site, seawater conditions and other design requirements, detailed cost assessment models, nevertheless, indicate that savings typically on the order of 10–15% in plant capital cost and 10–20% in water production costs are achievable.

3.2.1.3. PBMR desalination concepts

The PBMR cogeneration desalination configuration is based on a multi-module PBMR plant of 1500 MW(th) capacity producing steam for a power cycle, using a back-pressure steam turbine generator exhausting extraction steam into a thermal desalination plant. The steam that is extracted from the turbine is used as the heating source for desalination, with the back-pressure value being specific to the desalination technology. The three desalination plant technologies considered for this cogeneration configuration are MED, MED with TVC, and MSF.

A schematic of the possible coupling is shown in Fig. 3.49. It should be noted that coupling a thermal desalination system to a back-pressure turbine eliminates the need for a condenser and a cooling system, however, it does result in a lower electrical output than a full condensing Rankine cycle solution. It is not necessary to use a dump condenser since there are multiple trains in the desalination system. It can also be assumed that if one or two units fail, the rest of the units can accommodate extra steam mass flow. However, in the event of failure of a significant number of units, the PBMR plant would have to reduce its output.

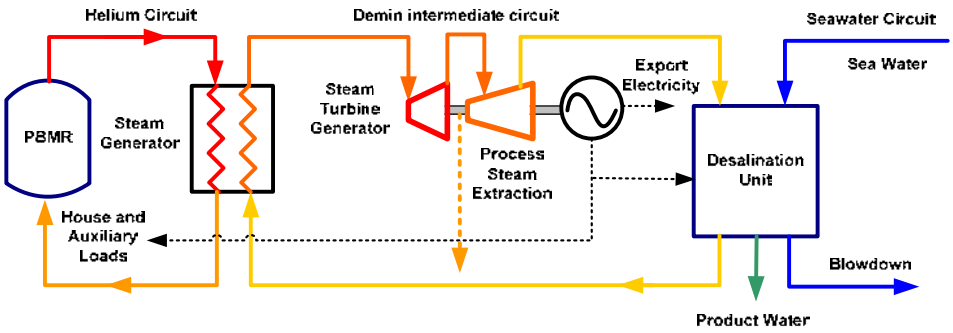

FIG. 3.49. Integrated cogeneration desalination schematic.

The amounts of water and power that could be produced by such a cogeneration configuration depend much on the desalination technology and the associated turbine back-pressure value. For the MED and MED-TVC desalination technologies, the minimum required turbine back-pressure value was assumed, as a higher back-pressure than the minimum required results in a significant reduction in power production, which is not outweighed by the insignificant increase in desalination water production. For the MSF desalination technology, two turbine back-pressure values are considered (0.1646 MPa and 0.09 MPa).

This production is also affected by the number of effects used in a desalination unit and the temperature rise in the desalination unit condenser. Having more effects or a smaller temperature rise in the condenser reduces the temperature drop of steam across each effect and significantly increases the amount of desalinated water that can be produced. This increase in desalinated water production, however, requires a significantly larger heat transfer surface area (and corresponding higher equipment costs). In this comparison of cogeneration configurations, additional MED and MED-TVC cases were considered with twice as many effects (ten effects instead of five effects) and a reduced condenser temperature rise (10°C instead of 20°C) to mitigate the higher equipment costs. A comparison of these different technologies and the associated parameters is illustrated in Table 3.21.

TABLE 3.21. COGENERATION CONFIGURATION SYSTEM DESIGN AND PERFORMANCE SUMMARY

	Case A	Case B1	Case B2	Case C1	Case C2	Case D1	Case D2
Desalination technology	—	MED	MED	MED-TVC	MED-TVC	MSF	MSF
Turbine back-pressure (MPa)	0.003	0.032	0.032	0.138	0.138	0.165	0.090
Number of desalination effects	—	5	10	5	10	—	—
Number of desalination stages	—	—	—	—	—	21	6
Number of desalination units in plant	—	13	25	18	30	4	4
Desalination production capacity (km^3/d)	0	145	277	198	339	223	155
Export power production capacity (MW(e))	655	549	543	476	469	419	447

— data not available.

3.2.2. Waste heat (thermal/RO)

Waste heat is defined as the released heat from the nuclear power plant after it has been used to drive the turbine to produce electricity. Some designs are listed below have useful applications for the waste heat.

3.2.2.1. Helium cooled GT-MHR with MED

A great advantage of the GT-MHR is that its design allows the utilization of waste heat from its intercooler and precooler exchangers at ideal temperatures for desalination (80 to 100°C). Because this heat is sent to the heat sink anyway, it is considered virtually free for desalination. However, calculations show that at the Skhira site in Tunisia, for seawater temperature of 21°C and helium temperature of 26°C at the output of the intercooler or the precooler, the maximum amount of heat available to the MED plant is about 43 MW(th) for two GT-MHR modules. This would correspond to a production of 43 500 m^3/day [149] as shown in Fig. 3.50.

3.2.2.2. Experimental work on BARC LTE plant

A 30 m^3/day low temperature evaporation (LTE) desalination plant using nuclear waste heat from the primary coolant water system of the nuclear research reactor CIRUS was installed for production of fresh water (Fig. 3.51). The unit operates at 41°C and 94.7 kPa. The LTE unit was operated at different temperatures of heating medium ranging from 50–65°C. Conductivity of the product water is in the range of 5 μS/cm. This water is used as make-up water for the reactor. Table 3.22 gives the performance of the desalination plant at various hot water temperatures for reactor rating varying from 20–40 MW [157].

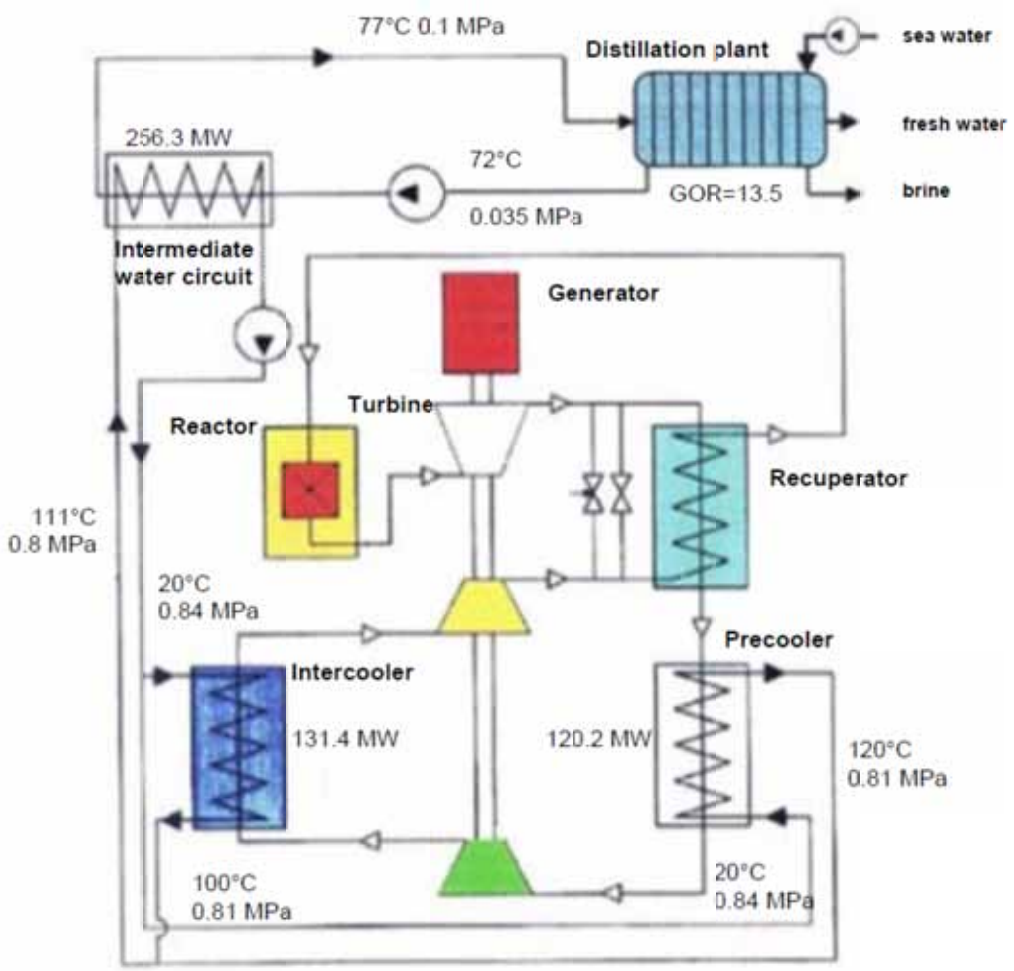

FIG. 3.50. Principal diagram of the GT-MHR plant coupled with a MED desalination plant.

FIG. 3.51. LTE desalination plant using waste heat of CIRUS nuclear reactor in BARC Mumbai for seawater desalination.

TABLE 3.22. OPERATIONAL DATA OF THE BARC LTE UNIT

Sl. No.	Production rate of desalted water (m^3/d)	Temperature of heating medium (°C)	Heat load (MJ/h)
1	9.0	50	910.4
2	15.8	55	1586.6
3	25.2	60	2633.5
4	31.7	62	3173.2

Recently an innovative modification to this technology has been made and the technology of a two-effect LTE desalination plant with cooling tower has been developed (Fig. 3.52).

In this plant total raw water requirement has been significantly brought down (by a factor of 30). This plant utilizes low grade waste heat as energy source for desalination [158].

FIG. 3.52. Two-effect LTE desalination plant with cooling tower.

3.2.2.3. Preheating of the feed water for RO system

This concept utilizes low grade heat that is otherwise lost in such essential but environmentally unfriendly power production elements as condenser cooling systems where very large quantities of water, typically 10 degrees and more above ambient, are discharged into the environment. The operation of RO systems at higher temperatures increases the efficacy of production. Cost savings are found at all temperatures where waste heat can be used to preheat the feed water. But the overall savings depend on a number of factors that is site specific including the TDS of the feed water, the size of the plant, etc. A criticism of preheated feed water that has sometimes been expressed is the fact that, as the temperature goes up, the TDS of the product water rises. This is, of course, correct if all other factors remain the same. However, this effect is manageable with a correct system design [157].

3.2.2.4. Coupling of RO and CANDU-6

An advanced concept for the design and operation of RO seawater desalination systems was first presented by CANDESAL in 1993 [159]. Preheated feed water is one of the key features of this concept, which is a feature now being considered for a number of current desalination systems. The use of reactor plant condenser cooling water as a preheated feed stream for the desalination plant allows for substantial gains in fresh water production efficiency, resulting in reduced plant capital cost as well as reduced energy consumption per unit of water produced. In addition to the condenser cooling water, the design of the CANDU reactors allows for the use of waste heat from its moderator cooling water system giving an additional temperature rise to the RO system feed water. Other reactors which do not offer this source of waste heat, are restricted to the availability of waste heat from the condenser cooling water resulting in a maximum feed water preheat available of only about 40°C. An analysis carried out by CANDESAL showed that this additional source of waste heat can be used to further increase the temperature rise of the feed water stream by as much as 9°C under the design conditions of the specific case analyzed. This results in significant performance improvement. A schematic of the CANDU-6/RO nuclear desalination system is shown in Fig. 3.53.

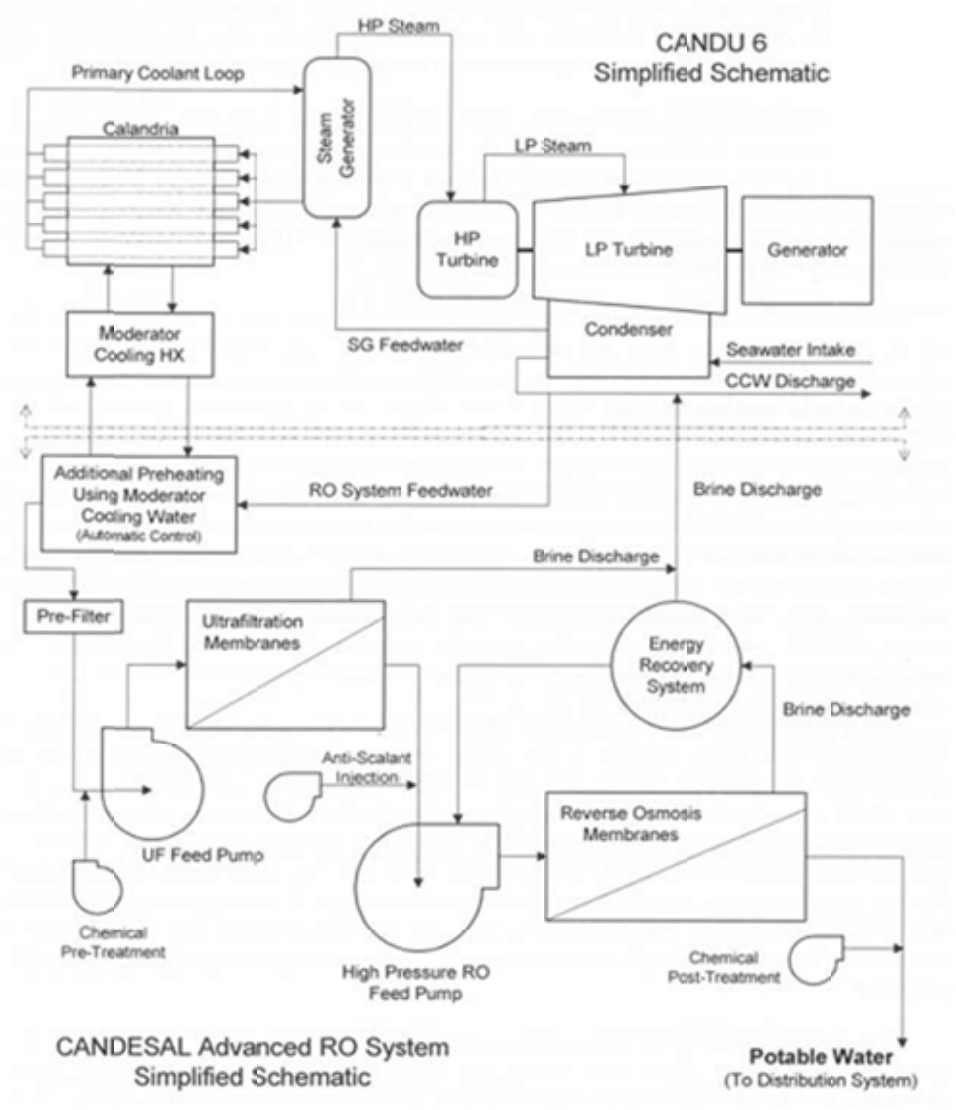

FIG. 3.53. Simplified schematic of the CANDU-6 CANDESAL nuclear desalination system.

3.2.2.5. PBMR power plant with MED

The waste heat utilization desalination configuration is based on a 400 MW(th) PBMR power plant configuration that uses a Brayton cycle for its power conversion through a single shaft recuperative Brayton cycle with helium as working fluid. The Brayton cycle uses a precooler and intercooler to cool the helium before entering the low pressure compressor (LPC) and the high pressure compressor (HPC) respectively. The precooler and intercooler together rejects ~218 MW(th) of waste heat at ~73°C and ~63°C, respectively. This waste heat is ideally suited for some low temperature desalination processes and can be used without negative impact on the power output and efficiency of the nuclear power plant.

In order to aid decision making regarding the feasibility of a PBMR coupled with desalination technology, a comparative economic study is performed. This comparative study includes an LT-MED desalination plant utilizing the rejected waste heat as well as an RO plant for water production. An LT-MED plant was selected based on the utilization of waste heat together with recent advances in lower capital costs. A preliminary design was conducted to determine the maximum water production associated with different configurations. Figure 3.54 illustrate a typical coupling arrangement of an LT-MED plant to the initial proposed PBMR.

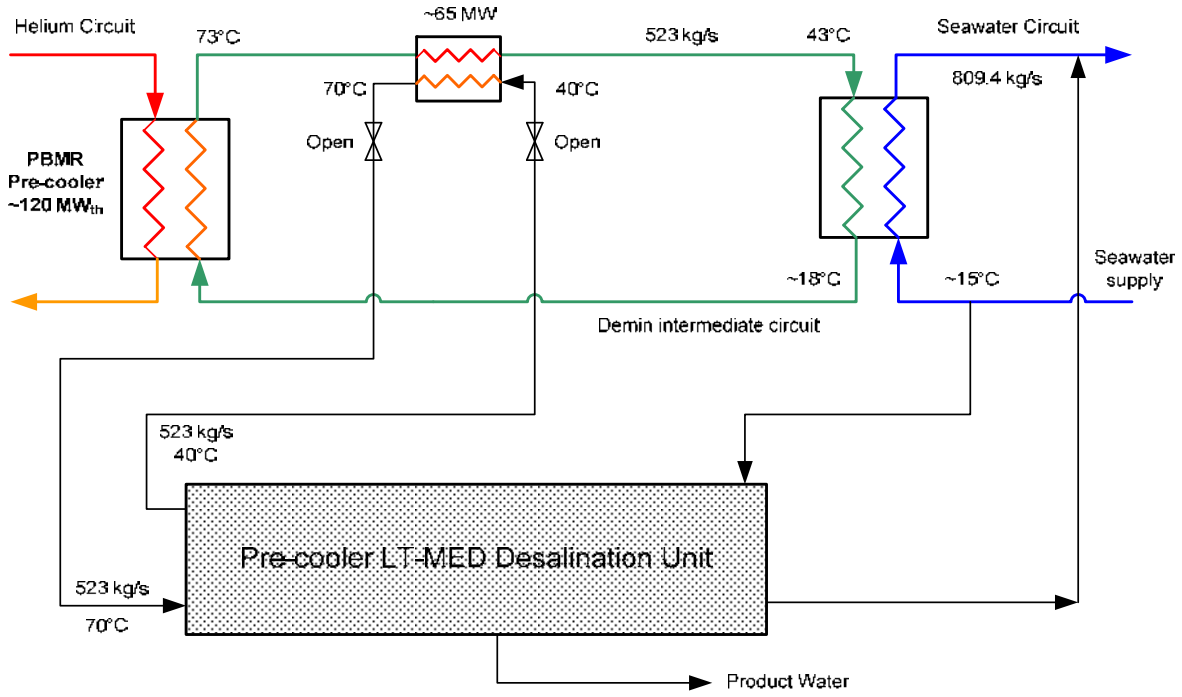

FIG. 3.54. PBMR coupled LT-MED layout.

An RO plant can also be coupled to the initial PBMR utilizing a portion of the electricity generated by the this plant, as well as the rejected water from the ultimate heat sink system as feed water to the desalination plant. The ultimate heat sink system rejects 2475 kg/s of heated seawater at 39°C through the existing Koeberg outfall structure. The elevated temperature of the seawater feed to the RO plant results in an increase in the flux of desalted water through the RO membranes. This results in less membrane area required compared to an RO plant that utilizes cold feed water directly from the ocean. The reduction in the required membrane area reduces the capital and membrane replacement cost of the RO plant substantially. A proposed integration of such a plant is illustrated in Fig. 3.55.

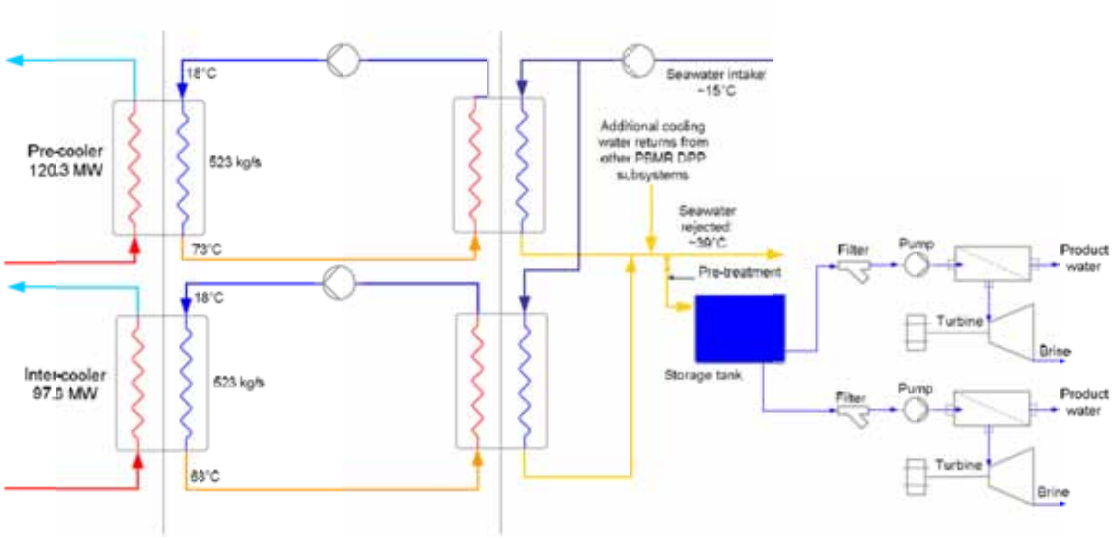

FIG. 3.55. PBMR coupled RO layout.

3.2.3. Techno–economics: elements and methodology of costing

3.2.3.1. Methodology of desalination cost

There are several factors which affect desalination costs and thus determine the successful implementation of desalination systems, using nuclear or other energies. These factors include [151, 153, 160]:

- Site characteristics: The main parameters at a given site are the availability of adequate land and its proximity to the water source and of the concentrated brine discharge locations. The geological nature of the terrain may also be a factor influencing pumping costs and the costs of pipe installations. Yet another factor influencing land cost could be the local regulatory requirements and the costs associated with the acquisition of permits, etc.
- Plant capacity: This is an important design factor in that according to the size effect law, the desalted water costs is reduced as plant capacity is increased, even though large capacity plants require high initial investment, larger sizes of treatment units, pumps, water storage tanks and water distribution systems. Generally these effects are offset by the modularity of the system and economy of scale.
- Feed water quality: it is obvious that the lower the salinity (TDS) of the feed water, the lower would be the energy consumption of the system. Low TDS would also lead to high conversion rates and less dosing of antiscalant chemicals. Similarly, the pretreatment of surface waters (e.g. tidal waters) will be more costly as compared to brackish ground water or water from beach wells.

In most methodologies, the construction cost of a desalination plant, for example, is the sum of the direct and indirect costs:

Direct costs include

- land and site permit cost which depend on the local site characteristics and plant ownership (public or private);
- cost of production wells which depends on plant capacity and well depth;
- surface water intake structure cost which depends on plant capacity and local environmental regulations;

- process equipment cost including the cost of water treatment units, instrumentation and control systems, pre and posttreatment systems, and cleaning systems;
- auxiliary equipment cost which includes the cost of open water intakes, wells and storage tanks, generators, transformers, pumps, pipes, valves, electricity, etc.;
- cost of building offices, control room, laboratories, workshops, and other structures.

Indirect costs are mainly the costs of

- freight and insurance, which is typically 5% of the total direct costs;
- construction overheads, which include labor costs, fringe benefits, field supervision, temporary facilities, construction equipment, small tools, contractor's profits, and miscellaneous expenses. Typically this cost is about 15% of the direct material and labor costs;
- owner's cost, representing the costs of land acquisition, engineering and design, contract administration, commissioning and legal fees, etc.;
- contingency cost, representing from 4 to 10% of the total direct costs.

Methodology of costing:

The specific water cost is defined as the annuity of potable water expenditures divided by the annuity production of water [155, 160].

The annuity of potable water expenditures (C_0) includes capital cost C_{ca} and operation and maintenance $C_{O\&M}$ and power consumption C_P.

$$C_o = C_{ca} + C_{O\&M} + C_P$$

where the annuity capital cost, C_{ca}, is defined as:

$$C_{ca} = C_{TO}\, a_n \text{ with } a_n = \frac{r \times (r+1)^n}{(1+r)^n - 1}$$

where

r is the discount rate,
n is the lifetime of the plant.

It is assumed that r = 7% and n = 30 years, therefore, $a_n = 0.11$. C_{TO} is given by:

$$C_{TO} = \left(C_{VO} + C_o\right)\left(1 + IDC\right)$$

where

C_{VO} is the vendor overnight cost,
C_o is the owner's cost.

IDC is the factor for the 'interest during construction' which is written as:

$$IDC = (1 + i_{cs})^{\frac{i_{cs}}{2}} - 1$$

where i_{cs} is the interest rate during construction.

Local prices for items and labor, foreign supplier prices, and the cost methodology mentioned above are used to calculate the specific water cost for the Syrian case study in the IAEA coordinated research programme (CRP) on 'economics of nuclear desalination — new developments and site specific studies' as shown in Table 3.23.

TABLE 3.23. COST EVALUATION FOR THE DESALINATION PLANT

Item	Value
RO Water plant total construction cost (M US $)	177.96
RO Water plant O&M cost (M US $/a)	9.81
Pumping power (HP + seawater and booster pump) (MW(e))	50
Specific power consumption for RO (kW(e)/m^3)	6.72
Specific cost for RO (US $/$m^3$)	0.2
Water cost (power cost 0.03 US $/kWh and I=6%) (US $)	0.55
MVC total construction cost (US $)	17 433 672
MVC Annual O&M cost (US $/a)	784 512
Energy (consumption & cost) for the MVC electric (kW(e)/m^3) thermal (kW(t)/m^3)	 10.5 —
Water cost (power cost 0.03 US $/kWh and I=6%) (US $)	0.48
MEE total construction cost (US $)	20 131 539
MEE annual O&M cost (US $/a)	905 919
Energy consumption for MEE electric (kW(e)/m^3) thermal (kW(t)/m^3)	 2.1 47.5
Power cost electric (US $/kW(e)) thermal (US $/kW(t))	 0.03 0.005
Water cost (power cost 0.03 US $/kWh and I=6%) (US $)	0.66
TVC-MEE total construction cost (US $)	28 500 000
TVC-MEE annual O&M cost (US $/a)	784 000
Energy (consumption & cost) for the TVC-MEE electric (kW(e)/m^3) thermal (kW(t)/m^3)	 2 38.64
Water cost (power cost 0.03 US $/kWh and I=6%) (US $)	0.55
Charge rate a_n and IDC for I_s = 6% for I_s = 8% for I_s = 10%	 a_n = 0.066 IDC = 0.0017 a_n = 0.084 IDC = 0.0030 a_n = 0.102 IDC = 0.0045

— data not available.

The three parameters interest rate, power cost, and plant availability were chosen to carry out sensitivity analysis as shown in Figs 3.56, 3.57, and 3.58. A comparison of water cost for MEE versus TVC-MED is given in Fig. 3.59.

3.2.3.2. PBMR desalination system

i. Capital and O&M costs

The cogeneration desalination systems were compared as incremental investments superimposed on a base PBMR power plant. The capital and O&M costs of desalination plants were partially offset by reduced amount of equipment that is needed if a desalination system is integrated with a PBMR power plant. With an integrated desalination plant, the condenser, cooling water system, and a feedwater heater in the power cycle were no longer required. Additionally a smaller steam turbine and a less expensive electrical system were needed. The O&M costs of the desalination plant were similarly partially offset by the elimination of the condenser and cooling water system O&M costs. The incremental capital and O&M costs (i.e. the costs of desalination plant minus the cost savings associated with integrating the desalination plant with a PBMR plant) are shown in Table 3.24 for each case.

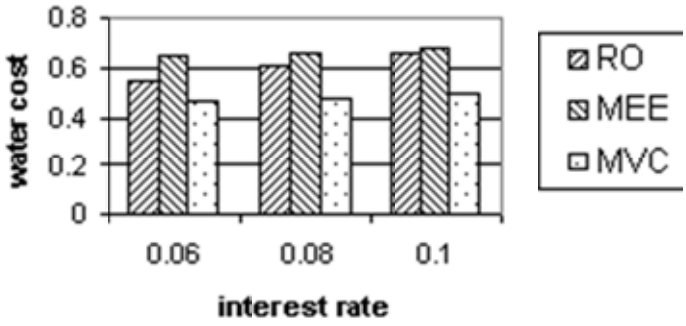

FIG. 3.56. Water cost vs. interest rate.

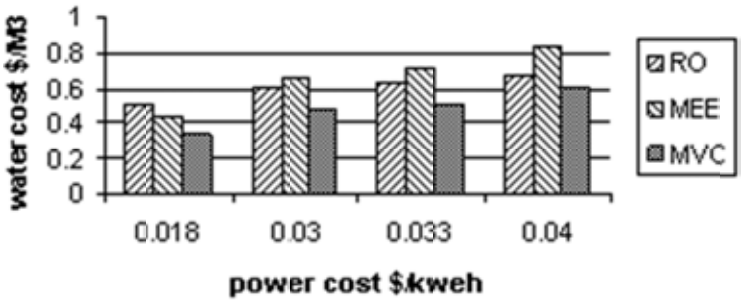

FIG. 3.57. Water cost vs. power cost.

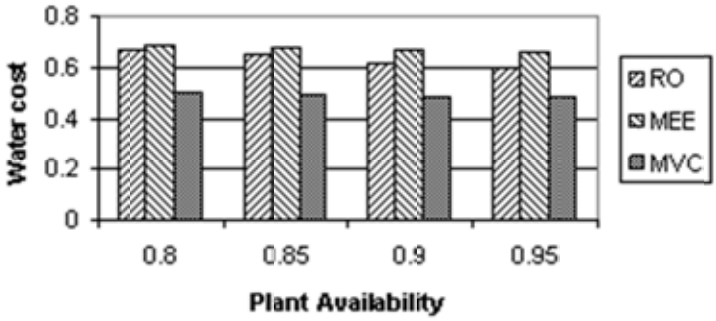

FIG. 3.58. Water cost vs. plant availabi

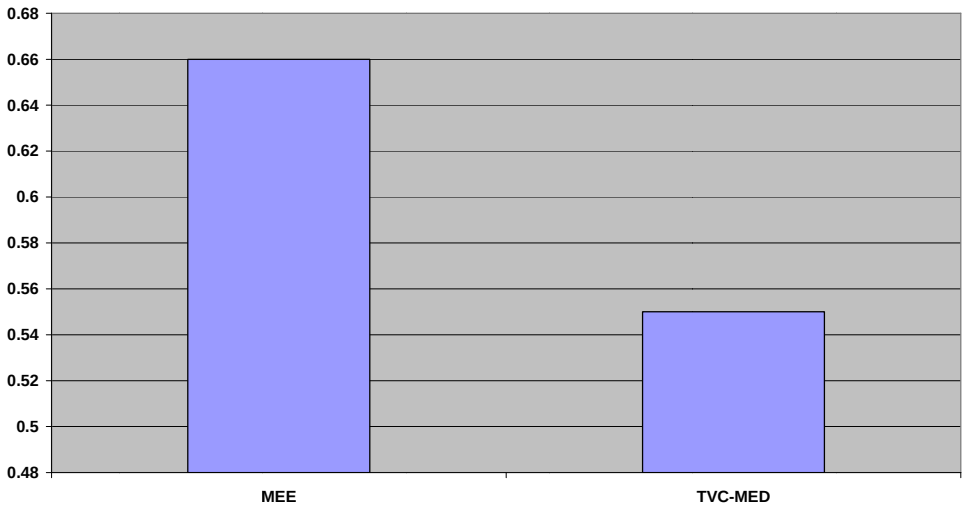

FIG. 3.59. Water cost for the MEE and TVC-MED assuming power cost of 0.03 US $/kWh.

TABLE 3.24. INCREMENTAL CAPITAL AND O&M COSTS

	Case B1	Case B2	Case C1	Case C2	Case D1	Case D2
Desalination technology	MED: 5 effects	MED: 10 effects	MED-TVC: 5 effects	MED-TVC: 10 effects	MSF: 0.165 MPa	MSF: 0.09 MPa
Incremental capital cost (M US $)	21	389	87	528	58	23
Incremental O&M cost (1st a) (M US $)	4	8	5	10	8	5

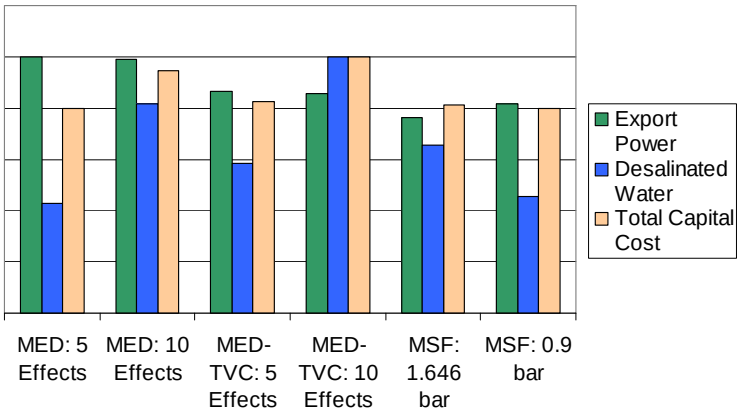

FIG. 3.60. Visualization of trade-offs.

The cases considered illustrate the trade-offs that exist when extraction steam is used to produce desalinated water. For the MED and MED-TVC technologies, increasing the number of effects will increase the water production as well as the capital cost. Reducing the turbine back-pressure will slightly increase the export power amount but will reduce the water production. Using the MED-TVC technology instead of the MED technology will increase the water production but reduce the amount of export power. Using the MSF technology instead of the MED or MED-TVC technologies will similarly increase the water production but reduce the amount of export power. These trade-offs are visualized in Fig. 3.60.

ii. Lifecycle cost

In order to compare these trades-offs quantitatively, a lifecycle economic analysis was performed. The lifecycle costs of each case were compared on a present value basis. The relative present values of the cases considered were highly sensitive to the values of export power and desalinated water. Because these values can vary greatly, depending on the specific location, the cases were considered for a variety of power and water values. Figure 3.61 shows the break-even water value for a range of power values. The power values are shown on the figure in 2008 Dollars, but are escalated through the life of the plant. Similarly the break-even water values are also shown in 2008 dollars and escalated through the life of the plant. For each power value, the breakeven water value is the value of water that must be obtained in order for the lifecycle present value of the cogeneration configuration case to equal the lifecycle present value of the power-only configuration case.

At power values below US $60/(MW·h), the MED technology with 5 effects requires the lowest water values to breakeven with the power-only configuration, varying from US $0.63/$m^3$ to US $1.12/$m^3$. With higher power values, the MED technology with 10 effects

becomes the more economical option as the increased capital cost is offset by the increase in revenue from the additional desalinated water production. It is critical that this economic analysis is on an incremental basis; for the entire project to be economical, the base case of the PBMR power plant must be covered by a sufficient amount of power sales. This economic analysis also assumes that a region needs all the desalinated water that is being produced in every case while the water production varies greatly depending on the case. In selecting a desalination technology, the water production needs of a region must be considered. While the largest desalination plants in the world have capacities above 500 000 m^3/d, there are many more plants with capacities in the 100 000 m^3/d to 200 000 m^3/d range, less than the capacities in several of the cases.

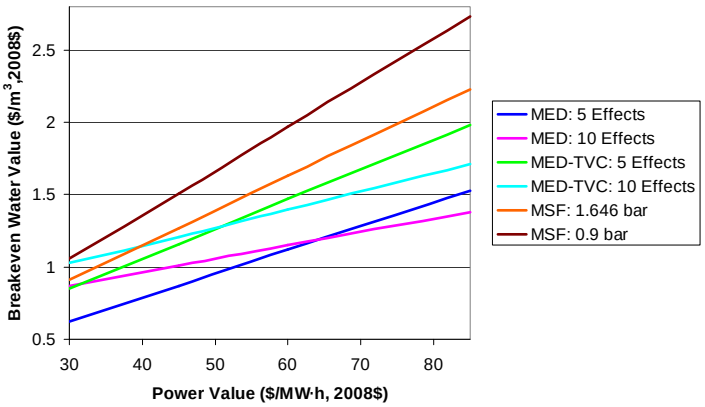

FIG. 3.61. Break-even water value versus power value.

iii. Waste heat option

A net present value (NPV) comparative study has been performed in order to assist the decision making with regards to adding a waste heat desalination plant to the Brayton cycle-based PBMR. This study has been performed between the proposed LT-MED process as well as RO for variations in specific capital cost as well as specific electric consumptions (in the case of the RO). A list of the general assumptions in this analysis can be found in Table 3.25, while it was also assumed that the PBMR base costs are covered by the selling of electricity.

TABLE 3.25. ECONOMIC PARAMETERS

Description	Value
General inflation	5
Capital escalation (%)	5.53
Electricity price escalation (%)	8
O&M escalation rate	5
Water price escalation rate (%)	5.53
Commercial start-up date	2015
Economic life (a)	25
Discount rate (%)	13.7
Tax (%)	35
Owners cost	5% of EPC [a] + $100k per month of construction
Contingency	10% of EPC [a]
Construction interest rate (%)	12.5

[a] EPC = energy performance certificate.

From these assumptions, a break-even water price analysis has been performed for both the LT-MED case with a specific capital cost of 1300 and 2000 US $/(m^3·day) and a RO system with capital cost of 700 and 900 US $/(m^3·day), respectively. The electrical consumption of the RO plant has also been varied between 3 and 5 kWh/m^3 while the electrical usage of the LT-MED has been fixed on 1.5 kWh/m^3.

Figure 3.62 illustrates the results from this break-even analysis and from it can be concluded that a LT-MED with low capital cost provides marginal better opportunities than all other options. The sensitivity of the LT-MED capital cost can, however, be seen from the fact that the 2000 US $/(m^3·day) option lies to the top of the graph. Another aspect worth noticing is the fact that as long as electricity cost are below 50 US $/MWh, the break-even point is still in the feasible range of ~1 US $/m^3. In agreement with these results are also the NPV graphs (Fig. 3.63) indicating the feasibility of a desalination scheme coupled to the initial PBMR as the major increase in NPV resulting from a higher water price.

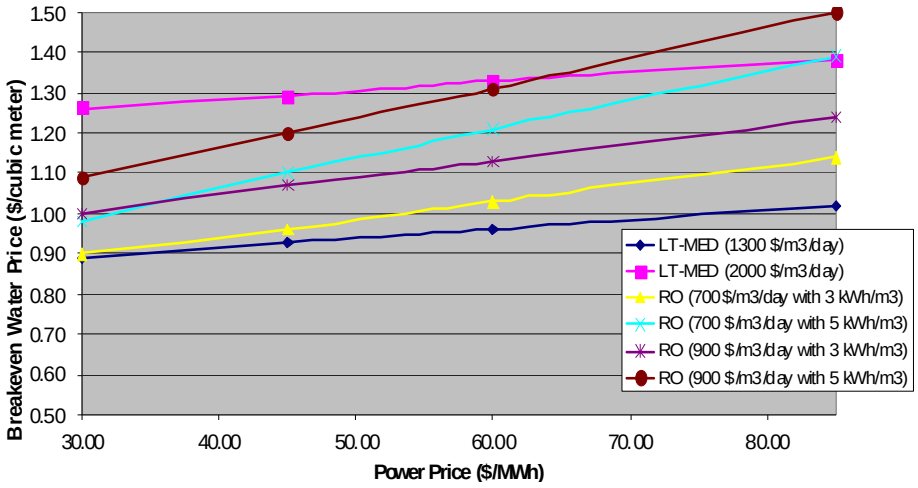

FIG. 3.62. Break-even water price vs. power.

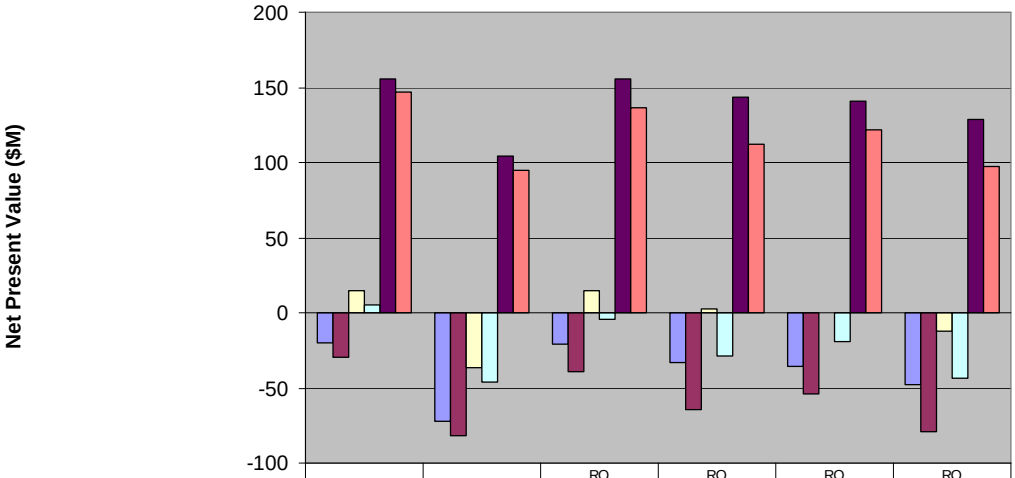

	LT-MED (1300 $/m3/day)	LT-MED (2000 $/m3/day)	RO (700$/m3/day - 3kWh/m3)	RO (700$/m3/day - 5kWh/m3)	RO (900$/m3/day - 3kWh/m3)	RO (900$/m3/day - 5kWh/m3)
Power = $30/MWh, Water = $0.75/cu meter	-20	-72	-21	-33	-35	-48
Power = $60/MWh, Water = $0.75/cu meter	-30	-81	-39	-64	-54	-79
Power = $30/MWh, Water = $1/cu meter	15	-37	15	2	0	-13
Power = $60/MWh, Water = $1/cu meter	6	-46	-4	-29	-19	-44
Power = $30/MWh, Water = $2/cu meter	156	104	156	143	141	128
Power = $60/MWh, Water = $2/cu meter	147	95	137	112	122	97

FIG. 3.63. Net present value for different power and water cost scenarios.

Based on these results, the overall conclusion is that the break-even analysis indicates a feasible value of ~1 US $/m^3 while an increased water price shows a significant higher net present value. This higher value is coupled to a water selling price of 2 US $/m^3 which has already realized in and around Cape Town (South Africa) region during dry seasons.

3.3. OTHER APPLICATIONS

Since the beginning of the development of nuclear power, the direct use of the generated heat for district heating or in industrial processes has been considered convenient and practiced in many countries. Still, it is less than 1% of the nuclear heat worldwide which is presently used for non-electric applications, but there are signs of increasing interest.

The experience up to now gained with nuclear process heat/steam extraction is from 60 reactors and about 600 reactor-years, respectively [161]. Most present nuclear non-electric applications are found in the lower process temperature range with experience obtained, e.g. from district heating (most in Eastern Europe), desalination of seawater (most in Japan) or D_2O production (Canada). Cheap off-peak electricity from LWRs for electrolytical hydrogen production could be another low temperature application.

3.3.1. District heating

District heating is predominantly applied in climate zones with relatively long and cold winters. It is usually provided in form of hot water (commonly used in Europe) or steam (e.g. USA, also Germany) at 80–150°C and at low pressures. Depending on local heat demand, it requires decentralized units, since heat transport over long distances is not efficient. With the improvement of hot water transportation, however, larger CHP grids could be realized, whereas steam transport is limited to a maximum of about 5 km. Typical district heating networks are in the range of 600–1200 MW(th) in large cities down to 10–50 MW(th) in smaller communities.

If nuclear power plants are used as primary energy source, heat is extracted from the low pressure turbine. An intermediate heat transfer loop is employed to avoid a transition of radioactivity into the heat/steam circuit. Major drawback of nuclear systems is their usually insufficient economy. As of 1998, 46 commercial nuclear plants in 12 countries are being used or have been used for heating purposes with a heat output between 5–240 MW demonstrating a safe and reliable operation. Among these plants were two dedicated plants in the Russian Federation (Obninsk) and China (NHR-5) [162].

One example is the nuclear station Beznau in Switzerland which supplies since 1983 heat in form of 85°C hot water to over 2300 clients. The main heating network has a length of 31 km, from which the heat is transferred to local secondary networks with a total length of 99 km. Most recent example of nuclear district heating is the operation of the Chinese HTR-10 research reactor at the Tsinghua University in Beijing to contribute to local heating in winter time. It is actually the first high temperature reactor used for the purpose of ‘process heat’ supply.

Also at PBMR, the possibility of district heating was briefly investigated as an alternative waste heat coupling scheme. This work has not yet been completed but initial indications clearly indicated that various favorable conditions need to exist in order to justify the additional capital expenditure and that application would be quite limited.

3.3.2. Oil recovery

One example with near term prospects is the provision of high temperature heat/steam and electricity in the tertiary oil recovery process increasingly applied with decreasing recovery of conventional oil resources. Particularly in this sector, massive amounts of H_2 will be required in future for the conversion of heavy oils, tar sands, and other low grade hydrocarbons [163]. Due to the increasing share of 'dirty fuels' such as heavy oils, oil shale, tar sands entering the market, the need for both process heat and hydrogen will also increase significantly. Figure 3.64 shows a schematic of the so-called 'steam assisted gravity drainage' process where a bituminous ground is flooded with steam at 200–340°C and 10–15 MPa, and the oil produced is retrieved through a separate well.

For larger resources, nuclear could represent a large centralized steam source to be injected at several locations. Fluctuations in oil production could be compensated by cogeneration of electricity. Canada appears to be an ideal candidate for such a combined system due to its vast amounts of oil sands and its established CANDU nuclear plants.

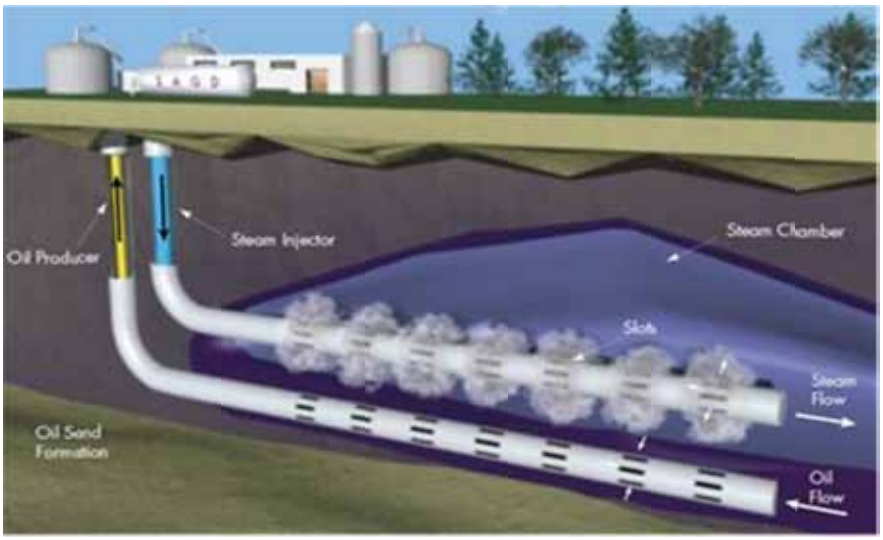

FIG. 3.64. Steam assisted gravity drainage for enhanced oil recovery.

3.3.3. High temperature process heat in the chemical industries

In the high temperature process heat range, CHP market penetration by nuclear power could be seen, e.g. in the chemical and petrochemical industries. The processes of splitting hydrocarbons are presently widely applied production methods for synthesis gas and hydrogen. The most important ones established on an industrial scale are steam reforming of natural gas, the extraction from heavy oils, and the gasification of coal.

The worldwide throughput of crude oil of 3×10^9 t/a requires a total energy of approximately 200 GW(t) or 8% of its energy contents. A refinery with a throughput of 6–7 million t/a of crude oil consists of a large number of individual plants which need a steady supply of typically about 400 MW(th). Due to the complex interaction of the different chemical processes optimized to a very high degree, the potential supply of energy by nuclear power may not be dedicated to a specific process, but rather cover the overall cogeneration of process steam, process heat, and electricity. An additional approach will be the important hydrogen generation. Process heat must be transmitted using an intermediate heat transfer loop.

Steam reforming of natural gas covering worldwide about half of the hydrogen demand, is one of the essential processes in the petrochemical and refining industries. The coupling with nuclear as process heat source may be an ideal starting point for nuclear power to penetrate this market in the near and medium term saving up to 35% of the methane feedstock, and a reasonable transition step towards a fossil-free hydrogen production in the long term.

4. SAFETY AND ENVIRONMENTAL CONSIDERATIONS

With regard to combined nuclear and chemical facilities, apart from their own specific categories of hazards, a qualitatively new class of events will have to be taken into account which is characterized by interacting influences. Arising problems to be covered by a decent overall safety concept are the question of safety of the nuclear plant in case of a flammable gas cloud explosion, or the tolerable contamination by a transition of radioactive substances into the product gas. In addition, there are the comparatively more frequently expected situations of thermodynamic feedback in case of a loss of heat source (nuclear) or heat sink (chemical). Potential hazardous events in connection with a process heat application system extensively investigated were

- fire and explosion of flammable mixtures;
- atmospheric vapour cloud explosion in the vicinity of the reactor;
- ingress of flammable gases into the reactor building;
- tritium transportation from the core to the product, e.g. hydrogen and methanol;
- thermodynamic interaction between nuclear and chemical plant;
- isolation of desalination plant.

4.1. SAFETY ISSUES OF NUCLEAR HYDROGEN PRODUCTION

There are two significant safety issues originated in the thermochemical hydrogen production system to be coupled to the HTGR. One is hydrogen release and the other is toxic gas release. Basic safety design approach is to prevent accidental release of there materials and to mitigate their effect on the HTGR safety items and operators. Provision of separation distance between the HTGR and the hydrogen production system is simple and reliable safety approach. But a long separation distance requires a long helium piping and a larger plant site, which results in an increase of the plant constr
the economic point of view.

4.1.1. Fire and explosion hazard

4.1.1.1. General recommendations

In case of initiating events such as accidents in the process plant or on industrial sites, releases of process raw stock or derived products are possible. From the viewpoint of protection measures, the worst safety implications will be produced by an air shock wave resulting from the explosion of such substances.

Allowable releases of explosive substances from the process plant are characterized by acceptable positive pressures in the shock wave front, complying with the limits established for NPP containment, systems and elements. The distance from the explosion point to the containment is accepted with account of the worst consequences for the nuclear island (reactor, spent fuel storage, etc.). In order to meet these requirements, the process plant

systems and elements important for NPP safety should be designed in accordance with the same principles as nuclear power equipment, primarily, the ‘single failure’ and the ‘conservative approach’ principles.

In order to reduce the risks associated with placing a nuclear reactor and a hydrogen production plant on one site, it is necessary to

- minimize the amount of H_2 and other explosive gases located close to the reactor plant;
- reduce the amount of gas released from the process plant in case of possible leaks from equipment or pipelines;
- create conditions preventing formation of explosive mixtures.

The following technical solutions can be recommended:

- modular design of the power–technological complex (not one, but four independent hydrogen production lines, each having its own nuclear source);
- burial of nuclear reactor modules in the main building below the ground level; arrangement of pipelines and equipment carrying explosive substances in the open air or, if it is impossible, in rooms filled with inert gases;
- maintenance of a safe distance between the hydrogen production plant and above ground electric engineering and radiation hazardous objects of the power–technological complex.

The modular design of the power–technological complex will permit to:

- reduce the amount of hydrogen and other explosive substances located close to the reactor plant, owing to the optimal number of fast-response shutoff valves isolating the leaky sections, and reduced pipeline cross sections and equipment dimensions;
- arrange the intermediate heat exchanger and the pipelines connecting it to the process plant in rooms protected against internal and external impacts, including possible explosions of process plant working fluids;
- provide for emergency relief of excessive pressure from the IHX room and from the pipeline gallery connecting the IHX to the process plant through vents releasing the steam–gas mixture into the environment;
- create conditions preventing formation of explosive mixtures in the rooms; in particular:
    - equip process plant equipment and systems with diagnostic tools;
    - provide for a control system to timely detect ingress of explosive gases into the compartments where process plant equipment is located, and effective systems to extract the explosive gases from these compartments;
    - fill the rooms where flammable and explosive gas concentrations can build up with inert gases, or equip them with reliable ventilation systems.

  Independence of all reactor modules from one another in all accidents accompanied with radioactive emissions is provided through:

- inherent safety features and passive safety systems that do not rely on supporting and auxiliary systems to function;
- arrangement of each reactor plant and radiation hazardous objects inside the building underground in individual reinforced concrete containments. The containments are designed to withstand emergency internal and external impacts (airplane crash, air

shock wave, explosion of fluids in the process plant, accidents in adjoining compartments, including nuclear reactor compartments);

- establishment of a safe distance between the hydrogen production plant and above ground electric engineering and radiation hazardous facilities of the power–technological complex.

4.1.1.2. Nuclear power plant safety requirements

i. Safety issues of an HTGR-based hydrogen production complex

Combination of the nuclear and hydrogen technologies in one facility poses a number of problems related to:

- maintenance of purity of the end product (hydrogen);
- necessity of protection of the nuclear power source against the air shock wave in case of possible hydrogen explosion.

In this connection, it is necessary to analyze the dependence of NPP safety on all possible stationary and mobile sources of accidental detonation, including industrial objects involved in production, processing, storage and transportation of chemicals and explosives.

The main parameters describing the process of explosion on the object are (Fig. 4.1) [164]:

- excessive pressure in the shock-wave front;
- trinitrotoluene (TNT) equivalent;
- distance to the object;
- design concentration, toxic dose near the object;
- possibility that the explosive cloud will drift towards the object; probability of cloud inflammation.

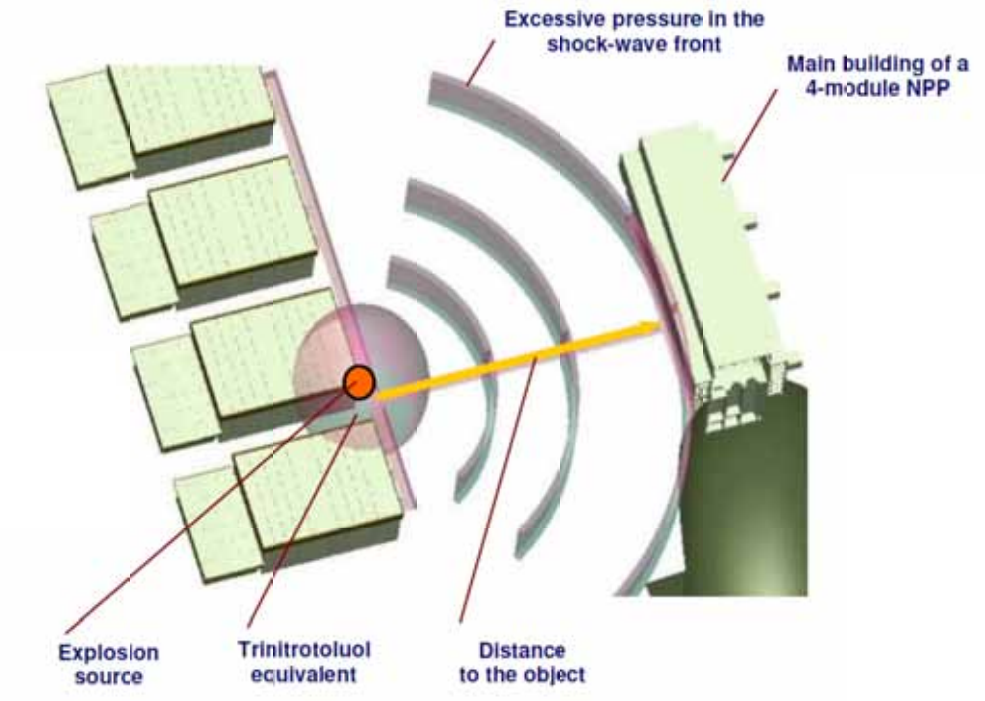

FIG. 4.1. Main parameters describing the process of explosion on the object.

The basic criteria for assessing explosion effects on the NPP building are [165]:

- Pressure in the shock wave front; if there are (or supposed to be) any external explosion sources at a distance of up to 5 km from NPP structures of category I (Table 4.1), this pressure is calculated or assumed equal to 30 kPa;
- Duration of compression phase up to 1 s;
- Horizontal propagation of the air shock wave.

ii. NPP safety requirements imposed by the hydrogen production plant

The technical measures on object protection against a blast wave are [164]

- explosion souroce removal or screening;
- building structure reinforcement (increased stiffness and inertia of cross-sections);
- technical solutins aimed at decreasing the energy potential of explosive process units.

TABLE 4.1. EXPLOSION HAZARD CATEGORIES OF PROCESS UNITS [166]

Explosion hazard category	Relative energy potential of released gas cloud, Q_v	Mass of released gas cloud, m (kg)
I	> 37	> 5000
II	27–37	2000–5000
III	< 27	< 2000

The energy potential, Q_v, of the process units intended for hydrogen production through water electrolysis shall be calculated on the basis of design solutions ensuring $Q_v < 27$ (explosion hazard category III).

For nuclear power plants, pressure in the shock wave front should be assumed equal to 10 kPa, with account of explosion sources located on the NPP site (storages of fuel and lubricants, hydrogen receivers, acetylene production in the scope included into the NPP design). During the entire operation period, it is prohibited to arrange explosion sources which can create more than 10 kPa pressure on category I structures at the NPP site. If there are (or supposed to be) any external explosion sources (oil refineries, basic storehouses of fuel and lubricants or explosives, gas mains, heat accumulators, navigable river routes, general purpose railroads etc.) at a distance of less than 5 km from an NPP structure of category I, the pressure in the shock wave front is to be calculated or assumed equal to 30 kPa.

Permanent stay of the servicing personnel in the electrolysis compartment is not recommended. Continuous monitoring of the progress of technological processes is performed by the operator from the control panel room. Automated shutdown takes place if the emergency protection thresholds are reached.

iii. Layout solutions [166]

The territory of an enterprise including explosive production facilities should be free of any natural cloughs. It is prohibited to lay pipelines carrying flammable and gaseous liquids and liquefied gas fuels in trenches or on the surface in artificial or natural cavitations.

Process facilities, production, administrative and domestic buildings as well as permanently or temporarily attended rooms located in the hazardous area in case of emergency should be equipped with effective systems for notifying the personnel about emergency situations on the process object.

Designed explosion and fire hazardous facilities shall meet the following requirements:

- Buildings accommodating control rooms (operator's rooms) should be constructed outside the destruction area or be capable of withstanding shock wave impact; in the latter case, they should be equipped with independent means to support normal systems operation and personnel activity in emergencies.
- Permanently attended administrative and other buildings should be constructed outside the destruction area.
- Plant-shared facilities (power, steam and water supply etc.) should be constructed outside the destruction area or be capable of withstanding shock wave impacts.
- For each object containing process units of any explosion hazard category, it is necessary to calculate zones in which the concentration of fuel in the vapour cloud that forms in the emergency remains below the explosion limit. The emergency response plan shall specify actions to be taken by the personnel in case of emergency to prevent ignition of the steam–gas or gas cloud sources within the calculated zones.

In accordance with the 'Safety rules to be obeyed in production of hydrogen by water electrolysis', hydrogen storage should be located at a distance of at least 15 to 30 m from the storehouses and production buildings, and at least 100 m from administrative buildings [167].

4.1.1.3. Design approach for hydrogen release

Fire and explosion of hydrogen is the most significant consequence of hydrogen release. Pressurized hydrogen is released as a jet from a failed pipe. If ignited during leakage, a jet flame is formed and components close to the flame may be damaged by overheating. According to the safety design regulations for chemical plants, leak detectors and emergency shutoff valves shall be provided for detecting and stopping a leakage of hydrogen as soon as possible. Components shall be arranged with an appropriate separation distance to eliminate secondary failure. The length of the jet flame may be several meters and the safety items in the HTGR are placed a hundred meters away from the hydrogen production system, so the jet flame does not directly damage the nuclear safety-related items.

If hydrogen does not ignite during leakage, a combustible hydrogen–air cloud is formed. It may cause a flash fire or an explosion. The flash fire is a deflagration without overpressure and emits strong heat. Temperature of the building and the components installed outside may not significantly increase because the burning period of the hydrogen–air cloud is short and thermal capacities of the building and equipments are large. The operators in the control room remain in a safe condition and are able to continue the safe operation of the HTGR.

The overpressure resulting from a hydrogen vapour cloud explosion may damage the reactor building or the components installed outside of the HTGR. Several tests were performed to identify the characteristics of hydrogen explosion [168]. A 300 m^3 volume of hydrogen–air mixture with stoichiometric concentration can generate a blast overpressure of 30 kPa in the open field. Densely arranged obstacles can accelerate the burning velocity of the hydrogen–air cloud and generate stronger overpressure. Vessels and pipes in the hydrogen production system shall be arranged with suitable space to eliminate acceleration of the burning velocity. Also dense arranged obstacles shall not be placed between the HTGR and the hydrogen production system.

The reinforced concrete wall of the HTGR reactor building and components placed outside must be designed to withstand severe external loads such as wind force of a typhoon and ground motion of an earthquake. In German and Russian design codes of the nuclear power plant for the explosion accident, the design limit of overpressure on the safety plant structures

is 30 kPa. Therefore, in this case, the fire and explosion in the open field should not affect to safe operation of the HTGR. If the blast overpressure of hydrogen explosion seems to exceed 30 kPa by acceleration of burning velocity of hydrogen–air cloud, a detailed analysis shall be performed to verify the structural integrity of the HTGR reactor building and components placed outside.

An explosion within a vessel or a pipe generates strong overpressure and may break it. Hydrogen and oxygen are produced simultaneously in the water splitting hydrogen production system so that there is a possibility of an internal explosion if hydrogen and oxygen are mixed. But hydrogen and oxygen are produced in different processes in the thermochemical water splitting system so that they are physically separated. Operation pressure of the hydrogen production system is higher than ambient pressure to minimize the plant scale and to enhance the hydrogen production efficiency. The air does not flow into the vessels and pipes in the event of pipe failure of the hydrogen production system. After the pressure in the hydrogen production system becomes ambient pressure, air ingress by natural convection may occur. To prevent an internal explosion, an emergency purge system shall be provided to purge hydrogen from pipes and vessels. Hence internal explosions and blast generated missiles can be excluded.

4.1.1.4. Fire and explosion hazards

i.Unconfined explosion

Fire and explosion hazards resulting from the leakage of flammable materials such as hydrogen, carbon monoxide, and methane or other flammable gases must be considered because they have the potential of causing significant damage to safety components. Within the PNP project, a gas explosion programme was conducted to improve understanding of the complex processes in vapour cloud explosions and their effects on the environment, in particular on nuclear plants. It included comprehensive experimental series employing representative combustible gases to examine flame speeds, overpressures, as well as criteria for the transition from deflagration to detonation (DDT), and on the other hand, the identification of PNP typical accident scenarios. Potential flammable gas mixtures accidently released into the atmosphere will if ignited, most probably undergo a deflagrative combustion connected with a non-damaging pressure wave.

As part of the experimental programme of the PNP safety programme, the Institute for chemical technology of the Fraunhofer Gesellschaft [169] have conducted in 1978 explosion experiments with unconfined, premixed stoichiometric hydrogen–air mixtures in hemispherical balloons of different sizes (3–20 m diameter). Maximum overpressures resulting from flame acceleration were observed to range between 1.3 and 6.3 kPa corresponding to a flame speed in the hydrogen–air mixture of 84 m/s. Flame velocities showed a certain dependence on cloud size and state of turbulence in the cloud [170]. Other tests with methane–air, methane–ethane–air, methane–oxygen-enriched air, propane–air mixtures in 1988 were investigating the effect of unconfined flat cloud geometry of rectangular or cylindrical shape. Initial turbulence was created by obstacles and fans. Weak point ignition resulted in hemispherical flame propagation which ended at the cloud boundary. Obstacle configurations increased flame speeds by a factor of 2–3. More tests were conducted by Pförtner in an arrangement with two parallel walls forming a 10 m × 3 m × 3 m lane and with rich hydrogen–air mixtures as fuel. After generating fan-induced turbulence, flame acceleration to a detonation was observed [171]. Explosive-initiated detonations have been observed in ethylene, propylene and propane mixtures with air by using 8 g, 30 g, and 80 g, respectively of high explosives, but never in premixed methane–air mixtures [170].

ii.Confined explosion

Fire and explosion events inside the reactor building may cause severe damage to nuclear safety systems. It is, therefore, required that the possibility of an ingress and ignition of flammable gases inside the reactor building should be low enough to avoid any fire and/or explosion at this location. Ingress of product gases into the reactor building requires a scenario with the simultaneous failure of the secondary helium pipe and the gas generator or reformer tube. The only cause of the simultaneous failure of these components is conceived to be an earthquake. Therefore, helium piping and chemical reactor should be designed according to the highest level of reliability and for a high seismic safety level. Furthermore, a qualified closure of the helium lines by diverse high temperature shutoff valves and the emergency shutoff valves in the process feed lines to disconnected from the chemical unit, and thus limiting the leaked quantity. Other countermeasures are an additional inerting of areas in the reactor building containing the secondary circuit piping. The employment of separation systems, segments of pipes which act as high pressure helium buffers, further helps to prevent a leakage of radionuclides to the outside.

An experimental programme at the research center Karlsruhe (FZK) to investigate the combustion behavior of hydrogen–CO–air mixtures and to quantify the influence of CO concentration on the combustion process of the hydrogen–CO–air mixtures under different conditions [172] has been conducted in a 12 m detonation tube. The results have clearly demonstrated a damping effect of CO on the turbulent combustion speed of hydrogen–CO–air mixtures when compared to turbulent combustion in pure hydrogen–air mixtures. This effect is probably caused by the relatively long induction and reaction time of the complicated oxidation mechanism of CO. This process requires as an initiating component OH-radicals, which have to be provided in a sufficient amount by the H_2 oxidation. The resulting time delay between hydrogen and CO oxidation could be detected in the hydrogen–CO–air experiments with the installed photodiodes, which showed two spatially separated flame zones moving along the tube.

With respect to safety analysis, the mitigation effect of CO additions on the observed flame speed and the resulting pressure loads should be taken into account. Treating CO simply as H_2 in the analysis would lead to overconservative load estimates.

4.1.1.5. Safety distance

There is a wide variety of possibilities for the definition of ‘safety distance’ and it is largely depending on country or document [173]. As commonly understood, a safety distance is the required minimum separation distance between a potential hazard source, e.g. the location of a flammable gas leakage, and the vulnerable object to be protected from an external impact. But apart from the difficulty in providing a precise definition, another problem arises with the necessity to select the appropriate method for quantifying a separation distance. Fixing of numerical values could be done by estimations assuming severe accident conditions or the application of probabilistic risk assessment methods taking account of mitigation measures such as, e.g. fire walls. And last but not least, there is a need for harmonization of the various approaches of quantification among the countries.

The separation distance is usually determined as a function of the quantity of hydrogen involved (quantity–distance relationship). It may be fixed on the basis of credible events taking account of – if referring to hydrogen – the evolving flammable atmosphere as well as of the heat and pressure wave resulting from a possible ignition. The separation distance can then be defined according to physically defined criteria, e.g. the dose of thermal radiation or the peak overpressure, to have reached a certain threshold value. A particular aspect is the risk

of projectiles which may be thrown much further away than the blast pressure-based safety distance. A basic prerequisite is the knowledge of the source term which is dependent on leak size and thermal dynamic conditions of the leaking substance. Small, hardly quantifiable leakages, e.g. from cracks in welding seams, will be a safety issue.

It should be noted that during transportation of high temperature fluids it is vital that the distance between the nuclear power source and the hydrogen production site is as short as possible. This is conditioned by the need to preserve the high temperature potential and to reduce the coolant pumping requirement and capital costs. However, from the viewpoint of safety assurance, the hydrogen storage, hydrogen production plant and reactor plant should be located at a distance from one another. Consequently, it is necessary to find a reasonable compromise when analyzing the economic effectiveness and safe arrangement of the mentioned objects.

One of the consequences from the experimental activities in the PNP vapour cloud programme was the guideline on the 'protection of nuclear power stations from shock waves arising from chemical explosions', drafted by the German Federal Ministry of the Interior (BMI) in 1976 [174] which defined a pressure–time history to be sustained by any future nuclear containment as well as a safety distance relation

$$R = 8 \times M^{1/3}$$

where

R is the safety distance, m;
M is the mass of the flammable substance, kg,

for nuclear power plants (Fig. 4.2). The guideline is valid for nuclear plants of present design; it is explicitly mentioned that "no statement can be given at present concerning its application to future nuclear process heat plants". A major reason is that, as a rule, the chemical process units such as the gas generator or steam reformer do not meet the additional requirement given by the guideline, which is a 100 m minimum distance to the nuclear reactor.

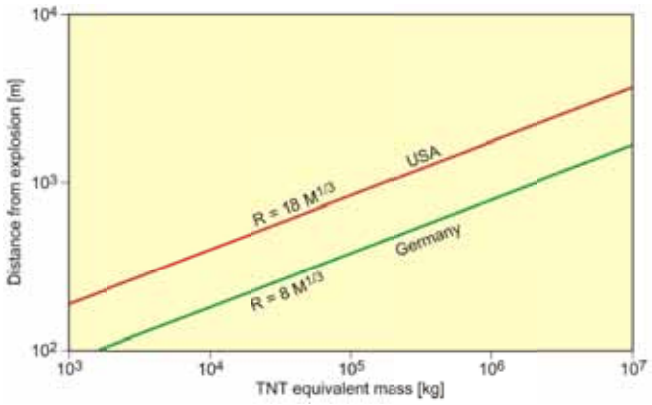

FIG. 4.2. Safety distance as a function of the quantity of released liquefied gas according to the BMI guideline and the US regulatory guide 1.91 [176].

A corresponding regulation in the USA, the US-AEC Regulatory Guide 1.91, applies a more conservative relationship for the safety distance with a k-factor of 18 instead of 8 (Fig. 4.2). No additional measures need to be taken if the equation is met. If, however, it is not met, lower distances will be allowed if a sufficiently low risk can be proven by probabilistic safety assessment methods [175].

In the Russian Federation there are some regulatory documents related to arrangement of explosive production facilities near nuclear power plants that cover:

- Factoring external natural and man-caused impacts on nuclear and radiation hazardous facilities (NP-064-05) [164];
- Codes for construction of NPPs with various type reactors (PiN AE-5.6) [165];
- General explosion safety rules for fire and explosion dangerous chemical, oil chemical and oil refining facilities (PB 09-540-03) [166];
- Safety rules to be observed in production of hydrogen by water electrolysis (PB 03-598-03) [167].

4.1.1.6. JAEA evaluation of safety distance

JAEA performed preliminary analysis of the separation distance for hydrogen explosion [177]. The computational fluid dynamics code STAR-CD was used to evaluate the concentration of hydrogen in the field. The computational domain and the layout of release point and protective wall are shown in Fig. 4.3 and Fig. 4.4. A three-dimensional rectangular coordinate system is adopted. The release point is set at x = 30 m, y = 0 m. The vertical position of z-direction is an input parameter. The symmetry model of x–z plane is employed to reduce the mesh number.

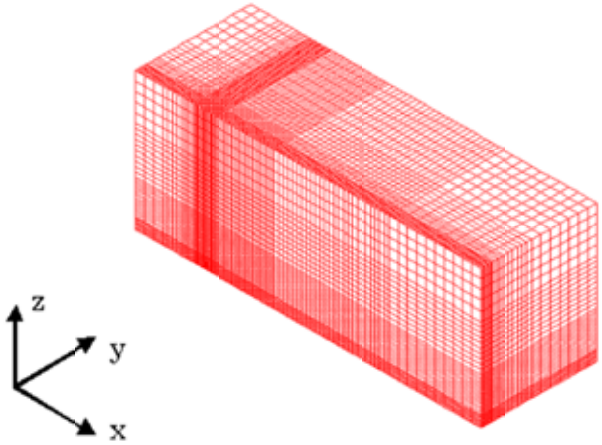

FIG. 4.3. Computational domain for hydrogen dispersion analysis.

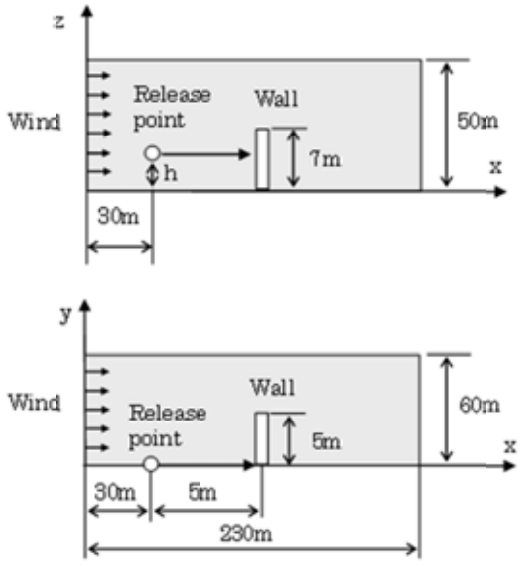

FIG. 4.4. Layout of release point and the wall.

(a) Hydrogen release rate

Pressurized hydrogen gas blows out from a failed pipe like a jet at critical speed. Mass flow rate of m_c can be calculated from the following equation by assuming isentropic flow of an ideal gas.

$$m_c = A\frac{p_0}{\sqrt{R\,T_0}}\sqrt{\kappa\left(\frac{2}{\kappa+1}\right)^{\frac{\kappa+1}{\kappa-1}}}$$

where

p_0 and T_0 are pressure, Pa, and temperature, K, of the hydrogen in the pipe,
A is the cross section area of the pipe, m^2,
R is the gas constant of hydrogen, = 4124.6 J/(kg·K), and
κ is the ratio of specific heats, = 1.403.

The mass flow rate depends on the pressure. The pressure of hydrogen gas in the pipe actually decreases according to the hydrogen leakage. In this analysis, however, a constant pressure is assumed during leakage at the initial condition. Duration of the gas release is given by dividing the amount of hydrogen released by the mass flow rate.

Pressurized hydrogen gas is compressible. The pressure dependence of density should be considered to analyze the detailed behavior of the hydrogen flow. Compressibility affects the gas concentration only close to the opening of the pipe. This analysis, however, focuses on analyzing the dispersion behavior in the open field so that the compressibility of hydrogen gas is not considered in this analysis.

(b) Atmospheric condition

The atmospheric condition is an important factor of the diffusion analysis. The standard k–ε model is adopted in the turbulent flow model of this analysis. A steady-state analysis for each wind speed is conducted to determine the initial atmospheric condition.

(c) Result of dispersion analysis

Analytical parameters which are the amount of hydrogen released, the pipe diameter, height of the release point, the wind speed, and the horizontal angle of jet, are listed in Table 4.2. Wind flows in x-direction in Fig. 4.3. Physical properties of the air–hydrogen mixture are calculated by the weighted average method.

Figure 4.5 shows the results of hydrogen gas concentration analysis. In this case, the amount of hydrogen gas released is 100 kg, the pipe diameter is 100 mm, the height of release point is 2.5 m and the wind speed is 1 m/s. The upper figure shows the cross section of the x–z plane at y = 0 m and the lower one shows the cross section of the x–y plane at 2.5 m.

TABLE 4.2. ANALYTICAL CONDITIONS OF THE HYDROGEN DISPERSION

Item	Condition
Amount of hydrogen released (kg)	Max. 100
Pressure (MPa)	4
Pipe diameter (mm)	20, 100
Height of release point (m)	0, 2.5, 5
Wind speed (m/s)	1–15
Horizontal angle of jet (°)	0–90
Atmospheric stability category	Stable

Figure 4.6 shows the effect of the amount of hydrogen released on the moving distance which is defined as the projected distance on the ground from the release point to the edge of the explosive hydrogen cloud. Increase of hydrogen amount extends the release duration. A small amount of hydrogen gas is released instantaneously and a large amount of hydrogen gas is released semi-continuously. Increase of the maximum moving distance is not proportional to the amount of hydrogen released. The difference of distances estimated for 58.1 and 96.8 kg is only 9 m.

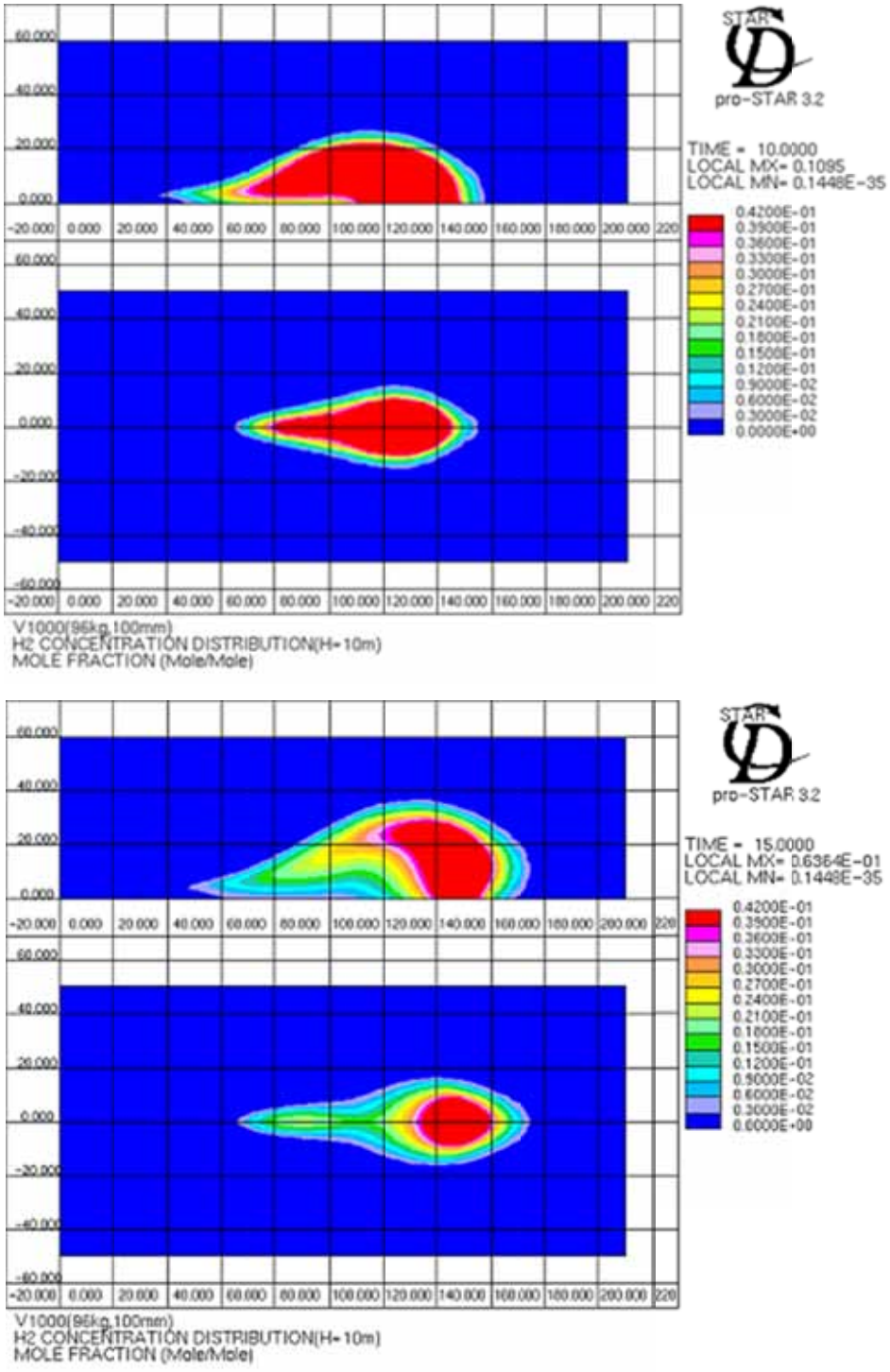

FIG. 4.5. Hydrogen gas concentration distribution after 10 s (top) and 15 s (bottom) of hydrogen gas release with the red color indicating the area of H_2 concentrations within the flammability limits, x–z cross section in upper part, x–y cross section at height z=2.5 in lower part.

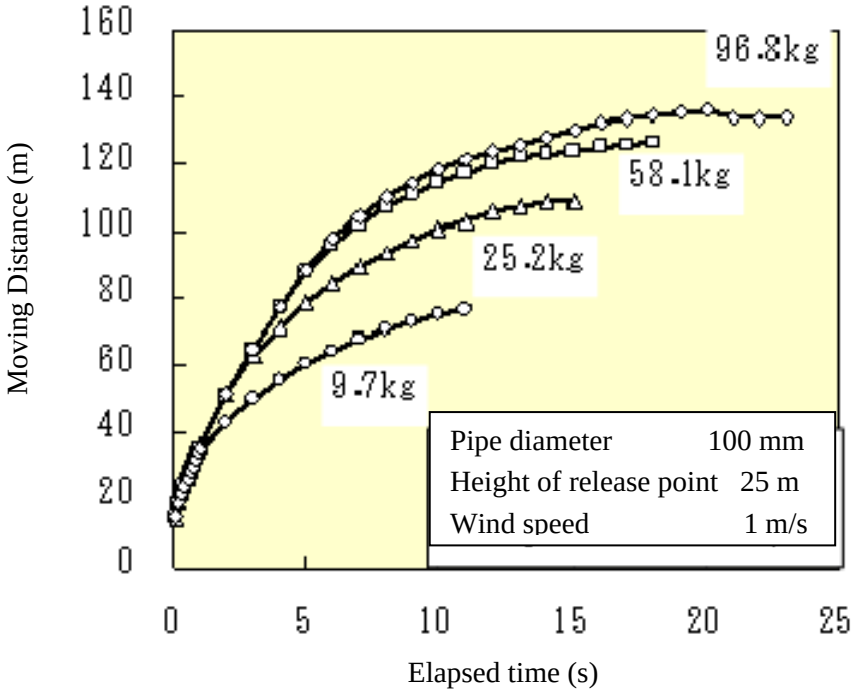

FIG. 4.6. Effect of amount of hydrogen released.

Figure 4.7 shows the relationship between the moving distance and the mass of explosive hydrogen cloud. During hydrogen release, the mass of the explosive hydrogen cloud increases. After the gas release is finished, mass decreases gradually by dispersion. Maximum explosive hydrogen mass is about 45 kg at the end of the release phase. Half of the hydrogen is diluted to 4% or less during release.

The pipe diameter has a direct effect on the release rate and the duration. Release mode for small pipe diameters is a continuous release and its moving distance is the shortest as shown in Fig. 4.8. This figure demonstrates that a large-size pipe rupture is more significant for the moving distance.

Hydrogen transport pipes are generally installed overhead to prevent gas retention and accumulation under vessels and structures and to enhance dispersion of the hydrogen gas because it is a light gas. Figure 4.9 shows the effect of the height of release point on the moving distance. The ground release is the longest moving distance because dispersion in z-direction is restricted. The results for the heights of 2.5 m and 5 m are almost same. Conclusion from this result is that an installation of the hydrogen pipe on the ground should be excluded.

Wind force dilutes the gas concentration but carries the cloud over a long distance. Figure 4.10 shows the effect of the wind speed on the moving distance. Maximum moving distance increases linearly with the wind speed.

It is difficult to predict which direction the hydrogen gas blows out to from a failed pipe. Figure 4.11 shows the effect of the horizontal angle of jet on the moving distance. Increase of the horizontal angle decreases the maximum moving distance. There is also a linear correlation obtained between the horizontal release angle and the maximum moving distance.

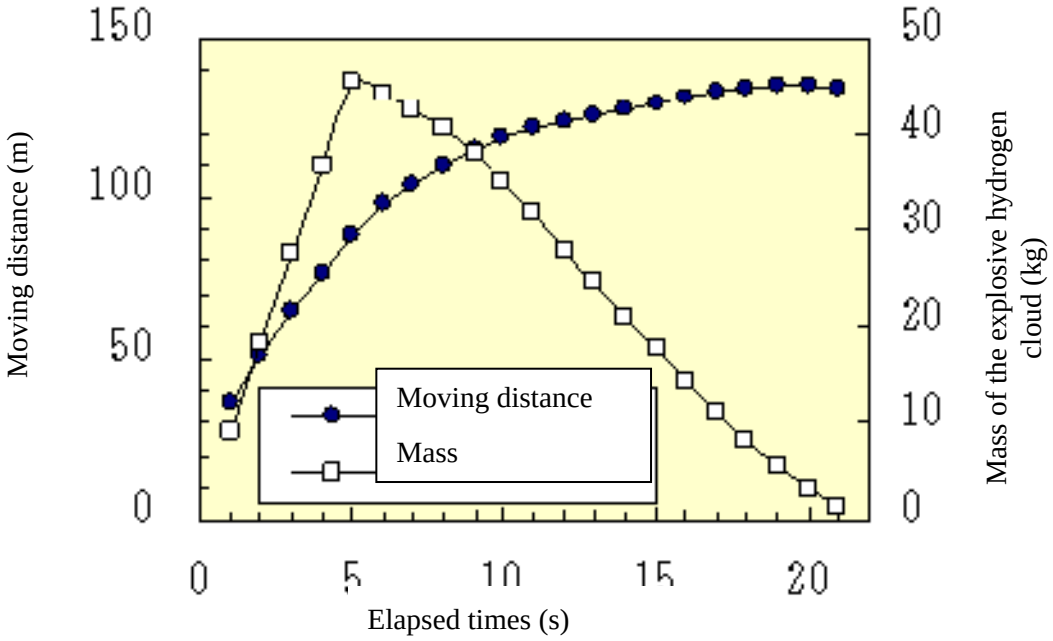

FIG. 4.7. A relation between moving distance and mass of explosive hydrogen cloud.

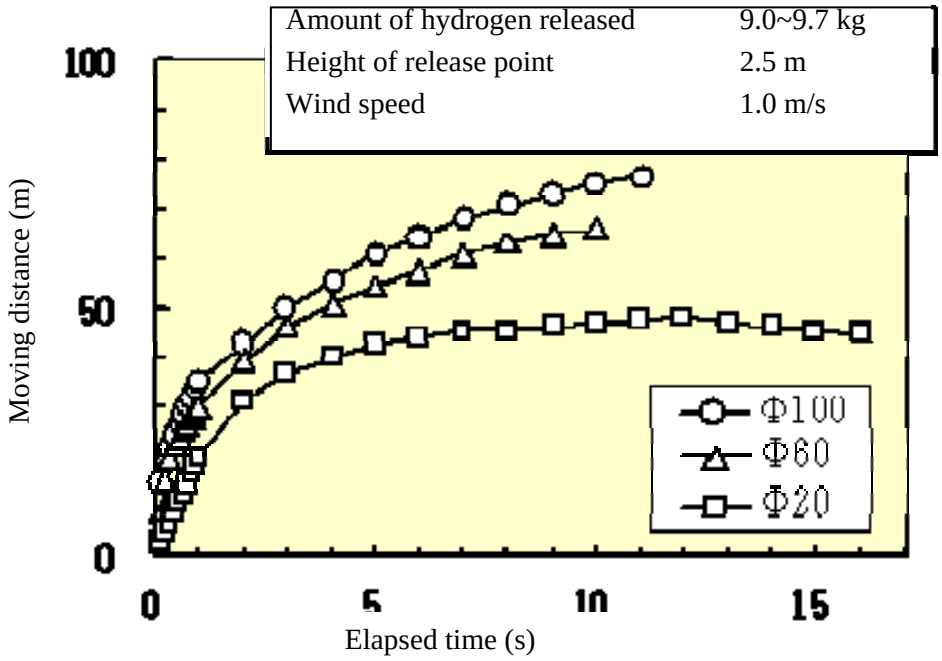

FIG. 4.8. Effect of pipe diameter.

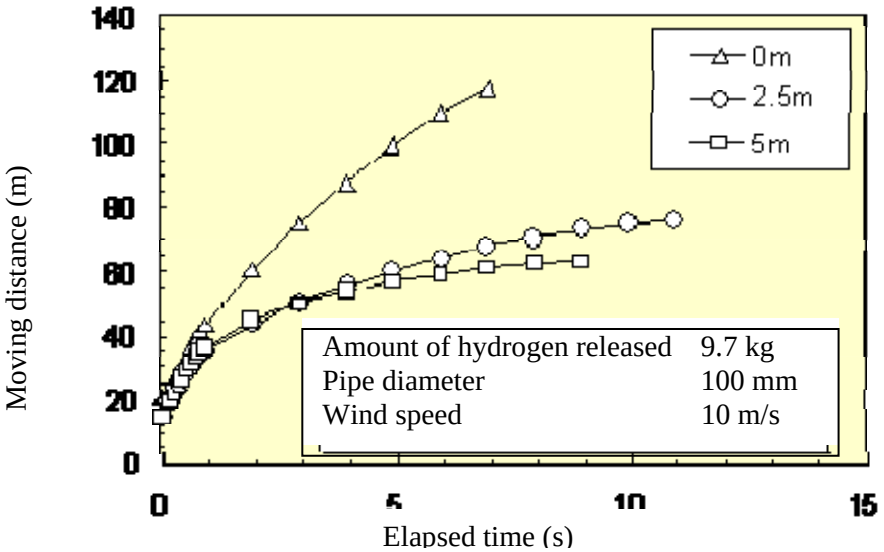

FIG. 4.9. Effect of the height of the release point.

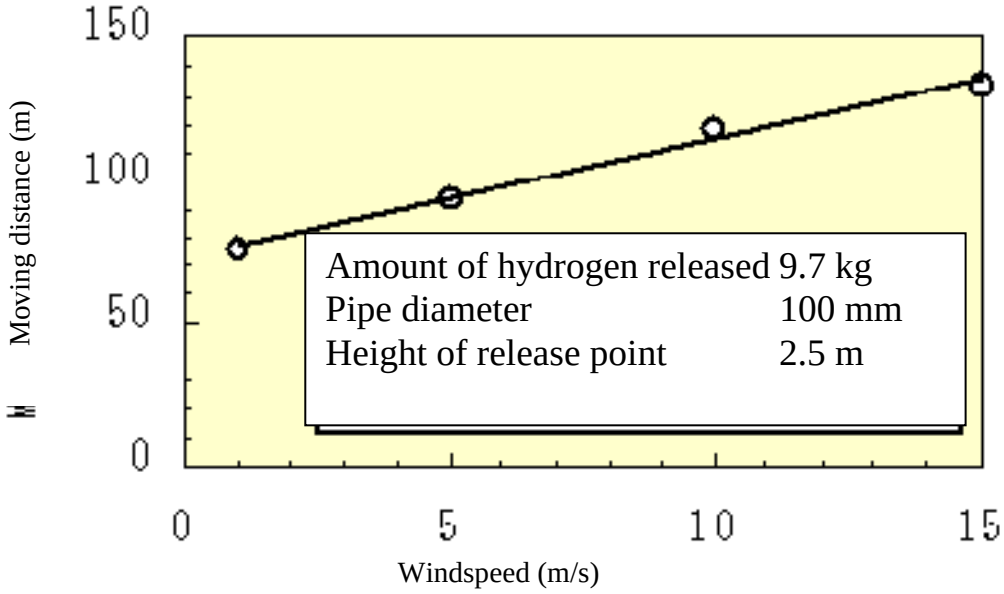

FIG. 4.10. Effect of the wind speed.

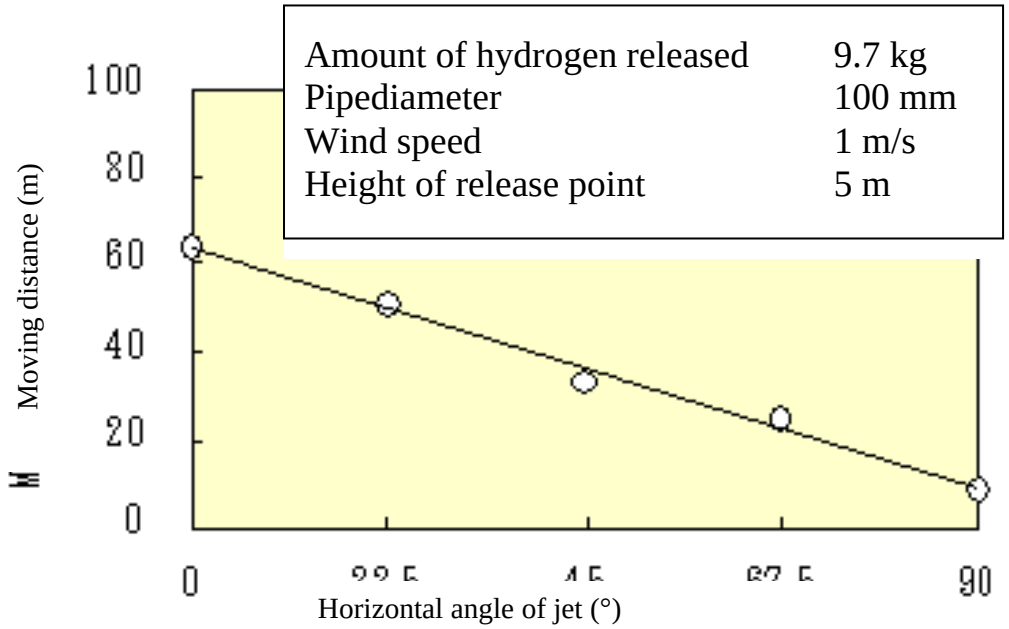

FIG. 4.11. Effect of the release angle

A physical barrier is an effective means to reduce the moving distance of the hydrogen cloud. The effect of the wall installed near the hydrogen transportation pipe is analyzed. Layout of the wall is shown in Fig. 4.12. The wall height is 2 m higher than the release point and is installed 5 m away from the release point. The thickness of the wall should be determined to withstand the load of blast overpressure generated by the hydrogen explosion. For example, the minimum thickness of the blast-proof wall made of reinforced concrete is 12 cm in Japanese industrial codes. Figure 4.13 shows an analysis result of the dispersion behavior. The effect of the wall on the moving distances is shown in Fig. 4.14. The moving distance with a wall drastically decreases. But the effect of the wall over 45° of the jet angle disappears because a hydrogen cloud goes over a wall in this case.

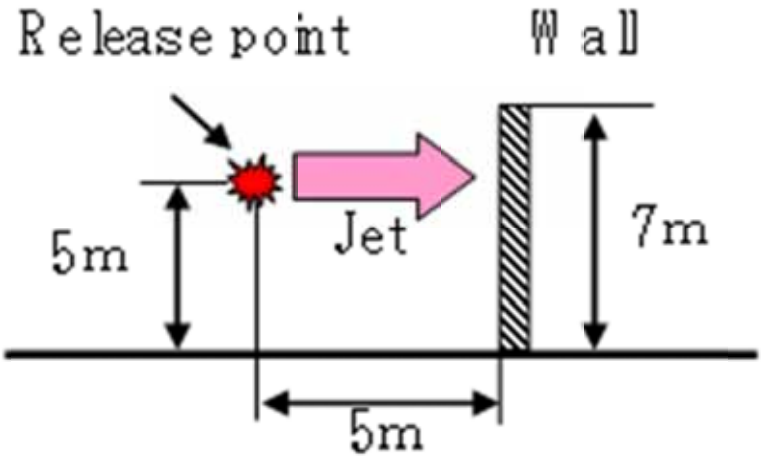

FIG. 4.12. Layout of the wall.

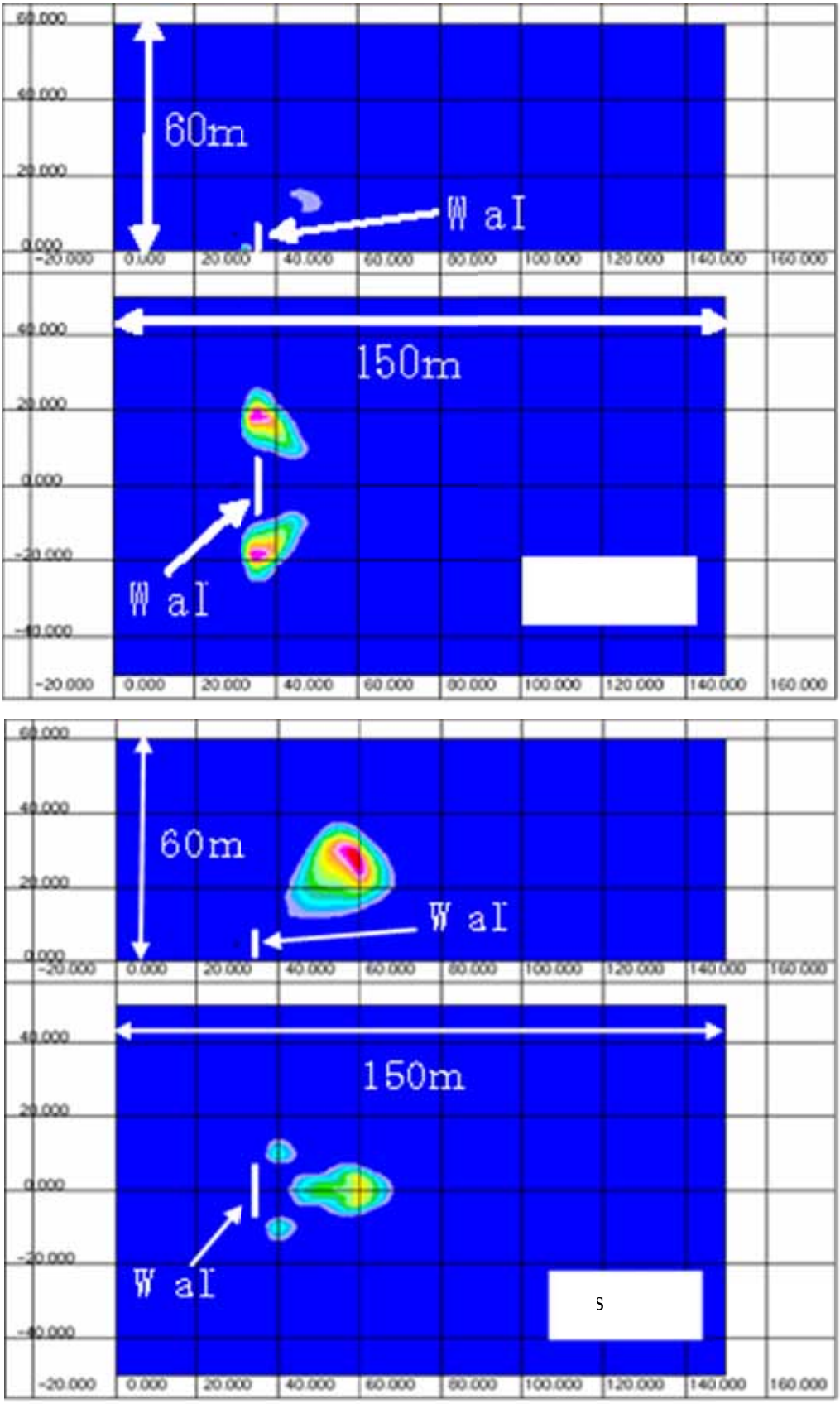

FIG. 4.13. Hydrogen dispersion at presence of a wall assuming a release angle of 0 degree (top) and of 22.5 degree (bottom).

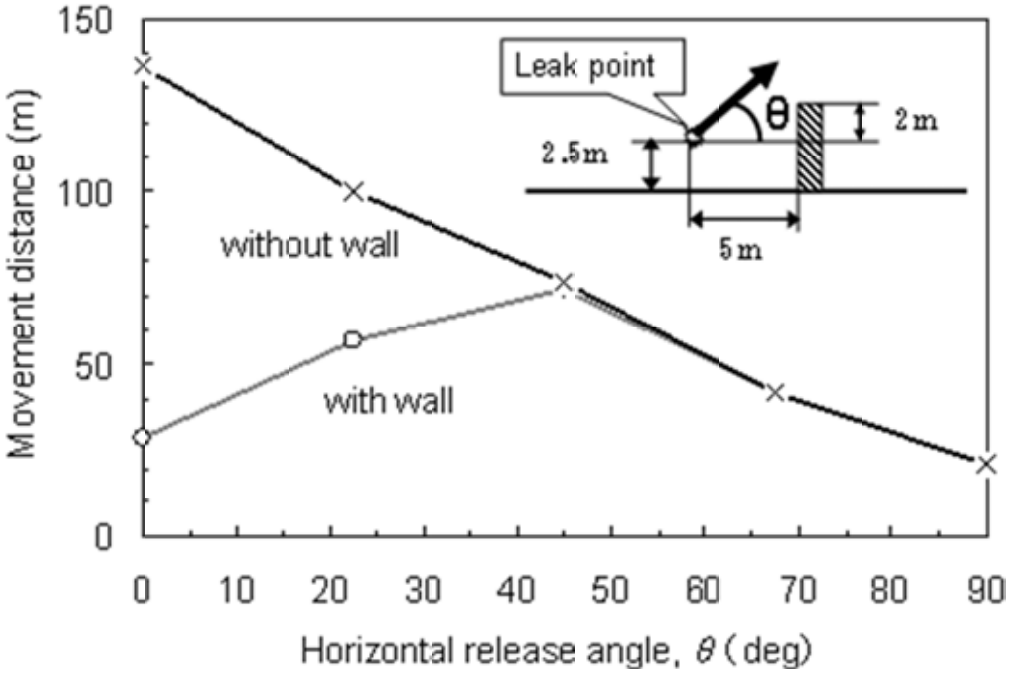

FIG. 4.14. Effect of the wall.

The hydrogen gas cloud can move over a long distance depending on the release condition and the atmospheric condition. The separation distance between the hydrogen production system and the HTGR plant should be determined to prevent ingress of an explosive hydrogen cloud into the reactor building through the ventilation system of the HTGR in consideration with dispersion of hydrogen cloud.

(d) Result of explosion analysis

The effect of the blast overpressure generated by a hydrogen explosion is not a significant issue if the structures and equipment are designed to withstand such overpressure. To reduce the possibility of damage by a hydrogen explosion, overpressures should be evaluated by the following methods and effect on the structures be analyzed. There are two major indicators which are peak overpressure and impulse to estimate damage of the structures. The peak overpressure is employed as the indicator in many codes and guidelines because of its simplicity. Intensity of the overpressure can is calculated by TNT equivalent method [178]. The equivalent mass of TNT is calculated with the following equation:

$$Q_{TNT} = \alpha \frac{Q_f \cdot E_{mf}}{E_{mTNT}}$$

where

Q_{TNT} is equivalent mass of TNT, kg,
Q_f is mass of fuel, kg,
E_{mf} is the combustion energy of the fuel, J/kg,
E_{mTNT} is the combustion energy of TNT, J/kg, and
α is a factor including yield and efficiency.

The peak overpressure is derived as a function of distance by the TNT explosion blast chart test as shown in Fig. 4.15.

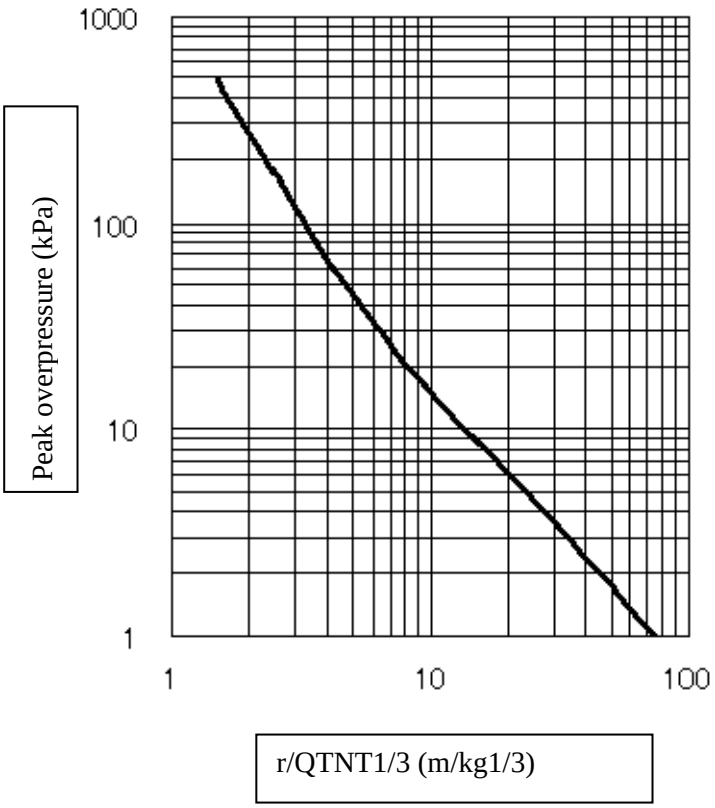

FIG. 4.15. TNT explosion blast chart; peak overpressure.

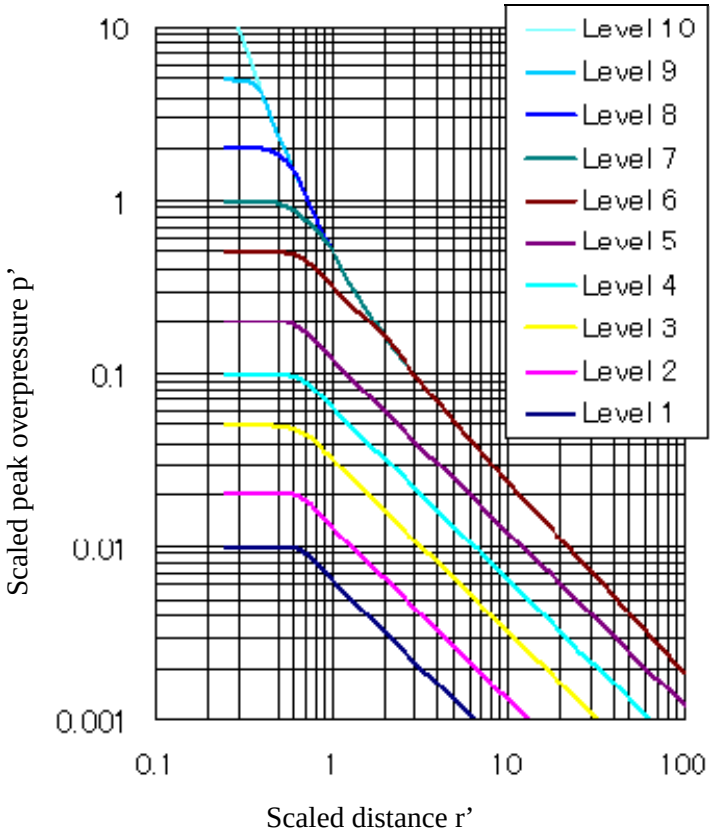

FIG. 4.16. Multi-energy method blast chart with peak overpressures.

The multi-energy method can also be applied to estimate the blast overpressure of hydrogen explosion [178]. The chart as shown in Fig. 4.16 is made from the idealized gas explosion analysis in which a combustion energy of 3.5 MJ/m^3, stoichiometric concentration of charge–air mixture, and a semi-spherical shape of the cloud are assumed. There are ten classes in the chart identified by the initial blast intensity. Class 10 represents a detonation. Class 5 represents a hydrogen explosion with low ignition energy and several obstacles. This is the most likely explosion in the open field. An explosion in the hydrogen production system may correspond to a level between class 5 and class 7 which represents a strong deflagration.

Scaled distance r' and scaled peak overpressure p' are given by the following equations:

$$r' = \frac{r}{(E/P_0)^{1/3}}$$

$$p' = P/P_0$$

where

r is the distance from the center of explosion, m,
E is the combustion energy, J/m^3,
P_0 is the ambient pressure, Pa, and
P is the peak overpressure on the target item, Pa.

The combustion energy of hydrogen is 142 MJ/kg or 12.75 MJ/m^3 (HHV) and the ambient pressure is 101.3 kPa.

The upper limit of the peak overpressure of structures is an important item to determine the safe distance in the safety design. Russian design code prescribes that the building should be designed for a shock wave of 30 kPa. But the NRC regulatory guide recommends ~7 kPa (1 psi) from the viewpoint of no significant damage on the safety related structures. Japanese industrial code recommends 10 kPa from the viewpoint of no significant damage to the public. The design limit of peak overpressure of hydrogen explosion will be 10 to 30 kPa.

In this preliminary analysis, design limit is tentatively set at 10 kPa to evaluate a conservative separation distance. The separation distance is defined by a sum of the moving distance of the explosive hydrogen gas cloud and the distance of the peak overpressure of 10 kPa derived from explosion of the explosive hydrogen gas cloud evaluated from the calculation of moving distance. Figure 4.17 shows the evaluation result of separation distance of a hydrogen release of 97 kg from a hydrogen transportation pipe of 100 mm. Other parameters are wind speed of 1 m/s, height of the release point of 2.5 m and the release angle of horizontal. When hydrogen of 97 kg is exploded at the release point which is a conventional evaluation method, a required separation distance is 62.5 m. However, the required separation distance greatly increases considering the moving distance.

Much hydrogen gas can move over a long distance by dispersion so that the moving distance of hydrogen gas cloud extends the separation distance. The conventional evaluation method which does not consider the dispersion process may give an uncertain separation distance under some conditions. The separation distance between the HTGR and the hydrogen production system in the cogeneration system should be minimized with adequate safety margin.

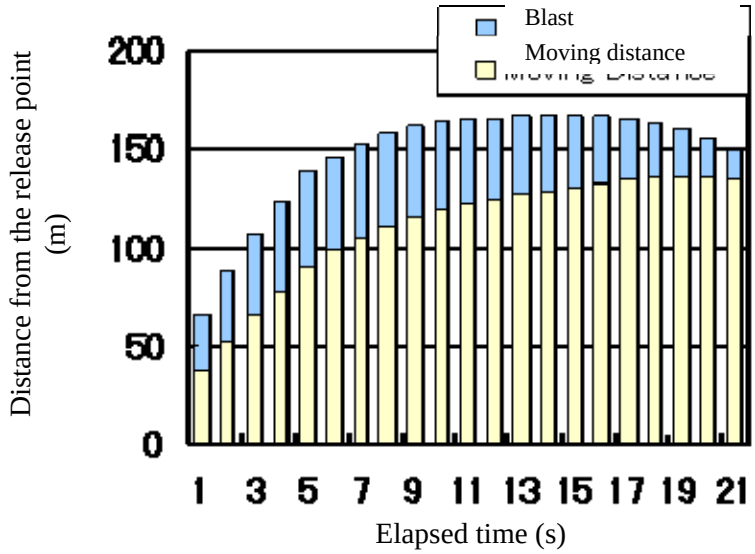

FIG. 4.17. Distance from the release point suffering an overpressure of 10 kPa.

4.1.1.7. Russian approach of determination of safe distance between reactor plant and hydrogen production plant

JAEA conducted a computer simulation of the release, dispersive transport, and explosion of a hydrogen cloud in the atmosphere. It was concluded that a relatively small distance between the reactor plant and the hydrogen production plant should not pose any risk to the overall safety, especially if the reactor and the process plant are separated with an earth mound or any other type of wall. However, building a high and wide earth mound or wall near the reactor plant is very expensive. In the opinion of the Japanese researchers, a wall rising 2 m above hydrogen pipelines would be enough to cut the safe distance in half [179]. Such barrier would prevent the hydrogen cloud from drifting towards the reactor plant and contribute to its dispersion in the atmosphere.

The performed research has confirmed that it is technically feasible to safely arrange the reactor plant and the hydrogen plant at a distance of 100 m from each other [177]. The layout of a GTHTR300C-based, power–technological complex for hydrogen production is illustrated in Fig. 4.18.

An estimation conducted for the MHR-T reactor plant in the Russian Federation supports the above conclusions. However, there is one important comment to be made. If the high hydrogen productivity of one reactor module only (6760 kg/h in the high temperature steam electrolysis (HTSE) technology and 12 500 kg/h in the SMR technology) is taken into account, it would be unsafe to store the produced hydrogen on the territory of the NPP or hydrogen plant located at a distance of maximum (in view of criteria of profitability) 100 m. All produced hydrogen should be continuously transported via pipelines to gas holders outside the power–technological complex.

The radius of destruction at explosion of hydrogen can be defined by formula (calculation based on PB 09-540-03 [166]) and also are shown in Fig. 4.19:

$$R = 9.6 \times (13.47\,m)^{1/3} \times \left(1+\left(\frac{3180}{1347\,m}\right)^{2}\right)^{-1/6}$$ at m ≤ 5000 kg, ΔP=28 kPa (Fig. 4.19, left);

$R = 9.6 \times (13.47\,m)^{1/3}$ at m ≥ 5000 kg, ΔP=28 kPa (Fig. 4.19, right);

where

m is the mass of hydrogen participating in explosion, kg, and
ΔP is the pressure in the shock wave front, kPa.

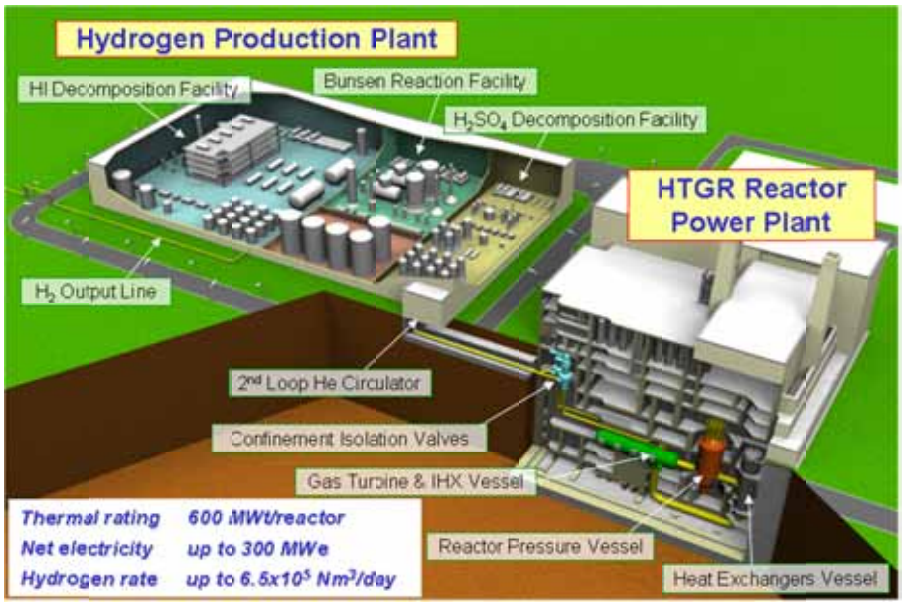

FIG. 4.18. Layout of a power–technological complex based on the GTHTR300C reactor plant.

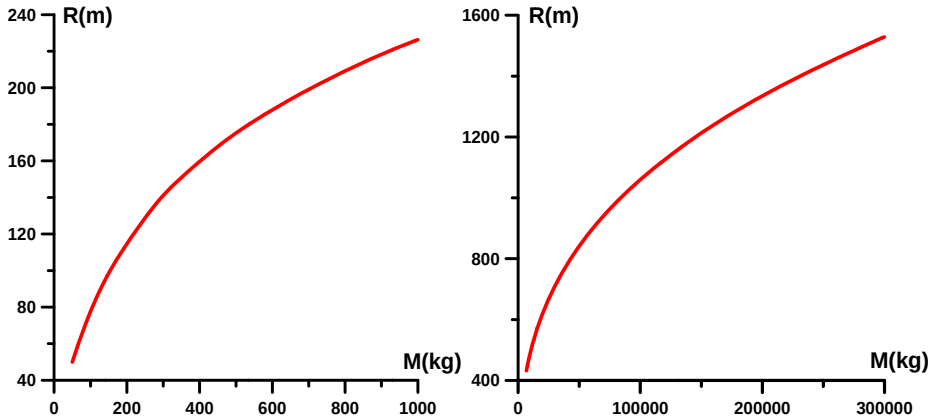

FIG. 4.19. Radius of destruction at explosion of hydrogen for m ≤ 5000 kg (left) and m ≥ 5000 kg (right).

Analysis of air shock wave impacts on the reactor plant should take into account possible leaks of hydrogen and explosive gases or gas mixtures in the chemical plant; leaks from the pipelines supplying explosive gases (e.g. natural gas for the SMR process) to the chemical plant; leaks from pipelines carrying the end product (hydrogen); and, in case of HTSE, leaks from pipelines carrying oxygen which is flammable and explosive. In all cases, design measures should be taken to prevent and minimize possible leaks of explosive gases and gas mixtures.

Explosive concentration of a gas cloud forms only at a certain height above the leak point. Vertical propagation speed of the hydrogen cloud is rather fast since hydrogen is much lighter than air. Moreover, cloud concentration in the atmosphere constantly decreases. These

properties of the hydrogen mixture allow reducing the safe distance between the nuclear and chemical plant.

In order to preserve the nuclear heat and to reduce the power required to pump the coolant along the pipeline, the hydrogen production plant should be arranged as close to the RP as possible. The reactor building should be, if possible, buried relative to the process plant. In another variant, it is necessary to arrange screening with an earth mound, a reinforced wall, or (which is less costly) a rising wall in the place of possible hydrogen leak from the pipeline. It therefore looks possible to arrange the hydrogen process plant and the reactor building at an acceptable distance from each other (not exceeding 100 m), observing all technical measures ensuring safety of such arrangement.

The mass flow during the release of hydrogen or other explosive gases located in close proximity to the RP can be reduced owing to the modular equipment design, optimal number of fast-response isolation valves sealing off the leaking sections, and reduced cross sections of pipelines and overall size of equipment that may contain explosive fluids.

According to the analysis of the MHR-T based SMR process, high concentration of water steam in the steam gas mixture transport area, even in case of leaks, prevents formation of explosive mixtures in any initiating events or meteorological conditions. Detonative mixtures can form only in chemical plant compartments not connected to the reactor plant, and therefore, these compartments can be removed to the required safe distance from the NPP main building.

In summary, the distance between the nuclear reactor and the hydrogen production plant is determined by the following main factors:

- air shock wave impact;
- capital costs;
- heat losses;
- coolant pumping power requirements.

The modular equipment design and interfaces between the four-module NPP and the chemical plant should prevent failures that may disable more than one MHR-T module. Therefore, an accident in one reactor module would not affect the safety of the remaining modules, and an uninterrupted operation of the entire power complex, in turn, would support a high availability factor.

The cost of screening depends on the screening type:

- An earth mound or a reinforced wall around the reactor building will be rather costly because the wall must be about 30 m high even if the reactor equipment is arranged underground;
- A wall at the point of possible hydrogen pipeline leak should rise about 2 m above the pipeline [177], and it does not have to be as thick as in the first option because its primary purpose is not protecting against the air shock wave, but preventing the hydrogen cloud from drifting towards the nuclear building.

Accordingly, if the second screening option is used, optimal structural strength of the other buildings can be selected. Besides, it would be expedient to analyze possible air shock wave impacts and economic effectiveness of protection options for a case with complete burial of the reactor plant. This will help to entirely prevent possible accidents associated with air shock wave impact on the reactor and to optimize hydrogen production plant arrangement relative to the NPP.

Due to the modular design of the high temperature electrolyzer, it is necessary to select optimal diameters of pipelines and hydrogen/oxygen collectors based on safety and economy considerations. This necessity is conditioned by the pumping power requirement on the one hand, and safety requirement (i.e. mass of possible hydrogen or oxygen leaks) on the other. Metal consumption will depend on the number of isolation valves and pipeline lengths and diameters.

It is more economically effective to arrange hydrogen/oxygen pipelines on the surface than underground.

One of the key conditions to the effectiveness of hydrogen production and radiation safety of the end product is selection of the optimal number of circuits. Germany, the USA and the Russian Federation [180] conducted research on different variants of HTGR with SMR, comparing, in particular, the variant with heat transfer to the thermal conversion unit through an intermediate helium circuit, and the variant with direct heat transfer to the thermal conversion unit in the primary circuit. According to the results of these studies, in the option without intermediate helium circuit, the capital and operation costs decrease by about 30%, and the net cost of generated heat decreases by 28% [181].

Removal of the intermediate circuit is quite acceptable from the viewpoint of end product activity. MHR-T calculations performed by Russian experts show that without the intermediate helium circuit, there will be no dangerous factors leading to abnormal operation, violation of nuclear and radiation safety norms, or revision of the basic technical solutions [180].

Exclusion of the intermediate helium storage would be reasonable not only from the safety considerations associated with high productivity of the hydrogen production plant based, for example, on a 600 MW(th) HTGR. A complex analysis of such factors as hydrogen storage form, equipment costs, and expenses related to maintenance and safety assurance shows that presence of the intermediate hydrogen storage can increase the end product cost by 30 to 300% [182].

Taking into account the analysis of Russian regulatory documentation and the corresponding calculations, this section can be concluded with the following statements:

- The required distance between the NPP and the hydrogen production plant, which is a potential explosion source, depends on the energy potential of the gas cloud released into the atmosphere. The nuclear reactor main equipment buildings should be designed to withstand a pressure of 30 kPa in the shock wave front. Process plant buildings containing hydrogen production and handling equipment should have a fire protection category not lower than II.
- Estimations of a 28 kPa shock wave impact on the boundary of the destruction area demonstrate that in order to maintain the 100 m distance between the nuclear and chemical plant, the mass of hydrogen taking part in the explosion should be limited to about 100 kg (without consideration of atmospheric conditions) (Fig. 4.19).
- The NPP control panel room should be in all cases located outside the explosion and fire hazard area.
- The upper limit of the safe distance can be lowered owing to the following technical measures:
    - Screening of the explosion source and underground arrangement of the reactor (the refueling mechanism should also be protected against shock wave impacts);

- Reinforcement of building structures;
- Development of technical solutions to reduce the energy potential of explosive process units.

- The power–technological complex design should be based on specific site conditions and should take into account the following factors:
  - climate in the selected region;
  - special external impacts such as seismicity, aeroplane crash impact, or shock wave impact.

4.1.2. Safety aspects of thermochemical (hybrid) cycles

In the hybrid sulphur process, the process feed material is water and a small amount of 50 wt% of sulphuric acid. The process products are hydrogen and oxygen gas. Process intermediates include large amounts of sulphur dioxide, sulphur trioxide, and sulphuric acid. Sodium hydroxide (NaOH) is used as a scrubbing agent.

HyS is a process in which 50 wt% of sulphuric acid from the electrolyzers, which contains dissolved SO_2, is stripped of the sulphur dioxide, and further concentrates the sulphuric acid to 75 wt%. The sulphuric acid is then decomposed to steam, oxygen, and sulphur dioxide at high pressure and high temperature. The product and stripped SO_2 is dissolved in water and sent as anolyte to the electrolyzer. Water is supplied to the cathode where it is separated into hydrogen and oxygen ions converting the SO_2 water solution into sulphuric acid.

The HyS process involves many hazardous chemicals that are commonly used in chemical processing and manufacturing, and the process products are either explosive or an oxidizer. A summary of the preliminary hazard assessment that formed part of the NGNP hydrogen plant alternatives study HPAS-Shaw (HPAS) study [183] is included in Table 4.3.

4.1.3. Toxic gas release

4.1.3.1. Design approach for toxic gas release

Some toxic materials such as sulphur dioxide, sulphur trioxide, sulphuric acid and hydrogen iodine are treated in the thermochemical water splitting hydrogen production system. The control room of the HTGR plant shall be protected against these materials to operate safely in all operational states [151]. When these materials are released and dispersed toward the HTGR, they can enter the control room through the ventilation system. To maintain the control room in a safe state or to bring it back into a safe state, appropriate measures shall be provided to decrease the toxic gas concentrations in the control room to below the acceptable limits.

Gas detectors shall be provided to detect toxic gas concentrations at the air intake of the ventilation system. When a gas concentration exceeds the acceptable limit, the ventilation system shall be shutdown to isolate the control room from the outside air. The control room and the ventilation shutdown system shall be low leakage construction to keep safe state. However, the toxic gas concentration in the control room will slightly increase due to in leakage of air. If the toxic gas concentration seems to exceed the acceptable limit, the recirculation air filter system in the control room will operate to reduce the toxic gas concentration to below the acceptable limit.

TABLE 4.3. PRELIMINARY HAZARD ASSESSMENT FOR THE HYS H_2 PRODUCTION PROCESS

Item	Hazard	Discussion
Concentrated H_2SO_4 at high pressure and temperature	Loss of containment of highly corrosive acid resulting in a release to the environment. High pressure can result in jet or spray release	Handling of concentrated H_2SO_4 is industrial practice. However, the high pressure employed in this process have the potential that personnel may come into contact with the liquid at a significant distance from the leak point. Corrosion resistance of metals to sulphuric acid is a strong function of temperature, fluid velocity, and concentration. Care must be taken to ensure that operating conditions are well understood before equipment is specified, and that actual operating conditions do not significantly vary from design. Joints should be minimized to reduce potential for leaks. Splash guards should be employed around pumps and joints near personnel.
Concentrated SO_2 at high pressure	Loss of containment of toxic gas resulting in a release to the environment. High pressure can result in jet or spray release	Large quantities of SO_2 at high pressure represent a serious toxicity hazard. Industrial experience with the safe operation of Claus plants may be a useful reference. The possibility of the release of large quantities of SO_2 from the anolyte solution in case of a change in temperature or pressure should be considered.
H_2 purification and compression	Loss of containment of flammable gas at high temperature and pressure resulting in fire or explosion	The conditions of these operations are within the experience of the industrial gases industries. Standard safety measures should be incorporated into the design. Due to the flammability of the H_2, joints and fittings should be avoided in the piping system. The possibilities of a jet fire or confined vapour cloud explosion in the region of potential leak points should be considered in the development of the plant layout.
O_2 purification and compression	The enhanced flammability of materials in O_2 resulting in equipment fire	All piping, fittings, and equipment exposed to > 25% oxygen must be oxygen-clean before startup. Fittings that are oxygen-cleaned at the factory must be shipped sealed. The use of soft materials and lubricants in contact with oxygen-enriched streams should be minimized. Fluorinated compounds such as Teflon and Viton are normally used for seals and per-fluorinated materials as lubricants. The use of O_2 as the regeneration gas for the TSAs will require that the maximum regeneration temperature and pressure be considered in the specification of the materials of construction for the adsorber vessels and piping that will be exposed to the hot gas. It is standard industry practice to place O_2 compressors inside of barriers for containment and personnel protection in case of a fire. The frequency of fires in such equipment should be considered in plant layout.
Sulfuric acid decomposer	Loss of containment of high pressure He. Contamination of He stream due to tube leaks and acid corrosion of He heat exchange equipment	Keeping the pressure of the He stream above that of the decomposer should minimize acid leakage into the He in the event of a leak.
Water treatment	No extra ordinary risk	This system should be standard equipment routinely used in industry with standard safety measures.

4.1.3.2. Evaluation of separation distance for toxic gas

Upper limits of the toxic gas concentration for human being are presented in many guidelines. The limits in the control room can be determined based on such authorized values. US-NRC regulatory guide recommends the upper limit from ‘immediately dangerous to life and health’ (IDLH) issued by the National Institute for Occupational Safety and Health (NIOSH) [184].

The IDLH limits are the values for 30 minutes exposure limit to eliminate death or permanent adverse health effects. Physical incapacitation does not occur within 2 minutes of exposure. The US-NRC considers that a control room operator will take a self-contained breathing apparatus within 2 minutes. Although operators maintain their safety actions, the hydrogen production system seems to be dangerous for a safe plant operation.

JAEA considers another safety approach in which operators are not expected to take breathing apparatus to reduce the risk of own health damage. The upper limit of toxic gas concentration in the control room has been decided to permit 60 minutes exposure. The 'emergency response and planning guideline' (ERPG) by the American industry health association (AIHA) and 'acute exposure guideline level' (AEGL) by the US-EPA are employed [185]. In the EPRG guideline, three levels of gas concentration limits for sulphuric acid, sulphur dioxide and sulphur trioxide for one hour exposure are defined as shown in Table 4.4.

TABLE 4.4. GAS CONCENTRATION LIMITS IN EPRG

Gas	Condition		
	ERPG-1	ERPG-2	ERPG-3
SO_2 (ppm)	0.3	3	15
(mg/m^3)	0.9	8.6	25.7
SO_3 (mg/m^3)	2	10	30
H_2SO_4 (mg/m^3)	2	10	30
Weight average (mg/m^3)	1.6	9.4	28.3

ERPG-1 is the limit without experiencing mild and transient adverse health effects. ERPG-2 is the limit without experiencing serious health effects or symptoms which could impair an ability to take protective action. ERPG-3 is the limit without experiencing life-threatening health effects. The weight-averaged limits corresponding to the released gas composition in the sulphur–iodine process where the fractions of SO_2, SO_3 and H_2SO_4 are estimated to be 0.25, 0.35 and 0.4, respectively, are also listed in the table. AEGL defines five levels for exposure period from 10 minutes to 8 hours. AEGL-1 is for 8 hours exposure limit and AEGL-2 is 1 hour exposure limit. Table 4.5 shows the comparison of these exposure limits.

TABLE 4.5. UPPER LIMITS OF TOXIC GAS CONCENTRATION [Mg/m^3]

Chemical Name	IDLH	EPRG-2	AEGL-2 (1 h)	AEGL-1 (8 h)
SO_2	262	8.6	—	0.5 (0.2 ppm)
SO_3	15	10	8.7	0.2
H_2SO	15	10	8.7	0.2
HI	—	—	115	5.2
I_2	21	5.2	—	—

— data not available.

The separation distance against toxic gas is determined by the results of atmospheric dispersion analysis. JAEA employs SLAB model which considers density effect of released gases. Table 4.6 shows the analytical conditions [186] and Fig. 4.20 shows the analytical result. The distribution of gas concentrations varies with time. Toxic gas cloud carries dangerous concentrations far away from release point. Trend of the gas concentration at the

point of 227 m (which is the minimum distance to meet design limits.) from the release point is shown in Fig. 4.21. High gas concentration level continues for 20 minutes. The gas concentration in the control room is evaluated under the condition of a control room air exchange rate of 0.06 per hour, which has low leakage construction features and automatic isolation system. Figure 4.22 shows the analysis result. The maximum concentration of the sulphuric acid mixed gas is 9.3 mg/m^3 which is lower than the upper limit of ERPG-2. But duration is longer than 60 minutes.

TABLE 4.6. ANALYTICAL CONDITIONS OF TOXIC GAS CONCENTRATION

Item	Condition
Amount of gas released (kg)	1000
Pressure (MPa)	0.1
Release mode	
Wind speed (m/s)	1
Atmospheric stability category	Stable
Gas composition H_2SO_4 : SO_2 : SO_3	0.4 : 0.25 : 0.35

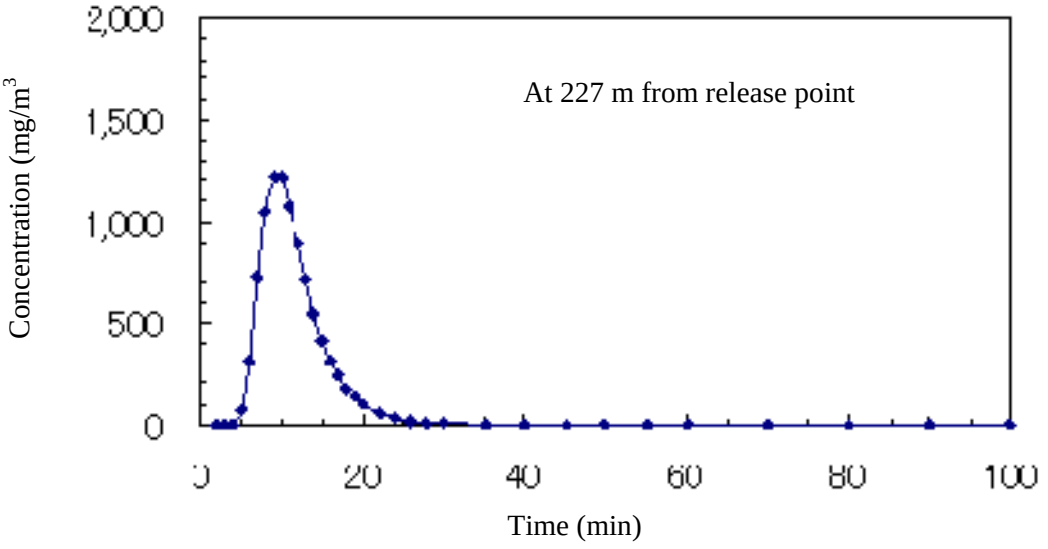

FIG. 4.20. Transient concentration at 227 m distance from release point during toxic gas dispersion.

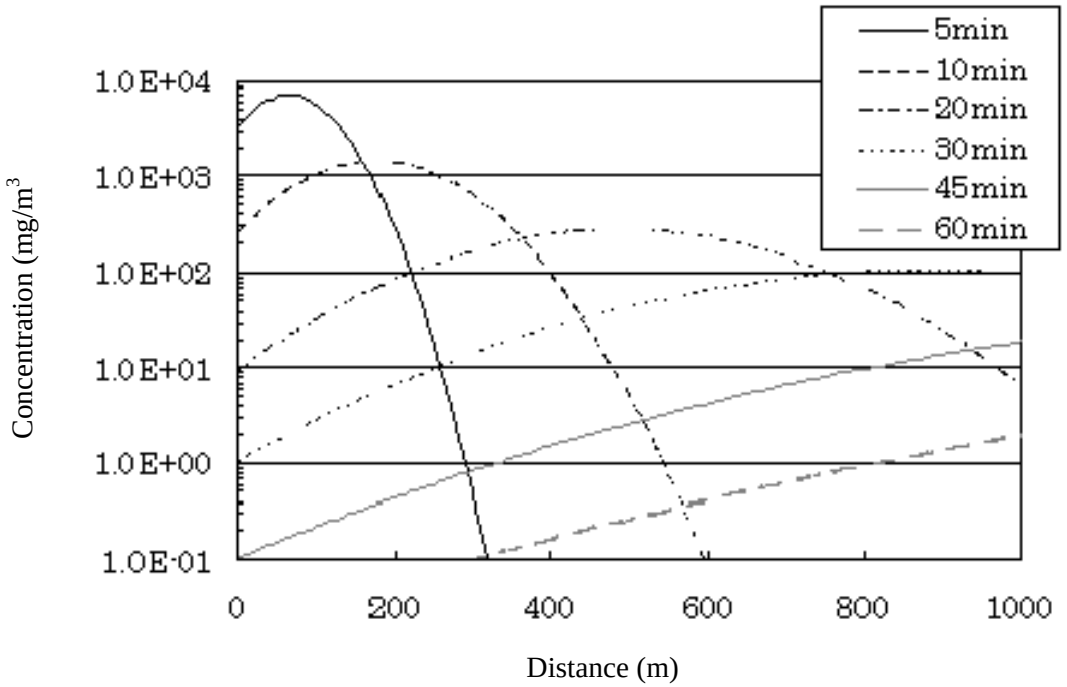

FIG. 4.21. Trend of the gas concentration at 227 m from the release point.

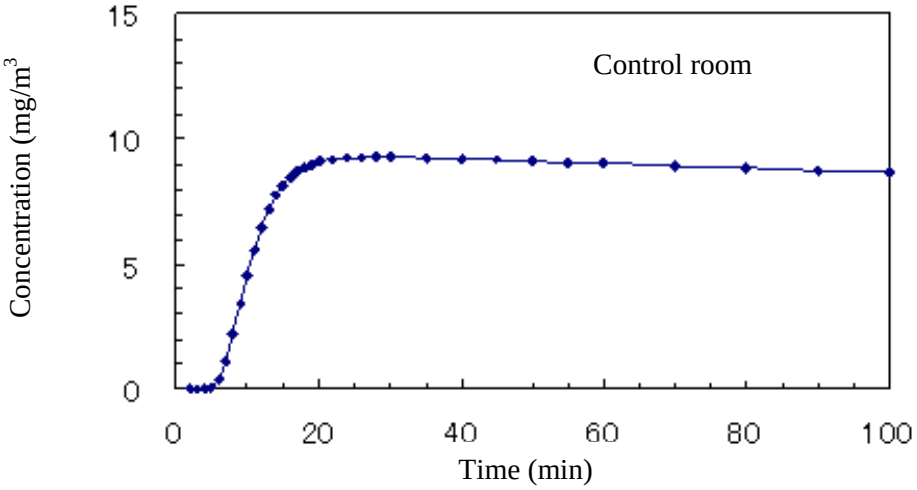

FIG. 4.22. Trend of the gas concentration in the control room.

To reduce the duration of high toxic gas concentration level in the control room, intake of the fresh air should be considered after the gas concentration outside the control room becomes lower. Figure 4.23 shows the trend of gas concentration in the control room. The toxic gas concentration in the atmosphere decreases of 10 mg/m^3 after 30 minutes, then the isolation system is deactivated to take fresh air into the control room. The gas concentration in the control room decreases at the level of EPRG-1 after 40 minutes and at AEGL-1 after 60 minutes according to the atmospheric concentration The exposure period to the gas mixture for concentrations ranging from 1.6 mg/m^3 (ERPG-1) to 9.4 mg/m^3 (ERPG-2) is about 35 minutes, which allows the operators in the control room to perform actions without any serious health separation distance of 227 m is sufficient for 1000 kg of toxic gas release from sulphuric acid decomposition process in the S–I process H_2 production system.

Gas concentration in the field depends on the meteorological conditions and the concentration in the control room depends on the air exchange rate. So the safe distance strongly depends on these conditions. After completion of the detailed design of the cogeneration HTGR, the separation distance shall be evaluated under realistic accident conditions.

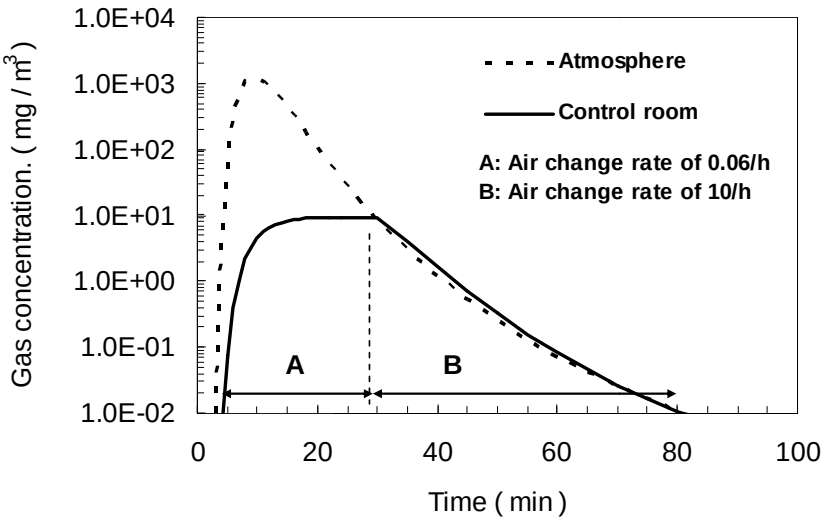

FIG. 4.23. Gas concentration in the control room at 227m from the release point.

4.2. SAFETY ISSUES FOR DESALINATION SYSTEM

From the HTGR thermodynamic cycle it can be seen that the HTGR overall thermal process disposes almost all of its waste heat via two large heat exchangers from the helium gas to buffered demineralized water: the precooler and the intercooler. HTGR waste heat at precooler and intercooler can be used as a source of thermal energy for the desalination plant.

4.2.1.1. Safety objectives

The safety of a desalination system mainly depends on the safety of the nuclear reactor and the interface between the nuclear plant and the desalination system. Adequate safety measures must be introduced to ensure near zero radioactivity release to the product water. The risk for accidental radioactivity carry-over is to be assessed. The basic objective is to prevent radioactive contamination of the desalination system and/or the atmosphere. It is necessary to ensure that the desalination plant should not cause any disruption and malfunction in the nuclear power plant. At the same time, perturbations to the desalination plant due to the nuclear power plant need to be analyzed.

4.2.1.2. Safety analysis of nuclear desalination plant

Safety analysis is the tool for confirming the adequacy and efficiency of the provisions in defense in depth. The most commonly accepted techniques of deterministic safety analysis used in the safety analysis of HTGRs are adequate for nuclear desalination plants (NDP). In a deterministic safety analysis, response of an NDP is predicted and analyzed for postulated initiating events (PIE), which can be anticipated, operational occurrences, or design basis accidents (DBA) [187].

The safety analysis of a NDP can be performed by

- Identification of the defense-in-depth barriers in the NDP;
- Construction of the postulated initiating event list (limited to design basis accidents);
- Analysis of the accident scenarios and its consequence;
- Verification of design with respect to acceptance criteria.

There are two aspects to implement the defense in depth. One is to provide barriers that would have to be successively breached for radioactive material to escape outside the plant. The other is to prevent the barriers from being breached. As stressed, the first aspect of defense in depth in the design is the provision of a series of physical barriers to confine the radioactive material at specified locations. The integrity of these barriers is ensured by conservative design margins and by high quality in manufacture, inspection and maintenance. In the case of failure of one or more of these passive barriers, active engineered safety systems are provided to ensure the integrity of the remaining barriers. The second aspect of the defense-in-depth strategy is to prevent the barriers from being breached. This is accomplished by the design of the plant operational systems.

An examination of the defense-in-depth barriers and a look at the NDP as a whole, six main barriers can be identified to avoid contamination of the fresh water product. These are

1. Tri-structural-isotropic (TRISO) coated fuel particles;
2. Ceramic layer of silicon carbide (SiC). It provides fission product confinement capability up to temperatures as high as 1600°C. The ability of TRISO fuel particles to contain fission products at high temperature help greatly in designing safety system

and mitigation measures and make it possible to eliminate adverse consequences of many severe accidents by design.

3. Precooler/intercooler tube walls;
4. Isolation heat exchangers;
5. Desalination plant;
6. Desalination plant isolation system (between the plant and distribution-piping grid).

The desalination plant itself also acts as a barrier in preventing radioactive contamination of the fresh water product as if any radioactive isotopes did enter the desalination system feed water stream, it would be left behind in the concentrate in MED desalination system. This means that, in case there is a release of fission products due to the catastrophic damage of the fuel matrix and fuel element cladding, contamination could reach the fresh water product only by a chain of failures. The precooler and intercooler tube would need to rupture, the reactor trip would have to fail, isolation heat exchanger tube walls would have to break simultaneously, and other safety systems would have to fail to perform its function.

Safety aspects with regard to desalination system coupling include the fact that desalination systems connected to critical systems should be included in the appropriate safety analysis reports (SAR). This would require the equipment to be seismically designed and qualified, which could have an adverse effect on the capital cost of the plant. Waste heat coupling schemes seems to be the only arrangement where this additional aspect could be designed to have a minimal impact. This aspect, however, has not been studied or incorporated into the costing analysis of the previously mentioned configurations.

4.2.1.3. Safety analysis of isolation system in HTGR

The isolation system design should ensure the performance of the isolation function that is fulfillment of safety requirements during all foreseen conditions, without relying on non-categorized components, in the required time and with the required reliability. BARC has carried out the safety analysis of the isolation system of a hybrid MED–RO desalination system coupled to HTGR as shown in Fig. 4.24.

i. Design basis of isolation system

The design basis of the isolation system covers the following postulated initiating events:

A. Operational transient in HTGR and desalination plant in terms of flow, pressure and temperature, etc.;
B. Leaks in the precooler and intercooler heat exchangers;
C. Leaks in the isolation heat exchangers working as barriers;
D. Failures in the IL pressure control;
E. Failures in the IL circulating pump.
F. Failures in the IL circulating pump in desalination plant loop
G. Failure of MED desalination plant
H. Failure of RO desalination plant

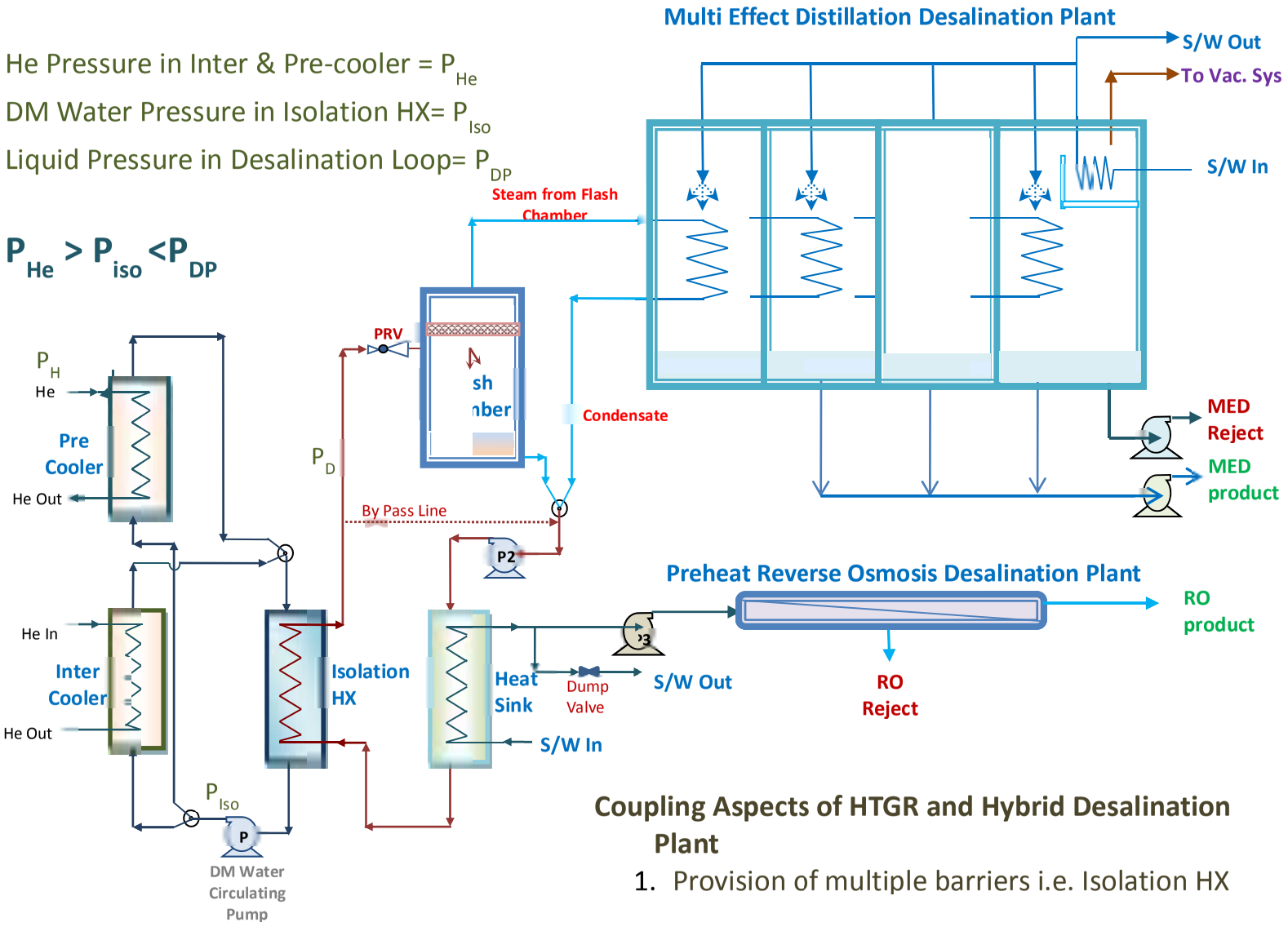

FIG. 4.24. Coupling of HTGR plant with hybrid MED–RO plant.

ii. Predicted response to postulated initiating events

A. Operational transient in HTGR and desalination plant in terms of flow, pressure and temperature, etc.

HTGR waste heat at precooler and intercooler is used as a source of thermal energy for the desalination plant. In case of sudden decrease or cessation of steam requirement in the MED desalination plant due to transients or shutdown of the desalination plant, a bypass line in the desalination loop will be used to divert hot water from the isolation heat exchanger directly to the heat sink. Heat will be rejected at the heat sink, so it will not affect HTGR operation.

It is to be mentioned that this transient can result a minor feedback of thermal transient in the HTGR loop also. But these transients are expected to be similar to the transients already considered in HTGR design, such as loss of heat sink, loss of load. So no transient more severe than those already addressed in the HTGR design are expected to occur as a result of addition of this desalination plant.

Passive heat removal in HTGR can be accomplished by the heat conduction through the graphite holding the TRISO particles, followed by convection and radiation in the structures and other media in absence of the primary coolant. Also due to large heat capacity of graphite in the HTGR core, HTGRs have slow and stable response in transients caused by initiating events, facilitating better reactor self control at all levels of defence in depth.

Likewise transients originated in HTGR will have an impact on operational stability and availability of the desalination plant, but it would not cause any radiological consequences. One of the most severe transients for the reactor core is the depressurization which happens very rapidly for the coolant. But even in the case of a depressurization, it has been shown that the maximum temperature of the fuel particles will remain below 1600°C, due to the very high thermal conductivity and heat capacity of the graphite assemblies, and to the choice of a non-thermally insulated metallic primary circuit, since the residual power will be removed by radiation heat transfer through the pressure vessel.

B. Leaks in the precooler & intercooler heat exchangers

Although severe accidents involving core melting should not occur in HTGRs, it will be important to avoid a major helium leakage, because reactor investment could be lost if fission products are released inside the primary circuit. For these reasons, leak-before-break procedures, evaluating if it is possible to detect a crack by leakage during normal operating state, far before the crack becomes unstable during a transient, are very important for gas cooled reactors.

C. Leaks in the isolation heat exchangers working as barriers

In the desalination plant loop, the pressure is higher than the IL pressure. Any leak in the IHX will cause demineralized water to leak into the IL. But there will be no carry-over of radioactivity from the isolation loop to the desalination plant loop in case of a failure in the isolation heat exchanger tubes. A leak will reduce the differential pressure between these two loops and the operator will be informed for a safe shutdown of the desalination plant.

D. Failures in the IL pressure control.

An isolation loop pressure control is necessary to maintain pressure reversal. The intermediate loop is pressurized by the demineralized water circulating pump, and this pressure is controlled by a pressure relief valve (PRV) at the flash tank inlet. The pressure reversal can also be monitored by installing a desalination plant transmitter between the shell side and tube side liquid of the isolation heat exchanger.

E. Failures in the IL circulating pump

The isolation loop is to be provided with feed pumps (2×100%) to prevent a loss of circulation in the IL due to failure in one IL feed pump.

F. Failures in the IL circulating pump in desalination plant loop

Desalination is to be provided with feed pumps (2×100%) to prevent a loss of circulation in the desalination plant due to failure in one feed pump [187].

G. Failure of MED desalination plant

In case of failure of the MED desalination plant, a bypass line in the flash loop will be opened and all heated water will be bypassed to the heat sink for heat rejection.

H. Failure of RO desalination plant

In case of failure of the RO desalination plant, the dump valve will be opened and heated sea water in the heat sink will be dumped to the sea.

4.3. COUPLING SCHEMES AND CONTAMINATION OF END PRODUCTS FOR HYDROGEN PRODUCTION

4.3.1. End product purity and public radiation safety

If the two power–technological complex options, with and without the intermediate circuit, are compared in terms of end product purity, the latter option might be preferred since it avoids such negative effects of the intermediate circuit as

- reduction of the grade of heat transported to the process plant;
- reduction of the plant efficiency.

The possibility of excluding the intermediate circuit is supported by the HTGR safety concept which provides

- containment of radioactivity inside fuel particles with multilayer coatings;
- guaranteed coating integrity;
- use of helium as the primary coolant because helium is not activated in the core;
- maintaining the required primary coolant purity using the coolant purification system.

Integrity of the reactor fuel, in turn, is possible due to:

- reactor inherent safety based on negative feedback and natural heat transport mechanisms;
- reactor transfer to subcriticality when control and compensation rods are inserted into the core by gravity;
- reactor core protection against deformation (or damage) in case of internal or external impacts (airplane crash, shock wave, hydrogen explosion in the interfacing systems);
- removal of decay heat to maintain fuel safe operational temperatures in all accidents, including full loss of coolant accidents (LOCA), by the natural mechanisms of heat conduction, radiation and convection.

Consequently, the required end product purity can be provided by:

- retention of fission products in the fuel;
- introduction of an intermediate circuit;
- introduction of effective purification systems;
- minimization of neutron radiation impact on the process circuit;
- pressurization of structures;
- use of proper materials;
- application of coatings and provision of specific equipment operating conditions to reduce tritium permeability of working surfaces (such as oxide film formation on heat exchange surfaces [180];
- maintenance of the pressure gradient directed from the process circuit to the primary circuit; and possibility of fast reactor isolation from the process circuit in abnormal operating conditions on alarms indicating excess of allowable radioactive/chemical contamination limits or reduction of the pressure gradient between the primary and process circuits.

Besides, it is necessary to take measures to protect the personnel against toxic effects of substances released from the damaged process plant equipment.

4.3.2. Coupling of GTHTR300C to sulphur–iodine cycle

Hydrogen production system is coupled with the HTGR via a heat transfer loop. Safety requirements are common for all types of reactor system, which is to protect people and the environment from harmful effects of ionizing radiation. The exposure of the public remains as low as reasonably achievable (ALARA) in operational states, and radiological risk is acceptably low in accident states. The defense-in-depth concept is employed to prevent accidental release of radioactive materials.

Hydrogen production system coupled with the HTGR should be a non-nuclear grade chemical plant to reduce construction and maintenance cost because hydrogen produced by the cogeneration HTGR system must have economic competitiveness with hydrogen produced by the conventional fossil system. Figure 4.25 shows an image of the design classification of the GTHTR300C designed by the JAEA [24]. With the following requirements, a non-nuclear grade hydrogen production system in a cogeneration HTGR is achievable:

- The HTGR can continue safe operation independent of operational conditions of the hydrogen production system.
- The heat transfer loop, which provides hot helium gas from the IHX to the hydrogen production system, is not required to perform any nuclear safety function to prevent anticipated operational occurrences and accidents.
- Events originating in the hydrogen production plant do not affect the safe operation of the HTGR.

The functions of the heat transfer loop are primary helium cooling, pressure load control on the IHX heat exchanger tubes, and impurity concentration control during normal operation.

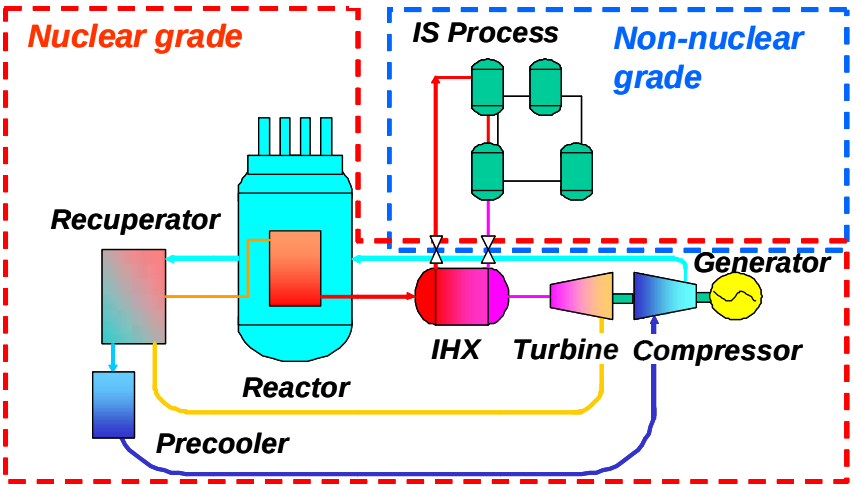

FIG. 4.25. Design classes of the GTHTR300C.

4.3.2.1. Primary helium cooling

A change of thermal load of the hydrogen production system causes a variation of the gas turbine inlet helium temperature. The safety functions mitigate the thermal transient to prevent an emergency shutdown of the gas turbine system. The gas turbine system has four control valves (Fig. 4.26), which are the turbine bypass flow control valve (CV1), the recuperator inlet temperature control valve (CV2), the turbine inlet temperature control valve (CV3), and the turbine bypass valve (V4) for an emergency shutdown of the gas turbine. The CV1 can control the turbine rotation speed by reducing the flow rate in the core and the gas turbine as the generator load decreases. The CV2 can control the recuperator inlet helium temperature below the design limit of the recuperator heat exchanger tubes which is 650°C in the GTHTR300C by injecting low temperature helium gas from the compressor outlet. The CV3 can control the turbine inlet temperature at the rated gas turbine operation condition which is 850°C in the GTHTR300C. The V4 is a backup valve for CV1, and is designed to open at loss of generator load and after turbine trip.

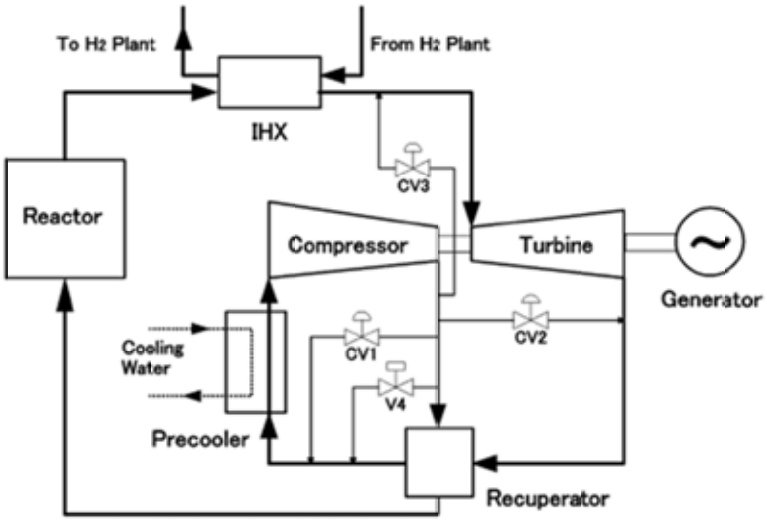

FIG. 4.26. Arrangement of control valves in the GTHTR300C.

Thermal load degradation of the hydrogen production system can be detected as a temperature increase at the turbine inlet. The operation sequence of this event is shown in Fig. 4.27.

At first, the CV3 opens to control the turbine inlet helium temperature. The load balance between the gas turbine, the compressor, and the generator changes and the turbine rotation speed increases. Then the CV1 opens to control the turbine rotation speed. Actuation of these control valves decreases the helium flow in the core. The reactivity control system reduces the reactor power to keep the reactor outlet helium temperature at rated operation condition of 950°C.

Thermodynamic analysis of the loss of thermal load of the hydrogen production system in the GTHTR300C was performed. The analytical result is shown in Fig. 4.28. In this event, the flow rate at CV1 and CV3 are 4 kg/s and 34 kg/s at 1000 s, respectively. The increase of turbine rotation speed is only 6 rpm at 12 seconds. The flow rate in the core decreases to 88% of the rated condition. And the reactor power decreases to 505 MW. CV1, CV3, and the reactivity control system can control the nuclear power plant within the operational limit, so that the nuclear power plant can continue the power generation operation independent of the hydrogen production system operation. This result shows an availability of the control valve system to continue safe reactor operation independent of the hydrogen production system.

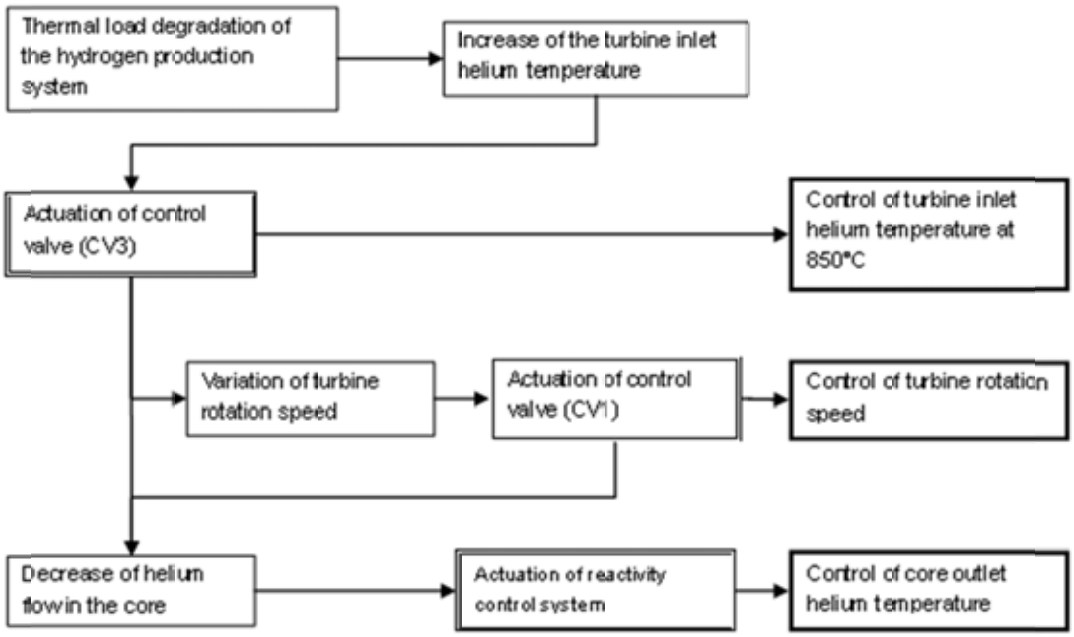

FIG. 4.27. Operation sequence of thermal load degradation of the hydrogen production system.

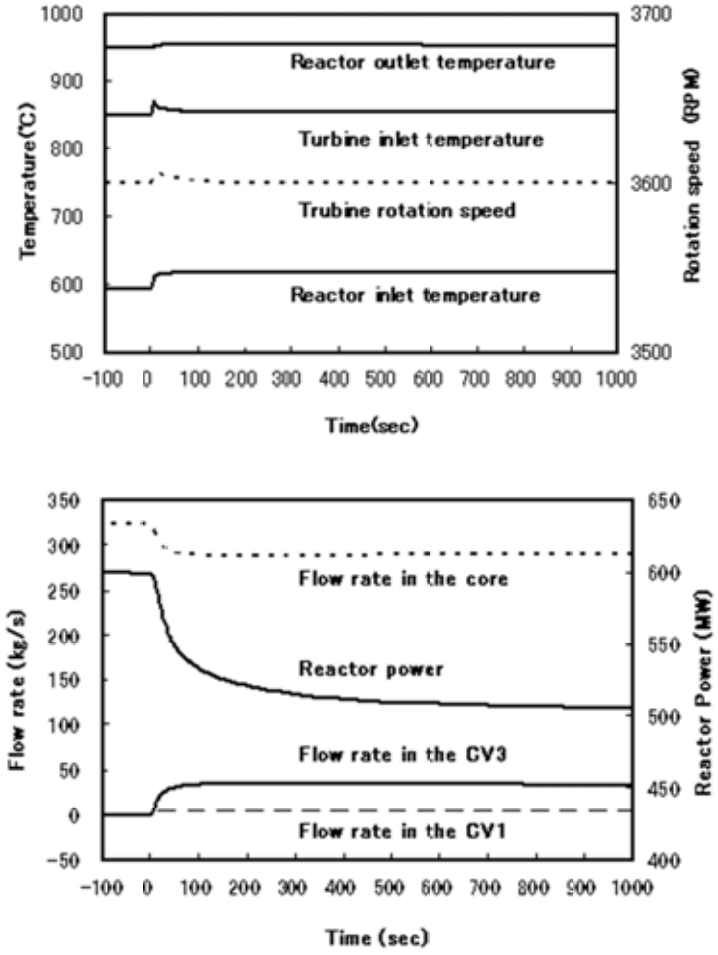

FIG. 4.28. Analytical result of thermal load degradation of the hydrogen production system.

4.3.2.2. Pressure load control

Temperatures of the IHX heat exchanger tubes are over 900°C in rated operation condition. A large pressure load on the tubes for long time periods increases creep damage, and results in shortening the operation lifetime. JAEA employs differential pressure control method in which the pressure of the secondary helium flowing inside the tubes of the IHX is controlled slightly higher than that of the primary helium in the rated operation condition. The pressure of the process fluids in the hydrogen production system is lower than that of the secondary helium to prevent ingress of the flammable and toxic materials into the secondary helium loop in the event of heat exchanger tube failure of the chemical reactor heated by the secondary helium. The secondary helium pressure decreases and the pressure load on the IHX heat exchanger tube increases in this event.

As discussed previously, the HTGR with gas turbine power generation system can continue operation when the hydrogen production system is shutdown. To continue long term power generation after secondary helium depressurization, the differential pressure of the IHX heat exchanger tubes must be controlled. The GTHTR300C provides isolation valves on the heat transfer loop to ensure confinement of the reactor system and isolate the hydrogen production system from the HTGR. After closing the isolation valves, the helium supply system supplies helium gas between the IHX and the isolation valves to recover the secondary helium pressure and to control the differential pressure. The operation sequence in the secondary helium depressurization is shown in Fig. 4.29.

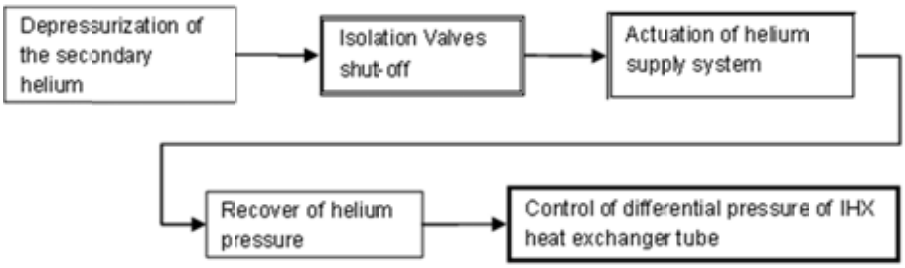

FIG. 4.29. Operation sequence of depressurization of the secondary helium in the heat transfer loop.

4.3.2.3. Tritium contamination

With regard to radioactive contamination of the product gas, the principal hazard is considered to be the extremely mobile tritium. While a pipe rupture may be excluded by a proper design and quality control, the transition of hydrogen or its isotopes by permeation through intact walls is easily possible.

There are two basic mechanisms of radioactivity transport from the primary circuit into adjoining ones:

- diffusion and leaks through micro defects in the barriers between the radioactive and nonradioactive circuits;
- depressurization of heat exchange surfaces separating the circuits [180].

The major contaminant of produced hydrogen is tritium because of its high diffusion permeability and relatively short half-life. Being a most important biologically relevant nuclide, tritium is referred to the group of most important dose-forming nuclides. It is well-known that nuclear reactors are a source of man-made tritium. Tritium generated in nuclear reactors gets into the environment with gas releases and liquid wastes. Different reactor types generate tritium at different rates. Tritium generation in HTGRs equals about 19 GBq (0.5 Ci) per year per 1 MW of thermal power. In the wastes from nuclear power plants, tritium exists in three main forms: tritiated water (HTO), tritiated hydrogen (HT), and tritiated methane (CH_3T). The life of tritiated hydrogen and tritiated methane in the atmosphere equals 5 to 10 years. Main mechanisms of tritium extraction from the atmosphere are bacterial oxidation and photochemical oxidation, and the end product in both cases is tritiated water.

Tritium is constantly produced by ternary fission of the fuel and neutron capture reactions of ^{3}He, ^{6}Ll, ^{7}Li and ^{10}B in the core and permeates through the heat exchanger tubes of the IHX from the primary helium into the secondary helium. The tritium concentration in the secondary helium shall be controlled at levels lower than the acceptable limit. Because tritium is a low energy beta radiation emitter, exposure via inhalation and ingestion are of most concern. The dose limit for the public is recommended at 1mSv/a according to the IAEA safety standard [188]. Dose coefficients of HT and HTO for people 18 years old and older are 1.8×10^{-15} Sv/Bq and 1.8×10^{-11} Sv/Bq, respectively. Thus the acceptable limits of the average concentration of HT and HTO in the air are 62.5 Bq/cm^3 and 6.3×10^{-3} Bq/cm^3 when the breathing rate is 1 m^3/h. The limit of HTO in the water is 60 Bq/cm^3 when the water ingestion is 2.5 L/d [189].

(i) Germany

Within the frame of the PNP project in Germany, experimental investigations were made on the permeation process in high temperature alloys. Test facilities allowed both long term (1000–3000 h) at temperatures up to 1000°C and pressures up to 3.2 MPa. Short term

analyses were used for preselection of materials. Results have shown that in-situ oxide layers show a large inhibition of permeation at temperatures above 650°C. Still, the uncertainty is relatively large at lower temperatures and also if looking at respectively measurements from operated HTGRs.

Assuming a gas purification system in the IHX cycle of the PNP reactor, the tritium release rate was estimated to be less than 0.2 GBq (5×10^{-3} Ci) per MW(th). For the product hydrogen, this translates into a contamination of less than 0.37 Bq (10 pCi)/g of H_2. This figure was deemed tolerable in the PNP-project in comparison to other allowed levels of radioactive contamination. Other countermeasures to be taken are a reduction of the lithium contents in the reactor graphite structures, an enhancement of the purification rate in the helium circuits, doping of the secondary circuit with oxidizing impurities, or the employment of an additional intermediate circuit.

For the H_2 transportation process in the opposite direction, as a typical result, around 50 mL/(m²·h) of H_2 were measured at 900°C for typical steam reformer applications. These quantities of hydrogen could be easily removed by the gas purification plant. Of course, the stability of oxide layers during transients and other loads have to be considered and may influence the data.

According to the German 'preventive radiation protection ordinance', neither licensing nor announcement is required for the use of fossil products refined by nuclear process heat, whose tritium content does not exceed 5 Bq/g. This special case is the exception from the rule, where for any fabricated product, the specific radioactivity limit is lower by a factor of 10 compared to the above figure, i.e. 500 mBq/g [190]. The background for this special rule resulting from discussions in the context of the PNP project is the fact that, depending on the origin of the feed natural gas, the natural activity content would be already close to the free limits given by the law. In the new German preventive radiation protection ordinance issued in 2001, the free limit for tritium has been raised to an activity of 1 TBq or alternatively a specific activity of 1 GBq/g [191].

(b) Russian Federation:

In accordance with Russian radiation safety norms (NRB-99) [192], it is necessary to observe the following limits of allowable personnel exposure to tritium (Table 4.7).

In ongoing nuclear power plant projects, the annual exposure doses for the public in normal operating conditions are limited to 10 μSv for aerosols and 10 μSv for liquid wastes [193].

Taking into account the experience of prototype HTGR operation in the USA and in Germany, and the experience of Russian MHR-T reactor designing, we can reasonably expect that a HTGR with a thermal power of 600 MW will release about 9 250–11 100 GBq/a (250–300 Ci/a) of tritium into the primary circuit. Tritium formation is illustrated in Fig. 4.30 for the example of the HTTR circuit [143].

TABLE 4.7. LIMITS OF PERSONNEL EXPOSURE TO TRITIUM [192]

Nuclide	Half-life (a)	Compound type, inhalation	Maximum yearly intake (Bq/a)	Allowable yearly average volumetric activity (Bq/m$^{3)}$
^{3}H	12.3	G1 (tritiated water steam)	1.1×10^{9}	4.4×10^{5}
		G2 (gaseous tritium)	1.1×10^{13}	4.4×10^{9}
		G3 (tritiated methane)	1.1×10^{11}	4.4×10^{7}

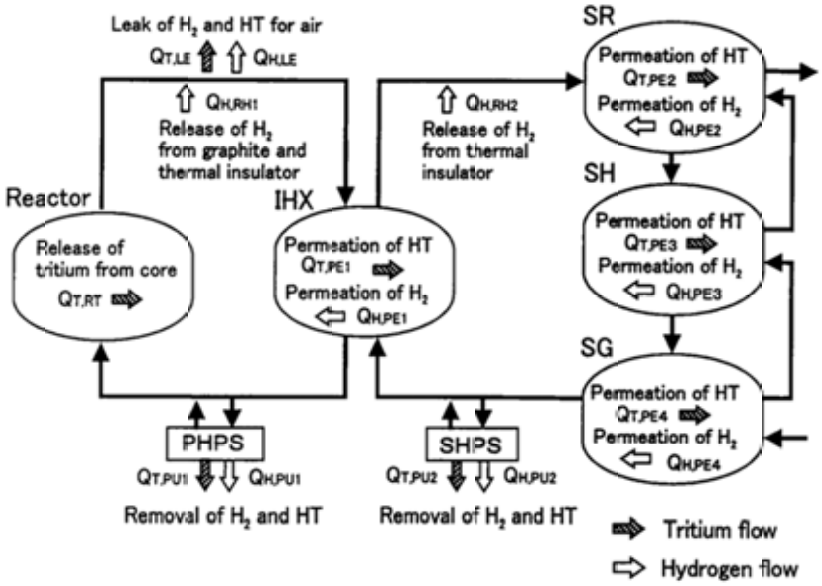

FIG. 4.30. Tritium flow paths in the HTTR circuit.

In accordance with the legislation of Germany, the allowable concentration of tritium in any product should not exceed 0.5 Bq/g (see previous section). Since the conservative concentration of tritium in the gas product equals ~9300 Bq/m^3, hydrogen production at an MHR-T-based power–technological complex using steam methane reforming (SMR) with direct heat transport and without an intermediate circuit is believed to meet the criteria established in the radiation safety norms (NRB-99) [180].

Activity estimations performed for the end product (ammonium nitrate) of Russian VG 400 reactor showed that the public exposure dose for tritium from the NPP was almost three orders of magnitude lower than the from the background radiation [180].

Analytical estimations performed by General Electric for an HTR-1170-based NPP with SMR show that even if the converted gas is contaminated with tritium with the activity of as high as 2775 GBq/a (75 Ci/a), the allowable limits of end product contamination will not be exceeded [180].

In the SMR process, there is a possibility of converted gas leaks, and this will require intensive ventilation in enclosed rooms and extra fire and explosion safety precautions (such as use of catalytic oxidizers) etc. to ensure additional protection against tritium contamination. A similar analysis performed for HTO leaks shows that the concentration limits will be observed with a considerable margin even in conservative estimations.

(c) Japan

Tritium production rate in the GTHTR300C is estimated at 1.5×10^8 Bq/s. Tritium circulating in the primary helium loop is removed by the primary helium purification system or permeates the heat exchanger tubes of the IHX. The concentration in the primary helium is estimated at about 6×10^5 Bq/(g He) (≈ 100 Bq/cm^3), where the helium inventory is 10 000 kg, the flow rate of purification system is 1000 kg/h and the tritium permeation of IHX is 10% of the birth rate. The concentration in the secondary helium is about 3×10^5 Bq/(g He) (≈ 50 Bq/cm^3), where secondary helium inventory is 1000 kg, the flowrate in the purification system is 200 kg/h and the permeation rate to the hydrogen production plant is 10% of permeated tritium from primary loop. This estimate strongly depends on the flow rate the purification system. Tritiated water (HTO) in the helium gas is several orders of magnitude lower than elemental hydrogen (HT) [194].

Even if the HT concentration in the secondary helium is 50 Bq/cm^3, it is lower than the acceptable limit in the air to achieve the dose limit of the public. Helium leakage during operation is very small so that the effective dose against operators of the hydrogen production plant is negligibly low. A much larger quantity of helium is released in case of the secondary helium pipe failure. The operator may inhale the released helium gas for several hours during inspection tour or maintenance activities. The effective dose by HTO inhalation is estimated to be about 2μSv/h when the concentration of HTO is 0.5 Bq/cm^3, which is two orders of magnitude lower than that of HT, and the helium gas concentration in the air is diluted by 10%.

Tritium can also permeate to the hydrogen production system through the heat exchanger tubes of the chemical reactors. The permeated tritium reacts with water and hydrogen in the hydrogen production system and becomes HT and HTO. HT is released from the hydrogen production system with the product hydrogen, but HTO circulates in the hydrogen production system. The tritium concentration in the circulating water will be higher than in the secondary helium [194]. Circulating water is not drinking water so that operators and public do not directly ingest this water. However, from the safety design point of view, the concentration of HTO in the circulating water in the hydrogen production system must be as low as reasonably achievable. Draining the circulating water and injection of fresh water are effective means to reduce the HTO concentration. Product hydrogen containing HT shall be exempted from radiation management requirements. The exemption criterion is that the effective dose of public shall be lower than 10 μSv/a [188].

4.4. COUPLING SCHEMES AND CONTAMINATION OF END PRODUCTS IN DESALINATION SYSTEM

4.4.1. Heat supply from nuclear reactor (coupling)

When an integrated system is based on the utilization of a contiguous RO process, the coupling between the reactor and the process does not require any further optimization, except for the adaptation to local site conditions.

The most promising process, LT-HTME distillation, and the most widespread process, MSF, need heat. The heat could be obtained from the nuclear reactor by coupling the exhaust steam of the power plant with the brine heater.

For a thermal process such as the MED, the coupling is more complex. It is necessary that the thermohydraulic characteristics of such a coupling be determined precisely. In order to elaborate and optimize a given coupling scheme, it is necessary to determine the conditions which allow the transfer of the right amount of heat to the process with the least possible impact on the plant performance.

The formulation of thermodynamic equations concerning the heat and mass balances at different nodes of the coupling and their subsequent resolution with appropriate boundary conditions then leads to the determination of the basic parameters such as mass flow rate of the extracted vapour, and its ideal temperature for a given amount of desalted water production.

It should be recalled that in accordance with the safety analysis an intermediate circuit, comprising a heat exchanger, a flash tank, and a recirculation pump, is absolutely essential to the coupling. The dimensioning of these components is then obtained by resolving the appropriate heat and mass balance equations.

There are four different types of steam coupling which have different steam pressures [152]:

(1) *Highest permissible brine temperature with pressure of 0.2–0.37 MPa and condensing temperature of 120–140°C*

This case is suitable for MSF and MED, but the brine temperature should not exceed 120°C to avoid scale problems. The ideal arrangement is to obtain a large amount of heat from a dual purpose plant, by condensing all steam from the exhaust of the power unit turbine and releasing its latent heat to the desalted process. This could be possible if the turbines were designed to operate at an exit pressure of 0.2–0.37 MPa. Suitable extraction condensation turbines are already used in many dual purpose fossil fired plants and this could be used for turbines in water cooled reactors.

Another alternative is to extract some steam after partial expansion, then several relatively small back-pressure steam turbines connected in parallel, and designed to operate at 0.2 to 0.3 MPa exhaust pressure, may replace the original large condensing turbine. The smaller such back-pressure turbines are, the lower is their efficiency and the more expensive is the investment.

Thermal coupling

The thermal coupling consists of a heat exchange system between the nuclear reactor and the desalination plant, which has the function to eliminate any possibility of radioactive trace penetration into the desalination plant. There should be at least two barriers between the primary coolant and the saline water. The steam generator is the first barrier, and the brine heater is the second barrier, plus the pressure reversal where the brine pressure should be maintained at a higher level than the heating fluid, so if there were any leakage, it would go away from the desalination system, not into it.

Another sufficient barrier is the isolation loop as shown in (Fig. 4.31). This closed loop ia placed between the nuclear steam and the brine. In this system, the exhaust steam is condensed and heat is transferred to a medium within the loop which is used to heat the brine. This pressurized closed loop is expensive.

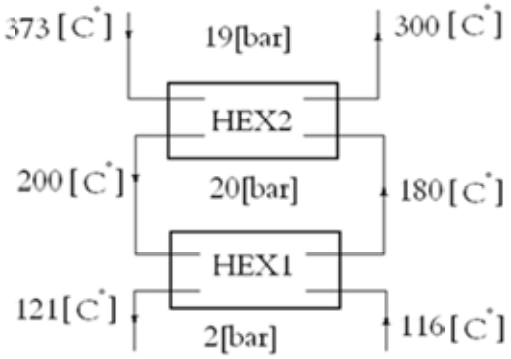

FIG. 4.31. Isolation loop.

Water cooled reactors suffer some disadvantages compared with conventional fossil fuel units:

1. The thermodynamic efficiency is lower than in conventional fossil fuel units because of the low steam temperature and pressure, and the wet steam. Thus more heat is released per kW(e) produced, so more energy losses.

2. The pressure in the steam cycle is lower than in the primary reactor cycle. Thus leakage may carry radioactive traces to the power–water interface.

As an example of energy consumption: a typical water cooled reactor of 600 MW(e) discharges about 1150 MW(th) at ambient temperature. If the steam expands in the turbine to a pressure of 0.25 MPa, the heat discharged by its condensation is about 1400 MW(th) and the electricity generated is about 350 MW(e). The amount of desalted water with a GOR of 12 is 624 000 m^3/day.

Pressurized water cooled reactors (PWR) and pressurized heavy water cooled reactors (PHWR) are safer as they have an additional barrier fluid between the reactor coolant and the desalination plant motive steam. Boiling water reactors are less attractive for thermal desalination as the reactor coolant reaches the condenser. An example of a water cooled reactor is the 'Thermos' reactor which is cooled by 0.9–1.0 MPa pressurized water at a maximum temperature of 137–140°C. The primary coolant is cooled by a secondary cycle of pressurized water having a pressure of more than 1.1 MPa and a maximum temperature around 128°C [152, 195].

(2) *Medium brine temperature with pressure of 30–40 kPa and condensing temperature of 69–76°C*

This case is suitable for most of low cost evaporators with aluminum heat transfer surface. Larger steam turbines of about 300 MW(e) are available that are capable of operating at the exhaust pressure of 30–40 kPa. Such turbines are designed to operate with dry cooling tower heat rejection.

For the thermal coupling in this case, the conditions in the brine heater are milder than in the previous case. Because of the low pressure in the desalination system, the isolation becomes more difficult. As the temperature is lower, the corrosion rate is slower. The Canadian reactor 'Slowpoke' with power sizes of 2–20 MW(th) is an example for this case. A thermal power of 10 MW(th)can desalt up to 4500 m^3/day [152].

(3) *Low brine temperature with pressure of 17–18.6 kPa and condensing temperature of 56.5–58.5°C*

In this case, there is no problem of producing a large amount of desalted water because of the availability of large turbines, minimum penalty on the power unit, maximum flexibility, simplicity, reliability, and safety. But due to the low temperature, at which this heat is supplied to the desalination plant, the GOR is smaller compared to the previous two cases. For instance, assuming 26°C seawater temperature and 56.5°C steam condensing temperature (17 kPa), the GOR of the MSF will be 3.5–4.5. For MED with aluminum heat transfer surfaces, the GOR could be 5.5–6.4.

While for the thermal coupling is the same as described in case 1. For MSF the steam condenser serves as the brine heater. The probability of leakage in this temperature is very small comparing with the previous two cases because of maintaining pressure reversal is very easy [152].

(4) *Cold brine temperature with pressure of 4–8 kPa and condensing temperature of 30–40°C*

The sea water here should be cold (20°C), so it is possible to adapt a special version of MSF, but number of stages is reduced and the GOR is as small as 0.5 to 2 [152].

4.4.1.1. Coupling aspects in nuclear desalination plant

In the case of nuclear plants that cogenerate heat and electric power, thermal energy can be extracted at suitable points in the power plant for use in the desalination plant. However, protective barriers must be included in all cogeneration modes to prevent potential carry-over of radioactivity [196].

(i) Thermal coupling to thermal desalination plant

Thermal energy can be supplied to the desalination plant via an intermediate heat transfer loop. In order to transfer thermal energy in such a configuration, there is a direct fluid coupling between nuclear reactor and desalination plant. This introduces the risk of radioactive contamination of the product water.

(ii) Electrical coupling to RO desalination plant

In the case of an RO desalination plant, the only energy supplied by the nuclear power plant is electricity to operate the desalination pumps. Since there is no thermal coupling between the reactor and the desalination plant, there is no direct path for a carry-over of radioactive materials from the reactor to the product water. However, as the RO plant shares common resources with the nuclear power plant such as common seawater intake, an outfall, and the effect of this on the possible contamination of the product water must be evaluated [197].

(iii) Thermal and electrical coupling to hybrid desalination plant

A hybrid desalination plant consists of both thermal and membrane-based desalination processes. Coupling hybrid desalination plant with a nuclear power plant is more complex as it involves both couplings.

It can be advantageous to use part of the electricity generated by the nuclear cogeneration plant to operate RO or MVC desalination plants in addition to thermal desalination plants. The hybrid system at the same location can play an important role in bringing down the water cost as well as making multiple product water qualities available. Fig. 4.32 shows a schematic of the coupling arrangement for a hybrid MED–RO plant [187].

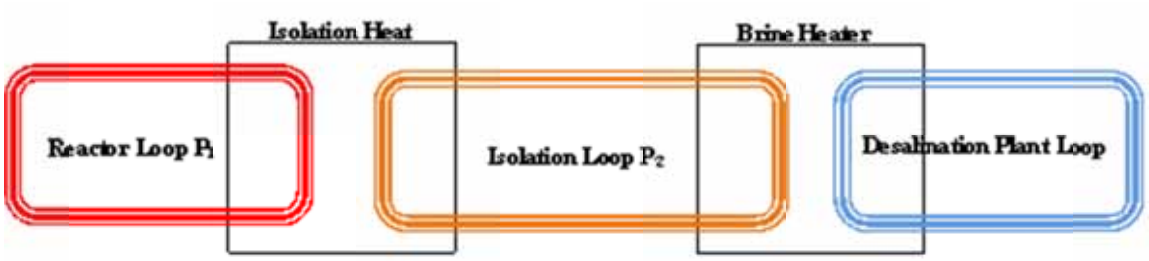

FIG. 4.32. Coupling of desalination plant to nuclear reactor by an isolation loop.

4.4.1.2. Safety design requirements for the coupling

Safety objective in nuclear desalination is translated into safety design requirements under defence in depth principle:

- Provision of multiple barriers between potentially radioactive material and product, i.e. isolation heat exchanger loop in between desalination plant and HTGR;
- Provision of engineered features preventing the radioactive material from reaching the product water, even in case of any credible sequence of failure.

4.4.1.3. Engineered safety features for prevention of the radioactive contamination of product water

Assuming a three loop system (i.e. an IL between reactor loop and desalination loop as shown in Fig. 4.31), pressures in these loops (P1, P2, and P3) may be adjusted in such a way that transfer between loops is in the favorable direction.

The best way, which is difficult in practice, is an arrangement where the reactor loop pressure is lower than the IL pressure which, in turn, lowers the product loop pressure. In this case, the transfer between loops is always in the safe direction.

In practice, systems are usually engineered in two ways:

(1) High–Low–High (H–L–H) configuration

The reactor loop pressure P_1 is higher than in the isolation loop P_2; the desalination loop pressure P_3 is higher than in the isolation loop, so (H–L–H). In this case, a pressure barrier against undesired transfer exists between the product loop and the isolation loop.

Advantages of this configuration are:

(a) Any leakage in the isolation heat exchanger will be directed to the isolation loop and not to the desalination loop.

(b) The allowed radioactive contamination for the isolation loop is slightly higher and more easily monitored.

Disadvantage is that the operating pressure in the desalination plant loop is higher which is difficult to use, as pressure of the desalination plant is dictated by the process and it is not very high.

(2) Low–high–low (L–H–L) configuration

The reactor loop pressure P_1 is lower than in the isolation loop P_2; the desalination loop pressure P_3 is lower than in the isolation loop P_2, so (L–H–L). In this case, a pressure barrier against undesired transfer exists between the reactor loop and the isolation loop.

Advantage of this configuration is that the radioactivities are enclosed inside the primary loop. Disadvantage is that is difficult to monitor the possible contamination of the IL and exclude the possibility of leakage from the IL to the final product.

4.4.2. Design of coupling system for HTGR and hybrid desalination plant

4.4.2.1. Coupling of LT- MED desalination plant with HTGR

An MED desalination plant is coupled to an HTGR nuclear power reactor along with an intermediate heat exchanger as an additional isolation loop (Fig. 4.33). It uses the flash loop to transfer heat to the desalination plant.

Buffered demineralized water is used as cooling media in the precooler and intercooler. This water is heated in the loop depending on the heat rejected in the precooler and intercooler. Also it is essential to ensure that no localized boiling is allowed to take place within these heat exchangers. Therefore, pressure in this loop should always be greater than the saturation pressure of the water at the temperature where it was heated up to.

In order to have the pressure reversal (H–L–H), pressure in the desalination plant loop should be greater than the intermediate loop pressure. Therefore, a higher pressure is maintained in this loop compared to the IL pressure. This is ensured by the demineralized water circulating pump.

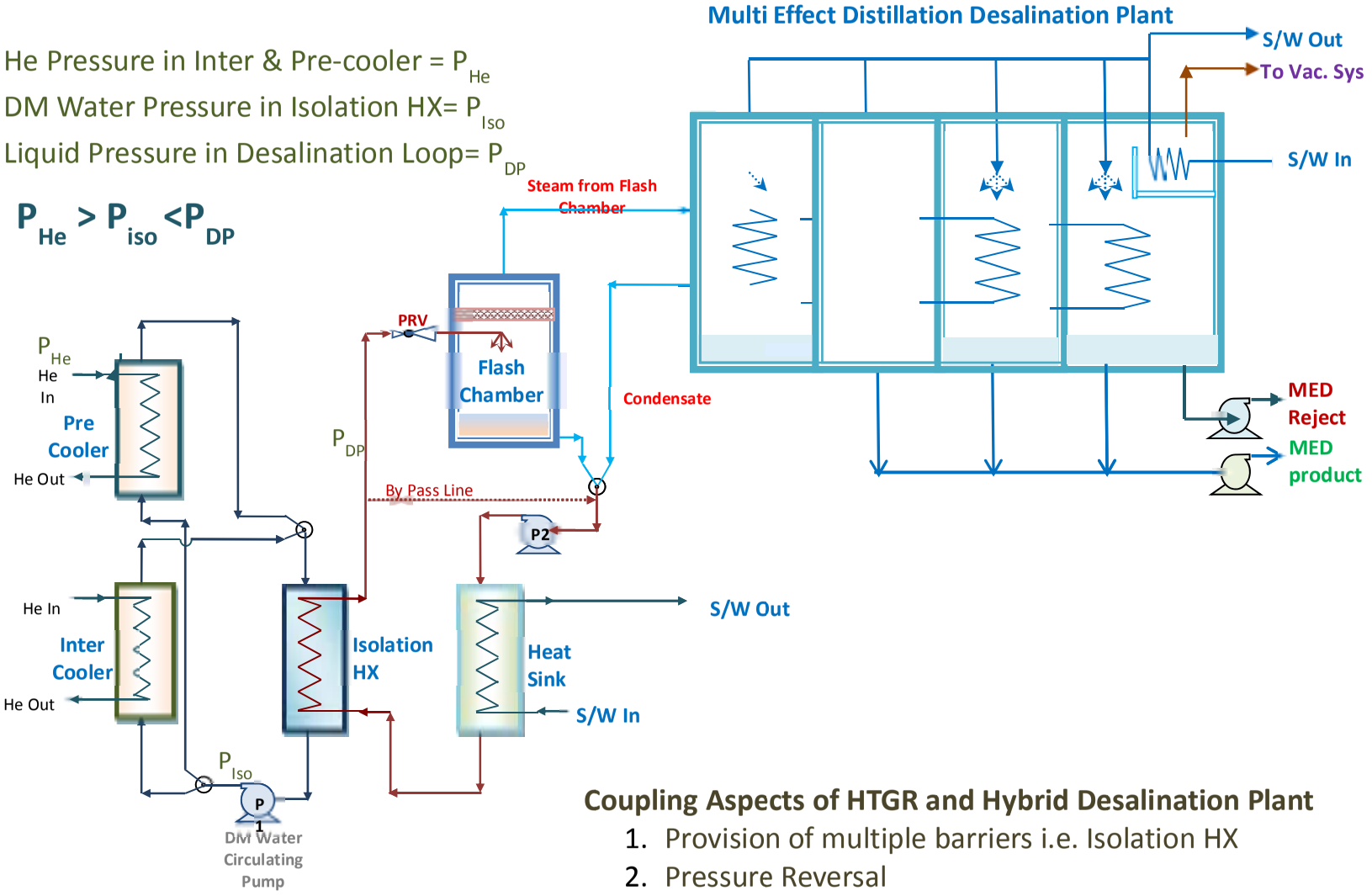

FIG. 4.33. Coupling of LT-MED desalination plant with HTGR.

One PRV is installed in the loop prior to the flash tank to reduce the pressure. After flashing in the flashing chamber, hot water is cooled by giving away the latent heat for vapour generation. Then this water is pumped through a demineralized water-to-seawater heat exchanger, i.e. a heat sink for rejecting the rest amount of heat.

A bypass line in the desalination loop is also provided to divert all the hot water from the isolation heat exchanger directly to heat sink in case of non-availability of the MED desalination plant.

4.4.2.2. Coupling of RO desalination plant with HTGR

The electric power generated by the HTGR can be used to power a reverse osmosis (RO) desalination plant. This is direct electrical coupling of the power plant to RO desalination plant without going through a transformation/ transmission/distribution process. So it will have some cost benefit.

RO with feed preheating:

In the heat sink, heat is rejected to the sea water. This rejected sea water is at high temperature (nearly 40^{o} C). So it can be used as feed stock for a reverse osmosis desalination plant. The only physical coupling between the two plants is a pipe connection between HTGR sea water discharge and RO plant's water intake. This piping connection would incorporate a 'dump' valve to enable HTGRs to continue normal operation in the event that the RO plant was non-operational.

4.4.2.3. Coupling of hybrid MED–RO desalination plant with HTGR

A schematic of the coupling system of HTGR nuclear reactor with hybrid MED–RO plant can be seen in Fig. 4.34.

4.4.3. Engineered safety features in coupling of hybrid desalination plant to HTGR

The process logic of coupling of a hybrid desalination plant to an HTGR is shown in Fig 4.34. An isolation heat exchanger is provided in between the desalination plant flash loop and the coolant loop for precooler and intercooler.

Helium in the precooler and intercooler is at considerably higher pressure than the pressure of coolant water in this heat exchanger. The coolant loop operates only marginally above atmospheric pressure in the precooler and intercooler. This is to ensure that any possible leakage is always 'helium-outwards' rather than 'water-inwards'. So there will be no leakage of water to the nuclear core. But in case of a leakage, the isolation loop will be contaminated.

The coolant in the isolation heat exchanger operates at higher pressure than the coolant in the loop for precooler and intercooler. Therefore, this interface provides a pressure reversal. In case of a leakage, the flow will be from the desalination plant loop to the isolation loop. So there will be no carry-over of radioactivity from the isolation loop to the desalination plant loop in case of a failure of tubes in the isolation heat
safety feature.

4.5. ENVIRONMENTAL ISSUES OF DESALINATION

Environmental issues related to desalination are a major factor in the design and implementation of desalination technologies [198]. Desalination plants along with fresh water (clean water) also generate concentrate (reject or residual stream). Major environmental issues are related to the disposal and management of the concentrate.

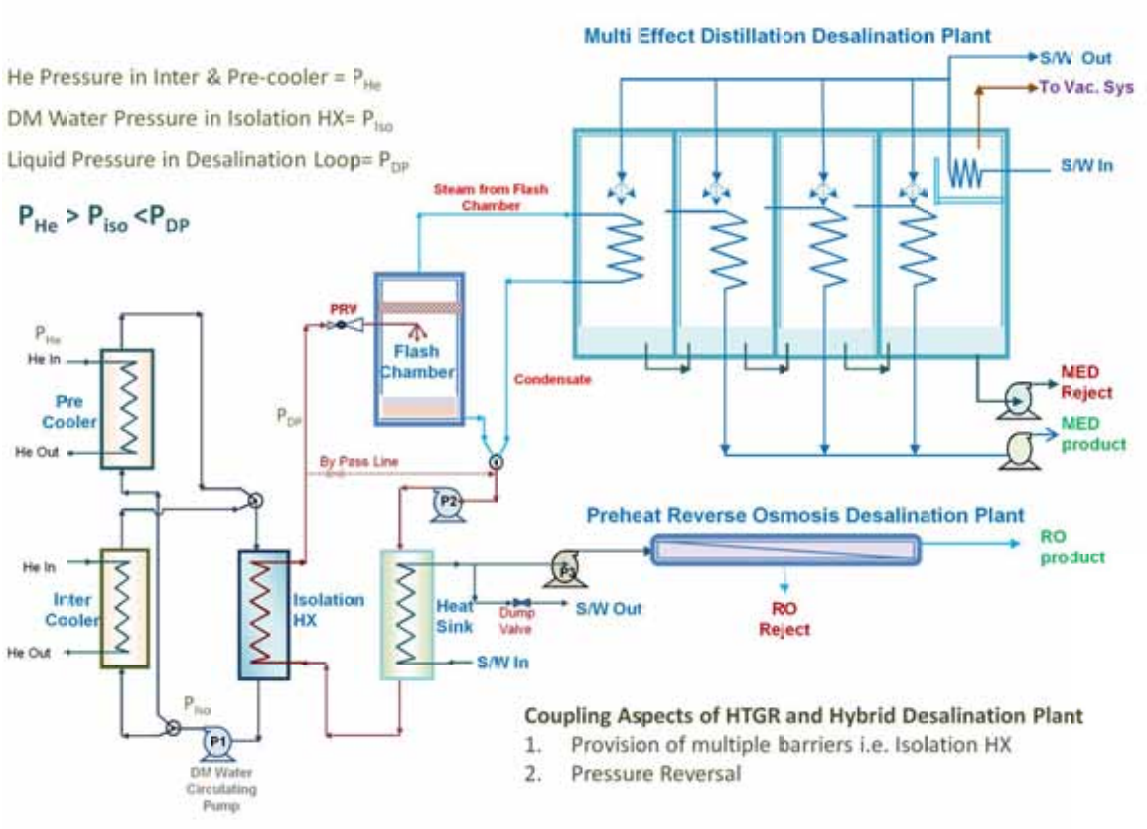

FIG. 4.34. Coupling diagram of HTGR plant with hybrid MED–RO plant.

4.5.1. Concentrate composition and characteristics

Concentrate is the byproduct from desalination. Characteristics of the generated concentrate depend on the type of desalination technology used. Table 4.8 shows the characteristics of concentrates from various types of desalination plants. The amount of concentrate produced from a desalination plant is a factor of the desalination process recovery rate (product water/feed water). Concentrate produced from seawater desalination plants can have an up to two times higher salt concentration than the receiving water. Concentrate from distillation processes is typically warmer, 5–8°C above the ambient water temperature. It may also contain low amounts of certain chemicals used during pretreatment and posttreatment (cleaning) processes such as chlorination, clarification, coagulation, acidification, and degasification to minimize algae growth, scaling, and corrosion. These chemical agents remain in the concentrate before disposal.

TABLE 4.8. CONCENTRATE CHARACTERISTICS.

Process	RO	RO	MSF/MED
Feed water	Brackish	Seawater	Seawater
Recovery (%)	60–85	30–50	15–50
Temperature (°C)	Ambient	Ambient	5–8
Final concentration factor	2.5–6.7	1.25–2.0	< 1.15

Critical concentrate parameters are TDS, temperature, and specific weight (density). The specific weight or density is a critical concentrate parameter. Compared to freshwater, concentrate has a higher density due to the increased salt concentration. When concentrate with a higher density is disposed into waters of lower salinity (lower density), the concentrate tends to sink. In comparison, a typical discharge from wastewater treatment plants will float, because its density is normally less than the receiving water. The tendency of the concentrate to sink when interacting with the receiving water introduces problems for the marine environment [198].

Typically a desalination plant concentrate consists of the following components or groups of components, respectively [199]:

- high salinity (depends on the recovery rate);
- heat (in thermal desalination);
- antiscaling additives (poly-carbonic acids, polyphosphates);
- antifoaming additives;
- antifouling additives (mainly chlorine and hypochlorite);
- halogenated organic compounds formed after chlorine addition;
- acid;
- corrosion products (metals).

4.5.2. Environmental issues related with concentrate disposal

4.5.2.1. High salinity

Desalination plants discharge the same load of seawater constituents as taken in. The only difference is the increased salinity. The salinity of a concentrate is a function of the desalination process recovery rate (product water/feed water).

Marine organisms exist in an osmotic balance with their environment. Higher salt concentrations in this brine plume affect benthic organisms (living near the seabed), as increase in the concentration of salt in the environment results in a dehydration of the cell, decrease of the turgor (or osmotic) pressure, and death (mainly of the larvae and young individuals) [200]. The magnitude of these environmental impacts on marine life also depends on the natural hydrodynamic conditions as well as biological factors of the local marine environment [201].

4.5.2.2. Heat

Thermal desalination plants discharge the concentrate usually with a temperature 5 to 8°C above ambient seawater temperature.

The elevated temperature of a concentrate discharge from a thermal desalination plant is known to have an impact upon marine organisms in a number of ways with certain communities, such as those at the limit of their geographical range being particularly affected. For instance, elevated temperatures and increased salinity reduce the overall concentration of dissolved oxygen in the water which restricts the life forms to those able to exist at lower oxygen levels. Furthermore, at the level of the individual organism, extreme temperatures may result in death, whilst sublethal temperature can modify the rate at which biological processes occur, thus influencing movement, the onset of maturity, life stage development,

and growth and size. At the species level, excessive temperatures may lead to changes in individual abundance and population diversity [202].

4.5.2.3. Antiscaling additives

Polyphosphate is an early antiscaling agent. It has a temperature sensitivity and is hydrolyzed to orthophosphate at temperatures above 90°C. Presently the most widely used antiscaling additive is BELGARD EV2000®, a polymer of maleic acid ($C_4H_4O_4$) [203]. These polymers prevent the dissolved material from precipitating, settling, and baking on surfaces, impair crystal growth by distorting the lattice structure so that soft sludge may be formed that does not adhere to or grow on metal surfaces. After [202], a typical BELGARD discharge concentration in concentrate is 0.53 mg/L.

Orthophosphate, the hydrolysis product of polyphosphate, is a macronutrient (besides nitrogen compounds) enhancing primary productivity. In sea, discharge of a macronutrient may have drastic consequences: eutrophication, i.e. algal blooms. It will cause a dramatic deterioration of the operation condition of the plant itself: increased bio-fouling, increased content in organic matter, increased filter problems, increased need of anti-foulants and so on [199]. All these effects are bound to a severe deterioration of the environmental quality. After [203], BELGARD does not give rise to any toxic hazard in the drinking water.

4.5.2.4. Antifoaming additives

Antifoaming agents typically are alcylated polyglycols, fatty acids, and fatty acid esters. A frequently used brand is ‘Belite’. The agents exhibit surface activity at the water steam interface and prevent foam formation. Fatty acids and their esters are non-toxic. Foaming is a function of organic seawater constituents, which are mainly excretion and degradation products of planktonic algae. Generally the need for antifoaming agents is seasonally different. It depends largely on the raw water quality.

Antifoaming agents are detergents. Detergents have adverse effects on organisms disturbing the intracellular membrane system.

4.5.2.5. Antifouling additives

Fouling is a multistage process in which many groups of organisms are involved. It starts with the adsorption of polymeric matter from the raw water to solid surfaces which allows film-forming pioneer-bacteria to settle. This first bio-film is then joined by secondary periphytes, which become the major part of the bacterial population. In a third step, microalgae, protozoa and fungi colonize, and finally, adhesion of debris, detritus and inorganic particles occur. These stages cannot be separated from each other, they rather form a continuous process. It is obvious that bio-fouling depends largely on the raw water properties, mainly on its contents of particulate matter and dissolved nutrients. Among the broad-effect agents, chlorine is preferred because it is cheap and much experience exists. A typical chlorine addition is 2 ppm. Good process guidance aims at a chlorine concentration zero at the outlet. Hypochlorite produced at the site of use by seawater electrolysis is an alternative to chlorine.

Chlorine exhibits broad effects on the environment, when it is discharged with the brine. The effects are of biological nature — the sterilizing activity itself, as well as of chemical nature — halogenations of organic seawater constituents. Seawater contains 70 ppm bromide. Chlorine transforms bromides to bromine while the chlorine itself is transformed to chloride. The result is that the reactive bromine is present in addition to the chlorine, and the variety of halogenated products becomes larger. In the presence of ammonia, chlorine and bromine form

chloramines and bromoamines. They are stable and survive 90°C for one hour. Chlorine and bromine form halogenated organic compounds [199].

4.5.2.6. Halogenated organic compounds

Chlorine is highly reactive. Natural and added organic seawater constituents may be chlorinated and metabolized. In addition, chlorine converts bromide and iodide to elemental bromine and iodine which, in turn, may react with organic matter. This means that chlorination starts avalanches of secondary reactions which form an unknown number of products, e.g. tri-halomethanes [204]. The situation becomes worse if the seawater content in organic carbon is enhanced, e.g. by pollution with hydrocarbons or by addition of antifoaming additives.

Chlorine interaction with oil products produces a variety of halogenated hydrocarbons, some of which (e.g. the halomethanes) are potential carcinogens and mutagens [205].

4.5.2.7. Acid

In addition to antiscaling additives, acid addition is a means to minimize scaling. Usually sulphuric acid is added. The original pH value of seawater is 8.3. The pH value is lowered to expel a part of the dissolved carbonate. Occasional removal of scaling remains necessary. This is done by conducting an acid wash at pH 2.0 [205].

The acid solution is discharged into the sea followed by fresh seawater used to rinse the distiller. The alkalinity of seawater amounts to ca. 150 ppm. From this, it can be calculated that 20 000–25 000 m^3 seawater are necessary to neutralize the 5000 m^3 acidified seawater discharged. This needs considerable time and damage to organisms cannot be excluded.

4.5.2.8. Corrosion products

Corrosion causes liberation of heavy metal ions with the consequence of heavy metal pollution of the desalted product as well as of the concentrate. Corrosion products reach the sea with the concentrate. Thermal desalination plants discharge copper, nickel, iron, chromium, zinc and other heavy metals depending on the alloys present in the process line. In terms of concentrations, copper and iron are highest. Copper concentrations in desalination effluents are 200 fold (and more) higher than natural copper concentrations in seawater.

The heavy metals will adsorb on suspended matter and will sink down causing an accumulation in the sediments. Since the problem is not the concentration, but rather the load, the consequences cannot be mitigated by dilution of the outfall [199]. Copper, nickel, chromium, manganese, and other potentially emitted metals exhibit biological adverse effects depending on organisms and their conditions and on the environment and its conditions.

5. CONCLUSIONS AND RECOMMENDATIONS

Conclusions can be drawn as follows:

- Nuclear power is a safe, reliable, clean, and economic energy source. The experience achieved and lessons learned from five decades of commercial nuclear power plant operation have resulted in a status of minimal risk of severe occurrences, thus representing a powerful option within the existing mix of energy sources. The next, fourth generation of nuclear plants will be even safer, more reliable, more economic, and more proliferation-resistant, and will supply more than just electricity.

- Many of the suggested designs of innovative nuclear reactors of the fourth generation are of small or medium power size (< 700 MW(e)), some even less than 300 MW(e). Among those, the VHTR, which is flexible in design, siting, fuel cycle and size, represents a promising concept. It clearly shows the features of a catastrophe-free reactor and is most advanced in terms of R&D works. It will provide coolant exit temperatures of up to 1000°C, which can be utilized in the cogeneration mode for a broad range of process heat applications.
- Nuclear CHP options and its market requirements should be investigated in more detail. Products others than electricity could significantly enlarge the energy market for nuclear CHP offering at the same time a considerable potential for fuel resource saving due to high overall efficiencies, improved economics and reduction of CO_2 emissions. There is already experience to couple nuclear energy to low temperature processes like district heating or desalination, but it still is lacking the demonstration on a larger scale. The petrochemical and refining industries represent another huge potential with their growing demand for hydrogen and process steam due to the increasing share of 'dirty fuels' such as heavy oils, oil shale, tar sands entering the market.
- In the high temperature heat market, nuclear is also applicable to the production processes of liquid fuels or of hydrogen by steam reforming or water splitting, compatible with the needs of the transportation sector. The feasibility of steam reforming of methane or coal gasification under nuclear conditions was already successfully demonstrated; technical and economical feasibility, however, remains to be demonstrated at a larger scale. The advanced water splitting processes of high temperature electrolysis and thermochemical cycles have still design challenges and not yet reached commercial scale.

Some recommendations regarding nuclear assisted hydrogen production are:

- Further work must be done on hydrogen production by water splitting in the area of pilot scale demonstration to develop an integrated cycle with automated control of operation including stability of the process, instrumentation and control required for the system, and the enhancement of the efficiencies of the processes.
- Separation and purification methods must be improved to obtain better quality (purity) of produced hydrogen.
- The safety of coupling for the overall nuclear hydrogen production plant must be thoroughly analyzed addressing the interaction of the reactor safety requirements and the chemical process safety requirements aiming at eventual establishment of safety criteria and standards related to nuclear hydrogen production.
- The energy economics of nuclear hydrogen must be analyzed.

Some recommendations regarding nuclear assisted desalination are:

- Further detailed design & economic analysis of the hybrid nuclear desalination technologies coupled to an HTGR utilizing the waste heat from it should be carried out to reflect the ongoing and future developments in HTGR technology.
- The safety of coupling the nuclear desalination plant with an HTGR must be thoroughly analyzed addressing the interaction of the reactor safety requirements and the product water quality.

APPENDIX I. NUCLEAR HYDROGEN PRODUCTION IN CHINA

I.1. INTRODUCTION

Since the 1980s, China's economy is rapidly growing. It is expected that the growth will continue in the next decades. But more and more energy demand and environmental problems caused by firing fossil fuels are key challenges for a sustainable development of China. In the period of 2000–2007, China's average growth rate of energy consumption was 8.9% per year and that of electricity consumption was as high as 13.0% per year. In 2007, China's total energy consumption was 2.66 billion tons of coal equivalent (TCE)[2]. The primary energy production was 2.23 billions TCE. The composition of primary energy production (as coal equivalent calculation) was: 76.6% raw coal, 11.3% crude oil, 3.9% natural gas, 7.3% hydro power and 0.9% nuclear power [206]. Such a primary energy mix resulted in the emission of large amounts of SO_2 and CO_2. In 2006, the emission amounts of CO_2 were 5.61 billion tons [207], and those of SO_2 from the industry sector were 22.35 million tons [208].

For meeting the challenge, China is developing clean energies including nuclear energy and renewable energies such as wind power, solar energy, and so on. In recent years, China's nuclear electricity production is increasing. Up to now, nuclear power plants with a total capacity of 9.11 GW(e) are in operation [209], new PWRs with a total capacity of over 10 GW(e) are under construction. The construction of Gen-III PWR, AP1000 and EPR, will start soon. According to the 'State Medium-Long Term (2005–2020) Development Programme of Nuclear Power' issued in Oct. 2007, the total capacity of operating nuclear power plants in 2020 will be 40 GW(e) plus 18 GW(e) under construction. Considerably increasing application of nuclear energy will greatly improve China's primary energy mix and effectively improve air quality.

Hydrogen is a clean energy carrier. China is taking a very active approach for developing hydrogen energy technology including production, storage, and application of hydrogen. In the 'Tenth Five-Year Plan (2001–2005)', funding for programmes related to electric vehicles and hydrogen and fuel cells added up to 40% of the total energy research budget. It mainly focuses on basic and technical aspects of hydrogen energy and related demonstration projects [210] such as fuel cell city bus, refueling station and a 'hydrogen park'. An example was the successful service provided by hydrogen powered automobiles during Beijing Olympic Games in August 2008.

Since the 1970s, the high temperature gas cooled reactor technology has been developed in China. A 10 MW(th) test reactor (HTR-10) with spherical fuel elements was constructed in 2000 and is now in operation. A number of safety related experiments have been conducted in the HTR-10. R&D on direct cycle helium turbine technology is being carried out. Coupling a helium turbine system to the existing 10 MW(th) test reactor is foreseen [211]. The construction of an industrial scale demonstration plant of modular HTGR (HTR-PM) is one of the so-called 'national major science & technology special projects'. The construction of the 200 MW(e) HTR-PM will be finished around 2013. The related design, construction, and R&D work has been started.

Hydrogen production by nuclear energy is a promising way for industrial scale production compared with other developing production methods. Among all nuclear reactors, the HTGR is most suitable for nuclear hydrogen process due to its potential of high efficiency electricity

[2] 1 TCE (ton of coal equivalent) corresponding to the energy content of 5.2 barrels of oil = 0.7 TOE (ton of oil equivalent) = 27.78 million BTU (British thermal unit) = 29 308 MJ = 8 141 kWh.

generation and supply of high temperature process heat. Therefore, R&D on nuclear hydrogen, as a part of the HTR-PM project, has started at the Institute of Nuclear and New Energy Technology (INET), Tsinghua University. The sulphur–iodine thermochemical cycle for splitting water and the high temperature steam electrolysis have been selected as potential processes for nuclear hydrogen production. Since 2005, INET has conducted preliminary studies on both the S–I process and the HTSE process. The laboratory of nuclear hydrogen with facilities for process studies has been established. HTR-10 constructed in INET will provide a real nuclear facility for future R&D of nuclear hydrogen technologies.

The development of nuclear hydrogen in China will be conducted in three phases:

- Phase I (2008–2012): Verification of H_2 production processes and bench scale testing;
- Phase II (2013–2020): R&D on coupling technology with reactor, nuclear hydrogen safety, and pilot scale testing;
- Phase III (after 2020): Commercialization of nuclear hydrogen production.

The current R&D activities on nuclear hydrogen at INET are focusing on realizing the target of phase I.

I.2. R&D ON SULPHUR–IODINE PROCESS

I.2.1. R&D plan for S–I process

The S–I process is generally considered as one of the most promising thermochemical water splitting processes for hydrogen production, which has been widely investigated in many institutes across the world, including INET. According to the general schedule, the final objective of the Chinese nuclear hydrogen programme is to achieve the commercialization of nuclear hydrogen production after 2020. With this consideration, a four-stage plan was made which is shown in Fig. I.1, also the features and main research topics in different stages.

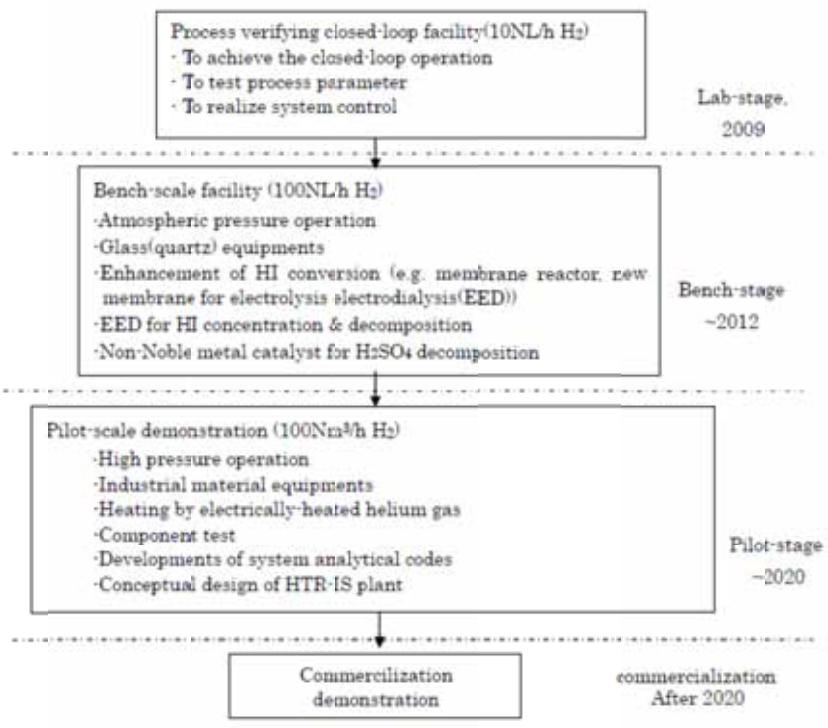

FIG. I.1. R&D plan of nuclear hydrogen production through S–I process in INET.

I.2.2. Fundamental research

Current R&D activities are covering: (1) researches on the three chemical reactions, i.e, Bunsen reaction, hydriodic (HI) acid decomposition, and sulphuric acid decomposition, and related technologies, (2) design and construction of a closed loop facility for verifying the process. The research topics are as follows [212–215]:

(1) *Process study on Bunsen reaction and separation characteristics of sulphuric acid phase and HI_x phase, purification of the two phases by reverse Bunsen reaction:*

A preliminary investigation of the kinetics of the reaction was conducted. The dependency of concentrations of various ions such as H^+, I^-, SO_4^{2-}, and I^{3-} on the reaction time was determined. Results show that the reaction proceeds rapidly, the concentrations of the ions quickly reach a stable level. The concentrations of various ions approximately meet the formula:

$$[H^+] = 2[SO_4^{2-}] + [I^-]$$

indicating that formation of the products keeps strict stoichiometry. In addition, it shows that the concentration of I^{3-} is two orders of magnitude lower than those of other ions, suggesting that the complex reaction between I_2 and I^- is negligible in the reaction.

In the Bunsen section, I_2 reacts with water and SO_2 forming H_2SO_4 and HI acids. With excess of iodine, the two acids will separate spontaneously. However, if the amounts of I_2 exceed the saturation, I_2 will be solidified out from the solution. In addition, the saturation is mainly affected by temperature, therefore, the influences of temperature and molar fraction of I_2 in the mixture of H_2SO_4, HI, I_2 and H_2O on the phase separation were investigated.

Although the two acids separate with excess I_2, they are cross-contaminated. i.e, the HI_x solution contains a small amount of H_2SO_4 and H_2SO_4 solution contains a little HI. If the two solutions as produced are fed to the distillation column for condensation, side reactions will occur and sulphur may form at the top of the column according to the following equation, by which 6 moles of HI are consumed per 1 mole of H_2SO_4.

$$H_2SO_4 + 6\ HI = S + 3\ I_2 + 4\ H_2O$$

More seriously, sulphur formed may lead to clogging of the pipe or unbalanced materials. In addition, mass balance will be poor. Therefore, it is necessary to purify the two acids. The two acids are purified by reverse Bunsen reaction shown in the following equation:

$$H_2SO_4 + 8\ HI = H_2S + 4\ I_2 + 4\ H_2O$$

The effects of temperature, flow rate of carrier gas, and feed rate on the purification (denoted with removal efficiency of impurities) were investigated. As Bunsen reaction is exothermic, raising temperature will be beneficial to the reverse reaction. In addition, a gaseous product, SO_2, forms in the reverse Bunsen reaction, therefore, removal of the gas will enhance the reverse reaction. These assumptions were confirmed by experiments. Results show that the two acid phases could be purified with higher removal efficiency of impurities under suitable conditions such as higher temperatures and a suitable carrier gas flow rate.

(2) *Pre-concentration of HI acid by EED to exceed azeotropic composition, and concentring of HI acid by conventional distillation:*

The concentration of HI acid in the HI_x phase produced in the Bunsen reaction is about 10 mol/kg H_2O, close to the azeotropic composition of HI acid solution, which is $HI : H_2O = 1 : 5$ (molar ratio), i.e. [HI] is ~11.1 mol/kg. Therefore, it is difficult to concentrate HI solution by conventional distillation. An EED technique was employed to concentrate HI solution. The influences of different materials such as electrode and membrane, and operational parameters such as temperature and initial composition of HI acid on the concentration effects were investigated. Results show that HI acid could be effectively concentrated through EED, and the concentration of HI could exceed the azeotropic composition. Higher operation temperature leads to lower cell voltage, which is beneficial to lower the energy consumption. However, the concentration efficiency will become lower as temperature increases.

(3) *Catalytic decomposition of HI acid; development of efficient catalyst/supporter and novel preparation method, such as electro-plating of Pt on various supporters [216]:*

The HI decomposition reaction is usually catalyzed by Pt catalysts which were prepared by an impregnation–calcination method or impregnation–H_2 reduction method. In INET, Pt catalysts were prepared by various methods including impregnation–H_2 reduction at high temperature, impregnation–calcination at high temperature, impregnation–hydrazine reduction at room temperature, and Pd-inducing electroless plating, and others. Much attention was paid to the Pd-inducing electroless plating method. The prepared catalysts were characterized, e.g. by XRD, TEM, BET, and their catalytic performance was evaluated.

(4) *Catalytic decomposition of sulphuric acid on Pt and non-Noble metal catalysts, including Fe/Cu oxides and Cr/Cu oxides:*

In this area, work was focusing on the development of non-Pt catalysts. Two composite metal oxides, $CuFe_2O_4$ and $CuCr_2O_4$, were prepared by sol–gel, vacuum freeze drying (VFD), and following calcination. These oxides were characterized by XRD, TEM and BET analyses. Their catalytic performance to the decomposition reaction of SO_3 was evaluated in a fixed bed reactor. Both copper ferrite and copper chromate show catalytic activities close to that of Pt/Al_2O_3. However, the stability and lifetime of these oxides need to be further explored.

(5) *System control technology for precise temperature and flow rate control*

(6) *Correlation between density and composition of $HI/I_2/H_2O$ and $HI/H_2O/I_2/H_2SO_4$ systems*

I.2.3. Process verifying closed loop facility

To verify the data acquired from the fundamental studies and obtain operating experience with the closed loop facility, a process-verifying facility (IS-10) was designed and established at INET. The main specifications of the facility are shown in Table I.1.

Figure I.2 shows a photograph of IS-10 which consists of the three main sections and the control device.

TABLE I.1. MAIN SPECIFICATION OF IS-10

Specifications	Contents
Capacity	Hydrogen production rate 10 Nl/h
Main parts	Bunsen reactor, H_2SO_4 decomposition reactor, HI decomposition reactor, EED, control system, pumps, etc.
Heating	electricity
Materials	quartz glass, B–Si glass, teflon
Size	3000 mm (L) × 2000 mm (W) × 2000 mm (H)
Features	• Automated temperature control and record; • Liquid flow rate control (diaphragmatic metric pump, mass flow controller); • Multi-running mode (section continuous, open cycle, closed cycle); • Protect I_2 from solidifying.

FIG. I.2. Process verifying IS-10 closed loop test facility at INET.

Many stand-alone experiments have been conducted with the IS-10 facility. The closed loop experiment carried out lasted for 8 hours. Among the three sections of the closed experiment, HI and H_2SO_4 sections run in continuous mode, while Bunsen section runs in batch mode. All temperatures and rates were kept constant. The hydrogen production rate was almost stable at 10 Nl/h, and the hydrogen and oxygen production ratio was approximately 2:1. Most of the reactors and processes were successfully operated. However, under some un-optimized conditions, problems such as clogging caused by iodine and formation of sulphur arose, leading to mass unbalance or failure of long time operation. To achieve longer and stable operation, further investigations are needed.

I.3. HTSE DEVELOPMENT AT INET OF TSINGHUA UNIVERSITY

I.3.1. HTSE development schedule

The R&D works on HTSE development are divided into four stages: (1) from 2008 to 2009, construction of HTSE test facilities and process verification, (2) from 2010 to 2012, bench scaled experimental study with hydrogen production yield of 60 L/h, (3) from 2013 to 2020, design of pilot scaled equipments and the pilot scale test with hydrogen production yield of 5 Nm^3/h as well as R&D on the coupling technology with HTGR, (4) commercial demonstration after 2020 [217].

Current research activities mainly focus on: (1) demonstration of the feasibility of using planar SOEC technology for high temperature electrolysis; (2) development of new materials with corrosion resistant and high performance HTSE; (3) analysis of the degradation mechanisms of SOEC cells used in HTSE mode; (4) optimization of HTSE cell and stack; (5) studies of system design to support cycle life assessment and cost analysis for HTSE plants.

I.3.2. R&D on HTSE

The research and development of HTSE technology was initiated at INET in 2005. In the past years, researchers mainly concentrated on preliminary investigations, feasibility studies, equipment development, and fundamental researches. Currently, two testing systems, one is for HTSE cell online testing and the other one is for high temperature electrochemical performance evaluation of SOEC components, have been designed and constructed [218]. In addition, the research on novel anode materials has obtained excellent results. Also the theoretical analysis of hydrogen production efficiency of HTSE coupled with HTGR has been carried out [219].

(1) *Study on conventional planar LSM-SOEC system*

The lab scale hydrogen production on a conventional LSM-SOEC system was investigated. The electrolyte layer made of YSZ (containing 8 mol% of Y_2O_3) was sandwiched between the porous cathode (Ni/YSZ) and anode layer (LSM). When the input voltage is 1.0 V and the temperature is 850°C, the hydrogen production rate is 0.315 mL/(min·cm^2). When the voltage increases to 1.3 V, the hydrogen production rate increases to 0.98 mL/(min·cm^2) correspondingly [216].

The 'area specific resistance' (ASR) is one of the most important characteristic parameters in measuring the electrolysis performance of SOEC for hydrogen production. The lower the ASR value, the better is the performance of the anode electrode. Testing results of LSM electrodes under SOEC and SOFC modes show that the ASR value of a Ni–YSZ/YSZ/LSM cell was only 0.76 Ω·cm^2, while it increased about 5 times, i.e. to 3.7 Ω·cm^2 when operating in the SOEC mode. Studies of the Risǿ National Laboratory, DTU (Denmark technical university), also showed similar results. Therefore, it can be seen that although HTSE is essentially a reverse process of SOFC, the conventional materials of SOFC are not suitable for operation in SOEC mode because of the high steam content, which is always over 70%, whereas it is only 3% in SOFC mode.

(2) *Development of novel anode ,aterials with low ASR*

The feasibility of the novel conductive membrane $Ba_{0.5}Sr_{0.5}Co_{0.8}Fe_{0.2}O_{3-\delta}$ (BSCF) used as oxygen electrode of SOEC was studied. Compared with other oxygen electrode materials, ASR data of the electrode BSCF/YSZ are 0.66 Ω·cm^2 at 750°C, 0.27 Ω·cm^2 at 800°C, and only 0.077 Ω·cm^2 at 850°C, remarkably lower than the common used oxygen electrode materials LSM as well as the current focus materials LSC and LSCF. When the voltage is 1.3 V and the current density is 300 mA, the hydrogen production rate of the BSCF cell is 147.2 mL·cm^{-2}·h^{-1}, about three times higher than that of the LSM cell (~49.8 mL·cm^{-2}·h^{-1}). It indicates that BSCF could be a potential candidate for the application of the SOEC anode [220].

(3) *Microstructure control of cathode electrode*

Previous analyses indicated that the coarsening and oxidation of nickel particles as well as the diffusion of steam were the limiting step in the whole electrolysis reaction.

As gas permeability and electrical conductivity of SOEC cathodes are strongly dependent on the cathode microstructure, the reasonable control of the microstructure is crucial for the optimization of the electrochemical performance of the cathode.

Nano-sized NiO powder on submicron-sized YSZ particles of functional layer was prepared via in-situ coating combustion method. XRD and FESEM analyses showed that the products were well crystallized with NiO coating on YSZ particles [221]. A SOEC single cell made from in-situ prepared NiO–YSZ exhibited better performance than the other samples with the electrolytic voltage of 0.92 V and showed excellent durability under the electrolytic currency of 0.33 A/cm^2 at a temperature of 900°C.

(4) *Design of the stack and the HTSE stack online testing system*

Figure I.3 is the design of the modular HTSE stack online testing system. The whole system mainly consists of three parts: measurement and control part, gas loop part, and hydrogen monitoring part. Construction has been finished.

Figure I.4 is the design of the planar stack. The short stack is designed to be composed of three planar individual cells with a hydrogen production rate of 1 L/h. Table I.2 indicates some of the cell configuration details that have been adopted for this conceptual design. The stacks have been assembled.

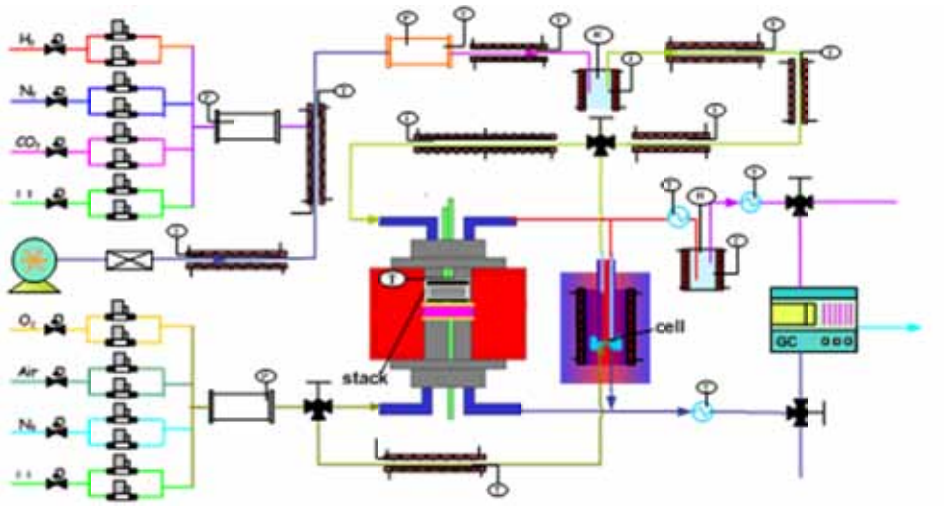

FIG. I.3. Design of the modular HTSE testing loop.

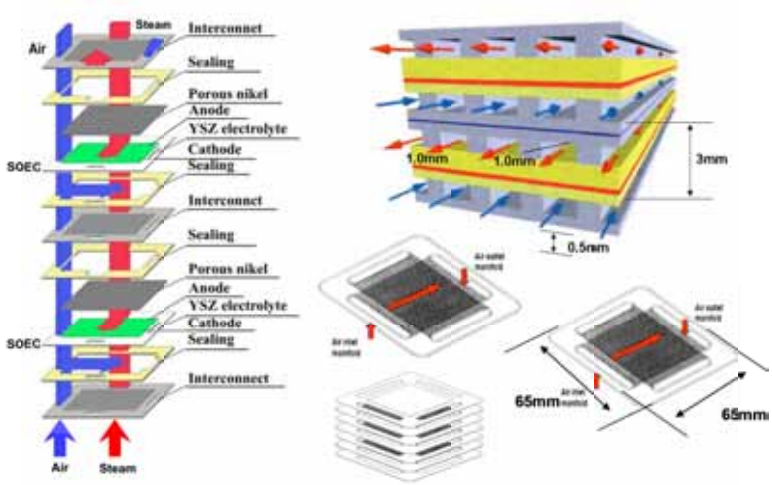

FIG. I.4. Design of the stack.

TABLE I.2. CELL CONFIGURATION AND TECHNOLOGICAL SPECIFICATIONS

Cell configuration					Specifications	
	Composition	Thickness (μm)	Size	Porosity/ density	Temp.	850°C
Electrolyte	YSZ	10–20	6.5 × 6.5	D > 95%	Input steam	> 70%
Anode	LSM	30–50	5 × 5	P > 20%	Efficiency	> 90%
Cathode	Ni–YSZ	1000	6.5 × 6.5	P > 35%	ASR-C	< 1 Ω.cm^2
Seal	Glass–Ceramic	3000		D > 95%	ASR-U	< 1.5 Ω.cm^2
Bipolar plate	Ferrite	—	6.5 × 6.5	—	—	—
Channel width	1.0 mm	Bipolar thickness	3.0 mm	—	Degradation rate	< 0.05 %/5h
Channel width	0.5 mm	Ridge width	1.0 mm	—	—	—

— data not available.

I.4. SUMMARY

It has been decided to develop nuclear hydrogen technologies in China. The R&D on nuclear hydrogen technology was initiated as a part of China's HTR-PM demonstration nuclear power plant project. The sulphur–iodine process and high temperature steam electrolysis were selected as potential production process of hydrogen, R&D on both processes is carried out at INET. It is expected to commercialize nuclear production of hydrogen after 2020, therefore, the coming decade is a key period to realize the target. There are many challenges on the way, and comprehensive international cooperation is necessary.

APPENDIX II. NUCLEAR COAL GASIFICATION RESEARCH IN GERMANY

The German PNP project was a cooperation between the HTGR industries (Hochtemperatur-Reaktorbau GmbH, Mannheim, and Gesellschaft für Hochtemperaturreaktortechnik mbH, Bensberg), the coal industries (Bergbauforschung GmbH, Essen, and Rheinische Braunkohlenwerke AG, Cologne), and the nuclear research center Kernforschungsanlage Jülich (today: FZJ). The project was funded by the Federal Government, the State Goverment of Northrhine Westphalia, and the participating industries.

Main objective was the development, design, and construction of an energy system based on a combination of German coal and nuclear power, including the developing and prototype testing of a nuclear heat generating system to be operated at a 950°C gas outlet temperature, intermediate circuit, heat extraction, coal gasification processes and nuclear energy transport.

II.1. NUCLEAR STEAM–GASIFICATION OF COAL

For nuclear coal gasification, a new component to be developed was the gas generator with allothermal heating. In 1973, a first device was tested on a small technical scale (~1 kg/h) to investigate kinetics and heat transfer characteristics, gas composition, and other parameters. The follow-on plant on semi-technical scale operated since 1976 at the Bergbau-Forschung, Essen, was a first-of-its-kind gas generator with a fluidized bed of about 1 m^2 base area and a height of up to 4 m, laid out for a coal throughput of ~200 kg/h. This unit was constructed as a vertically arranged cylindrical vessel (Fig. II.1) with the outer dimensions of 7.75 m (max.) diameter and 21.13 m height, designed for pressures up to 4 MPa. Its concept differed from the conventional one in that the coal was gasified indirectly by means of a tube-type immersion heater which was placed into the fluidized bed to transfer heat from a separate helium circuit. The helium was electrically heated up to 950°C with the heat transferred at a power of 1.2 MW. Characteristic data of the semi-technical plant are listed in Table II.1 [222].

The semi-technical plant was used for testing components, feeding devices, insulation, investigating broad ranges of operating conditions, and applying different types of coal. Reaction rates were observed to decrease with height of the fluidized bed which can be explained with the inhibiting effect of the product gases whose concentration increases with height. Due to the good heat transfer, half of the heat exchanging surface was already sufficient to decouple almost all of the heat from the helium.

Compared to the conventional case, the temperature provided by the helium is limited. Consequently reaction rates are slower which, however, could be enhanced by adding a catalyst. The catalytic coal gasification was also tested in the plant (Fig. II.2, left). The addition of 4 wt% of the catalyst potassium carbonate enhanced coal throughput by 44%. At the same time, the fluidized bed temperature was decreased. As the right-hand side of Fig. II.2 indicates, for constant helium temperature, the heat transfer decreases with increasing gasification temperature. On the other hand, heat transfer increases with increasing reaction rate (due to the addition of catalyst). This is compensated by a decrease in the gasification temperature [222].

Furthermore, residence times could be reduced from 7–9 h (anthracite) down to about 1.5 h. In addition, the H_2 production was significantly increased on the expense of CO (Table II.2). The catalyst, however, was found to be not effective until a certain threshold value of ~2 wt% due to bonding on the coal. Also corrosion effects were enhanced observing a strong inner oxidation at temperatures > 800°C.

TABLE II.1. CHARACTERISTIC DATA OF SEMI-TECHNICAL GAS GENERATOR FOR STEAM COAL GASIFICATION

Parameter	Value
Thermal power (MW)	1.2
Helium inlet temperature (°C)	< 1000
Helium flow (kg/s)	1.1
Heat exchanging surface (m^2)	33
Height (m)	< 4
Cross section (m^2)	0.8 × 0.9
Fluidized bed density (kg/m^3)	344
Coal input (kg/h)	233
Coal particle size (mm)	< 1
Steam velocity (m/s)	1.13
Gasification temperature (°C)	700–850
Pressure (MPa)	4
Raw gas production rate (Nm^3/h)	816
Conversion rate (%)	83

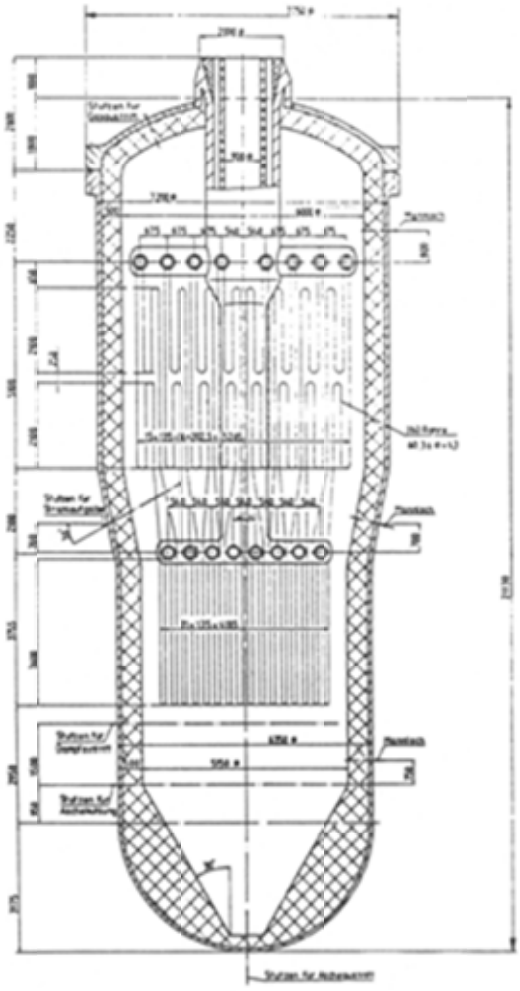

FIG. II.1. Schematic of allothermal gas generator.

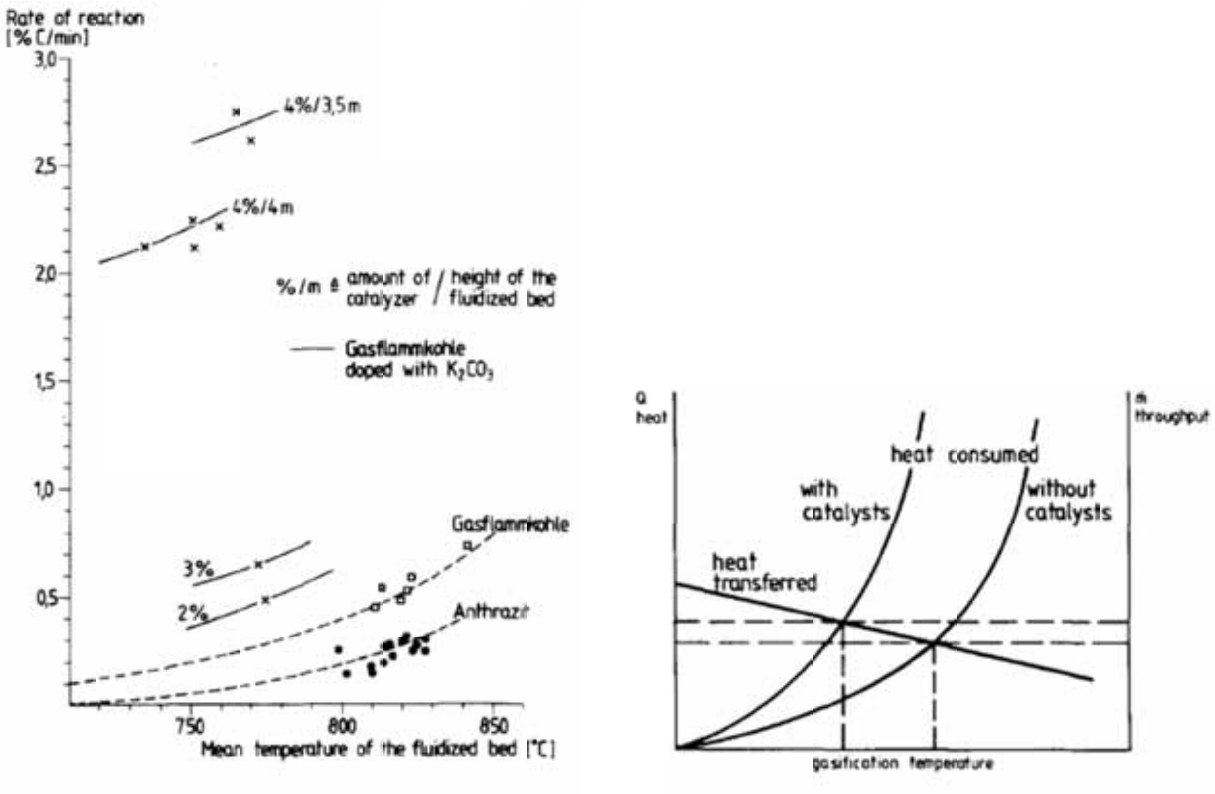

FIG. II.2. Influence of catalyst on reaction rates (left) and interaction between heat transfer and gasification kinetics in allothermal gas generator (right).

TABLE II.2. SOME RESULTS FROM CATALYTIC AND NON-CATALYTIC STEAM COAL GASIFICATION

Parameter	Non-catalytic		Catalytic	
	Pyrolysis	Gasification	Pyrolysis	Gasification
Helium temperature (°C)	895		895	
Gasification temperature (°C)	805		701	
Reaction enthalpy (kJ/kg coal)	2192	5678	2058	5148
Coal throughput (t/h)	27.3		69.3	
Raw gas production rate (Nm^3/h)	234 000		659 500	
Gas composition fractions (%) H_2:	44.2	53.5	57.6	57.2
CO:	11.1	12.7	1.1	2.4
CO_2:	19.2	25.8	25.9	32.7
CH_4:	23.7	7.4	14.5	7.3

The semi-technical plant was in hot operation for approx. 26 600 hours with more than 13 600 hours under gasification conditions (750–850°C, 2–4 MPa). Maximum capacity was 0.5 t/h of coal, the total quantity of coal gasified was 2400 t [222, 223]. Some results are summarized in Table II.2 regarding derived reaction enthalpy and product gas composition, distinguished between the non-catalytic and catalytic process and between the pyrolysis and gasification phase, and also compared with the autothermal process. It shows that the primary pyrolysis products are further converted in the steam atmosphere in the gasification phase. Overall result of the semi-technical scale operation was that an industrial scale gas generator in connection with a nuclear heat source was considered feasible.

Coal conversion programmes were accompanied by a qualification programme for high temperature metallic materials. Investigations under steam coal gasification typical conditions have shown that the degradation by corrosion was strongly depending on the contents of chromium and other elements. A minimum Cr content was identified to be necessary for maintaining a sufficient protective layer on the metal surfaces. Thinning by corrosion in the order of 0.01 mm/a should allow a satisfactory stability.

The commercial-size gas generator was foreseen to have a thermal power of 340 MW requiring three units for a 1000 MW nuclear process heat plant. It was designed, unlike the semi-technical plant, as a horizontal pressure vessel (Fig. II.3) to contain a fluidized bed with the shape of a long stretched channel to allow for long residence times. It consisted of four parts (modules) plus the two ending pieces. The coal passes through the reactor as a plug flow. It is introduced through several inlets in the first module where mainly the pyrolysis process takes place. The gasification zone spreads over the other three modules. In the fourth module, the remaining ash is cooled and removed. Each module contains steam inlets in the bottom section and an immersion heat exchanger bundle, through which heat is transferred from the hot helium to the fluidized bed. The dust formed in the pyrolysis zone is collected in a sieve and recirculated. Some characteristic data of the prototype gas generator for both the catalytic and non-catalytic version are given in Table II.3.

With the concept of an 'industrial plant coal gasification Ruhr', it was suggested to do the market introduction of nuclear in several steps: (i) construction of an autothermal Ruhr 100 gas generator with a coal throughput of 1 million t/a of coal for SNG production at a rate of 0.6 billion Nm^3/a; (ii) expand to three gas generators with one to be based on hydro-gasification; (iii) connection with a 700 MW(e) coal power plant for the supply of process steam and electricity; (iv) replacement of the coal power plant by an 1800 MW(th) HTGR to supply 400 t/h of process steam (400°C, 10 MPa) plus 600 MW of electricity.

In the 1980s, there was also a concept elaborated to convert the existing AVR reactor in Jülich to a process heat plant for steam coal gasification. The gas generator was planned to be integrated into the confinement of the AVR. Its vertical arrangement [224] has the advantage that in combination with a lower gasification pressure of 2 MPa less steam is required. Coal throughput was foreseen to be 7.8 t/h. Due to the low conversion rate of ~50%, a higher coal throughput and the production of a significant amount of fine coke (**4**.2 t/h), besides the 11 000 Nm^3/h of product gas, was expected.

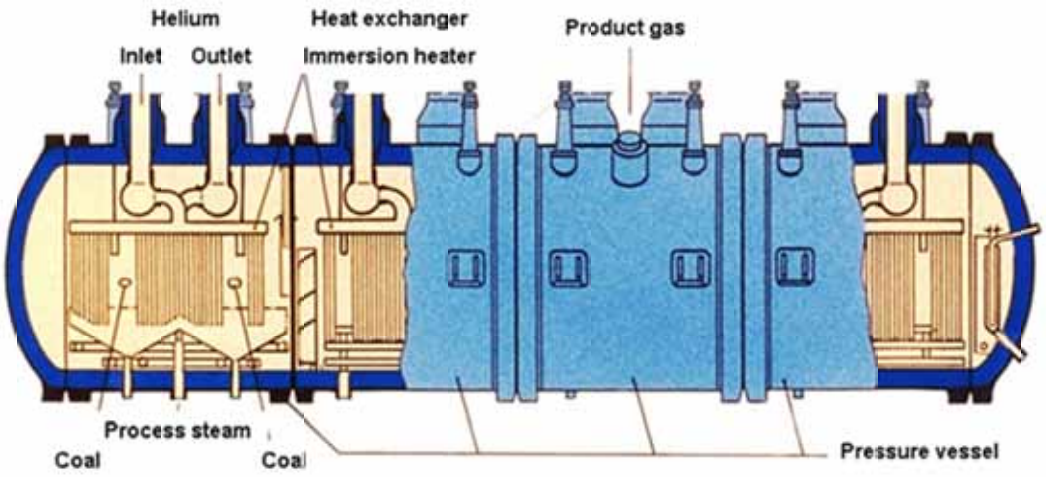

FIG. II.3. Schematic of an industrial scale gas generator for the PNP reactor for allothermal steam coal gasification.

TABLE II.3. MAIN DATA OF PROTOTYPE GAS GENERATOR FOR PNP STEAM COAL GASIFICATION

Parameter	Value	
	Non-catalytic	Catalytic
Thermal power (MW)	340	
Length (m)	~33	
Outer diameter (m)	7.2	
Heat exchanging surface (m^2)		
1st module (pyrolysis)	425	
2nd module (gasification)	535	
3rd module (gasification)	612	
4th module (gasification)	612	
Helium flow (kg/s)	94.4	
Helium inlet temperature (°C)	895	
Helium pressure (MPa)	~ 4.1	
Height of fluidized bed (m)	1.9–3.4	
Coal input (t/h)	27.3	69.3
Steam flow (t/h)	177	190
Catalyst (t/h)	—	3.27
Gasification pressure (MPa)	~4.3	—
Gasification temperature (°C)	800–900	—
Raw gas production rate (Nm^3/h)	77 923	219 818
Degree of gasification (%)	~ 93	—

— data not available.

II.2. NUCLEAR HYDRO-GASIFICATION OF COAL

Also the hydro-gasification process can be combined with a nuclear heat source. But unlike the steam–coal gasification, the nuclear heat is not coupled directly into the gasification reactor. Since two variants of hydrogen production exist, there are two alternatives of nuclear involvement [225]. The one variant is steam methane reforming, where a part of the product gas methane is drawn off and the high temperature nuclear heat is used for the endothermic reforming reaction. Still remaining low temperature nuclear heat is taken for steam and electricity generation. The produced hydrogen is routed at a relatively low temperature (~400°C) to the reactor where the gasification of coal takes place in an exothermal reaction at 800–900°C and 8 MPa. The partial pressure of the hydrogen strongly influences the methane production rate. About 40% of the H_2 reacts with the coal to methane, while 60% is recycled after gas treatment.

In the second variant, the nuclear heat is taken to preheat the hydrogen produced during the gasification process itself, i.e. by the water gas shift reaction which occurs at 100%. Due to the endothermic character of the shift reaction resulting in a much lower heat production in the reactor, the gasification agent hydrogen needs to be preheated to 800–950°C. Nuclear heat is also used for steam production and the residual power for electricity generation. Compared to the first variant, it has a simpler process scheme. A drawback is the fact that high gasification pressures (8 MPa) are needed, at least if the focus is on SNG production and high gasification rates, whereas the HTGR (PR-3000) would be operated at 4 MPa.

Between 1976 and 1982, the Rheinische Braunkohlenwerke, Wesseling, investigated the hydro-gasification process in a 1.5 MW semi-technical test facility with both lignite and hard coal [225–227]. The reactor of 8 m height contained a fluidized bed with 0.2 m diameter where the gasification agent hydrogen was injected. The hydrogen was electrically preheated to 750°C and could if necessary be further heated to 1000°C by partial combustion. System parameter could be varied in a broader range. A part of the hydrogen was used as a carrier medium for the coal input. Due to the exothermic character of the reactor, a direct heat input is not required. With residence times varied between 20–40 min gasification degrees (for lignite) were up to 75%.

The test facility was operated for about 27 000 h with more than 12 000 h under gasification conditions. The throughput was 320 kg/h of lignite or 160 kg/h of hard coal, the total quantity gasified was 1800 t.

From 1983 to 1985, a follow-up pilot plant was operated over 8300 h, with half of the time under coal gasification conditions with high availability. It included, unlike the semi-technical plant, all postprocessing components of gas treatment up to the stage of SNG production. The plant had a throughput of 9.6 t/h corresponding to a total power of 50 MW. Gasification of more than 17 000 t of brown coal was made to yield a total of 11 million Nm^3 of SNG, whose fraction in the raw gas was between 22 and 36%. The SNG production was at a rate of up to 6400 Nm^3/h. The characteristic data of both semi-technical plant and pilot plant are listed in Table II.4 and compared with a large scale commercial plant.

TABLE II.4. MAIN DATA OF HYDRO-GASIFIERS AT DIFFERENT SCALES

Parameter	Semi-technical plant	Pilot plant	Large scale plant
Operation	1976–1982	1983–1985	n.a.
Thermal power (MW)	1.5	50	3000
Length (m)	8	—	—
Inner diameter (m)	0.2	1.0	3.2
Dry coal input (t/h)	0.32 (lignite) 0.16 (hard coal)	9.6	2200 (lignite)
Coal grain size (mm)	< 1	—	—
Residence time (min)	9–80 (lignite) 28–38 (hard coal)	—	—
Hydrogen flow (Nm^3/h)	—	6000–12 500	—
Height of fluidized bed (m)	1.9–3.4	3–6	4.0
Gasification pressure (MPa)	5.5–9.5 (lignite) 8.0–8.7 (hard coal)	6.5–12	8
Gasification temperature (°C)	820–950 (lignite) 940–960 (hard coal)	850–930	850
Raw gas production rate [Nm^3/h] with fraction (%) of CH_4	≤ 48	< 16 000 22–36	380 000 (methane)
Degree of gasification (%)	≤ 82 (lignite) ≤ 47 (hard coal)	50–60	< 60

n.a. not applicable.
— data not available.

Both the semi-technical and the pilot plant were, apart from lignite, also used for testing whether or not hydro-gasification is feasible with the mostly caking hard coal using a gasification agent of either pure hydrogen or mixtures of H_2, CO, and steam. Results have shown that the reaction capability of hard coal is significantly smaller than for lignite. Due to the specific kinetics of hydro-gasification, residence times for complete gasification were comparatively long. Therefore, a degree of gasification of ~65% was considered reasonable requiring a residence time of about 30 min at 9 MPa and 900°C; beyond this value, residence times would be uneconomically long. Gasification degrees were higher for lignite and lower for anthracite coal. Also caking coals were found to soon lead to agglomeration near the coal inlet which resulted from poor mixing with the fluidized bed and eventually prevented a further operation.

The nuclear steam reforming as the alternative method to supply hydrogen was subject of extensive R&D work within the so-called NFE project, acronym for long distance energy transportation. The research center Jülich has developed in cooperation with the respective industries designs of a nuclear steam reformer for methane. The first test facility was a single splitting tube (EVA), and the follow-on facility consisted of a tube bundle (EVA-II) [22]. A similar experimental programme was recently conducted in Japan where the main focus was on the mutual thermodynamic interaction. was investigated in experiments conducted under the typical conditions of a nuclear reactor, i.e. in reformer tubes heated with helium of 900°C and 4 MPa with industrial scale dimensions (15 m in length, 130 mm inner diameter). Also EVA's counterpart, ADAM, a facility for the re-methanation of the synthesis gas generated in EVA, was constructed and operated, thus completing the system to a closed cycle and verifying the principle of a long distance energy transportation system based on hydrogen as the energy carrier.

APPENDIX III. NUCLEAR REACTOR

III.1. CAREM-D (ARGENTINA)

The project consists of development, design and construction of a prototype small nuclear power plant (100 MW(th), 27 MW(e)). A design alternative called CAREM-D has been developed for the cogeneration of electricity and potable water (preheated RO modules of 10 000 m^3/day) [151].

CAREM is a project for an advanced, simple and small nuclear power plant, conceived with new generation design solutions and standing on the large world wide experience accumulated in the safe operation of light water reactors, especially adequate for nuclear desalination of seawater. It is an indirect cycle plant with some distinctive and characteristic features that greatly simplify the reactor and also contribute to a higher level of safety. These distinctive features are:

Integrated primary cooling system.

- Primary cooling by natural circulation.
- Self-pressurized.
- Safety systems relying on passive features.
- Coupling system minimizing the risk of contamination.

III.2. KLT-40C (RUSSIAN FEDERATION)

The KLT-40C is a twin-reactor system intended to produce fresh water and electric power in different proportions. It may also be used for heat production in a cogeneration cycle. The KLT-40C design is based entirely on the serially produced marine nuclear steam supply system (NSSS) being used in the Russian nuclear-powered icebreakers [151].

The KLT-40C has the following original features:

- Primary piping length is minimized.
- Natural circulation is used in the primary and secondary circuits for all emergency modes.
- The containment is designed for high overpressure and includes a passive pressure suppression system.
- Safety is enhanced through fine-tuning of the engineered features proven by operation of the NSSS prototype and by the use of systems, which do not require external power sources.

III.3. SMART (REPUBLIC OF KOREA)

SMART (system integrated modular advanced reactor) is a small PWR with a rated thermal power of 330 MW. It is being developed by KAERI (Korea Atomic Energy Research Institute). The main objectives of the project are:

1. Development of a cogeneration system capable of producing 90 MW(e) and 40 000 m^3/day of desalted water [228].
2. Enhanced safety through a combination of inherent and passive engineered safety features.

3. Improved economics through system simplification, component modularization and construction time reduction.

The design of SMART is based on existing PWR technology and the fuel designs utilized in currently operating power reactors in the Republic of Korea. The prominent design feature of SMART is the adoption of integral arrangement. All the primary components such as core, steam generator, main coolant pumps and pressurizer are integrated into a single pressurized vessel. The integrated arrangement of these components enables the elimination of large-sized pipe connections between the components of the primary reactor coolant systems, and thus fundamentally eliminates the possibility of large break loss of coolant accidents. This integral arrangement, in turn, becomes a contributing factor to the safety enhancement of the SMART.

III.4. HELIUM COOLED GT-MHR WITH MED

The GT-MHR (gas turbine modular helium reactor) is an advanced high temperature gas cooled reactor which is being developed jointly by a consortium including Minatom of Russia, General Atomics, Areva NP, and Fuji Electric with the goal of burning weapons grade plutonium. It can, however, operate on uranium fuel and be competitive as a stand-alone electricity producer. By design, it releases waste heat at about 100°C. The recovery of 'free' heat for desalination lowers the price of the product water by a factor of 2, making the combination of GT-MHR and MED a very attractive economical option [151].

The nuclear reactor has a 600 MW(th) core with micro-particle fuel included into prismatic fuel elements. This type of core has been successfully employed in the Fort Saint Vrain plant in the USA. In the modular design, the safety of the concept is simplified by use of natural phenomena such as thermal radiation, which in any event maintains the fuel temperature below the temperature that leads to silicon carbide coating damage. This ensures that the nuclear material is confined within the fuel all the time.

With helium as a coolant, the core is coupled directly to a gas turbine in a Brayton cycle. Helium at 850°C is expanded in the turbine that drives two compressors and an alternator yielding a net electricity production of 285 MW(e) with an efficiency of 47.5%.

A special feature of the Brayton cycle, optimized for desalination operating conditions is the release of heat at the cold source via the precooler and intercooler at above 100°C. Normally this heat is released only through a cooling tower or to the river, but with proper adaptation it can be converted to useful heat to be used, for example to heat the feed water of an MED desalination unit.

APPENDIX IV. THERMODYNAMIC PROPERTIES OF PLANT MATERIALS

IV.1. SULPHURIC ACID

	H_2SO_4 @ 850°C
Heat capacity (kJ/(kg·K))	3.95
Heat conductivity (W/(m·K))	0.0032
Density (kg/m^3)	1840
Kinetic viscosity (m^2/s)	0.000015
Prandtl number	0.894

IV.2. HYDRIODIC ACID

	HI @ 450°C
Heat capacity (kJ/(kg·K))	0.83
Heat conductivity (W/(m·K))	0.0045
Density (kg/m^3)	976
Kinetic viscosity (m^2/s)	0.0000293
Prandtl number	0.894

IV.3. PRESSURIZED WATER

	PW @ 600°C
Heat capacity (kJ/(kg·K))	2.435
Heat conductivity (W/(m·K))	0.112
Density (kg/m^3)	20.58
Kinetic viscosity (m^2/s)	0.00000199
Prandtl number	0.894

IV. 4. THERMODYNAMIC PROPERTIES OF WATER

IV.4.1. Density

$$\rho = 10^3 (A_1 \times F_1 + A_2 \times F_2 + A_3 \times F_3 + A_4 \times F_4)$$

where [229]:

$$A_1 = 4.032219 \times G_1 + 0.15313 \times G_2 + 3.26 \times 10^{-4} \quad G_3$$

$$A_2 = -0.108199 \times G_1 + 1. \quad \times 10^{-3} \times G_2 - 4.23 \times 10^{-4} \times G_3$$

$$A_3 = -0.012247 \times G_1 + 1.74 \times 10^{-3} \times G_2 - 9 \times 10^{-6} \times G_3$$

$$A_4 = 6.92 \times 10^{-4} \times G_1 - 8.7 \times 10^{-5} \times G_2 - 5.3 \times 10^{-5} \times G_3$$

$$B = ((2S/1000) - 150)/150$$

$$A = (2T - 200)/160$$

$$G_1 = 0.5; \quad G_2 = B; \quad G_3 = 2 \times B^2 - 1$$

$$F_1 = 0.5; \quad F_2 = A; \quad F_3 = 2 \times A^2 - 1; \quad F_4 = 4 \times A^3 - 3 \times A$$

where T is the saturation temperature of water [°C] and S is the salinity of water [mg/L].

IV.4.2. Heat capacity

$$C_P = \left(A + BT + CT^2 + DT^3\right) \times 10^{-3}$$

where T is the temperature [°C] and

$$A = 4206.8 - 6.6197 \times S + 1.2288 \times 10^{-8} \times S^2$$

$$B = -1.1262 + 5.4178 \times 10^{-2} \times S - 2.2719 \times 10^{-6} \times S^2$$

$$C = 1.12026 \times 10^{-2} - 5.3566 \times 10^{-4} \times S = 1.8906 \times 10^{-6} \times S^2$$

$$D = 6.877 \times \quad ^{7} + 1.517 \times 10^{\ 6} \times S - 4.4628 \times 10^{-9} \times S^2$$

and S is the salinity of water [mg/L].

IV.4.3. Thermal conductivity

$$Log_{10}(\lambda) = Log_{10}(240 + 2 \times 10^{-4} \times S) + 0.434 \times \left(2.3 - \frac{343.5 + 0.037 \times S}{T + 273.15}\right) \times \left(1 - \frac{T + 273.15}{647.3 + 0.03 \times S}\right)^{1/3}$$

IV. 4.4. Dynamic viscosity

$$\mu = (\mu_W) \times (\mu_R) \times 10^{-3}$$

$$\mu_R = 1 + A \times S + B \times S^2$$

$$Ln(\mu_w) = -3.7914 + 604.129/(139.18 + T)$$

$$A = 1.474 \times 10^{-3} + 1.5 \times 10^{-5} \times T - 3.927 \times 10^{-8} \times T^2$$

$$B = 1.0734 \times 10^{-5} - 8.5 \times 10^{-8} \times T + 2.23 \times 10^{-10} \times T^2$$

APPENDIX V. ARGENTINA PHYSICO–CHEMICAL STUDIES ON THE THERMOCHEMICAL REACTION PROCESSES FOR HYDROGEN PRODUCTION

V.1. INTRODUCTION

The current and projected hydrogen demands are sufficient to justify massive investments in new methods to produce hydrogen that would be more cost-efficient than the actual large scale production methods. The objective of this project is to develop a suitable hydrogen production method based on high temperature chemical reactions for converting water to hydrogen and oxigen with a cost that is expected to be as low as 60% of that for nuclear hydrogen production by electrolysis of water. Even not specifically addressed in this project, it is believed that a high temperature nuclear reactor will provide the source of heat needed for the thermochemical water decomposition.

Three approaches have been identified for the efficient production of hydrogen using nuclear energy. The first one, nuclear assisted steam reforming of natural gas, uses nuclear heat to reduce the amount of natural gas needed to produce a given quantity of hydrogen. The second approach, hot electrolysis, involves the electrolysis of water at high temperature. Finally, thermochemical cycles use a series of high temperature chemical reactions for the water splitting and they are expected to have an overall efficiency of about 50%, receiving then the most attention.

Based on domestic capabilities developed for more than 50 years in Argentina, related with both nuclear energy and hydrogen production and applications technologies, the production of hydrogen using high temperature nuclear reactors is being seriously considered as a sustainable and environmentally friendly alternative for the country.

Since the majority of water splitting thermochemical processes requires heat supply at temperatures above 800ºC, several alternative cycles based on metallic chlorides are being investigated with the goal of reducing the process temperatures to the order of 500–600ºC. Lower operating temperatures reduce the costs of materials and maintenance, and they can effectively use low grade waste heat, thereby improving cycle and power plant efficiencies.

Research activities currently underway in Argentina are focused on the metallic chlorides family of thermochemical cycles. Theoretical and experimental investigations are addressed to elucidate the kinetics and mechanisms of thermochemical reactions at laboratory scale, in order to find the optimum conditions for increasing the efficiency of these cycles with the objective of a future scaling up of the experimental facilities.

A metallic chloride thermochemical cycle decomposes water into oxygen and hydrogen through intermediate metal and chlorine compounds. It is possible to employ a variety of chemical reaction steps so that the sum of them consumes water and heat, produces hydrogen and oxygen, and regenerates the chemical reactants within a closed system.

In addition to the sulphur–iodine process, four metallic chloride cycles have been recently identified in the so-called Nuclear Hydrogen Initiative to belong to the most promising thermochemical water splitting processes: (1) copper–chlorine (Cu–Cl cycle); (2) cerium–chlorine (Ce–Cl cycle); (3) iron–chlorine (Fe–Cl cycle); (4) vanadium–chlorine (Va–Cl cycle); and (5) zinc–chlorine (Zn–Cl cycle).

After considering factors such as availability and abundance of materials, simplicity, chemical viability and thermodynamic feasibility, the Fe–Cl, Zn–Cl and Cu–Cl family of cycles was selected to begin our investigations on water splitting thermochemical cycles.

A lot of studies have been performed in the past on these methods, but the kinetics and mechanisms of reactions are not completely understood yet and this project is expected to contribute to a better understanding of the critical problems identified for each cycle.

V.2. THERMODYNAMIC EQUILIBRIUM CALCULATIONS

At the beginning, a complete thermodynamic analysis was done in order to determine whether the iron chloride cycle may be replaced by another one that enhances the hydrogen production [230]. Using the software HSC for thermodynamic calculations, the equilibrium amount of the different species was evaluated for several experimental conditions.

First the well known iron–chloride system was analyzed considering that the most important reactions to be taken into account are:

$$FeCl_2(s,l) + H_2O(g) \rightarrow Fe_3O_4(s) + 6\,HCl(g) + H_2(g) \quad (I)$$

$$Fe_3O_4(s) + 8\,HCl(g) \rightarrow FeCl_2(s,l) + 2\,FeCl_3(g) + 4\,H_2O(g) \quad (II)$$

$$FeCl_3(g) \rightarrow FeCl_2(s,l) + Cl_2(g) \quad (III)$$

$$Cl_2(g) + H_2O(g) \rightarrow 2\,HCl(g) + 1/2\,O_2(g) \quad (IV)$$

$$2\,HCl(g) \rightarrow H_2$$

and H_2O (1:1 in moles). The equilibrium composition in the gaseous phase shows that the amount of H_2 increases with temperature from 2 mol% at 500˚C to 8 mol% at 950˚C. The total pressure considered was atmospheric pressure. So, using the ideal gas equation

$$p_{H2} = X_{H2} \times P_T,$$

where p_{H2} is the partial pressure of hydrogen, X_{H2} is the hydrogen mole fraction, and P_T the total pressure of the system, these percentages mean that the partial pressure of hydrogen is 0.02 and 0.8 atm, respectively. The other species in the gaseous phase are mostly unreacted water and undissociated HCl while less than 1% the $FeCl_2$, $FeCl_3$, Cl_2, and O_2 are also present as impurities. In the condensed phase, the only two species present are $FeCl_2$ with a minimum of reaction degree and a little amount of Fe_3O_4, but there is no Fe_2O_3 when equilibrium is reached.

TABLE V.1. $H_2O/FeCl_2$ (1:1)

Temp. (°C)	H_2O(g) (mol%)	HCl(g) (mol%)	$FeCl_2$(g) (mol%)	H_2(g) (mol%)	$FeCl_3$(g) (mol%)	Cl_2(g) (mol%)	O_2(g) (mol%)
500	84	14	3.475(-3)	2	8.859(-6)	3.282(-12)	2.698(-23)
700	48	44	1.261	7	3.357(-3)	4.246(-9)	6.340(-18)
950	21	46	27.15	8	4.953(-2)	5.263(-7)	2.826(-13)

If more water is added to the system, increasing the ratio between H_2O and $FeCl_2$ to 5:1 in moles, there are changes in the relative amounts of the different species. The changes with temperature of H_2O, H_2, HCl, $FeCl_2$, $FeCl_3$ and Cl_2 are less pronounced than in the previous case; for example, they are from 84 mol% to 64 mol% (instead 84 to 21 mol%) for H_2O, and from 2 mol% to 5 mol% (instead 2 to 8 mol%) for H_2 at 500 and 950˚C, respectively, while the relative change of O_2 increases from 3×10^{-23} to 2.5×10^{-11} comparing with 3×10^{-23} to

3×10^{-13} mol% for the previous case. It is expected that the percentage of water increases and the percentage of the other species decreases. Nevertheless, the final equilibrium amount of O_2 at 950˚C is greater than before. In the condensed phase, it is observed a less amount of $FeCl_2$ and a greater amount of magnetite, at all temperatures.

These results show that the presence of more water creates an oxidative atmosphere which is not convenient for the formation of hydrogen. Therefore, it is indicating that the dissociative reaction of HCl is not shifted by the presence of higher quantities of water. Meanwhile, the reactions I to IV are embraced by the Le Chatellier principle which establishes that, in a chemical reaction when a reactive is augmented, the equilibrium is shifted to the formation of the products.

On the other hand, if the amount of $FeCl_2$ is increased because the $H_2O/FeCl_2$ ratio used for calculations was 1:5 in moles, there is no change in the fraction of the gaseous phase. This result means that the condensed chloride does not affect the equilibrium amount, without beneficiation of the hydrogen reaction.

If the partial pressure of oxygen is diminished by its capture through an oxidation reaction, it is possible to produce more HCl that enhances the generation of H_2 by dissociation. The scavenger should react with O_2 but it should be almost unreactive with HCl. As it is well know that refractory metals have this characteristic, we considered the incorporation of metallic titanium to the system and we performed thermodynamic calculations for determining the possible species that may be formed with either oxygen or chlorine. Results of thermodynamic calculations are presented in Table V.2. As can be seen, a considerable amount of oxygen is generated. But if a refractory metal is added to the system for capturing this gas, the O_2 partial pressure diminishes remarkably and enhances hydrogen production.

TABLE V.2. $H_2O/FeCl_2$ (1:1) USING TITANIUM AS OXYGEN SCAVENGER

Temp. (°C)	H_2 (g) (mol%)	$FeCl_2$(g) (mol%)	HCl (g) (mol%)	H_2O(g) (mol%)	$FeCl_3$(g) (mol%)	$TiCl_4$(g) (mol%)	Cl_2(g) (mol%)	O_2(g) (mol%)
500	100	3.5(-3)	1.1(-11)	1.2(-12)	1.1(-18)	1.6(-27)	1.0(-34)	1.0(-34)
700	99	1.3	1.5(-11)	1.5(-9)	3.1(-16)	1.0(-34)	1.6(-34)	1.0(-34)
950	59	41.	1.6(-11)	2.4(-7)	4.2(-13)	1.0(-34)	9.7(-30)	7.1(-31)

After considering a starting system with 5 moles of $FeCl_2$, 1 mole of H_2O and 10 moles of Ti the results show that in the equilibrium the partial pressure of H_2 in the gaseous phase is 100 to 32% in the temperature range between 500 and 950ºC, while the other gaseous species are: 10^{-3} to 68 mol% for $FeCl_2$, 10^{-11} to 10^{-10} mol% for HCl, 10^{-12} to 10^{-7} mol% for H_2O, 10^{-18} to 10^{-7} mol% for $FeCl_3$, 10^{-27} to 0 mol% for $TiCl_4$, 0 to 10^{-30} mol% for Cl_2, and 0 to 10^{-29} mol% for O_2 at 500 and 950ºC, respectively. This shows that all H_2O has reacted and the HCl was dissociated, indicating that O_2 was completely consumed and the reactions I to V have shifted towards the right hand.

In the condensed phase, these hypotheses are confirmed because the amount of $FeCl_2$ is practically the same as at the beginning at low temperature, like is expected by reactions II and III. Otherwise, the decrease of Ti and the increase in the amount of TiO_2 confirm the evidence that the O_2 is captured by the metallic titanium. The null amount of Fe_3O_4 evidences that reaction II is very effective in the formation of $FeCl_2$.

If Fe is used as a reactive species instead of Ti and the formation of Fe_3O_4 is considered, the equilibrium calculation evidences that the performance of the cycle is less productive for the generation of H_2 and a greater amount of O_2 is present in the closed system (see Table V.3). But this oxygen is accompanied by smaller amounts of $FeCl_2$, and greater amounts of H_2O, HCl, and $FeCl_3$. In the condensed phase, a little quantity of Fe_3O_4 is formed.

TABLE V.3. $H_2O/FeCl_2$ (1:1) USING IRON AS OXYGEN SCAVENGER

Temp. (°C)	H_2 (g) (mol%)	H_2O(g) (mol%)	HCl (g) (mol%)	$FeCl_2$(g) (mol%)	$FeCl_3$(g) (mol%)	Cl_2(g) (mol%)	O_2(g) (mol%)
500	81	2.6	3.475(-3)	17	2.846(-7)	3.387(-15)	8.945(-28)
700	53	21	1.261	25	5.861(-4)	1.294(-10)	3.407(-20)
950	17	36	31.94	15	3.081(-2)	1.471(-7)	3.273(-14)

Other chloride cycles were also analyzed, like those in which participate the following chlorides: CuCl, $ZnCl_2$ and $MnCl_2$. taking into account the following reactions:

(a) Copper–chloride cycle

$$2\ CuCl(s,l) + 2\ H_2O(g) \rightarrow Cu_2O(s) + 2\ HCl(g) + H_2(g) + 1/2\ O_2(g) \quad (VI)$$

$$Cu_2O(s) + 2\ HCl(g) \rightarrow 2\ CuCl(s,l) + H_2O(g) \quad (VII)$$

$$2\ HCl(g) \rightarrow H_2(g) + Cl_2(g) \quad (VIII)$$

(b) Zinc–chloride cycle

$$ZnCl_2(s,l) + H_2O(g) \rightarrow ZnO(s) + 2\ HCl(g) \quad (IX)$$

$$ZnO(s) + 8\ HCl(g) \rightarrow ZnCl_2(s,l) + H_2O(g) \quad (X)$$

$$2\ HCl(g) \rightarrow H_2(g) + Cl_2(g) \quad (XI)$$

(c) Manganese–chloride cycle

$$3\ MnCl_2(s,l) + 4\ H_2O(g) \rightarrow Mn_3O_4(s) + 6\ HCl(g) + H_2(g) \quad (XII)$$

$$Mn_3O_4(s) + 6\ HCl(g) \rightarrow 3\ MnCl_2(s,l) + 3\ H_2O(g) + 1/2\ O_2(g) \quad (XIII)$$

$$2\ HCl(g) \rightarrow H_2(g) + Cl_2(g) \quad (XIV)$$

In the case of the copper chloride cycle, the amount of hydrogen obtained is various orders of magnitude less than in the iron chloride cycle (see Table V.4). It was also obtained that cycles with zinc chloride are not promising because the partial pressure of hydrogen is various orders of magnitude lower than the corresponding of the iron chloride cycle. Finally, when $MnCl_2$ is taken into account the situation is improved as a less oxidative environment is reached but, in any case, the H_2 production is not so satisfactory when compared with results of Table V.1.

TABLE V.4. $H_2O/CuCl$ (1:2)

Temp. (°C)	H_2O(g) (mol%)	HCl(g) (mol%)	CuCl(g) (mol%)	H_2(g) (mol%)	O_2(g) (mol%)	Cl_2(g) (mol%)
500	100	4.873(-3)	4.649(-8)	7.468(-8)	3.3733(-8)	1.246(-11)
700	99.9	5.829(-2)	5.186(-5)	1.446(-5)	7.226(-6)	3.794(-9)
950	99.6	0.4013	1.191(-2)	9.473(-4)	4.735(-4)	3.285(-7)

With this idea in mind, new thermodynamic calculations were performed, including the starting reacting species and an O_2 scavenger like titanium. The presence of titanium enhanced the production of hydrogen more than in the iron cycle, as can be seen from the following results: 100 to 99.9 mol% for Cu, 98.9 to 33.3 mol% for Zn, 100 to 85.8 mol% for Mn at 500 and 1000ºC, respectively. Therefore, it is concluded that the cooper chloride cycle is the best condition because there is the smallest amount of its chloride in the gaseous phase, and it condensed at room temperature with less tendency to its hydration. In the three cycles analyzed, the amount of the other gaseous species as HCl, O_2, $TiCl_4$ and H_2O, are insignificant.

But several others reactions may take place, due to the different interactions between gaseous and condensed reaction product phases. One of the most important interactions is the reaction between $TiCl_4$ and Fe_2O_3. Different Fe, Ti compounds can be obtained under varying temperature conditions, Cl_2 pressure, and atmosphere. A detailed study of this type of interference was done in the present research.

V.3. INTERFERENCE DUE TO INTERACTION BETWEEN FE_2O_3 WITH $TICL_4$

V.3.1. Starting materials and experimental setup

The starting materials used in this study were: metallic titanium (Aldrich Chemical Company, Inc., USA, 99.7%), Fe_2O_3 powder (Spex Industries Inc., USA), chlorine gas (Indupa, Argentina, 99.8%), argon gas (AGA, Argentina, 99.99%).

The samples were in different zones of a quartz capsule. The titanium sheet (0.5 mm × 10 mm × 0.18 mm, 75 mg) was in an alumina crucible and the Fe_2O_3 powder in a quartz crucible. Carbon powder was placed in the bottom of the capsule. The quartz capsule was then evacuated and materials were held in vacuum until they were completely outgassed. Finally, chlorine gas was introduced and the capsule sealed off. Figure V.1 shows the experimental setup, in which A and B denote the quartz capsule zones where the Ti sheet and Fe_2O_3 powder were placed. The amount used for experiments were 3.75×10^{-4} mole Fe_2O_3, 1.666×10^{-3} mole Ti and 6.165×10^{-4} mole Cl_2(g). Titanium was in excess with respect to the stoichiometric amount needed to convert all Fe_2O_3 into titanium oxides, and chlorine was in defect respect to the amount needed to convert stoichiometrically all Ti into $TiCl_4$.

The closed capsule was introduced in a preheated electric furnace at the reaction temperature (773, 873, 973 and 1073 K) and held there for a previously selected time. After heating, the encapsulated samples were cooled down to room temperature and finally the products were removed from the capsule. The capsules were opened in a glove box to prevent the hydrolysis of some reaction products. Then the solid products contained in A, B and C (Fig. V.1) were separated and analyzed.

Starting materials and reaction products were examined by scanning electron microscopy (SEM, Philips Electronic Instruments), energy dispersive spectroscopy (EDS, EDAX 9900), X ray diffractometry with Ni-filtered Cu Kα radiation (Philips PW 1310/01), and Mössbauer spectroscopy. The Mössbauer spectroscopy studies were carried out at room temperature using a ^{57}Co/Rh source in a constant-acceleration transmission spectrometer. The spectrometer was calibrated using a standard α-Fe foil and the reported isomer shift (IS) are relative to the center of the α-Fe spectrum. The spectra are least-square fitted with Lorentzian line shapes.

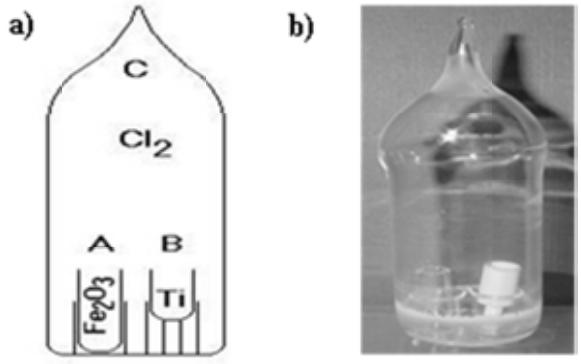

FIG. V.1: a) Schematic closed-capsule system showing the experimental disposition of Fe_2O_3 powder and Ti sheet in a chlorine atmosphere; b) Photograph of the capsule.

V.3.2. Structural and microstructure analysis of reaction products

(a) System Ti–Fe_2O_3–Cl_2

The structure of the reaction products was verified by comparing the experimental lines with those contained on PDF-1 (1997) [231] using PC Identify program (PW1776).

A XRD diffractogram of the reaction products at 773 K, corresponding to the sample withdrawn from A (quartz crucible), is shown in Fig. V.2a. It is seen that the phases detected at 771 K were TiO_2 (rutile) and $FeCl_2{\cdot}2H_2O$. The reference pattern of TiO_2 (card number 211276) and $FeCl_2{\cdot}2H_2O$ (card number 251040) [231] are shown in the same figure. These results are in agreement with the formation of solid TiO_2. Other diffraction lines of low relative intensities and attributed to magnetite, are also observed. To confirm the presence of this phase, a Mössbauer spectroscopy analysis was performed.

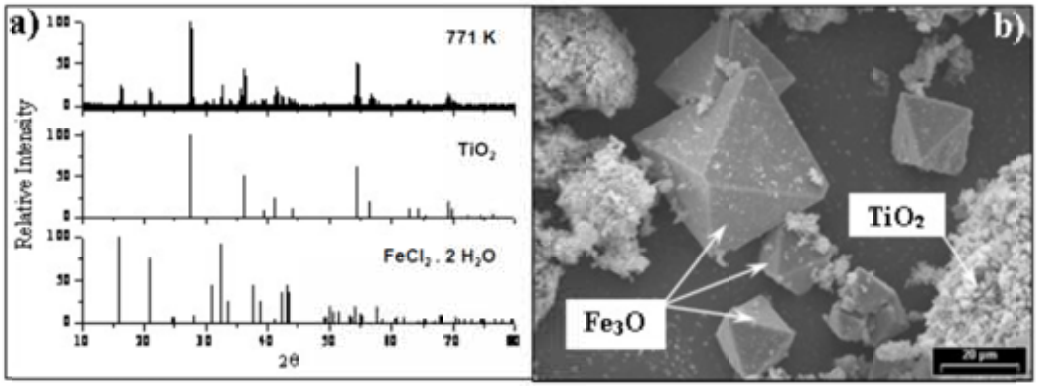

FIG. V.2. a) Diffraction and reference patterns of the reaction products at 773 K. b) SEM image of reaction products.

The Mössbauer spectrum of this sample has been fitted with two sextets with hyperfine fields of 493 and 458. These sextets suggest the presence of magnetite [232].

An SEM image showing the reaction products at 773 K is displayed in Fig. V.2b. The octahedrical particles were found to consist of Fe_3O_4, as shown by EDS analysis and Mössbauer spectroscopy. The TiO_2 forms aggregates of particles are less than 1 μm in size.

At 873 K, an ilmenite ($FeTiO_3$) — rutile (TiO_2) mixture (card numbers 290733–211276) [231] — was the final product. The XRD diffractogram along with the corresponding

diffraction patterns are, shown in Fig. V.3a. The formation of ilmenite can occur and the presence of O_2(g) and $FeCl_2$ are needed [233]. These reactants are thought to be supplied by direct chlorination. Nevertheless, ilmenite can be also formed by the reaction between O_2, $FeCl_3$ and $TiCl_4$ and the second reactant can be supplied by the reaction of Cl_2 with Fe_2O_3 [231]. An SEM image showing aggregates of particles of ilmenite less than 1 μm in size is presented in Fig. V.3b.

At 1073 K, the only phase detected in the zone indicated as A in Fig. V.1, is Ti_2O_3, (card number 431033) [231]. Since Ti is in excess over the maximum amount of Fe_2O_3 to form TiO_2, oxygen is in defect in the system, no other oxygen supplier is present. Then after removal of Fe from zone A of the capsule, only Ti is available to react with oxygen, but if this last substance is in stoichiometric defect to form TiO_2 at these temperatures, therefore, Ti_2O_3, a reduced species of TiO_2, is expected to be formed (Fig. V.4).

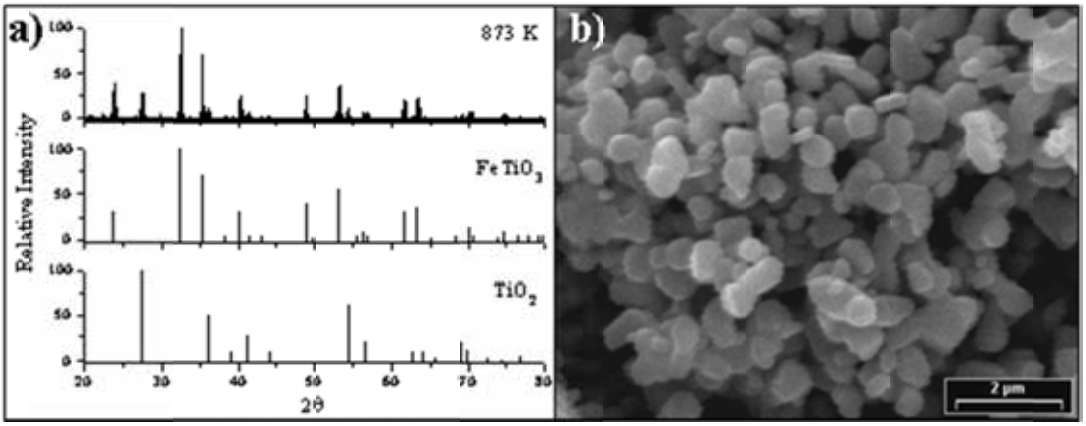

FIG. V.3. a) Diffractogram and reference pattern of the reaction products at 873 K. b) SEM image of the particles of ilmenite.

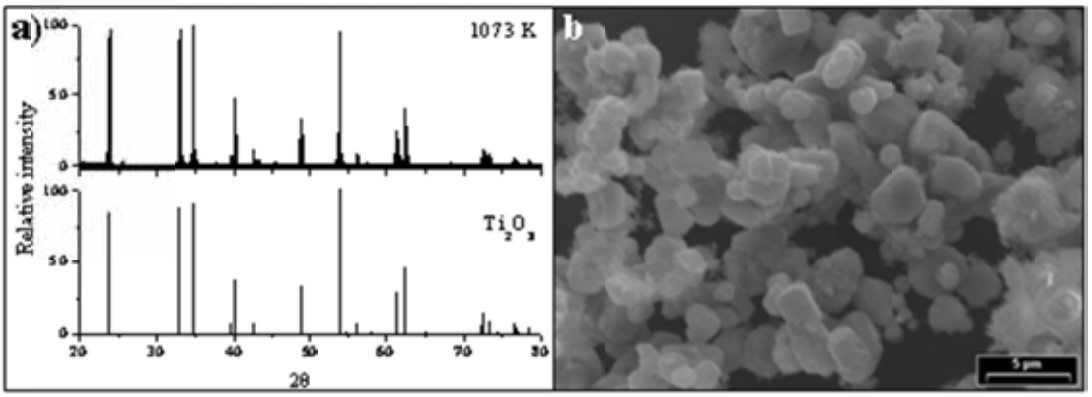

FIG. V.4. a) Diffractogram and reference patterns of the reaction products at 1073 K. b) SEM image of the particles of Ti_2O_3.

EDS analysis of the solid products and residues remaining in B (alumina crucible) allowed to confirm the deposition of iron on the Ti sheet, as shown in Fig. V.5. The XRD analysis showed that Fe was in its stable phase α-Fe, (card number 060696) [231], (Fig. V.5a). The iron deposited as a substrate over the remaining Ti sheet was observed at all tested temperatures.

The backscattered electron image obtained by SEM and displayed in Fig. V.5b, shows the Fe deposit covering the Ti sheet. The sheet was included in resin and polished. The Fe particles are the shinning dots observed over the substrate that cover the nucleus of remaining Ti.

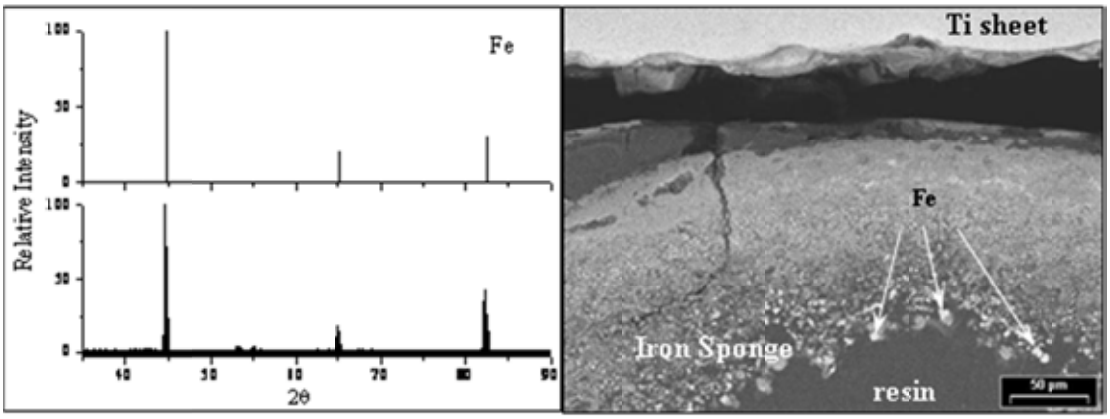

FIG. V.5. a) XRD of the Fe deposit covering the remaining Ti sheet. b) Backscattered electron image, showing the Fe deposit covering the Ti sheet

The gaseous reaction products condensed on the walls of the capsule by cooling from 773 and 923 K, were also analyzed. The formation of monoclinic ferric hexa-hydrated chloride ($FeCl_3 \cdot 6H_2O$) [234] and monoclinic ferrous di-hydrated chloride ($FeCl_2 \cdot 2H_2O$) were detected, (card numbers 330645–251040) [231], (Fig. V.6a).

The first compound is always present in a higher ratio than the second one. If both products are exposed to ambient, only $FeCl_2 \cdot 2H_2O$ was detected, indicating that the ferric chloride has been completely hydrolyzed.

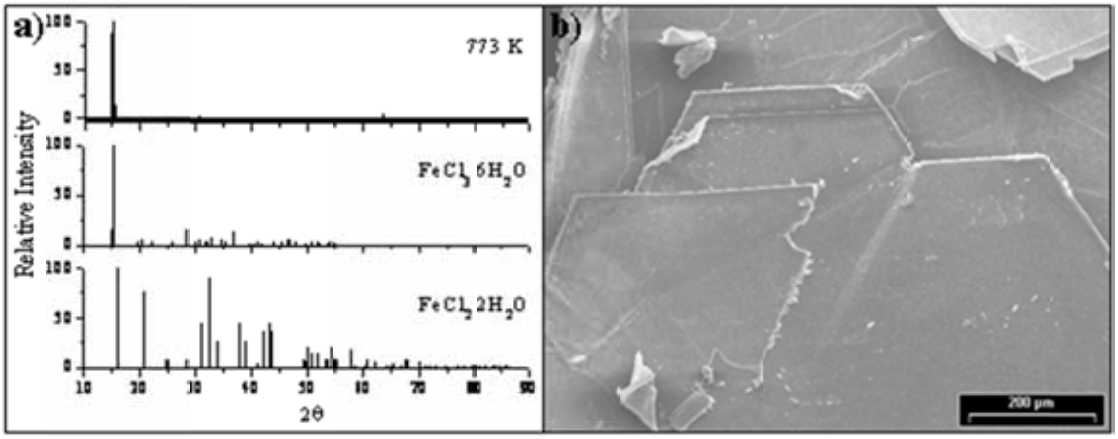

FIG. V.6. a) XR diffractograms of the gaseous products condensed by cooling on the walls of the capsule. b) SEM image of $FeCl_2 \cdot 2H_2O$.

Figure V.7 shows a Mössbauer spectrum of iron chlorides exposed to ambient. This spectrum is solved by a doublet with quadrupole splitting (QS) of 2.98 mm/s and IS(Fe) of 1.22 mm/s. The doublet parameters are in good agreement with those of hydrated $FeCl_2$ [235].

At temperatures above 923 K, no condensation of any phases was observed. An SEM image of the condensed chlorides on the capsule wall is presented in Fig. V.6b. Plates of 50 μm of width are observed. EDS analysis showed an average composition in atomic percentage (at%) of Cl (69 at%) and Fe (31 at%), indicating that the compound is the ferrous chloride.

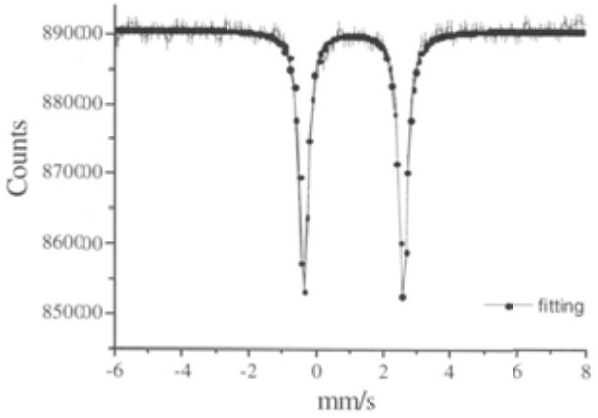

FIG. V.7. Mössbauer spectrum of iron chlorides exposed to ambient.

TABLE V.5. CONDENSED PHASES DETECTED BY XRD ANALYSIS IN THE $Ti–Fe_2O_3–C–Cl_2$ SYSTEM

Temperature [K]	Condensed phases detected by XRD analysis in zone A
773	TiO_2 (rutile), Fe_2O_3, $FeCl_3•6H_2O$, $FeCl_2•4H_2O$
873	TiO_2 (rutile), Fe_2O_3, $FeCl_2•2H_2O$, FeOCl
973	Ti_2O_3, FeOCl

Taking into account the phases detected at different temperatures (Table V.5) and according to the possible reactions that can be considered, the following picture is helpful to understand the process taking place to form titanium oxides. Titanium tetrachloride that is formed in B diffused along the capsule to region A for reacting with Fe_2O_3, producing titanium oxides and iron chlorides. The iron chlorides in the closed capsule go back to the region B and react whit the remaining Ti to produce $TiCl_4(g)$ and start a new transport cycle (Fig. V.8).

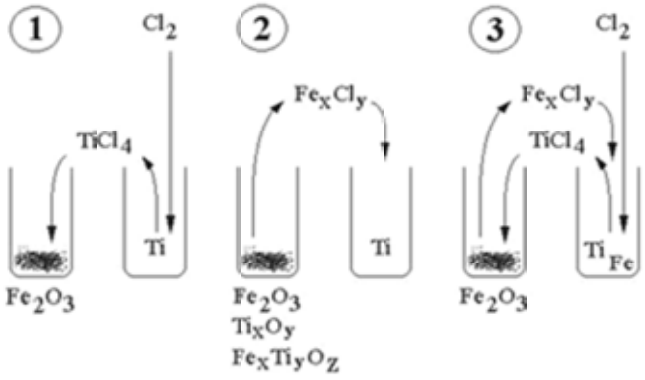

FIG. V.8. Schematic picture of the reaction mechanism: (1) Initiation: non-reversible formation of $TiCl_4(g)$ in B (alumina crucible). (2) Cyclic mass transport through gaseous phase to form titanium oxides or titanates in A (quartz crucible) and Fe(s) in B. (3) Finalization: the process is stopped when Fe_2O_3 has reacted completely.

V.3.3. Summary of the most important remarks

The most convenient cycle for the production of hydrogen was the iron chloride cycle in the presence of Ti at low temperatures and copper–chloride cycle along the whole temperature range.

The interaction between $TiCl_4$ and Fe_2O_3 was very important and the reaction takes place through a mass-transport mechanism by means of iron chlorides and $TiCl_4$(g) which are formed in situ within the closed quartz capsule.

In the system Fe_2O_3–Ti–Cl_2, there is a strong effect of the temperature on the characteristics of the reaction products. Due to the interaction of the $TiCl_4$(g) with Fe_2O_3, the reaction products in zone A (quartz crucible) were: TiO_2 (rutile) at 773 K, $FeTiO_3$ (ilmenite) at 873 K, and Ti_2O_3 at 1073 K. In the formation process of these oxides, gaseous iron chlorides diffuse along the capsule to zone B (alumina crucible) to react with remaining Ti, forming Fe and thereby regenerating $TiCl_4$(g). It makes the reaction a cyclic process until all the Fe_2O_3 is exhausted.

Moreover, in the system Ti–Fe_2O_3–C–Cl_2, the reductor atmosphere surroundings, generated by the presence of C with high specific area, bear to the majority formation of Ti_2O_3 at temperatures higher than 973 K without the presence of titanates.

Another significant interaction due to which the expected result of this thermocycle can deviate is the formation of iron oxychloride from the reaction of iron trichloride with iron oxide. The presence of iron trichloride is very posible due to the oxidative atmosphere present in the reactor.

V.4. THERMOGRAVIMETRIC STUDY OF COPPER CHLORINATION

V.4.1. Introduction

The chlorination reactions of copper or copper containing mixtures were studied for the development of separation methods in extractive metallurgy [236–240], for the recycling of metals from scraps [241, 242], or from spent catalysts [243, 244], and for preparation of anhydrous chlorides as precursors for further chemical industrial applications [245, 246].

Cuprous chloride is a colorless or grey cubic crystal, fairly stable on air or light [246]. The direct combination of the elements is the most common method of production. Remeika et al. studied the synthesis of CuCl from Cl_2 and CCl_4. They found that very pure and stoichiometric CuCl is produced by the reaction of copper with CCl_4 [247]. Cupric chloride is usually prepared by dehydration of the dehydrate $CuCl_2 \cdot 2H_2O$ at 120°C. It forms yellow to brown deliquescent monoclinic crystals [246].

The most complete thermogravimetric study of the chlorination of copper and copper chlorides was presented by Titi-Manyaka et al. [236] in 1976. They did non-isothermal thermogravimetric measurements for the chlorination of copper, CuCl and $CuCl_2$. According to their results, the chlorination of metallic copper proceeded by forming CuCl, followed by further chlorination of a part of CuCl to $CuCl_2$ above its melting point (430°C). However, the amount of $CuCl_2$ formed was limited, as indicated by a small weight decrease in the thermogravimetric analysis (TGA) curve at 537°C, its decomposition temperature. They say that in chlorine, metallic copper was converted to CuCl and fused at 220°C because of the highly exothermic nature of the reaction. In the cuprous chloride TGA curve, they distinguish four regions: accelerated chlorination after the fusion of CuCl, decelerated chlorination perhaps after the closure of the surface with solid $CuCl_2$, a rapid weight decrease by

decomposition of $CuCl_2$, and vaporization of Cu_3Cl_3. Finally for cupric chloride, they found that the TGA showed decomposition of $CuCl_2$ at 537°C followed by vaporization of CuCl.

The surface of reaction of copper at low pressures of chlorine (up to 1 kPa) was extensively studied by Sesselmann et al. [248, 249]. They found that upon chlorine exposure, a surface layer with an average stoichiometry $CuCl_x$ is formed and the value of x can vary continuously from 0 to almost 2 as a function of the gas pressure and the exposure time.

Bourhila et al. [245] studied the chlorination of copper foils in a flux of chlorine diluted in argon with a total pressure of 0.1 kPa. They found that the morphology and composition of the copper chloride deposited in a substrate holder near the chlorination chamber varied with the temperature of reaction. For temperatures above 420°C, they obtained only CuCl. As temperature decreases below 420°C, they found also $CuCl_2$. Finally at temperatures below 380°C, $CuCl_2$ was the only compound observed.

The chlorination of chalcopyrite concentrates has been studied by several authors as was reviewed by Kanari et al. [237]. Among other chlorides, they reported the formation of $CuCl_2$ for temperatures between 20 and 700°C and CuCl for 600 and 700°C.

The National Commission of Atomic Energy is investigating a suitable physicochemical process for the conditioning of spent nuclear fuel and treatment of the scrap of research reactors of the Al–U_xSi_y type. A possible way of processing is through dry chlorination of the cladding with the purpose of selective separation of the aluminum from the remaining elements such as Cu, Fe, Ni, Zn, etc., transforming them into volatile chlorides. To understand the chlorination reaction of metallic mixtures, it is necessary to study the chlorination of the different metals on their own. These studies are also the foundation for developing processes related with recycling valuable metals from complex metallic scraps. On the contrary to other metals, copper is mainly used as pure metal or as alloys with high copper content [250], consequently it may be recovered by a simple one-step process.

The chlorination of copper has not been studied systematically [236, 245, 247–249], and the kinetics and mechanism of the reaction are not well established yet for many reaction conditions. Consequently, the aim of this work is to analyze the kinetics of the copper chlorination reactions followed by TG measurements with the purpose of establishing a reaction model. In order to identify and quantify the products obtained at different temperatures between 100 and 750°C, microstructural characterization of solid and condensed phases were done. Volatilization of copper chlorides at temperatures above 400°C in chlorine and argon atmospheres has also been studied. Complete understanding of the volatilization processes is important for further development of a separation methodology based on the selective volatilization of the different compounds.

V.4.2. Experimental procedure

The gases used were Cl_2 of 99.8% purity (Indupa, Argentina) and Ar of 99.99% purity (AGA, Argentina). The solid reactants were circular sheets of 6 mm diameter of commercial copper (99.9% of purity). The chlorination reactions were carried out in a thermogravimetric analyzer (TGA), which is extensively described elsewhere [251]. This thermogravimetric analyzer consists of an electrobalance (Model 2000, Cahn Instruments, Inc.) suitable for working with corrosive atmospheres, a gas line, and an acquisition system. This experimental setup has a sensitivity of ±5 μg while operating at 950°C under a flow of 8 L/h.

Samples of about 20 mg were placed in a quartz crucible inside the reactor in an argon flow of 1.3 L/h. For the non-isothermal measurement, a chlorine flow of 0.8 l/h was introduced in the reactor and at the same time, the heating started with a ramp of 100°C/h. For the isothermal

reactions, the solids were heated until they reached the desirable temperature before chlorine injection. The partial pressure of chlorine was 35.5 kPa.

Due to the hygrospicity of the products, they were isolated into a glove box and were prepared in well sealed samples in order to characterize by XRD avoiding the absorption of moisture.

V.4.3. Thermodynamic analysis

According to the ΔG° values of all chemically possible copper chlorination reactions for temperatures below 100ºC, CuCl is the most likely product to be obtained for the reaction of copper with chlorine, whether in solid, liquid or vapour state. However, formation of $CuCl_2$ from metallic copper can not be excluded since it also has a negative value of ΔG°. The reaction of CuCl with Cl_2 to give $CuCl_2$ is straightforward for temperatures below 400°C. At higher temperatures, the decomposition of $CuCl_2$ is predictable since the ΔG° of this reaction becomes negative. There are some discrepancies in the literature about the $CuCl_2$ decomposition temperature; the values reported by different authors are between 300 and 537°C [236, 246]. For this reason, it is not obvious to determine which chloride would be formed.

According to the ΔG° value, formation of gaseous Cu_3Cl_3 from metallic copper is expected for all temperatures. Volatilization of CuCl although having a positive value of ΔG° for the whole range of temperatures, has to be taken into account in a flowing system because the flux conditions may enhance the volatilization process. The CuCl melting point is 422°C [246], its partial pressure is about 10^{-4} kPa for temperatures above 650°C for the trimmer and 750°C for the monomer [230], which suggests that the mass change will be detectable by thermogravimetric measurements.

V.4.4. Results and discussion

V.4.4.1. Non-isothermal thermogravimetry

For general characterization of the copper chlorination process, a non-isothermal TG measurement was carried out. The mass change vs. temperature is shown in Fig. V.9. As it can be seen there, the reaction starts at about 150°C with a mass gain followed by a mass loss starting at 500°C. Formation of CuCl produces a mass gain that corresponds to 55.8% of the initial mass of copper, whereas formation of $CuCl_2$ leads to a mass increase of 111.6%. The percentage of mass gain observed is indicating that in the maximum, there is mostly $CuCl_2$. The mass loss is due to $CuCl_2$ decomposition followed by CuCl volatilization. The presence of mostly CuCl in the last part of the curve was confirmed by XRD.

V.4.4.2. Calculation of the amounts of $CuCl_2$, CuCl, and CuCl(g)

Isothermal TG curves were obtained for temperatures between 100 to 825°C. In Fig. V.10, the curves obtained for three temperatures are shown to illustrate the different behavior observed as temperature increases. The chlorination reactions start with a mass gain which corresponds to the formation of condensed copper chlorides. After that, for temperatures above 500°C, the mass continuously decreases until complete volatilization, whereas for the lower temperatures, the mass tends to a constant value. For temperatures below 500°C, all reactions proceed without mass loss, and the amount of mass gained increases with temperature up to about 450°C. The mass gain in isothermal reactions is always smaller than the mass gain in the non-isothermal case. The mass gain for temperatures up to 625°C is higher than that needed for complete reaction to form CuCl, and the difference corresponds to $CuCl_2$ formation.

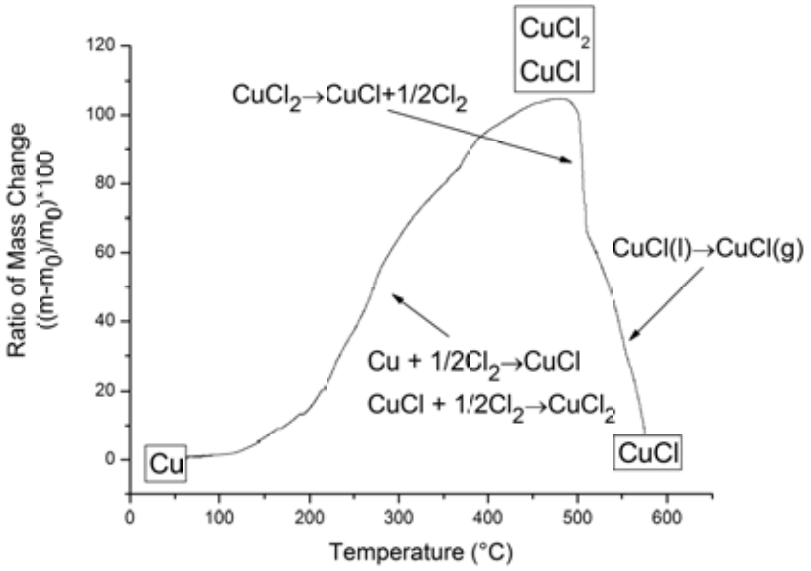

FIG. V.9. TG curve corresponding to non-isothermal copper chlorination reaction.

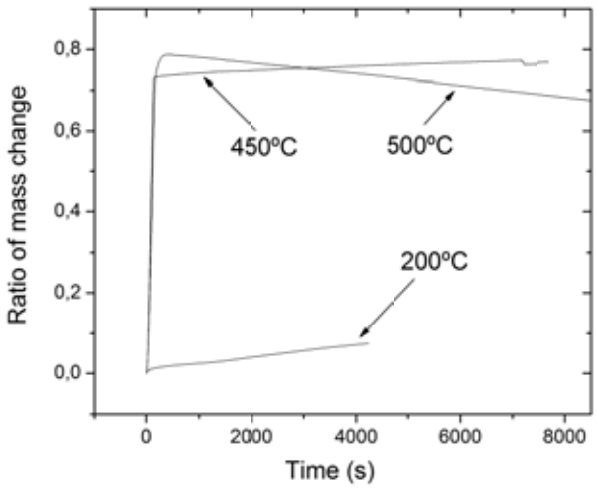

FIG. V.10. TG curves corresponding to isothermal copper chlorination reactions.

For temperatures between 400 and 750°C, a methodology of heating in argon [242] has been applied to decouple two processes taking place: decomposition of $CuCl_2$ and volatilization of CuCl in order to determine the amounts of CuCl, $CuCl_2$ and $Cu_3Cl_3(g)$ formed at each temperature. The results are shown in Table V.6 as percentage of initial mass of copper that forms CuCl, $CuCl_2$ and $Cu_xCl_x(g)$ with x=1 for the monomer and x=3 for the trimer.

These results were compared with equilibrium calculations made with the HSC software [230] in which arbitrary amounts of each reactant were used to simulate the different experimental conditions. At the beginning when chlorine arrives at the sample, it reacts quickly with copper due to the high temperatures leading to a chlorine deficiency condition on the reaction surface. According to thermodynamic calculations, only CuCl is expected for all temperatures when there is little chlorine to react with copper. However, formation of $CuCl_2$, which is not predicted by thermodynamics for these temperatures, can be understood considering that CuCl is being formed in a chlorine atmosphere. When the incoming flux of chlorine arrives at the sample, it first reaches the CuCl layer just formed, and the reaction of CuCl with excess chlorine to form $CuCl_2$ has a negative ΔG^o value up to 750°C.

TABLE V.6. PERCENTAGE OF INITIAL MASS OF COPPER THAT FORMS CuCl, $CuCl_2$ AND $Cu_xCl_x(g)$ (WITH x=1 OR 3) IN THE MAXIMUM OF THE TG CURVES (AFTER THE MASS GAIN) FOR DIFFERENT TEMPERATURES

Temperature (°C)	Mass of reacted Cu (mg)	Percentage of		
		CuCl	$CuCl_2$	$Cu_xCl_x(g)$
100	0.97	36.43	63.57	n/d
150	1.81	36.68	63.32	n/d
175	3.51	57.87	42.13	n/d
200	10.47	83.11	16.89	n/d
225	10.22	85.48	14.52	n/d
250	12.45	78.66	21.34	n/d
400	c/s	71.3	27.7	1
450	c/s	49.1	48.5	2.4
500	c/s	51.7	44.9	3.4
550	c/s	73.9	24.9	1.2
600	c/s	79.8	18.3	2
650	c/s	72.2	20	7.8
700	c/s	77.6	12	10.4
750	c/s	78.5	7.8	13.7

c/s complete sample of Cu reacted.
n/d non-detected.

The same can be applied to understand the non-isothermal reaction. As long as there is still metallic copper, there is a flux of chlorine passing through the layer of copper chlorides impelled by the gradient in chlorine partial pressure established between the top of the sample and the interface between metallic copper and the chloride ashes. In the interface, chlorine is being exhausted by the reaction with copper, whereas in the top of the sample, chlorine arrives from the bulk gas stream. The flux of chlorine prevents the decomposition of $CuCl_2$ even though it is unstable above 400°C. However, once copper finishes, the partial pressure of chlorine across the chloride ashes decreases leading to a decomposition of $CuCl_2$ from the inner side of the ashes. Mass balances indicate that the last part of the curve could not correspond to the volatilization of only CuCl because that would lead to an amount of copper bigger than the initial mass of copper. This means that after the change of slope point, there is still $CuCl_2$, probably because at the top of the sample, CuCl is in a chlorine atmosphere. However, towards the end of the reaction, volatilization of CuCl predominates which leads to the change of slope observed.

Table V.6 shows that for isothermal chlorination above 450°C, the amount of $CuCl_2$ decreases while CuCl increases with temperature. A possible explanation for the percentages observed is that during the mass gain, while there is still metallic copper, both processes occur: formation of CuCl from metallic copper and formation of $CuCl_2$ from CuCl. As temperature increases, the rate of formation of CuCl increases more than the rate of formation of $CuCl_2$ leading to formation of higher percentages of CuCl.

The formation of $CuCl_2$ at 600°C, although not being stable at that temperature, was confirmed by XRD of a sample obtained by interrupting the chlorination reaction during the mass gain by quenching with liquid air. For the lower temperatures up to about 275°C, the reaction rate reaches a near to zero value at intermediate stages. Although there is unreacted

metallic copper, the reaction practically stops. Therefore, the products of low temperature reactions consist of a brownish ash which can be easily removed; and below the ash, there is metallic copper. The composition of the products of reaction determined by mass balance for different temperatures expressed in percentage of each chloride is also shown in Table V.6.

Although there is not an immediate interpretation of these quantities, it is possible to appreciate that the amount of CuCl increases with temperature and also with the mass of copper that has reacted. This last quantity is a measure of the degree of reaction because the reaction area is constant for all samples regardless of the initial mass of copper.

Examination of the samples in the SEM reveals that the chloride ashes are formed by two layers (Fig. V.11) that belong to a reaction at 220°C. XRD profiles corresponding to the ash confirm that one layer is CuCl and the other one is $CuCl_2$, being the CuCl layer the one in contact with the unreacted copper. This indicates that in the copper surface, only CuCl is being formed and $CuCl_2$ is being produced by further reaction of CuCl with chlorine.

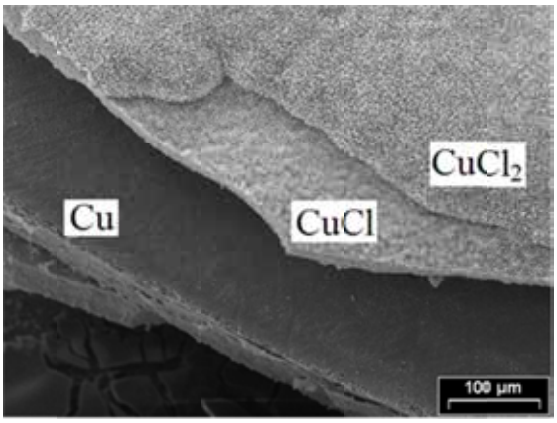

FIG. V.11. SEM photograph corresponding to a copper sample chlorinated at 225°C.

V.4.4.3. The volatilization process

The volatilization rate of the copper chlorides in chlorine atmosphere was determined between 500 and 825°C. The TG curves show an almost constant slope during the whole volatilization process. At the beginning of the mass loss, there is a liquid containing CuCl and $CuCl_2$, and decomposition of $CuCl_2$ occurs together with volatilization of CuCl. However, the velocities of these two processes are so similar that the change in the slope is almost imperceptible for the majority of the temperatures. The change in the slope is well evidenced for the non-isothermal measurement (see Fig. V.9). In such conditions, the amount of $CuCl_2$ formed reaches a maximum value indicating that almost all copper has formed $CuCl_2$. For this reason, the process of decomposition predominates in the first place. After that, volatilization takes place leading to the slope change.

An activation energy of 109±3 kJ/mol for the volatilization process in chlorine was calculated with the Flynn method [252] from the slope of the curve of ln$v$ (v = rate of reaction) versus 1/T (Fig. V.12, bottom). The volatilization of CuCl in argon atmosphere was also studied. Figure V.12, top, shows the ln$v$ versus 1/T plot, the value of the activation energy obtained was 97±3 kJ/mol.

The enthalpy of vapourization of cuprous chloride for temperatures between 450 and 800°C is 219 kJ/mol for the monomer (CuCl) and 50 kJ/mol for the trimer (Cu_3Cl_3) [230]. The intermediate values obtained could correspond to an apparent activation energy belonging to the formation of both species CuCl(g) and Cu_3Cl_3(g).

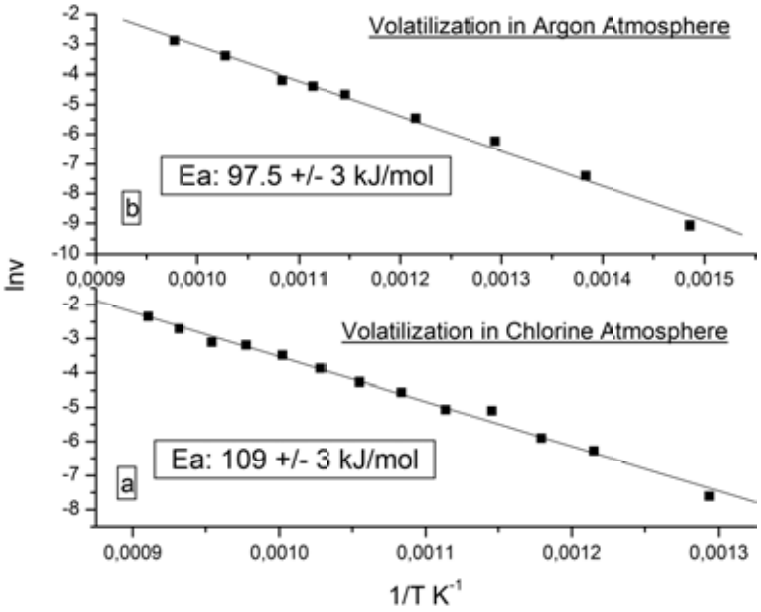

FIG. V.12. lnv versus 1/T plot for the calculation of the activation energy for volatilization in argon and chlorine atmosphere.

V.5. Conclusions

Copper chlorination reaction has been measured in the range between 100 and 800°C, and the starting temperature for the reaction was determined at 150°C. From the analysis of the TG curves obtained above 400°C in chlorine and argon atmospheres, the relative quantities of the different chlorination products, i.e. condensed and gaseous CuCl and condensed $CuCl_2$ were estimated. For the lower temperatures it was obtained that the metal reacts to form CuCl, and the $CuCl_2$ was only found over this CuCl. This indicates that it is being formed by further chlorination of CuCl and not directly from metallic copper. The relative amounts of CuCl and $CuCl_2$ were calculated with mass balances. The volatilization process was analyzed for the higher temperatures in chlorine and argon atmospheres. The activation energies obtained in both cases were around 100 kJ/mol. This value is intermediate between the vaporization enthalpies for Cu_3Cl_3 and CuCl. For this reason it may correspond to an apparent activation energy for the volatilization of both species.

V.6. CHLORINATION OF COPPER–ZINC ALLOY

V.6.1. Introduction

Metal chlorination reactions have been partially studied. Several works related with the chlorination of copper have been published [236, 244, 245, 248, 249, 253, 254] while little information is available regarding zinc dry chlorination reaction [255].

Chlorination processes have technological application for chloride synthesis [242, 243, 245, 247, 256–261] among others.

Basic research in alloy chlorination has shown that generally the reactivity of the alloy is different from that of the pure constituents [257–263]. Similarly, interactions between reaction products and solid reactants were observed in the chlorination of multi-component systems [230, 236, 260, 264–272].

V.6.2. Experimental

Commercial metals (99.9% purity) were used to prepare a CuZn alloy with the following composition: Zn: 48 wt%, Cu: 52 wt%. This alloy was chosen for the study, because the relative amount of each element ensures that the detection of reaction products and intermediate species is feasible by the different techniques available. Besides, we have considerable experience in our laboratory regarding its preparation and structural characterization. A powder of the alloy was prepared by mechanical abrasion with an electrical lathe (Black & Decker RT650). Thermal treatment at 300°C for 2.5 hours in air was performed to release possible residual tensions. The powder sample was well characterized by energy dispersive X ray fluorescence (ED-XRF), scanning electron microscopy (SEM), and X ray diffraction (XRD). The results are shown in Fig. V.13.

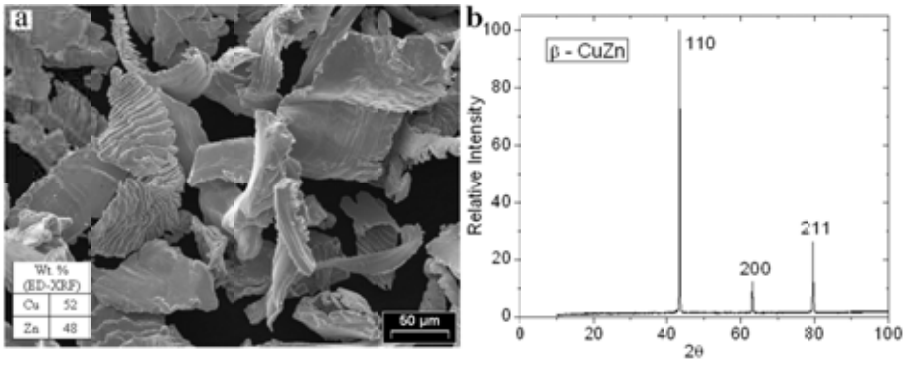

FIG. V.13. Morphology, composition, and structure of the initial sample: (left) SEM photograph of the Zn 48 wt%-Cu alloy powder and chemical composition obtained by ED-XRF; (right) XRD pattern of the initial sample.

Figure V.13, left, shows that the powder consists of shavings of 150 µm average size. XRD patterns (Fig. V.13, right) show that the alloy is in beta phase. This phase has a composition range of Cu–(36.7 to 59.8)Zn (wt%) [267].

The gases used were Cl_2 of 99.8% purity (Indupa, Argentina) and Ar of 99.99% purity (AGA, Argentina). Isothermal and non-isothermal chlorination reactions were carried out with samples of 20 mg in a TGA. The equipment as well as the methodology used to perform the chlorinations are extensively described elsewhere [259].

V.6.3. Results and discussion

V.6.3.1. Non-isothermal chlorination of CuZn alloy

The initial reaction temperature was determined at 225ºC by non-isothermal thermogravimetric measurements. The chlorination curve for the alloy together with the chlorination of the pure metal and oxides is shown in Fig. V.14. This figure shows the ratio between the mass change and the initial mass of the sample as a function of temperature.

The starting temperature for the reaction of the alloy is in between those of the pure metals. Copper and zinc chlorination reactions start at about 100 and 270ºC, respectively. Mass loss during oxide chlorination reactions starts at still higher temperatures above 350ºC.

Figure V.14 shows that the alloy chlorination reaction occurs with mass gain followed by mass loss above 450ºC. This is in accordance with the behavior observed in pure metal chlorinations. For both metals, an initial mass gain is observed due to the formation of condensed chlorides followed by a mass loss that indicates volatilization of the chlorides.

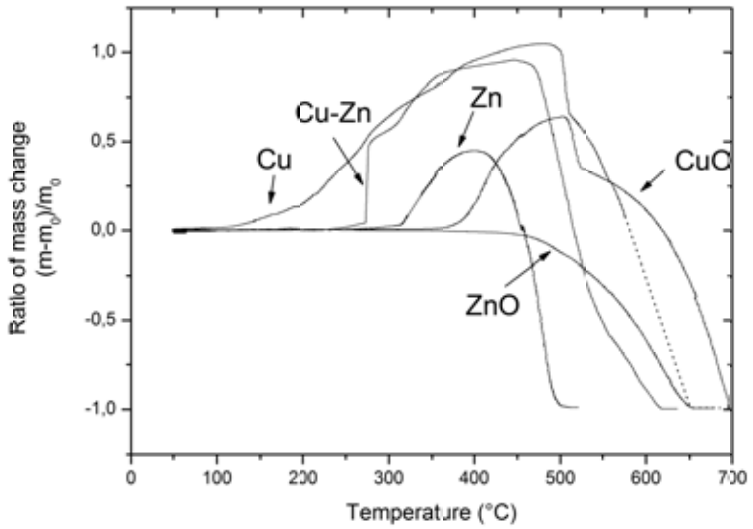

FIG. V.14. Non-isothermal TG curves for the chlorination of Cu, Zn and Zn 48 wt% -Cu alloy.

V.6.3.2. Isothermal chlorination of CuZn alloy

(a) Thermogravimetric analysis

Isothermal chlorination reactions were carried out at different temperatures between 250 and 500ºC. The corresponding TG curves are shown in Fig. V.15. The mass gains observed indicate the formation of condensed chlorides.

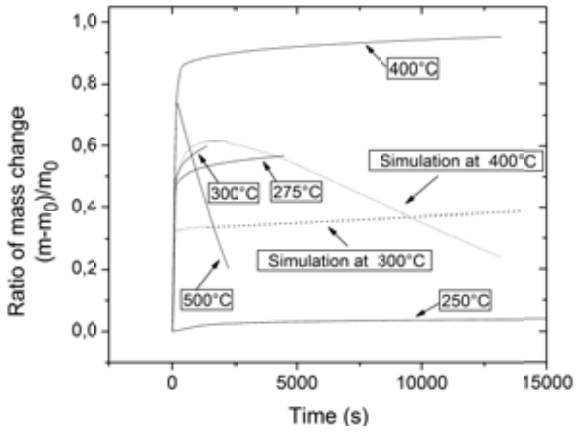

FIG. V.15. Isothermal TG curves for the chlorination of Zn 48 wt%-Cu alloy at 300 and 400ºC, together with the metal chlorination curves, and the simulated curve considering the individual contributions of the metal.

The ratios of mass gain observed in the alloy chlorinations at higher temperatures indicate that there are interactions between copper and zinc that lead to the formation of larger amounts of condensed zinc chlorides. To show this, simulated TG curves at 300 and 400ºC are also shown in Fig. V.15. These curves correspond to the weighted sum of the individual mass changes observed in the chlorination of each metal alone, weighted by the molar fraction of the metal in the alloy.

At both temperatures, it can be seen that the mass gain obtained in the alloy chlorination is higher than the one expected for the chlorination of the pure metals in the alloy ratio. Moreover, during chlorination of pure zinc at 400ºC, zinc chloride volatilization does occur. For this reason, there is a mass loss in the simulated curve. On the contrary, during alloy

reaction, volatilization of $ZnCl_2$ was not detected as evidenced in the TG curve for the alloy chlorination which only shows mass gain. These results show that at this temperature, retention of zinc chlorides in the condensed phase occurs, although the vapour pressure (see following equation) is high enough for its evaporation.

$$P_{vap} = 3\times10^{-8}\,T^3 - 6\times10^{-5}\,T^2 + 0.0412\,T - 9.8997 \qquad 673 < T < 873$$

where

P is the pressure, kPa, and
T is the temperature, K.

(a) Low-temperature behavior

At 250ºC, the low value of mass gain observed in the TG curve indicates that the reaction proceeds only to a very little extent. Sample morphology observed in SEM which is shown in Fig. V.16 confirms this. For comparison, the initial sample is presented in Fig. V.16a. Figure V.16b, which belongs to the chlorinated sample, shows that although the general sample shape of reacting particles is maintained, there are differences in the particle surface. In Fig. V.16c, a detail of the sample surface is shown. XRD analysis (Fig. V.16d) reveals that the crystallites that appear covering the sample surface, correspond to zinc oxichloride (Ref. Pat.: 45-0819, a:5.86, b:6.58 and c:11.36 [273]). Alpha phase (α-CuZn) a copper-rich phase which is not present in the initial sample, was also detected by XRD. This is a copper-rich phase with a maximum content of zinc of 39 wt%. Regarding Zn_2OCl_2, this compound is being formed from the thin layer of zinc oxide that covers the alloy. The reaction interruption is attributed to this species that forms a barrier which prevents further chlorination of the alloy.

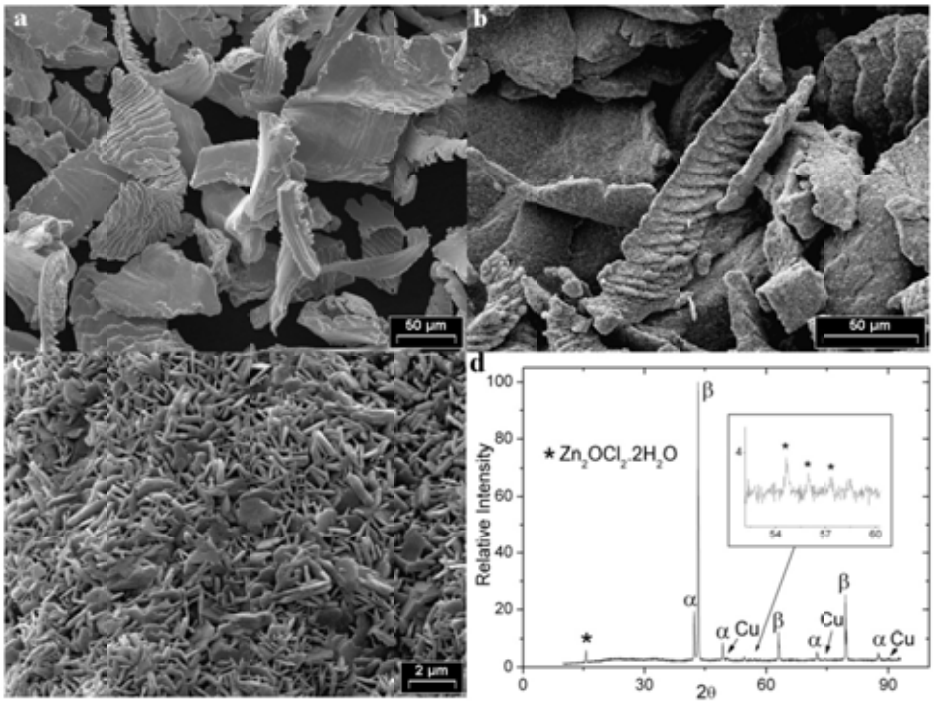

FIG. V.16. (a) SEM photograph of the initial sample (for comparison) (b) SEM photograph of the final sample from the chlorination at 250ºC, (c) surface of the sample shown in (b), (d) XRD pattern of the same sample.

(b) Interactions due to oxidation–reduction reactions

XRD analyses of the reaction products at 275 and 300ºC show that there is β-CuZn (initial sample), a copper rich phase α-CuZn, CuCl, and metallic copper. Zinc chloride is deliquescent, which is why it is difficult to detect this species by XRD.

Figure V.17 belongs to the samples chlorinated at 275 and 300ºC analyzed by SEM. The presence of well developed crystals can be observed, whose composition analyzed by EDS reveals that they correspond mainly to metallic copper. The presence of CuCl is not predicted by thermodynamic considerations below 400ºC where $CuCl_2$ is the most stable chloride. These results can be explained considering the electrochemical potentials of the different metal pairs which indicate that those species containing Cu^{+2} and Cu^{+} will be reduced to copper by metallic zinc. For this reason, copper chlorides formed during the reaction would not remain unreacted as long as there is zinc in the sample. It is expected that during the reaction, copper chlorides react with zinc leading to copper-reduced species (Cu^{+} and Cu).

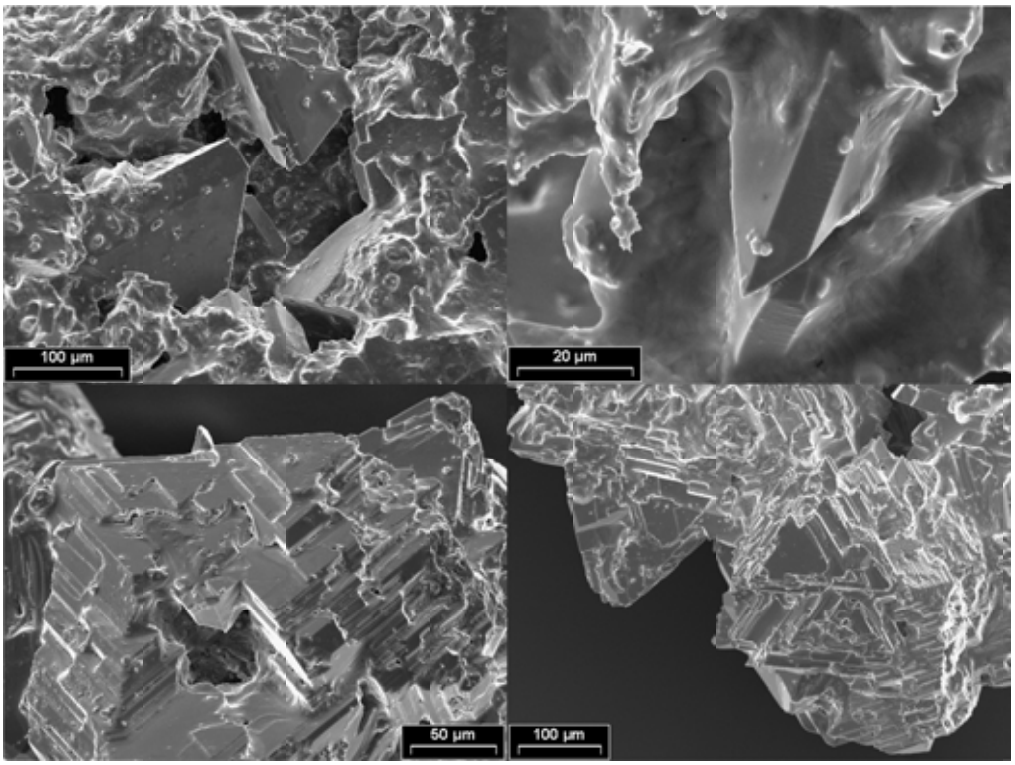

FIG. V.17. (a) and (b) SEM photograph of the final sample from the chlorination at 275ºC; (c) and (d) SEM photograph of the final sample from the chlorination at 300ºC.

The occurrence of these oxidation–reduction reactions between zinc and copper chlorides was confirmed by aging mixtures of powder of copper chlorides ($CuCl_2$, CuCl) and powder of CuZn alloy, at room temperature for different time periods in argon atmosphere. In those experiments, appearance of metallic copper and disappearance of $CuCl_2$ was observed. Therefore, during chlorination, the kinetics of these reactions will be faster due to high temperature condition.

(c) Reaction mechanism

Taking into account the results, the following reaction mechanism for the alloy chlorination is suggested:

$$(CuZn)_{\beta}(s) + ZnO(s) + Cl_2(g) \rightarrow Zn_2OCl_2(s,l) + (CuZn)_{\alpha}(s) + Cu(s) \quad (1)$$

$$Zn_2OCl_2(s,l) + Cl_2(g) \rightarrow 2\ ZnCl_2(s,l) + ½\ O_2(g) \quad (2)$$

$$(CuZn)_{\beta,\alpha}(s) + Cl_2(g) \rightarrow ZnCl_2(s,l) + CuCl(s,l) \quad (3)$$

$$(CuZn)_{\beta,\alpha}(s) + CuCl(s,l) \rightarrow ZnCl_2(s,l) + Cu(s) + (CuZn)_{\alpha}(s) \quad (4)$$

$$Cu(s) + Cl_2(g) \rightarrow CuCl_x(s,l)\ x=1,2 \quad (5)$$

$(CuZn)_{\alpha}(s)$ and $(CuZn)_{\beta}(s)$ correspond to alpha and beta phases of the CuZn alloy. The range of composition of these phases is Cu–(0 to 39)Zn (wt%) and Cu–(36.7 to 59.8)Zn (wt%), respectively [267].

The chlorination reaction starts at 250ºC with formation of zinc oxychloride from the thin layer of zinc oxide that covers the alloy surface and zinc from the alloy. The occurrence of α-CuZn and metallic copper can be due to zinc preferential elimination from the alloy. However, metallic copper can also arise from the reaction of CuCl formed initially according to:

$$(CuZn)_{\beta}(s) + ZnO(s) + Cl_2(g) \rightarrow Zn_2OCl_2(s,l) + (CuZn)_{\alpha}(s) + CuCl(s) \quad (6)$$

$$(CuZn)_{\beta,\alpha}(s) + ZnO(s) + CuCl(s) \rightarrow Zn_2OCl_2(s,l) + Cu(s) \quad (7)$$

All three species on the right hand side of equation (1) were detected by XRD in the chlorinated sample at 250ºC. CuCl as an intermediate species according to equations 6 and 7 has not been detected up to now. At 250ºC, the scale of oxychloride stops the reaction. At higher temperatures, due to the high reactivity of copper [254], large amounts of CuCl are quickly generated, which in turn reacts with zinc from the alloy inhibiting the protective effect of zinc oxychloride. Moreover, at high temperatures, the chlorination of Zn_2OCl_2 is kinetically feasible. Both events inhibit the protective effect of the zinc oxychloride layer.

V.6.4. Conclusions

- There are differences in the alloy and pure metal reactivity towards chlorine. Interactions were detected corresponding to oxidation–reduction reactions between copper chlorides and metallic zinc from the alloy. Volatilization of $ZnCl_2$ is diminished during alloy chlorination compared with chlorination of pure zinc.
- Formation of well developed copper crystals was observed.
- At low temperatures, the formation of a Zn_2OCl_2 layer inhibits the alloy chlorination reaction.
- A global mechanism was presented according to the different processes considered: reaction inhibition, interactions between chlorides and copper crystallization.

V.7. EXPERIMENTAL AND THEORETICAL ANALYSIS OF THE IRON–CHLORINE CYCLE

The iron–chlorine (Fe–Cl) family of thermochemical cycles was first proposed in the early of 1970 at the technical university (RWTH) Aachen in Germany. The Fe–Cl cycles consist of at least four different chemical reaction steps and employ auxiliary compounds selected from the group consisting of iron oxides, iron chlorides, chlorine, and hydrogen chloride [274–282].

V.7.1. Theoretical analysis

The following reactions are proposed for the iron–chlorine cycle, and the thermodynamic properties are presented in tables after each reaction:

(1) $FeCl_2(s) + 3\ H_2O(g) \rightarrow Fe_2O_3(s) + 4\ HCl(g) + H_2(g)$

T (ºC)	ΔH (kJ)	ΔG (kJ)	K
550	220.91	80.31	8.007×10^{-6}
650	223.75	63.07	2.697×10^{-4}
750	137.72	52.21	2.160×10^{-3}

(2) $HCl(g) \rightarrow H_2(g) + Cl_2(g)$

T (ºC)	ΔH (kJ)	ΔG (kJ)	K
550	187.77	199.32	2.242×10^{-13}
650	188.31	200.69	4.399×10^{-12}
750	188.78	202.01	4.854×10^{-11}

(3) $Fe_2O_3(s) + 3\ Cl_2(g) \rightarrow 2\ FeCl_3(g) + 3/2\ O_2(g)$

T (ºC)	ΔH (kJ)	ΔG (kJ)	K
550	298.11	127.99	7.542×10^{-9}
650	291.89	107.67	8.074×10^{-7}
750	286.45	88.04	3.198×10^{-5}

(4) $2\ FeCl_3(g) \rightarrow 2\ FeCl_2(g) + Cl_2(g)$

T (ºC)	ΔH (kJ)	ΔG (kJ)	K
550	226.26	112.58	7.171×10^{-8}
650	226.31	98.76	2.577×10^{-6}
750	226.35	84.95	4.602×10^{-5}

Thermodynamic calculations predict the formation of hematite during hydrolysis of $FeCl_2$ (instead of magnetite) and a low production of H_2, due to an oxidative atmosphere. A feasible way to enhance the H_2 production could be by removing the O_2 from the reaction site, for example with the presence of an O_2 scavenger like metallic Ti (Le Chatellier principle).

V.7.2. Experimental procedure

V.7.2.1. Materials

The solid reactants were $FeCl_2 \cdot 4H_2O$ powder provided by Fluka and the titanium sheet by Alfa Aesar Company. Typical sample sizes for the reaction were 150 mg and 80 mg, resp.

V.7.2.2. Procedure

The reactions for the study of thermochemical cycles were performed in a quartz reactor in vacuum conditions (Fig. V.18). The reactor was purged with a vacuum pump for two hours where the reagent loses two water molecules, with $FeCl_2 \cdot 2H_2O$ remaining in the reactor. Afterwards the reactor was heated until it reached the corresponding temperature of the experiment. The reactions were carried out at 650ºC at different times (see Table V.7). Then the gaseous products were condensed with liquid nitrogen, and hydrogen was analyzed by gas chromatography. The solid products were characterized by XRD and SEM.

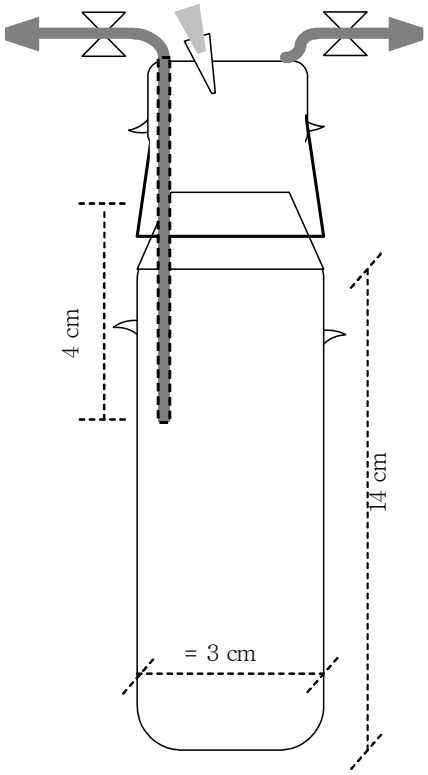

FIG. V.18. Schematic view of the thermo-cycle reactor used in the present study.

TABLE V.7. SUMMARY OF THE DIFFERENT EXPERIMENTAL CONDITIONS IN EACH EXPERIMENT

Experiment	$FeCl_2 \cdot 4H_2O$	$CuCl_2$	Ti	H_2O (20 µl)	Time (h)
1	×				48
2	×		×		5
3			×	×	24
4		×		×	24
5	×	×	×		24

V.7.3. Results and discussion

V.7.3.1. Analysis of samples by gas chromatography

SRI 8610C gas chromatograph (GC) was used for determining the contents of hydrogen in the reactor. It was equipped with Alltech® CTR 'concentric packed columns' which is essentially a column within a column. This permits to use two different packings for the analysis of the sample. The outer column is 1.83 m × 6.4 mm (6 ft × 1/4") packed with activated molecular sieve, and the inner column is 1.83 m × 3.2 mm (6 ft × 1/8") packed with porous polymer mixture. A thermal conductivity detection (TCD) system was employed. The pressure was equal to 83 kPa (12 psi) and the furnace temperature was 42ºC. The carrier gas (Argon) flow rate was 30 mL/min. The temperature of the TCD was 120ºC and the current was 125 mA.

The sample was taken from the reactor through a septum and introduced into the chromatograph by a 100 µl gas tight syringe (Alltech).

V.7.3.2. Solid products and residues

After the reaction at 650ºC, solid residues were found in the reactor.

(a) Experiment 1

This experiment was performed only with $FeCl_2 \cdot 4H_2O$ (Table V.7). After 48 hours of reaction at 650ºC, an important amount of white crystals were formed in the bottom of the reactor. XRD analysis revealed that they constituted of only one phase, hematite (Fe_2O_3). The formation of hematite during hydrolysis of $FeCl_2$ (instead of magnetite) and a low production of hydrogen may be due to the presence of an oxidative atmosphere. The yellowish gel on the reactor wall may be due to the formation of $FeCl_3 \cdot 7H_2O$. It is an amorphous phase that cannot be identified by means of XRD. Besides, it could be seen that the reaction was incomplete due to presence of water in the top of the reactor (Fig. V.19).

The gas chromatography (GC) analysis denotes that the hydrogen generation under this experimental conditions was very small, as can be seen in Fig. V.20.

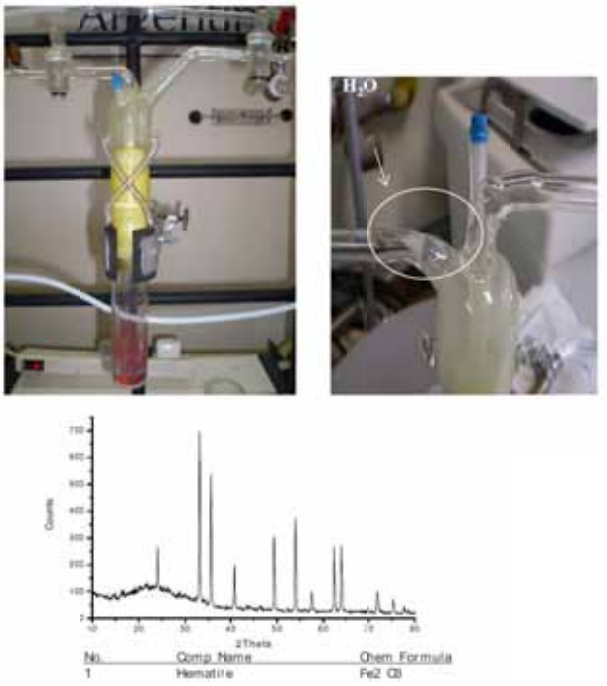

FIG. V.19. Experiment 1: (A) Photograph of the reactor after 48hs at 650°C, (B) XRD diffractogram of the solid residues at the botton of the reactor.

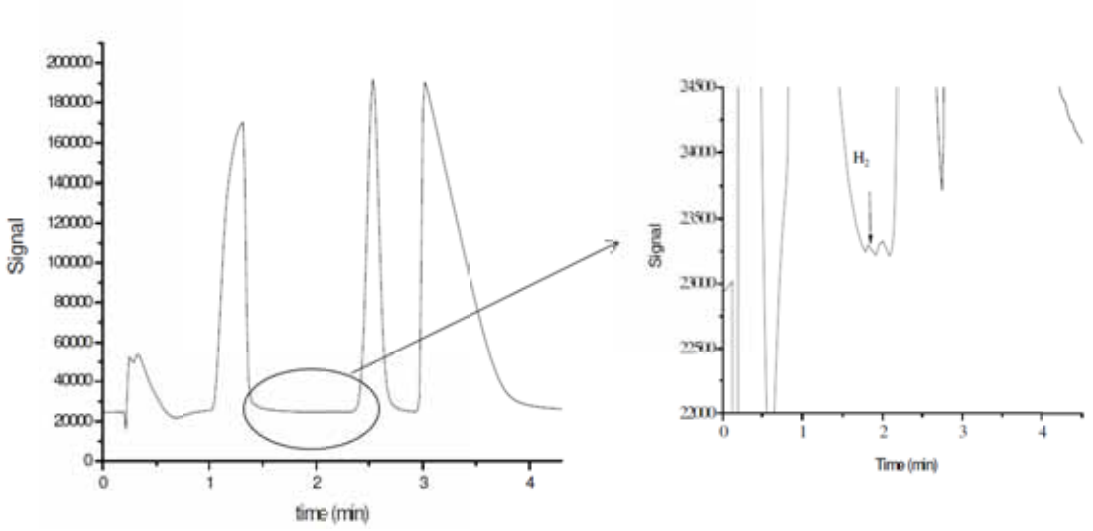

FIG. V.20. Experiment 1: (A) Completed gas chromatography curve; (B) Detail of the GC curve at the hydrogen time of retention.

(b) Experiment 2

In this experiment, a metallic titanium sheet was added to a reactor containing $FeCl_2 \cdot 4H_2O$. After the reaction at 650°C during 5 hours, a ring of condensed crystals was observed, located at a zone of lower temperature than the plateau of the reactor. These white crystals found around the reactor are exhibited in Fig. V.21. Their morphology is similar to the characteristic shape of anhydrous $FeCl_2$.

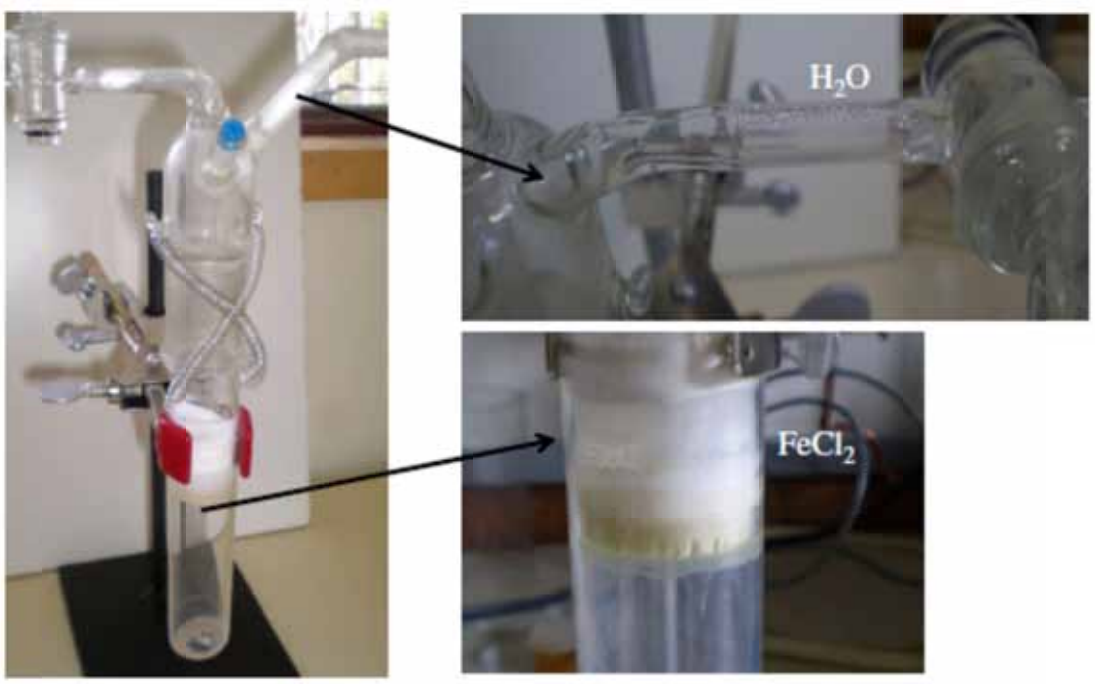

FIG. V.21(A). Experiment 2: Photographs of the reactor with a ring of white crystals condensed on the upper zone.

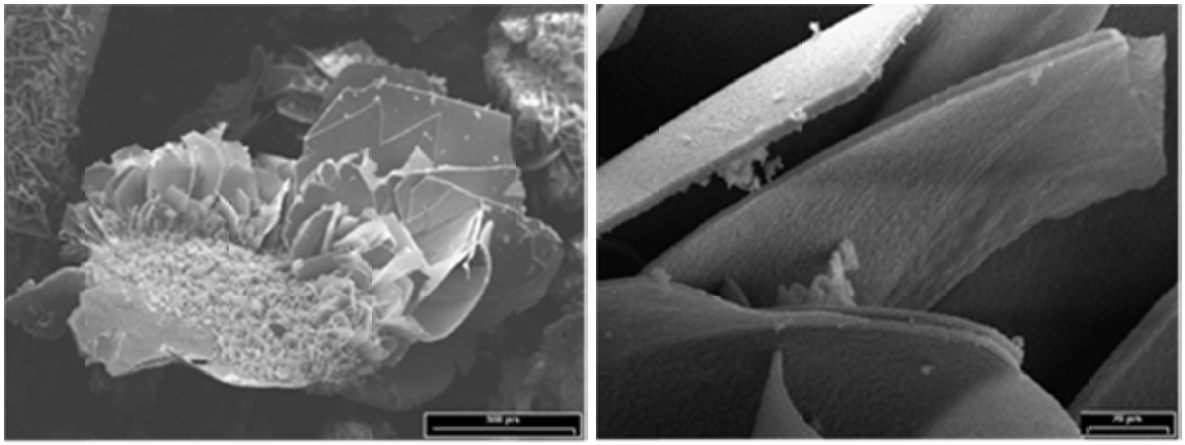

FIG. V.21(B). Experiment 2: Morphology of the white crystals obtained by SEM.

The analysis of XRD obtained from the titanium sheet after reaction shows the presence of unreacted titanium and titanium oxides (Fig. V.22a). Meanwhile the black powder found in the bottom of the reactor revealed that it constituted of a mixture of ferrite (Fe), titanium (Ti), pseudo-rutile ($Fe_2Ti_3O_9$), rutile (TiO_2), titanium oxide (Ti_2O) and magnetite (Fe_3O_4) (Fig. V.22b).

In Figures V.22c and d, the morphology of the titanium sheet after the reaction and the oxide formation upon it, is presented, indicating that the metal has performed as a good oxygen scavenger.

The GC analysis of the gaseous phase after reaction denotes that the increment in the hydrogen production. It could be due to the capability of titanium for removing the O_2 from the reaction site (Fig. V.23a).

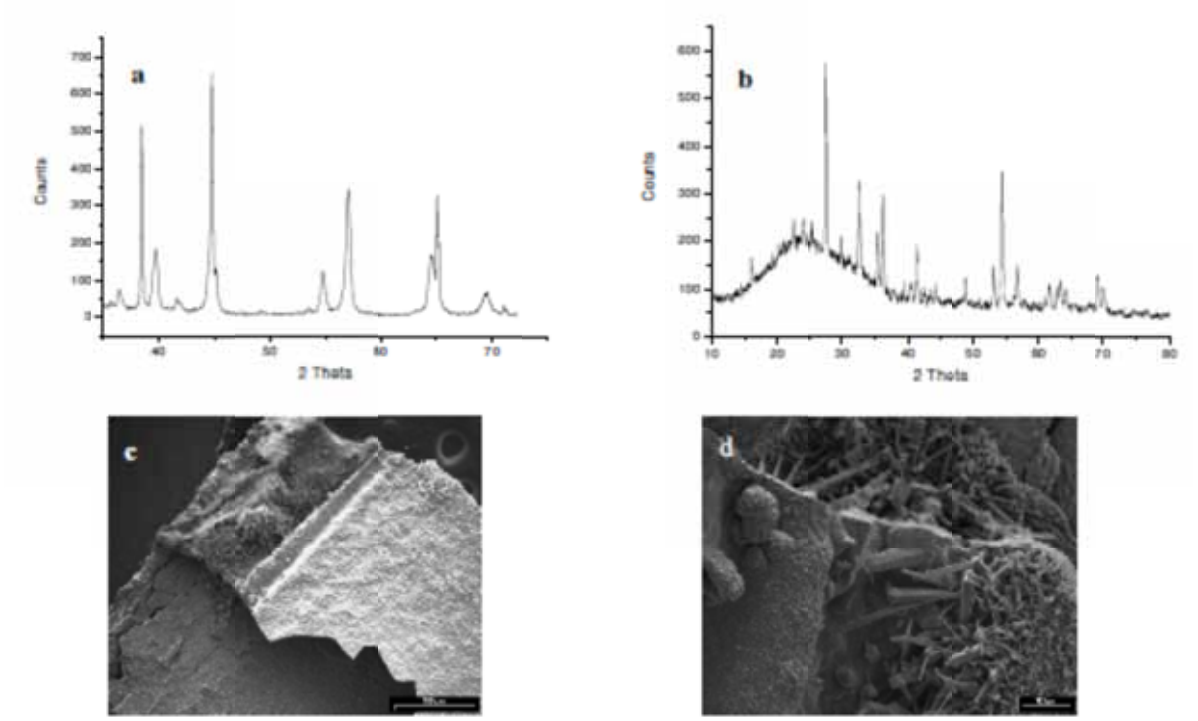

FIG. V.22. Experiment 2: (a) XRD of the titanium sheet after reaction, (b) XRD of the powder at the bottom of the reactor after reaction, (c) SEM image of the reacted surface of titanium sheet, (d) SEM image of the oxide formed on the titanium surface.

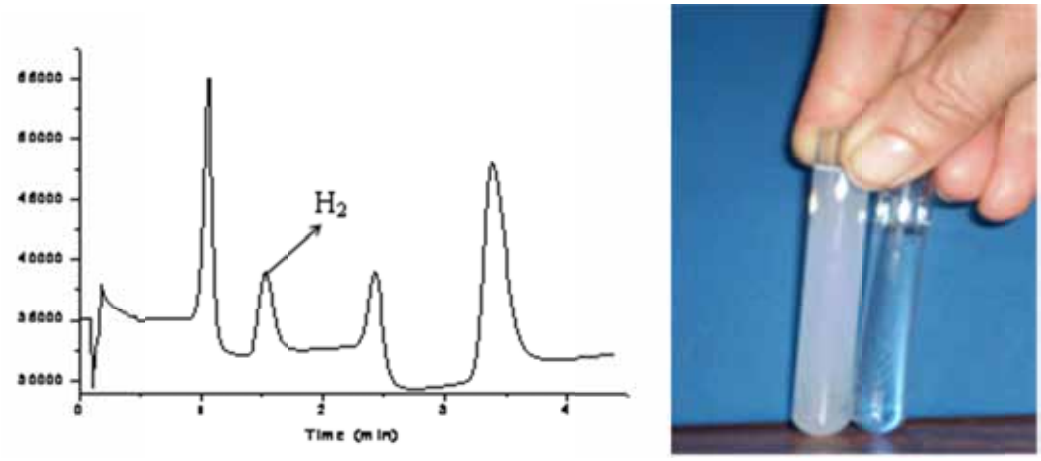

FIG. V.23. Experiment 2: (left) gas chromatography curve; (right) positive analysis for the presence of HCl.

Also the presence of HCl and Cl_2 was checked by bubbling, at room temperature, the residual gases of the reaction in a saturated solution of $AgNO_3$, where the formation of a white precipitate (AgCl) was observed (Fig. V.23, right).

(c) Experiment 3

The XRD and GC results obtained after the interaction of the titanium sheet with water during 24 hours at 950 ^oC showed the presence of rutile (TiO_2) and any hydrogen was detected in the gaseous phase. These results have demonstrated that the water oxidized the metal but did not generate hydrogen (Fig. V.24).

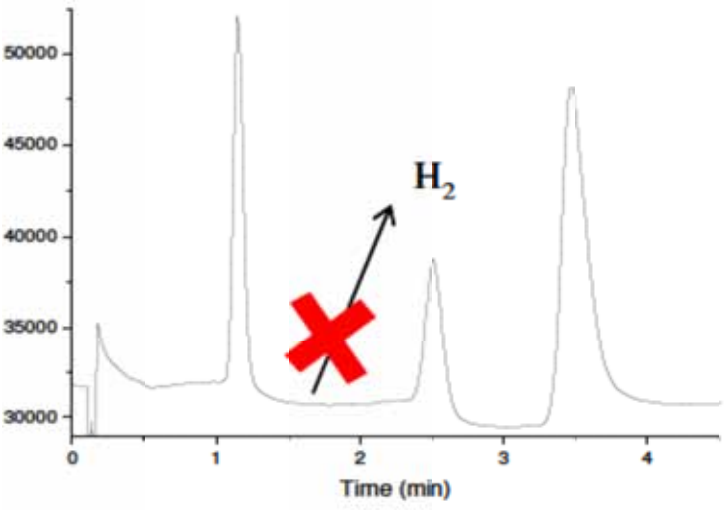

FIG. V.24. Experiment 3: XRD diffractogram of the titanium sheet after interaction with water.

(d) Experiment 4

In this experiment, it was necessary to add 20 µl of water because the $CuCl_2$ employed was dehydrated. After reaction with the GC analysis, it was able to observe the absence of the hydrogen peak although after 24 hours of reaction at 650^oC and in the presence of titanium. Also presence of water could be seen in the wall of the reactor (Fig. V.25).

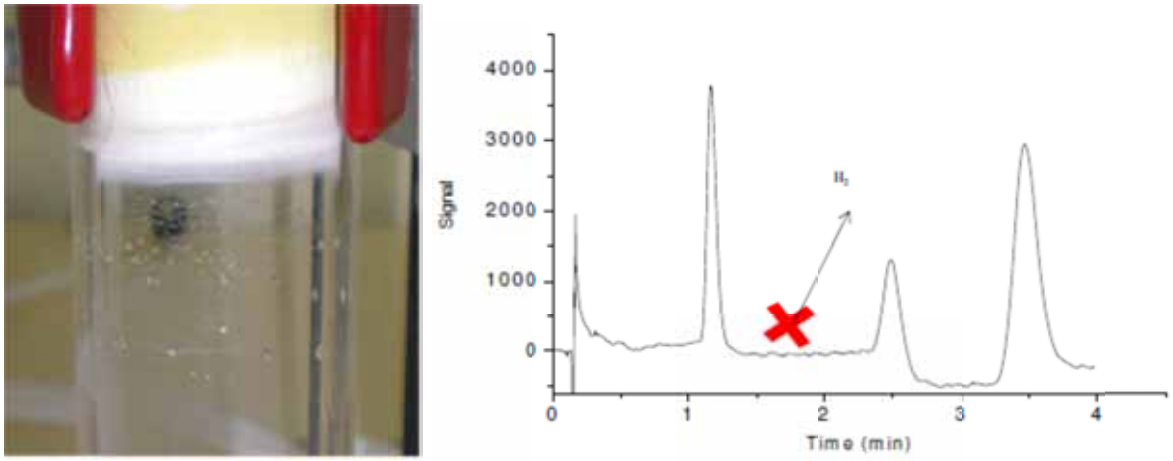

FIG. V.25. (A) photograph of the state of the reactor after 24 h at 650°C, (B) GC curve indicating the absence of hydrogen.

(e) Experiment 5

A mixture of $FeCl_2 \cdot 4H_2O$ and $CuCl_2$ in the presence of titanium was introduced in the reactor. After 24 hs at 650°C according to GC results (Fig. V.26), the increment of the hydrogen production could be observed. This behavior can be attributed to an interaction between $FeCl_2$ and $CuCl_2$. This behavior will be more deeply analyzed in further studies.

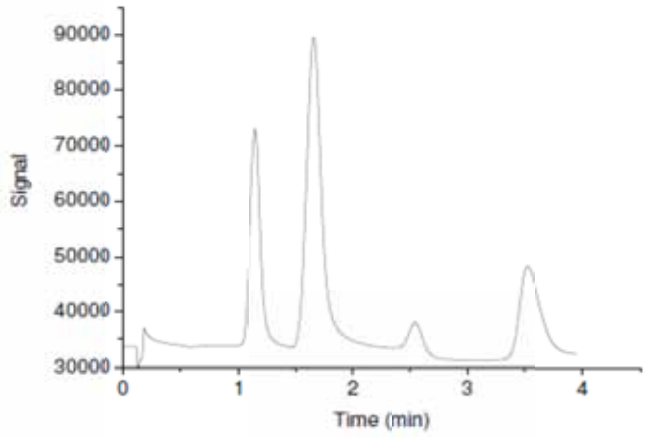

FIG. V.26. GC curve after reaction during 24 h at 650° C in the presence of titanium and a mixture of hydrated iron and copper chlorides.

V.7.4. Reaction mechanisms with metallic titanium

From previous results, it is evident that the presence of an oxygen scavenger drifts the reaction towards the formation of hydrogen. The following global mechanism for interpreting these experimental results was proposed:

(1) $3\ FeCl_2(s) + 4\ H_2O(g) \rightarrow Fe_3O_4(s) + 6\ HCl(g) + H_2(g)$

(2) $2\ HCl(g) \rightarrow H_2(g) + Cl_2(g)$

(3) $Fe_3O_4(s) + 4\ Cl_2(g) \rightarrow 2\ FeCl_3(g) + FeCl_2(g) + 2\ O_2(g)$

(4) $Ti(s) + 2\ Cl_2(g) \rightarrow TiCl_4(g)$

(5) $FeCl_3(g) \rightarrow FeCl_2(g) + ½\ Cl_2(g)$

(6) $TiCl_4(g) + FeCl_2(g) + 3/2\ O_2(g) \rightarrow TiFeO_3(s) + 3\ Cl_2(g)$

(7) $TiCl_4(g) + 3/2\ O_2(g) \rightarrow TiO_2(s) + 3\ Cl_2(g)$

In future experiments, the removal of oxygen and hydrogen using a diffusion ceramic membrane as a separation system will be improved in order to enhance the formation of hydrogen. But with the purpose of accelerating the reaction rates some catalysts must be incorporated and the temperature in the reaction zone could be increased.

APPENDIX VI. RECOMMENDATIONS CONCERNING REQUIREMENTS FOR COMPONENTS AND EQUIPMENT

VI.1. ANALYSIS OF LAYOUT AND DESIGN SOLUTIONS OF HIGH TEMPERATURE HEAT EXCHANGERS

HTGR plants use an intermediate helium circuit intended to transfer high grade heat from the reactor to the industrial application. The intermediate circuit prevents leakage of fission products into the industrial application circuit and contamination of the primary circuit with the industrial application products. It also improves plant safety and ensures flexibility in terms of application of different technologies. Direct transfer of heat to the process medium in high temperature heat exchangers is also applied. In both cases, the problem lies in the development of reliable high temperature intermediate heat exchangers for heat transfer from the primary to the intermediate circuit [283]. The problem is related to the fact that thermal stability of the HTGR graphite core is higher than the thermal stability of IHX structural materials. Fuel operating temperatures amount to 1200°C and can reach 1600°C for a short time in accidents. Heat exchange tubing temperatures in normal operating conditions can reach 950°C and higher. At such temperatures, the long term strength of the tubing materials, even if they are made of high nickel alloys, becomes very low (~10 MPa). The most typical IHXs developed in the Russian Federation, Japan, USA, Germany, and France are further analyzed in the report.

Main thermal engineering and geometric parameters of IHXs applied in different reactor plant designs are presented in Table VI.1.

VI.1.1. IHX design of the Russian Federation

The VG-400 and VGM reactor plants use an intermediate helium circuit where the pressure is higher than in the primary circuit. Two IHX designs were developed and tested. The first design is based on straight-tube shroudless cassettes, the second features cassettes with helical tubes [284]. Main characteristics and structural layouts of the two IHX designs are provided in Table VI.1 and Fig. VI.1.

The straight-tube IHX has an equilateral triangle arrangement of cassettes inside a profiled shroud, and an equilateral triangle arrangement of tubes in the cassettes in two rows around the central tube. All cassettes are arranged at two levels along the height in order to reduce pressure losses at the heat exchange surface inlet and outlet and to improve helium flow formation at the shell side inlet. In the IHX design with helical-tube cassettes, the heat exchange surface consists of 19 cassettes arranged in triangle inside a hexahedral shroud. Tubes are wound around the central load-bearing tube and form four multiple-turn coils with the diameter from 232 to 406 mm.

The IHX in the MHR-T plant is used to transfer heat at temperatures of up to 1000°C to the hydrogen production application and is separated into two heat exchangers due to limitations on the heat exchanger casing size. The heat exchanger is vertically arranged, pressurized, modular (with the possibility of plugging separate modules), see Fig. VI.2.

TABLE VI.1. MAIN CHARACTERISTICS OF IHXs USED IN REACTOR PLANTS IN THE RUSSIAN FEDERATION, JAPAN, GERMANY, USA, AND FRANCE

Parameter	Country, project designer, reactor plant						
	Russian Federation, OKBM				USA		
	VG-400	VG-400 VGM	MHR-T	GT-MHR	MHTGR-GT, (ind. cycle) GA	MGR-GTI, MIT	NGNP, GA
Power (MW)	110.5	76.9	105.5	302.5	454	355	65
Mean LTD (°C)	154	171	136	34.5	67.2	40	25
Primary circuit							
Coolant	Helium	Helium	Helium	Helium	Helium	Helium	Helium
Flow rate (kg/s)	85	59.1	135.5	159.3	239	149.2	34.7
Inlet/outlet temperature (°C)	950/700	950/700	1000/850	849/484	850/485	850/398.4	950/590
Inlet pressure (MPa)	4.9	5.0	6.42	7	7.0	7.0	6.23
Pressure loss (kPa)	23	12.8	33.4	16.2	40	180	31.2
Secondary circuit							
Coolant	Helium	Helium	Helium	Helium	Helium	Helium	Helium
Flow rate (kg/s)	38.6	24.2	38.65	171.4	250	149.2	34.7
Inlet/outlet temperature (°C)	350/900	290/900	450/975	460.8/800	425/775	358.4/810	565/925
Inlet pressure (MPa)	5.4	5.2	6.92	7.46	7.46	7.23	6.23
Pressure loss (kPa)	46	18.6	45	210	210	100	30.3

TABLE VI.1. MAIN CHARACTERISTICS OF IHXs USED IN REACTOR PLANTS IN THE RUSSIAN FEDERATION, JAPAN, GERMANY, USA, AND FRANCE (cont.)

Parameter	Country, project designer, reactor plant						
	Russian Federation, OKBM				USA		
	VG-400	VG-400 VGM	MHR-T	GT-MHR	MHTGR-GT, (ind. Cycle) GA	MGR-GTI, MIT	NGNP, GA
Geometrical characteristics							
Type of heat exchanger and tubes	Modular, straight-tube	Modular, helical	Modular	Coiled, helical	Coiled, helical	Coiled, helical	Heatric
Size of tubes (channels) OD×δ (mm) R×δ of bridge (mm) length (m)	 14 × 2 — 5.38	 21 × 2.5 — 10.9	 4	 30 × 4 — 49	 44.45 × 5.16 — 48.4	 25.4 × 2.5 — 35	 — 1.5 × 0.9 1.82
Number of tubes	163 × 42	19 × 132	252 × 121	2300	1120	3400	—
Tube material	CrNi55Mo WZr	CrNi55Mo WZr	SiC-based ceramics	CrNi55Mo WZr	Inconel 617	Inconel 617	Inconel 617
Bundle OD/ID (width/depth) (m)	—	0.435/0.20	3.35	4.88/1.544	4.896/1.892	3.56/0.96	—
Bundle height (m)	—	10.1	2	10.0	11	12.1	—
Casing OD (m)	—	2.3	5.7	~6	5.864	4.42	—

LTD log. Temperature difference.
OD outer diameter.
ID inner diameter.
δ wall thickness.
— data not available.

TABLE VI.1. MAIN CHARACTERISTICS OF IHXs USED IN REACTOR PLANTS IN THE RUSSIAN FEDERATION, JAPAN, GERMANY, USA, AND FRANCE (cont.)

Parameter	Country, project designer, reactor plant						
	Japan, JAEA		Germany				France AREVA
	HTTR	GTHTR300C	KVK Steinmüller	KVK Balcke–Dürr	HTR-Modul	HTR-Modul	ANTARES
Power (MW)	10	168	10	10.1	171.7	171.7	608
Mean LTD (°C)	113	154	61	64	69	69	50
Primary circuit							
Coolant	Helium	Helium	Helium	Helium	Helium	Helium	Helium
Flow rate (kg/s)	3.4	323.8	2.95	3.0	50.3	50.3	240
Inlet/outlet temperature (°C)	950/389	950/850	950/293	950/300	950/292	950/292	850/350
Inlet pressure (MPa)	4.06	5.02	3.99	3.99	3.99	4.38	5.5
Pressure loss (kPa)	9.2	—	55	50	20	190	< 100
Secondary circuit							
Coolant	Helium	Helium	Helium	Helium	Helium	Helium	Helium–nitrogen
Flow rate (kg/s)	3.0	81	2.85	2.9	47.3	—	614
Inlet/outlet temperature (°C)	237/869	500/900	220/900	220/900	200/900	200/900	300/800
Inlet pressure (MPa)	4.21	5.15	4.19	4.35	4.05	4.35	~5.5
Pressure loss (kPa)	50.2	—	165	100	60	160	< 200

— data not available.

TABLE VI.1. MAIN CHARACTERISTICS OF IHXs USED IN REACTOR PLANTS IN THE RUSSIAN FEDERATION, JAPAN, GERMANY, USA, AND FRANCE (cont.)

Parameter	Country, project designer, reactor plant						
	Japan, JAEA		Germany				France AREVA
	HTTR	GTHTR300C	KVK Steinmüller	KVK Balcke–Dürr	HTR-Modul	HTR-Modul	ANTARES
Geometrical characteristics							
Type of heat exchanger and tubes	Coiled, helical	Coiled, helical	U-shaped	Coiled, helical	U-shaped	Coiled, helical	Coiled, helical (backup sol.)
Size of tubes (channels) OD×δ (mm) R×δ of bridge (mm) length (m)	 31.8 × 3.5 — 21.5 × 22.9	 45 × 5 — 14	 22 × 2 — —	 20 × 2 — —	 22 × 2 — —	 20 × 2 — —	 — 0.3 × 0.7 —
Number of tubes	96	724	117	180	1612	2470	—
Tube material	HastelloyXR	HastelloyXR	Nicrofer 5520	Nicrofer 5520	Inconel 617	Inconel 617	Alloy 230, Alloy 617
Bundle OD/ID (width/depth) (m)	1.3/—	5.2/—	1.5/0.762	2.0/—	2.78/—	1.512/—	—
Bundle height (m)	4.87	2.6	—	—	—	—	1
Casing OD (m)	2	—	2.40	—	—	—	5.7

— data not available.

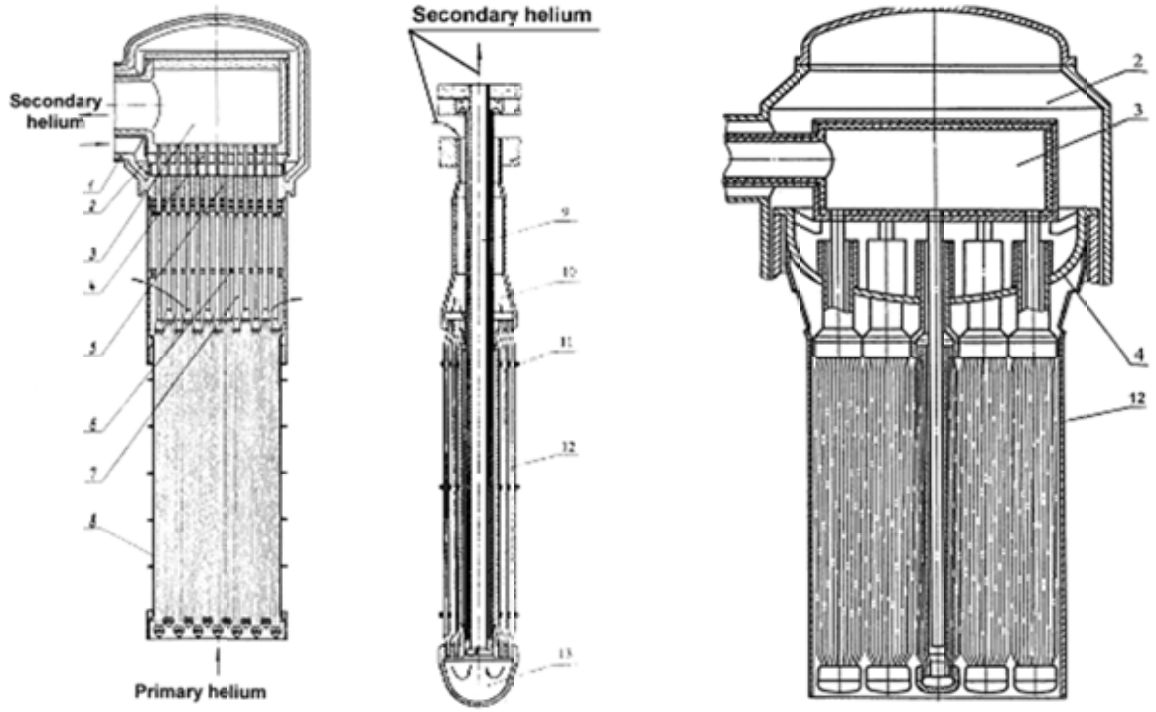

(a) (b) (c)

1: thermal insulation; 2, 3: secondary coolant inlet and outlet chambers;4, 5: top and bottom tube plates; 6: screen; 7: cassette; 8: profiled shell of the tube bundle; 9: central tube; 10, 13: secondary coolant headers; 11: spacer grid; 12: heat exchange tubes.

FIG. VI.1. Structural diagram of the straight-tube IHX design for the VG-400 (a) VGM power plants; (b) straight-tube cassette; (c) helical-tube IHX.

One IHX contains 121 modules. In order to reduce wall temperatures, the inner surface of the casing is fitted with thermal insulation and the outer surface is air cooled. In the cover, heat exchange modules are arranged in triangle at a pitch of 275 mm. Prospective materials for the IHX removable internals are the steels 12Cr18Ni10Ti, 08Cr18Ni9, 08Cr16Ni11Mo3, and high nickel alloy CrNi55MoWZr.

The module heat exchange surface is made of a heat-resistant ceramic compound. The heat exchanger consists of separate ceramic blocks with channels for the primary and secondary helium. The blocks are connected to one another end to end with special diffusion brazing. The primary helium flows in 30 slot gaps between the cylindrical holes where the heated secondary helium flows.

The IHX for the GT-MHR plant, which uses indirect (in the intermediate circuit) gas turbine cycle, was developed based on the IHX design with helical tubes wound in one coil (Fig. VI.3).

The IHX is inserted into the heat transfer unit casing where the primary circuit helium blower is located. Internal metal structures shape the circulation path between the IHX and the gas blower. This IHX design is more compact than the modular one. However, with the IHX power equal to the GT-MHR power, the IHX tube bundle does not fit into a casing of acceptable size and weight; that is why the IHX is divided into two parts. Besides, in the helical-tube IHX hydraulic resistance in the secondary circuit (on the tube side) is 3–5 times higher than in the primary circuit (on the shell side).

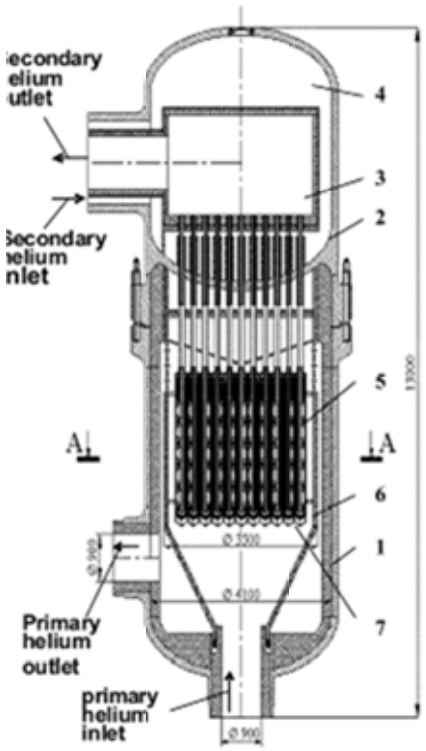

1: casing, 2: casing cover; 3: casing thermal insulation; 4: IHX casing internal metal structures; 5: removable internals; 6: “hot” header; 7: IHX “cold” header, 8: heat exchange module, 9: caisson pipe, 10: IHX removable internals shell, 11: tube sheet.

FIG. VI.2. General view of the MHR-T IHX.

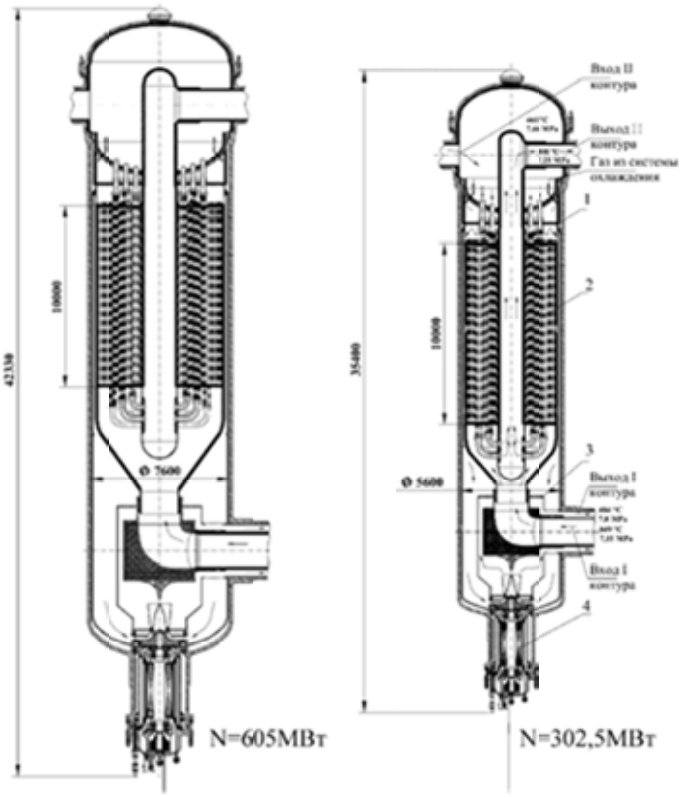

1: casing; 2: tube bundle of helical tubes; 3: internal metal structures; 4: gas blower.

FIG. VI.3. Variants of heat transfer unit designs based on the helical-tube IHX of different power for the GT-MHR with the indirect cycle.

VI.1.2. IHX design of Japan

Figure VI.4 shows the structural diagram of the Japanese IHX used in the experimental nuclear power plant with the HTTR reactor, where the entire tube system is replaced after expiration of its lifetime [285, 286]. The tube bundle of helical tubes is wound into one coil. Acceptable hydraulic resistance is ensured owing to the increased pitch of tubes arrangement in the bundle. Tubes and tube bundles which are subjected to high temperatures are made of Hastelloy-XR alloy (Russian analog is alloy CrNi55MoWZr). The IHX casing is cooled by the primary helium exiting from the gas blower at a temperature of 389°C.

The gas blower is located in a separate casing and is connected to the IHX by pipes. It was probably done so because the gas blower and the IHX were designed and manufactured by different companies, and this solution helped to join them in a simple way. At present, this heat exchanger operates in the experimental plant under inlet helium temperatures reaching 950°C. One of the most important tasks is to study and improve heat transfer efficiency.

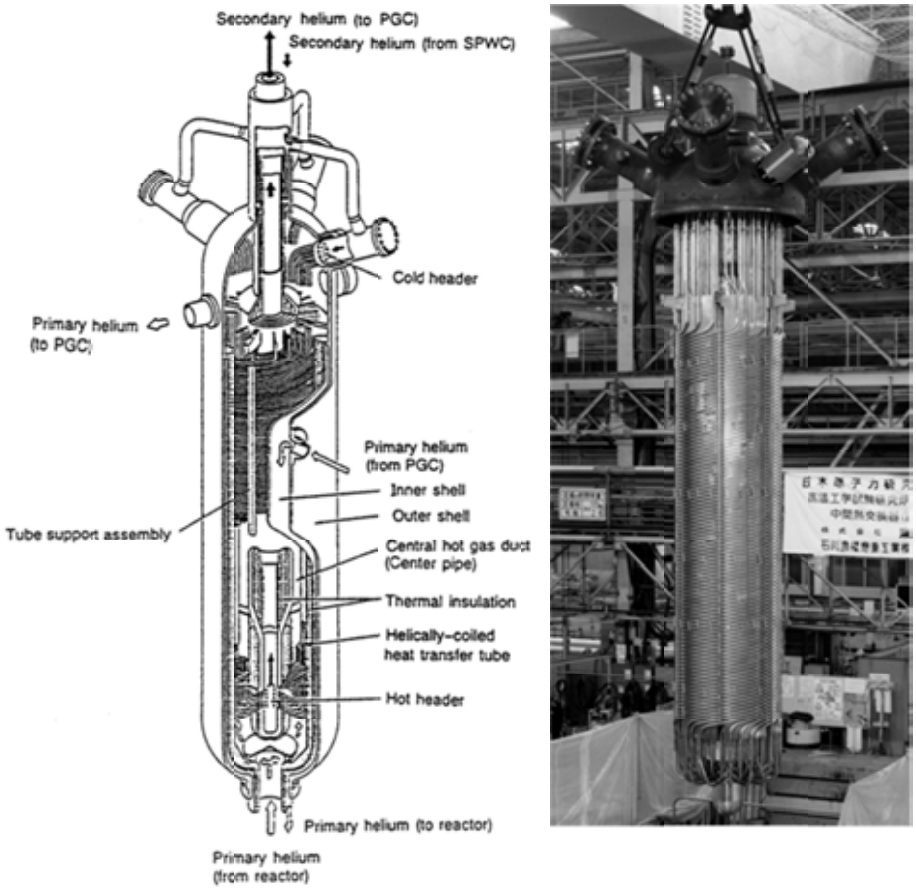

FIG. VI.4. IHX structural diagram and a manufactured HTTR IHX.

Based on the experience with HTTR IHX testing and operation, a heat exchanger design for the combined GTHTR300C plant was developed (Fig. VI.5). Unlike the HTTR IHX, this design has larger-diameter tubes, which reduces the total number of tubes and increases the tube bundle height. And vice versa, the use of small-diameter tubes increases the total number of tubes, decreases the tube bundle height, and intensifies creep deformation and damage of the pipe section connecting the coil part to the hot header.

In this design, the tube diameter is selected such as to ensure acceptable overall size of the tube bundle and structural integrity of the connecting pipe section. The tube bundle diameter was selected such as to ensure an about 5 kPa pressure loss in the primary and secondary circuits. In addition, helium flow velocity in the central tube, which influences the selection of tube bundle diameter, has been accepted equal to ~30 m/s in order to prevent flow induced vibrations.

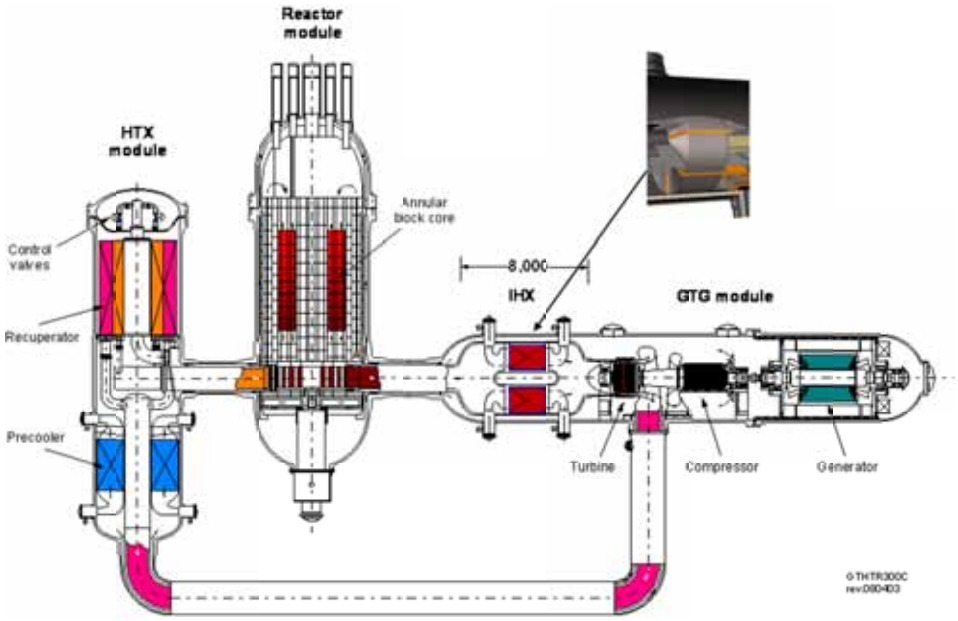

FIG. VI.5. IHX of the combined GTHTR300C plant.

VI.1.3. IHX design of the USA

In the USA, further evolutions of the IHX design can be observed in the developments of General Atomics (GA) for the MHTGR-GT and H2-MHR plants [52], and Massachusetts institute of technology for the MGR-GTI plant [287]. The IHXs with the single helical-tube coil for the MHTGR-GT and MGR-GTI (Fig. VI.6a) with the indirect gas turbine cycle are similar to the GTHTR300C IHX design of Japan. The distinctive feature of the US design is that the heat exchanger is located in one casing with the primary circuit gas blower arranged in the lower part of the casing. Because of that, helium is supplied and removed via a side coaxial gas duct. The high cycle and low cycle fatigue of the tube metal is reduced owing to the possibility of axial and radial thermal expansion of the tube bundle and embedding of the tubes in radial plates, thus reducing helium flow induced vibrations of the tubes. The MHTGR-GT IHX has tubes of larger diameter as compared with the MGR-GTI IHX.

For the H2-MHR plant designed for the production of hydrogen, GA developed an IHX design option which is based on the application of the HEATRIC heat exchange surface technology [288]. The HEATRIC heat exchanger consists of metal plates with straight or zigzag channels etched or mechanically formed on one side of the plates (Fig. VI.6b).

In the cross section, the channels are semi-circles with a diameter of about 0.5 mm and more. Plate thickness can be from one to several millimeters. The plates are stacked into a single module in such a way that the coolant passage is formed by the smooth surface of one plate and the channeled surface of the adjacent one. Plates in the module are diffusion bonded under high pressure and high temperature which stimulates grain growth between the surfaces of the plates.

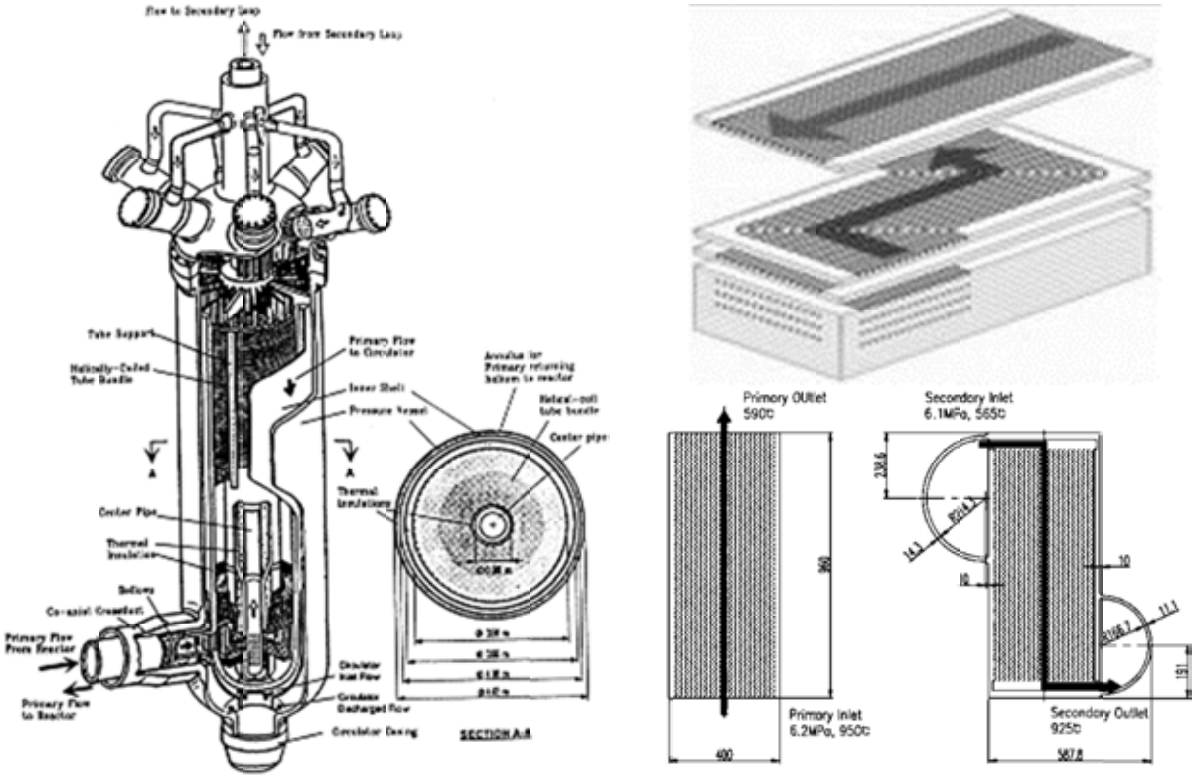

(a) (b)

FIG. VI.6. IHX heat transfer unit (a) with helical tubes for the MGR-GTI plant with the indirect cycle; (b) with Heatric technology for the H2-MHR plant.

VI.1.4. IHX design of Germany

During the development of high temperature heat transfer technologies for the HTR-Modul and nuclear process heat plants in Germany, two IHX components were tested under standard conditions at the 10 MW KVK helium test facility [22].

The IHXs differed from the standard IHX design in the number of tubes and diameter of tube bundles. The first model with a spiral-tube bundle was fabricated by Steinmüller company (Fig. VI.7a), and the second model with a U-tube bundle was fabricated by Balcke–Dürr company (Fig. VI.7b).

The maximum tube wall temperature amounted to 920°C at the maximum normal operation pressure difference of 0.2 MPa. In the depressurization mode, full pressure difference was observed for a short time. Both models operated for about 5000 hours without any problems.

Ultrasonic inspection of the tube material after 4700 hours of testing did not reveal any damages. Furthermore, there was no damage of hot headers after dynamic tests during 656 cycles of temperature change from 950 to 710°C at 40°C/min, and after static tests during 455 hours at a pressure drop of 4.3 MPa and temperature of 970°C.

Based on the performed tests, it was concluded that the two tested heat exchanger layout variants could be used for the 170 MW IHX in the HTR-Modul plant with the lifetime of 100 000 hours.

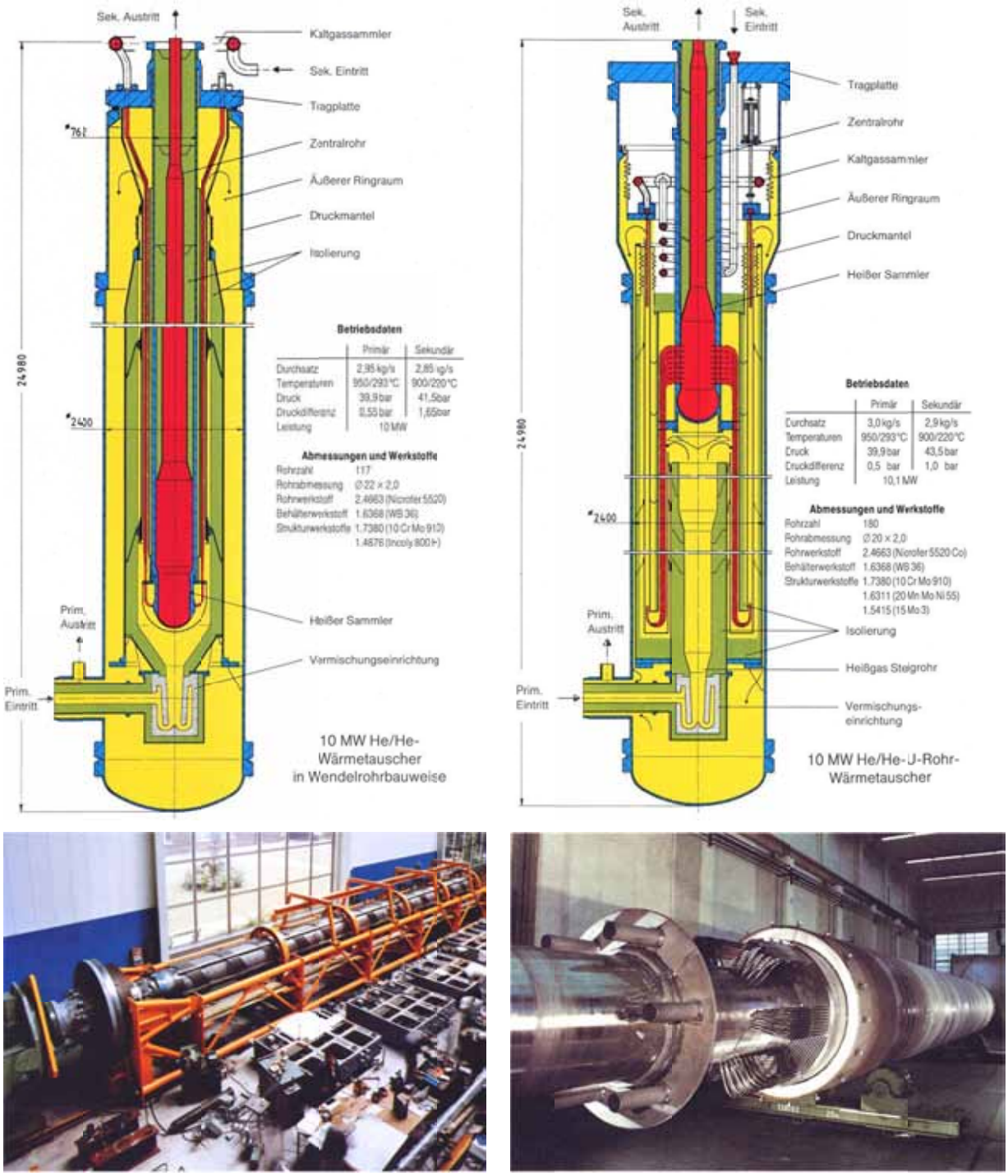

FIG. VI.7. Design and fabrication diagrams for IHX models for the KVK test facility (a) by Steinmüller; (b) by Balcke–Dürr.

All suggested and considered heat exchanger designs utilize countercurrent coolant flow. The secondary helium flows inside the tubes, and the primary helium flows between the tubes in the opposite direction. The secondary helium is supplied and removed from the top. From the upper headers with tube plates accessible for inspection and plugging, secondary helium flows down the tubes and gets heated. The hot helium then enters the bottom header, turns by 180° and is removed via the central tube.

Since all IHXs have short lifetime because of high operating temperatures, they are made repairable with a possibility of replacing the heat exchange surface. Owing to sectionalization of the heat exchange surface, it is made possible to find and isolate damages in the heat exchanger tubing when the reactor is shutdown.

VI.2. RECOMMENDATIONS CONCERNING DESIGN OPTIMIZATION

As a result of the performed analyses of existing IHX designs, main tendencies and directions of IHX development, a number of problems related to IHX designing were identified and recommendations for design optimization were formulated. Main difficulties in IHX development are first of all associated with the development (or selection) of structural materials operable at temperatures up to 1000°C and analysis of their properties.

Operation of AVR and THTR-300 high temperature reactors and tests at the KVK test facility demonstrated that the problem of structural materials compatible with helium at temperatures under 950°C can be solved [289, 290]. In HTGR nuclear power plant designs, this issue is solved by selecting high nickel steels and alloys (O5CrNi46MoWNb4, O3Cr21Ni32MoWNb, CrNi55MoWZr), which are characterized by high heat resistance at temperatures from 650 to 950°C, as the structural materials for heat exchange equipment. With the helium temperature increasing to 1000°C, the solution looks more problematic because of the need to ensure the maximum IHX lifetime of about 100 000 hours. In this case, the problem can be solved by using ceramic materials, e.g. materials based on SiC. There are additional problems caused by certain specific requirements to the IHX from the reactor: increased leak-tightness, accessibility for repairs, prevention of radioactive deposits, and reliability in all modes [291–293].

Another important problem is selection and validation of optimal and yet feasible IHX design and layout solutions. These problems stipulate solution of the following main tasks:

- ensure compensation of thermal deformations of tubes in the bundle and of the bundle relative to the casing;
- arrange load-bearing elements in areas with lower temperatures controlled by the inlet temperatures of heated helium;
- minimize hydraulic losses, especially on the heating coolant side;
- provide conditions for replacement of defective or spent structural elements;
- develop recommendations on the algorithms of nuclear power plant normal operation and accident modes from the viewpoint of ensuring heat exchanger operability;
- perform integrated investigations and model tests of main heat exchanger components.

The complex of investigations and tests, in particular, includes refinement of design, thermal hydraulic characteristics, and temperature conditions. Important tasks are the determination of tube bundle flow hydraulics, which is necessary to select design features and to reduce thermal irregularities, and calculation of heat transfer, temperature fields, pressure losses and non-steady-state operating modes.

The above mentioned tasks were investigated during calculations and experimental studies performed at high temperature helium test facilities in OKBM (Russian Federation). Similar experiments were actively performed in Japan and Germany.

The successful development of reliable and highly efficient IHXs largely depends on the correct selection of heat exchanger design layout, which determines the way of heat exchange

surface washing, heat exchange surface shape, arrangement of components, and coolant flow principles.

Analyses of different IHX designs, both existing and being developed, showed that in HTGR plants with inlet helium temperatures under 950°C, it is possible to apply metallic shell-and-tube vertical heat exchangers with top supply and removal of the heated coolant, constituted by helical tubes woven in a small or a single coil, with U-shaped/Field/straight tubes, with longitudinal or cross flow.

Heat exchangers with U-shaped heat exchange surfaces have self-compensation, but must include 'hot' load-bearing tube plates, which are thick-walled and therefore, manufactured or large-size forgings of heat resistant materials.

It is impossible to transport high grade heat from the reactor to the industrial application without insulating internal pipes to prevent heat recuperation. To eliminate heat recuperation, the internal pipes must be insulated with a manufacturable heat-resistant material with an effective heat conductivity coefficient in helium ≤ 0.2 W/(m·K). Recuperation problems must also be carefully addressed in high temperature heat exchangers with cold coolant supply and hot coolant removal via coaxial pipes. For example, methane conversion applications utilize intermediate heat exchangers based on field tubes with recuperation in the internal tubes, which has its advantages [294], namely recuperation decreases the temperature of outlet process gas from 800–850°C to 600°C and it allows simplification of secondary circuit valve designs and application of designs developed for power plant steam pipelines.

Sectionalization of the tubing system best meets the reliability and cost effectiveness requirements, improves design manufacturability and repairability, and decreases the size of IHX tube plates.

Analyses of different designs showed that the heat exchanger design which best meets these requirements is a vertical heat exchanger with self-compensation of axial and radial thermal deformations, with the heat exchange surface of helical tubes woven in a single coil.

Sectionalization of the heat exchange surface is ensured by grouping the tubes into separate headers with each tube being accessible. Hydraulic resistance on the tube side is 3 to 5 times higher than on the shell side, with equal helium flow rates on both sides. Therefore, the allowable resistance is ensured by selecting the internal diameter and number of tubes and, if possible, decreasing helium flow rate inside the tubes and simultaneously increasing helium heating. Such heat exchangers, similar to the developed and tested IHX for the HTTR plant (Japan), have found application in the majority of nuclear power plants in different countries. For the purpose of higher compactness and safety, such heat exchangers are arranged in one casing with the gas blower. From the viewpoint of safety, possible ruptures of pipelines connecting the IHX with the gas blower may be a concern. Among the advantages of the above described design is the application of proven manufacturing technologies for IHXs with the power up to 300 MW.

Current developments of more compact IHX designs with a power above 300 MW are based on the application of HEATRIC-type heat exchange surfaces. In such IHXs, which are designed to fit casings of reduced diameters, high hydraulic resistance in channels with small hydraulic diameters is avoided by organizing radial (relative to the vertical cylindrical casing) helium flow with vertical helium supply in one of the circuits. This flow pattern leads to a large temperature difference in the rigid heat exchange module matrix with restricted diameters and to possible irregularity of helium flow distribution in the circuit with vertical supply. These phenomena may contribute to an increase of stresses in the heat exchange module and a decrease of heat transfer efficiency.

In order to avoid these negative phenomena, the IHX design with compact heat exchange modules for the MHR-T plant suggests vertical helium flow in the circuits and arrangement of modules at two levels along the height. Cassette heat exchanger designs suggested for the VG-400 and VGM plants at the early stages of high grade heat transport technology development, when there was no operating experience or experimental data, were less compact but offered better possibilities of repairing, replacing, and testing the standard design.

As a result of analysis of design experience and operating heat exchangers [293, 295, 296], the following recommendations on optimization of IHX designs can be formulated:

1. IHX parameters at 100% power are determined by the process circuit and depend on the process parameters.
2. The design of IHX and its elements must have high technical and economic indicators and must ensure the assigned parameters in all reactor plant operating modes.
3. All IHX elements must have high reliability and meet all safety requirements.
4. The IHX design must have the required strength characteristics, including long term strength, and a lifetime up to 100 000 hours.
5. If inlet hot helium temperatures equal 950°C, the IHX heat exchange surface can be made of proven metallic nickel-based alloys; if inlet hot helium temperatures is 1000°C and higher, it is necessary to use ceramics, for example, SiC-based materials.
6. In order to reduce thermal stresses, IHX large load bearing elements must be shielded against the impact of high temperature gas flows.
7. The IHX design must be simple, compact, and easy to install and operate, with a possibility of detecting and eliminating damages. Analyses [285] showed that the optimal variant is the IHX design with a unit power up to 300 MW.
8. Connections between IHX elements must be leak-tight to prevent intercircuit and bypass leaks and must ensure compensation of thermal structural deformations.
9. Irregularity of temperatures in the heat exchanger cross section, temperature pulsations in elements, and element vibrations induced by high velocity gas flow must be eliminated or minimized.
10. The IHX is one of the most heat-stressed components of the nuclear power plant, therefore, plant control algorithms in normal operating modes and in accidents must be aimed at maintaining heat exchanger operability and lifetime. Therefore, it is necessary to prevent, if possible, simultaneous impact of maximum temperatures and maximum pressure differences on heat exchanger elements.
11. IHX main design solutions must be validated by a complex of research, calculation and experimental activities.

VI.3. ANALYSIS OF LAYOUT AND DESIGN SOLUTIONS OF HOT GAS DUCTS

Hot gas ducts are designed to transport hot coolant from the reactor to the intermediate or process high temperature heat exchanger, and in case of multi-circuit heat transfer pattern – to transport coolant from the intermediate heat exchanger to the process (network) heat exchanger. It is obvious that the most severe operation conditions are present in gas ducts transporting helium from the reactor. In these hot gas ducts which shall operate within the entire reactor plant operation period (up to 60 years), helium may circulate at an average temperature of up to 950°C. Local temperatures may reach a level of 1000°C and higher due

to non-uniform helium temperature at the reactor core outlet and errors in reactor parameter maintenance. During emergency cooldown of the reactor these temperatures may reach 1200°C within 50 hours and then 1100°C within up to 100 hours.

Two design options are possible for gas ducts: coaxial design or design with separate tubes [297]. In the coaxial design, hot coolant circulates in the inner heat-insulated tube, and cold coolant in the annular gap between the inner and outer tubes (Fig. VI.8). In the design with separate tubes (Fig. VI.9), coolant circulates along two separate heat-insulated tubes. The coaxial design, as compared to the design with separate tubes, ensures higher mechanical stiffness, better compactness and lower heat losses to the environment. However, this design is more complicated and has lower repairability. For example, the THTR-300 (Germany) had some problems with repair of the coaxial gas ducts in the accident with separation of heat insulation coating sheets in the inner pipeline [284]. Due to the small distance between reactor and heat exchanger, higher temperatures, and necessary rigid connection of vessels, all reactor plants utilize coaxial gas ducts to transport helium from the reactor to the heat exchanger. Intermediate (secondary) circuits, as well as next circuits with lower coolant temperatures may utilize more simple gas ducts with separate tubes to transfer heat over long distances.

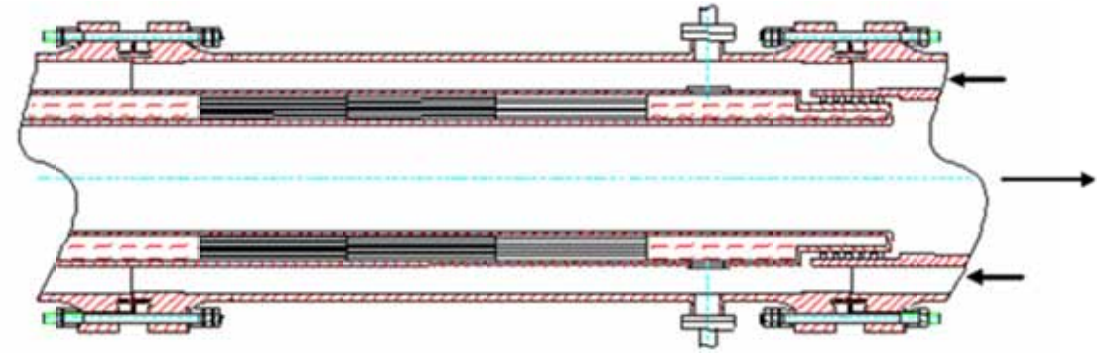

FIG. VI.8. Coaxial hot gas duct.

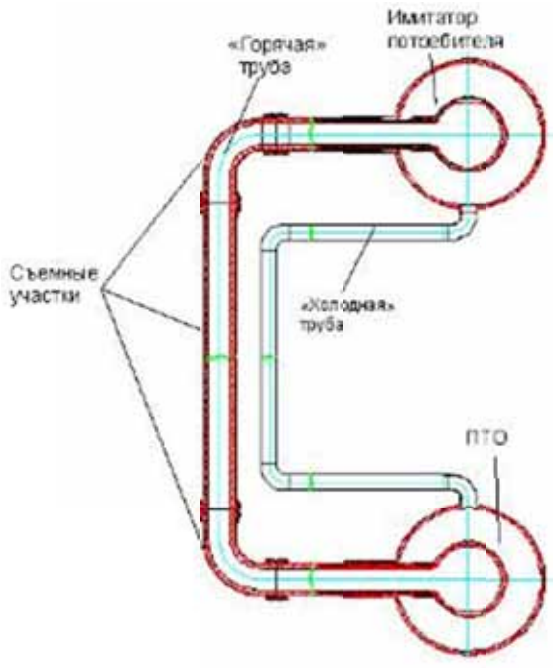

FIG. VI.9. Hot gas duct with separate tubes.

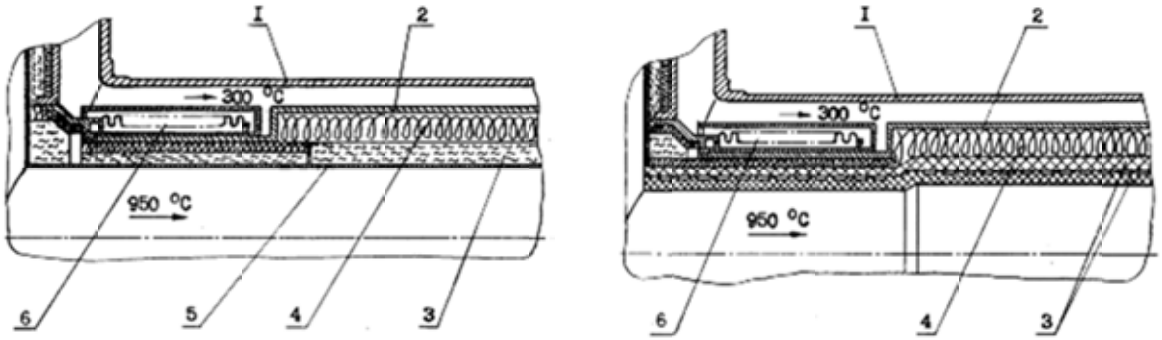

1: cross-vessel; 2: load-carrying metal structure; 3: inner heat insulation; 4: outer heat insulation; 5: protective liner; 6: bellows expansion joint

FIG. VI.10. Hot gas duct, (left) with carbon fiber inner heat insulation; (right) with pyrocarbon inner heat insulation.

High helium temperatures at the reactor outlet do not ensure long term operation of covering sheets of hot gas ducts, even if they are made of alloys with increased nickel content. One of the options improving operational reliability of gas ducts is a design (Fig. VI.10) where the components in contact with helium are made of pyrocarbon cylindrical units operated at temperature of 1000°C and higher.

Low heat conductivity and appropriate thickness (up to 50 mm) of pyrocarbon units allow a decrease of the temperature from 1000 to ~800°C, so that standard heat insulation (~60 mm) may be placed outside the graphite blocks. It can be based, for example, on foam cordierite, kaolin cotton, silica fiber, carbon fiber and operate at temperatures of ~800°C. Above this heat insulation, a stainless steel shell may be provided to withstand loads from the intercircuit pressure differences. Temperature compensation of deformations is implemented by large-diameter bellows or movable ring seals.

When designing the gas ducts, it is important to select and validate the operability of the heat insulation design. Operability of existing heat insulating materials under increased coolant temperatures at the reactor outlet within a long term period shall be confirmed by appropriate tests [298].

The following requirements for material database and tests may be defined. The data shall include:

- physical properties (heat conductivity and heat capacity);
- long term thermal and structural stability;
- mechanical strength at temperature fluctuations, pressure difference, vibration and acoustic loads;
- radiation stability, corrosion stability to moisture and air–helium environment;
- elimination of dust and gas emissions;
- possible tolerances for manufacturing and installation characteristics;
- preservation of stability and physical properties at external and mechanical impacts during normal operation and emergency cooling. Mechanical impacts on heat insulation are caused by non-uniform thermal expansion, acoustic vibration, helium flow friction, and rapid pressure variation in the circuit.

These data may be collected through tests of heat insulation samples or samples of small heat insulating panel assemblies. The requirements for test and experimental facilities include provision of helium flow rate and the availability of vibration and acoustic test equipment. Irradiation tests and hot chamber investigations will be required as well.

OKBM in cooperation with other enterprises performed a complex of investigations and tests of various types of heat insulation. Results are provided in Table VI.2 [15, 299]. Screen heat insulation was also tested.

As a result of investigations of heat insulation designs, it was demonstrated that in terms of heat conductivity and cost and under HTGR temperatures up to ~800–900°C, it will be optimal using heat insulation in the form of Al_2O_3 and Si_2O_3 ceramic fibrous mats to be arranged between metal covering sheets and the load-carrying tube. Ceramic fiber was used as heat insulation at FSV (USA) and other HTGRs in Germany and Japan. These plants passed tests to determine performance characteristics and mechanical load impact on kaowool and quartz-et-silice fibrous mats [299]. There are limited pilot data on irradiation results.

TABLE VI.2. FIBROUS MATERIALS HEAT CONDUCTIVITY IN HELIUM ENVIRONMENT

Material	Heat conductivity (W/(m·K))				
@ temperature (°C)	200	400	600	800	1000
Kaolin fiber [a]	0.26	0.28	0.32	0.36	0.40
Silicon fiber type	0.25	0.35	—	—	—
Quartz fabric	0.25	0.28	0.32	0.38	0.44
Graphite fabric	0.29	0.33	0.37	0.42	0.48
Foam cordierite [b]	0.65	0.7	0.8	0.95	—
Screen isolation from steel foil	0.18	0.23	0.29	0.35	—

[a] Density of 250 kg/m^3.
[b] Density of 600 kg/m^3, porosity of 79%.
— not available.

VI.4. ANALYSIS OF LAYOUT AND DESIGN SOLUTIONS OF GAS CIRCULATORS

To provide gas coolant circulation in main heat transfer loops, gas circulators are used in gas cooled reactor plants. Main characteristics of gas circulators are presented in Table VI.3. A brief description of gas circulators is given below. Their operation experience is still used when developing the new examples.

VI.4.1. China

Since the mass flow rate of the primary loop of HTR-10 is relatively small and the required pressure rise is quite high, a centrifugal fan was chosen as the helium circulator (Fig. VI.11) [300]. The helium circulator designed as single-stage radial compressor is vertically installed at the top of the steam generator inside the vessel and submerged in helium gas. The motor part in the upper region including motor, cooler, cooling fan remains at temperatures of 60–65°C, while the fan part in the lower region including impeller, diffuser, and gas inlet duct reaches 250°C. For a mass flow of 4.32 kg/s and a working temperature of 250°C, the pressure head of the blower required is 27.2 kPa.

TABLE VI.3. MAIN CHARACTERISTIC DATA OF GAS CIRCULATORS FOR DIFFERENT REACTORS

NPP	Country	Coolant					Type of gas circulator	Bearings
		Gas	Reactor inlet temp. (°C)	Inlet pressure (MPa)	Head (kPa)	Flowrate (kg/s)		
Calder Hall	United Kingdom	CO_2	150	0.69	—	890	—	—
Dungeness-A	United Kingdom	CO_2	250	1.96	—	—	axial	—
Sizewell-A	United Kingdom	CO_2	214	1.92	—	—	axial	—
G-2	France	CO_2	140	1.47	—	—	centrifugal	—
EDF-3	France	CO_2	240	2.45	156.9	2125	axial	oil
Latina	Italy	CO_2	180	1.35	—	—	axial	—
Tokaimura	Japan	CO_2	204	1.51	—	—	centrifugal	—
Vandellos	Spain	CO_2	217	2.60	—	—	—	—
Dragon	OECD	He	350	1.96	49.0	2.5	centrifugal	gas
AVR, Jülich	Germany	He	175	1.00	7.0	6.65 (m^3/s)	centrifugal	oil
Peach Bottom	USA	He	345	2.33	—	32	centrifugal	oil
Fort St. Vrain	USA	He	404	4.71	98.1	109.7	axial	water
Delmarva	USA	He	340	4.71	137.3	225	axial	water
THTR	Germany	He	250	3.82	98.1	14 (m^3/s)	centrifugal	oil
VG-400, VGM	Russian Federation	He	342	4.78	122.6	24.6 (m^3/s)	centrifugal	oil
HTTR	Japan	He	430	4.8	79.4 (PPWC) 107.9 (IHX)	4.2	centrifugal	—
HTR-10	China	He	250	3.0	60	4.32	centrifugal	oil

— data not available.

TABLE VI.3. MAIN CHARACTERISTIC DATA OF GAS CIRCULATORS FOR DIFFERENT REACTORS (cont.)

NPP	Shaft	Main drive			Flowrate control	Manufacturer	Operation startup
		Power (kW)	Rotation speed (rpm)	Type			
Calder Hall	—	1 500	940	DC motor	Variation of rotation speed	—	1956
Dungeness-A	—	6 560	—	Steam turbine	Variation of rotation speed	—	1965
Sizewell-A	vertical	6 500	—	AC motor	Bypass valve, guide blade rot.	—	1965
G-2	—	—	—	—	—	—	1959
EDF-3	horizontal	14 300	3 300	Steam turbine	Variation of rotation speed	Rateau	1966
Latina	—	3 500	—	AC motor	Variation of rotation speed	—	1963
Tokaimura	vertical	6 400	1 200	Steam turbine	Variation of rotation speed	—	1964
Vandellos	—	—	—	—	—	—	1971
Dragon	horizontal	—	1 100–12 000	AC motor	Variation of rotation speed	Brown Boveri	1966
AVR, Jülich	horizontal	—	3 500		Variation of rotation speed	Brown Boveri	1967
Peach Bottom	—	1 480	—	Motor	Hydraulic coupl		1966
Fort St. Vrain	vertical	4 100	9 550	Steam turbine	Variation of rotation speed	Gulf Gen Atomic	1973
Delmarva	vertical	10 000	6 750	Steam turbine	Variation of rotation speed	Gulf Gen Atomic	1975
THTR	horizontal	2 700	6 000	Motor	—	Brown Boveri	1976
VG-400, VGM	vertical	5 000	5 600	Motor	Variation of rotation speed	OKBM	n.a.
HTTR	vertical	300	12 000	Motor	Electric inverter/variable speed	—	1998
HTR-10	vertical	165	5 000	Motor	Variation of rotation speed	INET, Shanghai Blower Works	2000

— data not available.
n.a. not applicable.

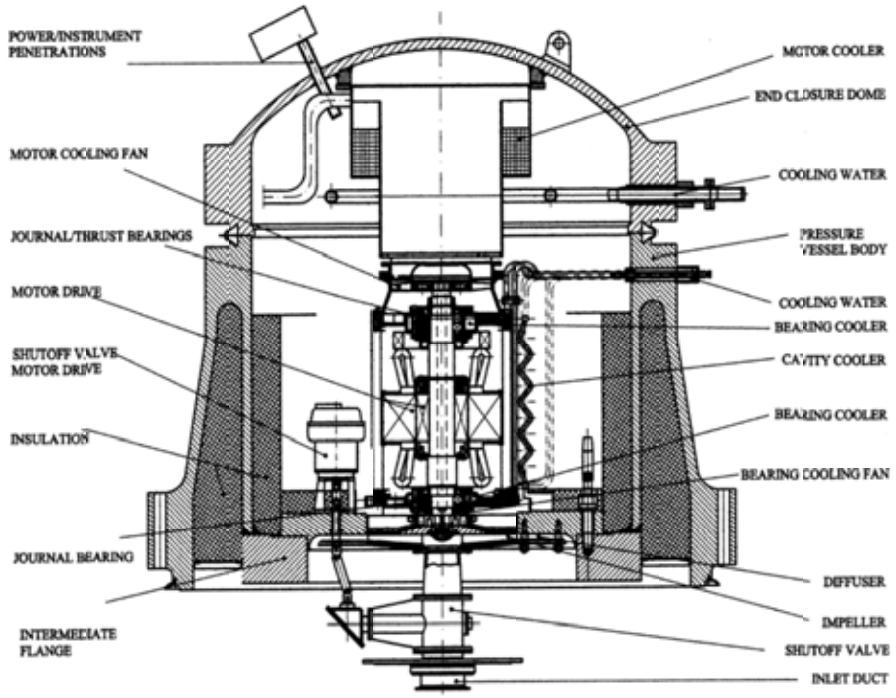

FIG. VI.11. Helium circulator in the HTR-10 [300].

In order to gain high efficiency, a centrifugal impeller is optimal for a high pressure rise and a low flow rate, as is the case for the HTR-10. The centrifugal impeller is designed as a closed type machine with 16 vanes to convey energy to the fluid and provide a smooth flow passage. Outside the impeller, there is a vaneless diffuser to further enhance pressure rise. The impeller is overhung at the lower motor shaft end. The shut off valve is mounted in the gas inlet duct. Compared with other HTGRs, the circulator for the HTR-10 is quite small, thus grease-lubricated bearings can be selected for the circulator for simplicity and reliability. A high performance grease of Molykote BG 20 was chosen, as it is suitable for a wide service temperature range (-45 to 180°C) and very high rotational speed.

Motor part and compressor part are separated by the partition plate on which a thermal insulation is fixed. Around the shaft, a labyrinth seal is equipped to increase the flow resistance of the annular gap between the compressor and motor part. Pressure rise and flow rate of the circulator are controlled by virtue of the variable speed of the motor drive.

As shown in the figure, two sets of bearings are installed at the upper and lower positions of the motor shaft. In the upper position, a pair of angular contact ball bearings is mounted face to face to carry a combination of radial and thrust loads, while in the lower position, a single angular contact ball bearing is mounted to carry mainly radial load. Since the lower bearing is near the impeller, the ceramic material of silicon nitride is used for the bearing balls instead of steel. Since it is a high speed and high temperature bearing system, cooling and lubrication are very important. Two bearing coolers are machined in the upper and lower bearing bases.

The motor is cooled by forced convection supplied by the motor cooling fan. The heat generated by the motor and transferred from the downside and outside is finally vented to the outside by the motor cooler and the cavity cooler. The grease lubricated ball bearings meet the requirements because HTR-10 is an experimental reactor and the design service life is short. In future, however, new type bearings have to be adopted in helium circulator to guarantee the long service life.

VI.4.2. United Kingdom

VI.4.2.1. Calder Hall gas circulator

The greatest experience in operation of gas circulators in closed loops is available. More than 150 centrifugal diagonal and axial gas circulators with vertical and horizontal shafts were installed in Magnox and AGR CO_2 cooled reactor plants (inside and outside the reactor vessel). These circulators operated during several million hours, most of them have constant-speed electric drives, and gas flowrate is controlled by variable vanes of outlet guide blades.

Four one-stage centrifugal circulators were installed at the first Calder Hall NPP with magnox reactor constructed in 1956 [301, 302]. Each circulator was driven by DC motor of 1.5 MW power at n = 750 min^{-1} via the reduction gear mechanism. Gas flowrate was 890 kg/s at 0.68 MPa pressure and temperature of 150°C. The CO_2 flowrate was controlled by impeller speed variation. Gas circulator rotation speeds were synchronized. The gas circulator design is given in Fig. VI.12.

VI.4.2.2. Hinckley Point-B gas circulator

Six axial circulators were installed at Hinckley Point-A NPP Magnox reactor (250 MW(e)), operating from 1965. Each circulator is driven by 6.15 MW motor at n = 2960 min^{-1}. The outer casing gas circulator is 3.6 m in diameter and 5.4 m in length (Fig. VI.13). The impeller has 11 blades. To improve flow structure, the guide blades and leveling device are installed at impeller inlet.

Eight centrifugal gas circulators with CO_2 driven by AC motor of 4.75 MW power at n = 2970 min^{-1} are used at Hinckley Point-B NPP with advanced gas cooled AGR. Gas flowrate through gas circulator is 500 kg/s at a pressure of 3.92 MPa and Δp = 0.29 MPa. The gas flowrate is controlled by variable blades, which are installed in the radial channel upstream the impeller. The outer impeller diameter is equal to 0.81 m. The rotor has plain bearings operating in oil under pressure exceeding 4 MPa. In case of lubrication system damage, it can be isolated by a valve system. Therefore, it is repaired without gas circulator depressurization. To eliminate oil ingress into the reactor, the pressure maintained in the motor cavity is less than that in the loop. All main components of gas circulator casing are designed for operation during 30 years without repair, and working components and gas circulator parts shall be visually inspected each five years. The accumulated gas circulator operating experience is more than 1 000 000 h. with availability coefficient of 0.994 over the period 1978–1985.

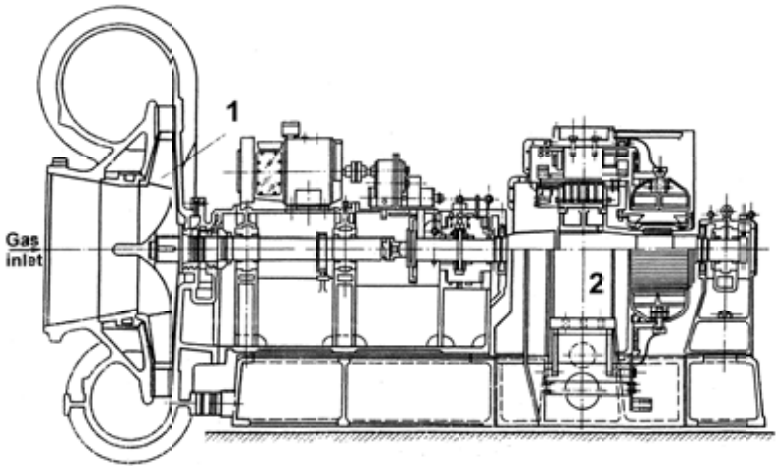

1: impeller; 2: drive.

FIG. VI.12. Calder Hall NPP gas circulator.

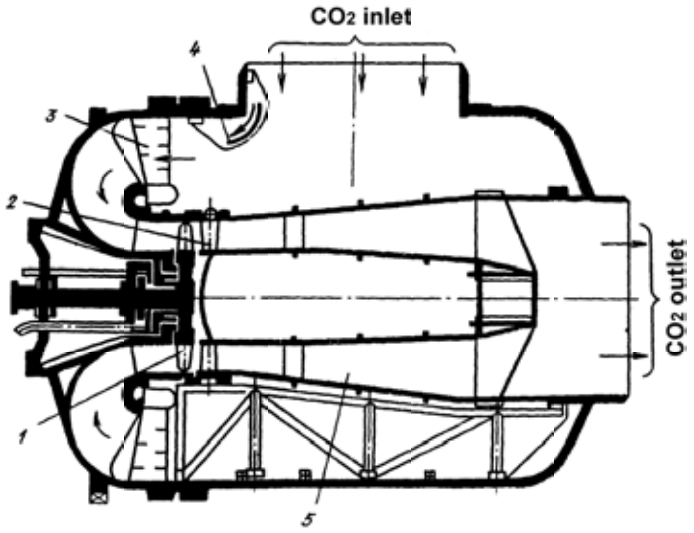

1: impeller; 2: straightener; 3: leveling device; 4: inlet blades; 5: diffuser.

FIG. VI.13. Hinckley Point–A Magnox reactor gas circulator.

VI.4.2.3. Dragon gas circulator

At Dragon HTGR NPP comn issioned in 1966, helium was circulated by six centrifugal gas circulators with AC motors. Motor rotation frequency varied within 1100–1200 min^{-1}. Helium flowrate was controlled by circulator rotor speed variation by means of a frequency converter. The inlet circulator pressure varied within 0.78–2.45 MPa, helium temperature attained 450°C, the impeller-developed head was 0.049 MPa. The gas circulator rotor rotated in gas supports. Dragon HTGR gas circulator diagram is given in Fig. VI.14. The circulators operated during 10 000 hours without failures.

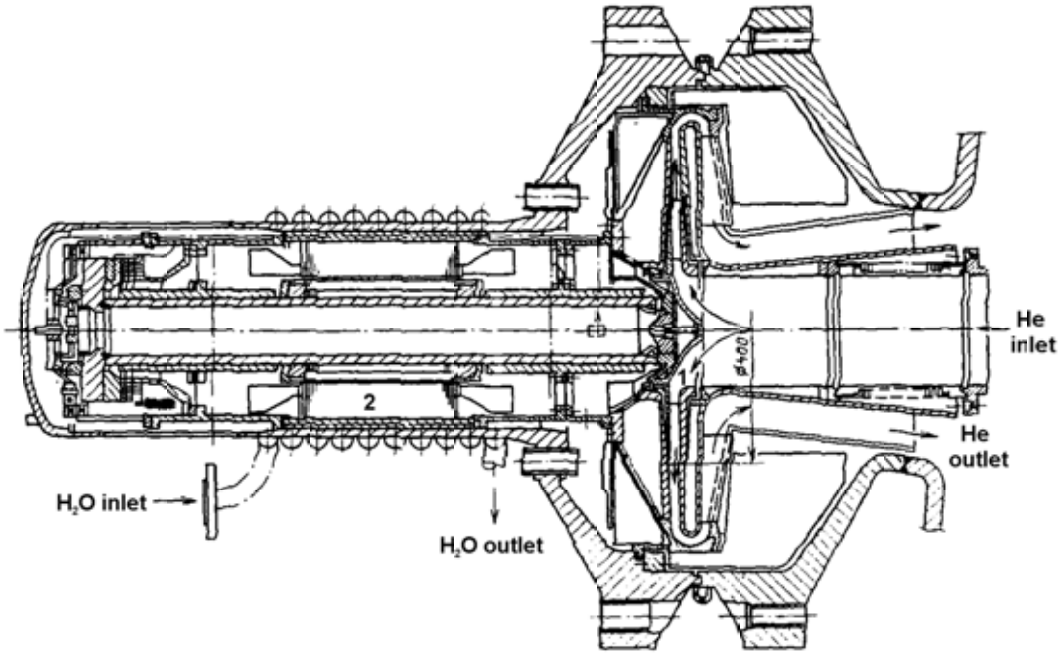

1: impeller; 2: moto

FIG. VI.14. Dragon HTGR gas circulator.

VI.4.3. France

VI.4.3.1. St. Loran-1 gas circulator

Four diagonal gas circulators of 2246 kg/s flowrate each at p_{inl} = 2.45 MPa and T_{inl} = 218°C circulate primary loop CO_2 at St. Loran-1 NPP. Steam turbine of 16 MW power at n = 2790 min^{-1} is gas circulator drive. Gas flowrate is controlled by impeller speed variation. Gas circulator diagram is given in Fig. VI.15. Gas circulator shroud (5) is bolted to load-bearing element (4) fixing the circulator to the reactor vessel wall. Gas flows to the diagonal impeller through inlet channel (1) and to the reactor loop – through diffuser (3). Bellows (2) seal the shaft between gas circulator inlet and reactor vessel, which are subjected to considerable temperature deformations. Journal and thrust plain bearings are oiled from turbine oil system. To replace the bearings and seals under working CO_2 pressure in the loop, the gas circulator impeller is displaced to sealing element 6, to prevent gas ingress to seal casing. After axial displacement of gas circulator impeller, its shaft is disconnected from the disk fixed by Hirt end teeth.

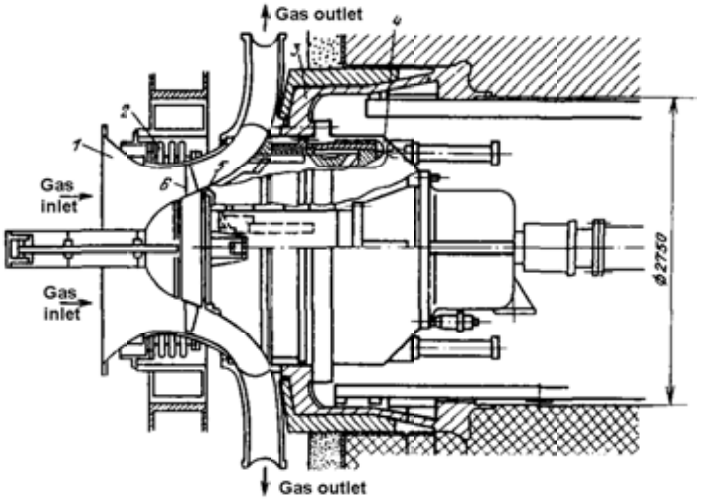

1: inlet channel; 2: bellows; 3: diffuser; 4: load-bearing element; 5: gas circulator shroud; 6: sealing element.

FIG. VI.15. St. Loran-1 NPP diagonal gas circulator.

VI.4.4. Germany

VI.4.4.1. AVR gas circulator

The experience in development and operation of centrifugal gas circulators acquired during HTTR operation is available. Thus, two small one-stage centrifugal gas circulators, with motor drive and oil lubrication, operated reliably during more than 100 000 hours at experimental AVR. The AVR gas circulator (Fig. VI.16) developed small head (Δp = 7kPa) under inlet pressure of 1 MPa and temperature of 200°C. Helium flowrate in the calculated point was 6.65 m^3/s and was controlled by rotation speed variation (n_{nom} = 3500 min^{-1}) of 77 kW motor rotor. Gas circulator impeller is fixed in cantilever fashion on shaft (5) of the motor rotating in oil plain bearings (6 and 11) with circulating lubrication system. To prevent oil ingress into the primary loop, labyrinth seal (4) is located directly downstream the impeller where pressurized blocking helium is supplied. Same helium is supplied to the other labyrinth seals of bearings (6 and 11). The minority of blocking gas flows to the primary loop and the most part – to bearing oil cavity. After passing through preliminary oil vapour purification system, helium is supplied to gas purification system for final purification. Blocking helium

flowrate is controlled such that the removed quantity of helium is always less than the supplied one.

As metal surfaces friction increases in pure helium, forced pressurized oil is supplied to improve bearing operation reliability during gas circulator startup and shutdown. Oil pipelines have valves, which allow dismounting and replacement of pipeline section in case of radioactive contamination. On one hand, gas circulator casing shall be sufficiently rigid and on and on the other hand, it shall allow considerable thermal deformations.

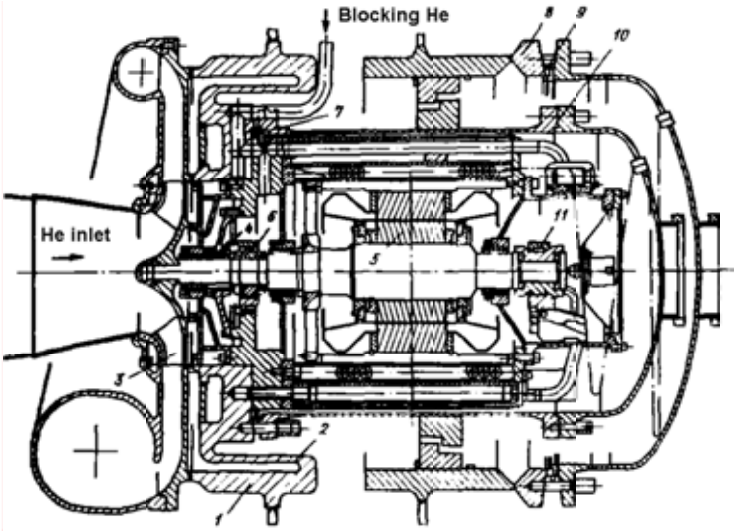

1: reactor vessel element; 2: expansion joint; 3: impeller, 4: labyrinth seals; 5: motor; 6: journal bearing; 7: flange welded seal; 8: main flange; 9: weld; 10: soft metal seal; 11: journal-thrust bearing

FIG. VI.16. AVR gas circulator.

VI.4.4.2. THTR-300 gas circulator

A one-stage vertical gas circulator with motor drive and oil bearings is used in THTR-300 plant. Six centrifugal gas circulators supply helium to the core and then to steam generators. Helium mass flowrate through one gas circulator is 50.75 kg/s at an inlet pressure of 3.8 MPa and temperature of 250°C; outlet pressure is 3.92 MPa. The gas circulator drive motor power is 2.297 MW, rotation speed is 5600 min^{-1}. The allowable difference in volumetric gas flowrate through gas circulators is 5% maximum in the area of rotation speed from 50 to 100% of n_{nom}. The flowrate through gas circulators is equalized by locking-control device (1), which is operated by servodrive (2) via the drawbar outside motor (3) (Fig. VI.17). Starting from 1982, small one-stage axial gas circulator with active electromagnetic supports was studied in experiments. These supports operated reliably during more than 11 000 h.

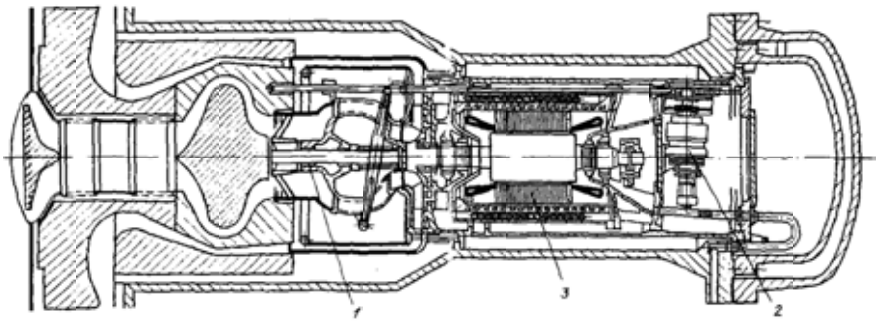

1: locking control device; 2: servodrive; 3: drawbar outside motor

FIG. VI.17. THTR-300 gas circulator.

VI.4.5. Japan

In the HTTR, the primary circuit has four gas circulators, while the secondary circuit of the IHX has one gas circulator [23, 303]. The former circulators are operated during both the parallel and single loaded operations and the latter during the parallel loaded operation. A cross-sectional view of gas circulator is shown in Fig. VI.18.

The primary gas circulator is a centrifugal, dynamic gas bearing type. It consists of an electric stator and rotor assembly, internal structure supports, axial thrust bearings and radial journal front bearings, an impeller unit, and a filter. The internal structures are contained in a casing which is cooled by a water jacket. The casing prevents primary helium gas from leaking into the atmosphere. Flow rate of primary helium gas is controlled by a variable speed motor using a frequency converter. The filter unit, which is on the top of the circulator, protects the impeller and rotating shaft from dust. The material of the casing and shaft is a low alloy steel.

The rotating assembly is fully floating on sets of dynamic gas bearing system during the operation condition. Gas bearings are used to maintain such a condition that the relative motion between the rotor and its stator obtains the lift. They acts on the principle that a pressure field, which depends on the viscosity, the linear speed, the load and the size of the bearing, builds up between two convergent surfaces in relative movement due to the viscosity forces that originate in the moving fluid. The gas bearing system consists of radial bearings mounted on either end of the motor and titling pad thrust bearings mounted on gimbals system. The rotating part consists of a stiff and a hollow shaft. It supports the motor; the single stage centrifugal impeller at its end and the motor compartment separates from the impeller compartment by a heat screen. The heat exchange with the outside cooling water system takes place at the location of the inner casing on which the motor is shrunk.

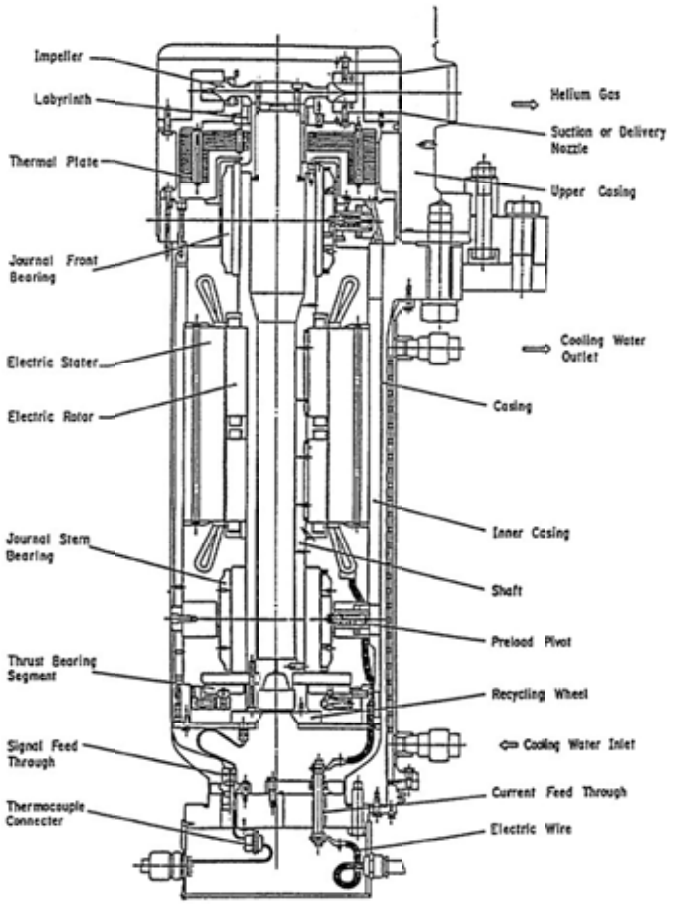

FIG. VI.18. Cross sectional view of primary gas circulator in the HTTR [303].

VI.4.6. USA

VI.4.6.1. Fort St. Vrain gas circulator

Experience was gained in operation of axial one-stage gas circulators with steam turbine drive and water supports at HTGR NPP. Fort St. Vrain NPP gas circulator operates already during more than 250 000 h. After the accident with water ingress into the primary loop, seal system reliability was additionally improved. In 1985, the third generation of water supports and seals was tested, which guaranteed against water ingress into the primary loop owing to installation of additional pump on gas circulator shaft and reliability improvement of the system for water removal from bearing body cavity. The results of the tests are positive. However, they proposed to change over to motor drive and active electromagnetic supports in advanced MHTGR plants.

Fort St. Vrain NPP was commissioned in 1973. It has four axial gas circulators with helium flowrate of 109.7 kg/s each under inlet pressure of 4.71 MPa and temperature of 400°C; pressure differential is 0.098 MPa. The main drive is steam turbine (9) with shaft rotation speed of 9550 min^{-1}, helium flow rate is controlled by shaft rotation speed variation. Pelton turbine (8) is used as an auxiliary drive (Fig. VI.19) which starts operating when steam is not supplied to the main drive and during reactor cooling down. Forces coming to gas circulator shaft (14) are transmitted to bearing casing with two journal bearings (6 and 12), thrust bearing (10), reversible thrust bearing (11), water seal (7), shutdown seal (15), and brake assembly (2) inside. Bearings (6, 10–12) are lubricated with water under pressure supplied through water inlet nozzle. The impeller labyrinth seal is pressurized with purified helium under the pressure exceeding water pressure.

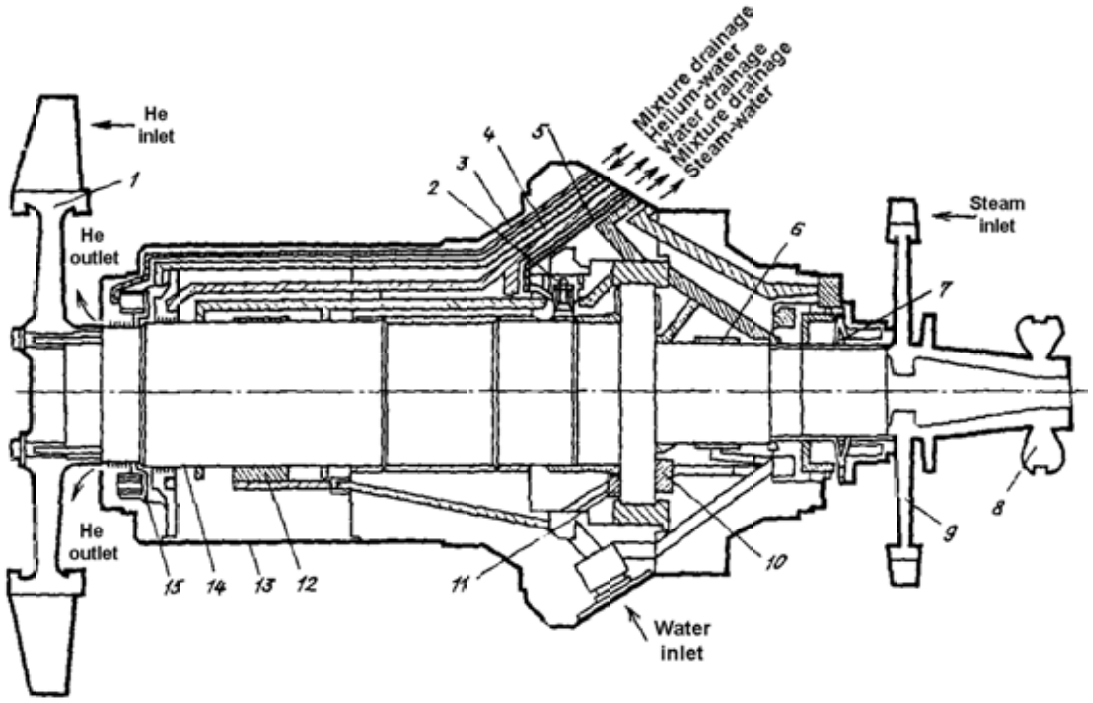

1: impeller; 2: shaft brake; 3: shutdown seal control (actuates during drainage);
4: blocking buffer helium supply; 5: shaft brake control (actuates during drainage); 6: journal bearing;
7: water seal; 8: Pelton turbine; 9: steam turbine; 10: thrust bearing; 11: reversible thrust bearing;
12: journal bearing; 13: bearing and seal casing; 14: shaft; 15: shutdown seal

FIG. VI.19. Fort St. Vrain NPP gas circulator.

In the middle of 1970s, the USA fabricated and tested full-size prototype axial gas circulator for Delmarva Project [304]. The gas circulator passed the tests and confirmed the design characteristics of water bearings and seals. As compared with Fort St. Vrain NPP, these gas circulators have the individual systems of water supply and removal from every gas circulator and ejector pump to activate drainage system for water removal from bearing body cavity.

VI.4.6.2. MHTGR gas circulator

Axial gas circulator design with canned motor drive and electromagnetic suspension was developed for MHTGR [305]. For drive power of 3.21 MW, helium flowrate and head are 158 kg/s and 91 kPa respectively. Temperature and pressure are 255°C and 6.29 MPa. Besides electromagnetic supports, the rotor has safety supports with less radial and axial gaps, which can take the rotor in case of main bearing electric system failure.

The cavity with gas circulator and drive motor is filled with pure helium under the pressure slightly exceeding primary loop pressure, which prevents ingress of contaminated helium from the primary loop to the motor cavity. During gas circulator operation, helium is circulated through the channels by two auxiliary fans. Cooling helium pressure is less than that one in water side of heat exchanger. Motor and EMB casings are cooled by water of heat exchanger arranged around motor stator.

Russian Federation. Development of VG-400 and VGM NPP with HTHR required comprehensive experimental study of main circulators (gas circulators) for heat transfer loops. For example, OKBM has designed, fabricated and supplied electric gas circulator EG-90/1.25 for benchmark tests, which was the baseline design for HTHR plants [306]. Vertical leak-tight centrifugal gas circulator (Fig.VI.20) with built-in motor consists of casing, active parts of drive motor, bearing assemblies, flow area and isolation valve.

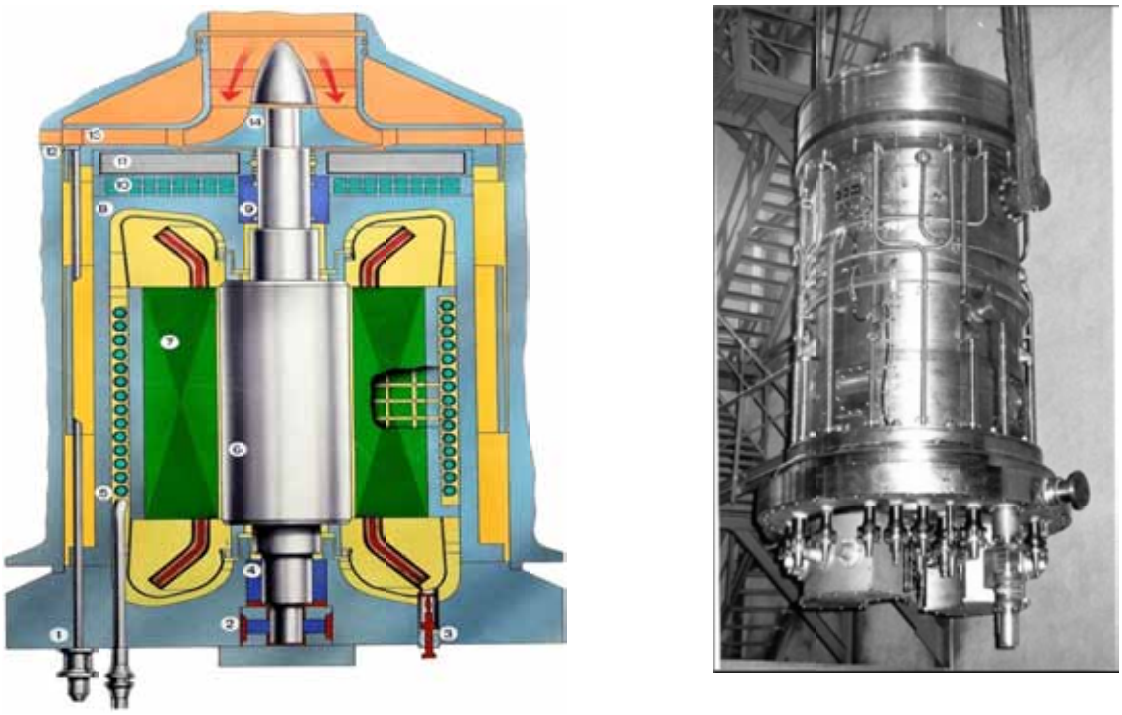

1: cover; 2: axial bearing; 3: electric lead-in; 4: radial bearing; 5: stator cooler; 6: rotor; 7: stator; 8: ca
radial bearing; 10: thermal insulation cooler; 11: thermal insulation; 12: isolation valve; 13: guide vane;
14: impeller

FIG. VI.20. Gas circulator EG-90/1.25 prototype.

The casing is a load-bearing component of gas circulator in the form of shell; the end heat exchanger, the support with thermal insulation and labyrinth seals and guide vane are fixed to the upper part of the shell; load-bearing sealing cover with electric lead-ins, nozzles for pipeline connection servicing and tachometric sensors are located from below.

The drive motor includes stator and rotor. The stator is made of sheet electric steel, it has channels for stator cooling by helium using built-in gas circulator cooling system. The short-circuited rotor is made of steel 38CrNi3MoVBe (GOST 4543-78). Power is supplied through special electric lead-ins from high voltage frequency converter. Motor rotor rotates in two radial hydrostatic bearings and in one axial hydrodynamic bearing. The design provides the possibility to install EMB with catcher bearings.

Gas circulator flow area consists of intake, impeller and guide vane. The isolation valve in the form of annular shell interrupts quickly helium circulation in the primary loop during emergencies and restricts backflow through the loop in case of shutdown. The isolation valve has forced pneumatic drive, which is located on gas circulator cover. The valve is automatically controlled by automated process control system of the reactor plant, and in the conditions of basic test facility – by automated test facility control system.

Development of main gas circulator requires large amount of R&D work, application of unit-by-unit procedure of design mastering and fulfillment of preliminary studies using models, analogues, prototypes and special test facilities. OKBM has performed the following tests: aerodynamic tests of gas circulator flow area and cooling circuit of gas circulator motor; tests of hydrostatic, hydrodynamic and electromagnetic bearings, isolation valve and tachometric complex; tests and studies of static frequency converter characteristics. Tests of models and analogues confirmed correctness of technical decisions used in gas circulator design. OKBM constructed multipurpose basic test facility for integrated tests of gas circulator; its diagram is given in Fig. VI.21.

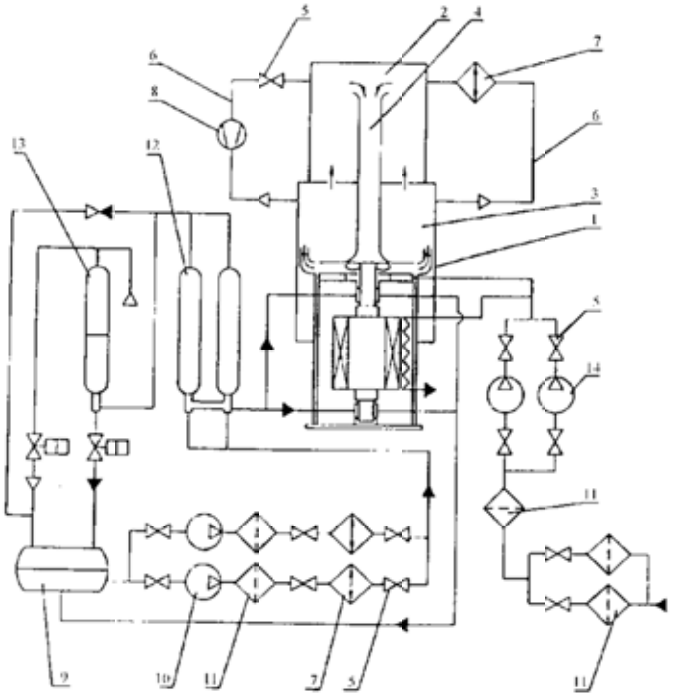

1: vessel; 2: suction plenum; 3: pressure plenum; 4: central duct; 5: valve; 6: bypass;
7: cooler; 8: flowmeter; 9: oil tank; 10: oil pump; 11: filter; 12: oil cylinder;
13: gas-oil accumulator; 14: pump.

FIG. VI.21. Diagram of basic circulator test facility ST-1383.

VI.4.7. *Recommendations for gas circulator design optimization*

Recommendations for design optimization can be formulated based on the analysis of experience in design development and gas circulators operation [301, 302].

The following recommendations are proposed for various stages of gas circulator design, development and operation.

1. It is necessary to take account of experience in design of various axial and centrifugal compressors in view of working fluid physical properties features.
2. All components of closed circuit shall be designed with account of mutual influence of parameters in the design point and in view of operation conditions at various power levels.
3. Specified parameters of flowrate, pressure and temperature shall be ensured both in standard and emergency operation conditions.
4. Gas circulator shall have stable response in wide range of rotation speed variation at $5 < n < 110\%$.
5. Gas circulator shall be arranged in the cold area of the loop, e.g. downstream the steam generator or heat exchanger.
6. Gas circulator shall use the drive with controlled rotation speed, which is leaktight against radioactive-contaminated pumped fluid.
7. P Gas circulator together with drive shall be located vertically.
8. Possibility of loop contamination from axial and radial supports shall be eliminated.
9. Gas circulator shall be fabricated and assembled in plant conditions, i.e. modular principle of assembling shall be used.
10. Gas circulator shall operate reliably under the earthquakes up to 0.15g; the entire plant shall shut down under the earthquakes up to 0.3g.
11. Service life shall be 60 years minimum starting from standard operation.
12. Easy and safe maintenance shall be ensured, diagnostics of remotely controlled and automatically served assemblies shall be provided.
13. Easy installation and replacement of assemblies shall be provided during scheduled repairs after reactor shutdown and cooling down.
14. Reliable operation shall be provided for operation period exceeding 7000 h per year.
15. To eliminate the risk of lubricant contamination to reactor circuit, gas bearing which is proven in the HTTR and HTR-10 is recommended for gas circulator units of limited reactor capacity (practically < 50 MW(th)), while electromaganetic bearing is recommended for gas circulator units of larger reactor capacity, say 200–600 MW(th).

REFERENCES

[1] LABAR, M., SHENOY, A., SIMON, W., CAMPBELL, E., The gas turbine modular helium reactor, Nuclear News **46** 11 (2003) 28–37.

[2] GOLOVKO, V.F., KODOCHIGOV, N.G., VASYAEV, A.V., SHENOY, A., BAXI, C.B., Ways to increase efficiency of the high temperature gas reactor coupled with the gas turbine power conversion unit, ASME J. Eng. Gas Turbines Power **131** (2009) 052903-1–052903-5.

[3] YAN, X., GTHTR300 Design and development, Nuclear Engineering and Design **222** (2003) 247–262.

[4] INL, Next generation nuclear plant pre-conceptual design report. Report INL/EXT-07-12967, Rev. 1, Idaho National Laboratory, Idaho Falls, USA (2007).

[5] KUNITOMI, K., Japan's future HTR – the GTHTR300, Nuclear Engineering and Design **233** (2004) 309–327.

[6] RICHARDS, M.B., et al., "The modular helium reactor for future energy needs" (Proc. Int. Congress Reno, USA) ICAPP'06, USA (2006) paper 6154.

[7] YAN, X., et al., Cost and performance design approach for GTHTR300 power conversion system, Nuclear Engineering and Design **226** (2003) 351–373.

[8] MATZNER, D., MULDER, E., PRETORIUS, P., "Review of the Pebble Bed Modular Reactor (PBMR) plant", Current Status and Future Development of Modular High Temperature Gas Cooled Reactor Technology, IAEA-TECDOC-1198, IAEA, Vienna (2001) 19–68.

[9] GOLOVKO, V.F. et al, "Features of adapting gas turbine cycle and heat exchangers for HTGRs", Gas Turbine Power Conversion Systems for Modular HTGRs, IAEA-TECDOC-1238, IAEA, Vienna (2001) 63–74.

[10] BREY, H.L., "Development history of the gas turbine modular high temperature reactor", Gas Turbine Power Conversion Systems for Modular HTGRs, IAEA-TECDOC-1238, IAEA, Vienna (2001) 21–43.

[11] LINNHOFF MARCH, Introduction to pinch technology, Linnhoff March Int. Ltd., Walton on Thames, UK (1998) 9–13.

[12] SMITH, R., Chemical process design and integration, John Wiley & Sons Ltd. (2005) 383–409.

[13] MUTO, Y., ISHIYAMA, S., SHIOZAWA, S., "Selection of JAERI's HTGR-GT concept", Gas Turbine Power Conversion Systems for Modular HTGRs, IAEA-TECDOC-1238, IAEA, Vienna (2001) 53–62.

[14] EPRI, "High temperature gas cooled reactors for the production of hydrogen: An assessment in support of the hydrogen economy", EPRI Report CA (2003) 92121–2767, Electric Power Research Institute, Palo Alto, USA (2003) 9–32.

[15] MITENKOV, F.M., et al., High-temperature gas-cooled reactor as an energy source for commercial production of hydrogen, Atomnaya Energiya **97** (2004) 432–446.

[16] VAN GOETHEM, G., et al., "EU research and training in reactor systems", FISA 2006, Directorate-General for Research Euratom, EUR 21231 (2006).

[17] VASYAEV, A.V., VLADIMIRSKY, M.K., KONSTANTINYCHEV, N.A., PANAIOTOVA, T.V., GANIN, M.Y., HTGR-based power sources for power-technological application. Design and structural solutions. Transactions from the International Forum on the Problems of Science, Engineering and Education, Moscow (2008).

[18] ZVEREV, L.D., et al., "Innovative technologies based on high-temperature gas-cooled reactors for the regional power industry", (Proc. Int. Congress on Advanced Fuel Cycles and Systems, GLOBAL'09), France (2009).

[19] WERKOFF, F., AVRIL, S., MANSILLA, C., SIGURVINSSON, J., Processes of hydrogen production, coupled with nuclear reactors: Economic perspectives. European Nuclear Conference, Versailles, France (2005).
[20] GOLOVKO, V.F., GUCHSHIN, U.L., KODOCHIGOV, N.G., KUZAVKOV, N.G., "Utilization of HTGR heat and its transfer to industrial facilities", Nuclear Heat Applications: Design Aspects and Operating Experience, IAEA-TECDOC-1056, IAEA, Vienna (1998).
[21] SCHULTEN, R., et al., Industriekraftwerk mit Hochtemperaturreaktor PR 500 – 'OTTO-Prinzip' zur Erzeugung von Prozessdampf, Report Jül-941-RG, Research Center Jülich, Germany (1973).
[22] HARTH, R., JANSING, W., TEUBNER, H., Experience gained from the EVA II and KVK operation. Nuclear Engineering and. Design **121** (1990) 173–182.
[23] SAITO, S., et al., Design of high temperature engineering test reactor (HTTR). Report JAERI 1332, Japan Atomic Energy Research Institute, Oarai, Japan (1994).
[24] KUNITOMI, K., JAEA's VHTR for hydrogen and electricity cogeneration: GTHTR300C, Nuclear Engineering and Technology **39** (2007) 9–20.
[25] YAN, X., GTHTR300 design variants for production of electricity, hydrogen and both. 3rd Information Exchange Meeting on Nuclear Production of Hydrogen, NSC/OECD/NEA, Oarai, Japan (2005).
[26] KATO, R., Design of the intermediate heat exchanger for the high temperature gas-cooled reactor cogeneration system, (1) Selection of the specification of heat exchanger tube and evaluation of the primary stress, Trans Atomic Energy Society of Japan **6** (2007) 141–148.
[27] YILDIZ, B., KAZIMI, M.S., Efficiency of hydrogen production systems using alternative nuclear energy technologies, International Journal of Hydrogen Energy **31** (2006) 77–92.
[28] LABAR, M., The gas-turbine modular helium reactor: A promising option for near-term deployment. ICAPP'02 Advanced Nuclear Power Plants (Proc. Int. Congress, Hollywood, FL, USA) ICAPP'02-ISBN: 0-89448-663-2 (2002).
[29] FORSBERG, C.W., Hydrogen production using the advanced high-temperature reactor, Presentation at the 14th Annual US Hydrogen Meeting, Washington DC, USA, 2003.
[30] KREUTER, W., HOFMANN, H., Electrolysis: The important energy transformer in a world of sustainable energy, International Journal of Hydrogen Energy **23** (1998) 661–666.
[31] HINO, R., HAGA, K., AITA, H., SEKITA, K., R&D on hydrogen production by high-temperature electrolysis of steam, Nuclear Engineering and Design **233** (2004) 363–375.
[32] HINO, R., MIYAMOTO, Y., "Hydrogen production by high temperature electrolysis of steam", High Temperature Applications of Nuclear Energy (Proc. TCM, Oarai, 1992), IAEA-TECDOC-761, IAEA, Vienna (1994) 120–124.
[33] BRISSE, A., SCHEFOLD, J., ZAHID, M., High temperature water electrolysis in solid oxide cells, International Journal of Hydrogen Energy **33** (2008) 5375–5382.
[34] HERRING, J., et al., Progress in high-temperature electrolysis for hydrogen production using planar SOFC technology, International Journal of Hydrogen Energy **32** (2007) 440–450.
[35] HINO, R., AITA, H., SEKITA, K., HAGA, K., IWATA, T., Study on hydrogen production by high temperature electrolysis of steam, Report JAERI-Research 97-064, Japan Atomic Energy Research Institute, Oarai, Japan (1997).

[36] O'BRIEN, J., STOOTS, C., HERRING, J., LESSING, P., "Performance measurements of solid-oxide electrolysis cells for hydrogen production from nuclear energy", ICONE-12 (Proc. 12th Int. Conf. on Nuclear Engineering, Arlington, USA, 2004).
[37] HERRING, J., et al., "Hydrogen production through high-temperature electrolysis in a solid oxide cell", OECD-NEA Information Exchange Meeting on Nuclear Production of Hydrogen, Argonne National Laboratory, USA (2003).
[38] SHIN, Y., PARK, W., CHANG, J., PARK, J., Evaluation of the high temperature electrolysis of steam to produce hydrogen, International Journal of Hydrogen Energy **32** (2007) 1486–1491.
[39] US-DOE, A technology roadmap for Generation IV nuclear energy systems, Nuclear Energy Advisory Committee and the Generation IV International Forum (2002).
[40] ANDERSON, R., Hydrogen research development and demonstration activities at the INEEL, 14th Annual US Hydrogen Conference, Poster Session, Washington, DC, USA (2003).
[41] DÖNITZ, W., DIETRICH, G., ERDLE, E., STREICHER, R., Electrochemical high temperature technology for hydrogen production or direct electricity generation, International Journal of Hydrogen Energy **13** (1988) 283–287.
[42] FUNK, J., Thermo-chemical hydrogen production: Past and present, International Journal of Hydrogen Energy **26** (2001) 185–190.
[43] MCQUILLAN, B., et al., High efficiency generation of hydrogen fuels using solar thermo-chemical splitting of water, Report GA-A24972, General Atomics, San Diego, USA (2002).
[44] LEWIS, M., TAYLOR, A., High temperature thermo-chemical processes, DOE Hydrogen Program, Annual Progress Report, Washington DC, USA (2006) 182–185.
[45] NORMAN, J., BESENBRUCH, G., BROWN, L., O'KEEFE, D., ALLEN, C., Thermo-chemical water splitting cycle, bench scale investigations and process engineering, Final Report DOE/ET/26225 and GA-A-16713, General Atomics, San Diego, CA, USA (1981).
[46] O'KEEFE, D., et al., Preliminary results from bench-scale testing of a sulphur-iodine thermo-chemical water-splitting cycle, International Journal of Hydrogen Energy **7** (1982) 381–392.
[47] ROTH, M., KNOCHE, K., Thermo-chemical water splitting through direct HI-decomposition from $HI/I_2/H_2O$ solutions, International Journal of Hydrogen Energy **14** (1989) 545–549.
[48] ÖZTÜRK, I.T., et al., A new process for oxygen generation step for the hydrogen producing sulphur-iodine thermo-chemical cycle, Transactions of the Institute of Chemical Engineers Part A **72** (1994) 241–250.
[49] ONUKI, K., et al., R&D program on thermo-chemical water-splitting iodine-sulphur process at JAERI, Proc. GENES4/ANP2003, Kyoto, Japan (2003) page 1072.
[50] KUBO, S., et al., "A bench scale hydrogen production test by the thermo-chemical water-splitting iodine-sulphur process", GLOBAL 2005 (Proc. Int. Conf. Tsukuba, Japan, October 2005) paper 474.
[51] SAKABA, N., KASAHARA, S., ONUKI, K., KUNITOMI, K., Conceptual design of hydrogen production system with thermo-chemical water-splitting iodine-sulphur process utilizing heat from the high-temperature gas-cooled reactor HTTR, International Journal of Hydrogen Energy **32** (2007) 4160–4169.

[52] RICHARDS, M.B., et al., “Conceptual designs for MHR-based hydrogen production systems”, GLOBAL 2005 (Proc. Int. Conf. Tsukuba, Japan, October 2005) paper 190.
[53] GIACONIA, A., et al., Survey of bunsen reaction routes to improve the sulphur-iodine thermochemical water-splitting cycle, International Journal of Hydrogen Energy **34** (2009) 4041–4048.
[54] NOMURA, M., et al., Application of an electrochemical membrane reactor to the thermochemical water splitting IS process for hydrogen production, Journal of Membrane Science **240** (2004) 221–226.
[55] NOMURA, M., et al., Development of an electrochemical cell for the efficient hydrogen production through the IS process, AIChE Journal **50** (2004) 1991–1998.
[56] LEE, B.J., et al., Development of a flowsheet for iodine-sulphur thermo-chemical cycle based on optimized bunsen reaction, International Journal of Hydrogen Energy **34** (2009) 2133–2143.
[57] SAKURAI, M., et al., Experimental study on side-reaction occurrence condition in the iodine-sulphur thermo-chemical hydrogen production process, International Journal of Hydrogen Energy **23** (2000) 613–619.
[58] SCHULTZ, K., Thermo-chemical production of hydrogen from solar and nuclear energy, Technical Report for the Stanford Global Climate and Energy Projects, San Diego, USA (2003).
[59] KUBO, S., et al., Corrosion test on structural materials for iodine-sulphur thermo-chemical water splitting cycle, AIChE Spring National Meeting, New Orleans, USA (2003).
[60] HADJ-KALI, M.K., et al., HI_x system thermodynamic model for hydrogen production by the sulfur-iodine cycle, International Journal of Hydrogen Energy **34** (2009) 1696–1709.
[61] LANCHI, M., et al., S-I thermochemical cycle: A thermodynamic analysis of $HI\text{-}H_2O\text{-}I_2$ system and design of the HI_x decomposition sections, International Journal of Hydrogen Energy **34** (2009) 2121–2132.
[62] LAROUSSE, B., et al., Experimental study of the vapour liquid equilibria of $HI\text{-}H_2O\text{-}I_2$ ternary mixture, Part 2: Experimental results at high temperature and pressure, International Journal of Hydrogen Energy **34** (2009) 3258–3266.
[63] VITART, X., et al., Thermochemical production of hydrogen, In: Chapter 4 “Nuclear production of hydrogen-technologies and perspectives for global development”, page 66, HORI M., SPITALNIK J., International Nuclear Society Council (INSC), Albuquerque, USA (2004).
[64] ÖZTÜRK, I.T., HAMMACHE, A., BILGEN, E., An improved process for H_2SO_4 decomposition step of the sulfur-iodine cycle, Energy Conversion Management **36** (1005) 11–21.
[65] BUCKINGHAM, R., et al., High efficiency hydrogen production from nuclear energy: Laboratory demonstration of S-I water splitting, Grant No. DE-FG07-03RL14520, INERI Report GA-C25006, San Diego, USA (2005).
[66] GOLDSTEIN, S., BORGARD, J.M., VITART, X., Upper bound and best estimate of the efficiency of the iodine sulphur cycle, International Journal of Hydrogen Energy **30** (2005) 619–626.
[67] KASAHARA, S., et al., Flow sheet study of the thermochemical water-splitting iodine-sulfur process for effective hydrogen production, International Journal of Hydrogen Energy **32** (2007) 489–496.
[68] DAVIS, M.E., et al., An entropy production and efficiency analysis of Bunsen reaction in the general atomic sulfur iodine thermochemical hydrogen production cycle, International Journal of Hydrogen Energy **5** (1980) 475–485.

[69] VITART, X., BORGARD, J.M., GOLDSTEIN, S., COLETTE, S., Investigation of the I-S-cycle for massive hydrogen production (Proc. 2nd OECD-NEA Information Exchange Meeting on Nuclear Production of Hydrogen, Argonne, USA, 2003), Report NEA No 5308 AEN, Nuclear Energy Agency, Paris, France (2004) 99–109.
[70] PRASAD, C.S.R., FANI, H.Z., MENON, S.B., Heterogeneous Bunsen reaction: Analysis & experimental study of chemical absorption of sulfur dioxide and dissolution of iodine into aqueous reacting system, Non-Electric Applications of Nuclear Power: Seawater Desalination, Hydrogen Production and other Industrial Applications, IAEA-CN-152-18, IAEA, Vienna (2009).
[71] PRASAD, C.S.R., Modeling and design of Bunsen reaction system - Issues, approaches and results (R&D on iodine-sulfur thermochemical process for hydrogen), Contribution to CRP on Advances in Nuclear Power Process Heat Applications, IAEA, Vienna (2007).
[72] DOKIYA, M., KAMEYAMA, T., FUKUDA, K., Thermochemical hydrogen preparation-part V. A feasibility study of the sulfur iodine cycle, International Journal of Hydrogen Energy **4** (1979) 267–277.
[73] DE BENI, G., PIERNI, G., SPELTA, B., The reaction of sulfurdioxide with water and a halogen. The case of iodine: Reaction in presence of organic solvents, International Journal of Hydrogen Energy **5** (1980) 141–149.
[74] MATHIAS, P.M., Modeling the sulfur-iodine cycle: Aspen plus building blocks and simulation model, AspenTech, Burlington, USA (2002).
[75] MATHIAS, P.M., Modeling the sulfur-iodine cycle: Aspen plus building blocks and simulation model, Final report to General Atomics, USA (2002).
[76] MATHIAS, P.M., BROWN, L.C., Thermodynamics of the sulfur-iodine cycle for thermochemical hydrogen production, Paper presented at 68th Annual Meeting of the Japan Society of Chemical Engineers, Tokyo, Japan (2003).
[77] MATHIAS, P.M., Report-4 preliminary flowsheets for SI cycle, General Atomics, San Diego, USA (2004).
[78] BROWN, L.C., MATHIAS, P.M., CHEN, C.C., RAMRUS, D., Thermodynamic model for the HI-I_2-H_2O system, AIChE Annual Meeting Reno, USA (2001).
[79] WANG, P., ANDERKO, A., SPRINGER, R.D., YOUNG, R.D., Modeling phase equilibria and speciation in mixed-solvent electrolyte systems: II. Liquid-liquid equilibria and properties of associating electrolyte solutions. Journal of Mol Liquids **125** (2006) 37–44.
[80] O'CONNELL, J.P., NARKPRASERTA, P., GORENSEK, M.B., Process model-free analysis for thermodynamic efficiencies of sulfur-iodine processes for thermochemical water decomposition, International Journal of Hydrogen Energy **34** (2009) 4033–4040.
[81] BELAISSAOUI, B., et al., Vapour reactive distillation process for hydrogen production by HI decomposition from HI-I_2-H_2O solutions, Chemical Engineering and Processing **47** (2008) 396–407.
[82] HONG, S.D., et al., Evaluation on the electro-electro dialysis to concentrate HI from HI_x solution by using two types of the electrode, International Journal of Hydrogen Energy **32** (2007)
[83] ONUKI, K., HWANG, G.J., ARIFAL, SHIMIZU, S., Electro-electro dialysis of hydriodic acid in the presence of iodine at elevated temperature, Journal of Membrane Science **192** (2001) 193–199.
[84] HWANG, G.J., ONUKI, K., NOMURA, M., KASAHARA, S., KIM, J.W., Improvement of the thermochemical water-aplitting IS (iodine-sulfur) process by electro-electro dialysis, Journal of Membrane Science **220** (2003) 129–136.

[85] ORME, C.J., STEWART, F.F., Pervaporation of water from aqueous hydriodic acid and iodine mixtures using nafion membranes, Journal of Membrane Science **304** (2007) 156–162.
[86] ELDER, R.H., PRIESTMAN, G.H., EWAN, B.C., ALLEN, R.W.K., The separation of HI_x in the sulphur-iodine thermochemical cycle for sustainable hydrogen production, Transactions of the Institution of Chemical Engineers Part B (2005).
[87] ORME, C.J., KLAEHN, J.R., STEWART, F.F., Membrane separation processes for the benefit of the sulfur–iodine and hybrid sulfur thermochemical cycles, International Journal of Hydrogen Energy **34** (2009) 6614–6624.
[88] CAPUTO, G., FELICI, C., TARQUINI, P., GIACONIA, A., SAU, S., Membrane distillation of HI/H_2O and H_2SO_4/H_2O mixtures for the sulfur-iodine thermochemical process, International Journal of Hydrogen Energy **32** (2007) 4736–4743.
[89] PENG, D.Y., ROBINSON, D.B., A new two constant equation of state, Industrial and Engineering Chemistry Fundamentals **15** (1976) 59–64.
[90] REDLICH, O., KWONG, J.N.S., On the thermodynamics of solutions, an equation of state, fugacities of gaseous solution, Chemical Reviews **44** (1949) 233–244.
[91] SOAVE, G., Equilibrium constants from a modified redlich-kwong equation of state, Chemical Engineering Science **27**(6) (1972) 1197–1203.
[92] CHEN, C.C., BRITT, H.I., BOSTON, J.F., EVANS, L.B., Local composition model for excess gibbs energy of electrolyte system, AIChE Journal **28** (1982) 588–596.
[93] ABRAMS, D.S., PRAUSNITZ, J.M., Statical thermodynamics of liquid mixers: A new expression for the Gibbs energy of partly or completely miscible systems, AIChE Journal **21**(1) (1975) 116–128.
[94] YAMAWAKI, M., et al., Application of nuclear energy for environmentally friendly hydrogen generation, International Journal of Hydrogen Energy **32** (2007) 2719–2725.
[95] RICHARDS, M.B., et al., Hydrogen production using the modular helium reactor, ICONE-13 (Proc. 13th Int. Conference on Nuclear Engineering, Beijing, China, May 16-20, 2005).
[96] RICHARDS, M.B., et al., H2-MHR conceptual designs based on the sulphur-iodine process and high-temperature electrolysis, International Journal Nuclear Hydrogen Production and Applications **1** (2006) 36–50.
[97] LE DUIGOU, A., et al., HYTEC: An EC funded search for a long term massive hydrogen production route using solar and nuclear technologies, International Journal of Hydrogen Energy **32** (2007) 1516–1529.
[98] ZHANG, Z., et al., Design aspects of the Chinese modular high-temperature gas cooled reactor HTR-PM, Nuclear Engineering and Design **236** (2006) 485–490.
[99] ZHANG, P., CHEN, S.Z., WANG, L.J., XU, J.M. Overview of nuclear hydrogen production research through iodine sulfur process at INET, International Journal of Hydrogen Energy **35** (2010) 2883–2887.
[100] ZHOU, J., et al., Thermal efficiency evaluation of open-loop SI thermo-chemical cycle for the production of hydrogen, sulphuric acid and electric power, International Journal of Hydrogen Energy **32** (2007)
[101] LEE, Y., et al., Development of HTGR-coated particle fuel technology in Korea, Nuclear Engineering and Design **238** (2008) 2842–2853.
[102] CHO, W., et al., Conceptual design of sulphur-iodine hydrogen production cycle of Korea Institute of Energy Research, Nuclear Engineering and Design **239** (2009) 501–507.

[103] MERRILL, A., LEWINSOHN, W., LEWINSOHN, C., ANDERSON, H., WRIGHT, E., High temperature ceramic heat exchanger materials for SI process, Paper presented at the AIChE Meeting, Cincinnati, OH, USA (2005).
[104] LEYBROS, J., ANZIEU, P., BORGARD, J.M., CARLES, P., RODRIGUEZ, G., CEA studies on S-I industrial scale process, UNLV Consortium Quarterly, University of Las Vegas, USA (2005).
[105] JONES, R.H., THOMAS, G.J., Materials for the hydrogen economy, CRC Press, Boca Raton, USA (2008).
[106] LIBERATORE, R., CEROLI, A., LANCHI, M., SPADONI, A., TARQUINI, P., Experimental vapour-liquid equilibrium data of HI-H_2O-I_2 mixtures for hydrogen production by sulfur-iodine thermochemical cycle, International Journal of Hydrogen Energy **33** (2008) 4283–4290.
[107] HARTMANN, J.M., et al., Speciation of the gaseous phase of the Hi section of the iodine sulfur thermochemical cycle by modeling and investigation of FTIR spectra, International Journal of Hydrogen Energy **34** (2009) 162–168.
[108] BRECHER, L., Electrolytic decomposition of water, US patent 3 888 750 (1975).
[109] BRECHER, L., SPEWOCK, S., WARDE, C., The Westinghouse sulphur cycle for the thermo-chemical decomposition of water, International Journal of Hydrogen Energy **2** (1977) 7–15.
[110] GORENSEK, M., SUMMERS, W., Hybrid sulphur flow-sheets using PEM electrolysis and a bayonet decomposition reactor, International Journal of Hydrogen Energy **34** (2009) 4097–4114.
[111] BARD, A.J., PARSONS, R., JORDAN, J., Standard potentials in aqueous solutions, CRC Press, New York, Marcel-Dekker (1985).
[112] ELDER, R.H., ALLEN, R., Nuclear heat for hydrogen production: coupling a very high/high temperature reactor to a hydrogen production plant, Progress in Nuclear Energy **51** (2009) 500–525.
[113] SUMMERS, W., et al., Hybrid sulphur thermo-chemical process development, DOE hydrogen program FY2007, Annual Progress Report, USA (2007).
[114] MCLAUGHLIN, D., et al., Hydrogen costs for the PBMR thermal reactor and the Westinghouse process, AIChE Annual Meeting, Cincinnati, USA (2005).
[115] BEGHI, G., A decade of research on thermo-chemical hydrogen at the Joint Research Center, Ispra, International Journal of Hydrogen Energy **11** (1986) 761–771.
[116] NATERER, G., et al., Recent Canadian advances in nuclear-based hydrogen production and the thermo-chemical Cu-Cl cycle, International Journal of Hydrogen Energy **34** (2009) 2901–2917.
[117] SADHANKAR, R., Leveraging nuclear research to support the hydrogen economy, International Journal of Energy Research **31** (2007) 1131–1141.
[118] CARTY, R., et al., Thermo-Chemical Hydrogen Production. GRI Report 80-0023, Vol. 1, Gas Research Institute for the Institute of Gas Technology, Chicago, USA (1981).
[119] WANG, Z., NATERER, G., GABRIEL, K., Multiphase reactor scale-up for Cu-Cl thermo-chemical hydrogen production, International Journal of Hydrogen Energy **33** (2008) 6934–6946.
[120] ORHAN, M., DINCER, I., ROSEN, M., Energy and exergy assessments of the hydrogen production step of a copper-chlorine thermo-chemical water splitting cycle driven by nuclear-based heat, International Journal of Hydrogen Energy **33** (2008) 6456–6466.

[121] ROSEN, M., NATERER, G., SADHANKAR, R., SUPPIAH, S., Nuclear-based hydrogen production with a thermo-chemical copper-chlorine cycle and supercritical water reactor (Proc. Canadian Hydrogen Association Workshop, Quebec, Canada, 2006).
[122] LEWIS, M.A., SERBAN, M., BASCO, J.K., Hydrogen production at <550°C using a low temperature thermochemical cycle (Proc. ANS/ENS Exposition. New Orleans, USA, 2003).
[123] EWAN, B., ALLEN, R., Limiting thermodynamic efficiencies of thermo-chemical cycles used for hydrogen production, Green Chemistry **8** (2006) 988–994.
[124] DOKIYA, D., KOTERA, Y., Hybrid cycle with electrolysis using a Cu-Cl system, International Journal of Hydrogen Energy **1** (1976) 117–121.
[125] WANG, Z., et al., Comparison of different copper-chlorine thermo-chemical cycles for hydrogen production, International Journal of Hydrogen Energy **34** (2009) 3267–3276.
[126] NATERER, G., et al., Thermo-chemical hydrogen production with a copper-chlorine cycle. I: Oxygen release from copper oxychloride decomposition, International Journal of Hydrogen Energy **33** (2008) 5439–5450.
[127] NATERER, G., et al., Thermo-chemical hydrogen production with a copper-chlorine cycle. II: Flashing and drying of aqueous cupric chloride, International Journal of Hydrogen Energy **33** (2008) 5451–5459.
[128] KAMEYAMA, H., YOSHIDA, K., Br-Ca-Fe Water decomposition cycles for hydrogen production (Proc. 2nd World Hydrogen Energy Conference, Zurich, Switzerland, 1978) 829–850.
[129] TADOKORO, Y., et al., Technical evaluation of UT-3 thermo-chemical hydrogen production process for an industrial scale plant, International Journal of Hydrogen Energy **22** (1997) 49–56.
[130] SAKURAI, M., TSUTSUMI, A., YOSHIDA K., Analysis of a reaction mechanism in the UT-3 thermo-chemical hydrogen production cycle, International Journal of Hydrogen Energy **21** (1996) 871–875.
[131] NAKAYAMA, T., et al., MASCOT - A bench-scale plant for producing hydrogen by the UT-3 thermo-chemical decomposition cycle, International Journal of Hydrogen Energy **9** (1984) 187–190.
[132] SAKURAI, M., et al., Adiabatic UT-3 thermo-chemical process for hydrogen production, International Journal of Hydrogen Energy **21** (1996) 865–870.
[133] LEMORT, F., LAFON, C., DEDRYVERE, R., GONBEAU, D., Physiochemical and thermodynamic investigation of the UT-3 hydrogen production cycle: A new technological assessment, International Journal of Hydrogen Energy **31** (2006) 906–918.
[134] LOTTES, S.A., et al., Modeling and analysis of calcium bromide hydrolysis. International Journal of Hydrogen Energy **34** (2009) 4155–4167.
[135] SIMPSON, M., UTGIKAR, V., SACHDEV, P., MCGRADY, C., A novel method for producing hydrogen based on the Ca-Br cycle. International Journal of Hydrogen Energy **32** (2007) 505–509.
[136] DOCTOR, R., WADE, D., MENDELSOHN, M., STAR-H2: A calcium-bromine hydrogen cycle using nuclear heat (paper presented at the Spring National Meeting of the American Institute of Chemical Engineers, New Orleans, USA, 2002).
[137] DOCTOR, R., et al., STAR-H2 with a calcium-bromine cycle: Delivering hydrogen, electricity and water from a modular reactor (paper presented at the Spring National Meeting of the American Institute of Chemical Engineers, New Orleans, USA, 2004).

[138] MURADOV, N., VEZIROGLU, T., From hydrocarbon to hydrogen-carbon to hydrogen economy, International Journal of Hydrogen Energy **30** (2005) 225–237.
[139] HORI, M., MATSUI, K., TASHIMO, M. YASUDA, I., Synergistic hydrogen production by nuclear-heated steam reforming of fossil fuels, Progress in Nuclear Energy **47** (2005) 519–526.
[140] KRUGER, P., Appropriate technologies for large-scale production of electricity and hydrogen fuel, International Journal of Hydrogen Energy **33** (2008) 5881–5886.
[141] YILDIZ, B. KAZIMI, M.S., Nuclear energy options for hydrogen and hydrogen-based liquid fuel production, Report MIT-NES-TR001, Massachussetts Institute of Technology (MIT), Cambridge, USA (2003).
[142] SANDELL, L., High-temperature gas-cooled reactors for the production of hydrogen, EPRI Report 1007802, Electric Power Research Institute, Palo Alto, USA (2003).
[143] VERFONDERN, K., NISHIHARA, T., Safety aspects of the combined httr/steam reforming complex for nuclear hydrogen production, Progress in Nuclear Energy **47** (2005) 527–534.
[144] NELSON, P., FLORES, A., FRANCOIS, J., A design-phase PSA of a nuclear-powered hydrogen plant, Nuclear Engineering and Design **237** (2007) 219–229.
[145] FRANCK, H.-G., KNOP, A., Kohleveredlung an der Schwelle der 80er Jahre, Die Naturwissenschaften **67** (1980) 421–430.
[146] TEGGERS, H., JÜNTGEN, H., Stand der Kohlevergasung zur Erzeugung von Brenngas und Synthesegas, Erdöl und Kohle – Erdgas **37** (1984) 163–174.
[147] TURNA, O., Sasol-lurgi fixed bed dry bottom gasification for fuels and chemicals, (paper presented at 2nd Int. Freiberg Conference on IGCC & XtL Technologies, Freiberg, Germany, 2007).
[148] VAN DYK, J.C., KEYSER, M.J., COERTZEN, M., Syngas production from South African coal using sasol-lurgi gasifiers, International Journal of Coal Geology **65** (2006) 243–253.
[149] MESSERSCHMIDT, H., Die Bedeutung nuklearer Verfahren für die Kohlenveredlung, Atomwirtschaft **26** (1981) 467–473.
[150] TAKEI, M., Economic evaluation on gas turbine high temperature reactor GTHTR300, Trans. Atomic Energy Society of Japan **5**(2) (2006) 109–117.
[151] INTERNATIONAL ATOMIC ENERGY AGENCY, Status of design concepts of nuclear desalination plants, IAEA-TECDOC-1326, Vienna (2002).
[152] INTERNATIONAL ATOMIC ENERGY AGENCY, Optimization of the coupling of nuclear reactors and desalination systems, IAEA-TECDOC-1444, Vienna, (2005).
[153] EL-DESSOUKY, H.T., ETTOUNEY, H.M., Multiple-effect evaporation desalination systems: Thermal analysis, Desalination **125** (1999) 259–276.
[154] WATANAWANAVET, S., Optimization of a high-efficiency jet ejector by computational fluid dynamics software, master thesis, Texas A&M University College Station, USA, 2005.
[155] INTERNATIONAL ATOMIC ENERGY AGENCY, Desalination Economic Evaluation Programme (DEEP): IAEA Computer Manual Series No.14, IAEA, Vienna (2000).
[156] DOW CHEMICAL COMPANY AND FILMTEC SOFTWARE, ROSA, 4.0, Midland, MI, USA (2000).
[157] TEWARI, P.K., RAO, I.S., Desalination utilizing waste heat from a nuclear research reactor, Desalination **150** (2002) 45–49.

[158] RAHA, A., RAO, I.S., SRIVASTAVA, V.K., TEWARI, P.K., Sea water desalination utilizing waste heat by low temperature evaporation, International Journal of Nuclear Desalination **2**(4) (2007) 342–352.
[159] HUMPHRIES, J.R. et al, A technical and economic evaluation of the CANDESAL approach in Indonesia using reverse osmosis and waste heat from the CANDU-6 nuclear power plant, Report, Rev. 1, Candesal Enterprises Ltd., Ottawa, Canada (1998).
[160] INTERNATIONAL ATOMIC ENERGY AGENCY, Technical and economic evaluation of potable water production through desalination of seawater by using nuclear energy and other means, Report IAEA-TECDOC-666, IAEA, Vienna (1992).
[161] INTERNATIONAL ATOMIC ENERGY AGENCY, Desalination Economic Evaluation Programme (DEEP): A user's manual, Vienna (2000), Market Potential for Non-Electric Applications of Nuclear Energy. Technical Report Series No. 410, IAEA, Vienna (2002).
[162] INTERNATIONAL ATOMIC ENERGY AGENCY, Nuclear heat applications: Design aspects and operating experience, IAEA-TECDOC-1056, IAEA, Vienna, (1998).
[163] Hydrogen energy and fuel cells — A vision of our future, European Commission, High Level Group Summary Report (2003).
[164] Factoring external natural and man-caused impacts on nuclear and radiation hazardous facilities, Regulatory Document NP-064-05, "Rostechnadzor", Russian Federation (2005).
[165] Rules of design & development of capital construction projects for nuclear plants with reactors of different types, Regulatory Document PiN AE-5.6, Russian Federation (1986).
[166] General requirements for explosion-proof conditions in the chemical, petrochemical and petroleum refining industries, Regulatory Document PB 09-540-03, Russian Federation (2003).
[167] Safety rules to be observed in production of hydrogen by water electrolysis, Regulatory Document PB 03-598-03, Russian Federation (2003).
[168] GROETHE, M., et al., Hydrogen deflagration at large scale (Proc. 15th World Hydrogen Energy Conference, Yokohama, Japan, 2004) paper 28F-01.
[169] SCHNEIDER, H., PFÖRTNER, H., Flammen- und Druckwellenausbreitung bei der Deflagration von Wasserstoff/Luft-Gemischen, Technical Note, Institute for the Chemistry of Fuels and Explosives of the Fraunhofer Gesellschaft, Pfinztal, Germany (1978).
[170] PFÖRTNER, H., The effects of gas explosions in free and partially confined fuel/air mixtures, Propellants, Explosives, Pyrotechnics **10** (1985) 151–155.
[171] BERMAN, M., A critical review of recent large-scale experiments on hydrogen-air detonations, Nuclear Science and Technology **93** (1986) 321–347.
[172] VERFONDERN, K., et al., Contributions to a safety analysis for a hydrogen production system with HTGR (paper presented at 1st Information Exchange Meeting on Nuclear Hydrogen Production, Paris, France, 2000).
[173] MARANGON, A., et al., Safety distances: Definition and values, International Journal of Hydrogen Energy **32** (2007) 2192–2197.
[174] Bekanntmachung der Richtlinie für den Schutz von Kernkraftwerken gegen Druckwellen aus chemischen Reaktionen durch Auslegung der Kernkraftwerke hinsichtlich ihrer Festigkeit und induzierter Schwingungen sowie durch Sicherheitsabstände, Bundesministerium des Innern, Bonn, Germany (1976).

[175] Evaluations of explosions postulated to occur on transportation routes near nuclear power plants, Regulatory Guide 1.91, Revision 1, U.S. Nuclear Regulatory Commission, Rockville, USA (1978).
[176] VERFONDERN, K., Nuclear energy for hydrogen production, Schriftenreihe des Forschungszentrums Jülich, Energy Technology **58**, Jülich, Germany (2007).
[177] NISHIHARA, T., KUNITOMI, K., MURAKAMI, T., Study on the separation distance in the HTGR hydrogen production system (GTHTR300C), HTR2006 (Proc. 3rd Int. Topical Meeting on High Temperature Reactor Technology, Johannesburg, South Africa) paper I00000126 (2006).
[178] VAN DEN BOSCH, C.J.H., WETERINGS, R.A.P.M., Methods for the calculation of physical effects, TNO Yellow Book CPR14E (Part 2), Committee for the Prevention of Disasters, The Hague, Netherlands (1997).
[179] NISHIHARA, T., Progress report Japan, Contribution to IAEA Coordinated Research Project on "Advances in Nuclear Power Process Heat Applications" (2008).
[180] STOLYAREVSKIJ, A.Y., Nuclear-technological complexes based on high-temperature reactors, Energoatomizdat, Moscow (1988).
[181] PONOMAREV-STEPNOY, N., STOLYAREVSKIJ, A., KODOCHIGOV, N., The concept of nuclear hydrogen based on MHR-T reactor, Fourth OECD-NEA Information Exchange Meeting on Nuclear Production of Hydrogen, Chicago, USA (2009).
[182] TAYLOR, J.B., Technical and economic assessment of methods for the storage of large quantities of hydrogen, International Journal of Hydrogen Energy **11** (1986) 5–22.
[183] SHAW, NGNP Hydrogen plant alternatives study, Report NGNP-HPS SHAW-HPA, Revision 1, Cambridge, MA, USA (2009).
[184] Evaluating the habitability of a nuclear power plant control room during a postulated hazardous chemical release, Regulatory Guide 1.78, U.S. Nuclear Regulatory Commission, Rockville, USA (2001).
[185] Emergency response planning guidelines (ERPG) & Workplace environmental exposure levels (WEEL) handbook. American Industrial Hygiene Association (AIHA), Fairfax, USA (2007).
[186] MURAKAMI, T., et al., Safety assessment of VHTR hydrogen production system against fire, explosion and acute toxicity, Transactions of the Atomic Energy Society of Japan **7** (2008) 231–141 (in Japanese).
[187] RAHA, A., et al., Safety aspects of nuclear desalination plant, reliability, safety and hazards, Narosa Publishing House, ISBN 81-7319-729-6 (2006) 717–723.
[188] INTERNATIONAL ATOMIC ENERGY AGENCY, International basic safety standards for protection against ionizing radiation and for the safety of radiation sources, Safety Series No. 115, IAEA, Vienna (1996).
[189] Estimated per capita water ingestion and body weight in the United States - An update, Report EPA-822-R-00-001, U.S. Environmental Protection Agency, Washington DC (2004).
[190] Verordnung über den Schutz vor Schäden durch ionisierende Strahlen (Strahlenschutzverordnung – StrlSchV) in der Fassung vom 30. Juni 1989 (BGBl. I S. 1321, zuletzt geändert 1997), Bundesministerium für Umwelt, Naturschutz und Reaktorsicherheit, Bonn (1989).
[191] Verordnung über den Schutz vor Schäden durch ionisierende Strahlen (Strahlenschutzverordnung - StrlSchV). Version of July 20, 2001, with latest changes made on August 29, 2008, BMJ, Berlin (2001).

[192] NRB-99, Ionizing radiation, radiation safety, Norms of Radiation Safety, SP-2.6.1. 58-99, Minzdrav, Moscow (1999).
[193] Sanitary rules for design and operation of nuclear plants, SANPIN 2.6.1.24-03, Moscow (2003).
[194] WICHNER, R., DYER, F., Distribution and transport of tritium in the peach bottom HTGR, Report ORNL-5497, Oak Ridge National Laboratory, USA (1979).
[195] INTERNATIONAL ATOMIC ENERGY AGENCY, Status of Non-Electric Nuclear Heat Applications: Technology and Safety, IAEA-TECDOC-1184, IAEA, Vienna (2000).
[196] ADAK, A.K., RAO, I.S., SRIVASTAVA, V.K., TEWARI, P.K., Nuclear desalination by waste heat utilization in an advanced heavy water reactor, International Journal of Nuclear Desalination **2** (2007) 234–243.
[197] PANICKER, S.T., TEWARI, P.K., Safety and reliability aspects of seawater reverse osmosis desalination plant of nuclear desalination demonstration project, International Journal of Nuclear Desalination **2** (2007) 244-252.
[198] YOUNOS, T., Environmental issues of desalination, Journal of Contemporary Water Research & Education **Issue 132** (2005) 11–18.
[199] HOEPNER, T., A procedure for environmental impact assessment (eia) for sea water desalination plant, Desalination **124** (1999) 1–12.
[200] EINAV, R., HARUSS, I K., PERRY, D., The foot print of the desalination processes on the environment, Desalination **152** (2002) 141–154.
[201] MEERGANZ VON MEDEAZZA, G.L., Direct and socially-induced environmental impacts of desalination, Desalination **185** (2005) 57–70.
[202] MORTON, A.J., et al., environmental impacts of seawater distillation and reverse osmosis processes, Desalination **108** (1997) 1–10.
[203] FINAN, M.A., SMITH, S., EVANS, C.K., MUIR, J.W.H., Belgard@ Ev - 15 Years' experience in scale control, Desalination **73** (1989) 341–357.
[204] TAWABINI, B., et. al., Trihalomethanes (THMs) formation in a distillation process, Desalination **66** (1987) 403–414.
[205] SHAMS EL DIN, A.M., et al., Electricity and water production in the emirate of abu dhabi and its impact on the environment, Desalination **97** (1994) 373–388.
[206] CHINA Energy Statistical Yearbook (2008).
[207] Statistical year text base, International Energy Agency, Paris (2006).
[208] CHINA Statistical Yearbook (2008).
[209] OUYANG Y, China Nuclear Power **1** (2008), pp 194–201 (in Chinese).
[210] SHI D., Chinese hydrogen update, Presentation at the 5th IPHE Steering Committee Meeting 28-29 March, Vancouver, Canada (2006).
[211] SUN, Y., XU, J., ZHANG, Z., R&D Effort on nuclear hydrogen production technology in China, International Journal of Nuclear Hydrogen Production and Applications **1** (2006) 104–111.
[212] BAI, Y., ZHANG, P., QU, Y.S., Fundamental study on the bunsen reaction in the thermochemical iodine-sulfur cycle, Applied Chemistry (in Chinese) **22** 3 (2009) 292–296.
[213] CHEN, S.Z., et al., HI concentration of HI_x ($HI-H_2O-I_2$) solution in iodine-sulfur water-splitting cycle by electro-electrodialysis, Xi'an Jiaotong University Xuebao **42** (2008) 2522–2555.
[214] JIN, M.M., ZHANG, P., WANG, J.C., Catalysts for decomposition of sulfuric acid in the iodine-sulfur process, Industrial Catalysis (in Chinese) **15** 8 (2007) 15-19.
[215] BAI, Y., et al., Purification of H_2SO_4 and HI phases in IS process, Chinese Journal of Chemical Engineering **17** (2009) 160–166.

[216] LIU, M.Y., et al., Thermodynamic analysis of the efficiency of high temperature steam electrolysis (HTSE) system for hydrogen production, Journal of Power Sources **177** (2008) 493–499.
[217] YU, B., et al., Research advance on highly efficient hydrogen production by high temperature steam electrolysis, Science in China Series B: Chemistry **51** (2008) 289–304.
[218] YU, B., et al., Status and research of highly efficient hydrogen production through high temperature steam electrolysis at INET, Paper presented at the Fourth International Hydrogen Forum, Changsha, China, 2008.
[219] LIU, M.Y., et al., Two-dimensional simulation and critical efficiency analysis of high-temperature steam electrolysis system for hydrogen production, Journal of Power Sources **183** (2008) 708–712.
[220] YU, B., et al., Microstructural characterization and electrochemical properties of $Ba_{0.5}Sr_{0.5}Co_{0.8}Fe_{0.2}O_{3-\delta}$ and its application for anode of SOEC, International Journal of Hydrogen Energy **33** (2008) 6873–6877.
[221] LIANG, M.D., YU, B., XU, J.M., Preparation of LSM–YSZ composite powder for anode of solid oxide electrolysis cell and its activation mechanism, Journal of Power Sources **190** (2009) 341–345.
[222] KIRCHHOFF, R., et al., Operation of a semi-technical pilot plant for nuclear aided steam gasification of coal, Nuclear Engineering and Design **78** (1984) 233–239.
[223] KUBIAK, H., VAN HEEK, K.H., ZIEGLER, A., Nukleare Kohlevergasung – Erreichter Stand, Einschätzung und Nutzung der Ergebnisse. Fortschritte in der Energietechnik, Monographien des Forschungszentrums Jülich, Vol. 8, Jülich, Germany (1993).
[224] BARNERT, H., SINGH, Y., Design evaluation of a small high-temperature reactor for process heat applications, Nuclear Engineering and. Design **109** (1988) 245–251.
[225] SCHRADER, L., STRAUSS, W., TEGGERS, H., The application of nuclear process heat for hydrogasification of coal, Nuclear Engineering and Design **34** (1975) 51–57.
[226] FLADERER, R., SCHRADER, L., Hydrierende Vergasung von Kohle – Neuere Betriebsergebnisse, Chemie-Ingenieur-Technik **54** (1982) 884–892.
[227] SCHARF, H.-J., SCHRADER, L., TEGGERS, H., Results from the operation of a semitechnical test plant for brown coal hydrogasification, Nuclear Engineering and Design **78** (1984) 223–231.
[228] CHANG, H.J., YEO, W., "Advanced design features adopted in SMART" (paper presente at IAEA International Seminar on Status and Prospects for Small and Medium Sized Reactors, Cairo, Egypt, 2001), IAEA-SR-218/28, IAEA, Vienna, (2002).
[229] EL-DESSOUKY, H.T., ETTOUNEY, H.M., Development and progress of the single and multiple-effect evaporation desalination process, Paper presented at the Water Desalination Workshop, Cairo, Egypt, 2000.
[230] ROINE, A., Outokumpu HSC chemistry for windows, 93001-ORGT version 2.0. Outokumpu Research Oy Information Service (1994).
[231] INTERNATIONAL CENTRE FOR DIFFRACTION DATA, Powder diffraction file, Joint Committee for Powder Diffraction Standards, Newtown Square, PA, USA, 1997.
[232] LONG, G.J., Mössbauer spectroscopy applied to inorganic chemistry, Plenum Publishing Corporation **2**, USA (1987) 513–514.
[233] SOHN, H.Y., ZHOU, L., The chlorination kinetics of beneficiated ilmenite particles by CO + Cl_2 mixtures, The Chemical Engineering Journal **72** (1999) 37–42.

[234] GENNARI, F.C., BOHÉ, A.E., PASQUEVICH, D.M., Effect of the temperature on the chlorination of Fe_2O_3-TiO_2-C mixture, Thermochimica Acta **302** (1997) 53–61.
[235] LONG, G.J., Mössbauer spectroscopy applied to inorganic chemistry, Plenum Publishing Corporation **1** (1984) 67–68.
[236] TITÍ-MANYAKA, R., IWASAKI, I., Chlorination behaviours of complex iron copper and nickel sulphides, Society of Mining Engineers, AIME **260** (1976) 282–288.
[237] KANARI, N., GABALLAH, I., ALLAIN, E., Kinetics of oxychlorination of chromite (Part I: Effect of Temperature, Part II: Effect of reactive gases). Thermochimica Acta **373** (2001) 75–93.
[238] KANARI, N., GABALLAH, I., ALLAIN, E., MENAD, N., Chlorination of chalcopyrite concentrates, Metallurgical and Material Transactions B **30B** (1999) 567–576.
[239] TAMAGAWA, T., FU, N.X., KOBAYASHI, M., IWASAKI, I., Extraction of copper from chalcopyrite concentrates without sulfuric acid generation via chlorination, Part 3: integration of gaseous chlorination and selective oxidation. Minerals and Metallurgical Processing **18**(4) (2001) 209–214.
[240] KUMAR, M. L., LI, K., WARREN, W.G., Kinetics and modeling of the gas-phase chlorination of chalcopyrite - I. reactions with powder, Canadian Metallurgical Quarterly **26**(1) (1987) 29–36.
[241] VIRČIKOVÁ, E., MOLNÁR, L., Recovery of copper from dump slag by a segregation process, Resources, Conservation and Recycling **6**(2) (1992) 133–138.
[242] MATSUMARU, K., SUSA, M., NAGATA, K., Removal of copper from iron-based scraps by O_2-Cl_2 gas mixtures, Tetsu-To-Hagane (Iron and Steel), Journal of the Iron and Steel Institute of Japan **82** 10 (1996) 1–6.
[243] SIEMENS, R.E., JONG, B.J., RUSSELL, J.H., potential of spent catalysts as a source of critical metals, Conservation & Recycling **9** 2 (1986) 189–196.
[244] GABALLAH, I., DJONA, M., MUGICA, J.C., SOLOZABAL, R., valuable metals recovery from spent catalysts by selective chlorination, Resources, Conservation and Recycling **10** 1–2 (1994) 87–96.
[245] BOURHILA, N., et al., Thermodynamic and experimental study of Cu-LPCVD by reduction of copper chloride, Applied Surface Science **91** (1995) 175–181.
[246] ULLMANN`s Encyclopedia of Industrial Chemistry, 6th Edition, Electronic Release (2002).
[247] REMEIKA, J.P., BATTLOGG, B., Synthesis of CuCl, Materials Research Bulletin **15** (1980) 1179–1182.
[248] SESSELMANN, W., CHUANG, T.J., The interaction of chlorine with copper, I. adsorption and surface reaction, Surface Science **176** 1–2 (1986) 32–66.
[249] SESSELMANN, W., CHUANG, T.J., The interaction of chlorine with copper, II. bulk diffusion, Surface Science **176** 1–2 (1986) 67–90.
[250] CAHN, R.W., HAASEN, P., KRAMER, E.J., refractory metals and their alloys, Materials Science and Technology, VCH, Germany (1996).
[251] PASQUEVICH, D.M., CANEIRO, A.M., A Thermogravimetric analyser for corrosive atmospheres and its application to the chlorination of ZrO_2-C mixtures, Thermochimica Acta **156** 2 (1989) 275–283.
[252] FLYNN, J.H., Thermal analysis kinetics problems, pitfalls and how to deal with them, Journal of Thermal Analysis **34** (1988) 367–381.
[253] RICHARDSON, H.W., Copper compounds - salts and basic salts, Ullmann's Encyclopedia of Industrial Chemistry, 6th Edition, Electronic Release (2002).
[254] DE MICCO, G., BOHÉ, A.E., PASQUEVICH, D.M., A thermogravimetric study of copper chlorination, Journal of Alloys and Compounds **437** (2007) 351–359.

[255] TITÍ-MANYAKA, R., IWASAKI, I., Thermogravimetric investigation of the chlorination behaviours of some common metals and their oxides, Transactions of the Society of Mining Engineers (SME) **252** (1972) 307–313.
[256] BELKNAP, L.S., Aluminum trichloride production, US Pat. 3 721 731, Cabot Corporation, Boston, Massachusetts, USA, 1973.
[257] LANDSBERG, A., Chlorination of binary alloys (SiGe, MoRe and AuPt), Journal of the Less-Common Metals **159** (1990) 163–172.
[258] CHANG, Y.N., WEI, F.I., High-temperature chlorine corrosion of metals and alloys - A review, Journal of Material Science **26** (1991) 3693–3698.
[259] DE MICCO, G., PASQUEVICH, D.M., BOHÉ, A.E., Chlorination of aluminium-copper alloys, Thermochimica Acta **457** (2007) 83–91.
[260] GONZÁLEZ, J.A., GENNARI, F.C., DEL CARMEN RUIZ, M., BOHÉ, A.E., PASQUEVICH, D.M., Kinetics of the carbochlorination of columbite, Transactions of the Institution of Mining and Metallurgy, Section C 107 (1998) 130–138.
[261] CHAUDHARY, J.A., DONALDSON, J.D., GRIMES, S.M., Heavy-metals in the environment, The use of high copper-zinc residues in the zinc-chloride process and the recovery of copper as anhydrous copper(II) chloride, Journal of Chemical Technical Biotechnology **61** (1994) 293–297.
[262] FERRY, D., CASTRILLEJO, Y., PICARD, G., Zinc metal electrodeposition reaction process in $ZnCl_2 \cdot 2NaCl$ melt, Electrochimica Acta **33** (1988) 1661–1667.
[263] FERRY, D., CASTRILLEJO, Y., PICARD, G., Acidity and purification of the molten zinc chloride (33.4 mol%)-sodium chloride (66.6 mol%) mixture, Electrochimica Acta **34** (1989) 313–316.
[264] CASTRILLEJO, Y., GARCIA, M.A., BARRADO, E., PASQUIER, P., PICARD, G., Chemical and electrochemical behaviour of indium ions in the $ZnCl_2 \cdot 2NaCl$ melt at 450°C, Electrochimica Acta **40** (1995) 2731–2738.
[265] CASTRILLEJO, Y., MARTINEZ, A.M., VEGA, M., BARRADO E., PICARD, G., Electrochemical study of the properties of iron ions in $ZnCl_2$ + 2NaCl melt at 450°C, Journal of Electroanalytical Chemistry **397** (1995) 139–147.
[266] GARCIA, M., CASTRILLEJO, Y., PASQUIER, P., PICARD, G., Molten Salt Forum 1993/1994 **1-2** (1993) 47.
[267] VILLARS, P., Pearson's Handbook of Crystallographica Data for Intermetallic Phases, page 3027, ASM International, Materials Park, USA (1991).
[268] HILDENBRAND, D.L., LAU K.H., Thermochemistry of ZnCl(g), Journal of Chemical Physics **111** (1999) 1337–1338.
[269] LIDE, D.R. (Ed.), CRC Handbook of Chemistry and Physics, 85th Edition 2004–2005, pages 4-95, CRC Press (2004).
[270] BOHÉ, A.E., ANDRADE GAMBOA, J.J., LOPASSO, E.M., PASQUEVICH, D.M., Zirconium recovery from zircaloy shavings, Journal of Materials Science **31** (1996) 3469–3474.
[271] GALVELE, J.R., DUFFÓ, G.S., Degradación de materiales corrosión, Monografía Tecnológica nro. 3., UNSAM, CNEA, Instituto Sabato, Buenos Aires, Argentina (2006).
[272] DE MICCO, G., FOUGA, G.G., BOHÉ, A.E., Chlorination of zinc oxide between 723 and 973 K, Metallurgical and Materials Transactions B **38** 6 (2007) 853–862.
[273] PDS, Powder diffraction file, Joint Committee for Powder Diffraction Standards, International Center for Diffraction Data (2001).
[274] VAN VELZEN, D., LANGENKAMP, H., Problems around Fe-Cl cycles, International Journal of Hydrogen Energy **3** (1978) 419–429.
[275] KNOCHE, K.F., CREMER, H., STEINBORN, G., A thermochemical process for hydrogen production, International Journal of Hydrogen Energy **1** (1976) 23–32.

[276] VAN VELZEN, D., LANGENKAMP, H., Development studies on thermochemical cycles for hydrogen production, International Journal of Hydrogen Energy **2** (1977) 107–121.
[277] DANG, V.D., STEINBERG, M., hydrogen production using fusion energy and thermochemical cycles, International Journal of Hydrogen Energy **5** (1980) 119–129.
[278] SOLIMAN, M.A., CONGER, W.L., CARTY, R.H., FUNK, J.E., COX, K.E., Hydrogen production via thermochemical cycles based on sulfur chemistry, International Journal of Hydrogen Energy **1** (1976) 265–270.
[279] KNOCHE, K.F., CREMER, H., STEINBORN, G., SCHNEIDER, W., Feasibility studies of chemical reactions for thermochemical water splitting cycles of the iron-chlorine, iron-sulfur and manganese-sulfur families, International Journal of Hydrogen Energy **2** (1997) 269–289.
[280] YALÇIN, S., A Review of nuclear hydrogen production, International Journal of Hydrogen Energy **14** (1989) 551–561.
[281] CREMER, H., et al., status report on thermochemical iron/chlorine cycles: a chemical engineering analysis of one process, International Journal of Hydrogen Energy **5** (1980) 231–252.
[282] ANDRESS, R.J., HUANG, X.Q., BEQUETTE, B.W., MARTIN, L.L., A systematic methodology for the evaluation of alternative thermochemical cycles for hydrogen production, International Journal of Hydrogen Energy **34** (2009) 4146–4154.
[283] GOLOVKO, V.F., et al., Development of a high-temperature intermediate heat exchanger for the VG-400 nuclear energotechnological plant, Issues of Nuclear Power and Engineering. Series: Nuclear Hydrogen Power and Technology **1** 11 (1982).
[284] MITENKOV, F.M., Designing of heat exchangers for nuclear power plants, Energoatomizdat (1988).
[285] YASUSHI, Elements of the experimental very high temperature gas cooled reactor. translated from Japanese, News of the BSSR Academy of Science. Series: Physics and Power Science **1** (1983).
[286] KUNITOMI, K., TAKEDA, T., HORIE, T., IWATA, K., "Development of compact heat exchanger with diffusion welding", Design and Development of Gas Cooled Reactors with Closed Cycle Gas Turbines, IAEA-TECDOC-899, IAEA, Vienna (1996) 165–176.
[287] LIDSKY, L.M., YAN, X.L., Modular gas-cooled reactors gas turbine power plant design (Proc. 2nd JAERI Symposium on HTGR Technologies, Oarai, Japan, 1992), Report JAERI-M 92-215, Japan Atomic Energy Research Institute, Oarai, Japan, (1993) 381–395.
[288] SOUTHALL, D., LE PIERRES, R., DEWSON, S.J., Design considerations for compact heat exchangers,(Proc. Int. Congress Anaheim, USA) ICAPP'08, USA (2008) paper 8009.
[289] WALRAVENS, M.J., MCIVER, R.F., HOSEGOOD, S.B., Preliminary orientation and parametric survey for very high temperature reactors with intermediate heat exchangers Gas-Cooled Reactors with Emphasis on Advanced Systems (Proc. Symp., Jülich, 1975), IAEA-SM-200/57, IAEA, Vienna (1976) 255–274.
[290] TAKIZUKA, T., "Reactor technology development under the HTTR project", Innovative Nuclear Energy Systems for Sustainable Development of the World (1st COE-INES International Symposium INES-1, Tokyo, 2004), Progress in Nuclear Energy **47** (2005) 283–291.
[291] GERASIMOV, V.V., MONAKHOV, A.S., Materials for nuclear engineering, Atomizdat (1973).

[292] DOLBENKO, Y.G., et al., Materials for VG-400 plant steam generators, Issues of Nuclear Power and Engineering. Series: Nuclear Hydrogen Power and Technology **1** (1983) 14.
[293] DUSHIN, Y.A., et al., Materials for high-temperature equipment in the helium coolant of power plants, Nuclear Hydrogen Power and Technology, Energoatomizdat **5** (1983).
[294] KUGELER, K., KUGELER, M., NIESSEN, H.F., HARTH, R., The development of helium-heated steam reformers, IAEA International Symposium on Gas-Cooled Reactors with Emphasis on Advanced Systems, paper IAEA-SM-200/29, Jülich, Germany, 1975.
[295] KUGELER, K., KUGELER, M., NIESSEN, H.F., HAMMELMANN, K.H., Steam reformers heated by helium from high temperature reactors, Nuclear Engineering and Design **34** (1975) 129–145.
[296] JONES, A.R., BOX, P.O., A very high temperature reactor (VHTR), Technology Record 1 of the Intersociety Energy Conversion Engineering Conference, Newark, USA (1975) 329–337.
[297] KIRYUSHIN, A.I., KUZAVKOV, N.G., BULYGIN, V.V., GOLOVKO, V.F., Design features of VG-400 and VGM reactor plant equipment (Bilateral Meeting with Specialists from Japan, OKBM, Nizhny Novgorod, Russia, 1992).
[298] DU TOIT, C.G., VAN RAVENSWAAY, J., PLESSIS, G., The impact of separation distance between reactor and process on the choice of secondary heat transport coolant for high temperature process heat applications (Proc. 3rd Int. Topical Meeting on High Temperature Reactor Technology HTR2006, Johannesburg, South Africa, 2006).
[299] KHARLAMOV A.G., KOREGIN YU.A., Thermal insulation, M.: IzdAT, 1998-224s, ISBN 5-283-86656, UDK 621.039.53 (1998).
[300] ZHOU, H.Z., WANG, J., Helium circulator design and testing, Nuclear Engineering and Design **218** (2002) 189–198.
[301] MAKSYANIN, A.I., NOVINSKY, E.G., TUMASHEN, R.Z., Gas circulators for NPP gas-cooled reactors, NIIEinformenergomash No. 2-80-01 (1980).
[302] MANUSHIN, E.A., BEKNEV, V.S., OSIPOV, M.I., SUROVTSEV, I.G., Nuclear gas-turbine and integrated plants, Energoatomizdadt (1983) 125–135.
[303] KAWASAKI, K., SAITO, K., IYOKU, T., Characteristics of DC electrical breaking method of the gas circulator to limit the temperature rise at the heat transfer pipes in the HTTR, Safety Related Design and Economic Aspects of HTGRs, IAEA TECDOC-1210, IAEA, Vienna (2001) 167–179.
[304] MCDONALD, C.F., NICHOLS, M.K., Helium circulator design considerations for modular high temperature gas-cooled reactor plant (paper presented at 32nd ASME International Gas Turbine Conference, Anaheim, USA, 1987) paper N 87-GT-138.
[305] MCDONALD, C.F., Active magnetic bearings for gas turbomachinery in closed-cycle power plant systems (paper presented at ASME International Gas Turbine and Aeroengine Congress and Exhibition, Amsterdam, The Netherlands, 1988) paper N 88-GT-156.
[306] KIRYUSHIN, A.I., KOSTIN, V.I., NOVINSKY, E.G., SMIRNOV, V.P., Experience in development of large HTGR helium circulator, Tyazheloye mashinostroyenie No. 11-12 (1998) 15–17.

ABBREVIATIONS

AC/DC	alternating current/direct current
AECL	atomic energy of canada limited
AEGL	acute exposure guideline level
AGR	advanced gas reactor
ASR	area specific resistance
BARC	Bhabha Atomic Research Centre
BET	Brunauer-Emmett-Teller N_2 absorption
BSCF	$Ba_{0.5}Sr_{0.5}Co_{0.8}Fe_{0.2}O_{3-\delta}$
CEA	Commissariat à l'energie atomique
CFD	computer fluid dynamics
CHP	combined heat and power
CRP	coordinated research project
EDS	energy dispersive spectroscopy
EED	electro-electro dialysis
ENEA	Agenzia nazionale per le nuove tecnologie, l'energia e lo sviluppo economico sostenibile
EPA	US Environmental Protection Agency
FESEM	field-emission scanning electron microscope
FTIR	fourier transform infrared spectroscopy
GCC	grand composite curve
GOR	gain output ratio
GTHTR300	Gas turbine high temperature reactor of 300 MW(e)
GTHTR300C	GTHTR300 cogeneration
GT-MHR	gas turbine - modular helium reactor
HHV	higher heating value
HP	high pressure
HPC	high pressure compressor
HPMR	hydrogen permselective membrane reactor
HTGR	high temperature gas cooled reactor
HTSE	high temperature steam electrolysis
HTTR	high temperature engineering test reactor
HyS	hybrid sulphur cycle
IDLH	immediately dangerous to life and health
IHX	intermediate heat exchanger

IL	isolation loop
INET	Institute for Nuclear and New Energy Technology
INL	Idaho National Laboratory
JAEA	Japan Atomic Energy Agency (former JAERI)
JRC	Joint research center
KAERI	Korean atomic energy research institute
LHV	lower heating value
LLE	liquid-liquid equilibrium
LOFC	loss-of-forced-convection accident
LP	low pressure
LPC	low pressure compressor
LSC	strontium doped lanthanum chromite $La(Sr)CrO_3$
LSCF	strontium and cobalt doped lanthanum iron oxide $La(Sr,Co)FeO_3$
LSM	$La(Sr)MnO_3$
LT	low temperature
LTE	low temperature evaporation
LT-HTME	low temperature – horizontal tube multi effect
MED	multi-effect desalination
MEE	multi-effect evaporation
MSF	multi-stage flash
MVC	mechanical vapour compression
NDP	nuclear desalination plant
NGNP	next generation nuclear plant
NHI	nuclear hydrogen initiative
NHSS	nuclear heat supply system
NOAK	N^{th} of a kind
NPV	net present value
NRC	US Nuclear Regulatory Commission
NSSS	nuclear steam supply system
PBMR	pebble bed modular reactor
PCHE	printed circuit heat exchanger
PCU	power conversion unit
PEM	proton exchange membrane
PHTS	primary heat hransport system

PNP	prototype nuclear process heat reactor
PRV	pressure relief valve
PTA	problem table algorithm
PTFE	polytetrafluoroethylene
PWR	pressurized water reactor
RCCS	reactor cavity cooling system
RO	reverse osmosis
RPM	revolutions per minute
SDE	SO_2 depolarized electrolyzer
SEM	scanning electron microscopy
SHTS	secondary heat transport system
S-I	sulphur-iodine cycle
SLE	solid-liquid equilibrium
SMART	system integrated modular advanced reactor
SMR	steam methane reforming
SNG	substitute natural gas
SNL	Sandia National Laboratory
SRNL	Savannah River National Laboratory
SOEC	solid oxide electrolysis cell
SOFC	solid oxide fuel cell
STAR	secure transportable autonomous reactor
TDS	total dissolved salts
TEM	transmission electron microscopy
TG	thermogravimetry
TGA	thermogravimetric analyzer
TNT	2,4,6-trinitrotoluene ($c_7h_5n_3o_6$)
TVC	thermal vapour compression
UT-3	University of Tokyo
VLE	vapour-liquid equilibrium
XRD	x ray diffraction
YSZ	yttria stabilized zirkonium

CONTRIBUTORS TO DRAFTING AND REVIEW

Bhanja, Kalyan	Bhabha Atomic Research Centre, Trombay, Mumbai, India
Bohé, Ana Ester	Comisión national de energía atómica, Bariloche, Argentina
Golovko, Vladislav F.	OKBM, Nizhny Novgorod, Russian Federation
Greyvenstein, Renée	PBMR, Centurion, South Africa
Herring, J. Stephen	Idaho National Laboratory, Idaho Falls, USA
Khamis, Ibrahim	International Atomic Energy Agency
Kodochigov, Grigory	OKBM, Nizhny Novgorod, Russian Federation
Malshe, Unmesh D.	Bhabha Atomic Research Centre, Trombay, Mumbai, India
Maphalala, Nhlanhla G.	PBMR, Centurion, South Africa
Mohan, Sadhana	Bhabha Atomic Research Centre, Trombay, Mumbai, India
Nassini, Horacio Elio Pablo	Comisión national de energía atómica, Bariloche, Argentina
Nisan, Simon	CEA, Cadarache, France
Nishihara, Tetsuo	Japan Atomic Energy Agency, Oarai, Japan
Platonova, Tatiana E.	OKBM, Nizhny Novgorod, Russian Federation
Prabhakar, S.	Bhabha Atomic Research Centre, Trombay, Mumbai, India
Prasad, Chaganti Santhi R.	Bhabha Atomic Research Centre, Trombay, Mumbai, India
Raha, Abhigit	Bhabha Atomic Research Centre, Trombay, Mumbai, India
Suleiman, Suheil	Damascus, Syrian Arab Republic
Sun, Yuliang	INET, Tsinghua University, Beijing, China
Suppiah, Sam	Chalk River Laboratories, Canada
Tewari, Pradip K.	Bhabha Atomic Research Centre, Trombay, Mumbai, India
Verfondern, Karl	Research Center Jülich, Jülich, Germany
Yan, Xing S.	Japan Atomic Energy Agency, Oarai, Japan
Zhang, Ping	INET, Tsinghua University, Beijing, China
Zhou, Zhiwei	INET, Tsinghua University, Beijing, China

Research Coordination Meetings

Vienna, Austria, 24–26 September 2007

Vienna, Austria, 1–3 July 2008

Vienna, Austria, 7–9 July 2009

Consultants Meeting

Vienna, Austria, 27–29 September 2010

IAEA
International Atomic Energy Agency

Where to order IAEA publications

In the following countries IAEA publications may be purchased from the sources listed below, or from major local booksellers. Payment may be made in local currency or with UNESCO coupons.

AUSTRALIA
DA Information Services, 648 Whitehorse Road, MITCHAM 3132
Telephone: +61 3 9210 7777 • Fax: +61 3 9210 7788
Email: service@dadirect.com.au • Web site: http://www.dadirect.com.au

BELGIUM
Jean de Lannoy, avenue du Roi 202, B-1190 Brussels
Telephone: +32 2 538 43 08 • Fax: +32 2 538 08 41
Email: jean.de.lannoy@infoboard.be • Web site: http://www.jean-de-lannoy.be

CANADA
Bernan Associates, 4501 Forbes Blvd, Suite 200, Lanham, MD 20706-4346, USA
Telephone: 1-800-865-3457 • Fax: 1-800-865-3450
Email: customercare@bernan.com • Web site: http://www.bernan.com

Renouf Publishing Company Ltd., 1-5369 Canotek Rd., Ottawa, Ontario, K1J 9J3
Telephone: +613 745 2665 • Fax: +613 745 7660
Email: order.dept@renoufbooks.com • Web site: http://www.renoufbooks.com

CHINA
IAEA Publications in Chinese: China Nuclear Energy Industry Corporation, Translation Section, P.O. Box 2103, Beijing

CZECH REPUBLIC
Suweco CZ, S.R.O., Klecakova 347, 180 21 Praha 9
Telephone: +420 26603 5364 • Fax: +420 28482 1646
Email: nakup@suweco.cz • Web site: http://www.suweco.cz

FINLAND
Akateeminen Kirjakauppa, PO BOX 128 (Keskuskatu 1), FIN-00101 Helsinki
Telephone: +358 9 121 41 • Fax: +358 9 121 4450
Email: akatilaus@akateeminen.com • Web site: http://www.akateeminen.com

FRANCE
Form-Edit, 5, rue Janssen, P.O. Box 25, F-75921 Paris Cedex 19
Telephone: +33 1 42 01 49 49 • Fax: +33 1 42 01 90 90
Email: formedit@formedit.fr • Web site: http://www. formedit.fr

Lavoisier SAS, 145 rue de Provigny, 94236 Cachan Cedex
Telephone: + 33 1 47 40 67 02 • Fax +33 1 47 40 67 02
Email: romuald.verrier@lavoisier.fr • Web site: http://www.lavoisier.fr

GERMANY
UNO-Verlag, Vertriebs- und Verlags GmbH, Am Hofgarten 10, D-53113 Bonn
Telephone: + 49 228 94 90 20 • Fax: +49 228 94 90 20 or +49 228 94 90 222
Email: bestellung@uno-verlag.de • Web site: http://www.uno-verlag.de

HUNGARY
Librotrade Ltd., Book Import, P.O. Box 126, H-1656 Budapest
Telephone: +36 1 257 7777 • Fax: +36 1 257 7472 • Email: books@librotrade.hu

INDIA
Allied Publishers Group, 1st Floor, Dubash House, 15, J. N. Heredia Marg, Ballard Estate, Mumbai 400 001,
Telephone: +91 22 22617926/27 • Fax: +91 22 22617928
Email: alliedpl@vsnl.com • Web site: http://www.alliedpublishers.com

Bookwell, 2/72, Nirankari Colony, Delhi 110009
Telephone: +91 11 23268786, +91 11 23257264 • Fax: +91 11 23281315
Email: bookwell@vsnl.net

ITALY
Libreria Scientifica Dott. Lucio di Biasio “AEIOU”, Via Coronelli 6, I-20146 Milan
Telephone: +39 02 48 95 45 52 or 48 95 45 62 • Fax: +39 02 48 95 45 48
Email: info@libreriaaeiou.eu • Website: www.libreriaaeiou.eu

JAPAN
Maruzen Company, Ltd., 13-6 Nihonbashi, 3 chome, Chuo-ku, Tokyo 103-0027
Telephone: +81 3 3275 8582 • Fax: +81 3 3275 9072
Email: journal@maruzen.co.jp • Web site: http://www.maruzen.co.jp

REPUBLIC OF KOREA
KINS Inc., Information Business Dept. Samho Bldg. 2nd Floor, 275-1 Yang Jae-dong SeoCho-G, Seoul 137-130
Telephone: +02 589 1740 • Fax: +02 589 1746 • Web site: http://www.kins.re.kr

NETHERLANDS
De Lindeboom Internationale Publicaties B.V., M.A. de Ruyterstraat 20A, NL-7482 BZ Haaksbergen
Telephone: +31 (0) 53 5740004 • Fax: +31 (0) 53 5729296
Email: books@delindeboom.com • Web site: http://www.delindeboom.com

Martinus Nijhoff International, Koraalrood 50, P.O. Box 1853, 2700 CZ Zoetermeer
Telephone: +31 793 684 400 • Fax: +31 793 615 698
Email: info@nijhoff.nl • Web site: http://www.nijhoff.nl

Swets and Zeitlinger b.v., P.O. Box 830, 2160 SZ Lisse
Telephone: +31 252 435 111 • Fax: +31 252 415 888
Email: infoho@swets.nl • Web site: http://www.swets.nl

NEW ZEALAND
DA Information Services, 648 Whitehorse Road, MITCHAM 3132, Australia
Telephone: +61 3 9210 7777 • Fax: +61 3 9210 7788
Email: service@dadirect.com.au • Web site: http://www.dadirect.com.au

SLOVENIA
Cankarjeva Zalozba d.d., Kopitarjeva 2, SI-1512 Ljubljana
Telephone: +386 1 432 31 44 • Fax: +386 1 230 14 35
Email: import.books@cankarjeva-z.si • Web site: http://www.cankarjeva-z.si/uvoz

SPAIN
Díaz de Santos, S.A., c/ Juan Bravo, 3A, E-28006 Madrid
Telephone: +34 91 781 94 80 • Fax: +34 91 575 55 63
Email: compras@diazdesantos.es, carmela@diazdesantos.es, barcelona@diazdesantos.es, julio@diazdesantos.es
Web site: http://www.diazdesantos.es

UNITED KINGDOM
The Stationery Office Ltd, International Sales Agency, PO Box 29, Norwich, NR3 1 GN
Telephone (orders): +44 870 600 5552 • (enquiries): +44 207 873 8372 • Fax: +44 207 873 8203
Email (orders): book.orders@tso.co.uk • (enquiries): book.enquiries@tso.co.uk • Web site: http://www.tso.co.uk

On-line orders
DELTA Int. Book Wholesalers Ltd., 39 Alexandra Road, Addlestone, Surrey, KT15 2PQ
Email: info@profbooks.com • Web site: http://www.profbooks.com

Books on the Environment
Earthprint Ltd., P.O. Box 119, Stevenage SG1 4TP
Telephone: +44 1438748111 • Fax: +44 1438748844
Email: orders@earthprint.com • Web site: http://www.earthprint.com

UNITED NATIONS
Dept. I004, Room DC2-0853, First Avenue at 46th Street, New York, N.Y. 10017, USA
(UN) Telephone: +800 253-9646 or +212 963-8302 • Fax: +212 963-3489
Email: publications@un.org • Web site: http://www.un.org

UNITED STATES OF AMERICA
Bernan Associates, 4501 Forbes Blvd., Suite 200, Lanham, MD 20706-4346
Telephone: 1-800-865-3457 • Fax: 1-800-865-3450
Email: customercare@bernan.com · Web site: http://www.bernan.com

Renouf Publishing Company Ltd., 812 Proctor Ave., Ogdensburg, NY, 13669
Telephone: +888 551 7470 (toll-free) • Fax: +888 568 8546 (toll-free)
Email: order.dept@renoufbooks.com • Web site: http://www.renoufbooks.com

Orders and requests for information may also be addressed directly to:

Marketing and Sales Unit, International Atomic Energy Agency
Vienna International Centre, PO Box 100, 1400 Vienna, Austria
Telephone: +43 1 2600 22529 (or 22530) • Fax: +43 1 2600 29302
Email: sales.publications@iaea.org • Web site: http://www.iaea.org/books